THE UNIVERSITY
of LIVERPOOL

LIMIT LOADS OF PIPING BRANCH JUNCTIONS WITH CRACKS

Thesis submitted in accordance with the requirements of the
University of Liverpool for the
Degree of Doctor in Philosophy

by

Michael Anthony Lynch

June 2001

Acknowledgements

I herein express my gratitude to all those involved with making this research such an enjoyable and rewarding experience. I would particularly like to thank my supervisors, Dr. D.G. Moffat and Dr. D.N. Moreton, whose guidance, encouragement and friendship have been central to the work. It has been a privilege to work with them.

I would like to thank Steve Pennington for his constructive advice and assistance with the experimental work. Thanks are due to Alan Smith for his many hours spent manufacturing the test components. I would also like to thank Dr. K. Yahiaoui for his friendship and advice, particularly with regard to my early understanding of FE modelling techniques.

Thanks are expressed to EPSRC and British Energy for funding the research. In particular, I am grateful to John Bouchard for his guidance throughout the project, and for ensuring that the time spent at Barnwood was so valuable.

I must thank all of my friends for their support. Regarding friends in the department, I particularly thank Themi Petridis, Minfu Hsieh and Antonis Dris, with whom I shared the research experience. Their friendship has been greatly appreciated.

I would especially like to thank my girlfriend, Susan, for her love and support over the last year, and for being with me through the highs and lows of the writing process. Finally, I am indebted to Mum and Dad. Without their love, encouragement and understanding throughout my years of study, this project and thesis would not have been possible.

Statement of originality

This thesis is submitted for the degree of Doctor in Philosophy in the Faculty of Engineering at the University of Liverpool. The research project reported herein was carried out, unless otherwise stated, by the author in the Department of Engineering at the University of Liverpool between October 1997 and October 2000.

No part of this thesis has been submitted in support of an application for a degree or qualification of this or any other University or educational establishment. However, some parts of this thesis have been published in co-authorship with Dr D.G. Moffat, Dr D.N. Moreton and Dr M.F.Hsieh in the following papers:

- M.A. Lynch, D.G. Moffat and D.N. Moreton. Limit Loads for Cylinders with Fully Circumferential Internal Cracks in Tension: Comparison of Analytical and Finite Element Data. *9th Int. Conf. Pressure Vessel Technology, Sydney*, 2000.
- M.A. Lynch, D.G. Moffat and D.N. Moreton. Limit Loads for Cracked Piping Branch Junctions under Pressure and Branch Out-of-plane Bending. *Int. Journal of Pressure Vessels and Piping*, 77:185-194, 2000.
- D.G. Moffat, M.F. Hsieh and M.A. Lynch. An Assessment of ASME III and CEN TC54 Methods of Determining Plastic and Limit Loads for Pressure System Components. *Journal of Strain Analysis*, 36(3):301-312, 2001.

Michael Lynch
May 2001

Limit Loads of Piping Branch Junctions with Cracks

by Michael Anthony Lynch

Abstract

The R6 procedure is the basis for assessing the integrity of structures with cracks, for the nuclear industry and other industries. A failure assessment diagram is used to evaluate a structure, consisting of a fracture component and a plastic limit load component. The presented work is concerned with the limit load aspect of the R6 procedure, for piping branch junctions with cracks. For many components, limit loads are available from existing solutions. However, for branch junctions there is little available information regarding limit load assessment, for either cracked or uncracked junctions.

The objective of the present work is primarily to provide recommendations for limit load assessment of cracked and uncracked branch junctions. Following some initial work on limit loads for cracked cylinders in tension, an extensive study of the limit and plastic loads for branch junctions is presented. This incorporates extensive finite element parametric studies and a selection of experimental cases. The main load cases are pressure, in-plane branch pipe bending, and out-of-plane branch pipe bending. A variety of diameter ratios (d/D), diameter to thickness ratios (D/T) and thickness ratios (t/T) are assessed.

An extensive finite element parametric study is detailed for uncracked junctions subjected to pressure. The junctions analysed were in the geometric range: $0.25 \leq d/D \leq 1.0$, $5 \leq D/T \leq 70$ and $0.75 \leq t/T \leq 1.5$. The influence of cracks on the limit loads of branch junctions is also presented through a finite element parametric study. This covers equal thickness ($t/T=1$) junctions in the range: $0.5 \leq d/D \leq 0.95$ and $10 \leq D/T \leq 30$. The cracks were located around the weld toe of the junction intersection, having various crack angles and depth to thickness (a/t) ratios. Typical crack positions were used for each of the three load cases mentioned above. Combined loading, for out-of-plane branch pipe bending and pressure, was also studied. Limit moments for uncracked junctions are also presented for the same parametric range analysed for the cracked study.

Assessment recommendations have been derived from the main findings of the above limit load studies. In summary, equations are presented enabling assessment of the limit pressure or moment for uncracked junctions within the relevant geometric range. For cracked junctions, the ratio of the cracked junction limit loads to the corresponding uncracked junction limit loads, for all three load cases, are shown to closely relate to the ratio of the cracked to uncracked limit moment solutions for a plain pipe (with the branch pipe dimensions). Considering the presented combined loading results, circular interaction is relevant for uncracked junctions, but as the crack length extends there is a distinct trend towards linear interaction.

The objective of the experimental study was to establish the validity of the finite element results presented in the limit load studies. A total of five tests have been performed, for a selection of uncracked and cracked junctions subjected to pressure or in-plane branch pipe bending. The experimental results generally agree well with the corresponding finite element analysis, thus reinforcing the validity of the parametric limit load studies.

Nomenclature

English Symbols

a	crack depth
a_n	polynomial multiplier
c	half crack length
d, D	branch, run pipe mean diameters
d_i, D_i	branch, run pipe inner diameters
d_o, D_o	branch, run pipe outer diameters
F_{AR}	area reduction factor
F_L	general limit load
F_{LU}	general uncracked limit load
K_r	R6 fracture mechanics component
l	crack length
L_r	R6 plastic load (or reference stress) component
L_{TES}	twice elastic slope limit load
L_{TI}	tangent intersection limit load
L_5	five times elastic slope limit load
M	general moment
M_L	limit moment
$M_{L(plain)}$	plain pipe limit moment
M_{TES}	plastic moment, using twice elastic slope method
M'	normalised limit moment, using plain pipe value
M'_U	normalised uncracked limit moment
P	general pressure
P_L	limit pressure
$P_{L(plain)}$	plain pipe limit pressure
P_{TES}	plastic pressure, using twice elastic slope method
P'	normalised limit pressure, using plain pipe value
P'_U	normalised uncracked limit pressure
r, R	branch, run pipe mean radii
r_i, R_i	branch, run pipe inner radii

r_o, R_o	branch, run pipe outer radii
R_{lig}	mean radius of crack ligament
t, T	branch, run pipe thickness

Greek Symbols

α	half crack angle
ϵ	general strain
σ	general stress
σ_a	axial stress
σ_h	hoop stress
σ_{ref}	reference stress
σ^R_{ref}	creep rupture reference stress
σ_U	ultimate tensile stress
σ_y	yield stress
θ	angular location around branch pipe

Abbreviations

15ES	fifteen times elastic slope
5ES	five times elastic slope
CNC	computer numerical control
CFOD	crack face opening displacement
COD	crack opening displacement
EDM	electric discharge machining
ESF	effective stress factor
FAD	failure assessment diagram
FE	finite element
IPB	in-plane branch pipe bending
LEFM	linear elastic fracture mechanics
NLGEOM	non-linear geometric analysis
OPB	out-of-plane branch pipe bending
PP	part-penetrating (crack)

TES	twice elastic slope
TW	through-wall (crack)

Contents

Chapter 1

Introduction

1.1 Motivation of Research

Safety reviews of piping networks require several different aspects to be considered, one of which is the assessment of cracked piping components. When cracks (or defects) are detected in piping components there are guidelines that can be adopted to enable the suitability for continued safe operation to be assessed.

The basis for assessing the integrity of structures with cracks for the the nuclear industry, and other industries, is the R6 procedure [1]. This procedure evolved from the 'two-criteria' approach introduced by Dowling and Townley [2], and is now used internationally. An analysis is carried out using a failure assessment diagram (FAD), such as that shown in Figure 1.1, consisting of a fracture component (K_r) and a plastic load component (L_r). K_r provides a measure of how close the structure is to failure in the linear elastic fracture mechanics regime and L_r is a measure of how close the structure is to the plastic limit load.

A FAD can be constructed for a particular cracked component using the procedures described in the R6 procedure. This requires a series of parameters, for example: the loading applied, the material tensile properties, the crack shape and size, and the fracture toughness. The limiting condition for the component is defined by the curve plotted on the FAD.

The presented work is focused upon the **limit load** aspect of the failure assessment diagram, rather than the fracture aspect. Often, the limit load for a structure is available from within one of the limit load compendia, recommended in the R6 procedure. There is a wide range of solutions available for straight pipes with cracks, and some data for elbows with cracks. However, there is little coverage of uncracked piping branch junctions in the databases and the data available for limit loads of cracked branch junctions is extremely sparse. Such is the lack of available data that approximations to cracked straight pipes are sometimes assumed for cracked piping branch junctions, often with little justification. The main reason for this lack of data, compared with straight pipes and elbows, is the large number of variables associated with branch junctions:

- There is a wide range of different geometric combinations in use.
- There is a large number of loads and combinations of loads than can be applied to branch junctions.
- Cracked junctions have further variables associated with the location and size of the crack.

It is, of course, possible to perform finite element (FE) analyses individually as problems arise with specific junctions. However, this is time consuming and impractical. A better solution would be to provide a reference that would enable straightforward evaluation of the limit load for a given geometry and crack. To cover all of the possible variations, including crack size, would prove to be an enormous undertaking. However, a better understanding of the issues involved in limit loads for cracked branch junctions would still be a considerable step from the present condition. The overall objectives of the presented research programme are discussed in Section 1.5.

1.2 Limit and Plastic Load Definitions

The definition of the term 'Limit Load' used herein is that recommended by Gerdeen [3]:

"An appropriate definition for the theoretical limit load is the maximum load solution to an analytical model of the structure which embodies the following conditions: (1) the

strain-displacement relations are those of small displacement theory; (2) the material response is rigid plastic or elastic/perfectly-plastic, with an admissible yield function; and (3) the internal stresses and applied forces are related by the usual equations of equilibrium which ignore changes in geometry due to deformations".
This theoretical limit load may be determined by calculation, or from FE analysis of a structure, using the above conditions.

Due to the difficulty in obtaining an exact limit load value, the limit load is often presented as either a lower or upper bound to the theoretical exact value, the lower bound theorem giving the most conservative value. The lower and upper bound theorems have been defined by Calladine [4]:
Lower-bound theorem: *"If any stress distribution throughout the structure can be found which is everywhere in equilibrium internally and balances certain external loads, and at the same time does not violate the yield condition, those loads will be carried safely by the structure".*
Upper-bound theorem: *If an estimate of the plastic collapse load of a body is made by equating internal rate of dissipation of energy to the rate at which external forces do work, in any postulated mechanism of deformation of the body, the estimate will be either high, or correct".*
The definition of limit load described by Gerdeen [3] is in keeping with the underlying principles of the R6 procedure [1], requiring the use of a lower bound, idealised limit load.

The limit load cannot be determined experimentally, as the above conditions cannot be satisfied in practice. In the experimental investigations and non-linear FE calculations the term 'Plastic Load' is used, again as recommended by Gerdeen [3]:
"At this plastic load, significant plastic deformation occurs for the structure or vessel as a whole. It has the same cause as the limit load, i.e., the plastic region in the vessel has grown to a sufficient extent that the surrounding elastic regions no longer prevent overall plastic deformation from occurring".

Limit loads and plastic loads are often evaluated from suitable FE or experimental load-displacement plots ('displacement' here meaning any relevant measure of change of shape). There have been several attempts to standardise the methods for obtaining the loads from such plots. These are assessed in Section 1.4.1.

1.3 General Information and Terminology

1.3.1 Types of junction

Branch junctions (or as they are also commonly referred to: cylinder-cylinder intersections, or tees) are often found in piping systems where combination or splitting of fluid flow is required. There are different types of branch junction configuration, the main two types being:

- Forged branch junctions - these are manufactured from a single piece of material. A typical forged junction is shown in Figure 1.2(a).
- Fabricated junctions - there are two principal methods of fabrication for attaching branch pipes to the run pipes of junctions:
    - 'Set-in: the nozzle is placed through a pre-machined outlet hole in the run pipe and welded in place, as shown in Figure 1.2(b)
    - 'Set-on': the nozzle is placed on the run pipe, aligned with a pre-machined outlet, and welded in place, as shown in Figure 1.2(c). This is the more common type of fabricated junction.

For the presented work, (set-on) fabricated junctions were selected as a basis for the FE work. The primary reason for this was to give the work broader appeal by avoiding the geometric variations associated with forged junctions, in terms of the many different specifications of forged components available. In addition, for the supplementary experimental work the large variability in nominally identical components for forged components is undesirable, as found by Yahiaoui et al. [5] in a study of forged components subject to pressure loading.

Machined junctions were used for the experimental work, in order to remove the complication of the weld material. These were machined from a solid billet of material. The FE models also excluded consideration of the weld material properties, although the geometry of the weld was modelled.

1.3.2 Junction Terminology

The branch junction terminology and nomenclature used herein is defined in Figure 1.3. The main non-dimensional parameter ratios used to define a particular junction geometry are: d/D, D/T and t/T.

1.3.3 Loading

Branch junctions may be part of a complex piping arrangement, consisting of various anchor points (such as large pressure vessels or machinery) and hangars, as well as other piping components (e.g elbows). Software is available to evaluate such a system (for example, [6]), using a piping flexibility analysis, thus determining the various forces and moments at any point in the system. Isolating a branch junction, this implies a system of nine forces and nine moments: three of each acting on each of the three limbs of the junction. Applying the equations of equilibrium to each of the three reference planes, the system reduces to a set of six forces and six moments. For a typical piping system, the moments will be of far more significance to the stresses in the junction than the forces (the axial force may be important for cases where the limb lengths are short). Hence, the loading situation may be reduced to that shown in Figure 1.4, described by Moffat [7], in addition to any internal pressure loadings.

Although these moments have been isolated into the six individual categories, in practice they are unlikely to occur unaccompanied. Obviously, it is likely that one additional load will be pressure but it is also likely that there will be a combination of moment loads present. However, in order to understand the effect of each load category on the plastic behaviour of a junction it is necessary to apply the loads individually.

In this study, limit loads for three of the main loads of concern have been assessed individually for branch junctions: internal pressure, out-of plane branch pipe bending, and in-plane branch pipe bending. The two moment categories were chosen as they are known to generally cause higher stresses than the others, and internal pressure is obviously a common load for most piping systems. Combinations of out-of plane bending and pressure have also been studied.

1.3.4 Cracked Junctions

The assessment of limit loads for cracked junctions was the main area of interest. Crack locations should be based upon peak elastic stress locations (as described by Moffat et al. [8]) and fatigue test data for branch junctions (e.g. using fatigue crack locations such as those described by Decock [9] or Yahiaoui et al. [10]). Some typical crack locations are shown schematically in Figure 1.5 for the load cases considered. In addition to the loads mentioned above, a small selection of cracked junctions subjected to in-plane run pipe bending were also studied. The locations used for the cracked junction study will be described in detail in Chapter 4.

1.4 Literature Survey

There is very little available data for cracked branch junctions, as discussed in Section 1.1. As this thesis includes both cracked and uncracked limit load analysis, any existing recommendations for evaluation are explored. Relevant experimental studies giving plastic loads are also discussed.

1.4.1 Determination of Limit and Plastic Loads

There are various methods for the evaluation of limit or plastic loads from load-deformation plots. Unfortunately, there does not appear to be a universally accepted method for evaluation. A detailed review of these methods has been presented by Kirkwood [11].

The techniques used for limit and plastic load assessment are quite similar, with the same techniques often used for each. There are two main techniques, for which there are several variations:

- **The Tangent Intersection Method.** This method defines the limit load as the intersection of the tangent to the elastic region with a tangent from the plastic region, as illustrated in Figure 1.6(a) (where L_{TI} is the tangent intersection limit load). This has been used in a large number of publications to evaluate the limit load, but can vary greatly due to the non-linear behaviour in the plastic region. The tangent in the plastic region can be constructed at a number of different points, because of the continually changing curvature of the response. The resulting limit load would largely depend upon the judgement of the analyst. In an attempt to remove this subjectivity, the CEN draft pressure vessel design code [12] recommends that a maximum principal strain value of 5% can be used to define the point on the plastic curve to which the tangent should be drawn (the load at 5% principal strain is marked L_5 in Figure 1.6(a)). This method has been evaluated by Moffat et al. [13], for both limit and plastic loads, concluding that a unique limit load level can be obtained, irrespective of the elastic behaviour of a component (i.e. regardless of the limb length). The method is valid for FE work, both for limit and plastic load assessment, although the load corresponding to 5% principal strain may vary considerably for FE models, depending on the mesh density around stress concentrations. However, it may be difficult to apply this technique correctly to an experimental case, unless the position and direction of the maximum principal strain can be monitored.

- **The Twice Elastic Slope Method.** This is an arbitrary method, recommended in the ASME III pressure vessel design code [14] to determine a 'collapse load' from a load-displacement plot determined using full non-linear analysis. The technique is illustrated in Figure 1.6(b), where the plastic load derived using this method is marked L_{TES}. The term 'twice elastic slope' is actually incorrect, as the slope of the load-displacement plot is halved to obtain this plastic load. Although the term 'collapse load' has been used, the correct term would be **'plastic load'**, as discussed in Section 1.2. ASME III warns that "particular care should be given to ensure that the strains or deflections that are used are indicative of the load carrying capacity of the structure", but does not specify the criteria upon which this decision should be based.

  For **limit load assessment** this technique has been adapted to derive the limit load from a well-established 'plateau'. The twice elastic slope tends to give load values that are below this plateau, and hence the 'five times elastic slope', or even 'fifteen times elastic slope', [15] have been used to obtain limit loads. These methods are purely arbitrary and are a means of comparing limit loads for similar components. The technique used for limit load assessment should not make a great difference, provided the load value derived lies on the plateau.

The limit loads throughout the presented work are evaluated using the 'five times elastic slope' method. unless stated otherwise. This method is shown schematically in Figure 1.6(c). Plastic loads have been assessed using the 'twice elastic slope' method.

1.4.2 General Limit Load Studies

The present work has emerged from a previous study on cracked piping components by Yahiaoui et al., consisting of experimental and FE work. The study concentrated on plain pipes and elbows, for which the published work included:

- Cracked plain pipes [16] - considering the effects of hoop and axial part-penetrating (a/t=0.5) cracks on the plastic loads of plain pipes.
- Cracked piping elbows [17] - limit load results were presented for elbows under pressure and opening bending, with axial and circumferential cracks. Experimental and FE Plastic loads were also presented [18].

In addition to this, some work was performed on a particular geometry of forged branch junction with cracks [19]. This work was limited in parametric variation and was quite specific to the geometry considered. The results are discussed in Section 1.4.4.

Limit load solutions for a variety of cracked components have been compiled by a number of authors, including Miller [20], Decock [9], Jones and Eshelby [21], and Al Laham [22] (the SINTAP compendium). However, there is very little mention of branch junctions in these reports, whether cracked or uncracked.

Miller [20] suggested that 'if the nozzle has been well designed, with suitable reinforcement' then the nozzle should not weaken the component and the analysis can take the form a plain cylinder assessment. Alternatively, Miller suggests, the analysis can be reduced to an uncracked junction with thickness equal to the crack ligament thickness. However, no comprehensive method was provided for uncracked junction assessment. Miller also briefly presents some limit pressure solutions for cracked cylinder-cylinder intersections. These were for the crack geometry shown in Figure 1.7(a) and the results were in the form of charts, an example of which is shown in Figure 1.7(b). These results are quite basic, and do not account for crack length, one of the most important parameters for evaluating limit loads.

The SINTAP compendium [22] presents some tubular joint solutions for both uncracked and cracked junctions, which are discussed in the following Sections.

1.4.3 Uncracked Branch Junctions

Single Loading

There is a range of articles available on limit and plastic loads for piping branch junctions subjected to single or individual loads. However, prior to examining branch junctions under plastic loading, the elastic behaviour of the junctions should first be generally appreciated.

Elastic stress analysis of four equal diameter branch junctions has been described in detail by Moffat [7], for all six external moment loadings mentioned in Section 1.3.3. This work was experimental, with strain readings recorded via an extensive array of strain gauges. The four junctions had D/T ranging from 11.4 to 41.4, and were tested in pairs. The setup for each test was such that each of the moment loadings satisfied the cantilever model. The locations for the maximum effective stress factor (ESF) in each junction were listed for the six moment loads. This work was subsequently extended by Moffat et al. [8], using FE data, to incorporate a much wider range of junction parameters. The junctions dimensions were in the range $0.2 \leq d/D \leq 0.8$ and $5 \leq D/T \leq 70$. The maximum ESF results were presented for the six moment loads and internal pressure in the form of polynomial equations in d/D, for the D/T ratios analysed (note that the ESF locations were not included in this wider study). The pressure results were later used by Moffat et al. [23] to develop a single parametric equation, enabling the ESF for any branch junction under pressure loading to be derived.

The maximum ESF locations are useful when considering crack locations for particular loadings, although there are also other factors to consider. There are many other elastic stress studies available for branch junctions, but these are not discussed here as they are not directly relevant to the presented research project. Aspects of some of these other elastic studies have been reviewed by Kirkwood [11] as part of an extensive survey of the available literature.

For plastic loading of branch junctions, and more specifically limit load analysis, there are a number of studies that are relevant. Again, Kirkwood [11] has evaluated many of these. This survey is not repeated, but some of the more significant publications are highlighted, for pressure and moment loading. As mentioned previously, the limit load compendia make very little mention of branch junctions and it seems that, despite all of the research, very little practical use has been made of existing data. This is not to say that there is no useful data, rather that there is no set of universally accepted guidelines derived from this data.

Limit (and plastic) pressures for branch junctions have been researched extensively over many decades - among the earliest published work on plastic testing of branch junctions was that by Blair [24] in 1946. Surprisingly, considering the quantity of publications on the subject, there is still no definitive formula or equation for deriving the limit pressure for a junction of a particular geometry. This research project has included a parametric study for limit pressures of uncracked branch junctions, described in Chapter 3. A selection of the references mentioned in this section are evaluated alongside these FE results, and are thus discussed in more detail in Chapter 3.

Cloud and Rodabaugh [25], have been among the most influential contributors to the field of branch junction limit analysis and presented a theoretical limit pressure solution derived from an upper bound limit analysis. The analysis was limited to junctions with $d/D \leq 0.5$ and was based on the postulation of four different mechanisms of collapse in the junction. Two of the mechanisms involved collapse of the individual run and branch pipes, for which the solutions are straightforward. For the other two mechanisms, the first consisted of two plastic hinges forming in the branch pipe (nozzle) and one in the run pipe, and the second mechanism had a single hinge in the branch pipe and two hinges in the run pipe. Solutions were calculated for these two mechanisms, followed by test data from a junction with a d/D ratio of 0.5, a D/T ratio of 25 and a t/T ratio of 1.0. The pressure was plotted against the radial deflection of the run pipe, and the authors noted that their theoretical limit solution was similar to the onset of large deformation of the junction.

Rodabaugh and Cloud [26] produced a subsequent publication which compared the solutions from [25] with 46 pressure tests. The solution was thought to give a good approximation to a junction's limit pressure. More recently, Rodabaugh [27] produced an extensive review of existing 'area replacement rules'. In this review, the solution from [25] was again cited, with the equation given for cases where the yield strength of the run an branch pipes are identical, as:

$$P_L = p^*(2\sigma_y T/D) \tag{1.1}$$

where,

$$p^* = \frac{[A(t/T)^2 + 228(t/T)(d/D) + B]\lambda + 155}{108\lambda^2 + [228(d/D)^2 + 228]\lambda + 152} \leq 1.0 \tag{1.2}$$

$A = 162$ for $t/T \leq 1.0$; $A = 54$ for $t/T > 1.0$

$B = 210$ for $t/T \leq 1.0$; $B = 318$ for $t/T > 1.0$

$\lambda = (d/D)(D/T)^{0.5}$

This equation was developed for $d/D \leq 0.5$, but Rodabaugh suggests that it may give reasonable guidance for all d/D values. Equation (1.1) is evaluated in detail in Chapter 3 for a broad range of parameters.

Limit pressure theory was also developed by Schroeder, generally from an upper bound aspect. One example of this was Schroeder and Rangarajan [28], with an upper bound solution presented for the limit pressure of branch junctions. The method was fairly complex and required a computer program to calculate the limit pressures. The authors presented validation of their solution by comparison with results from two experimental junctions. The plastic pressure was determined using the tangent intersection method, with the branch end deflection used as the deformation parameter. The upper bound solution was found to be approximately 20% higher than the experimental plastic pressure values.

Another key contributor, from the same period as Schroeder, was Ellyin. Using a lower bound analysis of the problem, Ellyin and Turkkan [29] utilised a similar approach to limit pressure analysis as Schroeder and Rangarajan [28]. The solution was again complex and was validated through comparison with existing experimental data, giving good comparison. The solution was also compared with other methods of analysis (including that of Schroeder and Rangarajan [28]) and was found to give a lower bound solution as expected.

In 1978, Robinson [30] presented an extensive parametric survey using another theoretical technique. Using a lower bound solution, limit pressures for a wide range of junctions were presented: ranging from d/D of 0.05 to 0.8, D/T ratio of 30 to 400 and t/T ratio of 0.05 to 2.0. A selection of these results are compared with the FE results in Chapter 3.

More recently, Tabone and Mallet [31] presented a study of a single branch junction (d/D=0.65, D/T=31, t/T=0.66) using FE analysis. This study concentrated on combined out-of-plane moment and pressure loading, but also presented individual pressure and out-of-plane moment results. For the pressure case the deflection of the node at the centre of the branch pipe end was used as the deformation parameter. For evaluation of the limit load, an extrapolation method was used by plotting the load against the inverse displacement. The technique required the load to be plotted against the inverse of the displacement parameter. The resulting curve was then extrapolated linearly to the load axis, using the slope at the end of the analysis. The limit load was defined as the intersection of this extrapolated curve with the vertical axis. There must be some doubt about this method of limit load evaluation, as the limit load will always be higher than the final load level of the analysis, and also depends upon the slope of the load-displacement curve at the point the analysis finished. The last point of the analysis may vary considerably, depending upon the method of analysis and the limits used. However, ignoring the concerns regarding the conservatism of this method, the limit pressure of 6.21MPa agreed well with a predicted value of 6.15MPa (obtained using the Cloud and Rodabaugh equation (1.1)). The combined loading work is discussed later.

Kirkwood and Moffat [32] presented experimental plastic loads for an equal diameter junction (d/D=1.0), with D/T ratio of 24 and thickness of 6.24mm. The pressure was plotted against volumetric change, as recommended by Gerdeen [3]. The plastic pressure, defined using the twice elastic slope method, was 38.2MPa. The result was part of a wider study on the interaction between pressure and in-plane moment loads. This work is discussed in more detail in the following combined loading section.

Sang et al. [33] presented analytical and experimental results for a branch junction with d/D ratio of 0.53, D/T of 101, and with equal wall thickness throughout. The spread of plasticity was studied, along with the burst pressure for the experimental junction. The authors state that limit pressures for both experimental and FE cases were presented. However, limit loads cannot be determined experimentally, using Gerdeen's [3] definition, and a full non-linear material response was used for the FE case, rather than elastic/perfectly-plastic material. It is believed that the term 'limit load' should be replaced with 'plastic load' in this work. This is a common finding with many publications: the limit load is often not defined correctly, leading to inappropriate comparison between data from different sources. The 'plastic loads' presented by Sang et al. were obtained from plots of pressure against strain at two different strain gauge locations. The tangent intersection method was used to obtain the plastic loads, but the resulting limit pressures appeared to depend largely upon the judgement of the authors (particularly for the experimental case) and were not convincing.

Results for another experimental case were presented by Yahiaoui et al. [5], alongside corresponding FE results. The junction studied was a forged equal diameter branch junction, and cannot be directly compared with results from cylinder-cylinder analyses. The plastic loads were obtained from plots of pressure against the diametral growth across the flank of the junction. The twice-elastic slope method was used. The comparison between the experimental and FE plastic loads was good. The comparison of the strain data between the experimental case and the FE model was not good. Yahiaoui et al. acknowledged that the geometrical inconsistencies of the forged junction resulted in difficulties in constructing an adequate FE model.

Two solutions for the limit pressure of an uncracked tee are provided by Zahoor [34] in the Ductile Fracture handbook:

Solution 1

$$P_L = p_r \left[1 - 7.3573 \times 10^{-2} \beta - 0.15147\ \beta^2\right] \tag{1.3}$$

Solution 2

$$P_L = p_r \left[1 - 7.6908 \times 10^{-2} \beta - 0.2332\ \beta^2\right] \tag{1.4}$$

where, $p_r = 2\sigma_u T/D$, and $\beta = (dt/DT)^{0.5}$

(Solution 2 represents an estimated lower bound to the data).

Although these solutions refer to the 'limit pressure', it is thought that they are actually solutions for the burst pressure of a junction, as there is no allowance made for the yield stress, σ_y. The above solutions could be evaluated by substituting σ_y for the ultimate tensile strength, σ_u. This assumes that the limit pressure can be scaled from the burst pressure solution, according to the ratio of the yield to ultimate strength of the material. However, this assumption is highly unsatisfactory for limit pressure analysis, where elastic/perfectly-plastic material is assumed with no consideration of the ultimate strength of the material. Hence, this method is not recommended and results were not presented alongside other methods in Chapter 3.

In the R5 procedure for high temperature assessments, advice for the assessment of uncracked and cracked piping branch junctions is given in Appendix A3 [35]. This appendix cites the recommendation of Budden and Goodall [36] to use the Inverse Code Method (as described by Booth [37]) as a useful approach for uncracked junctions under pressure. This method is described in detail in Chapter 3 and is compared with the FE parametric study results.

Budden and Goodall [36] also produced an FE correlation equation, based on the results of a parametric study on limit pressures, produced by Galt [38]. This equation is also evaluated in Chapter 3.

Considering external **moment loading** of uncracked branch junctions, there are less publications than for pressure loading. Schroeder [39] again made significant contributions to the literature, providing an upper bound analysis for in-plane and out-of-plane moment loadings on the branch pipe of junctions with d/D ratios up to 0.8. This work was expanded over the following years and has been described thoroughly by Kirkwood [11].

Ellyin and Turkkan extended their lower bound limit pressure analysis, using the same principles, to include out-of-plane branch moments [40] and later in-plane branch moments [41]. A wide d/D ratio was covered in their parametric study: from 0.1 to 1.0. Again, this work has been extensively reviewed by Kirkwood [11].

Rodabaugh [27] discussed the issue of limit moments, noting that out-of-plane limit moment appeared to be less than or equal to the in-plane and torsional limit moments of the branch pipe. Rodabaugh proceeded to discuss out-of-plane branch pipe moment loading, citing the ASME pressure vessel design code [42] from which a limit moment equation was presented:

$$M_L = \sigma_y \left(\pi/4\right) d^2 t/B_{2b} \tag{1.5}$$

where the B_{2b} index was defined as:

$$B_{2b} = 0.945 \left(D/T\right)^{2/3} \left(d/D\right)^{1/2} \left(t/T\right) \left(d/d_o\right); \geq 1.0 \tag{1.6}$$

Rodabaugh also presented an equation from [43] for the out-of-plane limit moment:

$$M_L = \left[1.4 + 9.8 \left(d/D\right)\right] dT^2 \sigma_y; \leq d^2 t \sigma_y \tag{1.7}$$

This equation was based on test data (implying that it is intended for plastic moments rather than limit moments) for tubular joints with D/T between 35 and 98 and d/D between 0.19 and 0.9. Rodabaugh then normalised the above equations using the limit moment for a straight pipe of branch pipe dimensions. The plain pipe limit moment, from simple shell theory, was used:

$$M_{L(plain)} = d^2 t \sigma_y \tag{1.8}$$

Hence, equations (1.5) and (1.7) were divided by equation (1.8), giving:

$$M_L/M_{L(plain)} = \left(\pi/4\right)/B_{2b} \tag{1.9}$$

$$M_L/M_{L(plain)} = \left[1.4 + 9.8 \left(d/D\right)\right] / \left[\left(D/T\right) \left(d/D\right) \left(t/T\right)\right]; \leq 1.0 \tag{1.10}$$

Rodabaugh compared these two equations with test data from a variety of publications, concluding that equation (1.10) compared well with the test data. This equation is discussed in Chapter 4, by comparison with the presented FE limit load data.

Tabone and Mallet [31] presented results for out-of-plane branch moment loading, alongside the pressure result described above. The limit moment was 2.37kNm, compared with a plain pipe value of 4.89kNm (calculated using equation (1.8)).

Kirkwood and Moffat [32] also presented plastic moment results for in-plane moment loading of the branch pipe of a junction. The junction, of the same geometry as that described previously for pressure loading, had a plastic moment of 32.75kNm (derived using the twice elastic slope method from a plot of the moment against the branch pipe rotation). This was a prelude to the combined loading work, which was the main objective of the work and is discussed in the following section.

Yahiaoui et al. [19] presented experimental and FE results for a forged piping branch junction. Although not directly comparable with cylinder-cylinder intersections, the difficulties associated with applying pure out-of-plane branch moment loading were tackled as part of a wider study into cracked junctions (discussed in Section 1.4.4). The agreement between the FE and experimental plastic moments was not good, with the FE result 33% higher than the experimental result. The geometric inconsistency in the forged junctions was probably a major factor in this large difference.

The use of tubular joint data and design codes in assessing branch junctions is quite common for external loads. Tubular joints are used in a variety of applications, from simple frameworks or supports, to offshore structures. The integrity of such joints is often as safety critical as for piping branch junctions, although the joints are not generally subjected to pressure loading and the most common load is axial compression of the brace (equivalent to the branch pipe). There is a considerable amount of data available in design codes for moment loadings, and this is often used by piping engineers.

In order to justify this, the strength of the extra 'plug' of material in the tubular joint (i.e. the run pipe is solid and does not have an opening) is assumed to be negligible. However, no publications were found that compare the strength of tubular joints with branch junctions. This is unsurprising, as the offshore and piping industries do not tend to work alongside each other. However, in order to justify the use of design codes from another field some validation is required. This issue is covered in Chapter 4 as part of the parametric study for moment loadings. Several of the branch junctions studied have been remodelled as tubular joints, including the 'plug' of material, and subjected to limit moment analysis. A comparison is then made with the branch junction limit moment results.

Three tubular joint solutions have been obtained from the literature. The first of these solutions was referred to in the **SINTAP compendium** [22] and originated in design guidance for offshore structures [44]. The limit moment solution is for in-plane and out-of-plane branch bending of a tubular T-joint, and is calculated as follows:

$$M_L = Q_u Q_f \sigma_y T^2 d_o \tag{1.11}$$

where,

Q_f = a factor to allow for the presence of axial and moment loads in the run pipe ($Q_f = 1.0$ for single branch moment loading)

Q_u = a strength factor which varies with the joint and load type

For in-plane bending: $Q_u = 5\beta\gamma^{0.5}$

For out-of-plane bending: $Q_u = (1.6 + 7\beta)\, Q_\beta$

$\beta = d_o/D_o$

$\gamma = D_o/2T$

Q_β = a geometric modifier defined as:

$Q_\beta = 1.0$ for $\beta \leq 0.6$ $\qquad Q_\beta = \frac{0.3}{\beta(1-0.833\beta)}$ for $\beta > 0.6$

The second solution is that from an **API publication** [45] covering working stresses for offshore platforms. This includes formulae for the calculation of allowable loads of tubular T-joints under axial loads and branch in-plane and out-of-plane moments. The allowable moment capacity (M_a) solution is presented and is of a similar form to that from [22] presented above.

$$M_a = Q_u Q_f \frac{\sigma_y T^2}{1.7}\, 0.8\, d_o \tag{1.12}$$

where the definitions are the same as for [22] with the exception of Q_u:

For in-plane bending: $Q_u = (3.4 + 19\beta)$

For out-of-plane bending: $Q_u = (3.4 + 7\beta)\, Q_\beta$

Finally, the **CIDECT design guide** [46] again includes formulae for the design strength of tubular T-joints under branch pipe moments. The formulae for the design moments for in-plane and out-of-plane bending (M^*_{zb} and M^*_{xb}, respectively) are as follows:

$$M^*_{zb} = 4.85\sigma_y T^2 \gamma^{0.5} \beta d_o \tag{1.13}$$

$$M^*_{xb} = \sigma_y T^2 \frac{2.7}{1 - 0.81\beta} d_o \tag{1.14}$$

where, β and γ are defined as above for [22].

The three tubular joint assessment methods described above, from [22], [45] and [46], are evaluated in Chapter 4 by comparing the predictions with the FE results obtained.

Combined Loading

There has been a considerable amount of elastic work published on combined loading of branch junctions. For example, Moffat and Mistry [47] published elastic interaction results for a range of branch junctions, subjected to various combinations of pressure and external moments.

Interaction diagrams are the most common means for illustrating the interaction between two different loads on a component. One load is plotted on the vertical axis with the other plotted on the horizontal axis. For elastic analysis, the axes often represent the first yield load for the component, normalised to the single loading values. A distribution would then be plotted to show how the first yield is effected by combinations of the two loads, as in [47]. For limit and plastic loads, the axes usually represent the limit or plastic load for the component, each normalised using the single loading limit load values. Again, a distribution would be plotted to show the limit or plastic load for the component when subjected to combinations of the two loads. A typical limit load interaction diagram is shown in Figure 1.8, considering just the positive aspects of two loads. Circular interaction and linear interaction are marked with two examples of possible interaction behaviour for a component. Calladine [4] presented the 'convexity theorem' which states:

"The locus in the independent loading space of the collapse loads of a structure is convex"

This indicates that limit load combinations that occur within the linear interaction line are not possible.

Available publications for plastic and limit load work are limited. Tabone and Mallet [31] described combined pressure and out-of-plane bending for a junction with d/D equal to 0.65, D/T ratio of 31 and t/T ratio of 0.66. The load was plotted on an interaction diagram, normalising each axis using the previously described individual limit load results, and was found to be close to circular interaction. To obtain a full interaction response several more load combinations would be required.

Kirkwood and Moffat [32] described experimental interaction results for combined pressure and in-plane moment loading of the branch or run pipes of equal diameter junctions (D/T=24, t/T=1). The plastic load results were obtained using the five times elastic slope method and then plotted in the form of an interaction diagram. Circular interaction was found to give a reasonable approximation to the results.

Nadarajah et al. [48] presented combined loading FE results from a parametric survey covering junctions in the range: d/D values of 0.1, 0.2 and 0.4, D/T values of 100, 200 and 400 and t/T ratio of either 0.5 or 1.0. The loads considered were internal pressure and in-plane branch moment. The study utilised the elastic compensation method to calculate the upper and lower limit loads from simple shell FE models. The elastic compensation method was devised as a means of simulating plastic analysis by altering the elastic modulus of the elements in an FE model, according to the ratio of stress in each element to a nominal stress. The method is more economical in terms of computing time required compared with an equivalent plastic FE analysis, although this is becoming a less important issue with the constant development of more powerful processors. The results of the study indicated that the interaction behaviour was generally circular.

Finally, the inverse code (described previously for pressure loading) can be used to assess combined moment and pressure loading for a branch junction. This procedure is assessed by comparison with a selection of combined loading FE results in Chapter 4.

1.4.4 Cracked Branch Junctions

Single Loading

There is little available literature for cracked branch junctions. Assessment methods often consist of crude approximations to cracked plain pipe solutions. It is suggested in [35] that the limit load for a cracked branch junction can be obtained from that for the uncracked junction by using a scale factor based on the ratio of the cracked to uncracked limit load for an equivalent plain pipe:

$$\frac{F_L\,(Cracked\ Branch\ Junction)}{F_L\,(Uncracked\ Branch\ Junction)} = \frac{F_L\,(Cracked\ Plain\ Pipe)}{F_L\,(Uncracked\ Plain\ Pipe)} = \frac{F_L}{F_{LU}} \quad (1.15)$$

This approach lacks the necessary validation, and is recommended with caution in [35]. In Chapter 4, a selection of FE model results are compared with results obtained using this method. Obviously, if the method were validated extensively, it would be extremely useful since limit load solutions for plain pipes are widely available, even for various defect shapes under combined loading (for example, Miller [20] and Jones and Eshelby [21]).

The literature specifically covering branch junctions is now examined. The earliest work found on branch junctions with defects was that of Schulze et al. [49], published in 1984. The work consisted of a series of tests on straight pipes and 'T-pieces'. The 'T-piece' (branch junction) study consisted of a series of tests on equal diameter (d/D=1) forged branch junctions with a variety of artificially inserted defects. The defect locations were chosen to be suitable for the load applied, and are shown in Figure 1.9. The branch junctions were loaded in five different ways, with loads applied up to 'realistic operating conditions'. The loads were as follows:

- Pressure loading, with crack running internally around the crotch of the junction in the axial direction - three part-penetrating cracks were tested with varying crack depth and length;
- Combined pressure and in-plane run pipe bending, with a crack on the flank orientated parallel to the branch pipe - one part-penetrating crack tested with constant pressure and increasing moment;
- Combined loading, as for the previous case, but with the moment direction reversed - one part-penetrating crack was tested with constant pressure and increasing moment;
- In-plane branch pipe bending with a crack at the crotch of the junction, orientated circumferentially - one through-wall crack was tested;
- Torsional moment applied to the end of the run pipe with the crack orientated diagonally on the flank of the junction - one through-wall crack was tested.

Unfortunately, the results of these tests were not presented in any detail. For the pressurised cases, the only results supplied were the pressures at which leakage, rupture or collapse occurred. For the moment-only cases, the maximum moment applied was stated, along with some details of crack extension and opening. The 'T-piece' study appears to have been supplementary to the primary study into plain pipes with defects.

Zahoor [34] presented some of the few solutions for limit loads of branch junctions. The source of the solutions was stated as an internal company report, which cannot therefore be examined. However, this report covered burst data from piping junctions, and so the solutions provided may not actually be for true limit load conditions.

Two solutions were presented:

1. Axial part-penetrating crack at the crotch, with internal pressure loading - Figure 1.10(a);
2. Part-penetrating cracks on the flank, with internal pressure loading - Figure 1.10(b).

The solutions were as follows:

1.

$$P_L = P_o \left[1 - 1.1x\left(1 - 0.2x\right)\right] / \left[1 - 1.1x^2/M\right] \tag{1.16}$$

where,
$P_o = \sigma_f T/R$
$x = a/t$
$M = 2.3 + 1.25\,(c/R)$

σ_f is the flow stress, stated as the average of the yield and ultimate strengths; 'c' is the crack half-length; 'a' is the crack depth. The applicability was stated as:

- Failure by ligament collapse
- d/D = 1, t/T = 1
- 0 ≤ c/R ≤ 0.5; a/t ≤ 0.8 and 10 ≤ D/T ≤ 20

2.

$$P_L = P_o\left[1 - 1.1\,(x)^{0.8}\,(1 - 0.4x)\right] / \left[1 - 1.2\,(x)^{1.4}/M\right] \tag{1.17}$$

Note that in the original text, the above equation was stated as:

$$P_L = P_o\left[1 + 1.1\,(x)^{0.8}\,(1 - 0.4x)\right] / \left[1 - 1.2\,(x)^{1.4}/M\right] \tag{1.18}$$

but it is believed that the first '+' sign is a mis-print, and should be negative as shown in equation (1.17). Also, the flank is mistakenly referred to as the crotch in the text.

The definitions were as for the crotch case, but with:
$M = \left[1 + 1.2987\gamma^2 - 0.026905\gamma^4 + 5.3549 \times 10^{-4}\gamma^6\right]^{0.5}$
$\gamma^2 = c^2/Rt$

The applicability for this case was stated as:

- Failure by ligament collapse
- d/D = 1, t/T = 1
- $0 \leq c/R \leq 2$; $a/t \leq 0.8$ and $10 \leq D/T \leq 20$

The fact that the solutions include reference to the flow stress, based upon an average of the yield and ultimate strength, implies that they are not intended for limit load analysis (for which the material properties are elastic/perfectly-plastic, and do not include the ultimate strength) but rather for estimation of experimental burst pressures. This solution was not compared with the FE data in Chapter 4, due to the limited geometric range covered (it was only specified for junctions with d/D=1).

Schwarz et al. [50] presented a set of results from tests on a series of five branch junctions with cracks located internally at one crotch corner of each junction. An uncracked junction was also tested. The results were part of a wider study which also included piping elbows. The loading was combined: constant pressure was applied with increasing in-plane moment. The junction dimensions are shown in Figure 1.11. The d/D ratio was 0.33, the D/T ratio 16.6 and the thickness ratio (t/T) was 0.86. The branch pipe was of a concentric design and became wider and thinner away from the intersection region (d/t ratio increased from 6.3 at the intersection to 18). The details of each test specimen are reproduced in Table 1.1. There were numerous variables, making the effect of each individual variable difficult to isolate:

- For junctions AZ2, AZ4 and AZ6 the materials for the branch and run pipes were different (materials A and B), although in the text the two materials were stated as being of similar yield strength and Young's modulus;
- A variety of temperatures were used for the tests. Three tests were performed at approximately room temperature (AZ1, AZ3 and AZ6), with junction AZ2 tested at 90°C and junction AZ4 tested at 130°C;
- The four cracks were elliptical in shape and were produced using spark erosion techniques (electrical discharge machining). However, two of the cracks were then extended (junctions AZ4 and AZ6) using cyclic internal pressure loading in order to produce 'pre-fatigue cracks'. The crack depth and length for the two spark-eroded cracks were constant (a/t=0.25, l=40mm) and one of the fatigued cracks was also similar (a/t=0.26, l=42mm). The remaining fatigued crack was considerably deeper (a/t=0.42, l=39.5mm).
- The pressure level was between 15-16MPa for four of the tests, but the fifth test (the junction with the deeper crack) had a lower pressure level of 11MPa.

The results of these tests were presented as moment-displacement plots for junctions AZ1, AZ4 and AZ6 (the displacement used is not stated, but is assumed to the displacement of the ram used to apply the moment). The maximum moment levels are stated in Table 1.1, but it is unclear if these were failure moments or merely the maximum moments applied. It is believed that they were the maximum moments prior to failure, although the uncracked junction may not have been tested to failure. Comparing the moment-displacement plots for each junction, it was found that there was no size effect of the flaw on the behaviour of the junctions until failure occurred. Prior to failure, each junction exhibited similar moment-displacement responses to the uncracked case, the differing ultimate moments being the only indication of the presence of a crack. Surprisingly, the junction with the largest flaw (AZ4) appeared to behave in the same way, although this may have been a result of the slightly lower pressure level for this test. Junction AZ6 had a lower moment compared to the other junctions, and clearly failed prior to the other junctions. Overall, the results show that relatively large cracks at the crotch corner of a junction under combined pressure and moment loading can have little effect on the failure moment of the junction. The results may have been of more interest if fewer parameters had been varied.

Schuler et al. [51] supplemented the work of Schwarz et al. [50] by producing finite element models of the cracked elbows and branch junctions. Considering the branch junctions, the primary objective of the work was a fracture mechanics evaluation of the junctions. However, a comparison of the FE and experimental moment-displacement response was provided for junction AZ6, with good agreement found.

Plancq and Berton [52] presented analysis of various cracked branch junctions, utilising the elastic compensation method, as described previously for [48]. Various uncracked junctions, subjected to pressure or out-of-plane branch bending, were analysed and verified by comparison with the work of various authors, including Nadarajah et al. [48] and Cloud and Rodabaugh [25]. Junctions with 'defects' were then examined, covering two types of cracked junction.

- The first cracked junctions studied were not illustrated in the publication, and only warranted a short paragraph of description. The loading case used was out-of-plane branch moment and the crack 'settled into the intersection between the branch and the run'. It is assumed that this was a through-wall crack on the flank of the junction, and also that the FE model was a shell model, as for the cracked junctions. The junction had d/D ratio equal to 0.5, t/T equal to 1.0 and D/T equal to 72. Results were presented as non-dimensional limit moment against 'half angle from the centre of defect' as shown in Figure 1.12(a). The results show a considerable reduction in limit moment for large crack angles.

- The second type of cracked junctions considered had cracks running longitudinally along the run pipe, centred at the flank of the junction, as shown in Figure 1.12(b). Six junctions were analysed for internal pressure loading, with d/D equal to 0.5 or 0.25, D/T equal to 50 or 100 and the value of t/T was stated as 1.25 or 2.5. The crack length was also varied between 15mm and 50mm. The dimensions for the six junctions are presented in Table 1.2 along with the resulting limit pressures, in non-dimensional form.

It is unfortunate that more detail was not provided for the study, for example the boundary conditions used, the means of applying the moment, and the exact location of the crack for the bending models. It is also significant that the weld was not modelled due to the use of shell elements. The purpose of the work was to illustrate useful applications of the elastic compensation method, rather than to provide extensive limit load data.

Results from another cracked branch junction study were presented by Chapuliot and Moulin et al. [53]. Seven out-of-plane bending tests were presented, with a number of variables used:

- Junctions with or without additional pressure application;
- Junctions with or without a notch (crack);
- Junctions with or without a weld at the intersection.

The test specifications are summarised in Table 1.3. The junctions were machined from thick pipe, with a short branch stub, and are shown in Figure 1.13(a) - the d/D ratio was 0.48, D/T was 19 and t/T was 1.38. Extension limbs were welded onto this machined junction. It is unclear if a weld profile was machined into the junctions. The crack location (the crack was sometimes referred to as a notch in the text) is also shown in Figure 1.13(a) for junctions without a weld, and for junctions with a weld. The cracks were machined at the junction boundary using a 1mm thick milling cutter to a width of 20mm and a depth of 1mm (compared with the run pipe thickness of 8.3mm - a/T=0.12). During testing, both ends of the run pipe were stated to be embedded, although no test setup was provided. Out-of-plane bending was tested using a hydraulic ram to apply a displacement at the end of the branch pipe extension limb. For the pressure loading cases, a pressure of 12MPa was maintained in the junction.

The load-displacement curves for all of the tests are shown in Figure 1.13(b), with the maximum load value, the excessive strain value and the crack initiation load listed in Table 1.3. The maximum load values for junctions 5.7 and 5.8 were not reached, but all of the other junctions reached a peak. The excessive strain load was defined by the load at which the imposed total displacement was equal to the twice the elastic displacement. The crack initiation load was listed for the cracked models, and referred to the load at which crack propagation started. It is clear from Figure 1.13(b) that all of the load-displacement responses were similar, with the exception of junction 5.7 which reached a considerably higher load than the other junctions. This junction was one of the two junctions with pressure applied (the other, junction 5.8, leaked before the entire load-displacement response was obtained) and appeared to have been strengthened by the pressure loading. The experimental results were followed by the presentation of FE results, concentrating on the fracture mechanics aspect of the tests rather than the global load-displacement response. However, global load-displacement FE results were presented in a later publication by Chapuliot and Moulin [54] for test numbers 2 and 3, showing good comparison between the FE and experimental results.

The cracked pressure test (test number 5.7) described above was discussed in more detail in another publication by Chapuliot and Moulin [55], in which it was stated that the internal pressure had a beneficial effect on the junction behaviour. It was postulated that the pressure increased the junction's global rigidity, particularly against local buckling of the run pipe by the displacement of the branch pipe. However, it was also found that the internal pressure increased the load imposed locally to the crack, hence increasing the tearing initiation. These findings were verified using FE models. The main conclusion from examining the work of Chapuliot and Moulin is that small cracks on the flank have very little influence on the global behaviour of the model.

Yahiaoui et al. [19] presented experimental and FE results for a forged piping branch junction, with cracks, subjected to pressure, out-of-plane moment and a combination of these two loads. Although not directly relevant to cylinder-cylinder intersections, these forged junction results may give some indication of the size of cracks required to produce significant reduction in strength. The junctions were equal diameter, with D/T ratio nominally equal to 15 and nominal thickness of 5.49mm. The crack length was constant for all cases (equal to half the pipe radius) and the crack was either part-penetrating (with a/t=0.5) or through-wall (a/t=1.0). The forged junction is shown in Figure 1.14(a) along with the crack position and strain gauge positions. The test program is listed in Table 1.4. For the out-of-plane bending tests it was decided to test pairs of junctions, due to the difficulties involved in applying the correct boundary conditions. The moment was applied by means of a controlled displacement at the end of the branch pipe with the resulting force and torque reacting at both ends of the run pipe, for each junction, as shown in Figure 1.14(b). The mass of the test assembly was supported at point 'A'. For combined pressure and bending, a steady pressure was maintained at the design pressure for the junction, with increasing moment applied.

One of the main issues with this study was the variation in thickness of the junctions, which was found to be up to 46% greater than nominal thickness. The FE models were created using the thickness in the region of highest stress (i.e. 7.5mm around the crack location). However, this variation in thickness led to difficulties when comparing the FE and experimental results, due to the reduction in thickness away from the intersection region of the junctions. The experimental results alone are discussed here. The bending tests resulted in plots of moment against applied displacement. For the uncracked pressure case, the diametral growth was used as the global deformation parameter. For the other pressure test no global parameter was recorded, only strain data was available. The crack opening displacement was also monitored for two of the tests using a displacement transducer mounted across the crack faces, on the outer surface of each junction.

Global plastic loads were calculated from the load-displacement curves using the twice-elastic-slope method. In addition, an attempt was made to derive a 'local' measure of plastic load, using the strain gauge data and the FE strains. The presented experimental results are shown in Table 1.4. The local plastic load results were presented as maximum and minimum values, showing the variation, depending upon the choice of strain gauge. In some cases the maximum local plastic load was higher than the global plastic load. For the pressure cases, the cracked pressure test failed (leaked) at a pressure 15MPa lower than for the uncracked test. The bending results showed a global plastic moment for the cracked junction in test 4 slightly higher than that for the uncracked junction. This was caused by the afore-mentioned dimensional variation. However, the results were within typical experimental error and the FE results confirmed that the crack would have little effect on the global plastic load. The combined loading case was found to agree with circular interaction.

The main problem with this work was the dimensional variation of the junctions. However, the study illustrated that these junctions were tolerant of fairly large cracks.

The remaining cracked branch junction literature obtained was fracture based, with little direct relevance to limit loads. However, as for the uncracked literature review, there were a number of **tubular joint** publications which may provide useful data. The relevance of tubular joint equations is discussed in Chapter 4 using results from tubular joint FE models compared with branch junction FE models. Some of the available publications are discussed below.

Stacey et al. [56] presented an extensive review of the available data in 1996. Publications prior to this date are not discussed individually here. A number of experimental and FE studies were listed for a variety of tubular joint configurations (including K-joints, Y-joints, double-T- joints and T-joints) subjected to various loads with a number of different crack configurations. T-joint data was cited from nine other publications, with the dimensions and loading listed for each. The majority of the test results were for axial tension or compression of the 'brace' (the 'brace' is equivalent to the branch pipe for a branch junction). Axial loading of the brace is the primary load for typical tubular joints, as they are often used as support members for large constructions. This is a load rarely reported for branch junctions, as they tend to be dominated by moment loadings. However, axial branch pipe loading may give a similar response to in-plane run pipe bending. In addition to these axial load results, some out-of-plane branch bending results were also presented. The cracks included through-wall and part-penetrating surface cracks. The positions of the cracks were not specified. The cracks were quantified by the percentage of the intersection area occupied by the crack: referred to as the % cracked area.

The resulting 'static strengths' for the cracked joints were compared with the uncracked T-joint solutions, as described in the previous section (using the HSE method [22], [44], and the API method [45]). Some uncracked results were presented but have not been discussed herein. There was a wide spread of static strength data for the cracked T-joints, ranging from results that were considerably lower than the predicted uncracked strength to those that were higher than this uncracked strength.

The main conclusion of Stacey et al. was that the the static strength reduced due to the presence of a crack, and that the reduction could be substantial. It was also found that the HSE and API methods for evaluating the static strength could be unreliable, as for specimens with a cracked area of up to approximately 30%-40% the measured strength in the cracked tubular joint could be equal to or higher than the predicted uncracked tubular joint.

Stacey et al. complemented the above review of data with another publication [57] in which the use of a reduction factor with uncracked predictions was discussed. This area reduction factor, F_{AR}, originated from the work of Cheaitani and Burdekin [58] and is widely quoted in standard assessment methods (for example, BS7910 [59] which covers the assessment of flaws in metallic structures). The definition of F_{AR} is:

$$F_{AR} = \left(1 - \frac{Crack\ area}{Weld\ length \times T}\right)\left(\frac{1}{Q_\beta}\right)^{m_q} \tag{1.19}$$

Q_β is a geometric modifier and has been defined previously for equation (1.11). m_q is the power allocated to Q_β and depends on the approach used to estimate the capacity of the uncracked joint. The method is based upon the assumption that the uncracked strength (for axial loading, in-plane branch bending or out-of-plane branch bending) will be evaluated using either HSE or API recommendations, as described in [44] and [45] respectively. For [44] m_q=1 is recommended while m_q=0 is used for [45]. In Chapter 4 the potential for using such a factor with uncracked FE limit load data is assessed.

Stacey et al. concluded that the area reduction factor was a useful means for predicting the static strength of cracked tubular joints (with the exception of brittle fracture cases).

Cao et al. [60] presented details of a technique for producing uncracked and cracked FE models of tubular joints, for fracture mechanics analysis. The technique did not use the usual approach of producing the joint geometry and then adding the mesh to this geometry. Instead, each mesh was produced in a two-dimensional plane, and then mapped to cylindrical coordinates using a set of equations. The branch and run pipe could both be created in this way and then connected together. The method appears to be a simple way of creating models that would otherwise be time consuming, and geometrically difficult, to create using conventional three dimensional techniques. The mesh generation procedure is shown, for an uncracked tubular joint, in Figure 1.15. The intersection mesh was created using the radii values of the branch pipe and weld

(Figure 1.15(a)) and then transformed into the correct oval profiles using the equations:

$$Y' = R \sin^{-1} \frac{v}{R} \tag{1.20}$$

$$Z' = \left[w - R \left(1 - \cos \frac{Y'}{R} \right) \cos\theta \right] \frac{1}{\sin\theta} \tag{1.21}$$

where R is the radius of the run pipe outer surface, and θ is the angle of the intersecting branch pipe (θ is equal to zero for a normal branch junction or tubular joint). Following this, the remaining mesh was generated on the plate, as shown in Figure 1.15(b). The mesh was then mapped onto a cylinder (Figure 1.15(c)) using the equations:

$$X = R \cos \frac{Y'}{R} \tag{1.22}$$

$$Y = R \sin \frac{Y'}{R} \tag{1.23}$$

Finally, the branch pipe was connected to the run pipe, having been constructed in a similar way, resulting in the uncracked model shown in Figure 1.15(d) (note that θ was non-zero for this example).

For a cracked case with a semi-elliptical crack, as shown schematically in Figure 1.16(a), the procedure was slightly more complex. The crack elements were created in a single plane, as shown in Figure 1.16(b) and then transformed into a curved profile (see Figure 1.16(c)) using the equations:

$$Y = r_1 cos \frac{z}{r_1} \tag{1.24}$$

$$Z = r_1 sin \frac{z}{r_1} \tag{1.25}$$

(It should be noted that the equations are for a circular weld profile).

The resulting elements were then inserted into the plate, as shown in Figure 1.15(a) and the remaining mesh constructed as for the uncracked case. This publication was only discovered at a late stage of the presented project, and so the techniques described were not used.

1.5 Scope of the Present Work

The primary objective of the current research programme was to provide limit load data for a range of cracked piping branch junctions, and hence to derive techniques for assessing such junctions. The results presented should add considerably to the available literature on limit loads for cracked piping branch junctions. The main types of crack studied were those that run around the lower weld-toe in the intersection region, as often found for internal pressure loading, in-plane branch pipe bending and out-of-plane branch pipe bending. Extensive FE parametric studies for these types of cracks are presented, considering the above loads and combinations of out-of-plane bending and pressure. Recommendations have been made for the limit load assessment of cracked junctions within the parametric range presented.

This FE work has been complemented with some experimental work, in which the plastic loads for branch junctions were considered. The purpose of the experimental work was to provide confidence in the FE results by testing a selection of cracked and uncracked junctions and comparing the test results with the corresponding FE results.

In addition to the cracked parametric study, an FE parametric study of the limit pressures for uncracked junctions is also presented. A wide range of junctions were included, and the results were compared with those from some of the literature described in the previous Section. This study enabled FE techniques to be established, which were subsequently used in the cracked branch junction work.

1.6 Structure of Thesis

- A preliminary FE study of the limit loads of plain pipes, with fully circumferential cracks, is presented in Chapter 2. The intention of this work was to gain an insight into the type of FE mesh required for limit load analysis, using a simple cracked geometry.

- Chapter 3 details an extensive FE parametric study for the limit loads of uncracked branch junctions subjected to internal pressure. The basic techniques used for the FE modelling of branch junctions are described in this Chapter.

- The primary objective of the work was the evaluation of limit loads for cracked branch junctions. Hence, Chapter 4 presents a parametric study of various cracked branch junctions subjected to individual loads and combined loading. The results are examined alongside some existing methods, and recommendations are made for cracked branch junction assessment.
- Chapter 5 introduces the experimental work on branch junctions, and describes the test component manufacture and test arrangements.
- Chapter 6 presents the results from the experimental work, comparing them with corresponding FE results.
- Conclusions and recommendations for future work are given in Chapter 7.

Table 1.1: Schwarz et al. [50] Cracked Branch Junction Tests

Junction:		AZ1	AZ2	AZ3	AZ4	AZ6
Run pipe material		A	B	A	B	B
Branch pipe material		A	A	A	A	A
Temperature	°C	20	90	20	130	30
Flaw		without flaw	inside corner, longitudinal (run pipe axis)			
depth a/t	mm	-	0.25	0.25	0.42	0.26
crack length	mm	-	40.0	40.0	39.5	42.0
Loading						
internal pressure	MPa	15	15	16	16	11
bending moment	MNm	2.2	2.2	2.4	2.3	1.7

Table 1.2: Plancq et al. [52] Limit Pressure Results for Cracked Branch Junctions

Junction:	A	B	C	D	E
d/D	0.25	0.25	0.25	0.5	0.25
D/T	50	50	50	100	100
Crack Length [mm]	15	20	50	35.35	28.2
$PD/t\sigma_y$	1.750	1.500	1.026	1.360	1.254

Table 1.3: Chapuliot and Moulin [53] Results for Cracked Branch Junctions under Out-of-plane Branch Bending

Branch junction	F_m (max) [kN]	F_e (excessive strain) [kN]	F_i (Crack Initiation) [kN]
2	28.0	23.4	-
3	27.7	23.4	21.0
4	27.8	23.8	21.8
5.5	28.5	23.3	-
5.6	28.4	23.8	22.6
5.7	-	23.1	15.9
5.8	-	23.3	19.2

Table 1.4: Yahiaoui et al. [19] Cracked Branch Junction Test Results for Out-of-plane Bending (M) and Pressure (P)

Junction	Defect	Load	Global TES	Local TES		Failure Pressure
				Max.	Min.	
1	No Defect	P	37.8	36.5	36.3	64.6
2	No Defect	M	12.9	15.7	10.7	-
3	PP	P	-	33.4	21.7	49.7
4	PP	M	13.8	13.8	10.7	-
5	PP	P + M	11.8	-	5.58	-
6	TW	M	11.9	11.6	5.82	-

(TW = through-wall crack; PP = part-penetrating crack; units: M in kNm, P in MPa)

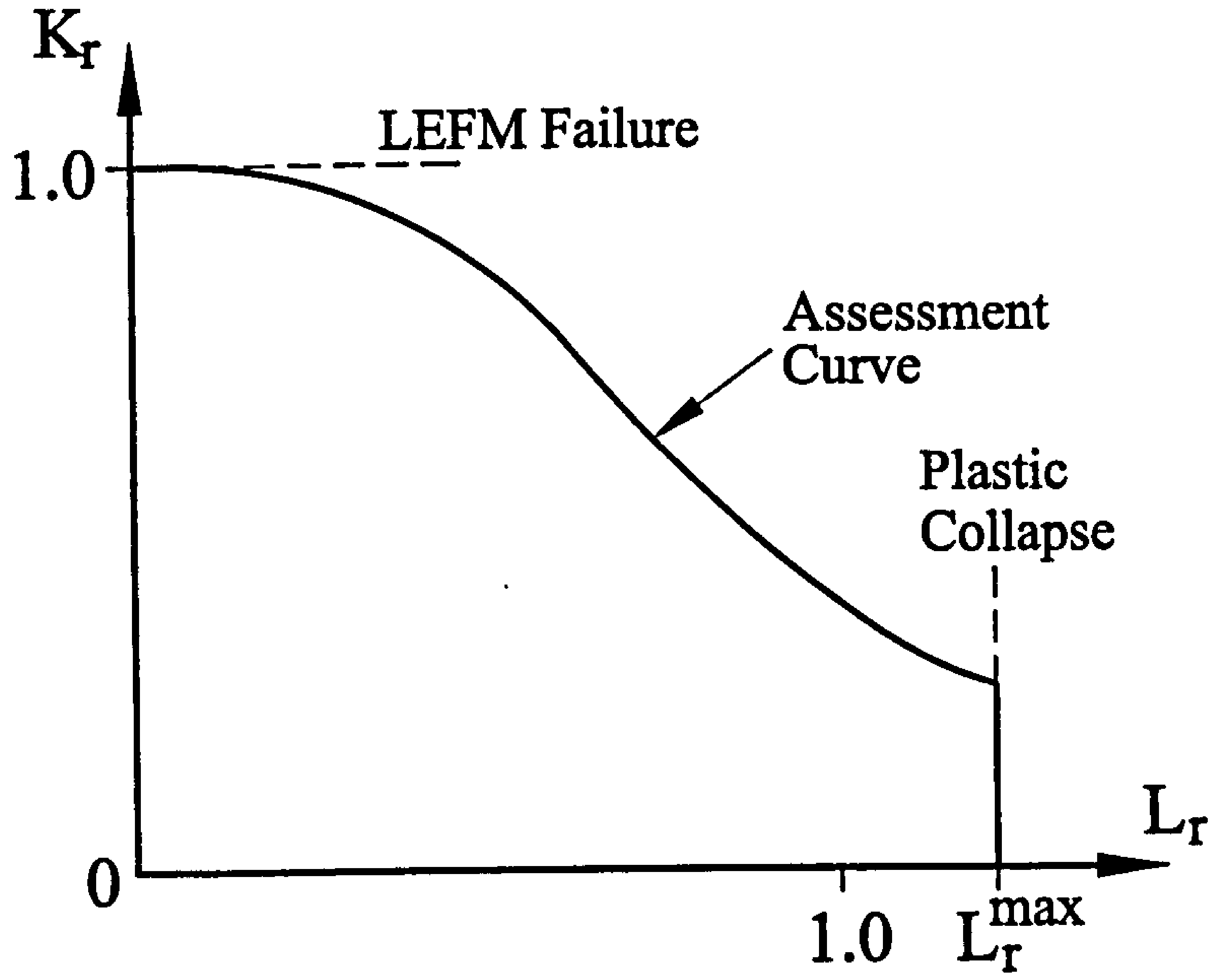

Figure 1.1: Failure Assessment Diagram

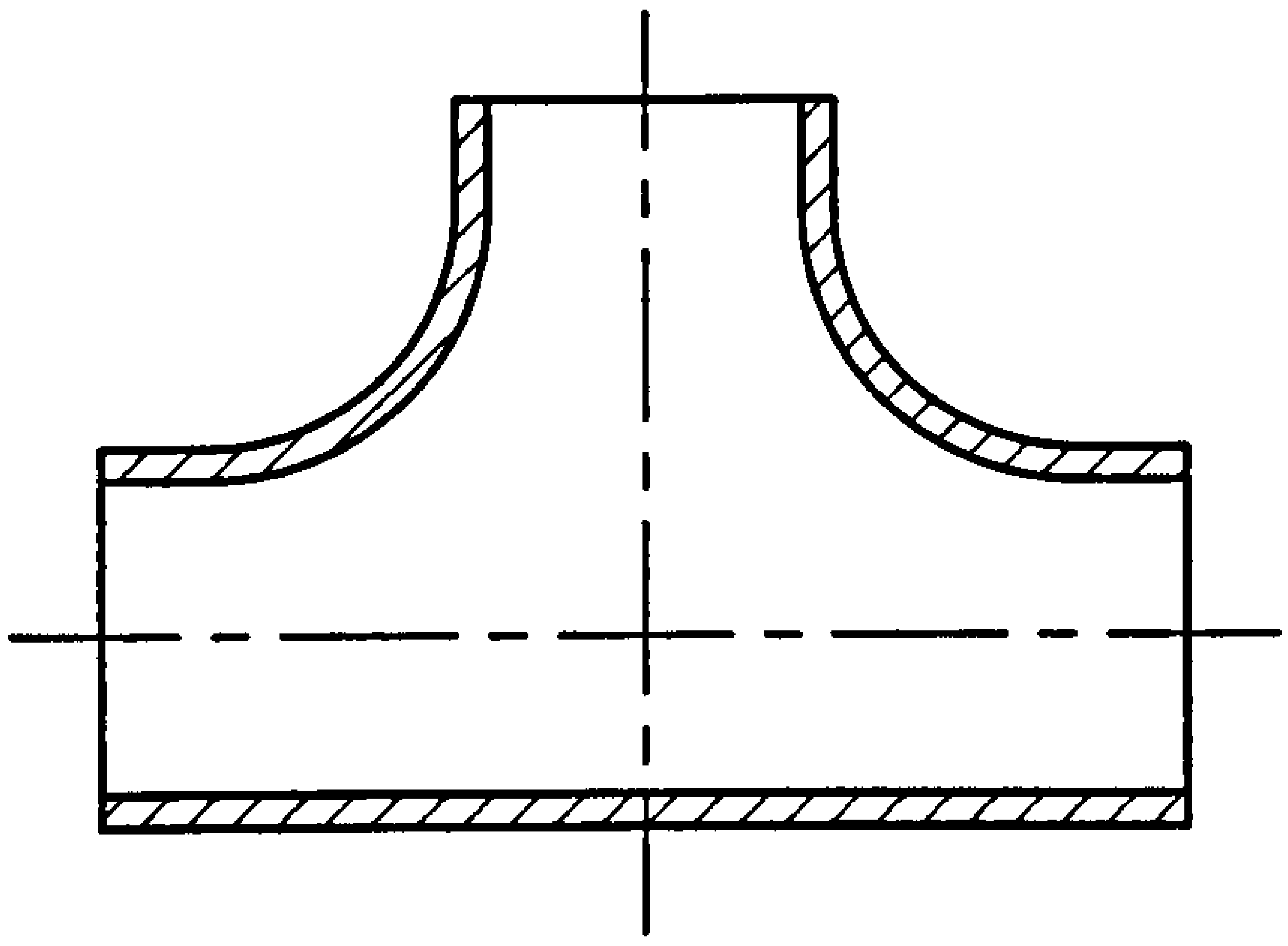

(a) Forged

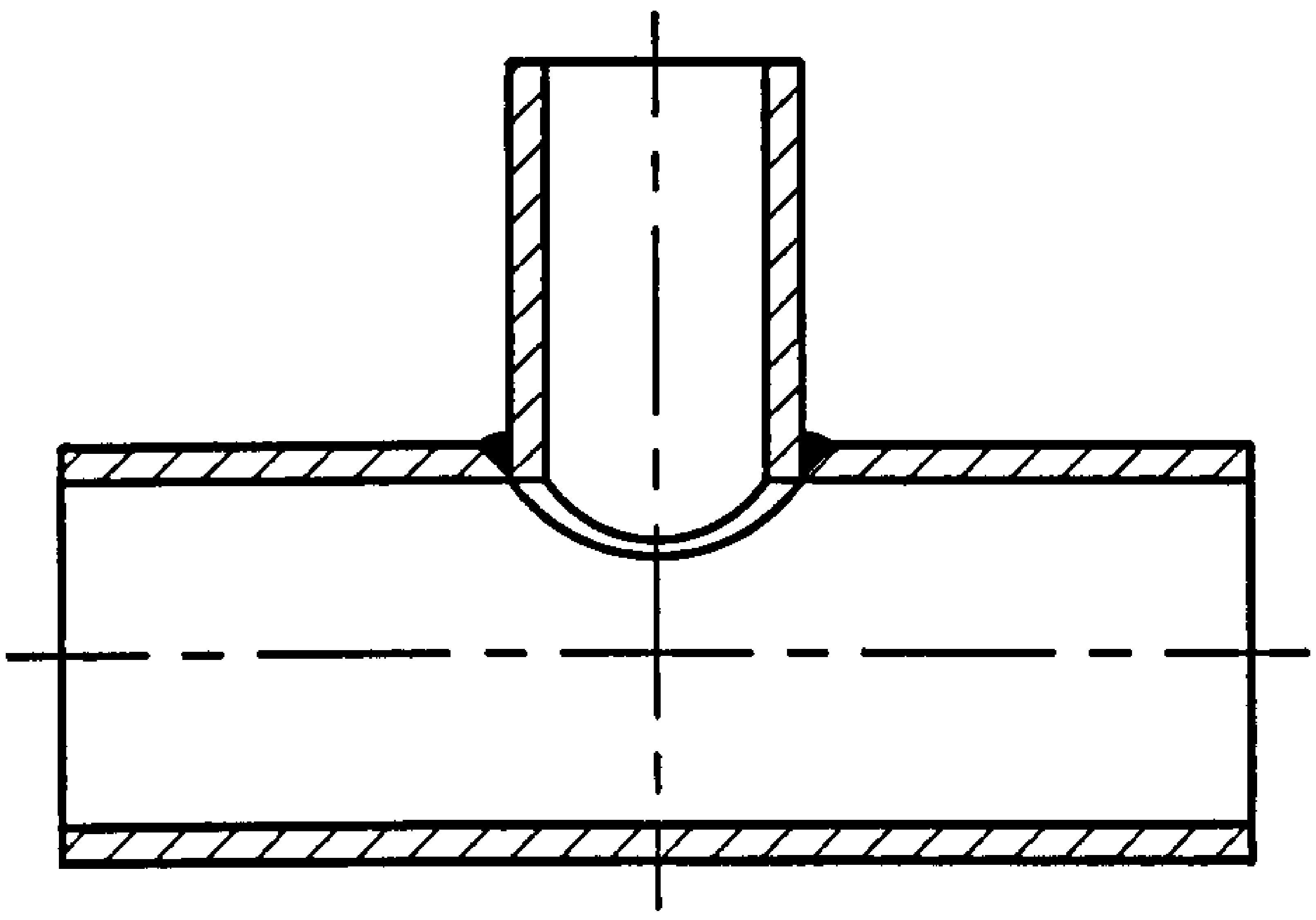

(b) Set-in

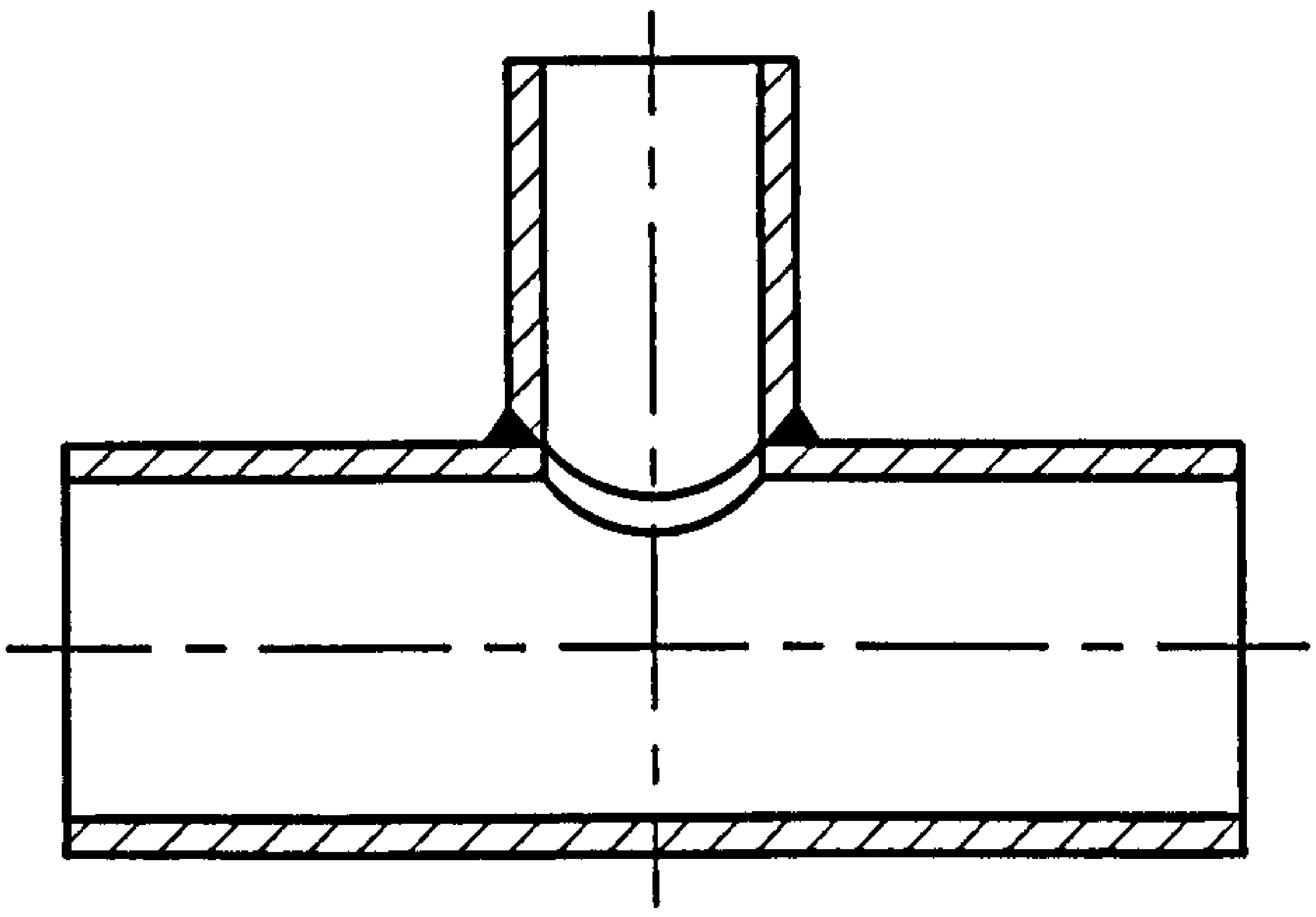

(c) Set-on

Figure 1.2: Main Types of Branch Junction

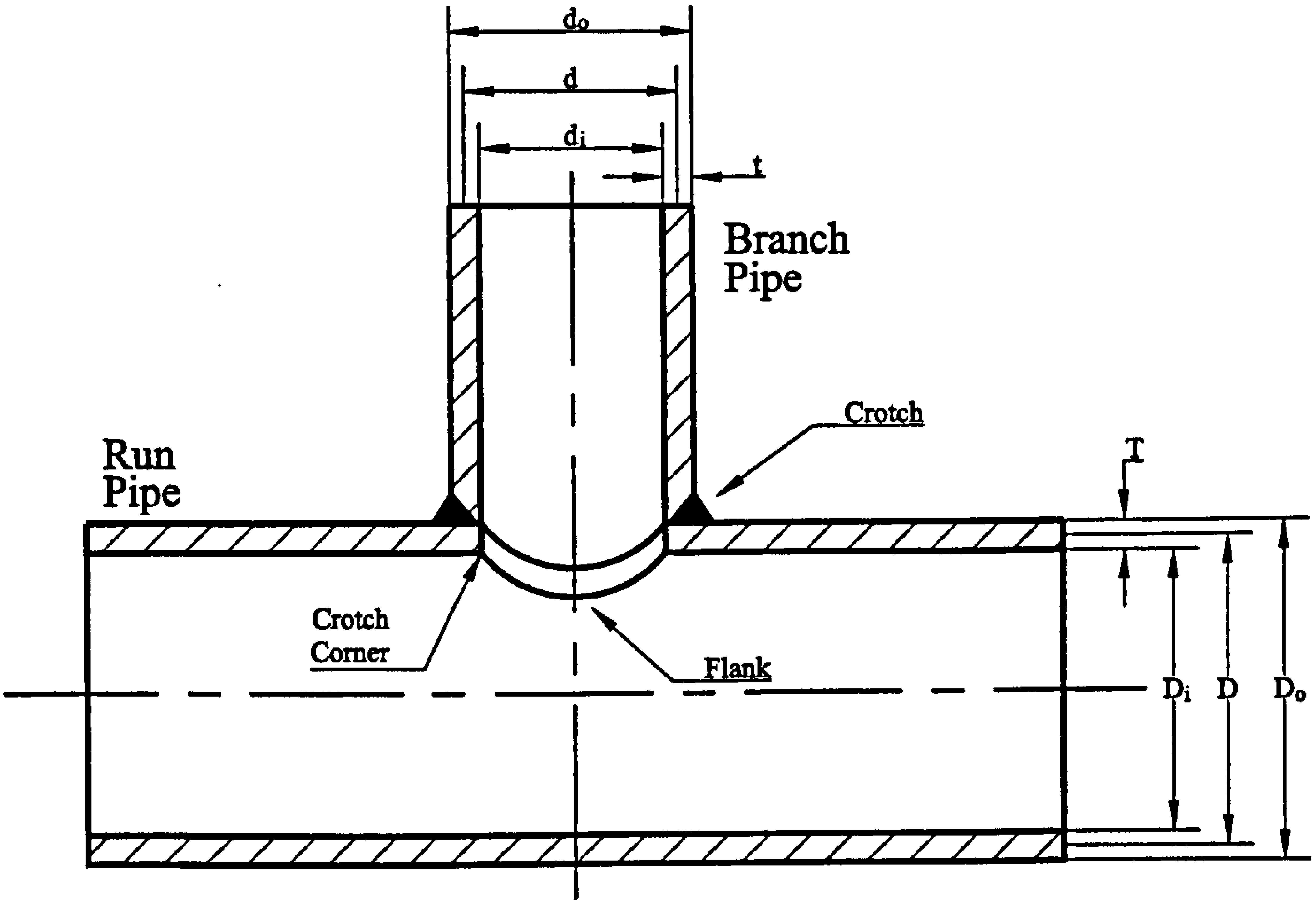

Figure 1.3: Terminology Used for Branch Junctions

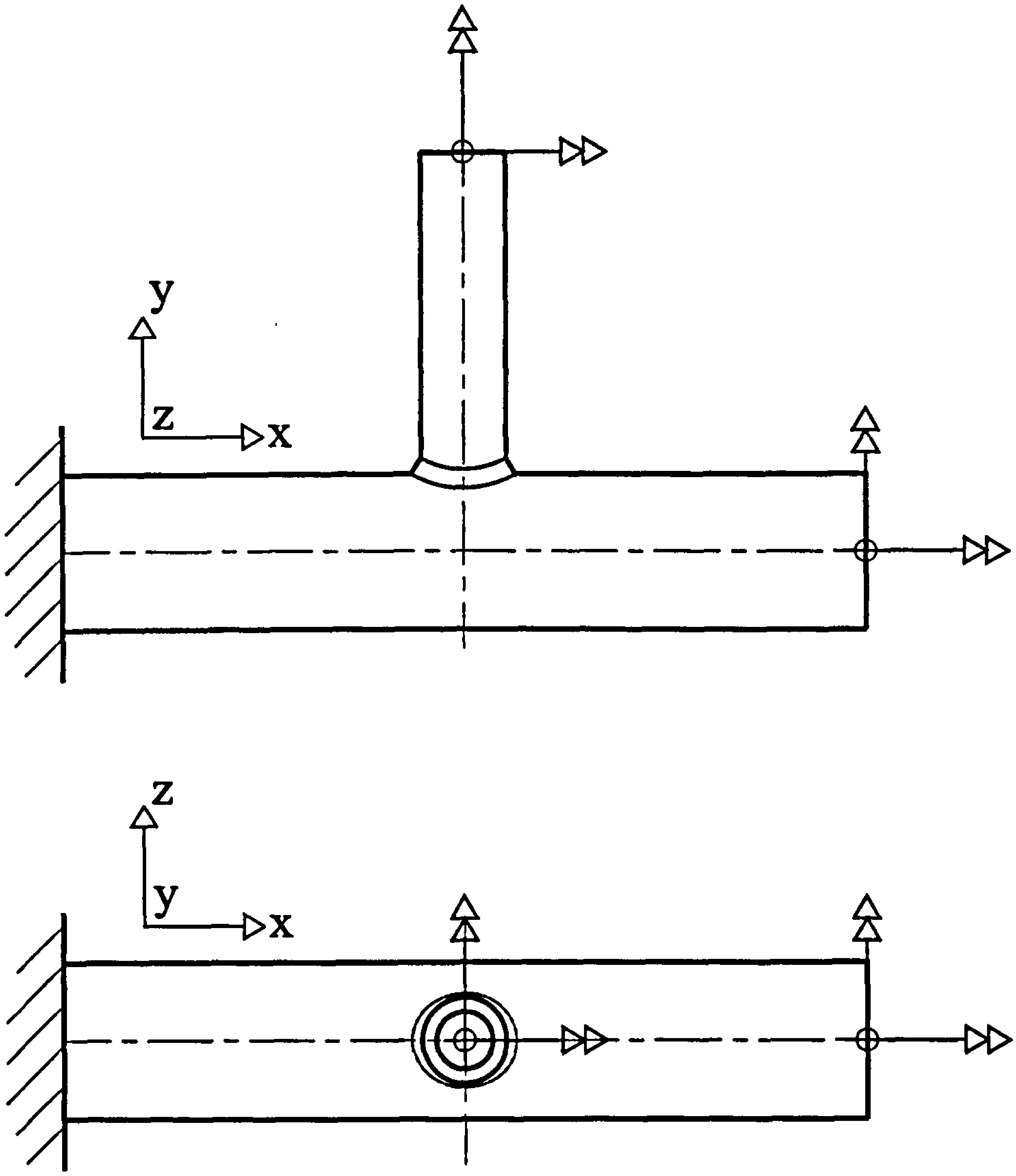

Figure 1.4: Possible Moment Loads for Branch Junctions - Moffat [7]

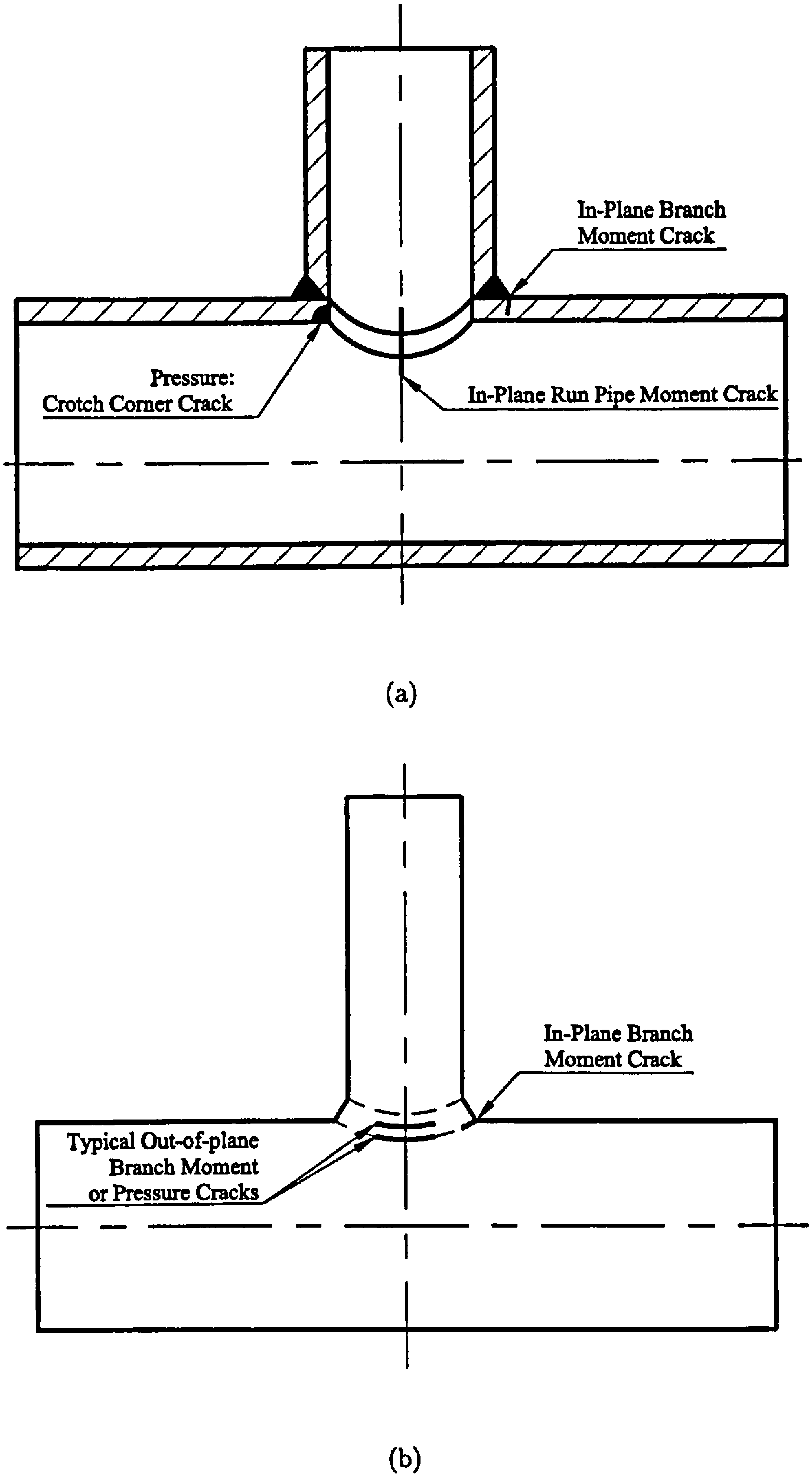

Figure 1.5: Typical Crack Locations

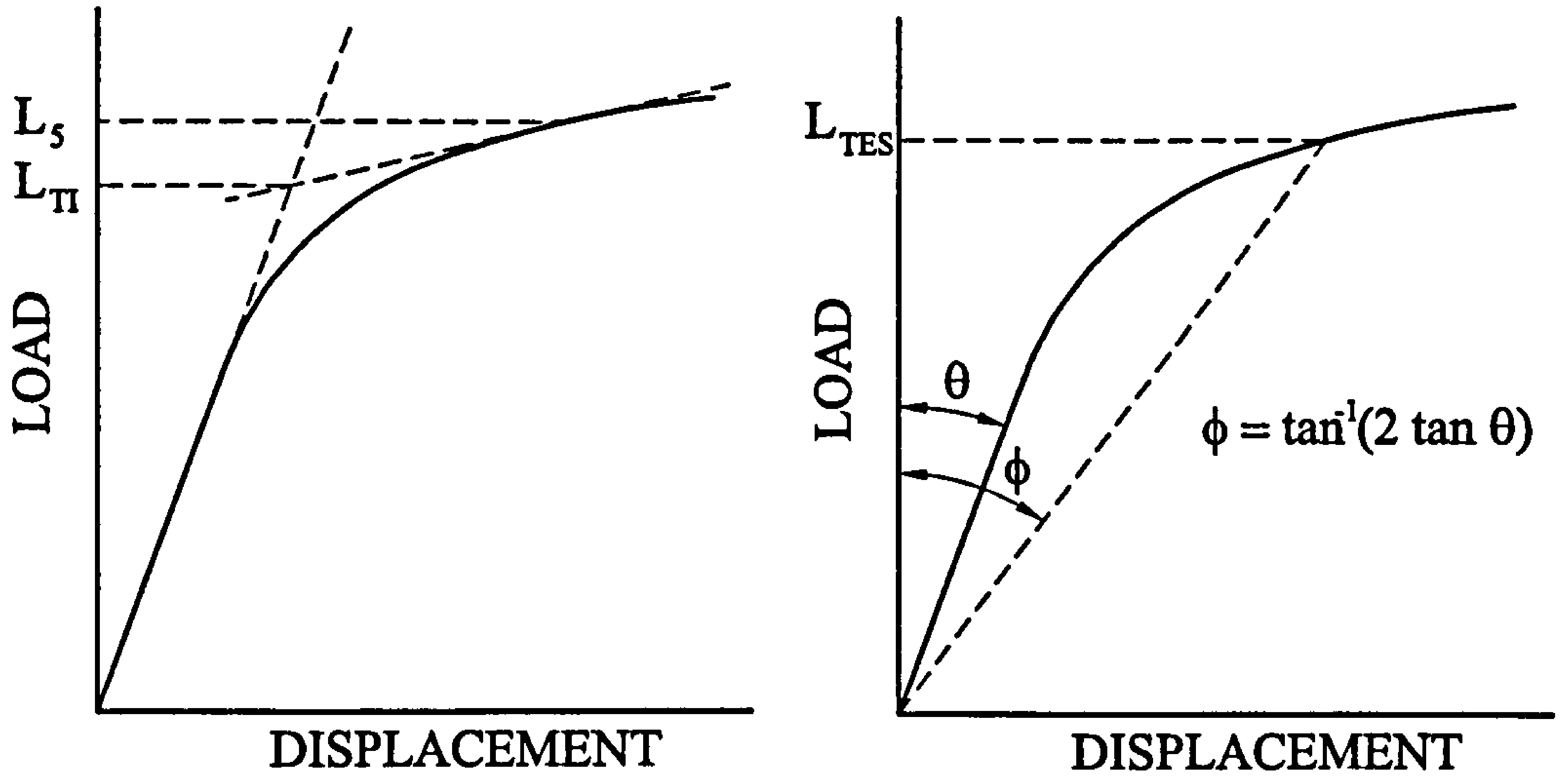

(a) Tangent Intersection Method

(b) Twice Elastic Slope Method

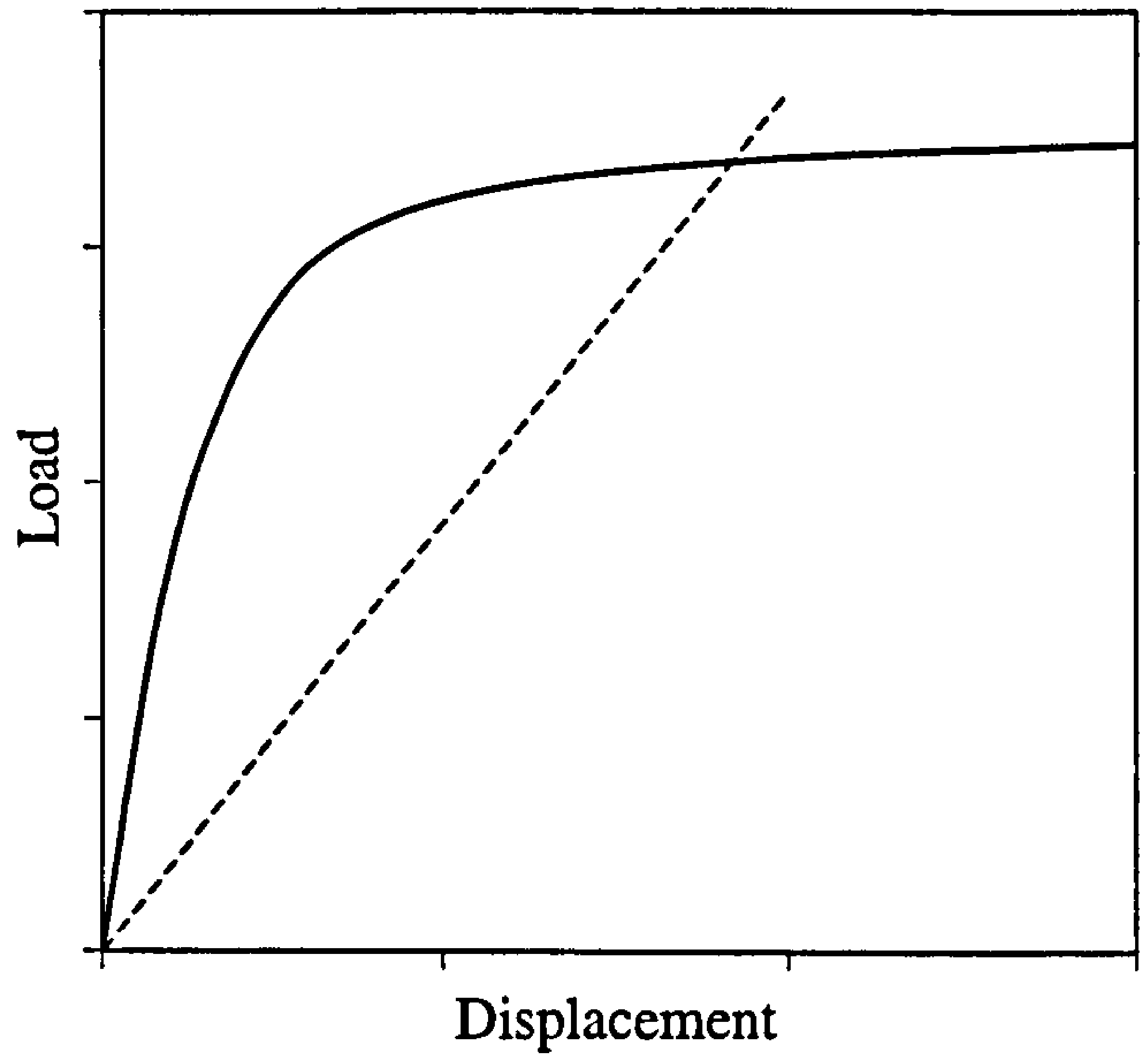

(c) Five Times Elastic Slope Method

Figure 1.6: Methods for Evaluation of Plastic and Limit Loads

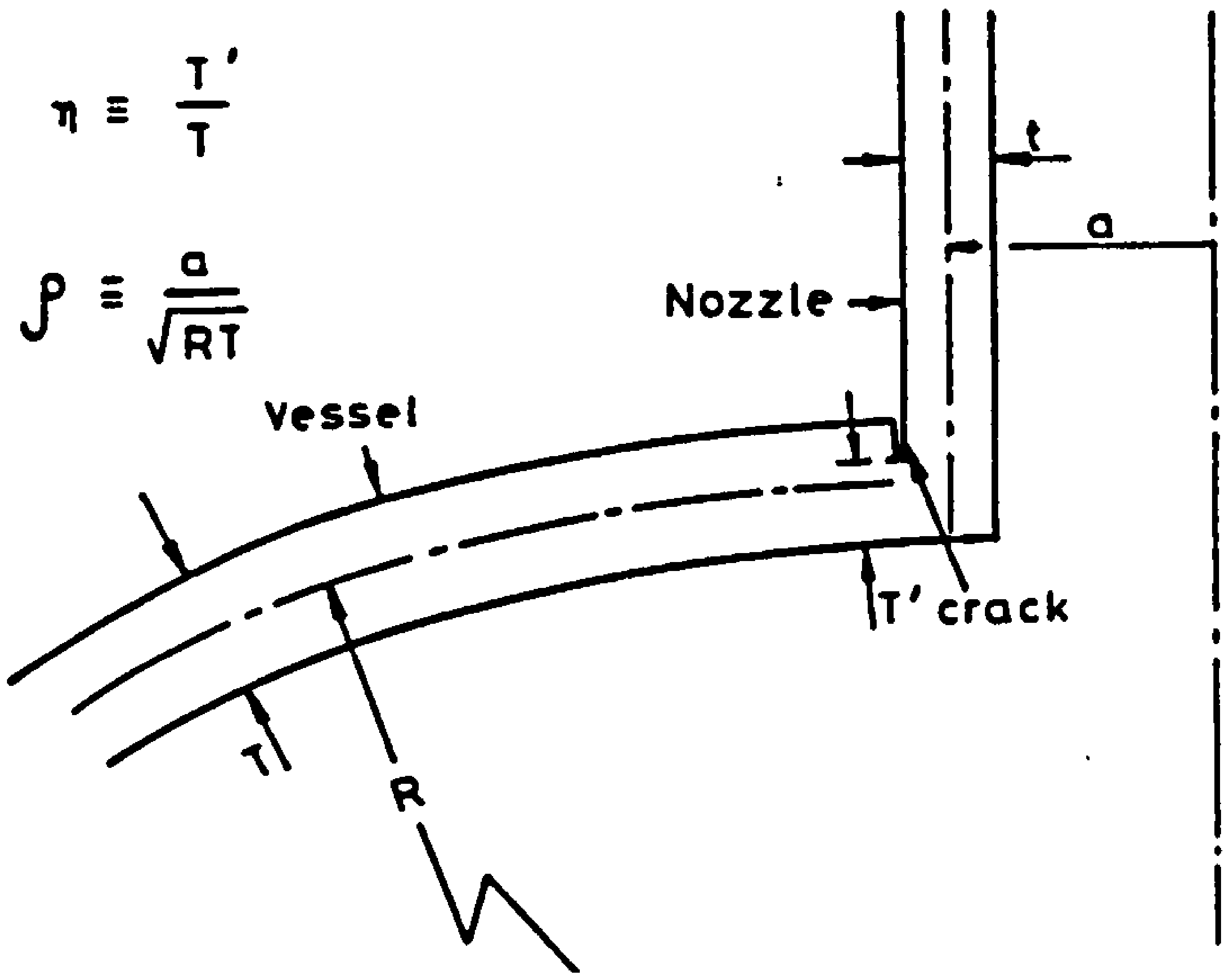

(a) Crack Location

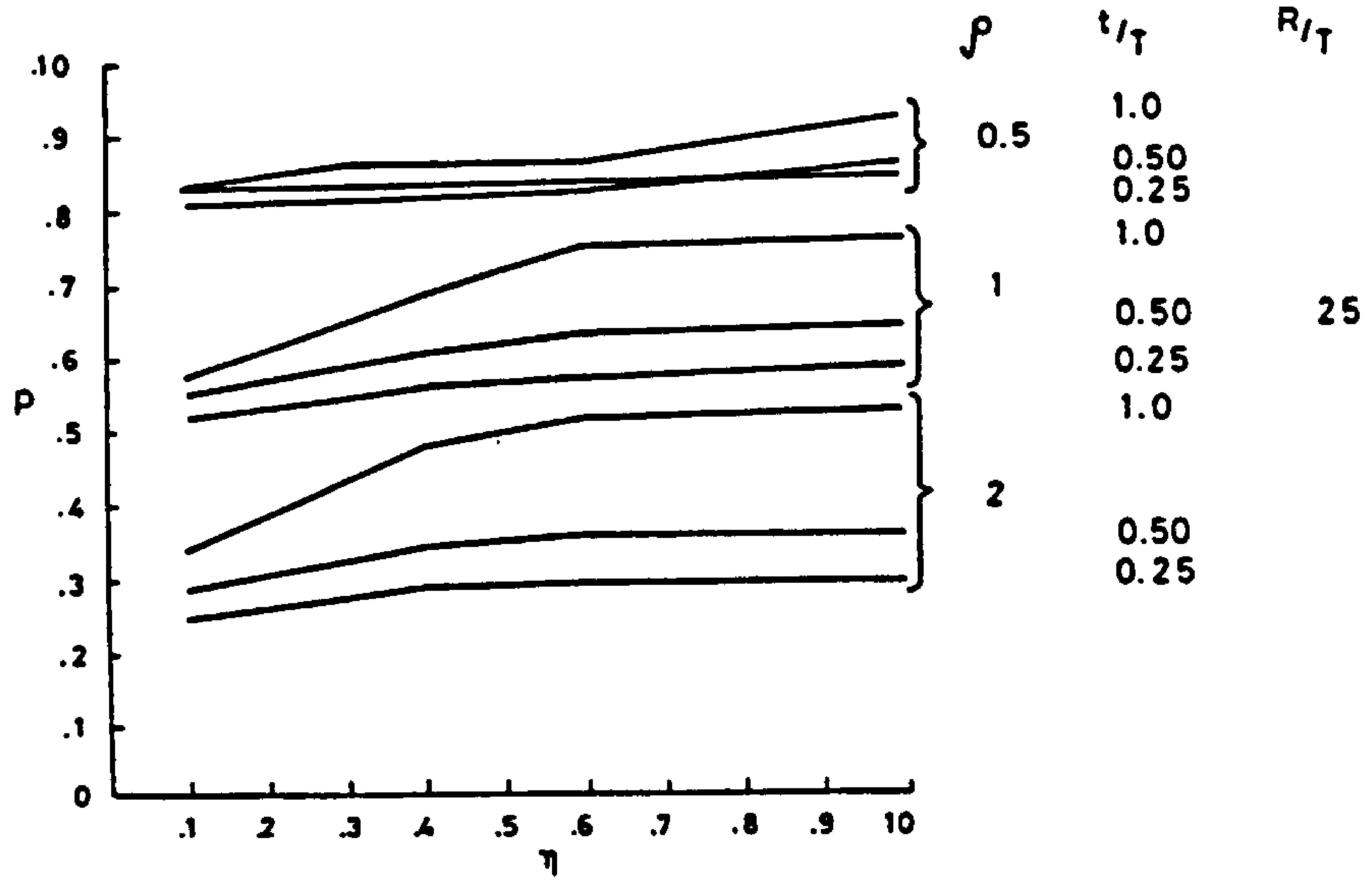

(b) Limit Pressure Solutions

Figure 1.7: Miller [20] Cracked Junction Solutions for R/T=25

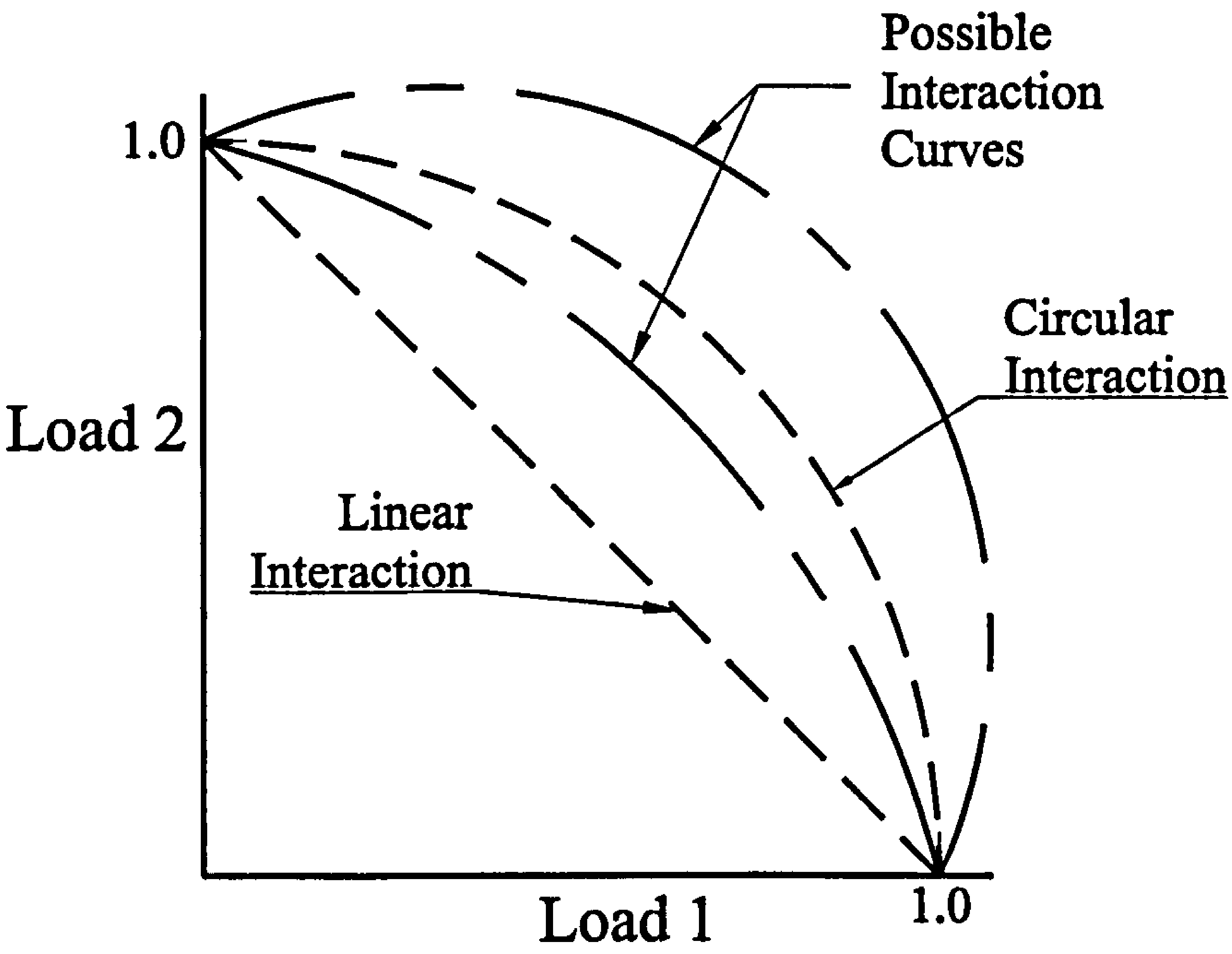

Figure 1.8: Interaction Diagram Format (Considering only Positive Loads)

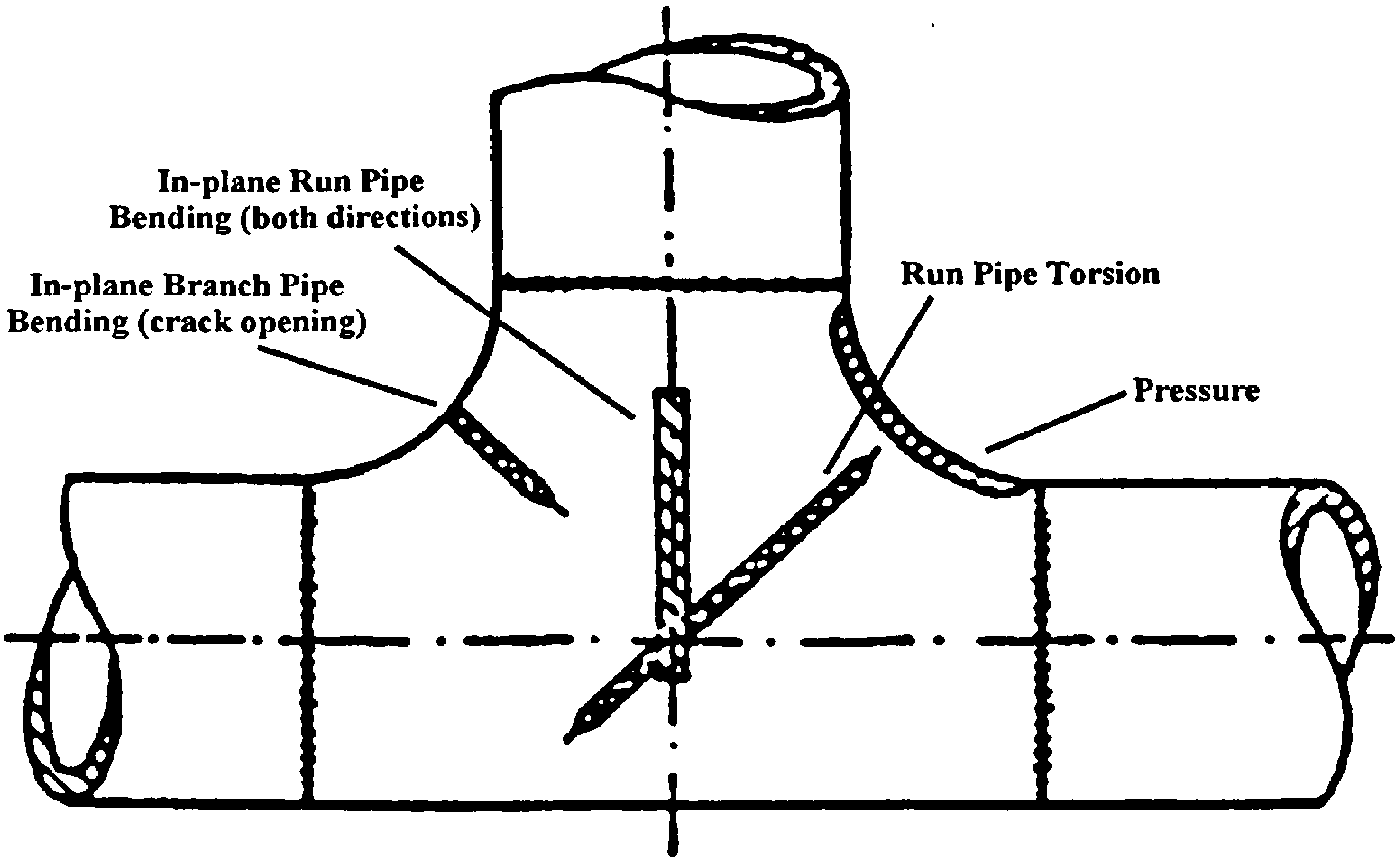

Figure 1.9: Schulze et al. [49] Crack Locations

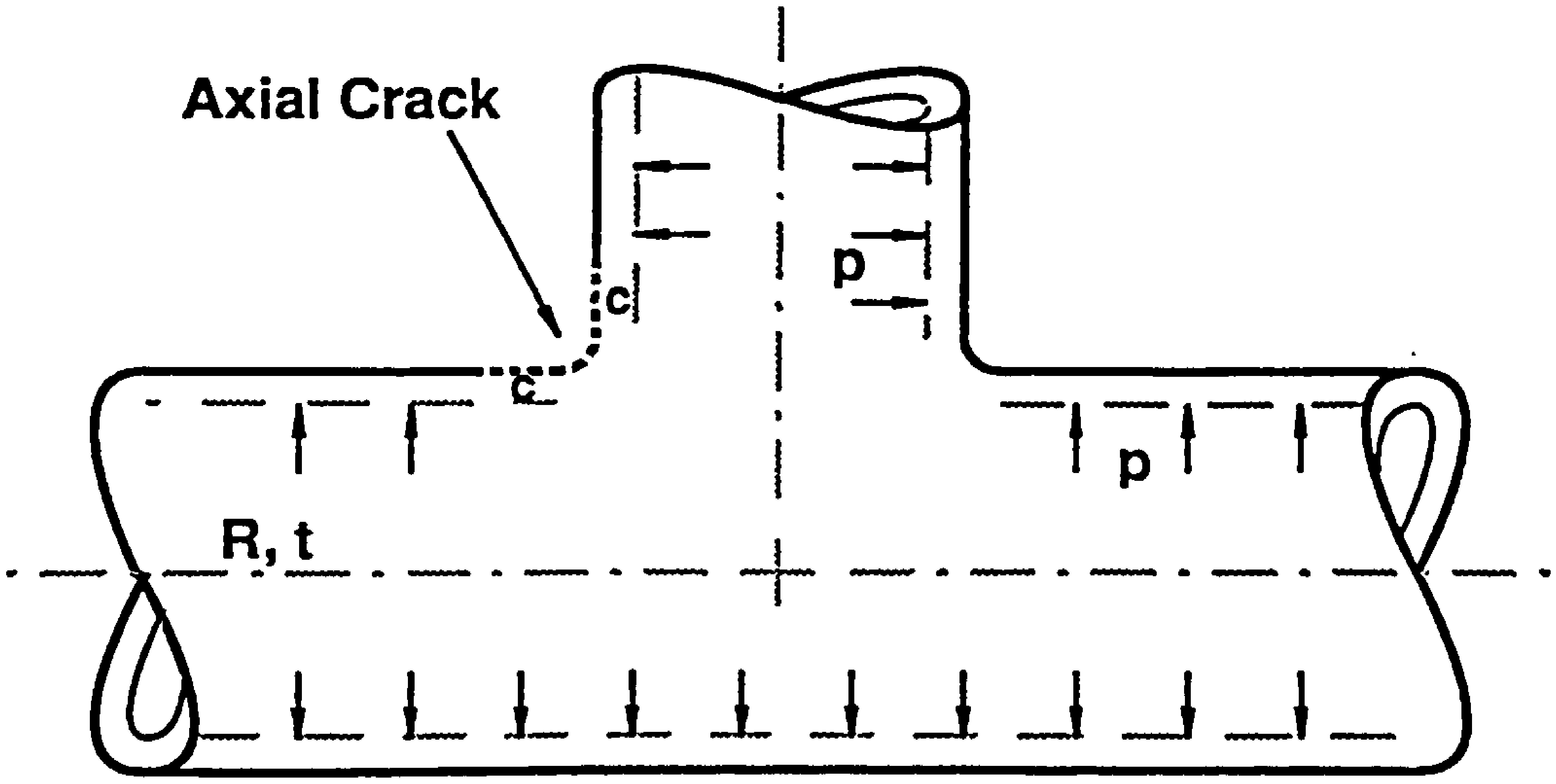

(a) Axial Crack

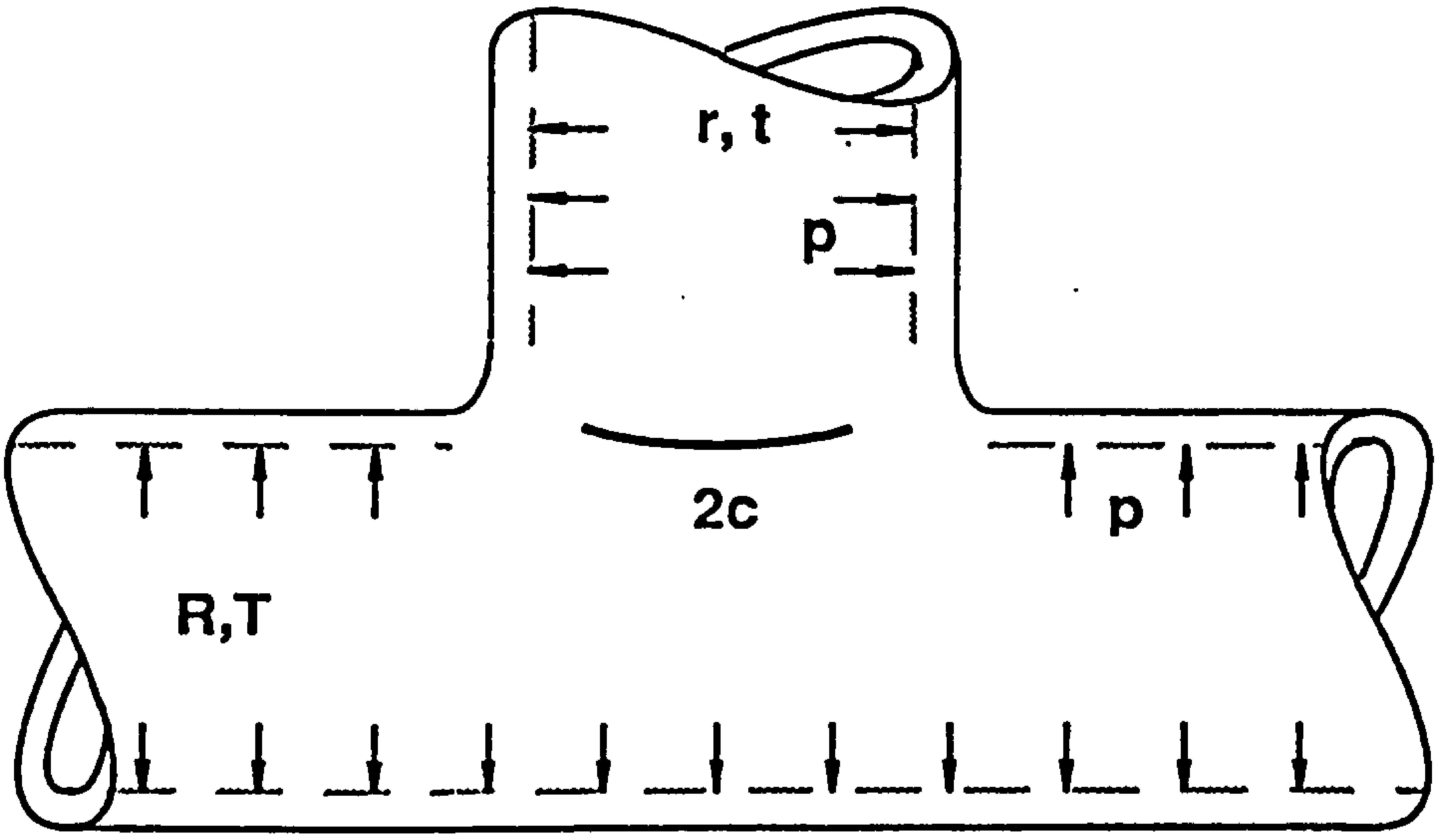

(b) Flank Crack

Figure 1.10: Zahoor [34] Crack Locations

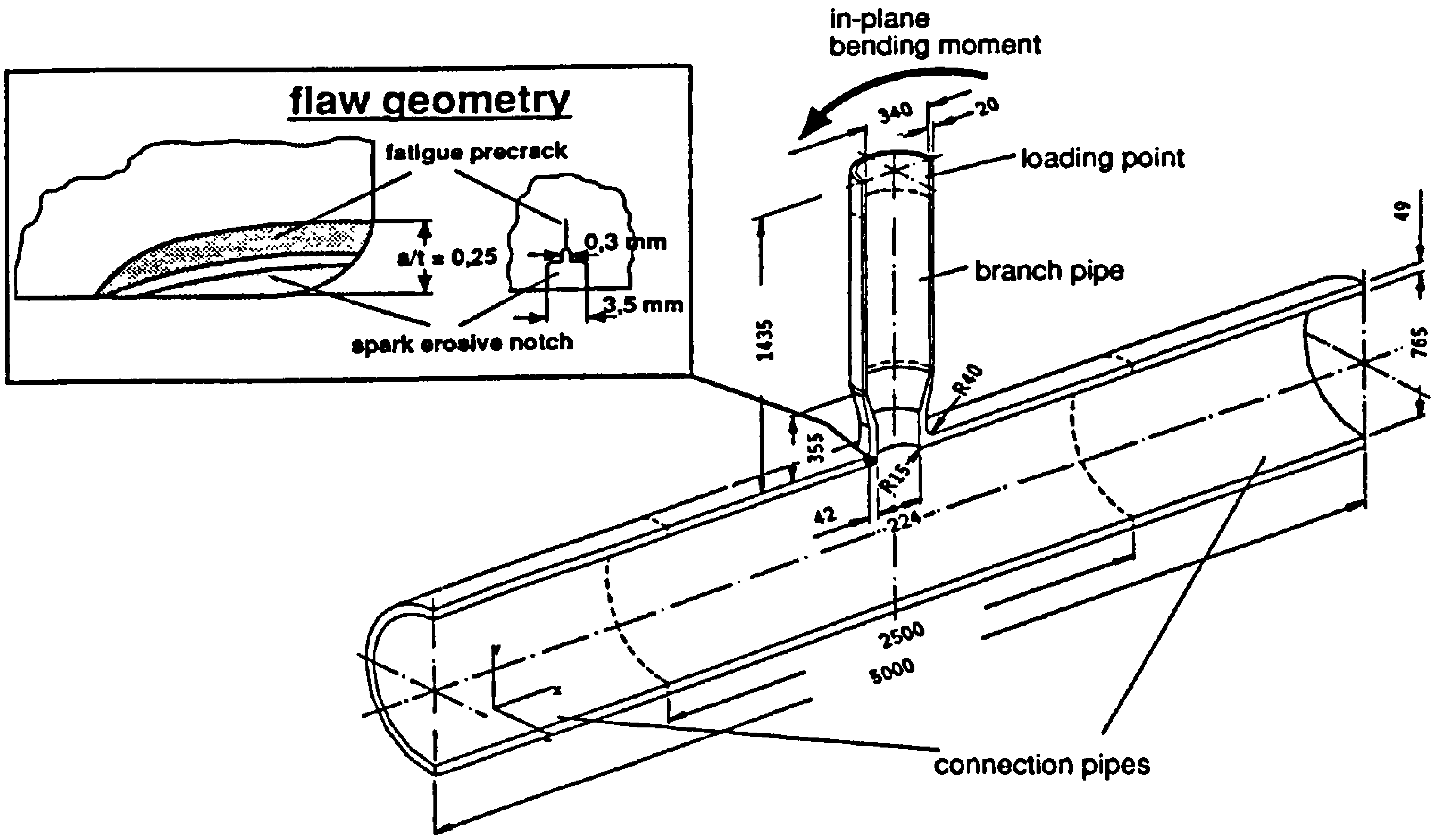

Figure 1.11: Schwarz et al. [50] Crack Location and Junction Geometry

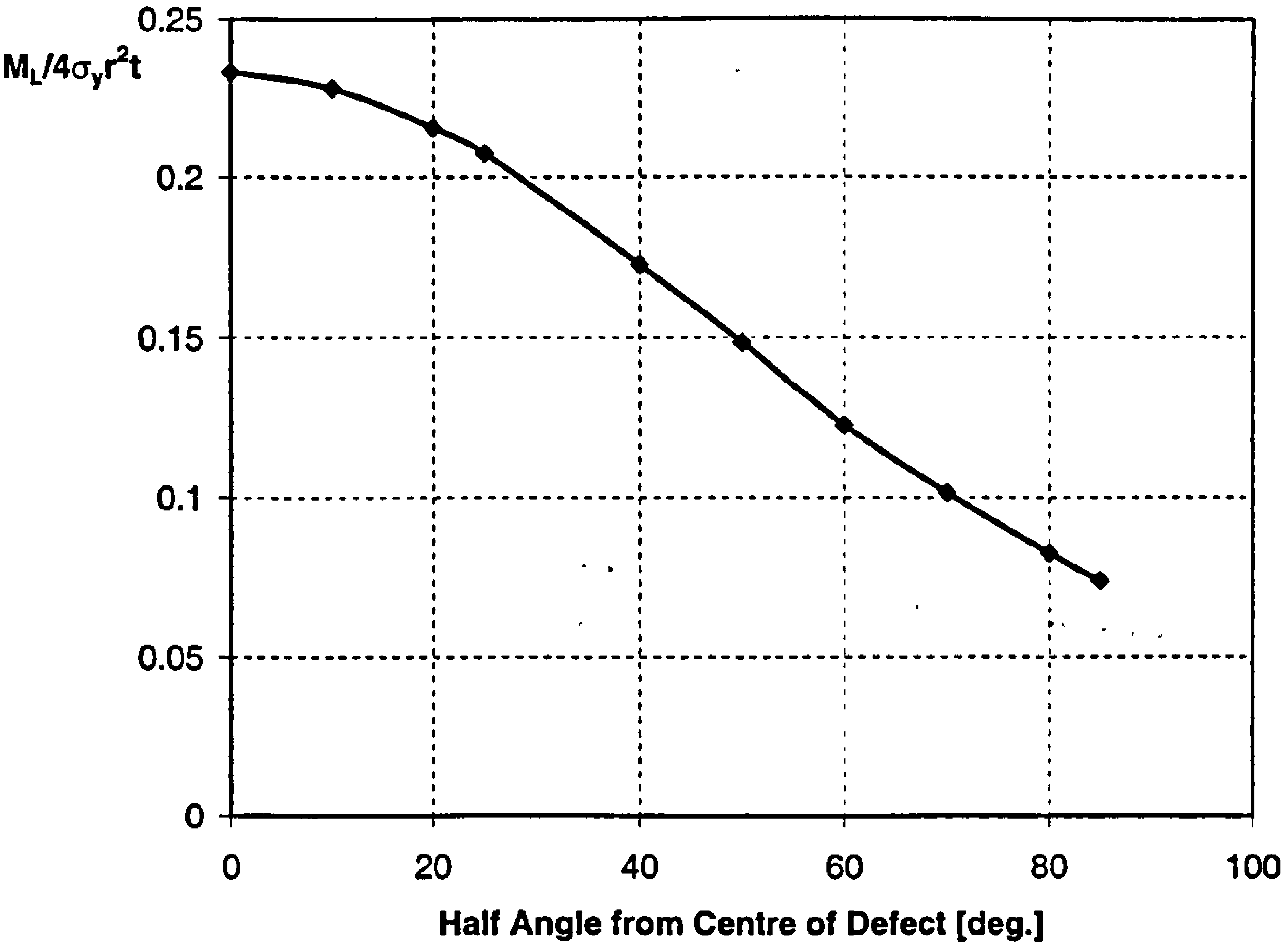

(a) Out-of-plane Branch Bending - Limit Moment Results

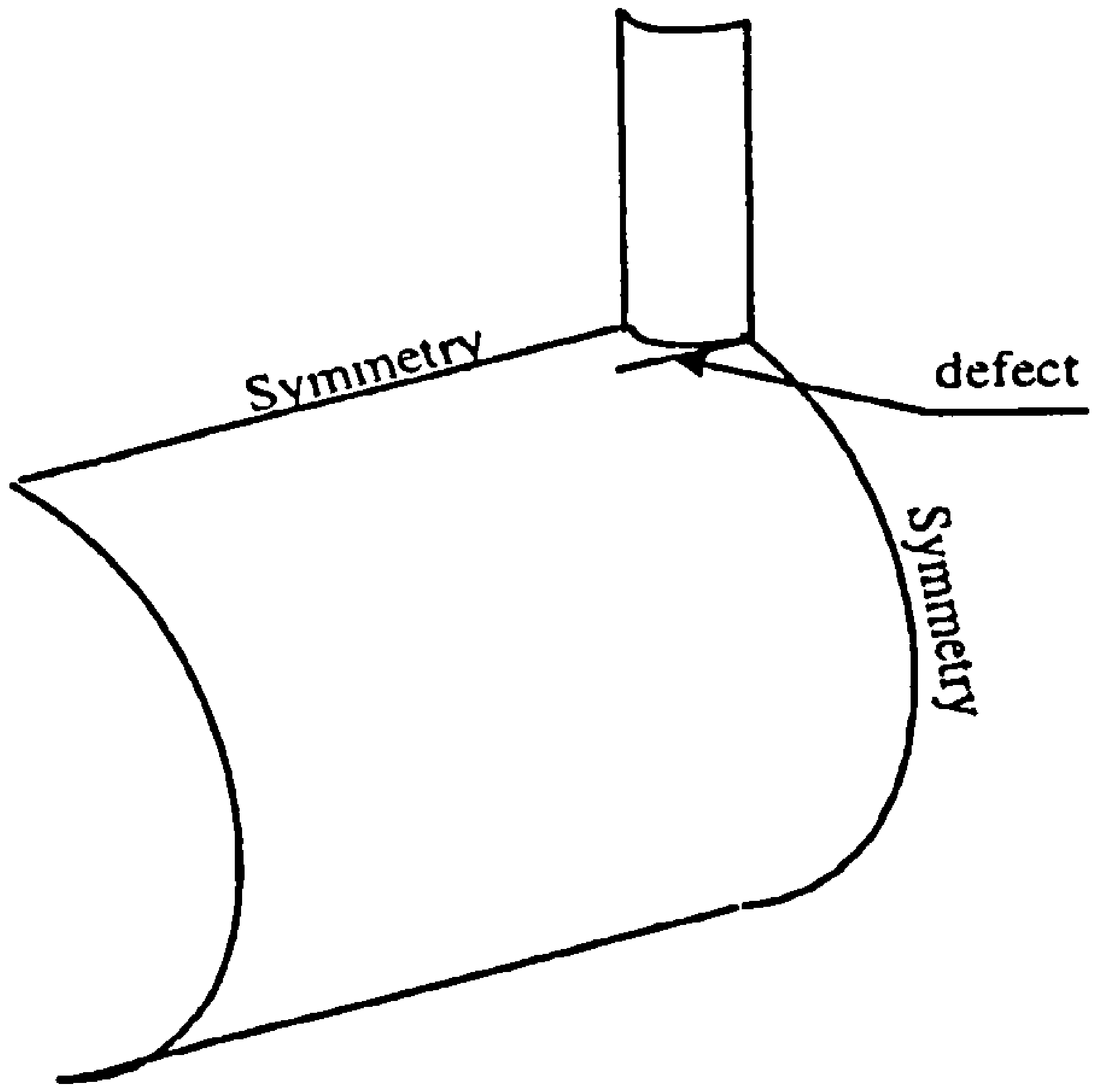

(b) Crack Location for Internal Pressure Loading

Figure 1.12: Plancq et al. [52] Branch Junction Analysis

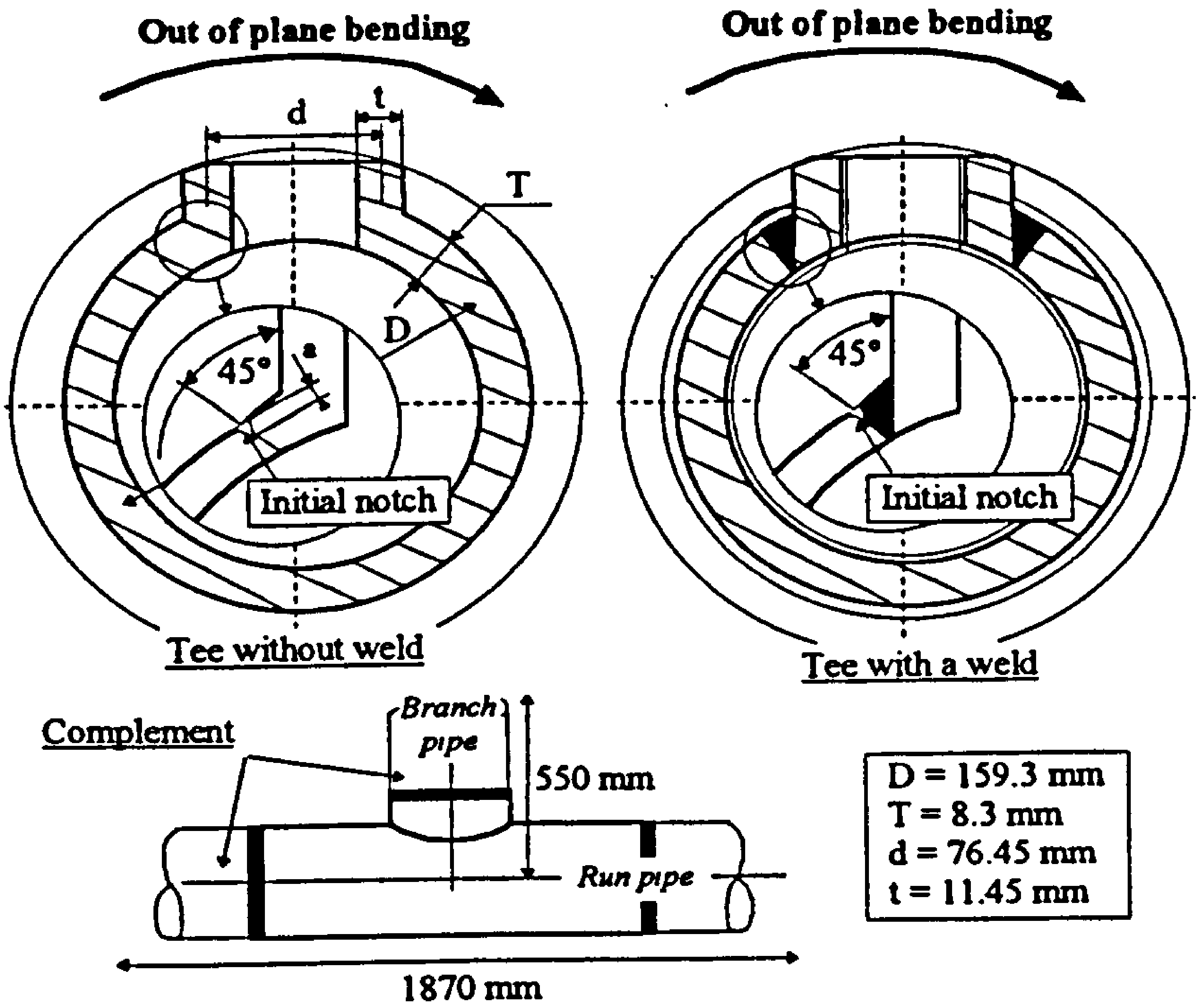

(a) Junction Geometry and Crack Locations

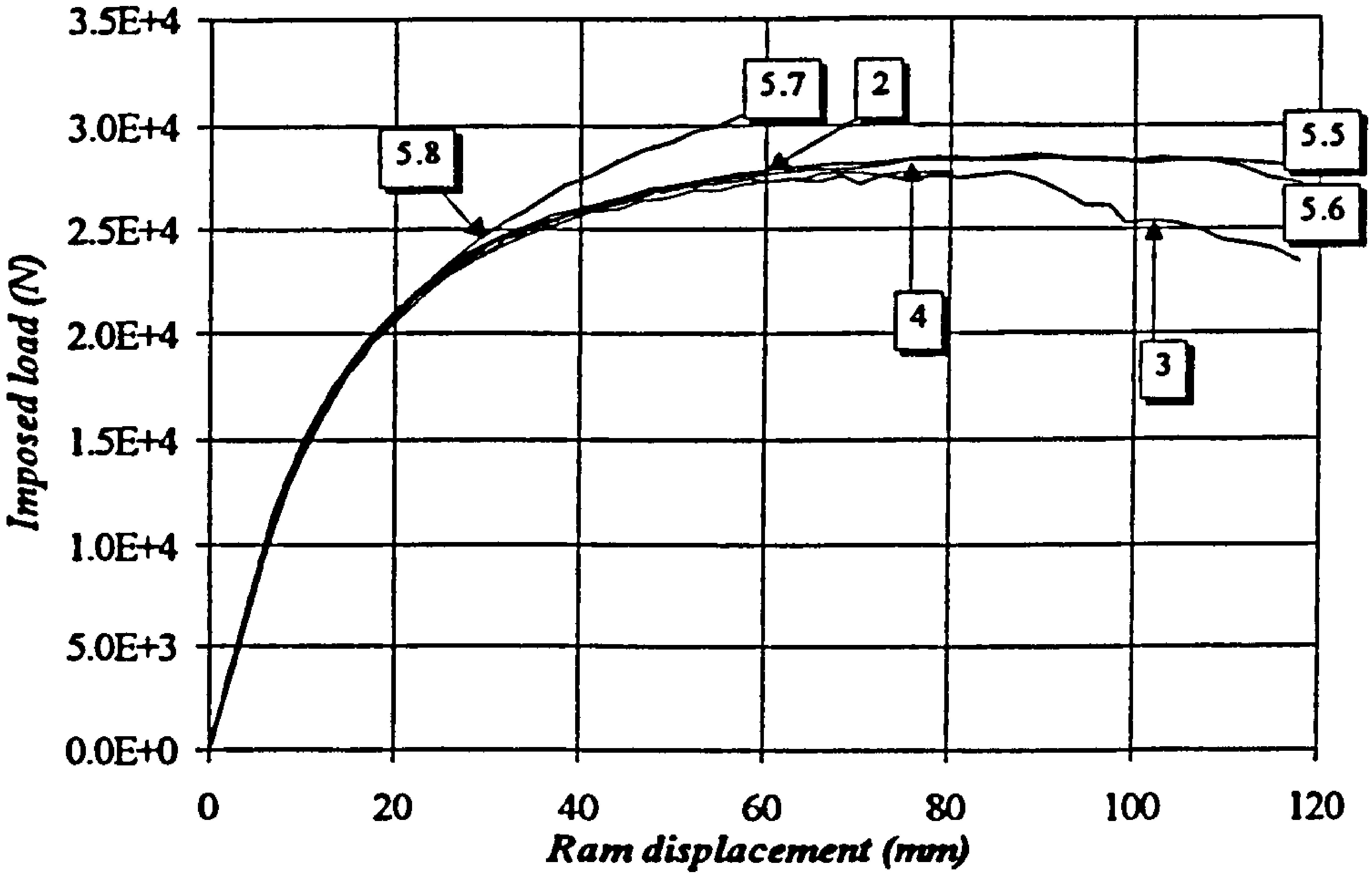

(b) Load-Displacement Behaviour

Figure 1.13: Chapuliot et al. [53] Out-of-plane Branch Bending Tests

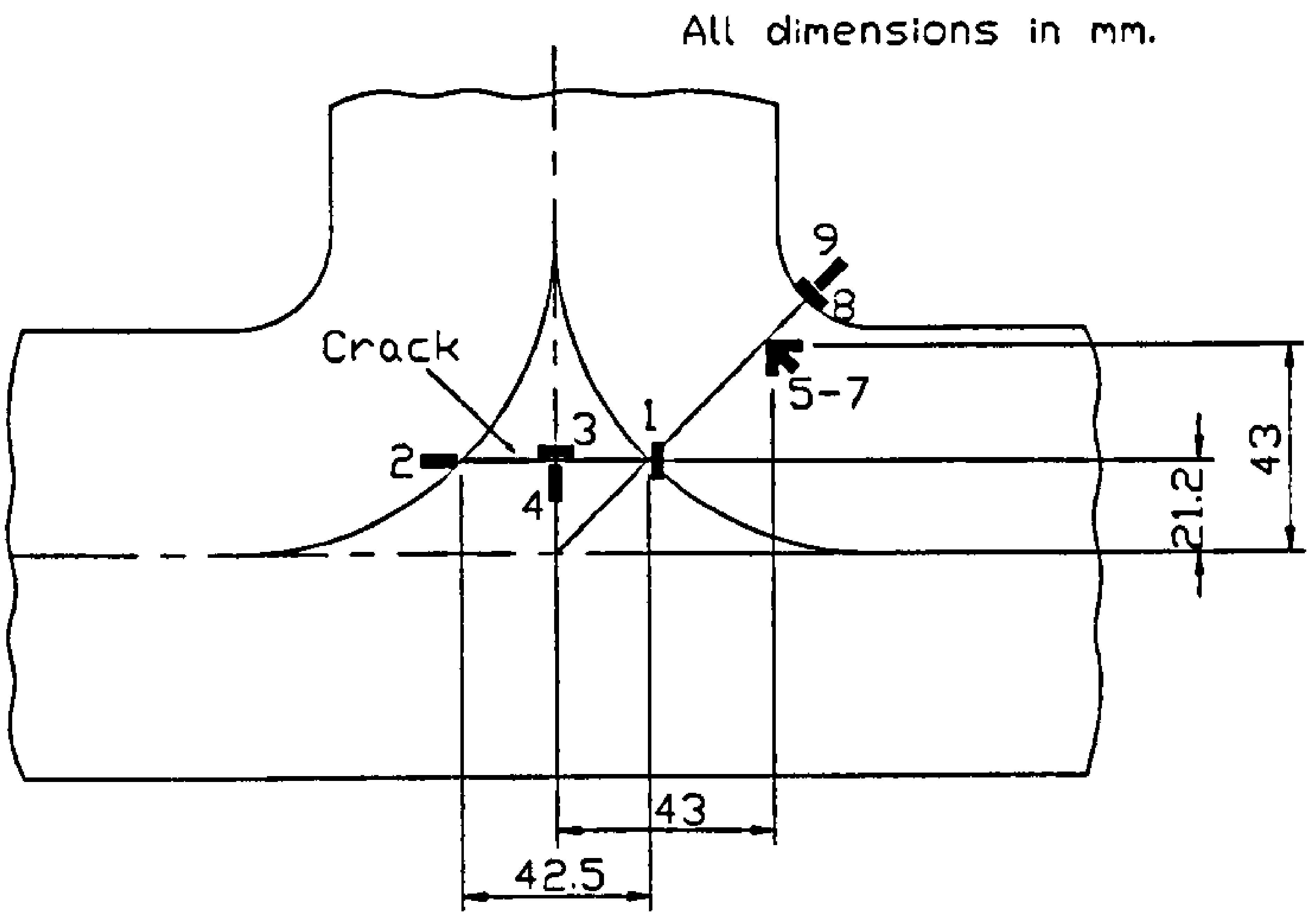

(a) Crack and Strain Gauge Locations

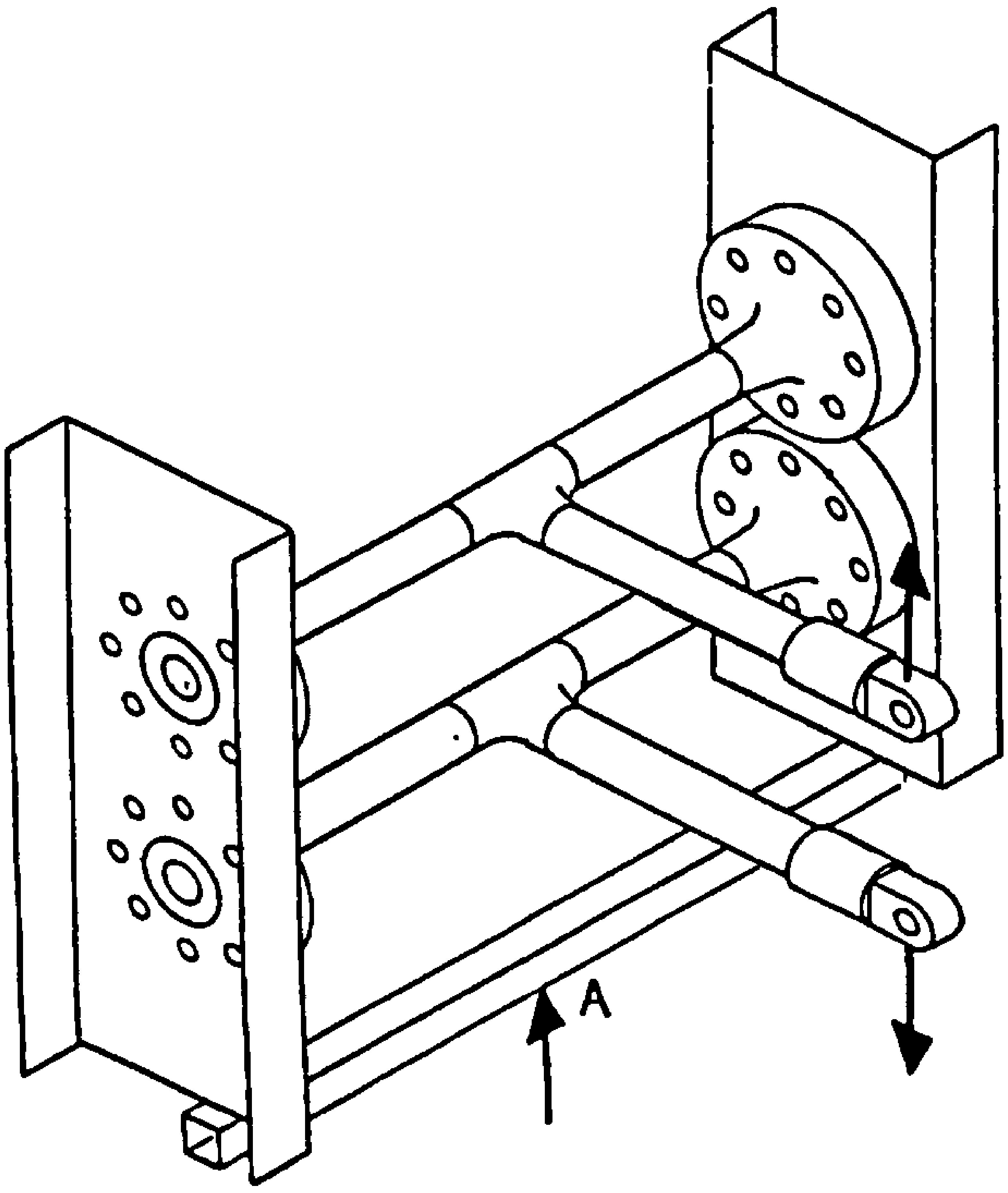

(b) Out-of-plane Branch Bending Test Setup

Figure 1.14: Yahiaoui et al. [19] Forged Branch Junction Study

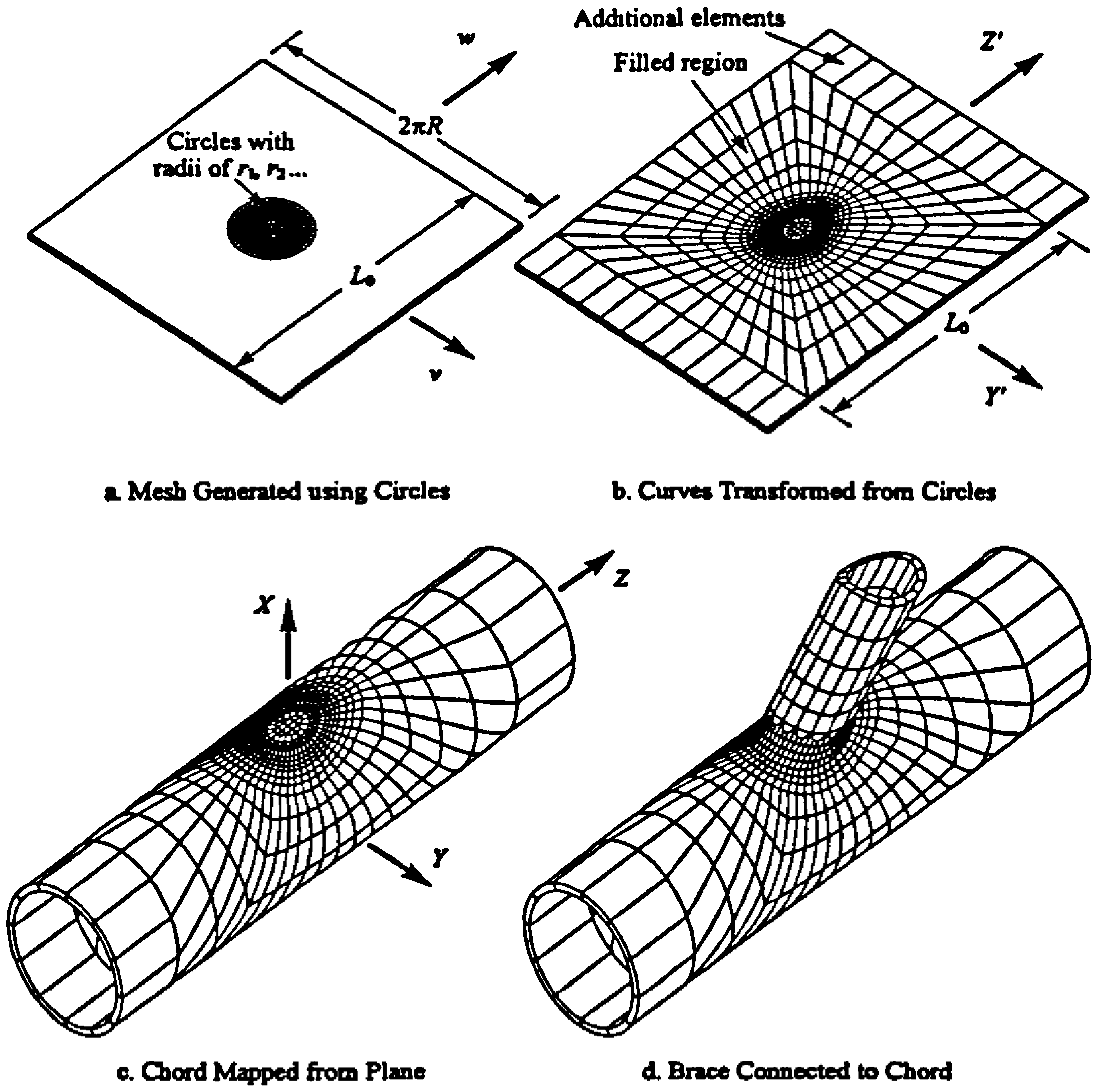

a. Mesh Generated using Circles

b. Curves Transformed from Circles

c. Chord Mapped from Plane

d. Brace Connected to Chord

Figure 1.15: Cao et al. [60] Tubular Joint Mesh Generation Method

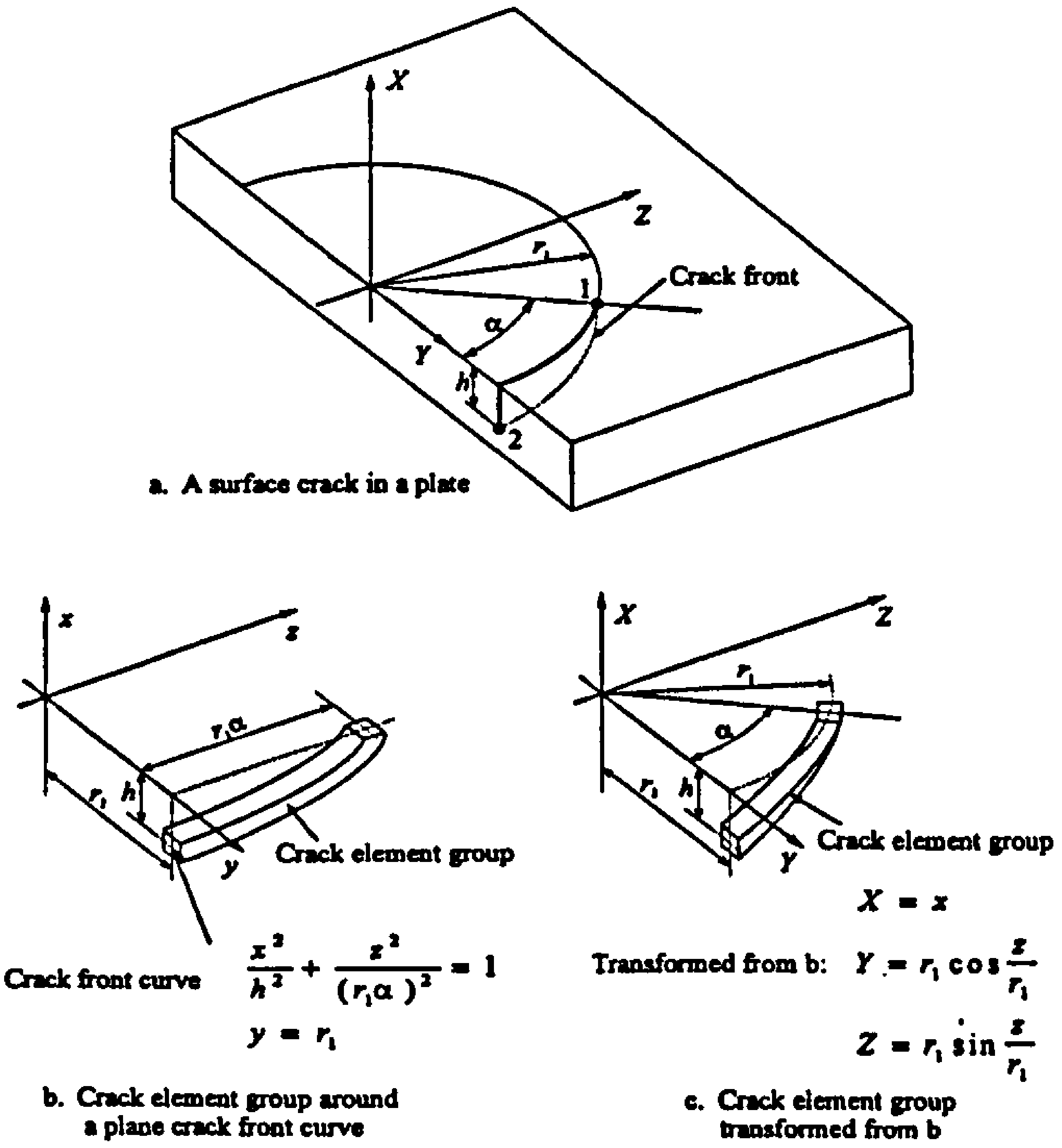

a. A surface crack in a plate

b. Crack element group around a plane crack front curve

c. Crack element group transformed from b

Figure 1.16: Cao et al. [60] Crack Generation Method

Chapter 2

Analysis and Experiments on Cracked Cylinders in Tension

2.1 Introduction

It has been observed previously, in a study on limit loads for cracked piping elbows [17], that it is possible to over-estimate the limit load using standard FE meshing techniques, particularly for components with long, deep cracks. Increasing the concentration of the mesh through the crack ligament for an elbow with a large, deep crack was shown to significantly reduce the limit load, under in-plane bending. The objective of the work in this Chapter was to step back from the relative complexity of piping elbows and to model a cylinder, with a **fully circumferential internal defect**, subjected to tensile axial loading (Figure 2.1). These results were then compared with full non-linear FE results and the corresponding experimental data. The intention was to gain a good understanding of the type of mesh that would be required for the later work on cracked piping branch junctions with part-penetrating cracks.

The first part of the work involved FE modelling of the limit load case, using elastic/perfectly-plastic material without non-linear geometric effects, as defined by Gerdeen[3]. This included a mesh convergence study, providing convincing evidence of the quality of mesh that is likely to be required to assess limit loads in piping components with large, deep cracks. A theoretical analysis for the cracked cylinder is also presented and the limit load predictions are compared with those from the FE study.

The second part of the work was experimental, using a series of five specimens with various crack depths. FE models of these specimens were produced and subjected to a full non-linear analysis. The results of the FE and experimental work could thus be compared with one another and with the analytical limit load predictions.

2.2 Stress Analysis

The recognised method (for example, see Carter [61]) for calculation of the limit load for a cylinder in tension, with a fully circumferential internal crack, is simply to calculate the load across the net-section of the remaining ligament, with the stress equal to the yield stress of the material. In other words, the limit load is the same as for an uncracked cylinder with dimensions equal to the ligament dimensions. Using the parameters defined in Figure 2.2, this is simply:

$$F_L = \sigma_y \left[2\pi R_{lig}(t-a)\right] \tag{2.1}$$

An alternative solution has been developed [62] (originally derived by Ainsworth[63]) for the limit load of a cracked cylinder using the equilibrium and yield conditions for the area surrounding the crack. The following assumptions were made:

1. The loading of the cylinder is purely axial.
2. A fully circumferential part-penetrating crack, of zero width, exists in the inside wall of the cylinder.
3. The material of the cylinder is elastic/perfectly-plastic and obeys the maximum shear strain energy (von Mises) theory of yield.
4. The radial stress is zero.

In Figure 2.2 the region around the crack is divided into three zones, enclosed within a short axial length, L. The crack width is shown for clarity, but was assumed to be zero for the analysis. Zone 1 includes the ligament and zones 2 are on either side of the crack as shown. In what follows, axial (σ_a) and hoop (σ_h) stresses in these areas are considered with secondary subscripts 1 and 2 to indicate the relevant zone. Referring to Figure 2.2, for hoop equilibrium:

$$\sigma_{h1}L(t-a) = -\sigma_{h2}aL \tag{2.2}$$

$$i.e., \sigma_{h1} = -\sigma_{h2}\left[\frac{a}{t-a}\right] \tag{2.3}$$

Clearly, in the cracked area σ_{a2}=0 and thus the von Mises yield criterion gives:

- For the cracked zone,

$$\sigma_{h1}\left[\frac{t-a}{a}\right] \leq \sigma_y \tag{2.4}$$

- For the ligament,

$$\sigma_{a1}^2 + \sigma_{h1}^2 - \sigma_{a1}\sigma_{h1} \leq \sigma_y^2 \tag{2.5}$$

There is now no reason to retain the second subscript for σ_a and σ_h in the above, since both refer to the ligament area. Thus the above equations become:

$$\sigma_a^2 + \sigma_h^2 - \sigma_a\sigma_h \leq \sigma_y^2 \tag{2.6}$$

$$\sigma_h\left[\frac{t-a}{a}\right] \leq \sigma_y \tag{2.7}$$

From the lower bound limit theorem (see [64], for example) the axial load,

$$F_L = \sigma_a 2\pi R_{lig}(t-a) \tag{2.8}$$

is a lower limit bound(where R_{lig} is the mean ligament radius), provided there are corresponding values of σ_a and σ_h which satisfy the yield criteria (2.6) and (2.7). One solution that satisfies equation (2.6) is:

$$\sigma_h = \sigma_y/\sqrt{3} \tag{2.9}$$

$$\sigma_a = 2\sigma_y/\sqrt{3} \tag{2.10}$$

Substituting (2.9) into (2.7), this also satisfies inequality (2.7) provided:

$$a \geq \frac{t}{1+\sqrt{3}} \tag{2.11}$$

The stress field of equations (2.9) and (2.10) is taken to be a solution for deep cracks since inequality 2.11 requires that the crack is deeper than 0.366t. For shallower cracks, it is assumed that equality holds in the yield criterion (2.7).

$$\text{Hence,} \qquad \sigma_h = \frac{a\sigma_y}{t-a} \tag{2.12}$$

Substitution into (2.6) gives the maximum axial stress, which satisfies the yield criterion in the ligament, as:

$$\frac{\sigma_a}{\sigma_y} = \frac{a}{2(t-a)} + \sqrt{1 - \frac{3}{4}\left[\frac{a}{t-a}\right]^2} \tag{2.13}$$

Hence, lower bound limit loads for the cracked cylinder are, from (2.8) and (2.10),

$$F_L = \frac{2}{\sqrt{3}}\sigma_y \left[2\pi R_{lig}(t-a)\right] \qquad a \geq t/(1+\sqrt{3}) \tag{2.14}$$

and from (2.8) and (2.13),

$$F_L = 2\pi R_{lig}(t-a)\sigma_y \left[\frac{a}{2(t-a)} + \sqrt{1 - \frac{3}{4}\left[\frac{a}{t-a}\right]^2}\right] \qquad a \leq t/(1+\sqrt{3}) \tag{2.15}$$

These relationships for the limit loads, normalised to the nominal yield load for the ligament, are plotted in Figure 2.3 as functions of a/t. There is clearly a considerable difference between the net-section value of the limit load (see Equation 2.1) and the above relationship, especially for deep cracks. The objective of the subsequent FE mesh convergence study was to confirm this result, and to explore the type and density of mesh required.

2.3 Finite Element Mesh Convergence Study

The mesh convergence study concentrated on three crack depth to thickness ratios: a/t=0.25, a/t=0.5 and a/t=0.75. The FE models were generated using PATRAN [65] and analysed using ABAQUS Standard [66]. The material properties were chosen to be consistent with the mild steel elbow study [17]. The cylinder dimensions and material properties used were:

Outer Diameter (D_o) = 34.29mm	Poisson's Ratio = 0.285
Inner Diameter (D_i) = 30.00mm	Young's Modulus = 210 GN/m^2
Mean Diameter to Thickness Ratio(D/t) = 15	Yield Stress (σ_y) = 308 MN/m^2

Two distinct types of mesh were used for the study:

1. 'Standard' limit load mesh, with nodes released to simulate a crack
2. 'Focused' mesh, similar to fracture mechanics mesh designs.

Globally the mesh structure for each case remained the same. However, the standard limit load mesh may not make any particular allowance for the position of the crack tip, although the element mesh may be biased towards the crack tip. Conversely, the focused mesh, as the name suggests, focuses the elements towards the crack tip. These two mesh techniques were used to evaluate the limit loads for the three different crack depths.

The cracked cylinder was axisymmetric, enabling the use of axisymmetric elements. The elements used throughout were 8-noded, biquadratic, reduced integration, axisymmetric solid elements (ABAQUS element: CAX8R). The use of such elements allowed modelling simply through the plane of the cylinder thickness. Additionally, only one axial half of the cylinder was modelled because of symmetry about the cracked section, as shown in Figure 2.4. The nodes at the ligament were constrained axially (i.e. in the 2-direction) to provide a symmetry face, with the tensile load applied by means of a pressure acting at the end of the cylinder, in order to provide uniform loading across the thickness. The crack was simply modelled by allowing the nodes along the crack face to be unconstrained: the crack was assumed to have zero width.

2.3.1 Standard Mesh

This mesh design used a standard rectangular mesh, with different numbers of elements through the thickness of the cylinder. Away from the crack, the mesh concentration was reduced to two elements through the thickness. Two types of standard mesh were assessed:

- Element size kept constant through the thickness at the crack position - this would be the case if an existing uncracked model was altered to create a cracked model.
- Refining the mesh so that the element size was biased towards the crack tip (referred to as 'non-uniform' standard mesh).

Typical standard mesh designs for both cases are shown in Figure 2.5, for a/t=0.75. For the non-uniform standard mesh the number of elements through the thickness was varied in the range 8 to 32 and the degree to which the element size was biased towards the crack tip was investigated by varying the 'non-uniformity ratio'. This ratio is defined as the ratio of the lengths of the smallest and largest elements along the crack ligament and could be adjusted easily in PATRAN [65].

2.3.2 Focused Mesh

The construction of this type of mesh was more complex than for the standard mesh. The mesh away from the crack position remained of the same form, but the elements surrounding the crack tip were generated such that the nodes could be 'collapsed' or 'focused' to the crack tip position, forming elements that shall be referred to as 'focused elements'. The reasons for using such a mesh are detailed by Anderson [67]. For elastic cases, a $\frac{1}{\sqrt{r}}$ singularity is present at the crack tip (i.e. the strain near the crack tip varies in proportion to $\frac{1}{\sqrt{r}}$ - 'r' being the distance from the crack tip). It is recommended in [67] that focused elements are used to model the singularity, with the mid-side nodes moved to quarter positions on the sides of the elements adjacent to the tip, and the nodes 'tied' at the crack tip. For elastic-plastic cases (e.g. limit load analysis), the $\frac{1}{\sqrt{r}}$ singularity is replaced by a $\frac{1}{r}$ singularity. For this case the recommendation [67] is again, that focused elements are used, but with the nodes at the crack tip untied (this allows blunting of the crack upon loading) and leaving the position of the mid-side nodes unaltered.

This technique resulted in there being several inter-connected nodes at the same geometric position at the crack tip, only one of which was constrained as part of the ligament boundary condition. Figure 2.6 shows the construction of the focused element mesh using a rectangular arrangement at the crack tip, followed by collapsing the elements to the crack tip and re-adjustment of the mid-side nodes to their correct positions. Figure 2.7 shows some typical focused mesh designs for a/t=0.75. The number of elements through the ligament, and hence the size of the focused elements, was varied, but was found to have very little effect on the limit load. Hence, the effect of the number of focused elements surrounding the crack tip was the main concern. The number of elements through the ligament was, however, increased with increasing elements around the crack tip in order to maintain reasonable element form away from the tip.

2.4 Experimental Work

The experimental work consisted of five specimens, with nominal values of a/t equal to 0.15, 0.3, 0.5 and 0.75 in addition to one uncracked specimen. The objective of the experiments was to compare the plastic loads of these specimens with their corresponding full non-linear FE results and with the theoretical limit load described previously (Section 2.2).

2.4.1 Specimen Manufacture

The five test specimens were machined from bright, mild steel bar. The bar was divided into seven sections - one additional specimen blank was kept in case of problems with the manufacture of any of the specimens (this specimen was machined alongside the others, but was not used in the test program), and another specimen blank was set aside for tensile test specimens. Initial rough external and internal machining was completed initially for each of the specimens, followed by heat treatment to stress-relieve the material and also introduce a clear 'perfectly-plastic' region, or 'lower yield plateau', to the material behaviour. (The heat treatment was necessary as the original material was bright bar, which generally has no distinct yield plateau). The specimens were subjected to one hour in a furnace at 650°C, followed by natural cooling of the specimens in the furnace to room temperature. The bore of the specimen was then honed to give a good surface finish (the honing was performed by a sub-contractor). Final external machining was then performed. Threads were machined on each end of the specimen to match existing end connections. The final specification is shown in Figure 2.8, along with the specified nominal crack location and dimensions. A dimensional survey was performed by the sub-contractor on each of the specimens, a summary of which is presented in Table 2.1. The results of this survey were checked, and were found to be satisfactory.

The defects, or cracks, were machined into the specimens using Electric Discharge Machining (EDM). All of the EDM work for the cylinders was sub-contracted to the same company that was responsible for honing the bores of the specimens. A rotary EDM machine was used, due to the fully-circumferential nature of the defects. The copper electrodes used were 0.3mm thick, in order to produce narrow defects. The defects were machined to provide uniform ligament thickness, rather than machining to a uniform defect depth. This was done because there was some ovality and eccentricity of the bores of the specimens, which could cause non-uniform ligament thickness if constant defect depth was required. The predominant factor in the loading calculations is the ligament thickness and so this was the controlling parameter. The electrode was mounted on the end of a bar and then centred inside the specimen, the centre determined from the external diameter of the cylinder. The cylinder was then eroded, as shown in Figure 2.9, by setting an electrode orbit about the centre of the cylinder. Initial rough machining was performed, followed by final machining with an unused electrode.

In order to inspect the profiles obtained, impressions were taken of the defects to check their depth and width. The used electrodes were also provided to show the extent of the erosion. The defect profiles, as provided by the sub-contractor, are shown in Figure 2.10. A summary of the actual crack depth values is given in Table 2.1, along with the values of a/t (calculated using the mean thickness values).

2.4.2 Material Properties

Three tensile test specimens were machined from a blank taken from the end of the bar. This blank had been subjected to the same heat treatment as the blanks used for specimen manufacture. The nominal dimensions of the specimens are shown in Figure 2.11. The specimens were routinely tested in a uniaxial tensile testing machine, using extensometer readings to calculate the strain values.

The results of these tensile tests are shown in Figure 2.12. It can be seen that the three curves are fairly consistent. For the purposes of the FE modelling a single true stress-strain curve was produced from an average of the three curves, as shown in Figure 2.13. The method for conversion of engineering stress-strain curves to true stress-strain curves is explained in [68]. The yield stress used for the experimental FE models was 290 MN/m^2 (Note: different to the mesh convergence study value).

2.4.3 Experimental Arrangement

Strain Gauges

The primary aim of the experiments was to produce load-displacement plots for each of the crack depths. In addition to this, strain readings were taken for each of the five specimens. Each specimen had strain gauging around the defect area, on the outer diameter of the cylinder. The aim was not to produce a complete strain distribution, but to gain an insight into the spread of the plasticity around the crack tip and to compare the strain readings with the corresponding FE results. The positions of the strain gauges were altered for each specimen, depending upon the depth of the crack. All of the strain gauges were orientated axially on the cylinder.

The uncracked specimen had a strain gauge arrangement as shown in Figure 2.14. There were four gauges around the centre of the specimen, used to measure the magnitude and direction of any bending. There were also two gauges towards each end of the specimen and another high elongation gauge between two of the bending gauges (gauge No. 5). This specimen was used to check the test setup, in an attempt to ensure that there was no excessive bending. Each of the cracked specimens also had a similar series of 4 bending gauges positioned away from the crack. The percentage bending was calculated for each diametrically opposite pair of gauges (e.g. 2 gauges giving strains ε_1 and ε_3) using the equation:

$$\%\ bending = \frac{1}{2} \times \frac{\varepsilon_1 - \varepsilon_3}{(\varepsilon_1 + \varepsilon_3)/2} \tag{2.16}$$

The peak strain positions for a selection of the existing cracked FE meshes from the mesh convergence study were studied. It was found that the axial strain on the outer surface tended to peak at approximately 45° from the crack tip, as would be expected with slip lines from a crack (see Anderson[67]). This effect is described later, in Section 2.6. Gauges were positioned approximately at these peak positions (taking into account the width of the crack, as the mesh convergence models had zero crack width). Gauges were also positioned alongside these gauges and over the crack ligament, in a staggered formation. The gauge arrangement is shown schematically in Figure 2.15, along with the actual measured positions for the various cracked specimens.

- Two of the specimens (with measured a/t = 0.16 and 0.73) had an arrangement of three gauges on one side, and on the opposite side they had a similar arrangement but with four gauges, as shown in Figure 2.15.
- The two remaining cracked specimens (measured a/t = 0.33 and 0.51) had three gauges on one side and a chain gauge on the opposite side, consisting of a strip of ten gauges (and one additional gauge, at the end of the strip). The chain gauge was positioned with one gauge centred over the crack ligament. The chain gauges were used to give a detailed strain analysis over a greater length of the two specimens - the arrangement is shown in Figure 2.15. Due to the logging capacity limitations of the data logger, not all of the gauges were used. The unconnected gauges are marked with an 'x'.
- The gauge length of all gauges used on the cracked specimens was 0.6mm.

Test Arrangement

The tests were conducted using a Dartec 250kN servo-hydraulic test machine. A set of universal joints were designed in order to minimise the bending in the test. These were connected, via existing connecting pins, to the base and crosshead of the Dartec. The specimens were attached to threaded 'clevis-eye' type connections and then connected to the universal joints. The test arrangement is shown in Figure 2.16. The load and displacement were recorded from the Dartec crosshead output throughout the tests.

A bending check was carried out for each specimen prior to testing. The specimens were loaded up to a fraction of their expected yield load and the bending strains were monitored. It was found that the positioning of the connections of the universal joints could be adjusted to reduce the bending to a minimum. The tests were then performed continuously at a set rate of displacement using the 'ramp' function on the Dartec.

2.5 Full Non-Linear FE Analysis

The FE analysis of the experimental cases is described in this section. Unlike the mesh convergence study in Section 2.3, full non-linear analysis was required. The true stress-strain data, shown in Figure 2.13, was used and material non-linear geometry was also accounted for (i.e. the NLGEOM parameter was used in ABAQUS [66]).

The model geometry and construction was very similar to that of the models described earlier. However, as there were only four experiments with cracks, the individual measured geometry (see Table 2.1) was modelled for each, including the crack width. The crack profiles shown in Figure 2.10 were used as a basis for the models. The cracks modelled had constant width, equal to the measured width at the crack opening (e.g. 0.33mm for specimen No. 2), with a radius used to connect the 'flat' at the bottom of the crack with the crack face. The four cracked FE meshes are shown in Figure 2.17. The mesh around the crack is of a slightly different form to the mesh convergence cases. The mesh was biased towards the crack tip radius, but no focused mesh was used as it was thought that this would make very little difference at a crack tip with a curved profile.

Another difference between the mesh convergence models and these experimental models is the boundary conditions that were applied. Due to the nature of the experimental specimens, they have a finite 'gauge' length (or parallel section), after which the cylinder was constrained from reducing radially by the thicker end connections. This effect was modelled by using the specimen 'gauge' length of 96mm (see Figure 2.8) and applying a radial constraint to the end of the model. The axial constraint on the nodes at the ligament was applied as before. This extra constraint was examined for the $a/t=0.508$ case, and was shown to have little effect. The various boundary conditions and possible analysis methods were compared - the relevant load-displacement plots are shown in Figure 2.18. The two full non-linear cases, with the cylinder end constrained and unconstrained, give virtually identical responses. The limit load case gives a clear plateau below the full non-linear value. Removing the non-linear geometry analysis from the full non-linear analysis gave a result that continued to rise and did not account for the tensile 'necking' of the crack ligament. Altering the material behaviour of the full non-linear case, from a true stress-strain response to an elastic/perfectly-plastic response, gave a load displacement curve that reached the limit load and then dropped immediately due to 'necking' of the ligament.

The method of applying load for these full non-linear cases was displacement control, as this was the method used experimentally. A series of load-displacement charts was produced for comparison with the experimental results. Strain values were also compared with the experimental strain results.

2.6 Results and Discussion

2.6.1 Mesh Convergence Study Results

The results of the mesh convergence study are summarised in Figure 2.19. Theoretical values from the net-section analysis (i.e. using yield stress × ligament area) and from the analysis described in Section 2.2 are compared, along with the standard and focused mesh results. The fifteen times elastic slope was used to determine the limit load, and is shown in Figure 2.20 for typical standard and focused load-displacement curves. The fifteen times elastic slope criterion is an arbitrary one that has been used with other limit load assessments at Liverpool (e.g. [15]). It is clear from Figure 2.19 that the FE results confirm the analysis described in Section 2.2 rather than the net-section value - both the standard and focused mesh results converge towards the Section 2.2 value.

For the limit load results shown in Figure 2.19, the focused mesh cases had the same number of focused elements around the crack tip (for a half model) as they had through the thickness. It was apparent that the focused mesh results were considerably closer to theory than standard mesh designs, particularly for coarse mesh designs with few elements through the thickness. Refining the standard mesh towards the crack tip ('non-uniform' standard mesh) provided limit loads closer to theory than the uniform standard mesh. Figure 2.21 illustrates the effect of altering the non-uniformity ratio upon the limit load, for a/t=0.75. The '% Variation' parameter used is defined as the % difference between the FE limit load and the theoretical value. Four different cases are shown with 8, 16, 24 and 32 elements through the thickness. The effect of using non-uniform elements tended to reduce as the number of elements through the thickness increased, although there was still a substantial difference from the standard mesh (ratio = 1.0) for each case. A non-uniformity ratio of 0.05 was used for the general limit load comparison in Figure 2.19, as the values reduced very little for smaller elements.

An alternative method of evaluating the results is to plot the % variation, as defined above, against the number of elements through the thickness. This method was used in Figures 2.22, 2.23 and 2.24, for a/t=0.25, 0.5 and 0.75 respectively. For a standard mesh, the greatest variation occurred for the deepest defect, with a/t=0.75. For this crack depth, the variation was as high as 38% for the coarsest mesh and was still over 5% with 32 elements through the thickness. Using a non-uniform standard mesh reduced the variation to a more acceptable level of between 10% and 1%, depending upon the number of elements used. However, the focused mesh provided a variation from theory of less than 3% for the coarsest mesh, reducing to just 0.3% for the finest mesh.

Similar results were shown for a/t=0.25 and a/t=0.5, but with less range of variation than for a/t=0.75. Using a non-uniform standard mesh for these cases gave variations of less than 5%, which may be deemed acceptable in many instances. However, the focused mesh always had a lower variation than the equivalent non-uniform standard mesh.

2.6.2 Experimental Results and Comparisons with FE Results

The main set of results obtained from the experiments was a series of load-displacement plots. The specimens tested were thin (t=2.15mm, with D/T=15) and the testing machine had a maximum capacity of 250kN. Due to the deflection of the machine, the end connections, and the threads at the ends of the specimens, the crosshead displacement would not give an accurate representation of the specimen response. This machine deflection was measured with a solid bar, using the same setup as for the test specimens. It was then theoretically possible to subtract the machine deflection from the overall crosshead displacement to give the specimen displacement. However, it was decided that each set of results should be adjusted so that the linear region had the same slope as the corresponding FE model (under elastic analysis). This enabled the plastic results to be directly compared between specimens and with the FE results, eliminating concerns about the accuracy of the elastic slope of the specimens. In any case, the difference between the slope of the FE results and the slope using the adjusted displacement (i.e. with the machine deflection subtracted) was not greater than 30%, which would have negligible effect on the plastic response.

The bending was recorded for each of the specimens using a set of four strain gauges, as described previously. Although universal joint connectors were used, there was still some bending present in the tests. This was probably caused by slightly uneven loading on the pins in the universal joints, as well as any slight differences in ligament thickness and symmetry of each specimen. The bending was plotted as a percentage value for each diametrally opposite pair of gauges, using equation (2.16). Typical bending responses for two of the tests are shown in Figure 2.25. The % bending was higher at low loads, but decreased to about 4% as the load level increased. This level of bending was not expected to have much influence on the results, although it would have caused specimen 'yielding' at a slightly lower than expected load, which would in turn affect the overall response.

In addition to the load-displacement results, the strain data has been used to study the strain distribution in relation to the distance from the crack. This data was also compared with results from the FE model. The results are presented and discussed below.

Load-Displacement Results

Overall comparisons of the load-displacement plots for each of the five specimens are shown in Figures 2.26(a) and 2.26(b), for the experimental and FE results respectively. These figures give a general idea of the reduction in strength with increasing crack depth.

The individual load displacement plots, comparing the experimental and FE results, are shown in Figures 2.27 - 2.31, for specimens 'A'-'E' respectively. The theoretical limit load (from Section 2.2) is also marked on each of the plots. Beneath the cracked model load-displacement plots, the axial strain results from the strain gauges and from the FE models are displayed, for a selection of load levels: these are discussed in the following Section.

For the uncracked specimen (Figure 2.27) the comparison between the FE and experimental results was very good, as would be expected for an uncracked tensile test. The lower yield plateau was clearly defined and was equal to the theoretical limit load. The ultimate load carried by the test specimen was 96.1kN.

For the shallowest crack (Figure 2.28(a)) the comparison was again very good, with the FE results giving a slightly higher plateau reading than the experimental results (approximately 7.5% higher than the theoretical value). The plateau was present up to approximately 1.8mm. The experimental plateau was 4.2% higher than the theoretical value. The comparison continued to be good for the entire plastic region. The ultimate load carried by the test specimen was 94.5kN.

The a/t=0.33 model load-displacement results are shown in Figure 2.29(a). Although the plateau of both load-displacement responses was well above the theoretical limit load (over 22% higher), the response first became non-linear (for both the FE and experimental results) just below this limit load value. In fact, the experimental response exhibited a slight yield peak just below the limit load, similar to an upper yield point for an uncracked tensile test. Overall, the FE results compared well with the experimental results. The ultimate load carried by the test specimen was 79.5kN.

The a/t=0.51 model (Figure 2.30(a)) again showed a good comparison between the FE and experimental results, with the FE results having slightly lower load values.

There was no distinct plateau value for this model, although there was a slight yield plateau experimentally (at 33.6kN), below the theoretical limit load value (marked in Figure 2.30(a)). The FE and experimental results both started to exhibit non-linear behaviour above this load level. The ultimate load carried by the test specimen was 60.7kN.

The deepest crack, with a/t=0.73, showed less satisfactory comparison between the FE and experimental results. There were problems with recording the displacement values for this specimen: because the displacements in question were so small, the resolution of the data logger for measuring displacement should have been adjusted accordingly. Unfortunately, this was not done for this specimen (or for the uncracked and a/t=0.33 specimens, although the displacements in these cases were larger and so the default resolution of the data was adequate). The original load displacement response is shown in the inset of Figure 2.31(a), along with a smoothed approximation to the response for ease of comparison with the FE data. Despite the poor quality of the original experimental results, it is clear that the FE data was considerably below the experimental response. There is no yield plateau apparent for either set of results, although any small plateau in the experimental results would not have been clear. The differences between the results may be due to this specimen having such a thin ligament compared with the other specimens, any measurement errors having a greater effect on the overall results. Having said this, the comparison between the two sets of data improved as the displacement and load increased. The ultimate load carried by the test specimen was 31.7kN.

The ratio of the ultimate load carried by the test specimens (P_{ult}) to the theoretical limit load is shown in Table 2.2. This ratio is fairly constant and may be assumed to be approximately equal to 1.6 for all of the specimens. Hence the ultimate load can easily be predicted from the calculated limit load.

Comparison of Strain Results

The contour plots of the axial strain are shown in Figures 2.32(a)-(d) for cracked specimens 'B'-'E' respectively. It is clear that the peak axial strain on the surface of the specimen was at approximately 45° to the crack tip. This should be confirmed by the strain data for each case. The strains have been plotted at a selection of load values for each specimen, for both experimental data and the FE analysis, in order to illustrate the spread of yielding around the crack tip location. The experimental data was plotted for the strain gauge positions described in Figure 2.15. The data was plotted against distance from the centre of the crack width, regardless of the side of the crack that the strain gauges were placed. Hence, the strain values for the same nominal locations could be easily compared with the FE values. The FE strain values were obtained from the node locations along the outer surface of each cylinder, using the 'averaged at nodes' location for strain values in ABAQUS [66].

The 45° location on the outer diameter of each of the specimens was also considered in the results presented below. This location was calculated from the FE models (see Figure 2.17) by extrapolating a line at 45°, from the midpoint of the radius between the ligament and the crack face to the outer surface of the model. This 'peak' location prediction was not expected to be exact, as the choice of the midpoint of the aforementioned radius was an arbitrary one.

For the shallowest crack the strain distribution is shown in Figure 2.28(b). At low loads the strain appeared constant (although adjusting the strain scale of the graph would show some variation) but as the load increased to 40.1kN a peak strain location became apparent. As the load increased further to over 60kN the peak was clear for both test and FE results. The FE data did not compare that well with the strain gauge values in terms of magnitude, but the peak strain locations were similar and were close to the 45° position.

For specimen C, the FE data compared very well with the strain gauge values throughout the test (Figure 2.29(b)). A chain gauge was used with this specimen, and so strain data was available for a greater length of the specimen. Even at the lowest load value, there was a significant difference between the strain at the centre of the ligament (distance = 0) and the strain away from the crack. A clear peak strain location formed at the highest load value, which was confirmed by the FE data. Both the FE and experimental results were close to the 45° position.

The strain distribution for Specimen D is shown in Figure 2.30(b). The FE data again compared well with the strain gauge data. As for the previous case, a chain gauge was used for this specimen. At a load of 30kN, the strain was actually compressive at the centre of the ligament, for both FE and test data. The location of the peak was clear at the highest load value (35.7kN), which was just above the plateau level marked in Figure 2.30(a). The strain gauge data gave a slightly higher peak value than the FE data. The only other major difference between the two sets of data was at the ligament centre for the highest load: the strain gauge data at this point was considerably higher than the FE data. Again, both the FE and experimental results were close to the 45° position.

For the deepest crack, specimen E, the strain distribution is shown in Figures 2.31(b) and (c). Figure 2.31(b) shows the overall strain distribution up to 9000 micro-strain, while Figure 2.31(c) examines the behaviour at lower strain values. The four lowest loads from (b) are presented in (c). Overall the FE results compared well with with the strain gauge data. The peak strain location at the highest load was confirmed by the FE data, although the magnitudes of the strains were different. It is interesting to note that the load of 18.9kN, at which this peak was clearly visible (meaning that plasticity had spread across the ligament), was still in the linear section of the load-displacement plot of test data in Figure 2.31(a). There may have been some response that was not detected due to the problems with recording displacement data, described previously. Figure 2.31(c) shows that for the lower load levels there was considerable negative strain at the centre of the crack ligament. It is also interesting to note that, for the FE results, the peak strain location for these lower loads was at a greater distance from the crack than for the highest load in Figure 2.31(b). In general, the peak FE and experimental results were close to the 45° position.

The compressive strain at the ligament position for specimens D and E is caused by the application of the tensile load being offset from the crack ligament. The load may be assumed to be acting through the centre of the wall thickness, as shown in Figure 2.33. For an uncracked specimen, this gives uniform loading, but for a cracked specimen the load is offset from the load-bearing section (the crack ligament). This load is actually equivalent to an axial load and a bending load acting in line with the centre of the ligament, as illustrated in Figure 2.33. Hence, there will be a tendency for compression to occur on the outer surface and tension on the inner surface. The net strain was positive for the shallower cracks, as the axial load caused tension across the ligament, offsetting the compressive bending strain. However, for the deeper cracks the compressive effect was recorded, as the axial loads were not initially sufficient to cause the net strain to be positive.

2.7 Concluding Remarks

The FE mesh convergence study has confirmed the theoretical limit load described in Section 2.2, as opposed to the usual net section limit load. A focused mesh was found to be the most economical method of evaluating the limit load accurately, in terms of number of elements used. A standard mesh with the elements biased towards the crack tip also gave results that were close to the theoretical limit load.

The overall agreement between the experimental and FE results was good, both in terms of the load-displacement response and the strain levels. The plateau of the load-displacement plots did not always coincide with the theoretical limit value, but the response usually began to be non-linear at approximately this limit load value. There was generally a factor of 1.6 between the theoretical limit load and the ultimate load of each specimen. The FE peak strain locations predicted in Figure 2.32 agreed well with the experimental strain peaks, as shown in Figures 2.27(b)-2.31(b).

The work presented gives a useful insight into FE meshing techniques for cracked models, both for limit load analysis and experimental comparisons.

Table 2.1: Dimensional Survey

Specimen	D_o(mean) [mm]	t(mean) [mm]	D_i (=D_o-2t) [mm]	a [mm]	a/t
A	34.267	2.125	30.017	-	-
B	34.263	2.125	30.013	0.33	0.16
C	34.268	2.100	30.068	0.70	0.33
D	34.267	2.125	30.017	1.08	0.51
E	34.259	2.110	30.039	1.55	0.73

Table 2.2: Experimental Ultimate Load Results

Specimen	P_L (theoretical) [kN]	P_{ult} [kN]	P_{ult}/P_L
A	62.2	96.1	1.55
B	57.3	94.5	1.65
C	48.3	79.5	1.65
D	36.5	60.7	1.66
E	19.9	31.7	1.59

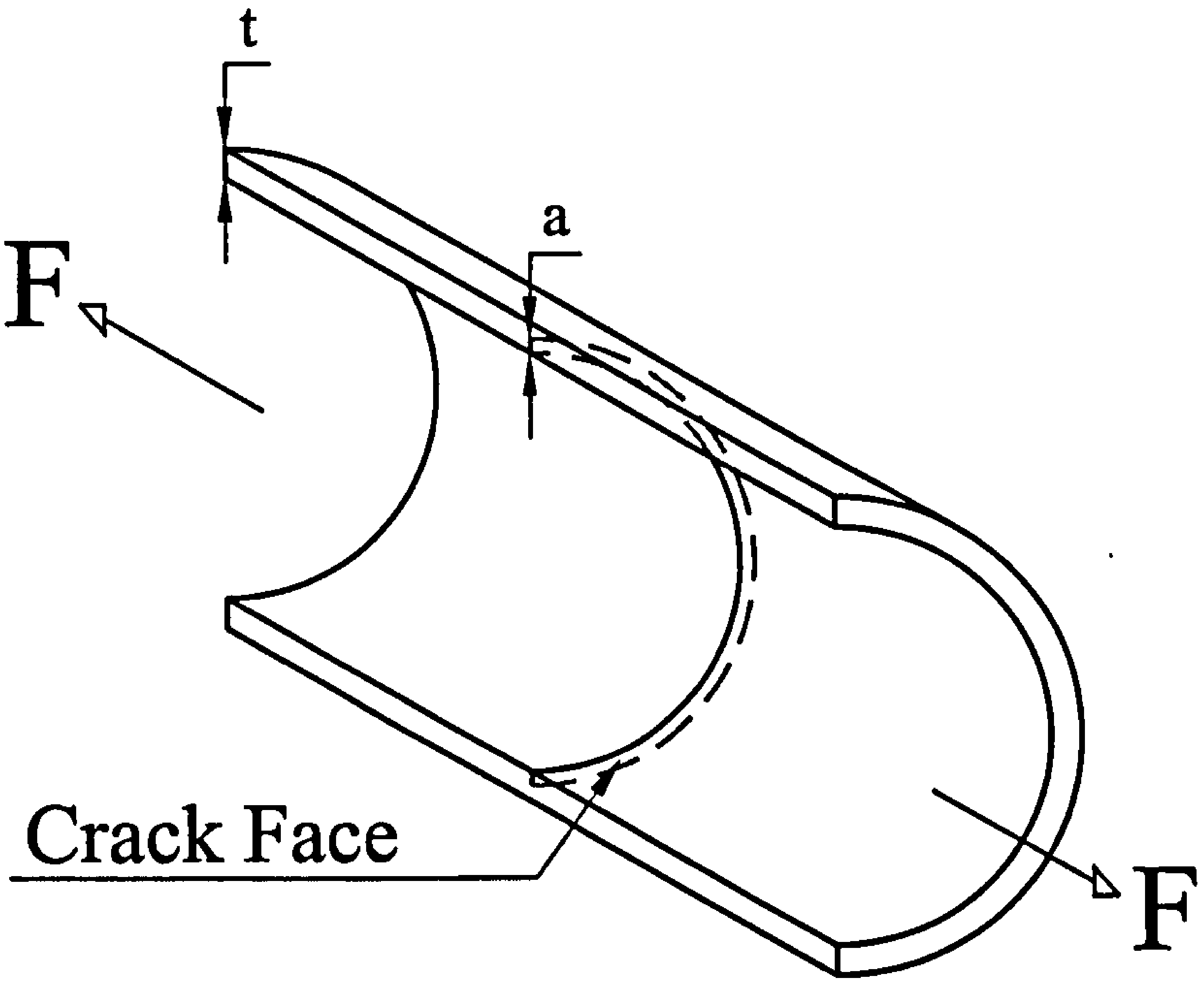

Figure 2.1: Section through Cracked Cylinder

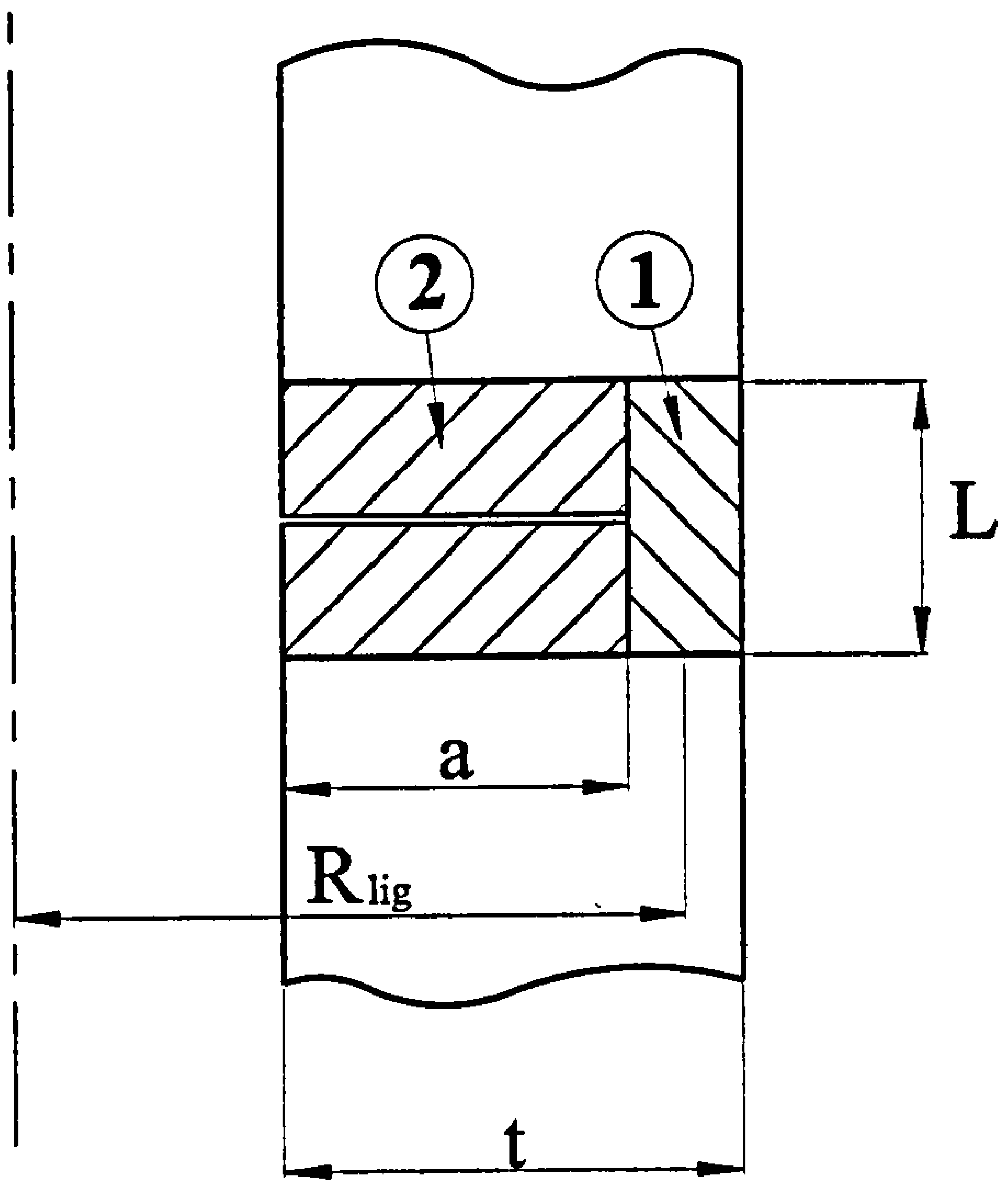

Figure 2.2: Notation for Cracked Area

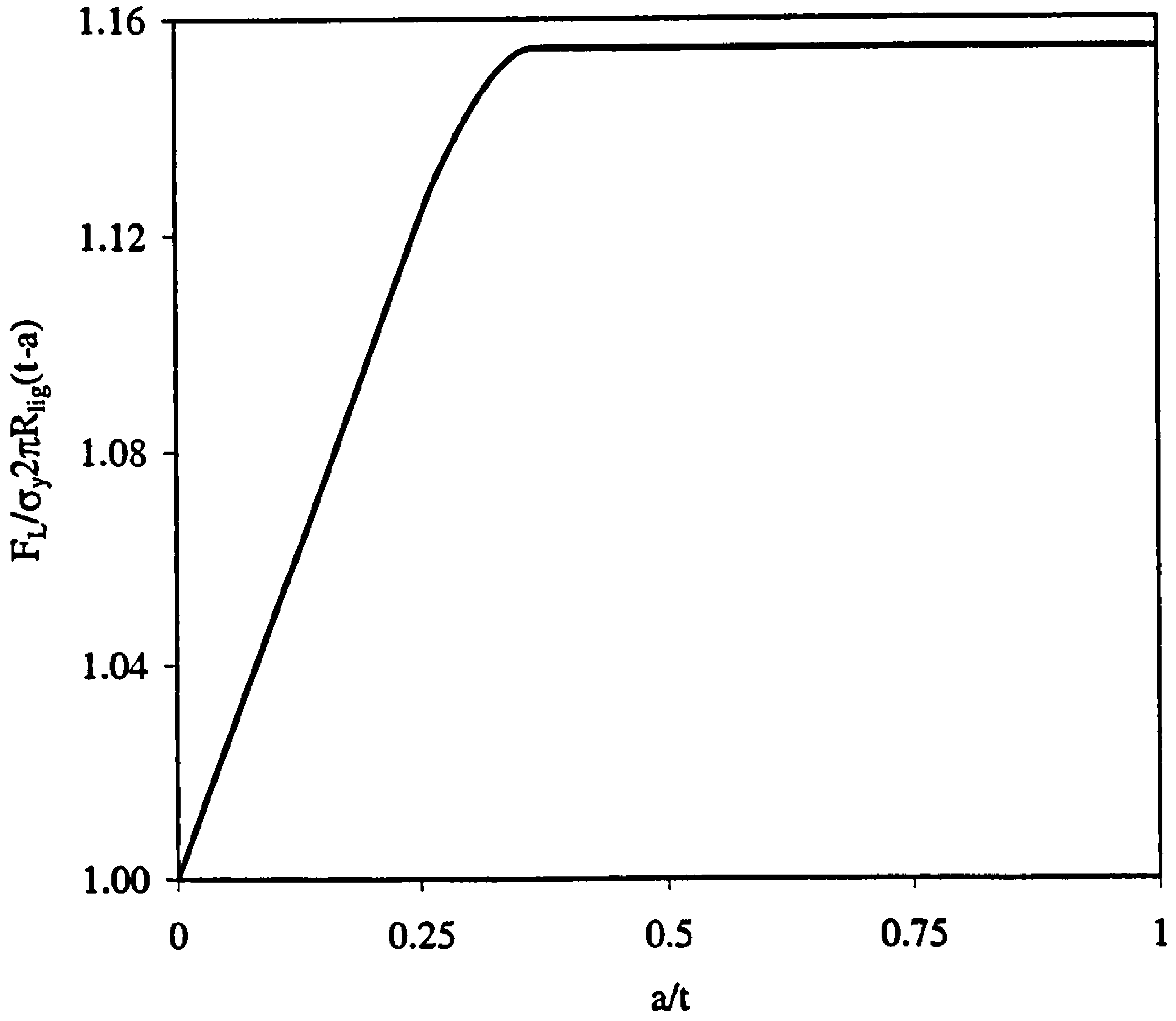

Figure 2.3: Limit Load - Defect Depth Relationship

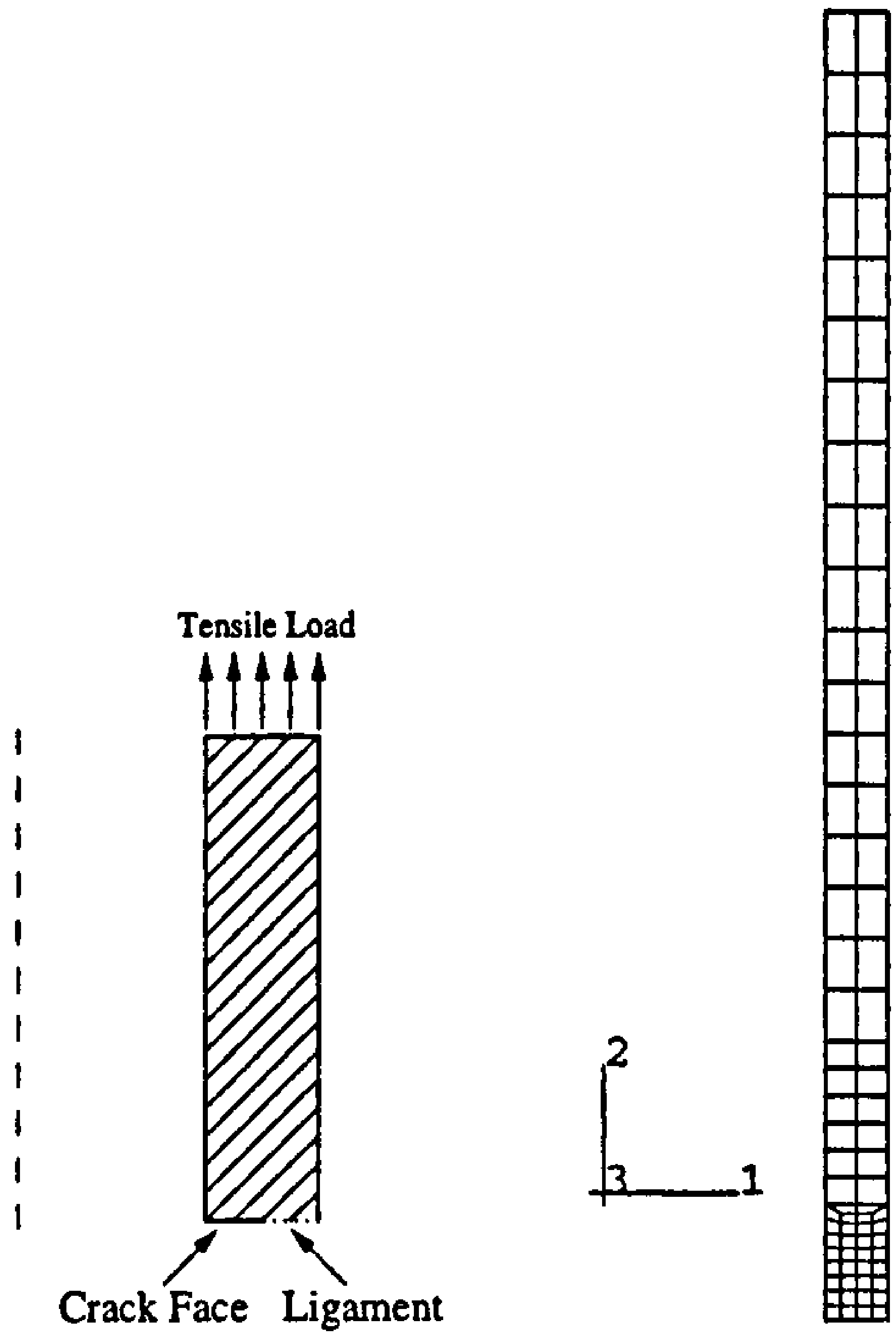

(a) (b)

Figure 2.4: (a)Schematic of FE Model Layout (b)Typical FE Model

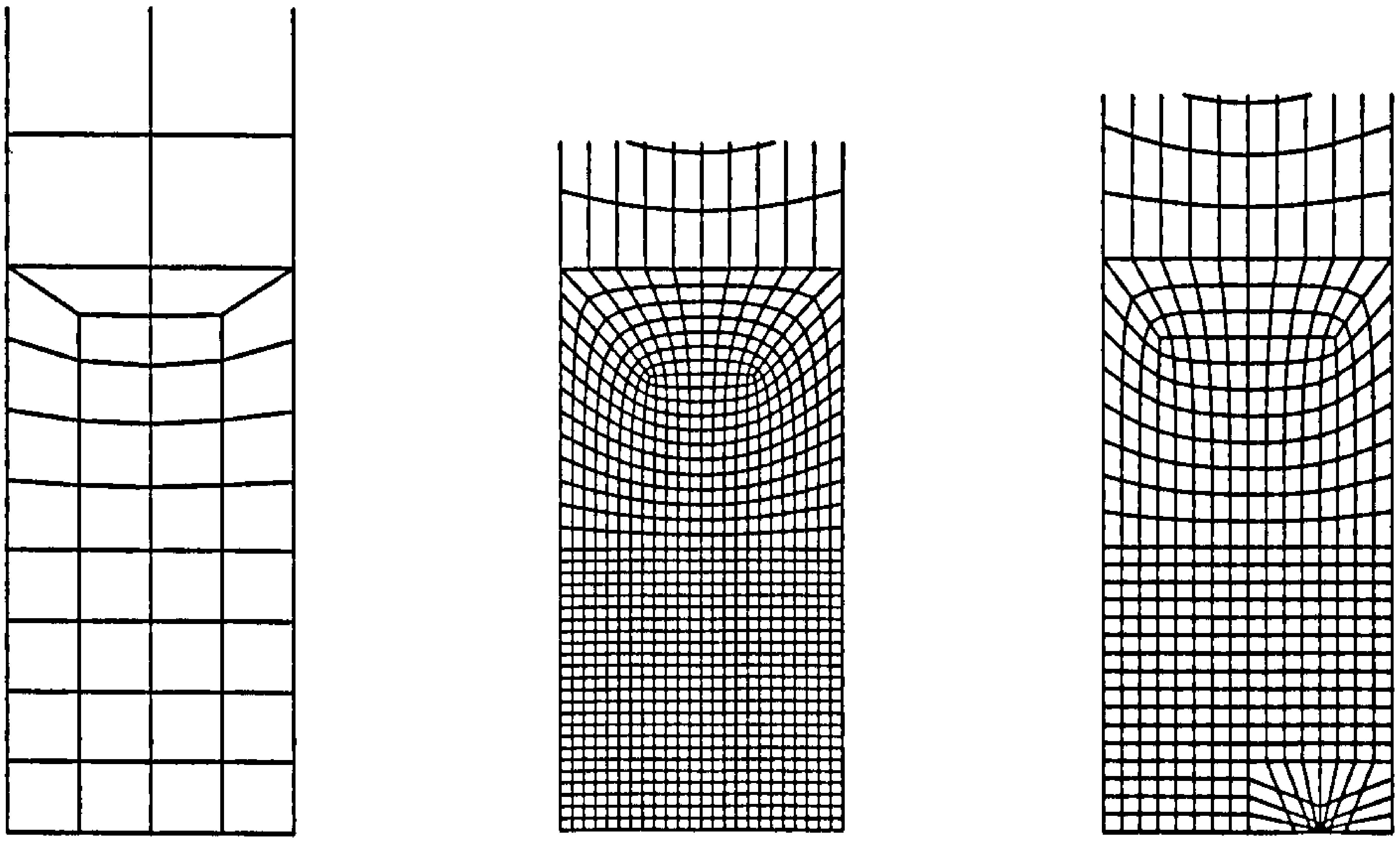

4 elements
Standard Mesh

24 elements
Standard Mesh

16 elements
Non-uniform Standard Mesh

Figure 2.5: Typical Standard Mesh Designs for a/t=0.75

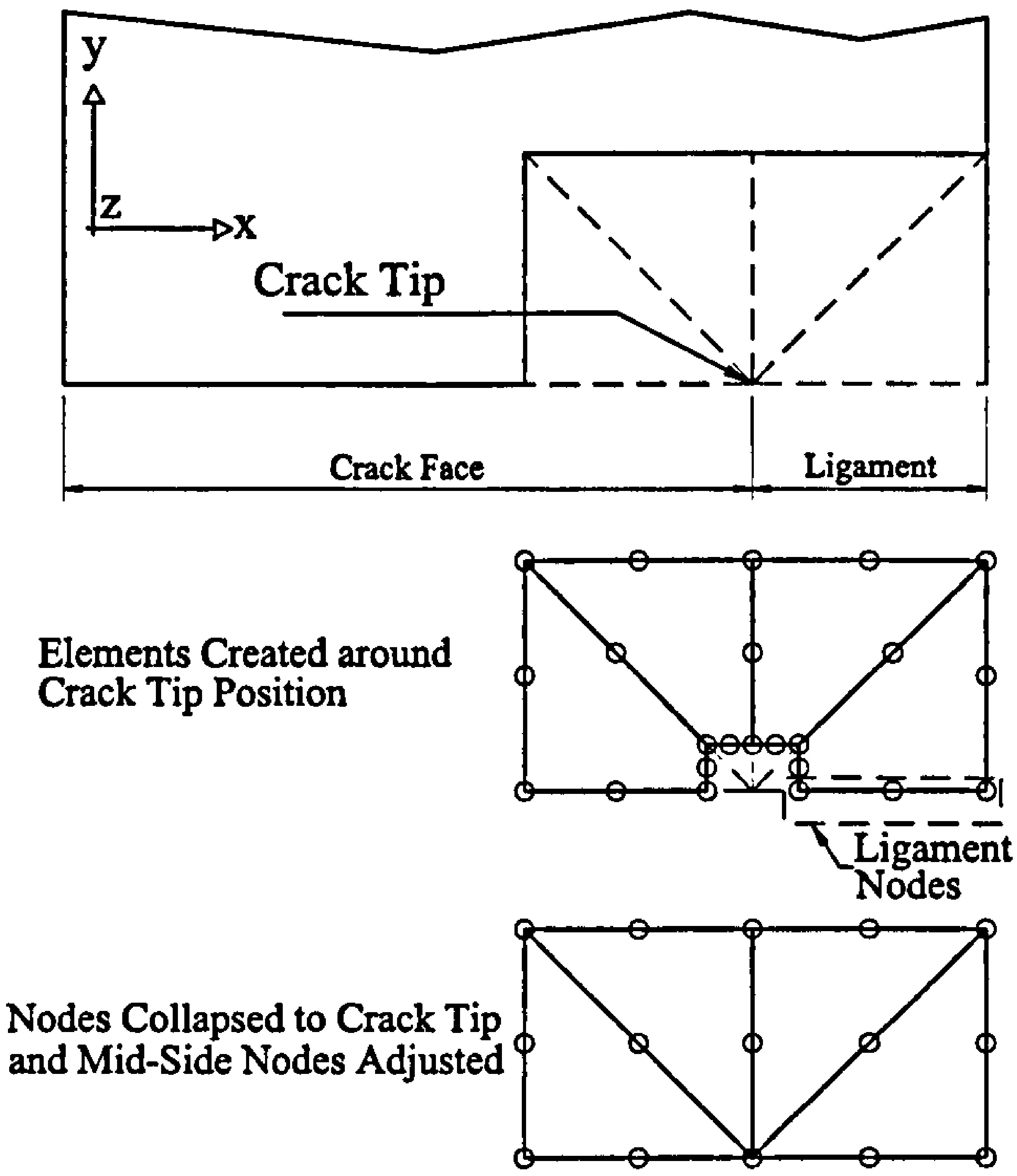

Figure 2.6: Focused Mesh Construction for a/t=0.75

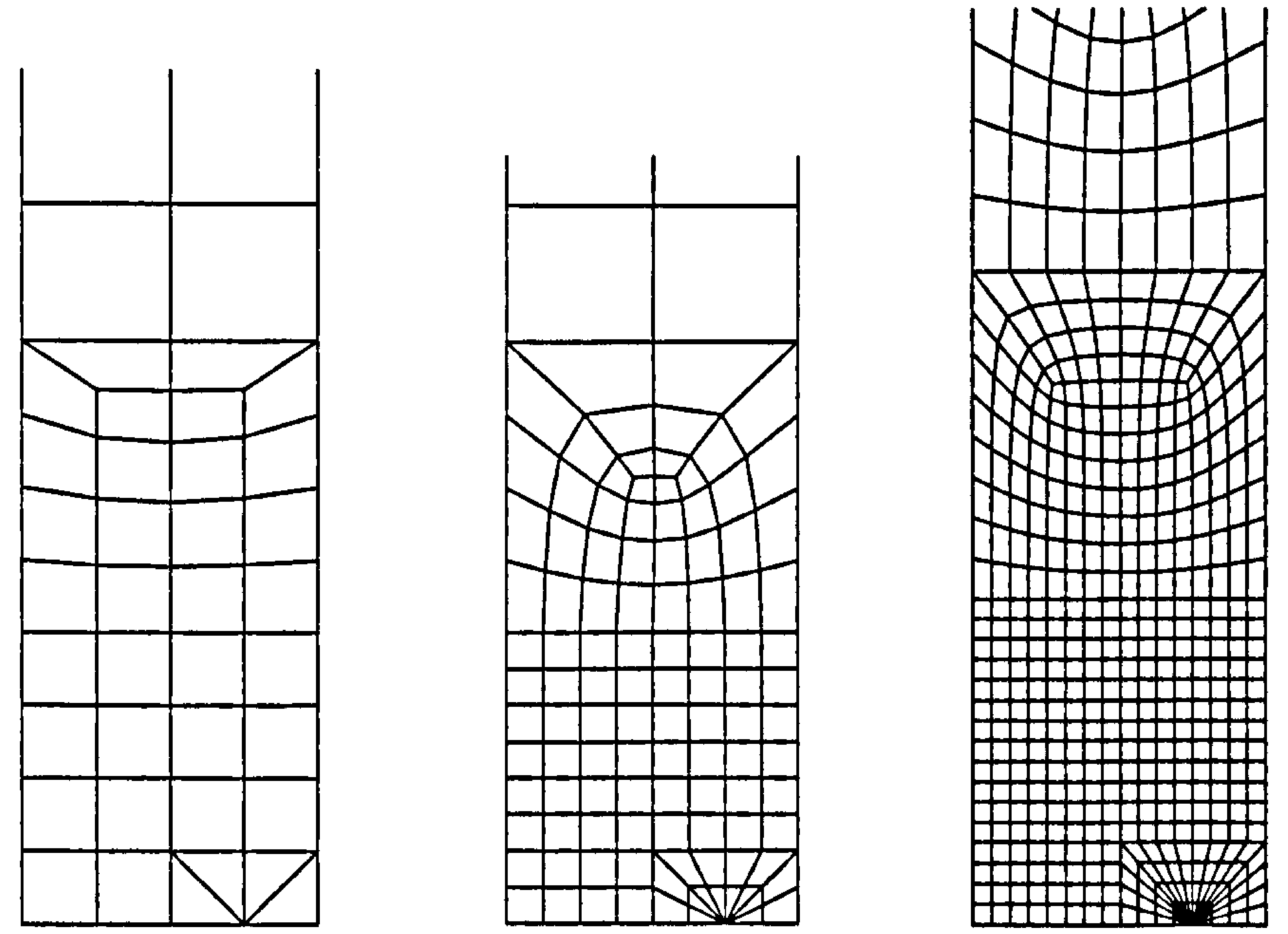

4 Focused Elements 8 Focused Elements 16 Focused Elements

Figure 2.7: Typical Focused Mesh Designs for a/t=0.75

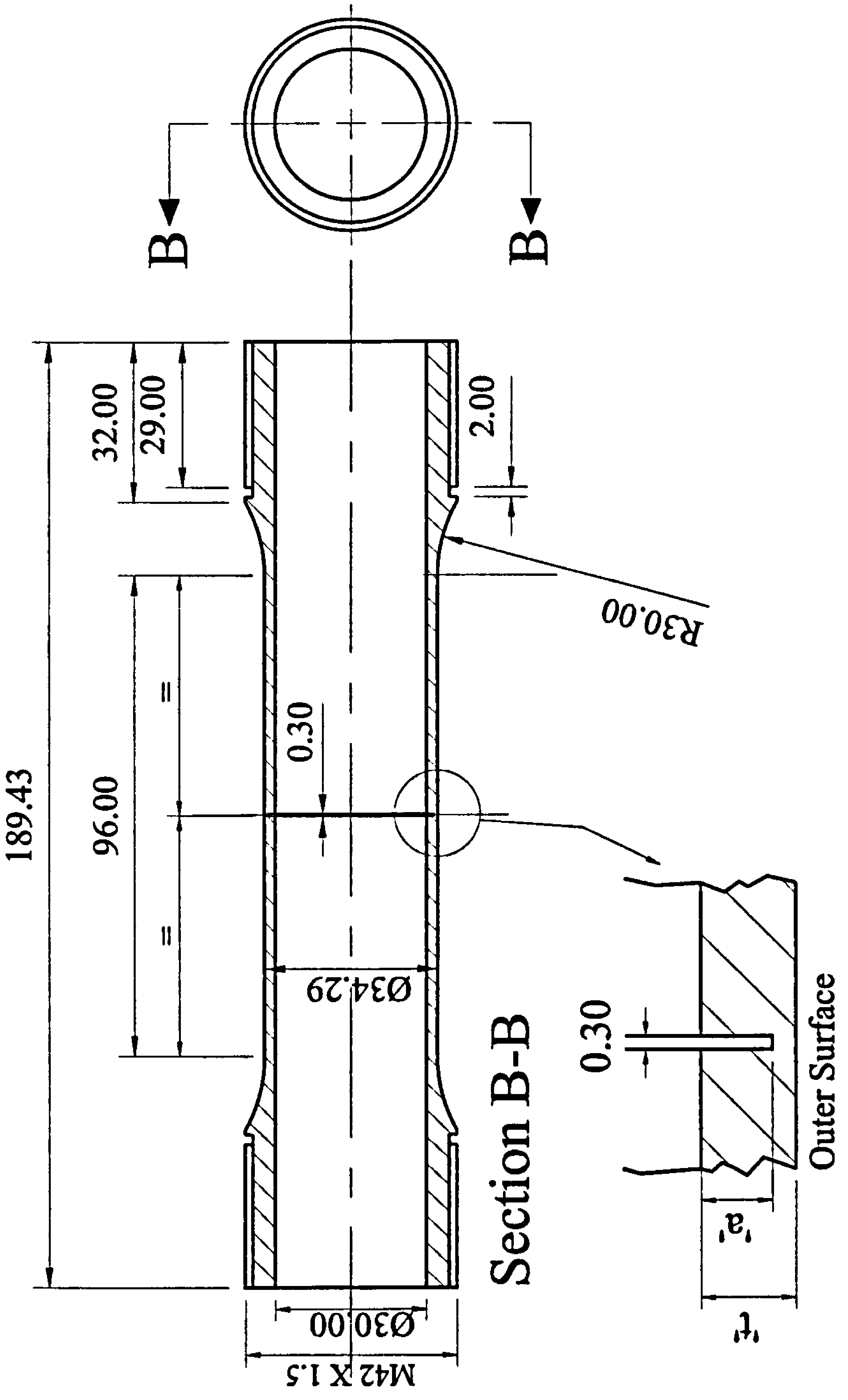

Figure 2.8: Manufacturing Specification for Cylinders

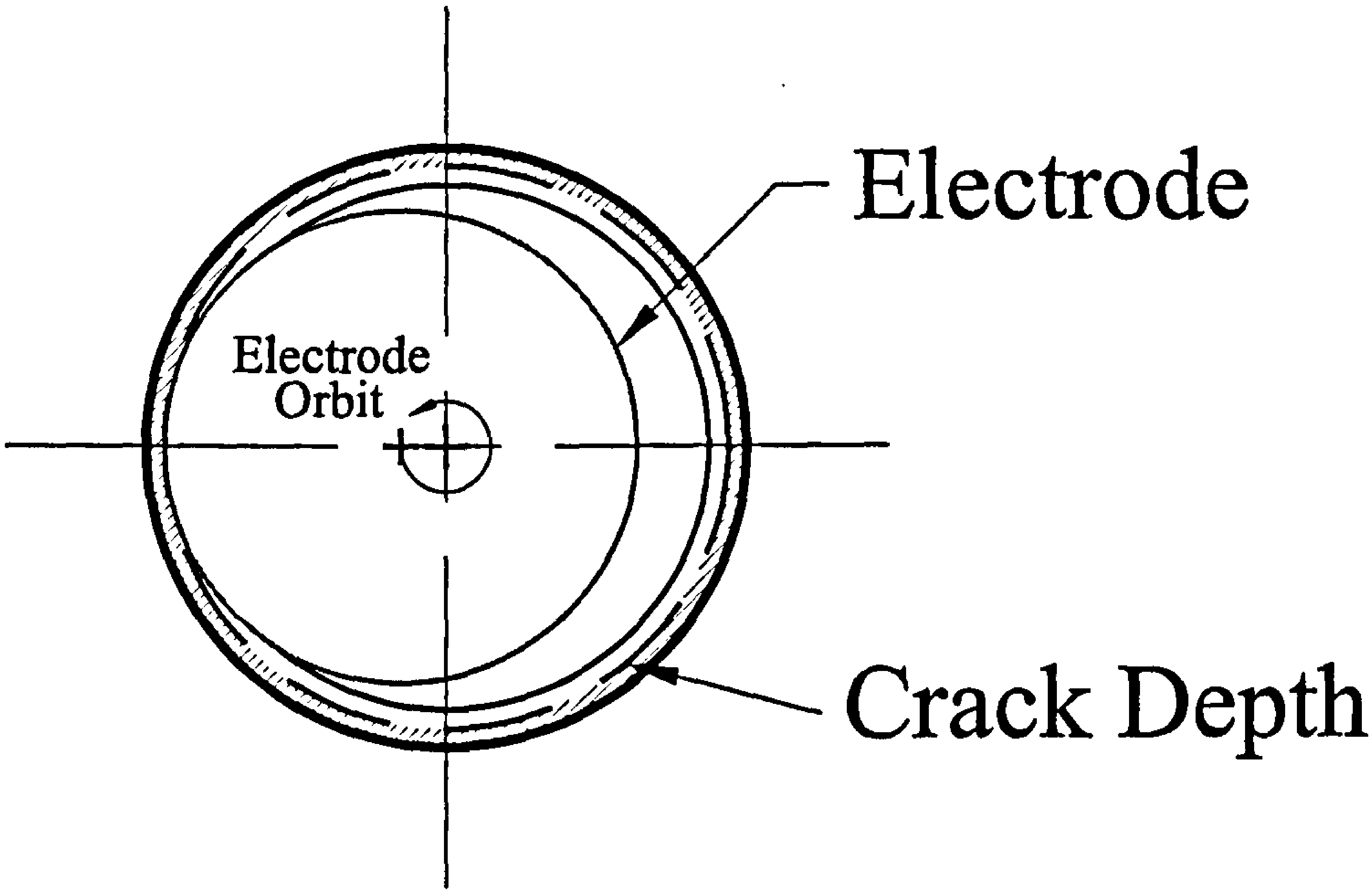

Figure 2.9: Section through Cylinder to show EDM Technique

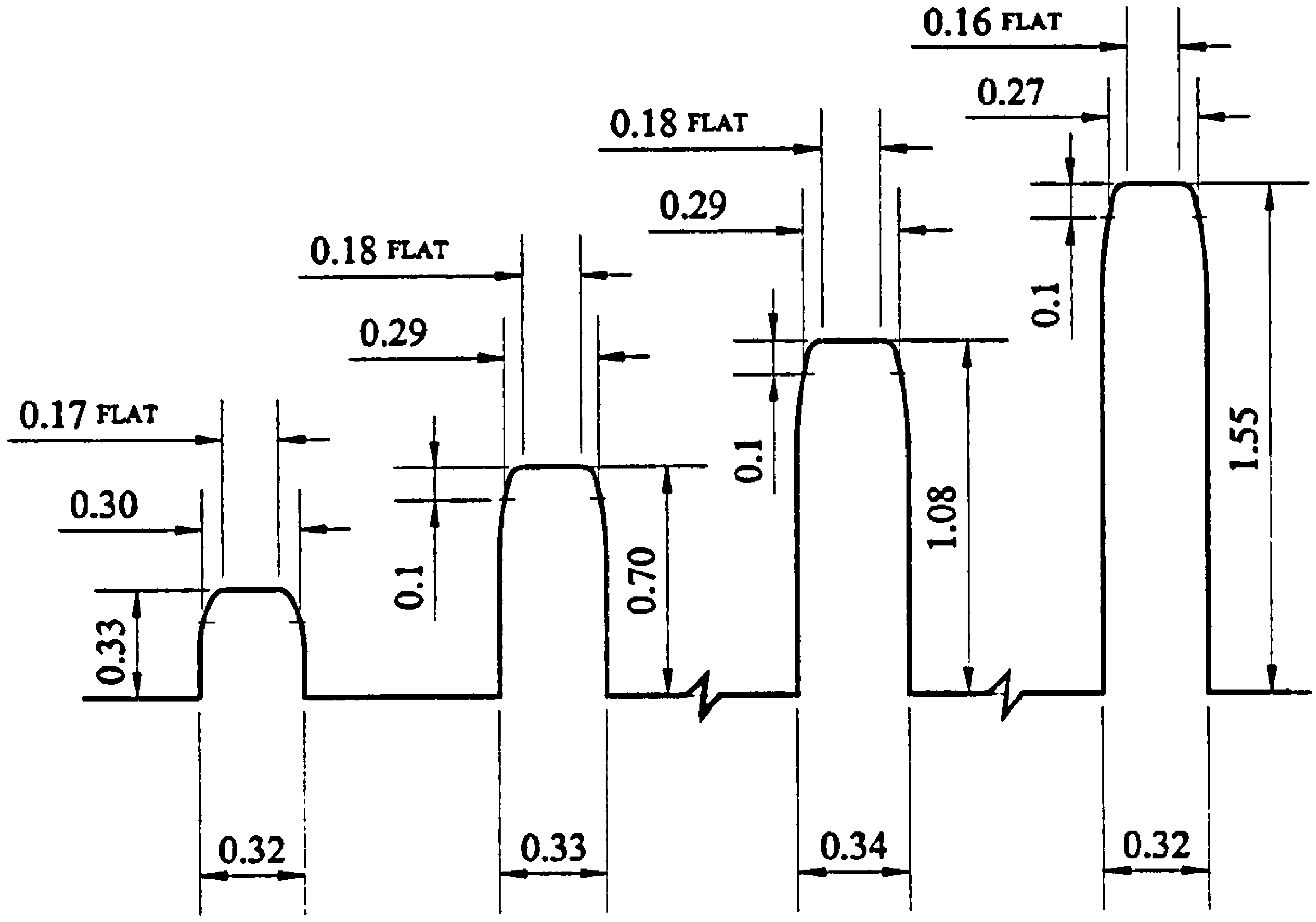

Specimen No.	B	C	D	E
a/t	0.16	0.33	0.51	0.73

Figure 2.10: Measured Crack Profiles

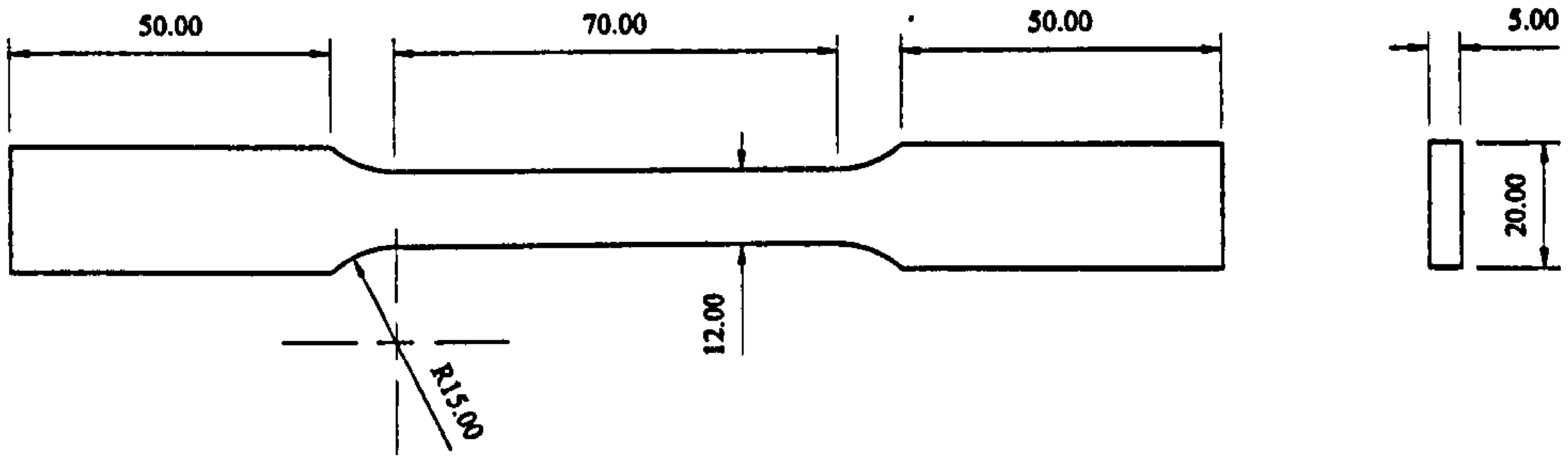

Figure 2.11: Tensile Test Specimen Dimensions

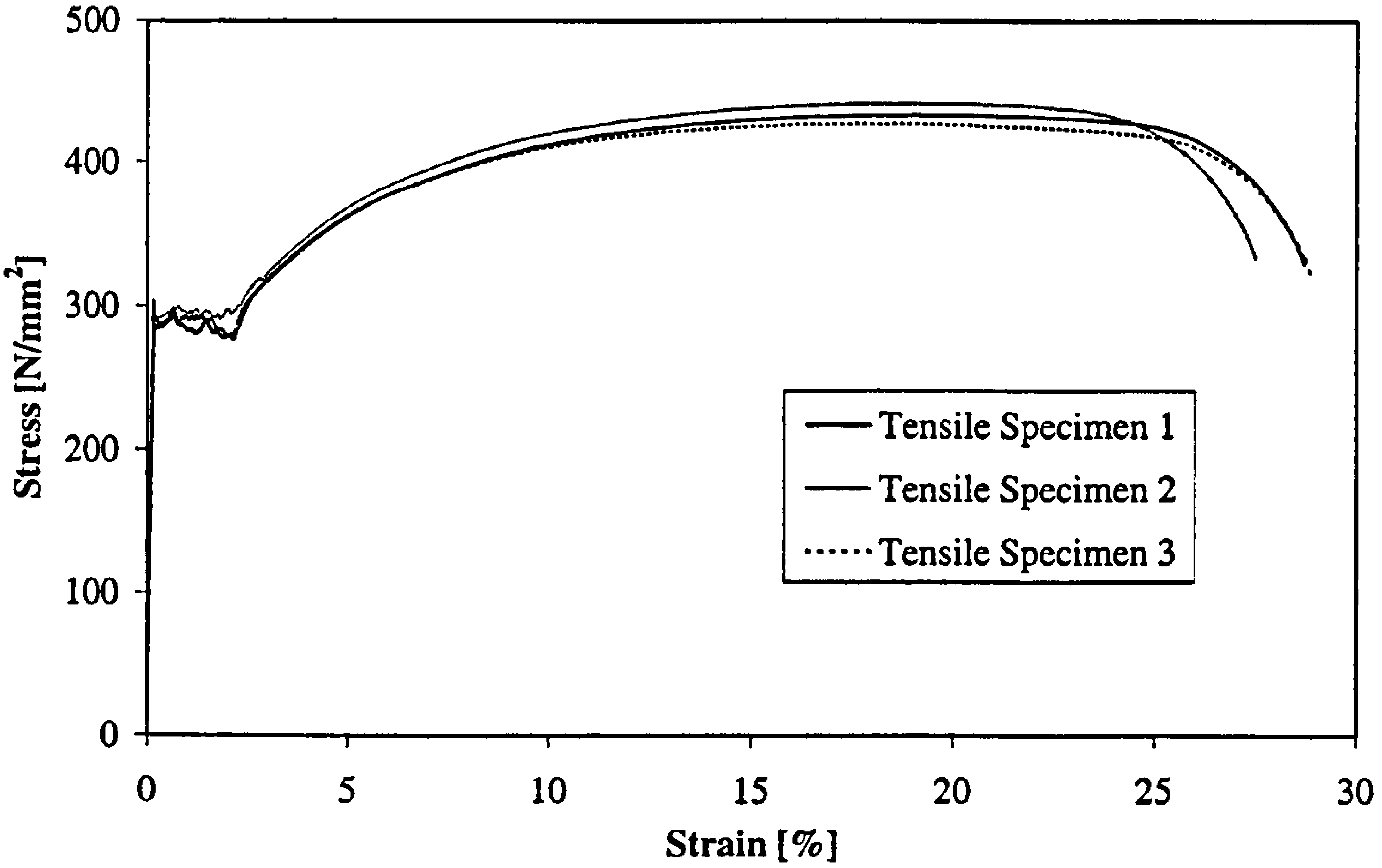

Figure 2.12: Tensile Test Engineering Stress-Strain Results

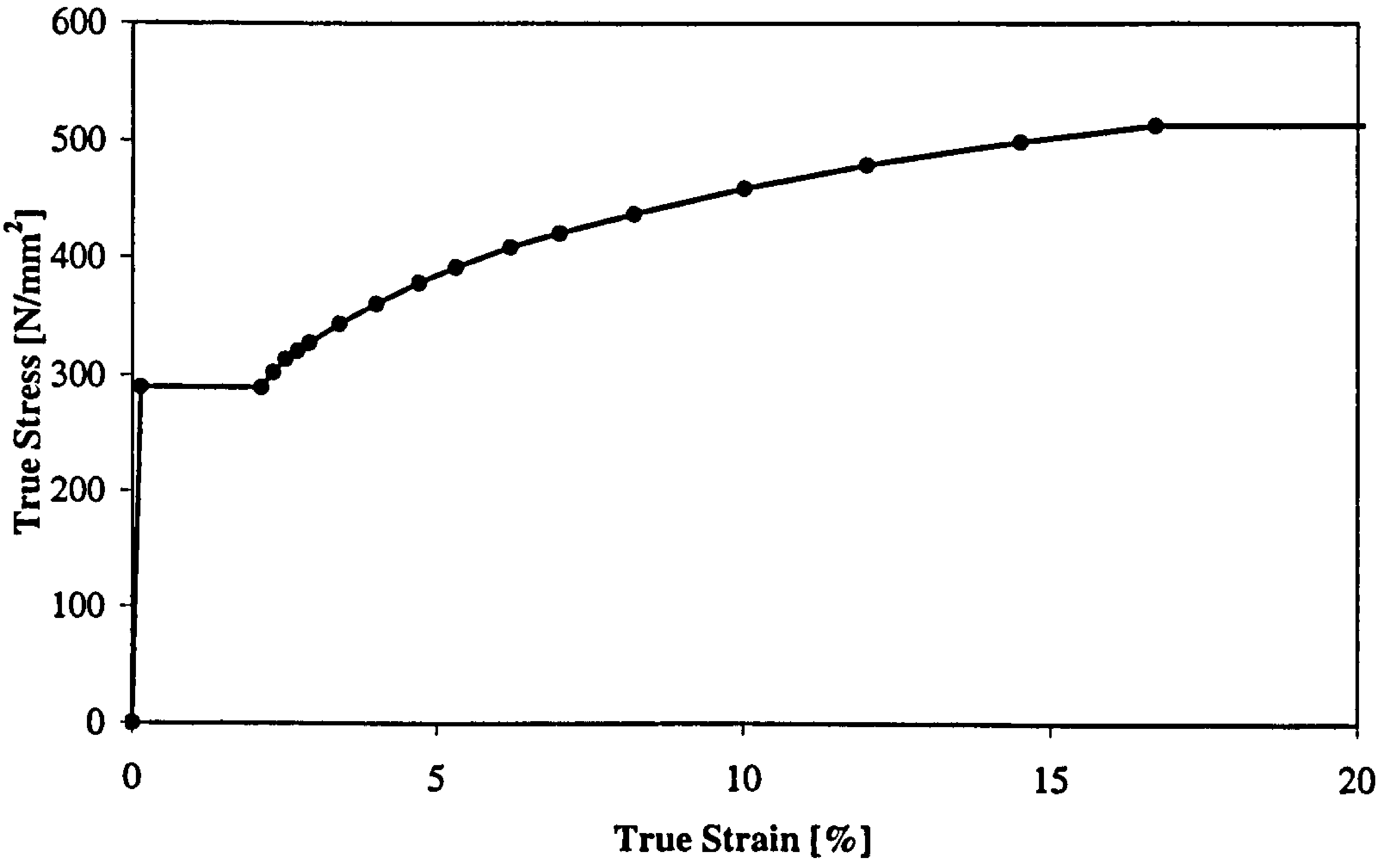

Figure 2.13: Averaged True Stress-Strain response for FE Work

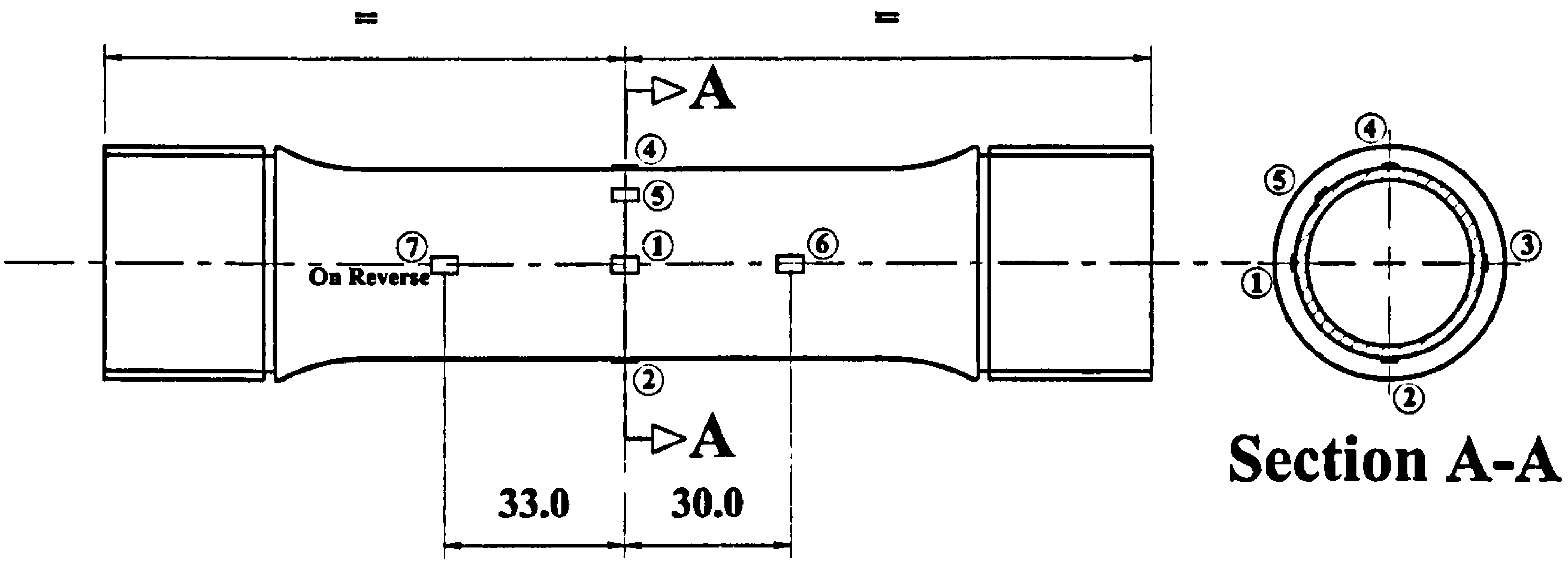

Figure 2.14: Strain Gauge Positions for Uncracked Specimen

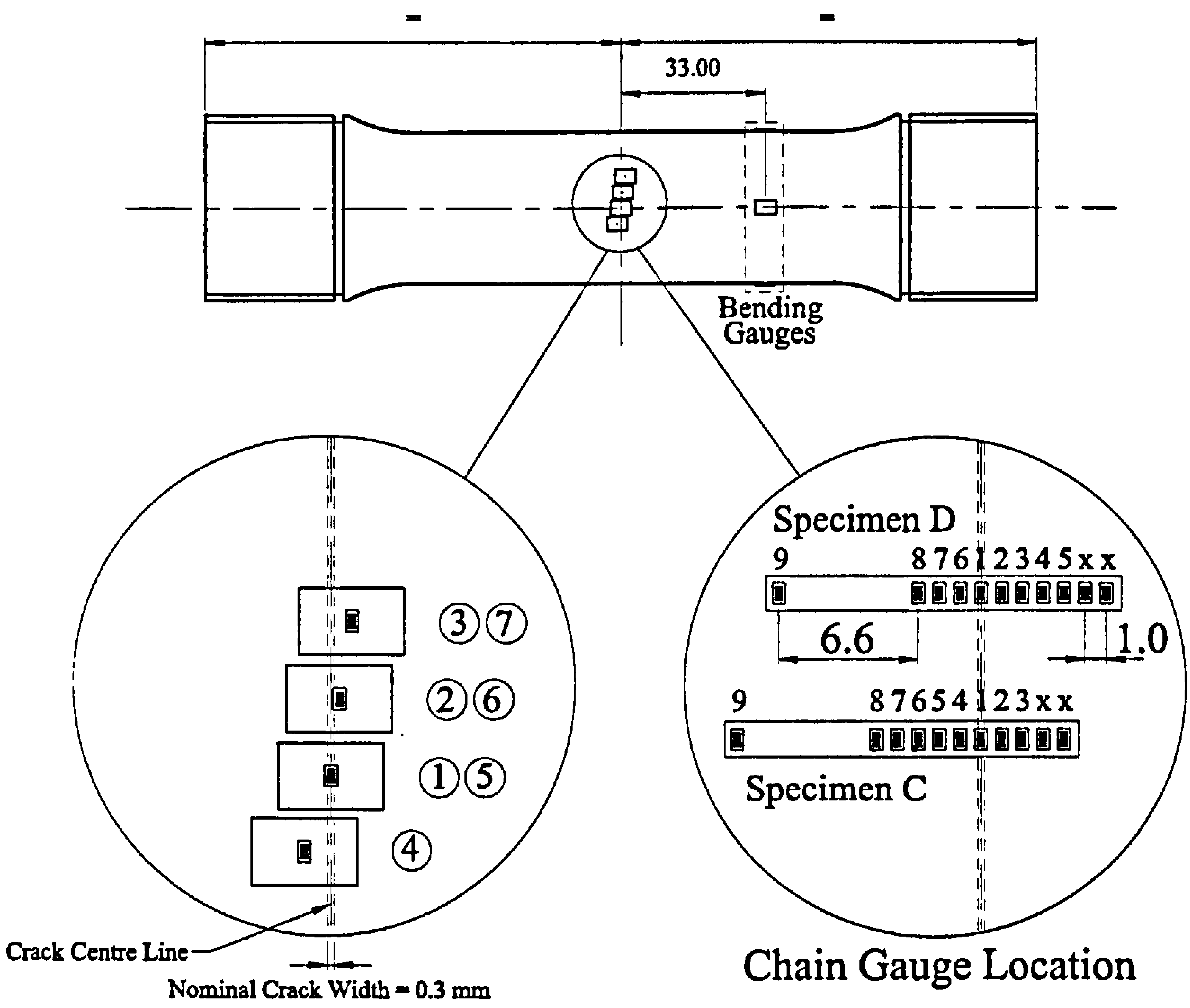

		Distance from Crack Centreline [mm]						
Specimen	a/t	1	2	3	4	5	6	7
B	0.16	0.0	1.59	2.16	-2.14	0.0	1.97	2.60
C	0.33	0.0	1.88	2.60	Chain Gauge Used			
D	0.51	0.0	1.25	2.20	Chain Gauge Used			
E	0.73	0.0	0.45	1.38	-0.83	0.0	0.76	1.63

Figure 2.15: Strain Gauge Positions for Cracked Specimens

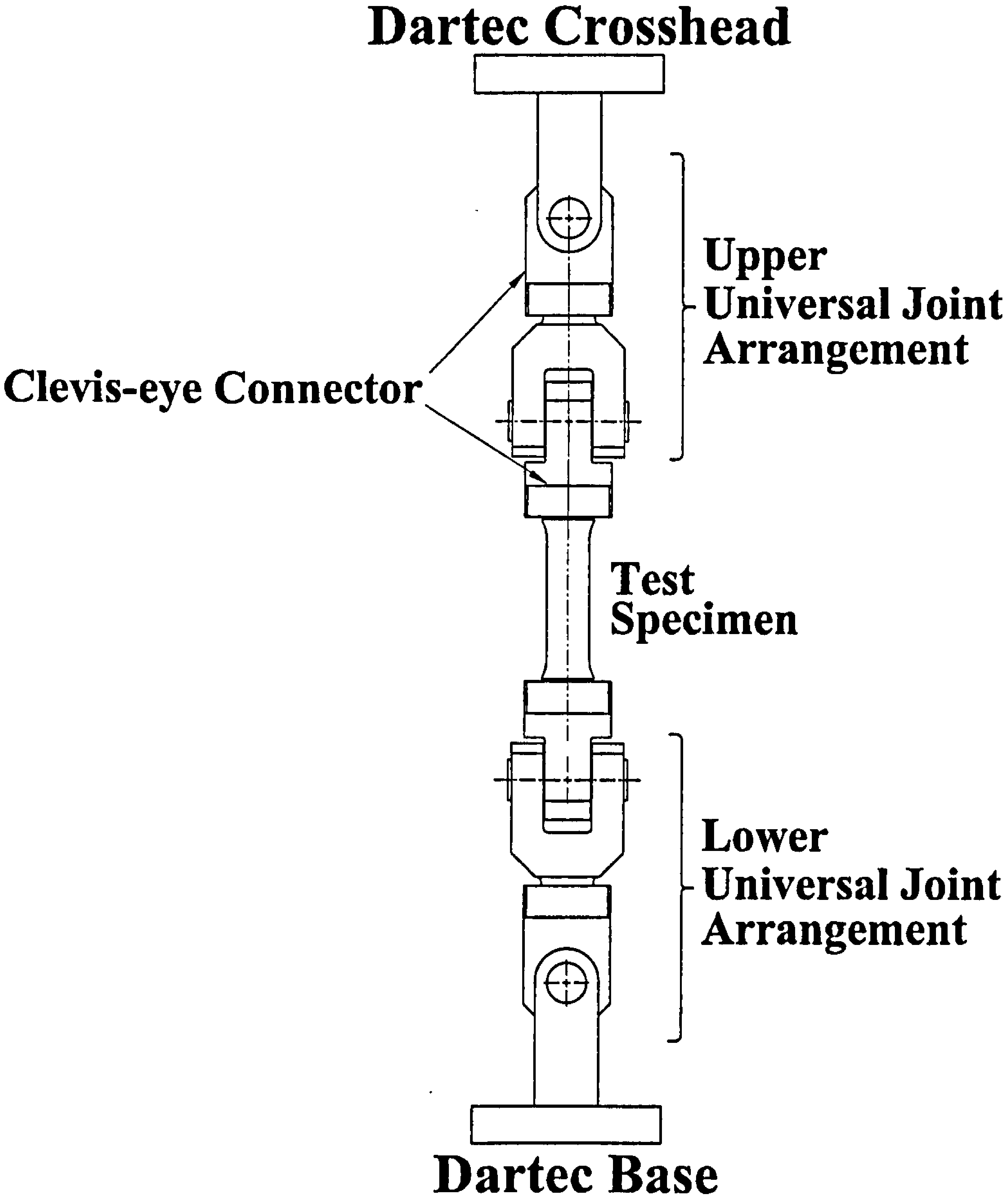

Figure 2.16: Experimental Arrangement

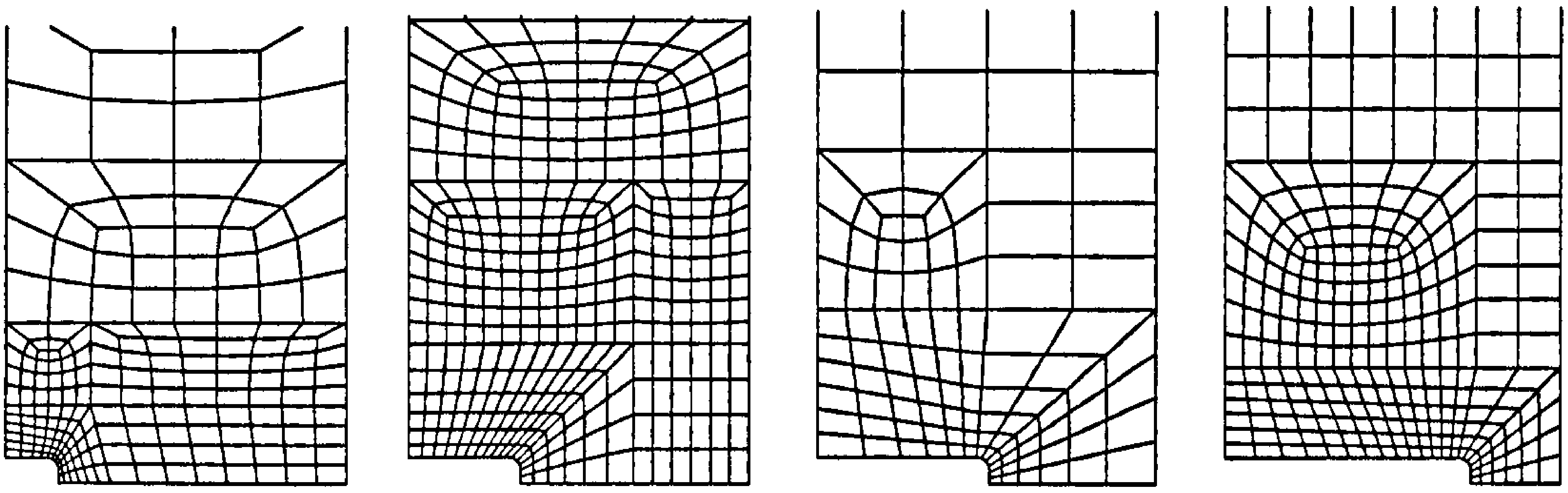

(a) Specimen B (b) Specimen C (c) Specimen D (d) Specimen E

Figure 2.17: Experimental FE Mesh Designs

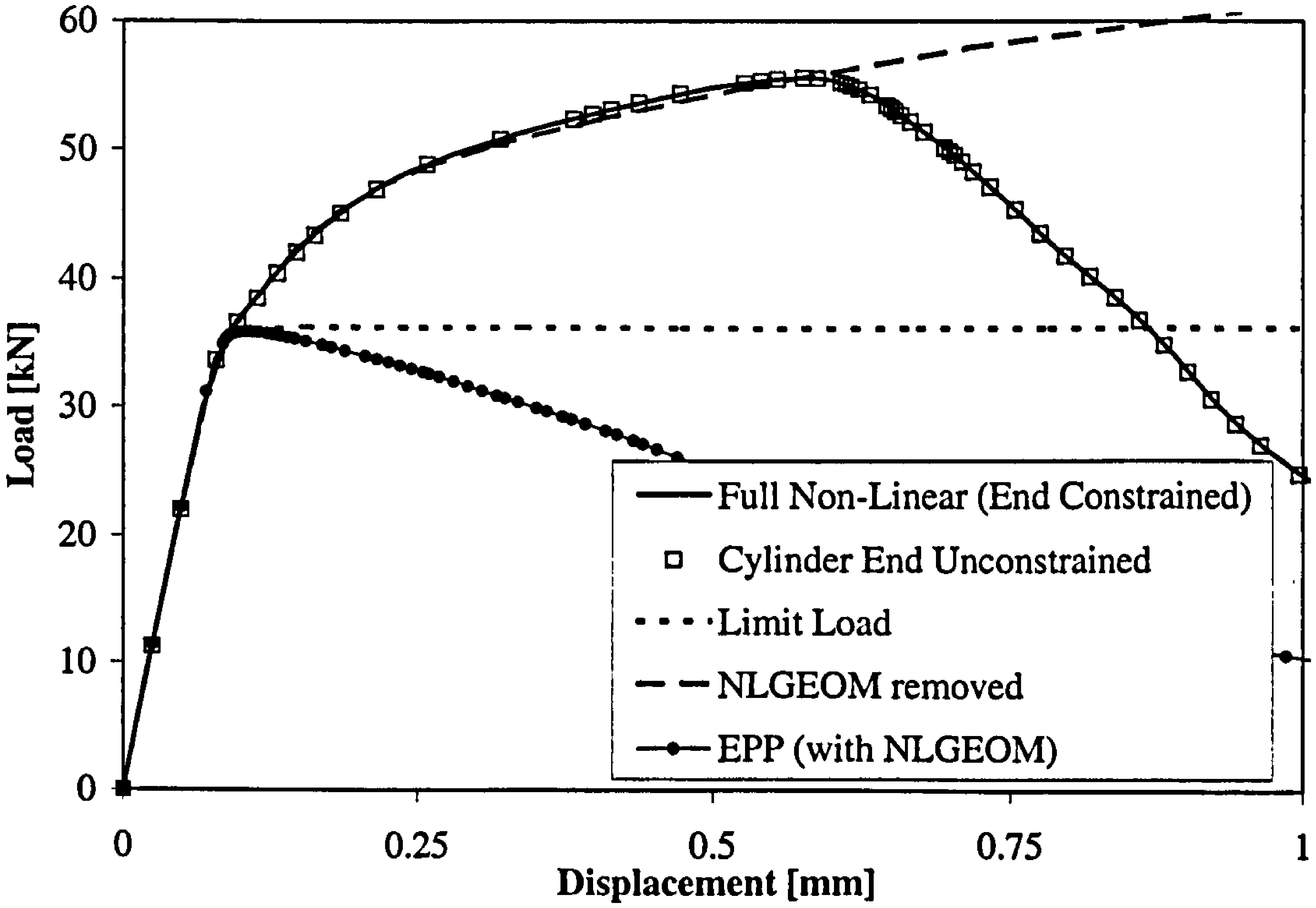

Figure 2.18: Comparison of FE Loading Cases (for a/t=0.51)

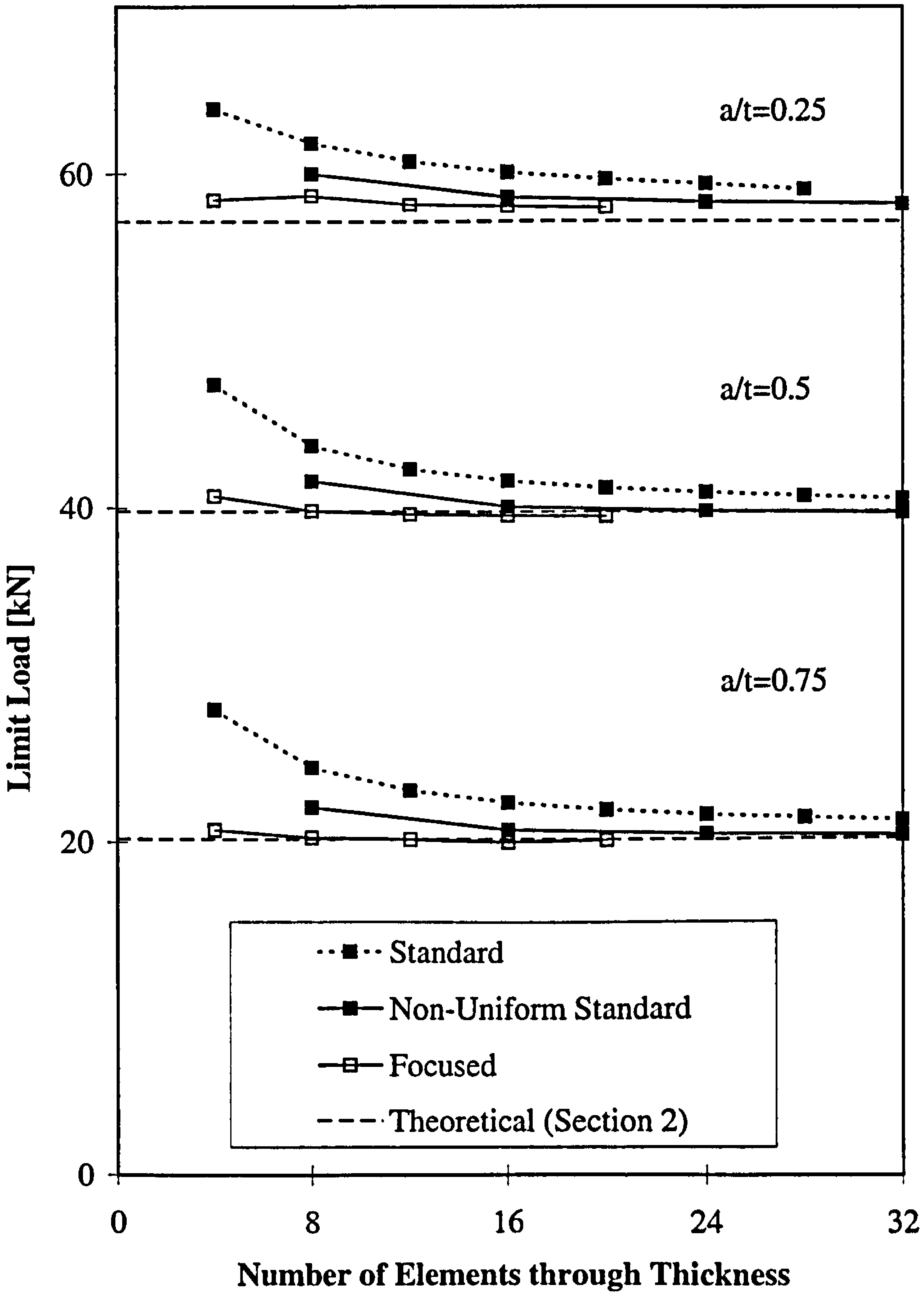

Figure 2.19: FE Limit Load Results

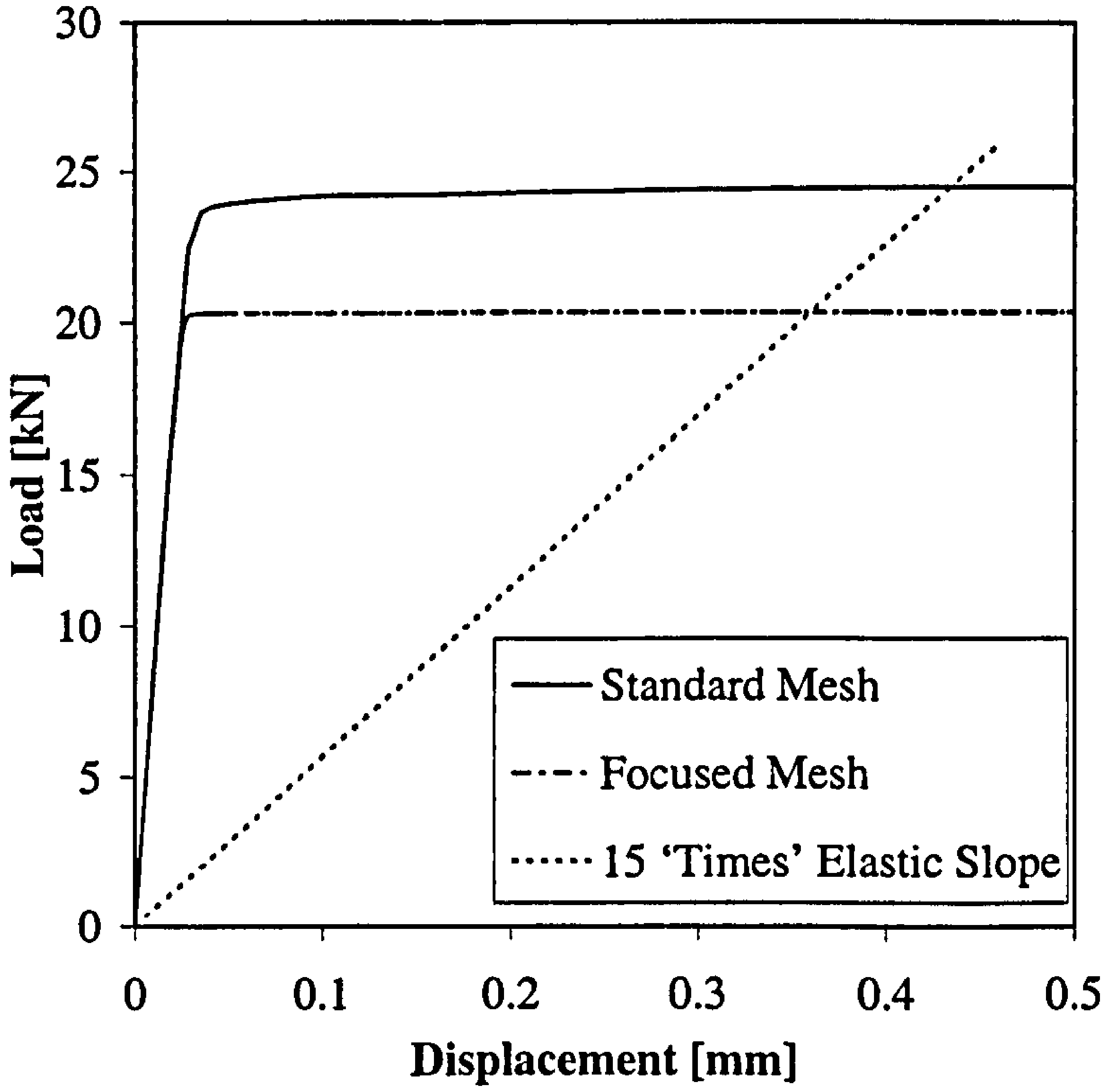

Figure 2.20: 15 'Times' Elastic Slope

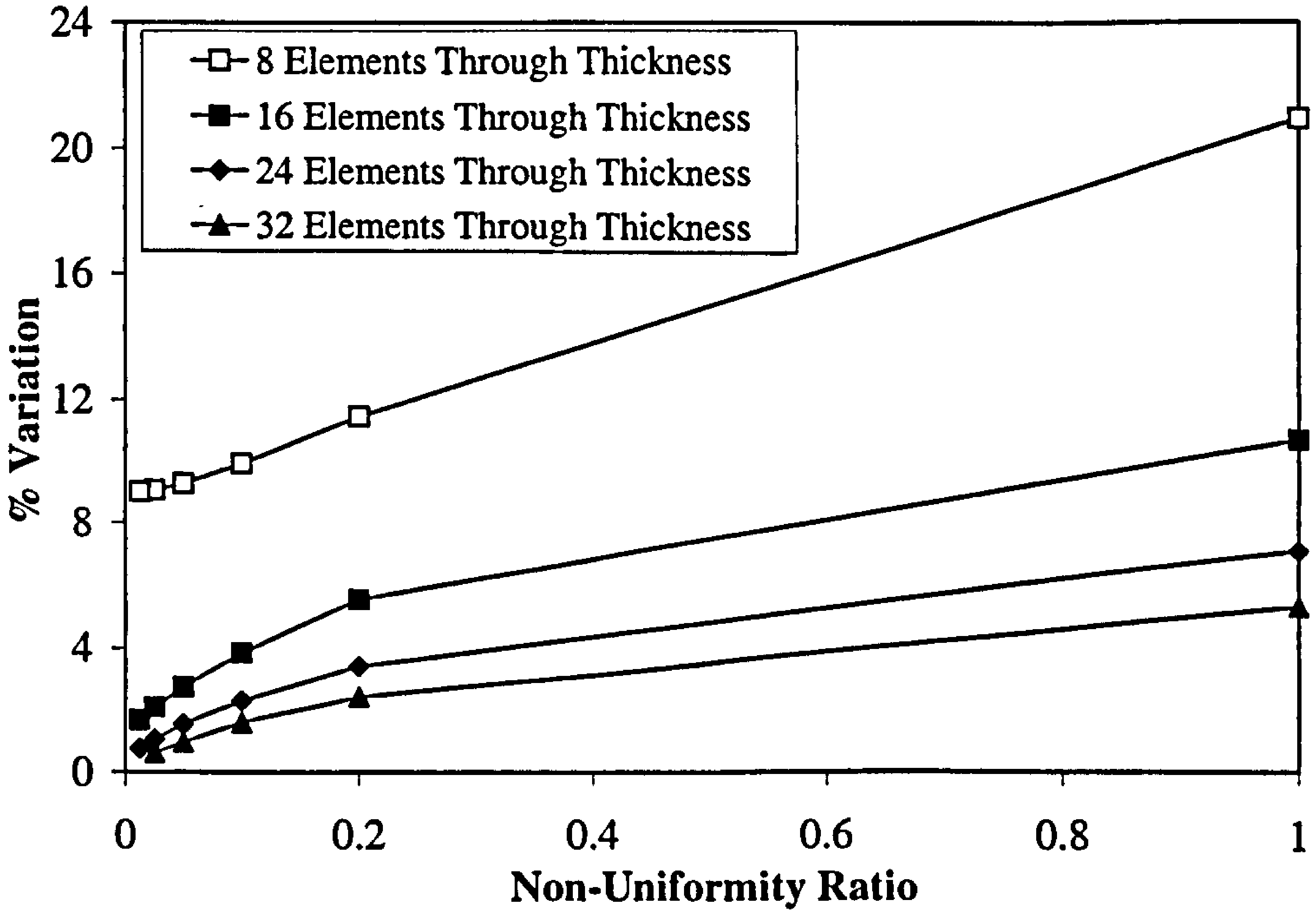

Figure 2.21: Variation of Non-Uniform Standard Mesh Results from Theory (a/t=0.75)

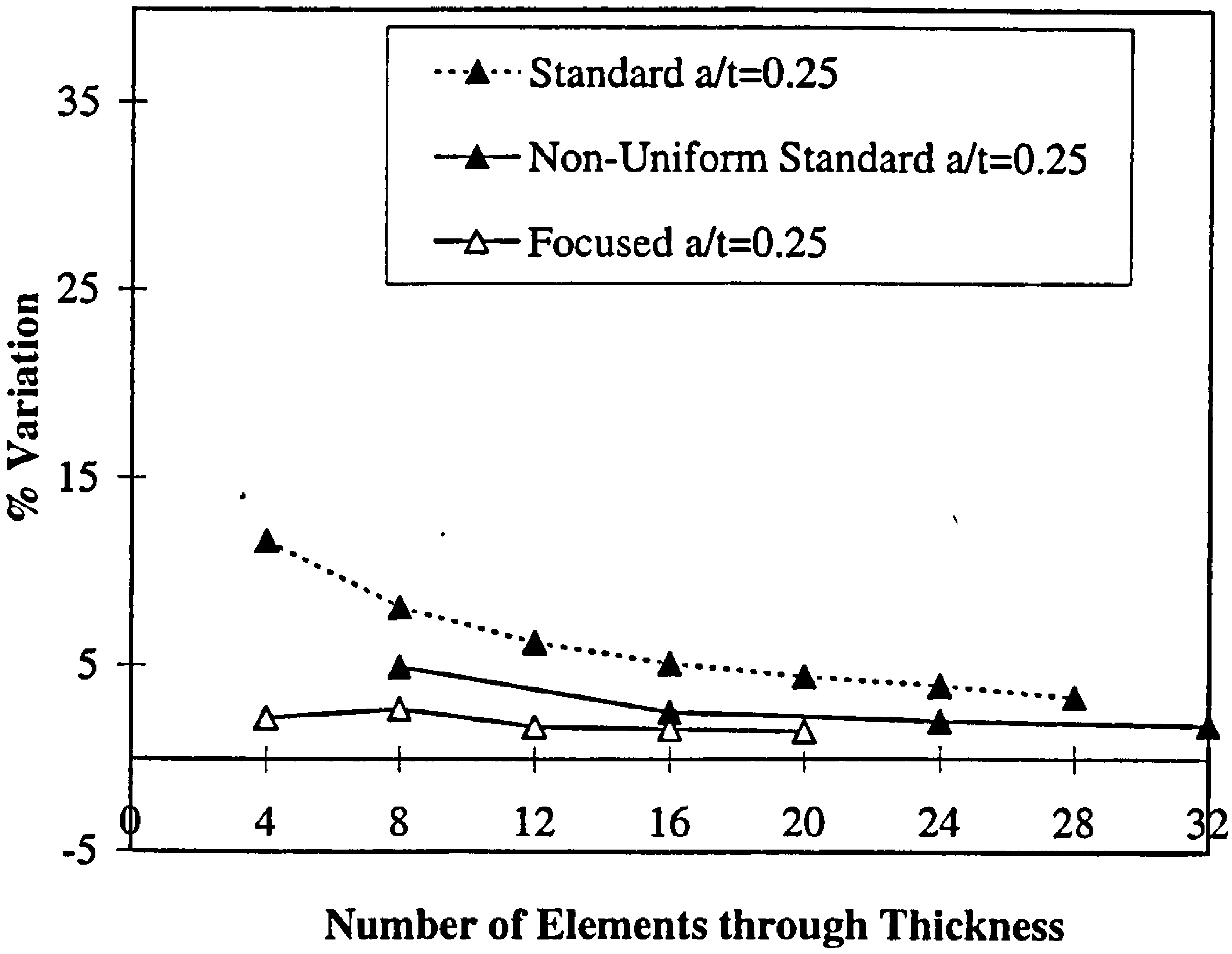

Figure 2.22: Variation of FE Results from Theory (a/t=0.25)

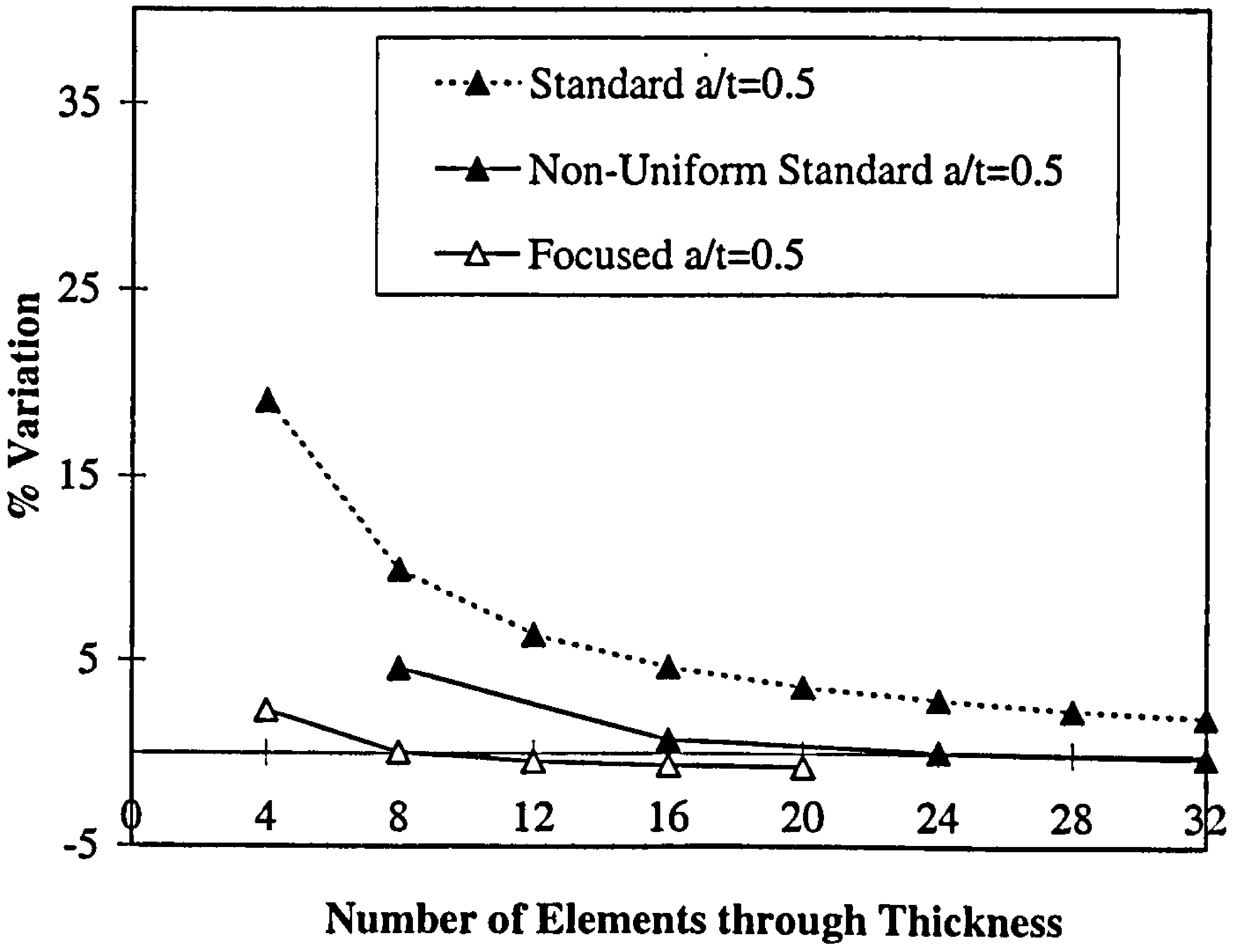

Figure 2.23: Variation of FE Results from Theory (a/t=0.5)

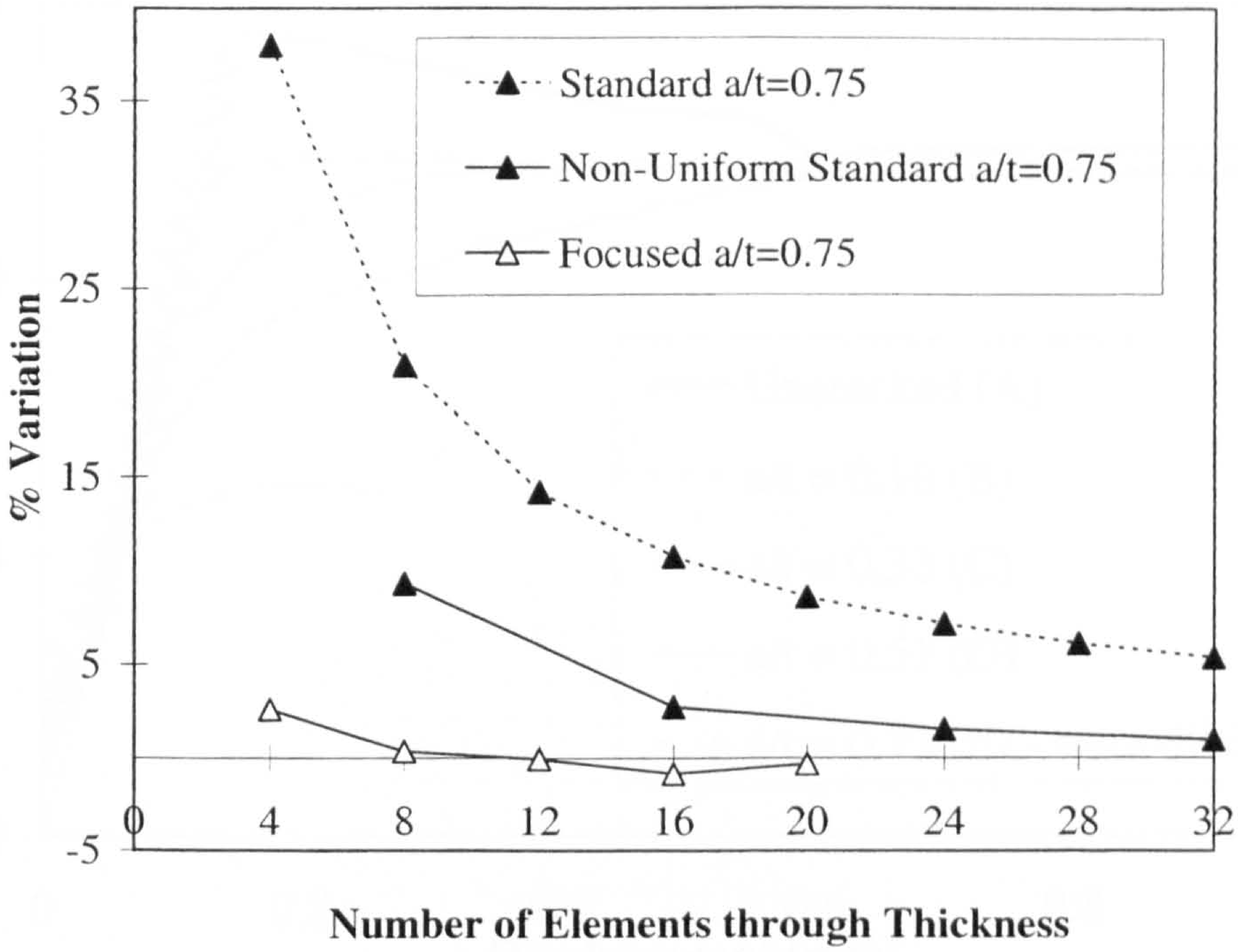

Figure 2.24: Variation of FE Results from Theory (a/t=0.75)

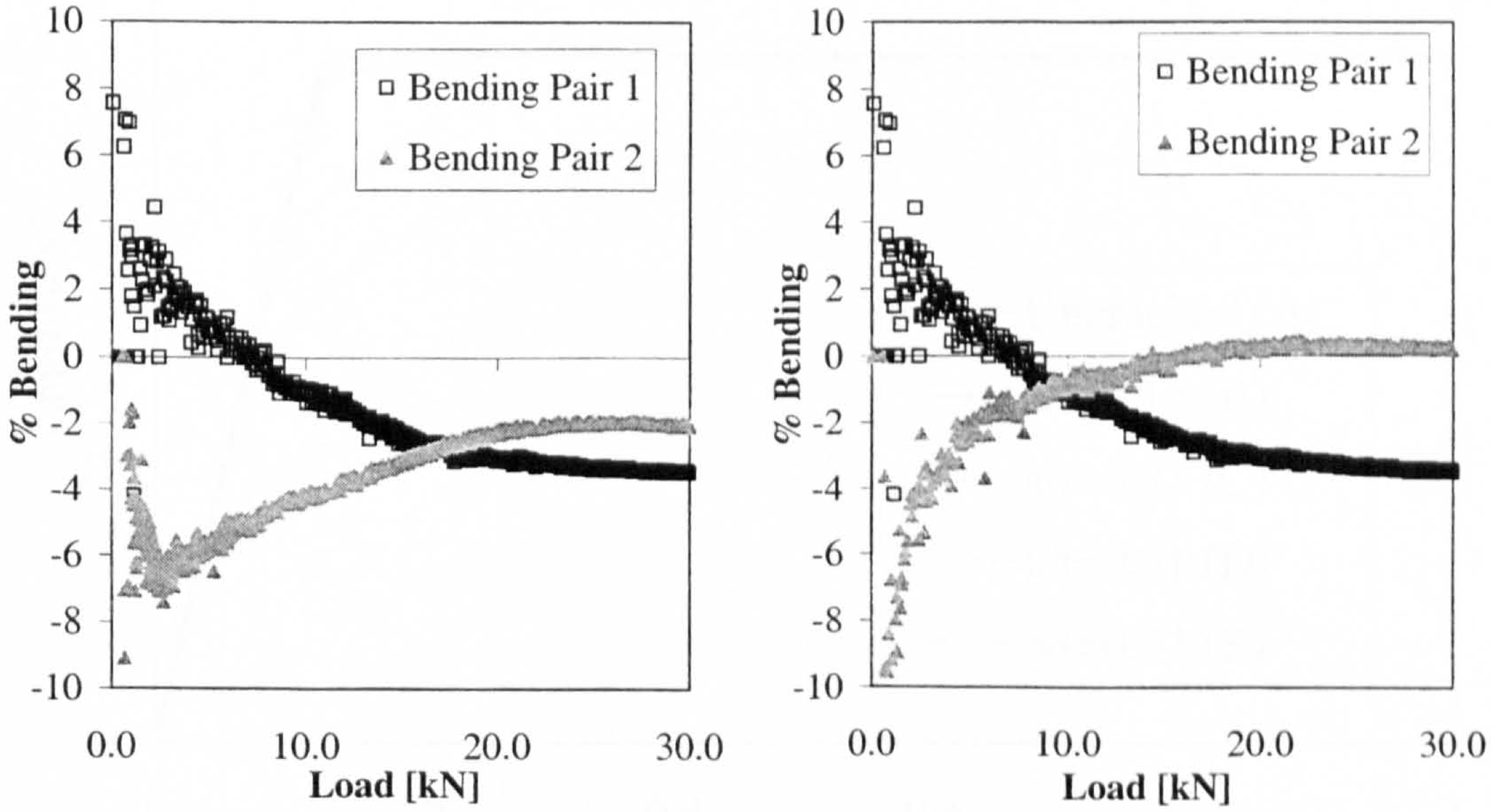

(a) Specimen C

(b) Specimen D

Figure 2.25: Typical Bending Response

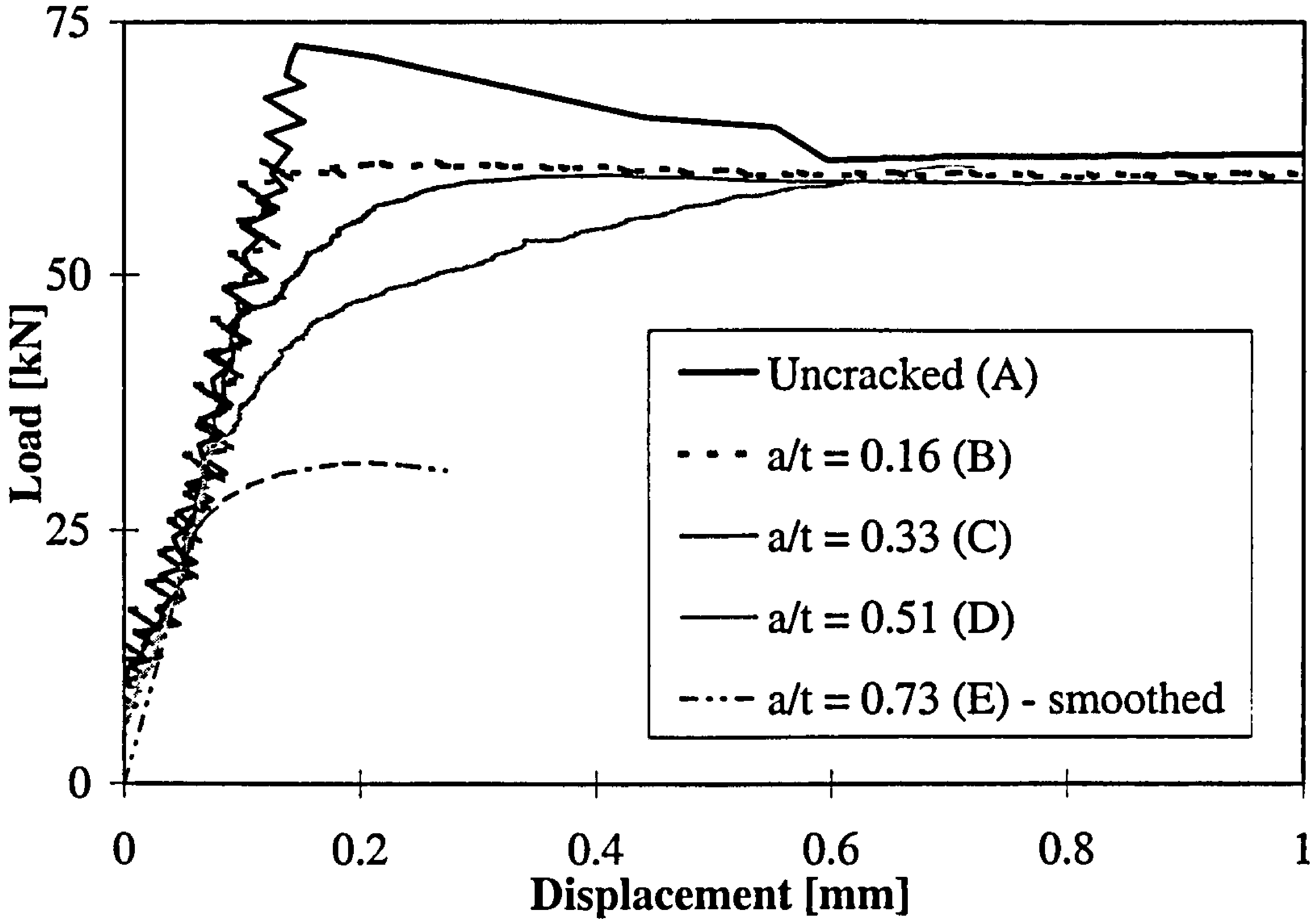

(a) Experimental Data

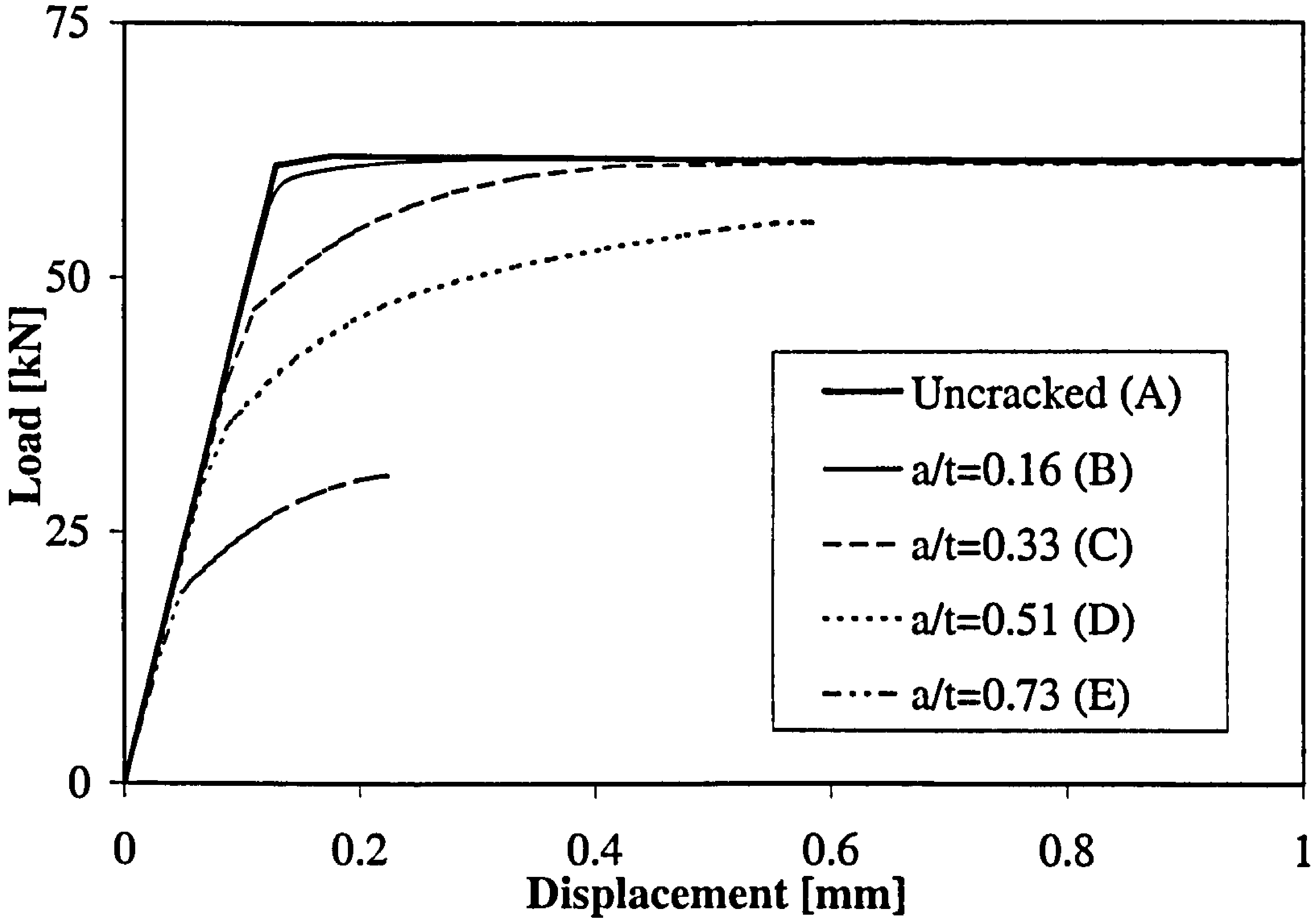

(b) FE Data

Figure 2.26: Overall Load-Displacement Results

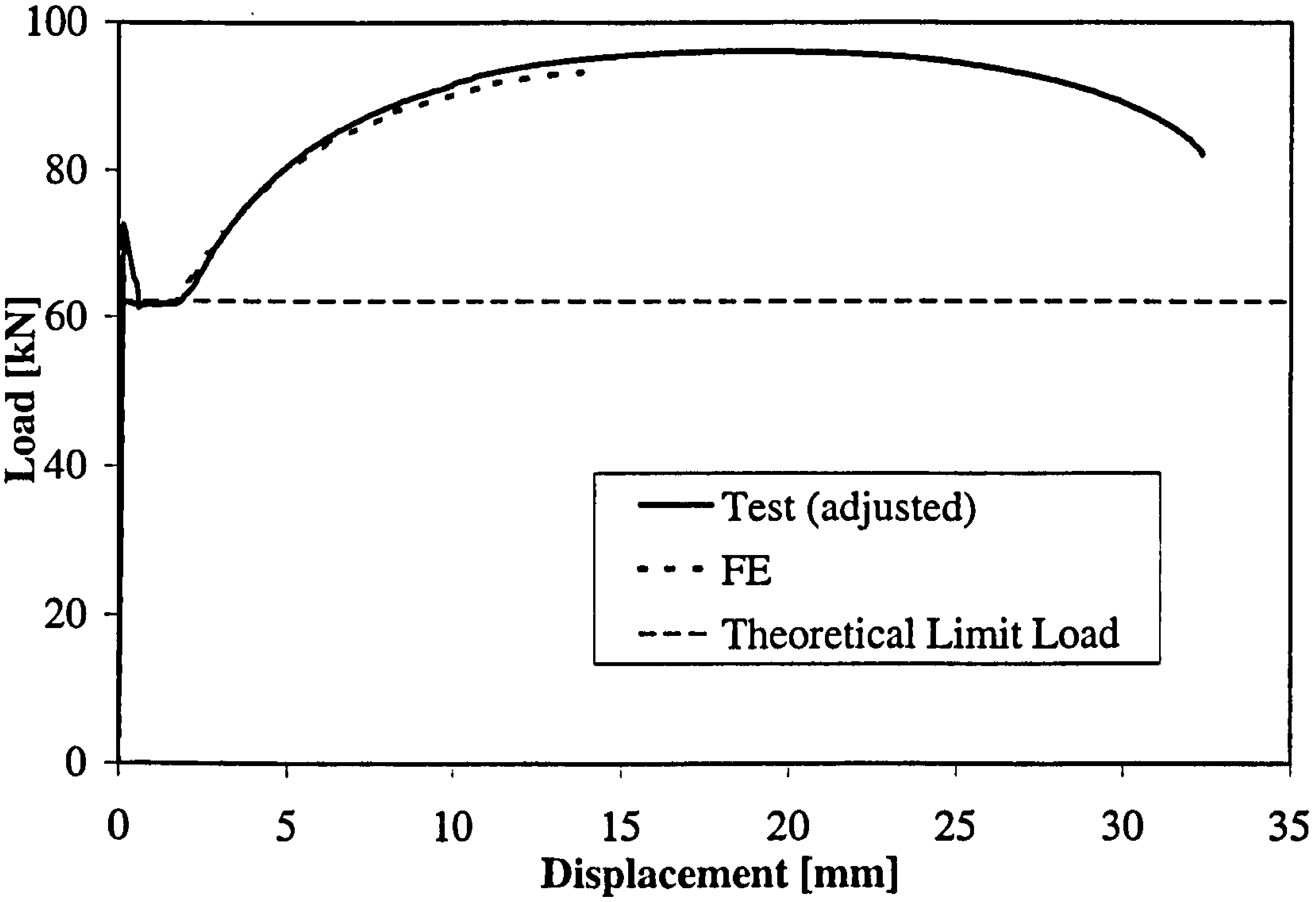

Figure 2.27: Test Specimen A (Uncracked) Results

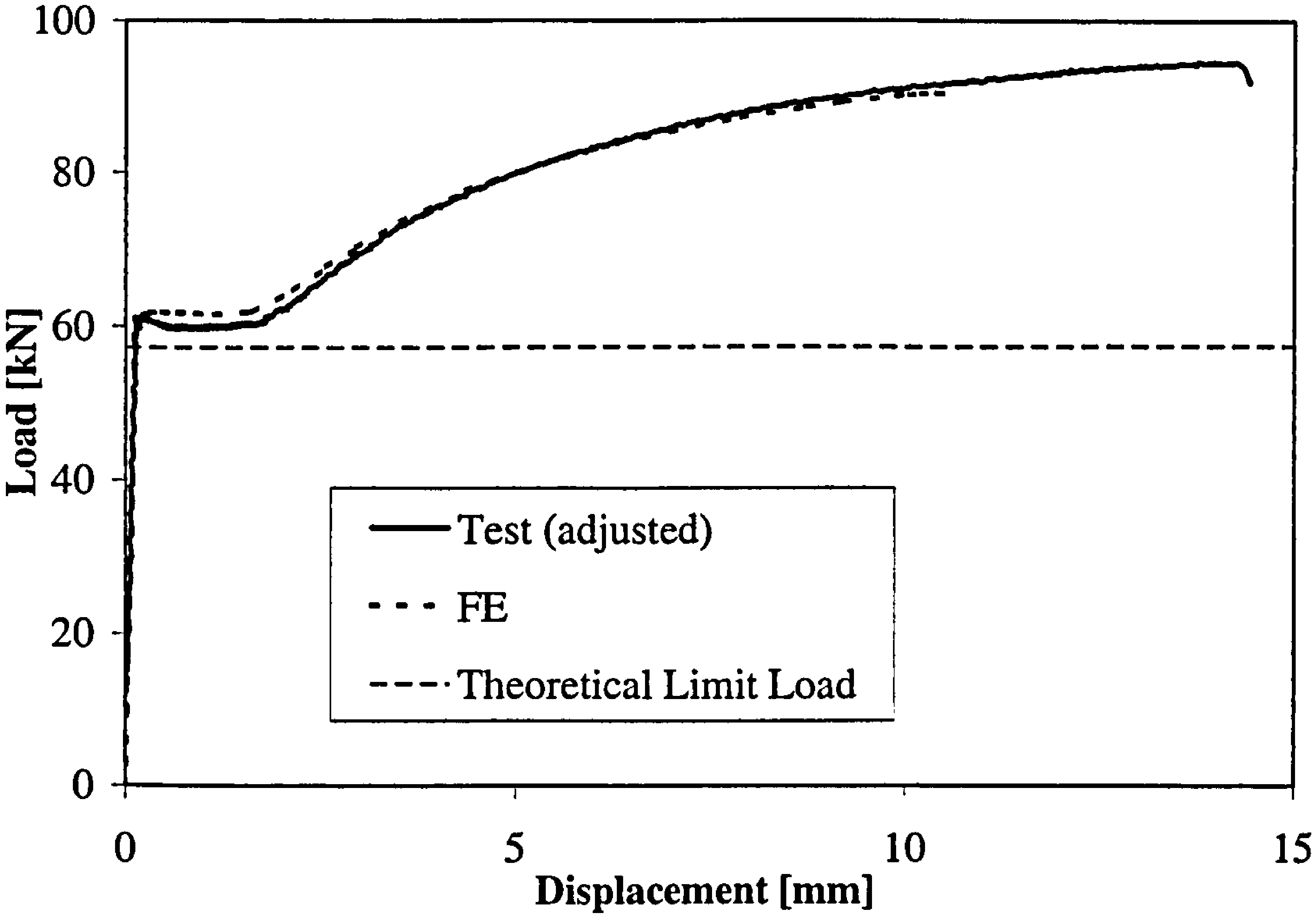

(a) Load v Displacement

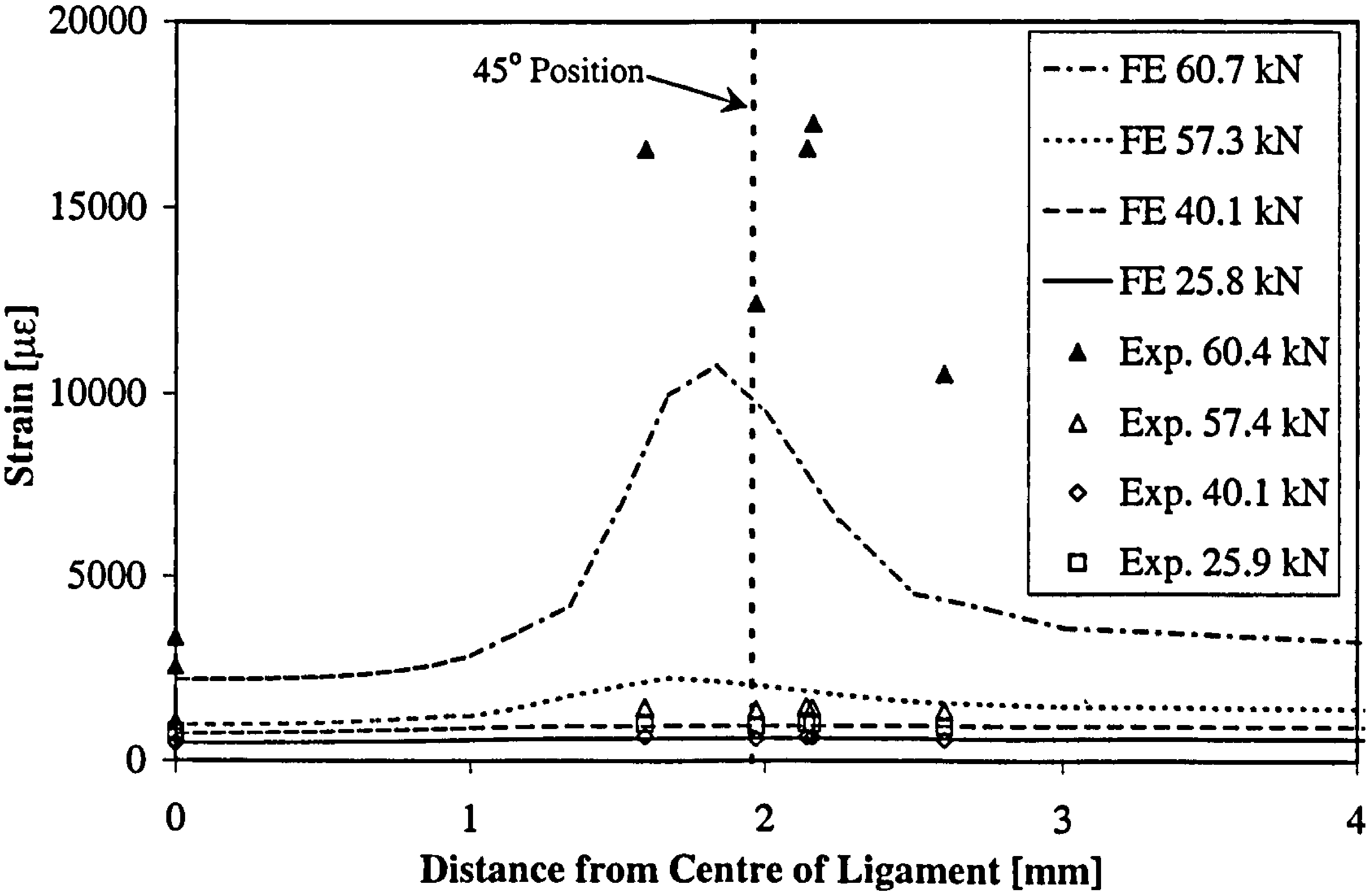

(b) Strain Distribution

Figure 2.28: Test Specimen B (a/t=0.16) Results

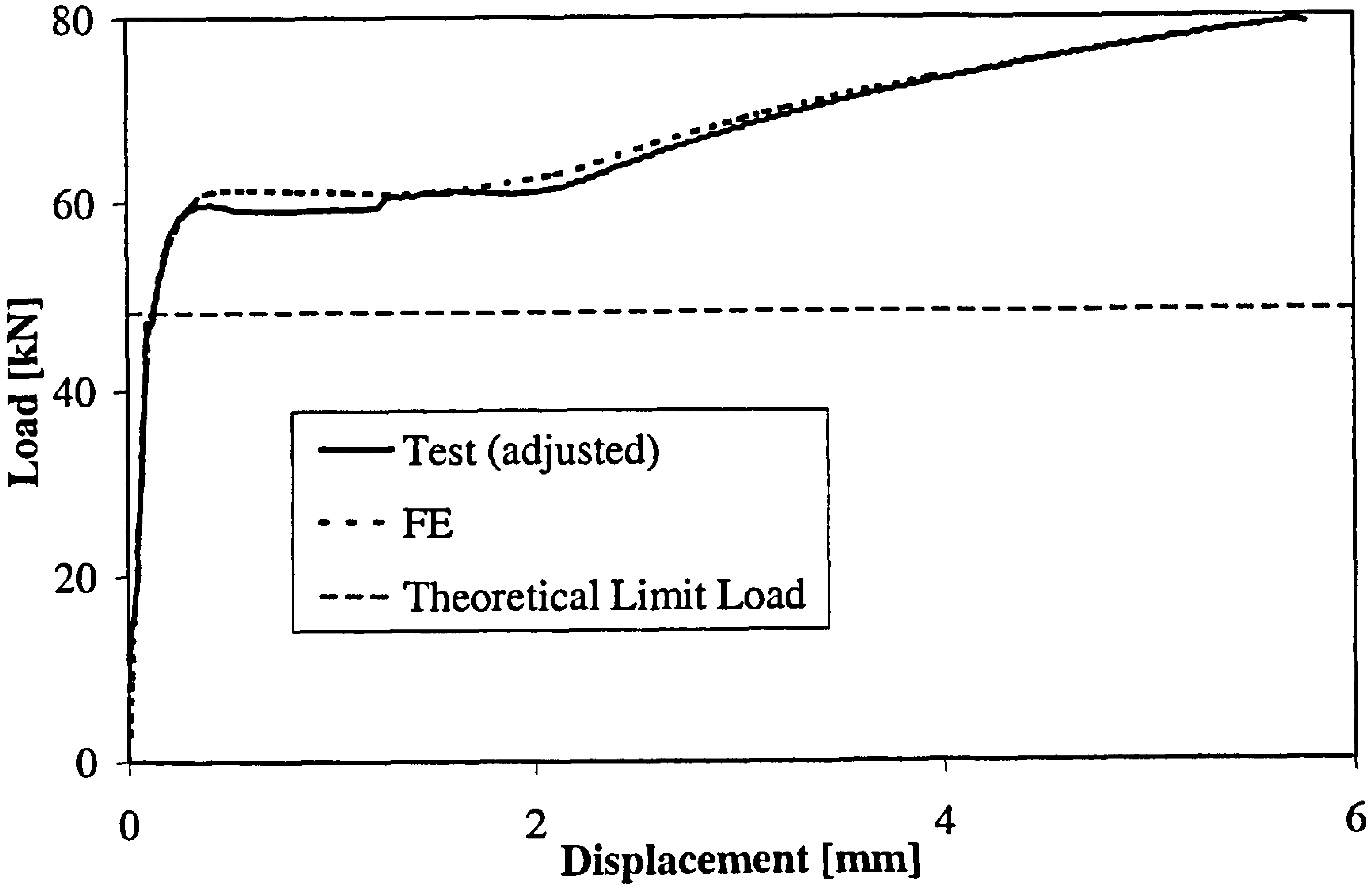

(a) Load v Displacement

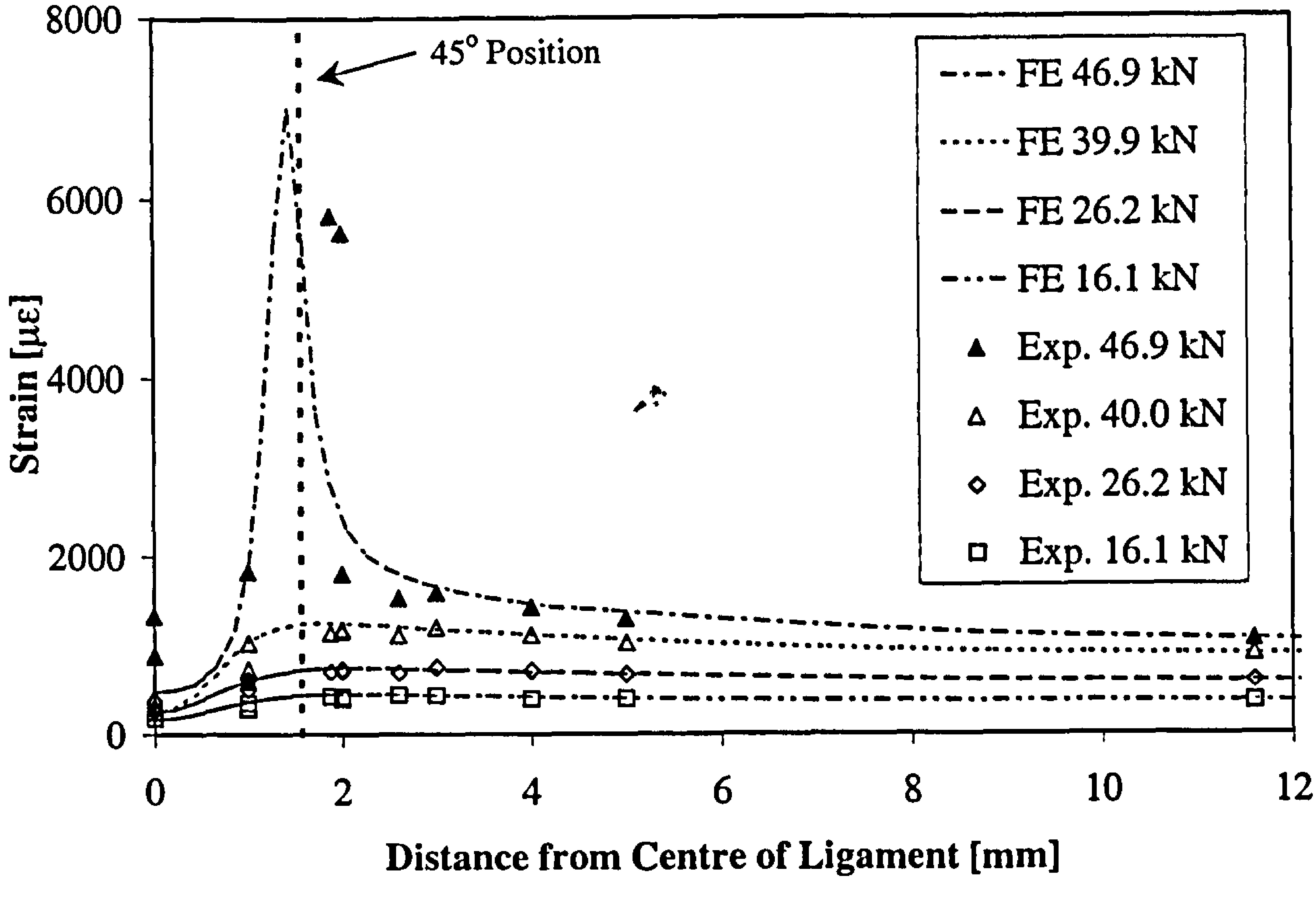

(b) Strain Distribution

Figure 2.29: Test Specimen C (a/t=0.33) Results

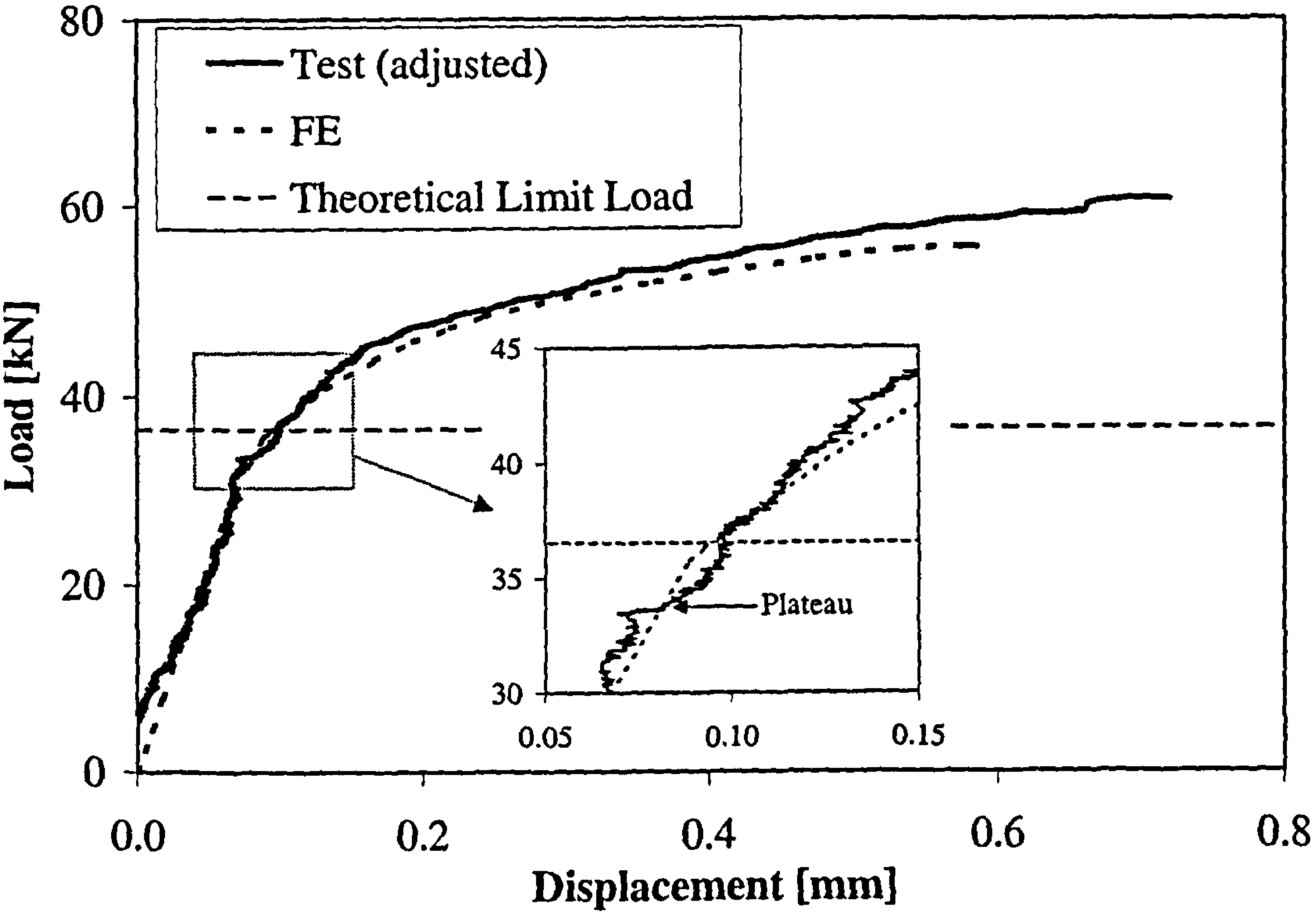

(a) Load v Displacement

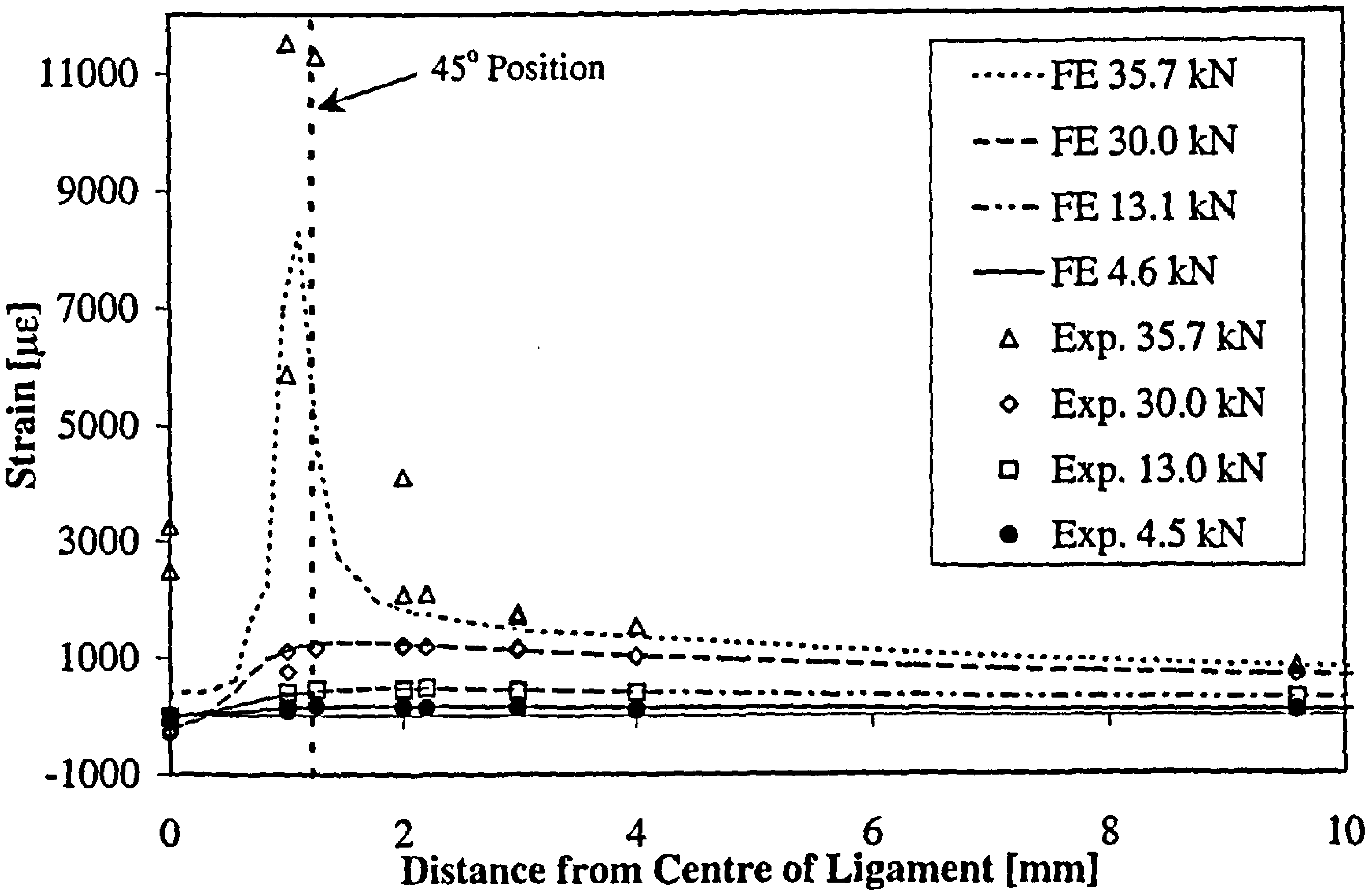

(b) Strain Distribution

Figure 2.30: Test Specimen D (a/t=0.51) Results

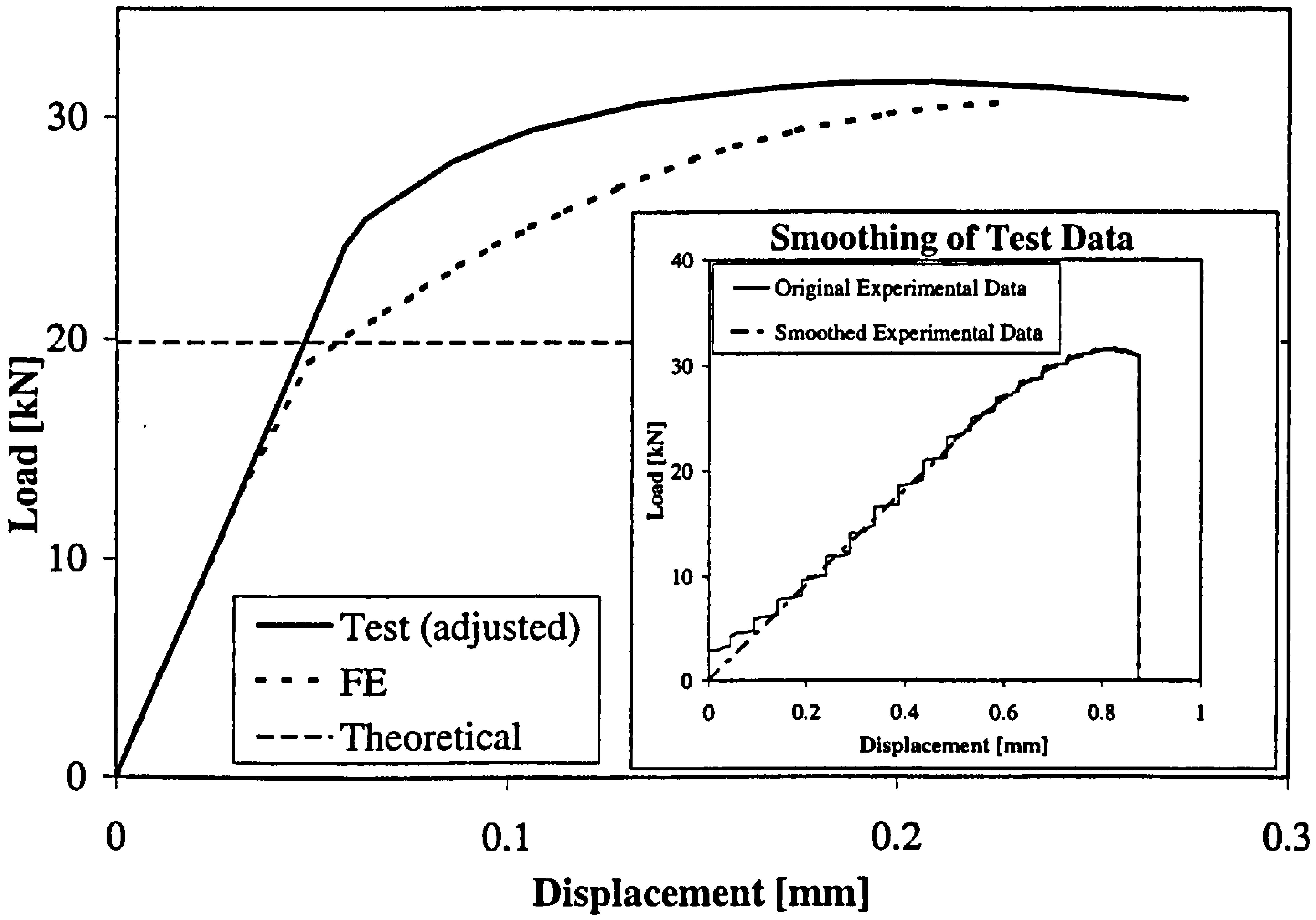

(a) Load v Displacement

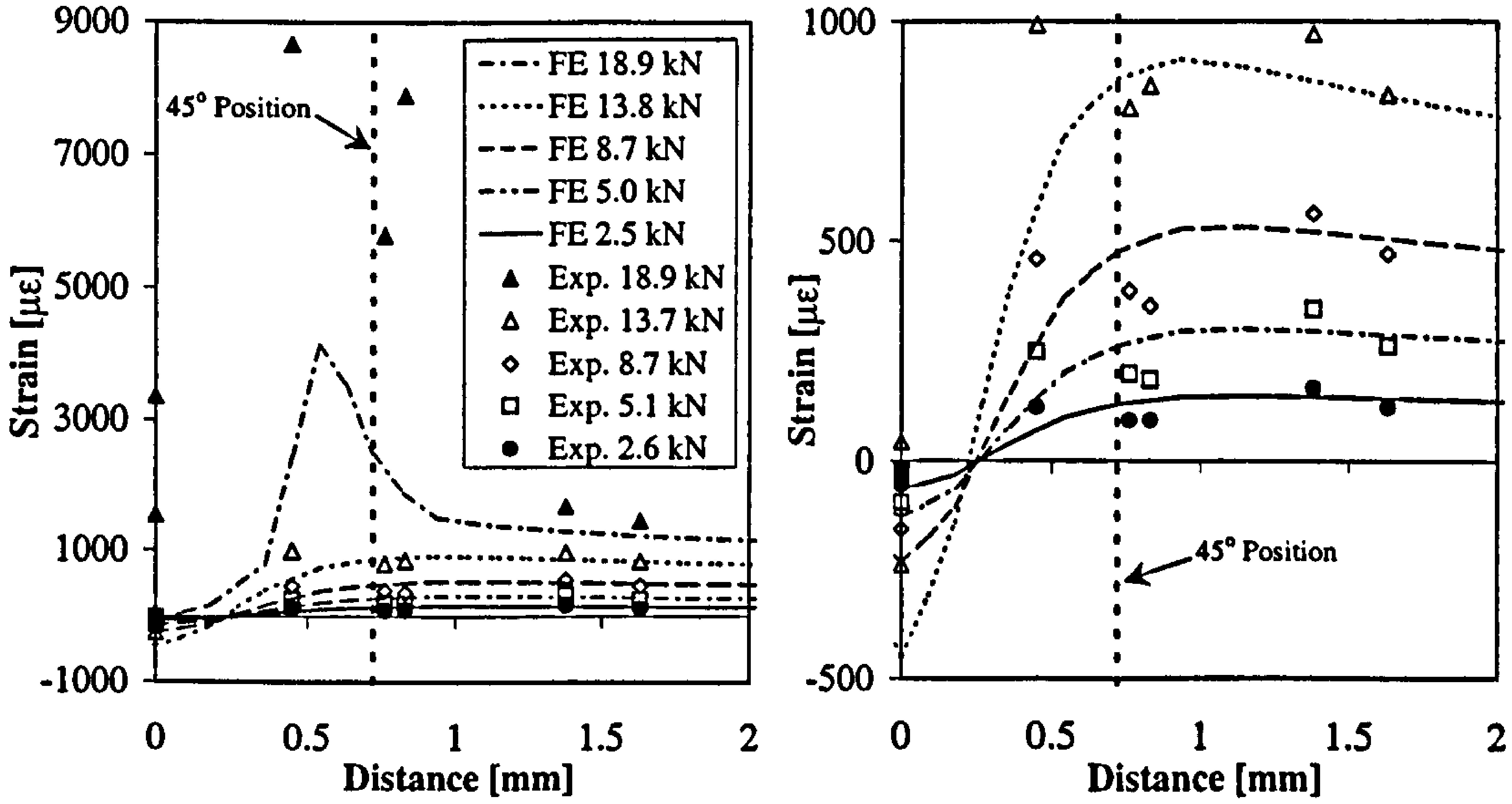

(b) Strain Distribution

(c) Strain Distribution (low strain)

Figure 2.31: Test Specimen E (a/t=0.73) Results

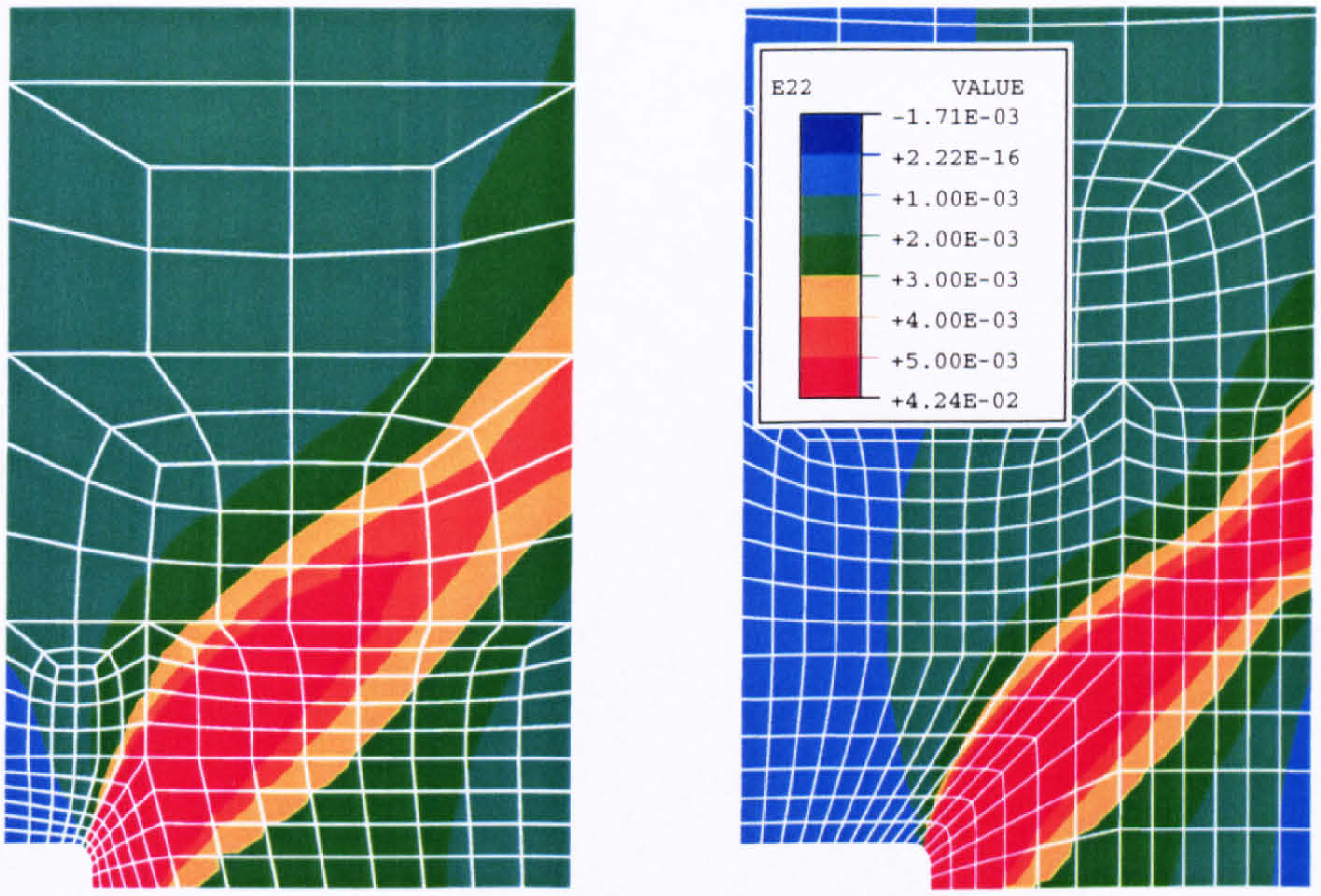

(a) Specimen B

(b) Specimen C

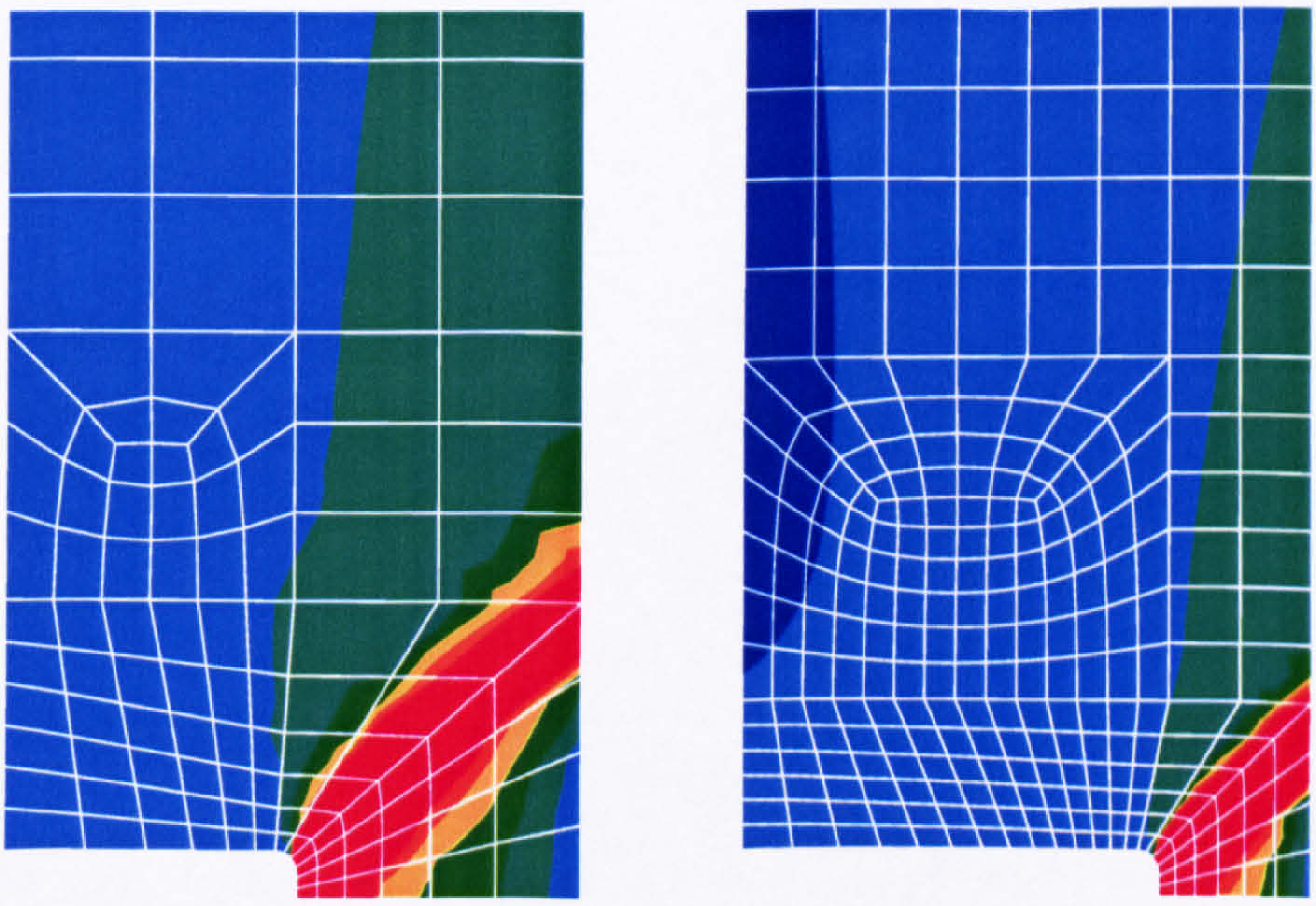

(c) Specimen D

(d) Specimen E

Figure 2.32: Axial Strain Contour Plots at Crack

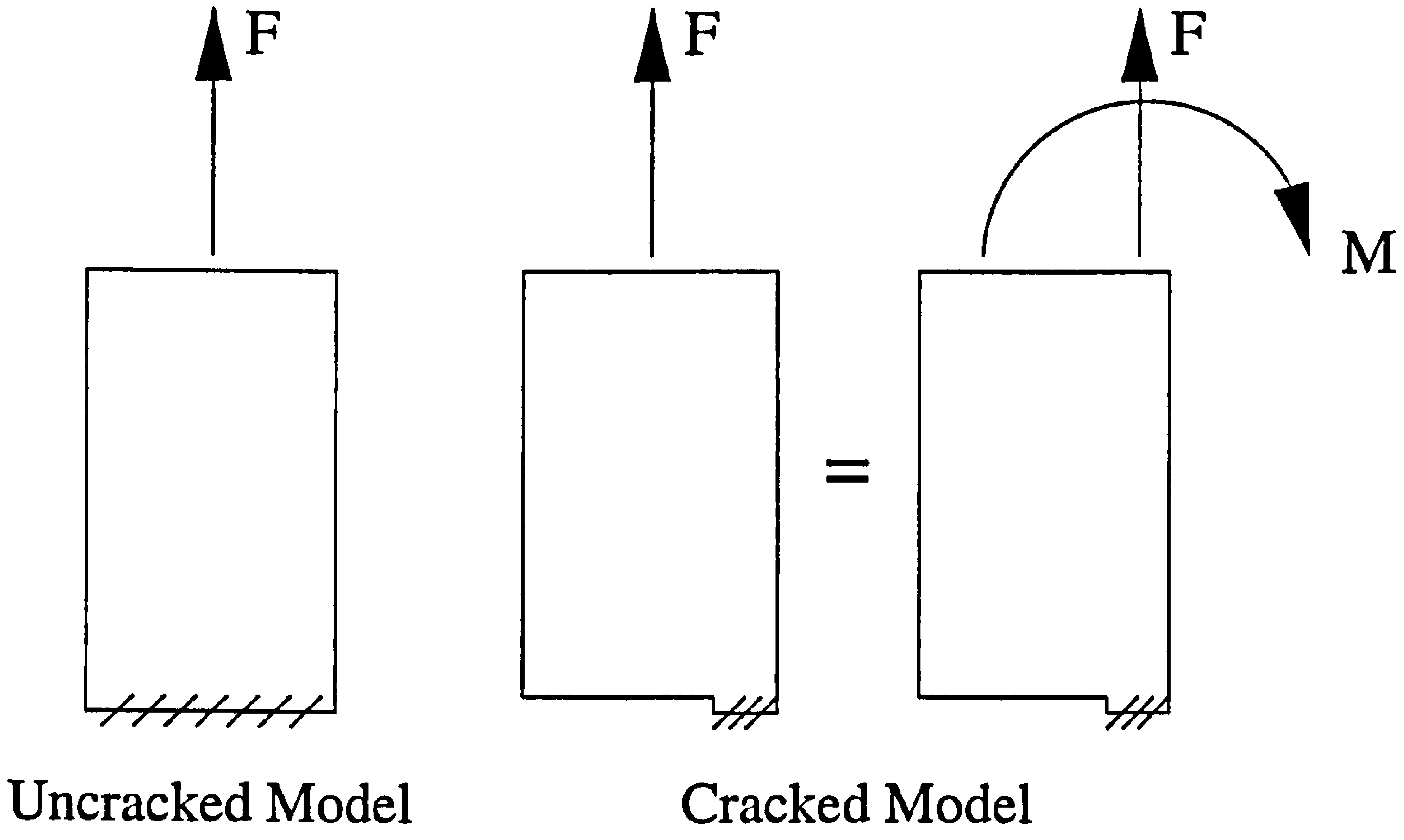

Figure 2.33: Bending of the Crack Ligament

Chapter 3

Uncracked Junctions: Parametric Study for Pressure Loading

3.1 Introduction

An extensive FE parametric study was carried out to assess the limit pressures of uncracked branch junctions subjected to internal pressure. The parameters varied were:

- d/D = 0.25, 0.5, 0.75, 1.0
- D/T = 5, 10, 20, 30, 50, 70
- t/T = 1.0 or d/D

The junction with d/D=0.25, D/T=5, t/T=1.0 was not modelled, as the branch pipe opening was unrealistically small. The range of parameters studied is shown in Table 3.1, along with the weld parameters: w_{hc}, w_{bc} and w_{bf}, described later. In addition to the main parametric study (t/T=1.0 and t/T=d/D), an additional set of models were constructed to study the effect of varying t/T (see Table 3.2).

The general meshing techniques are described in this Chapter, and these were also used as the basis for the subsequent cracked branch junction studies. A brief mesh convergence study is also described. The branch junction terminology used is shown in

Figure 3.1. Finally the results of the parametric study are presented in non-dimensional form, along with general equations to calculate the limit pressure. These FE results are compared with existing methods used to calculate the limit pressures of branch junctions, and are also compared with some published data.

3.2 Finite Element Method

The Finite Element method is widely used in the area of pressure vessels and piping, as described in Chapter 1, and is a useful tool for obtaining quick, accurate solutions to stress analysis problems. It is the only practical method by which the parametric study presented could be undertaken. In fact, for the evaluation of limit loads, as defined by Gerdeen [3] with elastic/perfectly-plastic material and small displacement analysis, it is the only generally available method for analysis of structures or components with complicated geometry. Experimental analysis of the variation of the large number of parameters presented here would be an extremely time consuming and expensive task.

However, the finite element method is just a tool and must be used correctly. The major concerns for FE users are issues including the types of elements available, the mesh density required and applying the correct boundary and loading conditions. Incorrect application of the FE method can give misleading results.

Mesh convergence is usually required to ensure that a mesh of sufficient density is used. For the modelling of pressurised components, shell and solid elements are both commonly used. The junctions studied covered a wide range of parameters, including some relatively thick junctions, and also incorporated detailed modelling of the weld. Shell elements are not suitable for thick branch junctions with complex geometry, such as a weld (or a crack, as in Chapter 4), and the limit load can be sensitive to such features. Hence, solid brick elements are recommended and have been used for all branch junction FE models.

3.2.1 Junction Geometry and FE Mesh Generation

Two FE packages were used: PATRAN [65] and ABAQUS [66]. PATRAN was used as a pre-processor for creating the geometry and finite element mesh of the models.

The node sets and element sets required for applying boundary conditions and loading were also identified using PATRAN. ABAQUS input files were then generated from PATRAN.

The analysis and post-processing were performed using ABAQUS. ABAQUS is capable of non-linear analysis, including the analysis of geometric and material non-linearity. The input files generated by PATRAN were refined to specify the desired loading, boundary conditions and results output and were then submitted for analysis using ABAQUS.

The type of elements used were specified in ABAQUS as 'C3D20R'. These are 20-noded, reduced integration, isoparametric brick elements with three translatory degrees of freedom at each node. Transition regions, used to reduce the mesh density away from the weld, sometimes required the use of the corresponding wedge elements (ABAQUS element type 'C3D15'). An aspect ratio of less than three is recommended [69] for elements in critical areas, but a ratio of between three and five is regarded as acceptable. The aim throughout the FE work was to adhere to this criterion, in order to ensure reliable results.

All of the models created for this study were quarter models, as branch junctions have two planes of symmetry for pressure loading, specified in Figure 3.1(a). The length of the pipe limbs, L, was measured from the intersection of the run pipe and branch pipe centre lines, and was equal to 200mm. The inner diameter of the run pipe was always equal to 63.6mm (to correspond with experimental models), and the external diameter was altered for different values of D/T. The value of L/D_i was therefore equal to 3.14, which should give a sufficient 'die-away' length for the stresses in each of the limbs.

The branch junction FE models included the weld, which was altered for each geometric variation. The weld preparation was assumed to be on the branch pipe and so the weld was scaled according to the thickness of the branch pipe. The parameters used to define the weld geometry (w_{hc}, w_{bc} and w_{bf}) are shown in Figure 3.1(b) and the values are listed in Table 3.1 (w_{hf} in Figure 3.1(b) is not listed as this was dependent upon w_{bf} in the model construction).

The weld was generated in PATRAN by means of an ellipse, which was constructed using a curve fitted to a series of points. This ellipse was used to define the run pipe weld toe by projecting its profile onto the surface of the run pipe (see plan view, Figure 3.1(a)). The profile of the ellipse was generated from the values of w_{bf} and w_{bc} for each model. The width of the weld at the flank w_{bf}, and hence the ellipse, was reduced with increasing d/D (this value was zero for d/D=1.0). The value of w_{bc} was dependent upon the branch pipe wall thickness. The upper weld toe was created by transforming the intersection line between the run and branch pipes by a distance equal to the weld height at the crotch, w_{hc}.

The methods of construction for all of the models were very similar, differing slightly for each d/D value, especially d/D=1.0. As there was a relatively large number of models, a program was written to allow a PATRAN journal file template to be altered for the required geometry. These journal files were then used to generate the geometry in PATRAN without any further input. The mesh was not generated in this way as each junction had different mesh requirements.

3.2.2 Loading and Boundary Conditions

As mentioned above, symmetry faces were applied to two faces of the model. The end of the branch pipe was fully clamped. Although this would stop the radial expansion of the pipe at the end, the branch was sufficiently long ($\geq$ 3d) that the behaviour of the junction intersection would not be affected. The end of the run pipe was free, and had a tensile axial stress applied to it equal to $PD_i^2/(D_o^2 - D_i^2)$, in order to simulate a closed end condition for the pipe.

The material properties used were similar to those used in Chapter 2: elastic/perfectly-plastic material with Young's Modulus = 210 GN/m^2, yield stress (σ_y) = 308 MN/m^2 and Poisson's ratio = 0.3. The 'Riks' method was used in ABAQUS [66], allowing ABAQUS to automatically determine the required load incrementation. This method was used in case of any unstable response from the analyses, although analysis of selected junctions without the use of the 'Riks' method gave the same limit load results.

The results are presented as normalised limit pressures, later in this Chapter, enabling the limit pressure for any yield stress to be calculated.

3.2.3 Determination of Limit Loads

Gerdeen [3] recommended that the deformation parameter for limit load analysis should be such that: 'the product of the load parameter and the deformation parameter should represent work'. For pressure loading, this implies that the deformation parameter used should be volumetric change. However, there is no facility in ABAQUS to calculate the internal volume of a component, and manual calculation from the displacement results, while possible, would be impractical for the number of models analysed. Hence, alternative **displacement** based parameters were used instead, as described below.

The limit load was determined from the pressure-displacement curve using a similar method to the fifteen times elastic slope method described in Section 2.6.1. Due to the displacements involved it was decided that the 'five times elastic slope' (5ES) should be used instead. This ensured that the levels of displacement were reasonable at the point at which the limit load was recorded, and that the limit load was on the plateau. This method was relatively straightforward to use for the analysis of the results from a large number of models. Alternative methods are described in Chapter 1.

The displacement parameter against which the pressure was plotted was altered depending upon the model analysed. Generally, the diametral growth of the intersection measured at the flank of the run pipe was used. However, in some cases this parameter could not be used as it reversed in direction before the 5ES value was reached. An alternative displacement parameter was used for these junctions: the displacement in the 1-direction (see Figure 3.1(a)) of the node at the bottom of the run pipe, in line with the branch pipe centreline, was recorded. Using this parameter, a limit load result for those cases in which the diametral growth parameter reversed was obtained. Conversely, this parameter often reversed for the cases in which the diametral growth could be used.

The effect described above is illustrated in Figures 3.2(a) and 3.2(b). The run pipe expands initially in both directions (Figure 3.2(a)) but, as shown in Figure 3.2(b), the vertical displacement becomes the predominant parameter. This was caused by the intersection near the weld becoming the main area of growth and the diameter across the flank eventually decreasing.

Figures 3.2(c) and 3.2(d) illustrate the alternative case for a much thicker branch junction, with the diametral displacement becoming the predominant displacement parameter. Pressure-displacement curves for both displacement parameters are plotted in Figure 3.3 for the two cases described (Note that in Figures 3.2(a)-(d) expansion in the 1-direction is defined as negative). It was obvious that a different parameter was suitable for each of the two models.

3.2.4 Mesh Convergence Study

The typical density required for internal pressure loading has previously been established at Liverpool by Yahiaoui et al. [5] for forged tee junctions. In this previous study, four elements through the thickness were used in order to be consistent with the cracked work, although it was found that one element through the thickness gave 'adequate accuracy'. In addition, a draft report [70], providing guidelines for FE modelling of intersections, recommends that a minimum of two elements through the thickness are used near the intersection area.

A mesh convergence study was performed for one of the branch junctions to ensure that the mesh used was of sufficient density. The branch junction studied had the parameters: d/D=0.5, D/T=10 and t/T=1.0. The number of elements through the thickness (at the intersection location) and around the weld circumference were varied. The limit loads were calculated using the method described in Section 3.2.3, using both of the two displacement parameters (for this geometry neither of the parameters reversed in direction). The number of elements through the thickness was varied between 1 and 5, the number around the junction intersection varied between 48 and 80, and the number of elements used in the weld height was varied between 4 and 10. The mesh was always reduced to one element through the thickness away from the intersection. Despite these large differences in the mesh density, and hence the total number of elements used, the maximum variation (measured from the limit pressure for the finest mesh) was just 1.1%.

It was decided that, for the thickest (D/T=5) cases, five elements through the thickness should be used, with 3 elements through the thickness for D/T=10, 20 and 30. The remaining thinner models had 2 elements through the thickness. The number of elements in the weld height and around the circumference were adjusted accordingly, to give an aspect ratio of no greater than five in the vicinity of the intersection.

A selection of the FE models used in the parametric study are shown in Figure 3.4.

3.3 Results and Discussion

3.3.1 FE Parametric Study

Following the derivation of the limit loads, the results were plotted using a series of curves, as shown for t/T=1.0 and t/T=d/D in Figure 3.5, with limit pressures plotted against D/T. However, it is easier to assess the effects of varying individual parameters if the results are presented in a non-dimensional form. Hence, each of the limit pressure values was divided by the corresponding plain pipe limit pressure, to give a non-dimensional limit pressure, P' - using thick shell theory:

$$P_{L(plain)} = \left(\frac{2}{\sqrt{3}}\right)\sigma_y \ln\left(\frac{R_o}{R_i}\right) \tag{3.1}$$

$$P' = \frac{P_L}{P_{L(plain)}} \tag{3.2}$$

All of the following results are presented non-dimensionally.

Junctions with t/T=1.0

The results for these junctions, with equal thickness in the branch and run pipes, are presented in Figure 3.6(a) plotted against varying D/T for four different d/D ratios. An alternative method of presenting these results is to plot the values of P' against d/D as shown in Figure 3.6(b). The two graphs provide a useful method of observing trends from the results.

Examining Figure 3.6(a), it is clear that for small branch pipe diameters (d/D=0.25) the limit pressures tended towards the plain pipe value (i.e. P'=1.0). The limit pressures also generally tended to the plain pipe value as the thickness increased, for any diameter ratio. The greatest difference from the plain pipe value was for the thinnest (i.e. D/T=70) d/D=1.0 and d/D=0.75 models, which have a limit pressure of just 0.42

of the plain pipe value. The thinnest d/D=0.25 model is still 0.77 of the plain pipe value.

Figure 3.6(b) shows that, for any given D/T value, the limit pressure reduced with increasing d/D. The only exception to this trend was for D/T=70 which was equal to the d/D=1.0 case for d/D=0.75. For the thicker junctions (D/T=5 and D/T=10) the relationship was virtually linear.

Junctions with t/T=d/D

The results for these equal pressure strength junctions are presented in Figures 3.7. Note that the values for the d/D=1.0 case are identical to those used for the t/T=1.0 results. Figure 3.7(a) shows a greater reduction in the limit pressure for small branch pipe diameters (d/D=0.25 and 0.5) than for the t/T=1.0 set in Figure 3.6(a). None of the results were close to the plain pipe limit pressure, although they all generally tended towards this value with decreasing D/T (increasing thickness). The greatest difference from the plain pipe value was for the thinnest d/D=0.75 model, with P'=0.34.

Figure 3.7(b) shows a different response to that for the t/T=1.0 set of results. The limit pressure did not always reduce with increasing d/D. It reduced in this way for the thickest set of models (D/T=5) but not for the remaining thinner models. In other words, the d/D=1.0 case did not always have the lowest P' values: the lowest values were often for d/D=0.75, usually followed by d/D=0.5 or d/D=1.0. As for the t/T=1.0 results, the d/D=0.25 models always had the highest P' values. The values all tended toward the plain pipe value with decreasing d/D, represented by the broken lines in Figure 3.7(b) (obviously if d/D=0 then the problem reduces to a plain pipe). This principle could not be applied to the t/T=1.0 models as there is the added complication of the constant thickness of the junction, regardless of the branch pipe diameter.

Effect of Varying t/T

Considerable data was already available from the above parametric study data for t/T=1.0 and t/T=d/D. However, in order to study the effect of t/T ratios other than these, a series of additional models, listed in Table 3.2, were constructed and analysed.

These additional models covered a limited selection of the parametric study, with t/T values of 0.75 and 1.25 added for some d/D=0.5 cases, and t/T values of 1.5 added for selected d/D=0.75 cases. The results for these models are presented in Figure 3.8(a). The relationship between the non-dimensionalised limit pressure and t/T was almost linear, for the range of t/T values presented. The results for all of the models are shown in Figure 3.8(b). The trend was always for the limit pressure to increase with increasing t/T, as would be expected. A straight line drawn between the lowest and highest t/T values for each case would give a reasonable estimate to the limit pressure for any intermediate t/T values. This estimate would always be conservative within the range of t/T values studied for any particular combination of d/D and D/T. However, the estimate is likely to be unconservative for t/T values outside of this range.

The gradient of this line can be used in combination with the polynomial equations for limit pressure, as presented in the following Section, to give results for t/T values other than those presented.

Equations for Branch Junction Limit Pressure

In order to quickly calculate the limit pressure for a particular junction configuration, a series of curves have been fitted to the parametric study results shown in Figures 3.6(a) and 3.7(a), using the polynomial curve fitting ('trendline') facility in Microsoft Excel. The curves that were generated are shown in Figure 3.9.

The curves were defined for each d/D value (for t/T=1.0 and t/T=d/D) in terms of P' and D/T in the following form:

$$P' = a_0 + a_1\frac{D}{T} + a_2\left(\frac{D}{T}\right)^2 + a_3\left(\frac{D}{T}\right)^3 + a_4\left(\frac{D}{T}\right)^4 + a_5\left(\frac{D}{T}\right)^5 \tag{3.3}$$

The values of a_n are given in Table 3.3. Linear interpolation could be used to obtain P' for values of d/D other than those presented.

For values of t/T other than t/T=1 and t/T=d/D, an adjustment factor ('m') has been calculated from the slope of a line joining the lowest and highest t/T values for each set of results shown in Figure 3.8(b). These 'm' values are shown in Table 3.4, along with the range of applicability, for each value of d/D and D/T. The adjustment factors should be used in conjunction with the **equal pressure strength results (t/T=d/D)**, as these are always the lowest t/T value available (i.e. $(t/T)_{min}$). Hence, the non-dimensionalised limit pressure can be calculated for a given t/T:

$$P' = P'_{eq} + m\left(\frac{t}{T} - \frac{d}{D}\right) \tag{3.4}$$

for $(t/T)_{min} \leq t/T \leq (t/T)_{max}$, where P'_{eq} is the equal pressure strength result from equation (3.3). This would give a conservative approximation of the limit pressure of the branch junction.

Worked Example

The procedure above will now be shown for an intermediate junction geometry. The limit pressure for a junction with d/D=0.5, D/T=40 and t/T=0.85 is estimated. The non-dimensionalised limit pressure for the equal pressure strength junction is first calculated. Substituting the values from Table 3.3 into equation (3.3):

$$P' = 9.548 \times 10^{-1} - [3.227 \times 10^{-2} \times (40)] + [8.677 \times 10^{-4} \times (40)^2] \ldots$$

$$-[1.198 \times 10^{-5} \times (40)^3] + [6.296 \times 10^{-8} \times (40)^4] = 0.447 \tag{3.5}$$

This value is then adjusted to account for t/T=0.85, using the 'm' values in table 3.4. Linear interpolation should be used between the values for D/T=30 and D/T=50 (i.e. between 0.383 and 0.397) to give 'm' for D/T=40. This gives m=0.390, which is then substituted into equation (3.4):

$$P' = 0.447 + 0.390\,(0.85 - 0.5) = \mathbf{0.584} \tag{3.6}$$

This procedure can be used for any junctions within the specified range of parameters. Limit pressures for other d/D values could also be extracted by linear interpolation between the values of d/D, although linear interpolation would not necessarily give a conservative estimate.

3.3.2 Comparison of Results with Existing Evaluation Methods

There are several existing methods used for calculating the limit pressure of branch junctions, some of which are equations derived using theoretical methods, others are equations based upon FE or experimental data. Some of these methods will now be discussed.

Rodabaugh Recommendation

Rodabaugh [27] discussed limit pressure solutions for branch junctions, concluding that the approximate solution of Cloud and Rodabaugh [25] gives a reasonable solution for all d/D values, when compared with test data. The solution of Cloud and Rodabaugh was calculated using a factor, p^* to adjust the Tresca plain pipe limit pressure equation:

$$P_{LP} = p^*(2\sigma_y T/D) \tag{3.7}$$

where,

$$p^* = \frac{[A(t/T)^2 + 228(t/T)(d/D) + B]\lambda + 155}{108\lambda^2 + [228(d/D)^2 + 228]\lambda + 152} \leq 1.0 \tag{3.8}$$

A = 162 for t/T $\leq$ 1.0; A = 54 for t/T $>$ 1.0

B = 210 for t/T $\leq$ 1.0; B = 318 for t/T $>$ 1.0

$\lambda = (d/D)(D/T)^{0.5}$

The results presented in Section 3.3.1 were non-dimensionalised using the von Mises plain pipe limit pressure solution for a thick pipe (see equation (3.1)). In order to compare the FE results with the Cloud and Rodabaugh results, the values obtained from equation (3.7) were divided by the corresponding values from equation (3.1) to give:

$$P' = \frac{p^*(2\sigma_y T/D)}{\frac{2}{\sqrt{3}}\sigma_y \ln\left(\frac{R_o}{R_i}\right)} \tag{3.9}$$

Equation (3.9) is shown plotted against d/D, alongside the FE parametric study results, in Figure 3.10. For the t/T=1.0 results, it is clear that the present FE parametric study and the Cloud and Rodabaugh equation exhibit similar trends, the limit pressure reducing with increasing d/D. Equation (3.9) generally gives slightly higher values than the FE limit pressures, although it always gives a lower value for equal diameter junctions (d/D=1.0). The overall comparison is considered to be good.

For the t/T=d/D results, the comparison between the FE results and the equation is not as good for thick junctions (i.e. with $D/T \leq 10$) but for thinner junctions the comparison is good. Again, the equation always gives slightly lower results for d/D=1.0. Overall, the equation gives reasonable agreement for t/T=d/D, except for junctions with both $D/T \leq 10$ and $d/D < 1.0$.

The Cloud and Rodabaugh equation appears to be a useful method of estimating the limit pressure. The general trend of the equation is similar to the FE parametric study. Although the results are not always conservative (except for d/D=1.0) compared with the parametric study results, in general they are close to them (usually within 10%, with the exception of the thick t/T=d/D cases described above).

Inverse Code Method (Creep Rupture Pressure)

The inverse code method, as described by Booth [37], is recommended by Budden and Goodall [36] as one of the methods for evaluating the creep rupture reference stress (σ^R_{ref}), which is useful for predicting the creep rupture of defect free (cylinder-cylinder) branch junctions made from ductile pressure vessel steels. The resulting creep rupture load from this method is compared with the parametric study limit pressure data. Although it is not strictly correct to compare these results, this method is often used in practice as an approximation to the limit load.

For isolated branch junctions subjected to internal pressure alone, the creep rupture reference stress [36] is given by:

$$\sigma^R_{ref} = P\left(\frac{R_i\,Ca_1}{T\gamma_{min}} + 0.5\right) \tag{3.10}$$

where Ca_1 is a stress concentration factor for the hole and any branch reinforcement, and γ_{min} is the minimum system load factor that accounts for global bending moments in the branch or run pipes (i.e. for pressure loading, $\gamma = 1.0$). P is the nominal pressure corresponding to the creep rupture reference stress.

For flush branches where $d/D \geq 0.2$, the stress concentration factor Ca_1 is approximated by:

$$Ca_1 = 0.8K\left(\frac{2K-1}{4K-3}\right) \tag{3.11}$$

where the geometric parameter K is defined as:

$$K = \frac{2.5}{\sqrt{\frac{t}{r}\sqrt{\frac{R}{T}}}} \tag{3.12}$$

The creep rupture pressure load (P_L^R) is given by:

$$P_L^R = P\frac{\sigma_y}{\sigma_{ref}^R} \tag{3.13}$$

This load is compared with the parametric study results in Figure 3.11. The creep rupture pressure has been normalised using the plain pipe limit pressure equation (3.1). For t/T=1.0 (Figure 3.11(a)) the inverse code results show the same trend as the FE results, with the pressure reducing with increasing d/D. The inverse code results are always conservative.

The t/T=d/D results (Figure 3.11(b)) show a constant limit pressure for each value of D/T. The inverse code method does not have a factor accounting for changes in d/D. Hence if t/r and T/R are constant, as they are if t/T=d/D, then the limit pressure remains constant. Although the method does not reproduce the effect of altering d/D, the predicted pressures are conservative for all of the cases analysed (with the exception of the d/D=0.75, D/T=70 case, which is slightly non-conservative).

Overall, the inverse code creep rupture pressure appears to provide a conservative approach for estimation of the limit pressure. In some cases the method is considerably over-conservative (over 30% lower than the FE result).

Inferred Inverse Code Method (Limit Pressure)

The global reference stress, σ_{ref}, for a branch junction under pressure load is defined by:

$$\sigma_{ref} = P\frac{\sigma_y}{P_L} \tag{3.14}$$

where P is the nominal pressure used to evaluate σ_{ref} and P_L is the global limit pressure.

When assessing creep damage, R5 Volume 2 Appendix A3 [35] states that the global reference stress (usually from finite element analysis) should be enhanced using the stress concentration factor χ. This approach accounts for the initiation of cracking at highly stressed regions or the presence of small defects around stress concentrations. Thus the creep rupture reference stress is calculated from:

$$\sigma_{ref}^{R} = [1 + 0.13(\chi - 1)]\,\sigma_{ref} \tag{3.15}$$

where $\chi = \sigma_{E,max}/\sigma_{ref}$ and $\sigma_{E,max}$ is the maximum elastically calculated value of equivalent stress in the branch junction. The values of $\sigma_{E,max}$ would normally be calculated from the FE results, taking care not to use values associated with sharp corners by using the gradient of the stress through the thickness. However, as such a large number of models has been included in the parametric study, the effective stress factor (ESF) for each model, from Appendix H of BS806 [71], have been used to calculate $\sigma_{E,max}$, using the relationship:

$$\sigma_{E,max} = ESF_{max} \times \frac{PR}{T} \tag{3.16}$$

The method described could be used to determine creep rupture limit pressures from the finite element results, for direct comparison with the inverse code results of the previous section. However, a 'reverse' procedure is often applied to infer the global reference stress from the creep rupture reference stress (σ_{ref}^{R}) of the previous section, using the above approach to calculate σ_{ref} values and hence the limit pressures. Expanding equation (3.15) and substituting in for χ gives:

$$\sigma_{ref}^{R} = \left(0.87 + 0.13\frac{\sigma_{E,max}}{\sigma_{ref}}\right)\sigma_{ref} \tag{3.17}$$

rearranging for σ_{ref}, gives:

$$\sigma_{ref} = \frac{\sigma^R_{ref} - 0.13\ \sigma_{E,max}}{0.87} \tag{3.18}$$

This gives a global limit pressure that can be compared with the parametric study FE data. The comparison is shown in Figure 3.12.

For t/T=1.0, this method was found to greatly over-estimate the limit pressure for thick junctions (D/T=5 and 10). The correlation improved for thinner junctions, but virtually all of the results were non-conservative.

For t/T=d/D, there was little agreement with the FE results. The curves tended to be conservative for d/D=0.25 and some d/D=1.0 cases, but otherwise non-conservative. The general trend of the curves was contradictory to that of the FE results.

The inferred inverse code method gives poor agreement with the parametric study data and is not recommended.

Budden and Goodall FE Correlation

Budden and Goodall [36] recommended the use of equation (3.19) based on finite element results from a previous parametric study by Galt [38]. This study covered 27 geometries, in the range: 0.4<d/D<1.0, 0.25<t/T<1.0 and 4<D/T<30.

$$P_L = \frac{\sigma_y T}{R}\left[\frac{A[1+B(1-r/R)][1-D(0.5-T/R)^2]}{[1+C(1-t/T)]}\right] \tag{3.19}$$

where, A = 0.641; B = 0.908; C = 0.608; D = 1.422

Although there are limits specified to the equation, the limit pressures for all of the cases in the FE parametric study have been calculated for comparison. The results from equation (3.19) have been normalised using equation 3.1 as before, and are shown in Figure 3.13. The out-of-range D/T values are represented by broken lines, and the applicable range for d/D is also marked.

The equation does not compare well with the FE results and is not recommended.

Robinson Parametric Survey

Robinson [30] presented data from a theoretical parametric survey for lower bound limit pressures. A wide range of junctions was covered, in the range: $0.05<d/D<0.8$, $30<D/T<800$ and $0.05<t/T<2.0$. A selection of the relevant results from this survey have been presented alongside the FE parametric study results in Figure 3.14. For some of the Robinson data it was necessary to use linear interpolation between the t/T values, as the exact values required were not available. D/T values of 30, 50 and 100 are presented.

The data for $D/T=30$ and $D/T=50$ compare well with the FE parametric study, generally being slightly conservative. The general trend of the two sets of data are also very similar. For $t/T=1.0$, the limit pressure reduces with increasing d/D. For $t/T=d/D$ the limit pressures reach a minimum at intermediate d/D values (≈ 0.6)

3.4 Concluding Remarks

An extensive parametric study has been successfully completed. From the equations presented in Section 3.3.1 it is possible to determine quickly a limit pressure for any branch junction within the range studied.

Several other existing methods of evaluating the limit pressure have also been compared with parametric study results. The most useful comparison methods were deemed to be the Cloud and Rodabaugh equation and the Inverse Code method for creep rupture pressure.

The main conclusions from this study are outlined in Chapter 7.

Table 3.1: Parameters Studied

t/T=1.0

d/D	D/T	w_{hc} [mm]	w_{bc} [mm]	w_{bf}[mm]
0.25				
	10	8.426	5.189	4.000
	20	3.992	2.459	1.895
	30	2.610	1.607	1.239
	50	1.549	0.954	0.735
	70	1.096	0.675	0.520
0.5	5	18.949	11.669	4.831
	10	8.426	5.189	2.148
	20	3.992	2.459	1.018
	30	2.610	1.607	0.665
	50	1.549	0.954	0.395
	70	1.096	0.675	0.280
0.75	5	18.949	11.669	2.924
	10	8.426	5.189	1.300
	20	3.992	2.459	0.616
	30	2.610	1.607	0.403
	50	1.549	0.954	0.239
	70	1.096	0.675	0.169
1.0	5	18.949	11.669	0.0
	10	8.426	5.189	0.0
	20	3.992	2.459	0.0
	30	2.610	1.607	0.0
	50	1.549	0.954	0.0
	70	1.096	0.675	0.0

t/T=d/D

d/D	D/T	w_{hc} [mm]	w_{bc} [mm]	w_{bf} [mm]
0.25	5	4.738	2.918	2.249
	10	2.109	1.299	1.001
	20	1.001	0.617	0.475
	30	0.655	0.404	0.311
	50	0.393	0.242	0.187
	70	0.274	0.169	0.130
0.5	5	9.474	5.835	2.416
	10	4.219	2.598	1.076
	20	1.969	1.229	0.509
	30	1.305	0.804	0.333
	50	0.775	0.477	0.198
	70	0.548	0.338	0.140
0.75	5	14.218	8.756	2.194
	10	6.316	3.890	0.975
	20	2.991	1.842	0.462
	30	1.954	1.204	0.302
	50	1.168	0.719	0.180
	70	0.822	0.506	0.127

Table 3.2: Additional Models

d/D	D/T	t/T	w_{hc} [mm]	w_{bc} [mm]	w_{bf} [mm]
0.5	10	0.75	6.316	3.890	1.610
0.5	20	0.75	2.991	1.842	0.763
0.5	30	0.75	1.954	1.204	0.498
0.5	70	0.75	0.822	0.506	0.210
0.5	10	1.25	10.535	6.488	2.686
0.5	20	1.25	4.993	3.075	1.273
0.5	30	1.25	3.265	2.011	0.833
0.5	70	1.25	1.371	0.844	0.349
0.75	10	1.5	12.695	7.787	1.951
0.75	30	1.5	3.921	2.415	0.605
0.75	70	1.5	1.645	1.013	0.254

Table 3.3: 'a' values for Limit Pressure Equation 3.3

t/T=1.0

d/D	a_0	a_1	a_2	a_3	a_4	a_5
0.25	1.033	-4.506×10^{-3}	1.828×10^{-5}	-3.489×10^{-7}	3.336×10^{-9}	
0.5	1.060	-2.316×10^{-2}	6.274×10^{-4}	-9.830×10^{-6}	5.810×10^{-8}	
0.75	1.004	-3.428×10^{-2}	1.331×10^{-3}	-2.925×10^{-5}	3.109×10^{-7}	-1.270×10^{-9}
1.0	8.769×10^{-1}	-2.616×10^{-2}	8.355×10^{-4}	-1.334×10^{-5}	7.733×10^{-8}	

t/T=d/D

d/D	a_0	a_1	a_2	a_3	a_4
0.25	9.958×10^{-1}	-2.116×10^{-2}	4.496×10^{-4}	-5.553×10^{-6}	2.756×10^{-8}
0.5	9.548×10^{-1}	-3.227×10^{-2}	8.677×10^{-4}	-1.198×10^{-5}	6.296×10^{-8}
0.75	8.631×10^{-1}	-2.034×10^{-2}	2.791×10^{-4}	-9.624×10^{-7}	-5.582×10^{-9}

Table 3.4: 'm' values for Limit Pressure Equation 3.4

d/D=0.25

D/T	m	$(t/T)_{max}$
10	0.222	1.0
20	0.313	1.0
30	0.360	1.0
50	0.387	1.0
70	0.390	1.0

d/D=0.5

D/T	m	$(t/T)_{max}$
5	0.291	1.0
10	0.270	1.25
20	0.371	1.25
30	0.383	1.25
50	0.397	1.0
70	0.348	1.25

d/D=0.75

D/T	m	$(t/T)_{max}$
5	0.357	1.0
10	0.295	1.5
20	0.363	1.0
30	0.308	1.5
50	0.471	1.0
70	0.265	1.5

Note: $(t/T)_{min}$ = d/D for all cases.

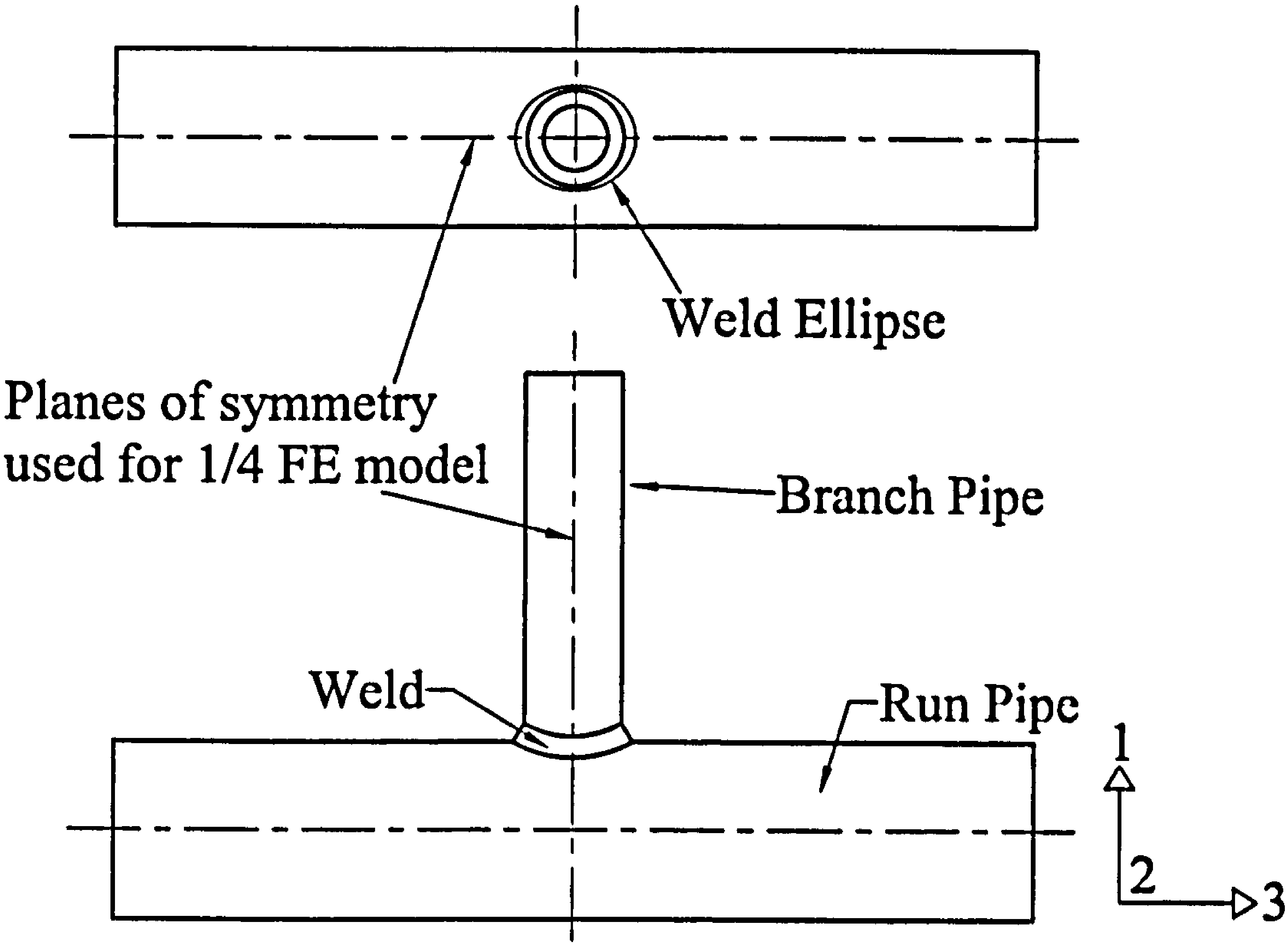

(a) Typical Branch Junction Modelled

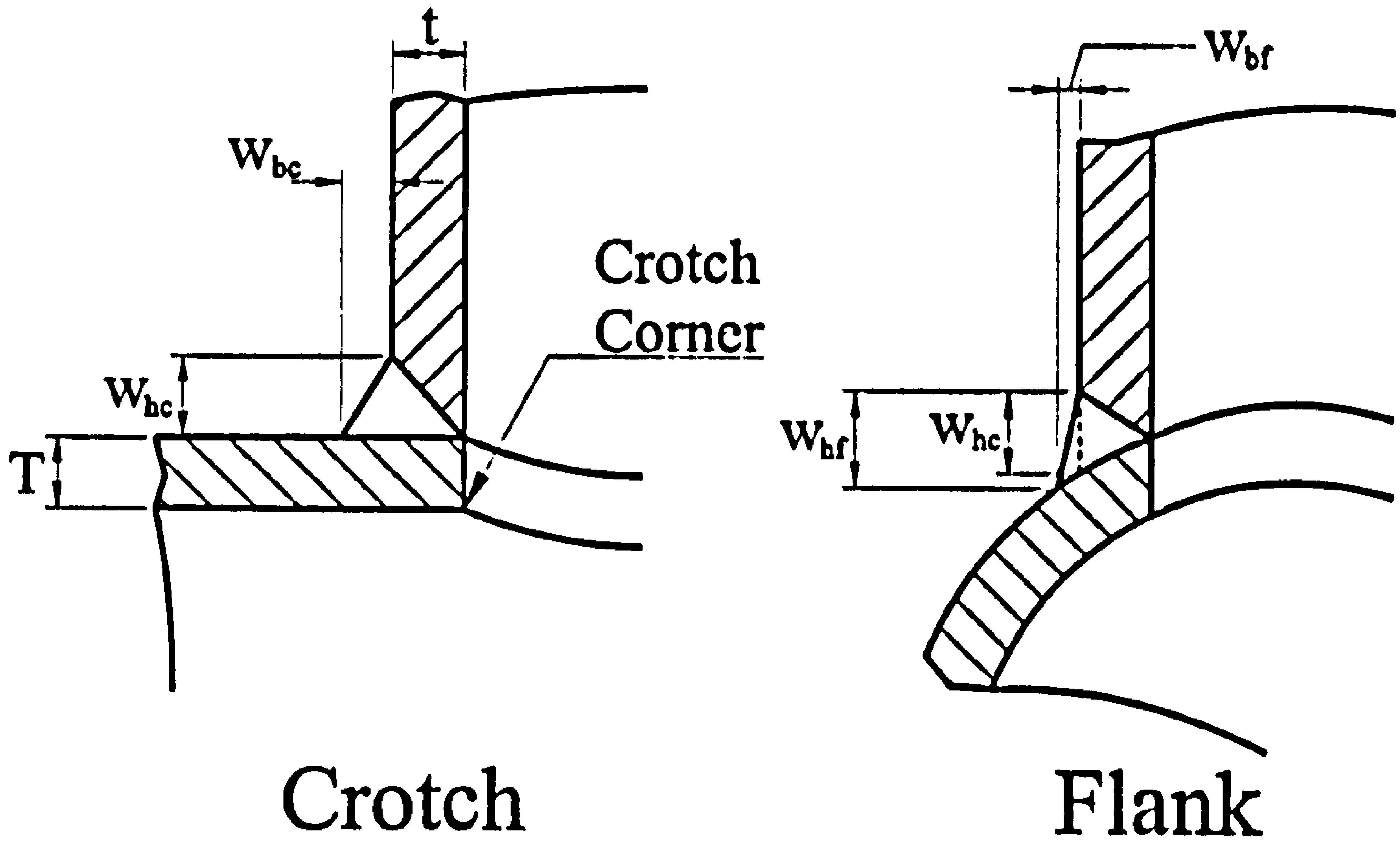

(b) Weld Details

Figure 3.1: Branch Junction Terminology

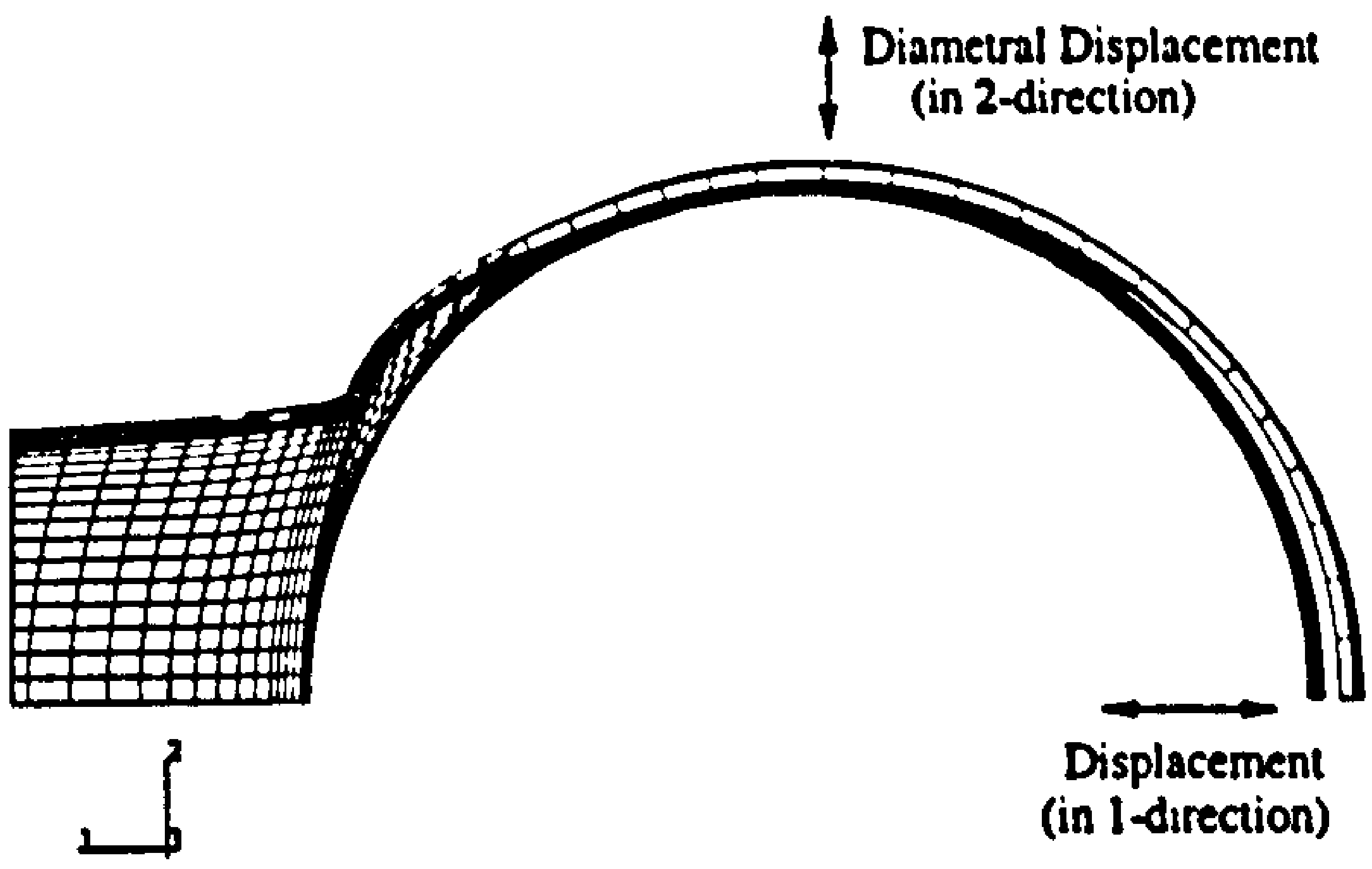

(a) d/D=0.5, D/T=70, t/T=1.0 - 1.44 MPa

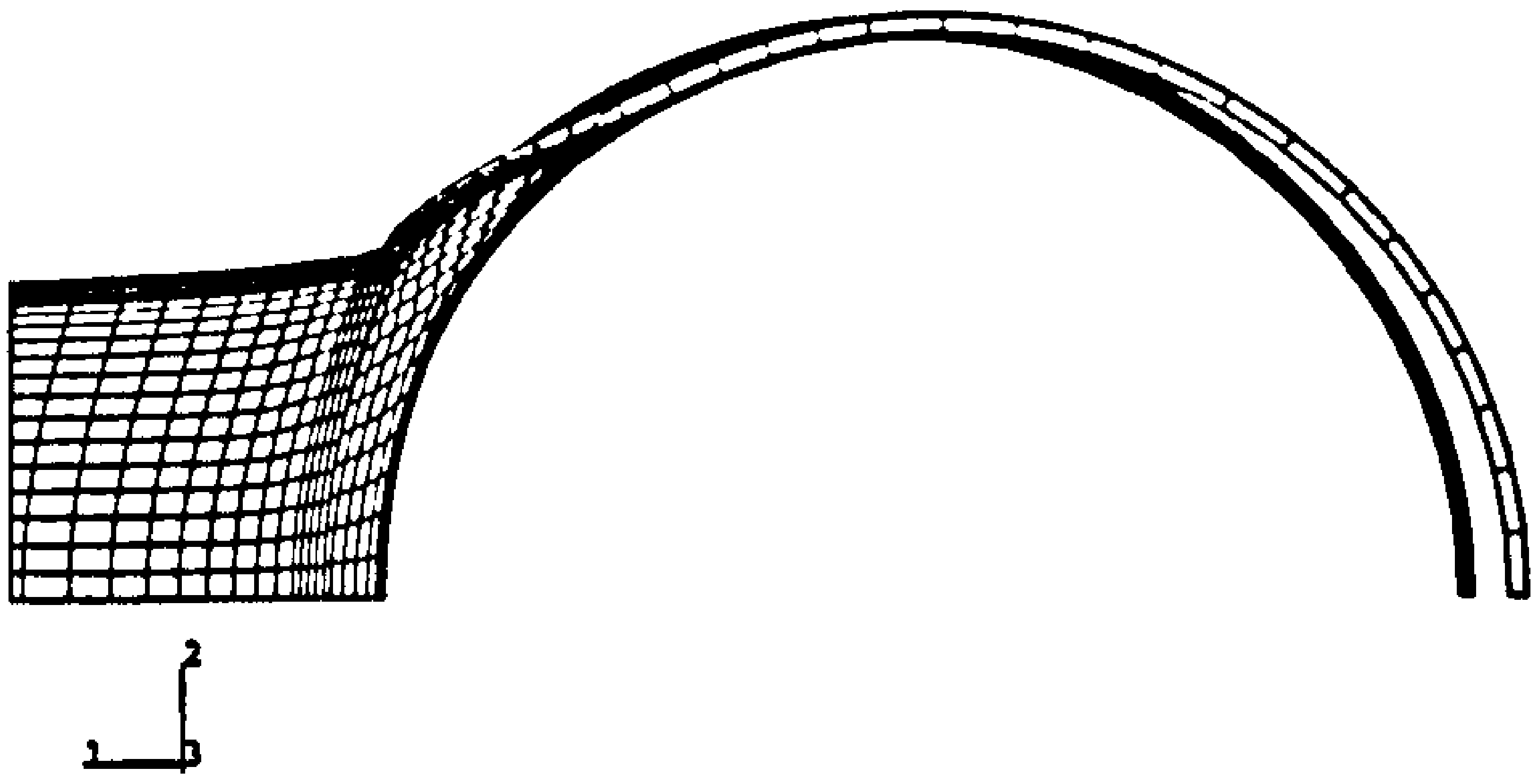

(b) d/D=0.5, D/T=70, t/T=1.0 - 5.80 MPa

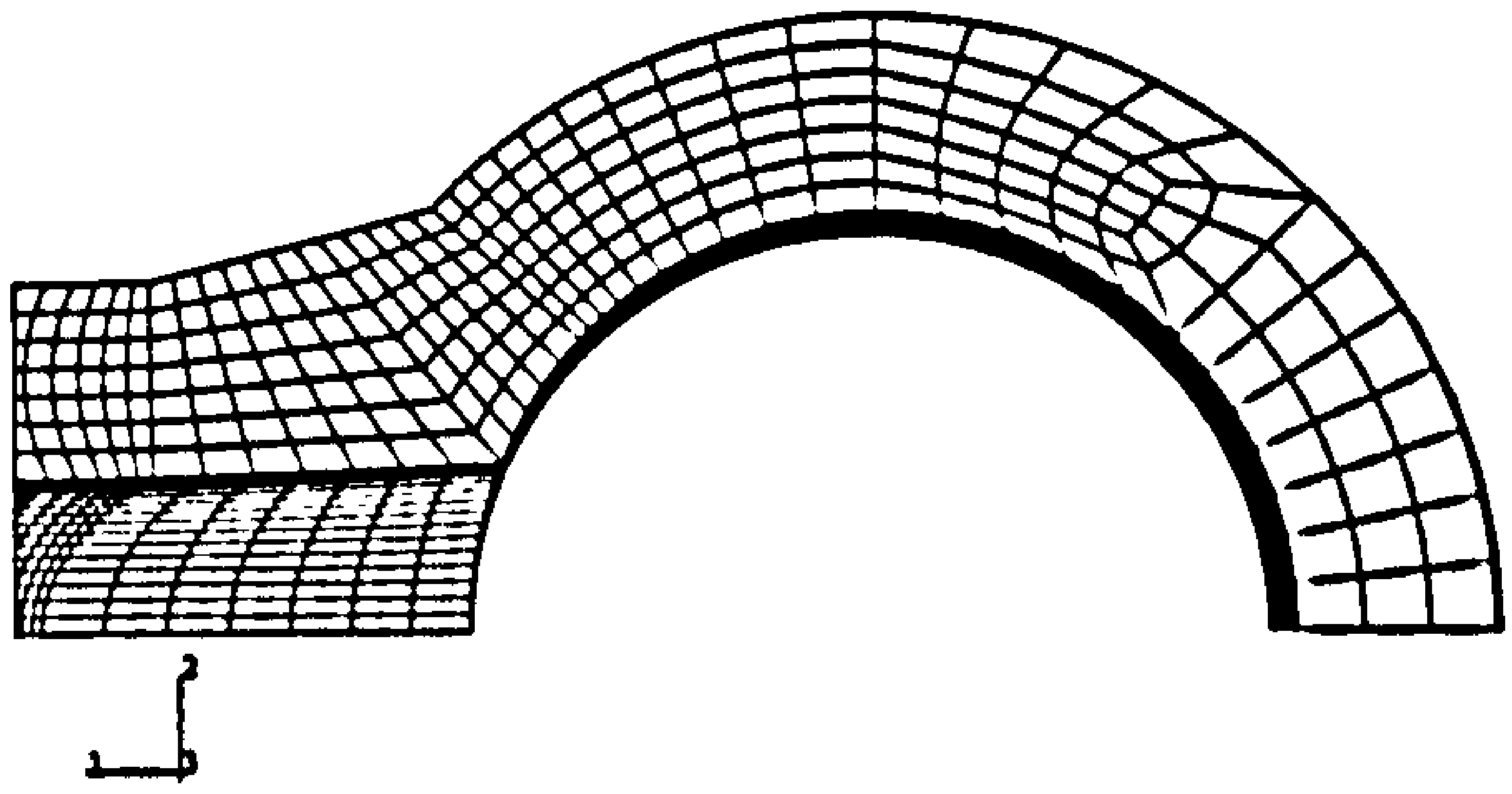

(c) d/D=0.5, D/T=5, t/T=1.0 - 28.8 MPa

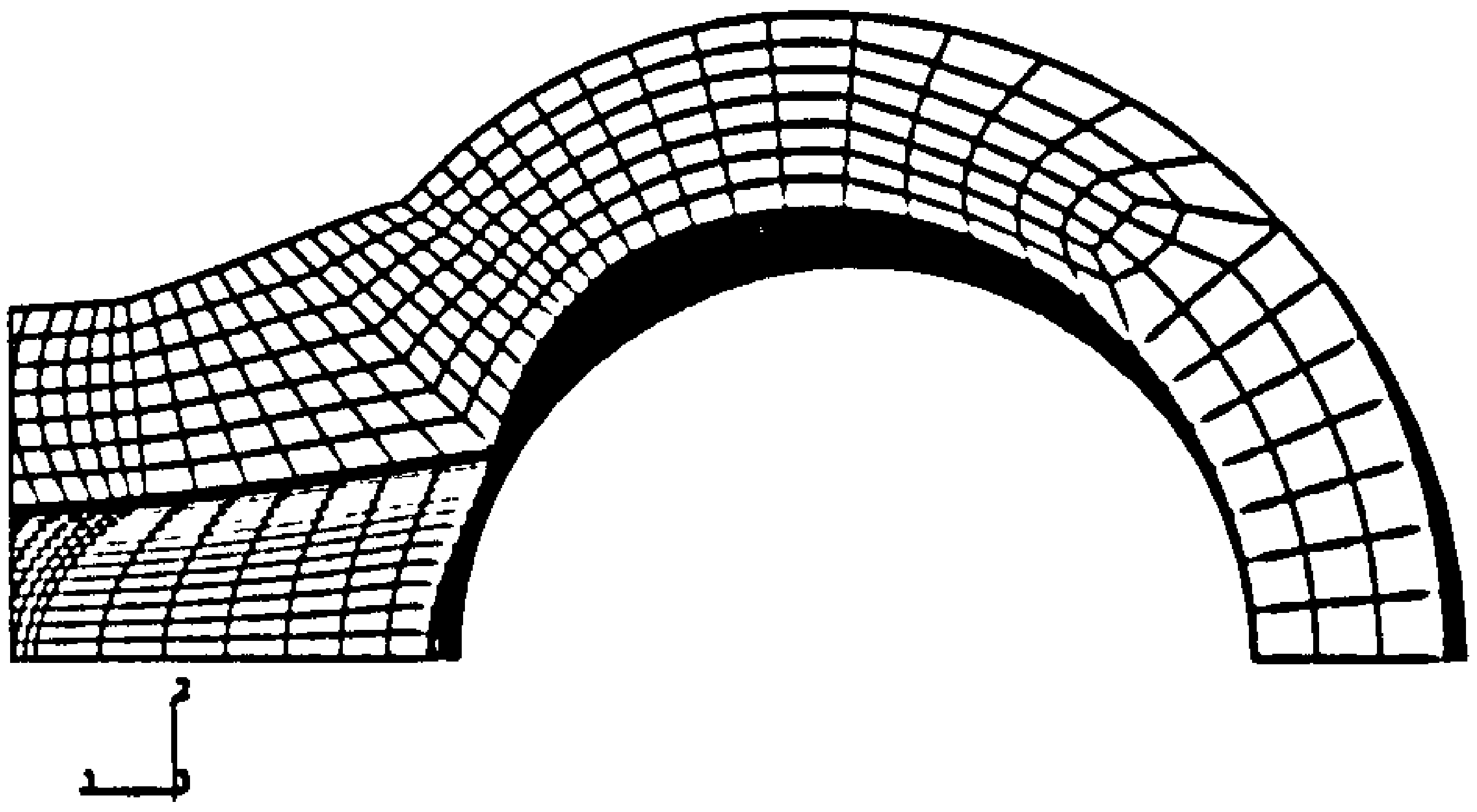

(d) d/D=0.5, D/T=5, t/T=1.0 - 139 MPa

Figure 3.2: Reversal of Displacement Parameters (n.b. displacements magnified)

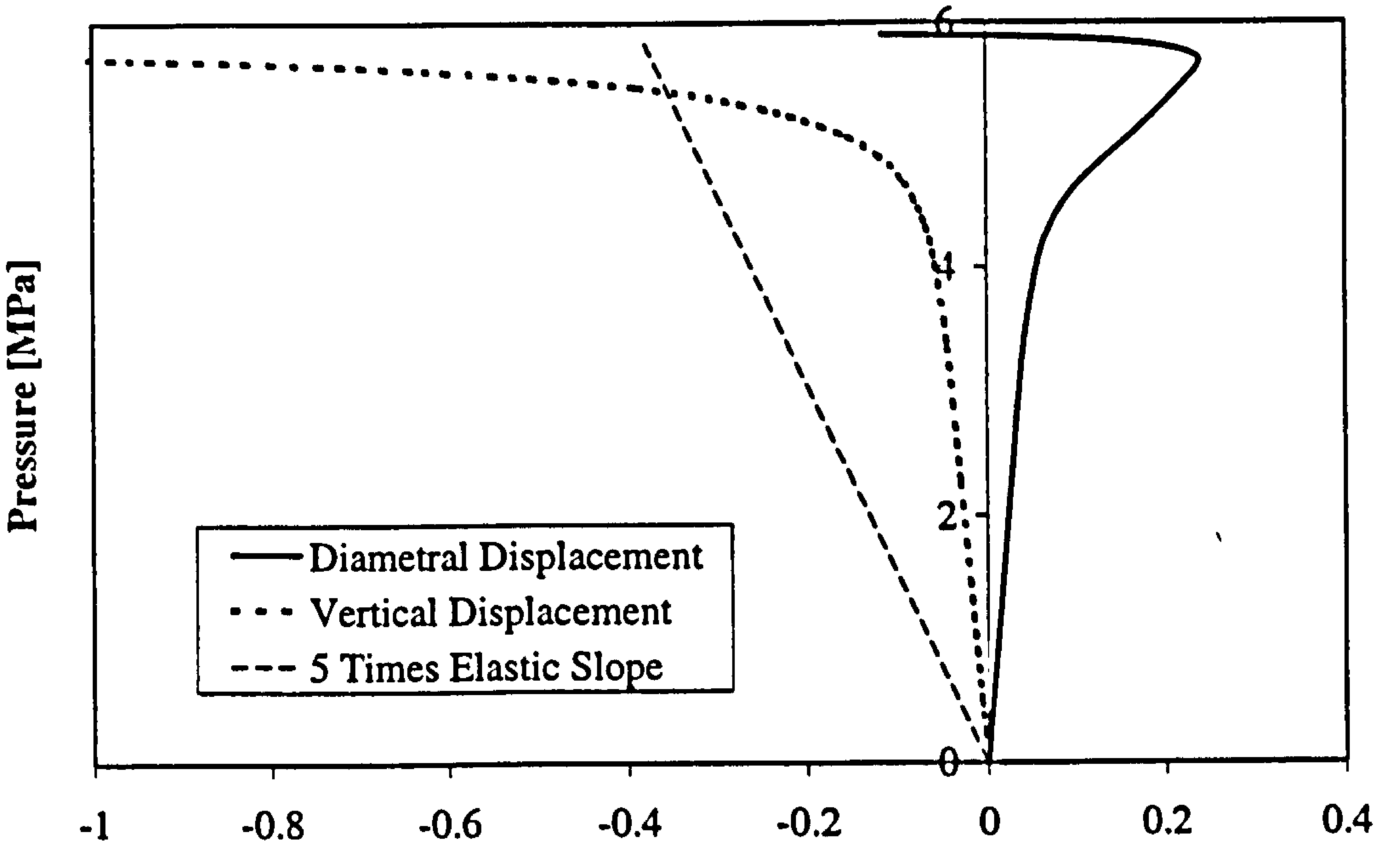

(a) d/D=0.5, D/T=70, t/T=1.0

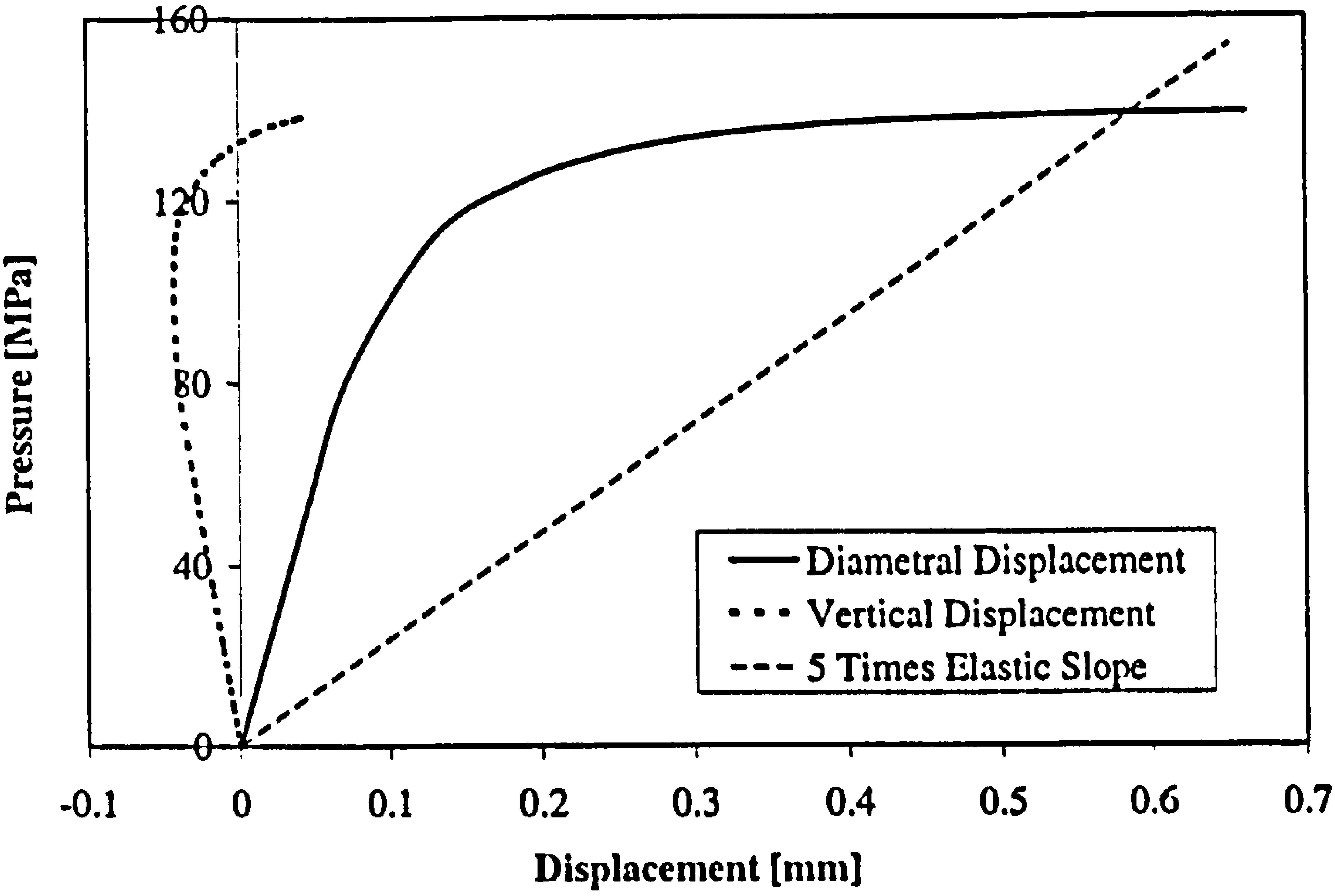

(b) d/D=0.5, D/T=5, t/T=1.0

Figure 3.3: Reversal of (a) Diametral Displacement and (b) Vertical Displacement

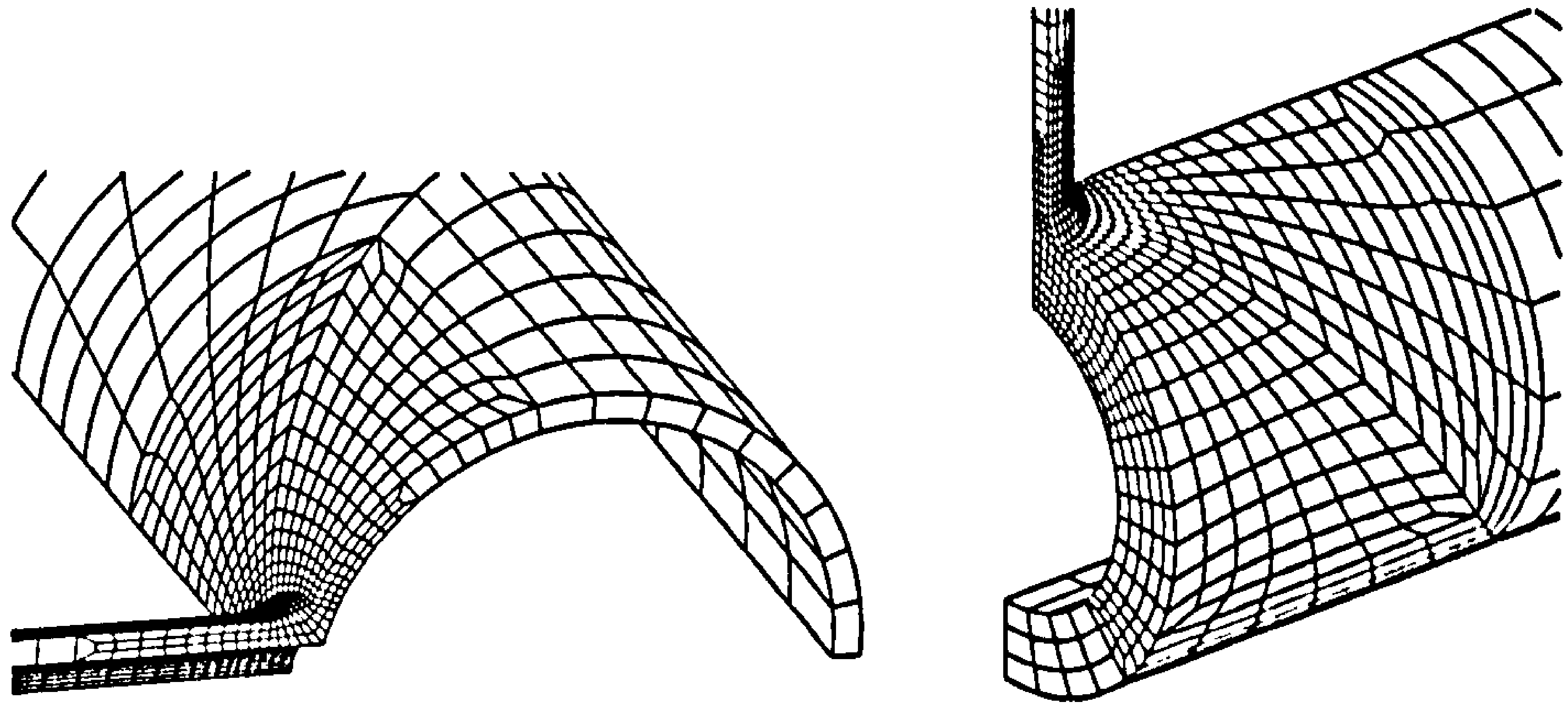

(a) d/D=0.25, D/T=20, t/T=1.0 (b) d/D=0.25, D/T=5, t/T=d/D

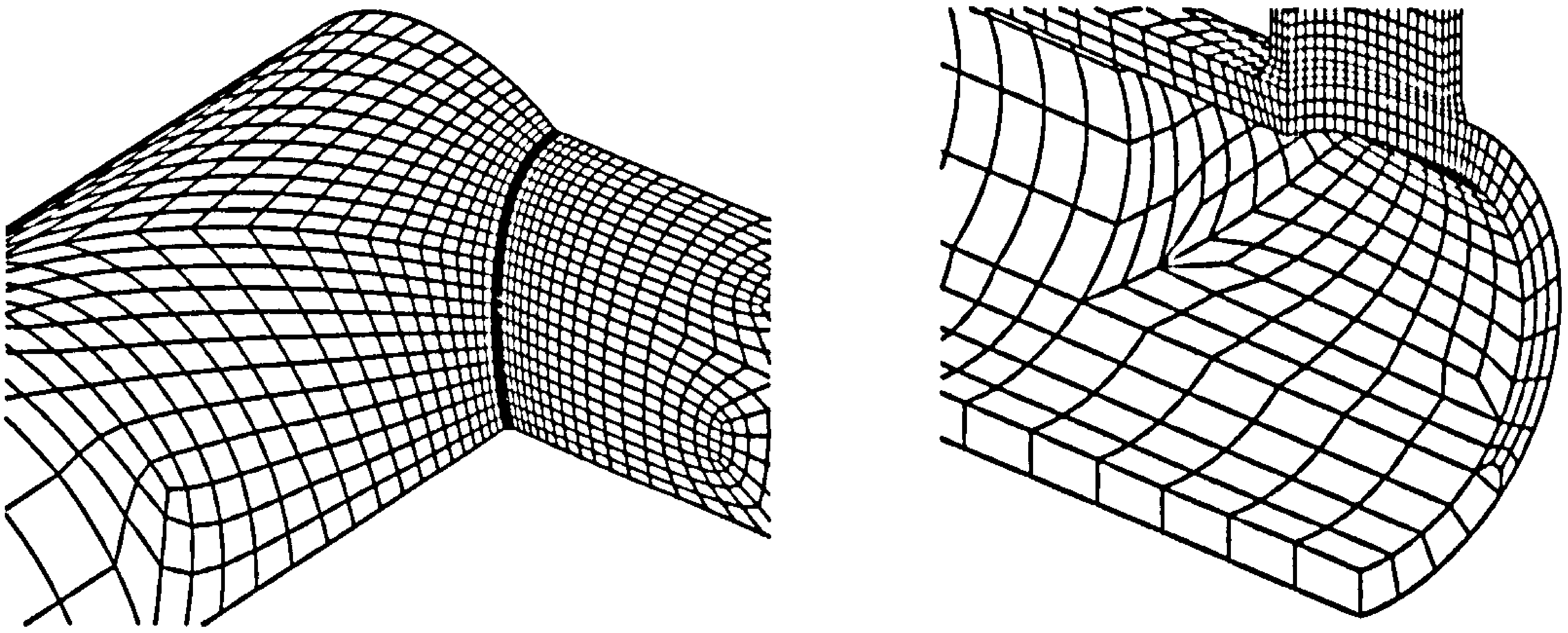

(c) d/D=0.75, D/T=70, t/T=1.0 (d) d/D=0.5, D/T=10, t/T=1.0

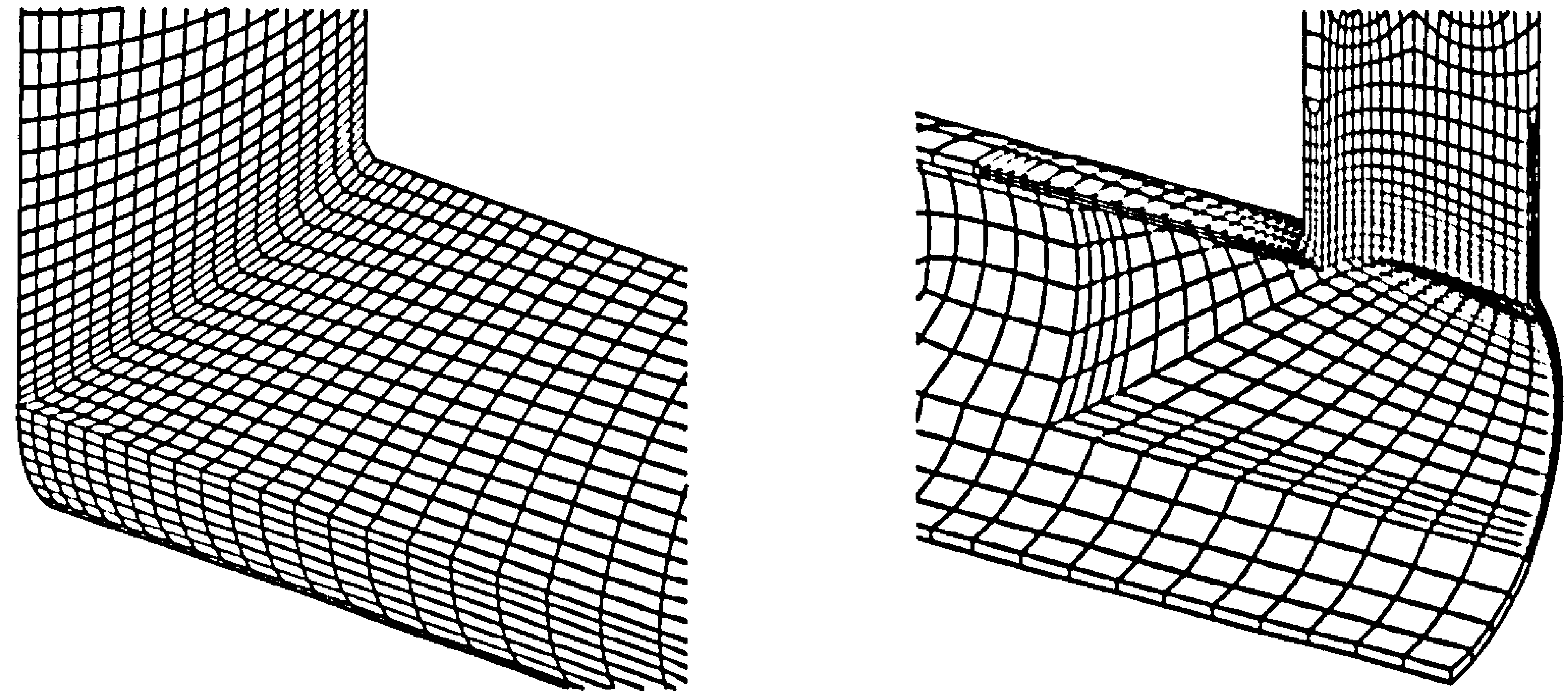

(e) d/D=1.0, D/T=30, t/T=d/D=1.0 (f) d/D=0.75, D/T=30, t/T=1.5

Figure 3.4: Typical FE Models for Parametric Study

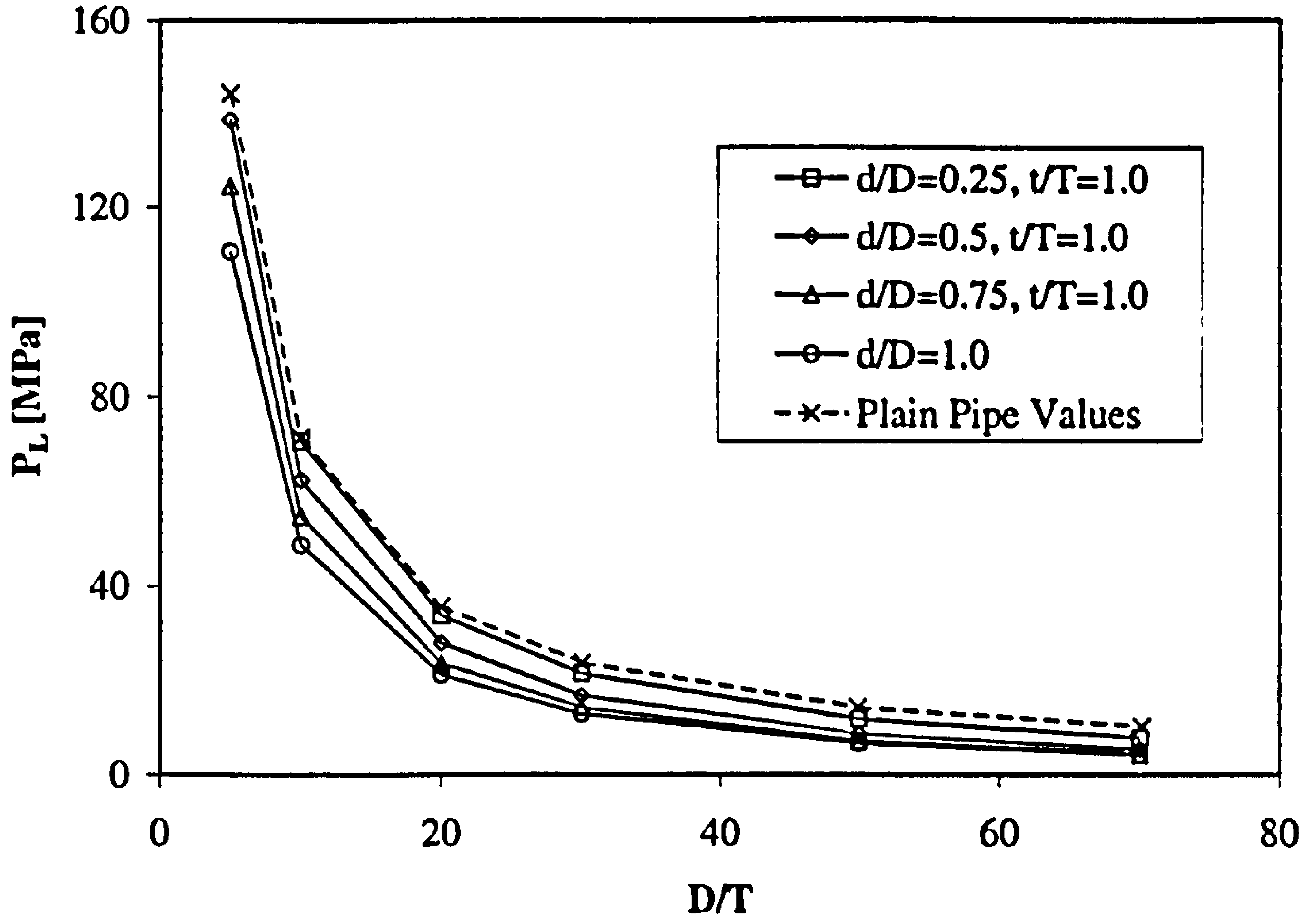

(a) Limit Pressure Results for t/T=1.0

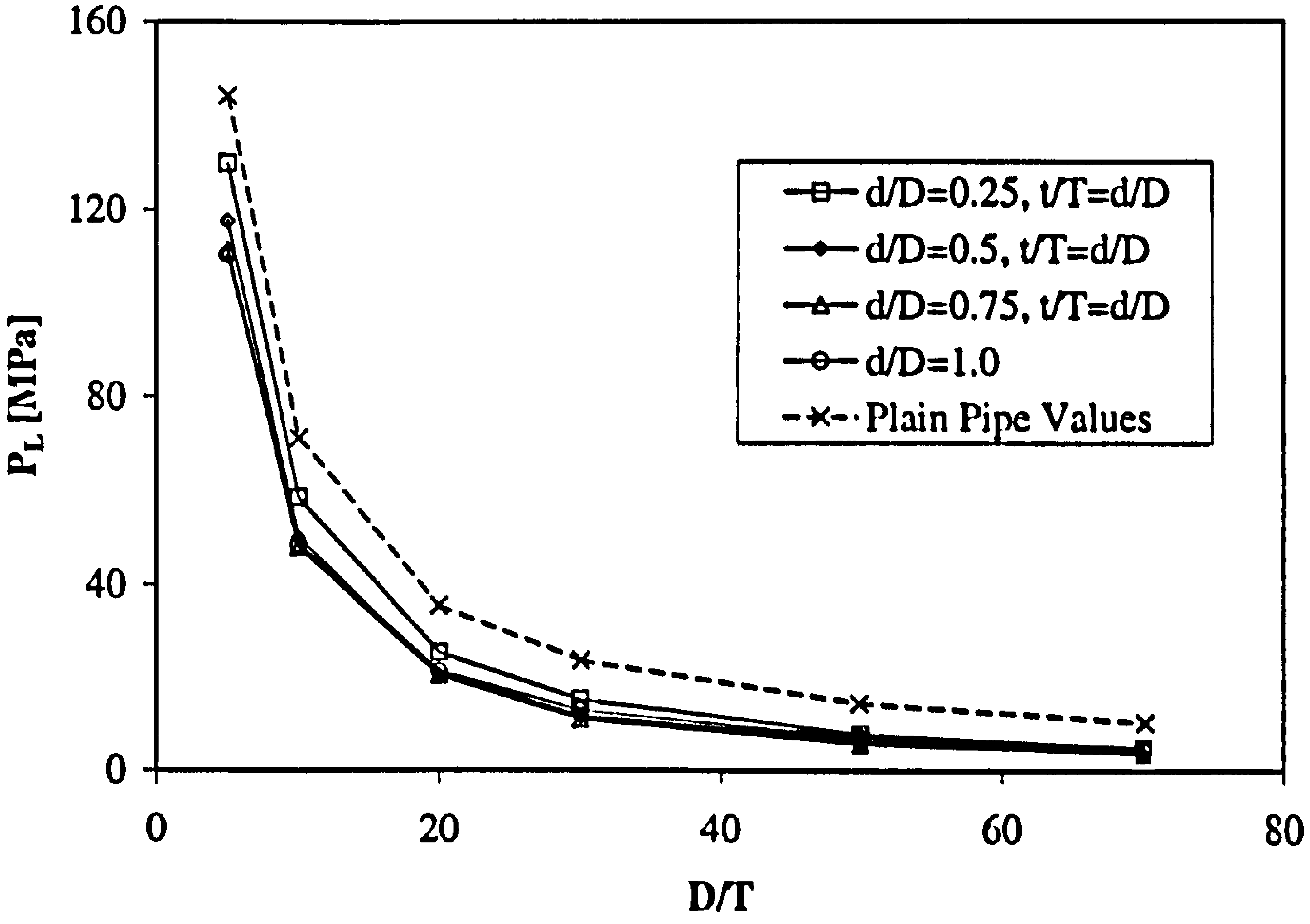

(b) Limit Pressure Results for t/T=d/D

Figure 3.5: Limit Pressure Results versus D/T

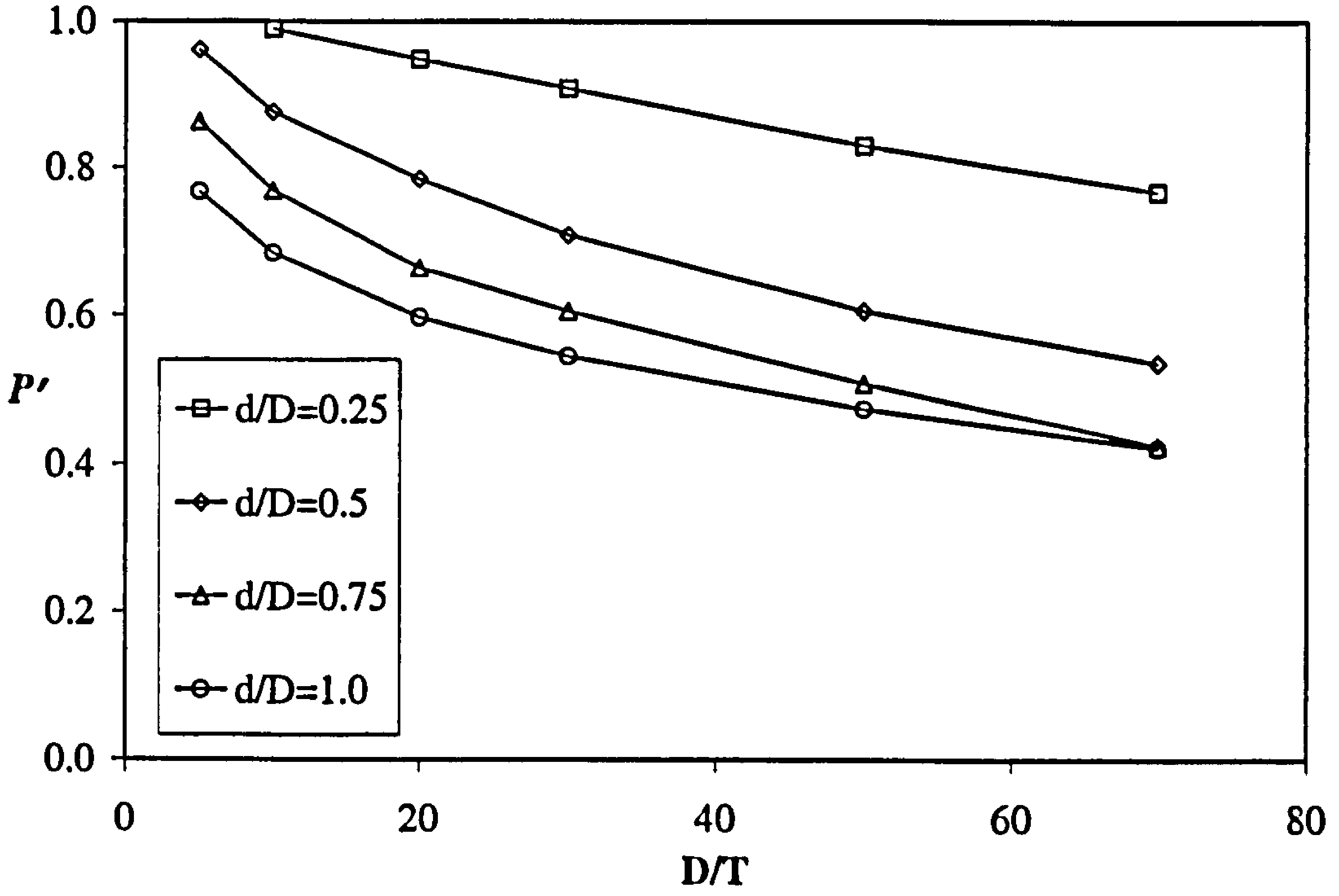

(a) t/T=1.0 Results plotted versus D/T

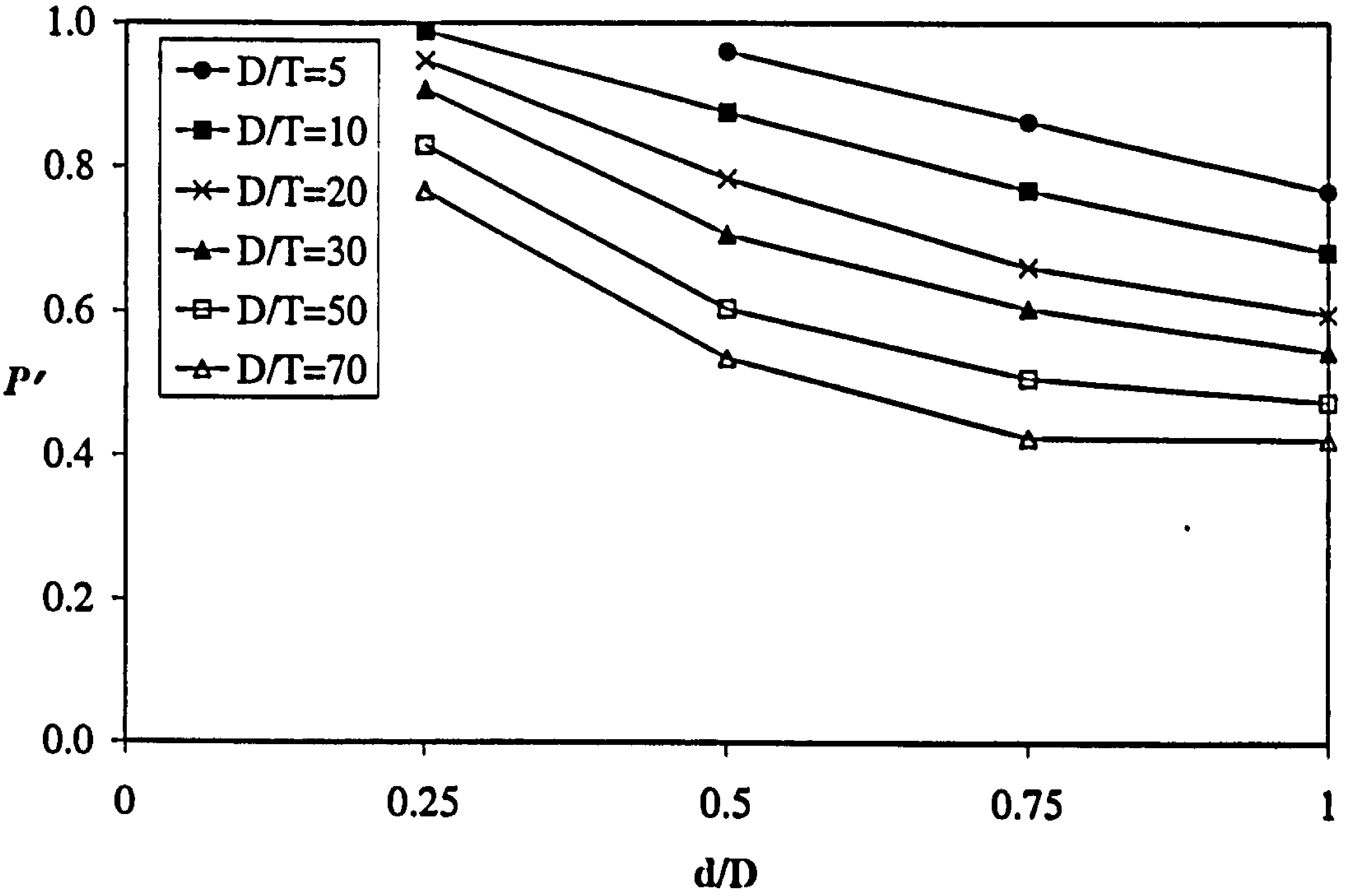

(b) t/T=1.0 Results plotted versus d/D

Figure 3.6: Normalised Limit Pressure Results for t/T=1.0

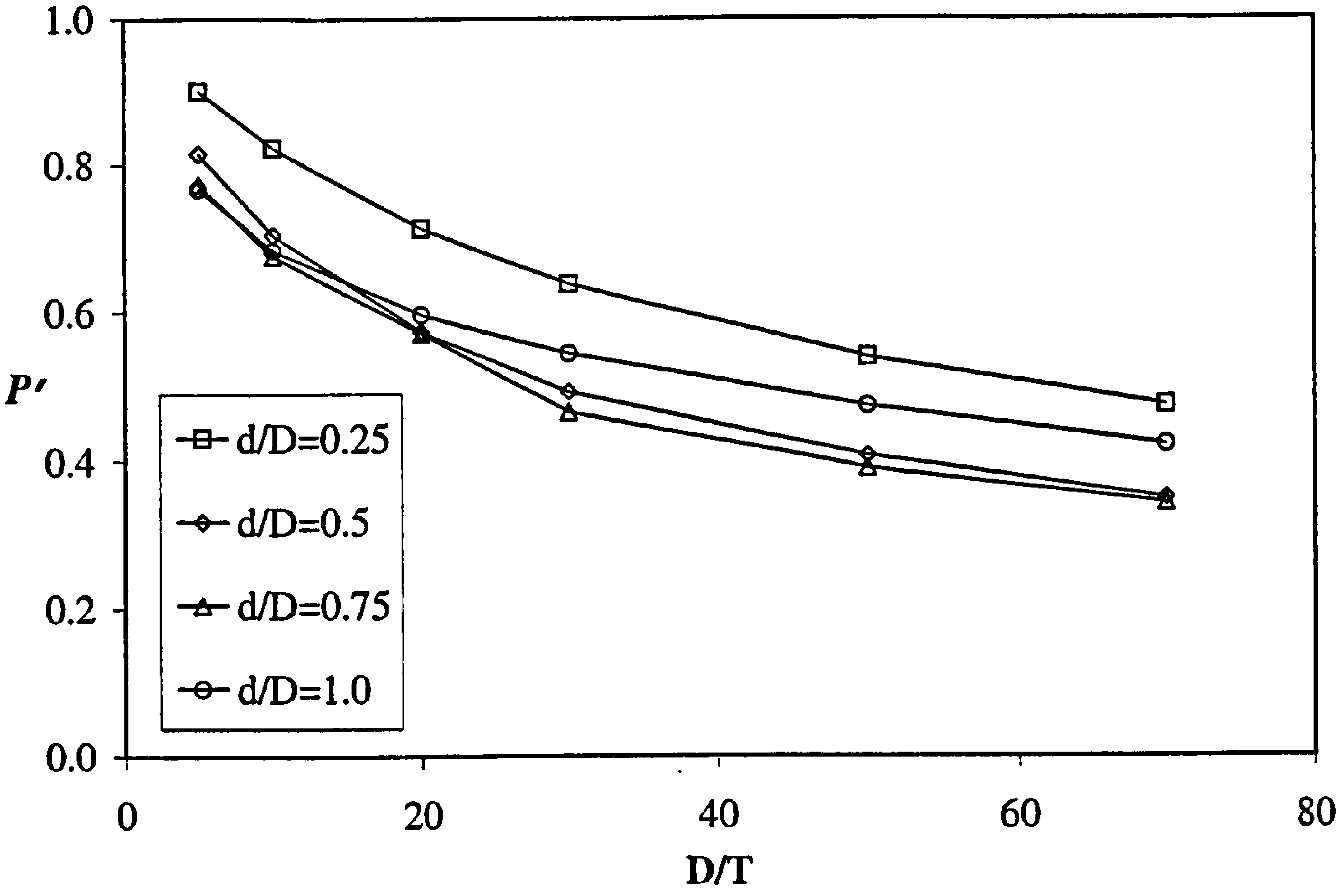

(a) t/T=d/D Results plotted versus D/T

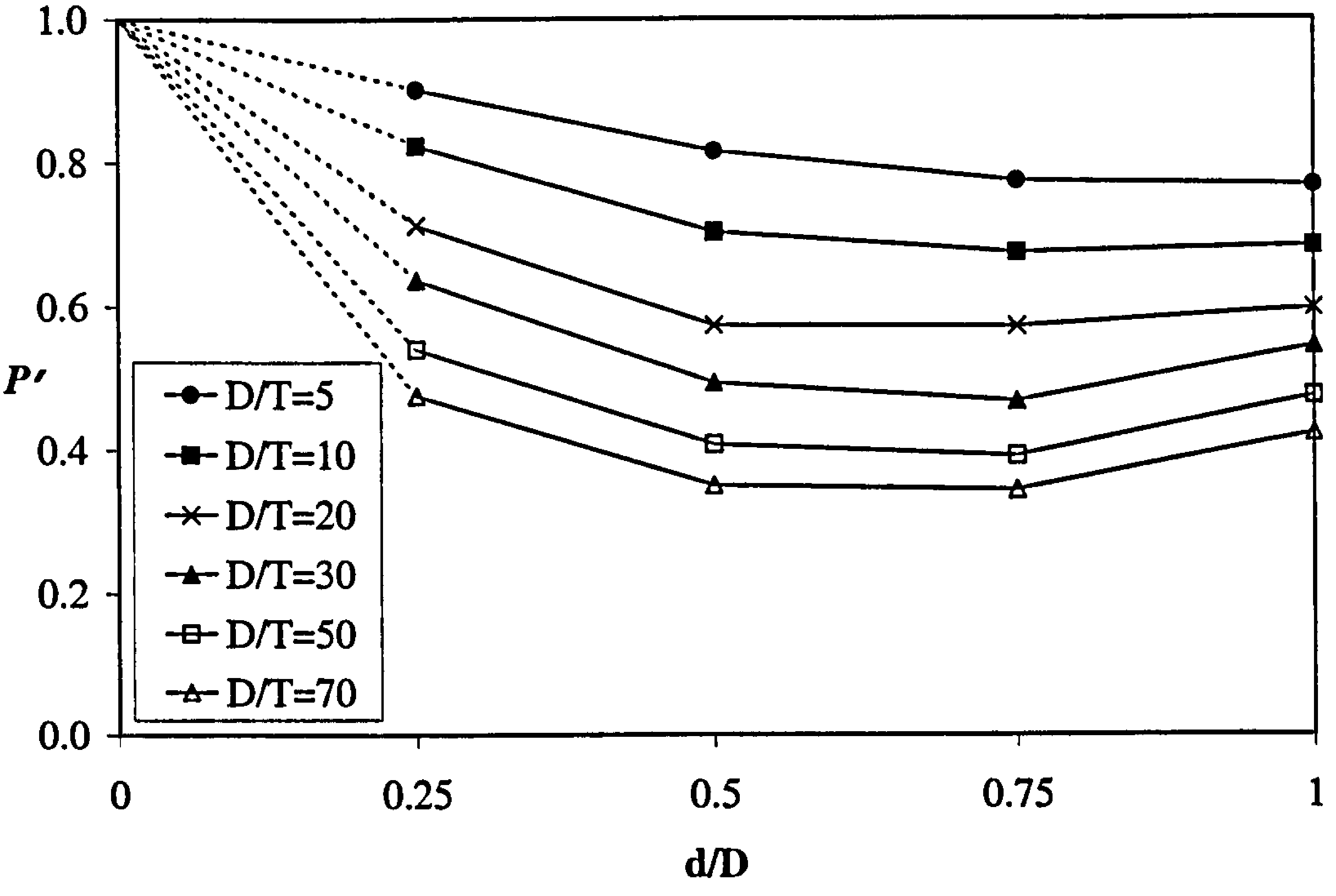

(b) t/T=d/D Results plotted versus d/D

Figure 3.7: Normalised Limit Pressure Results for t/T=d/D

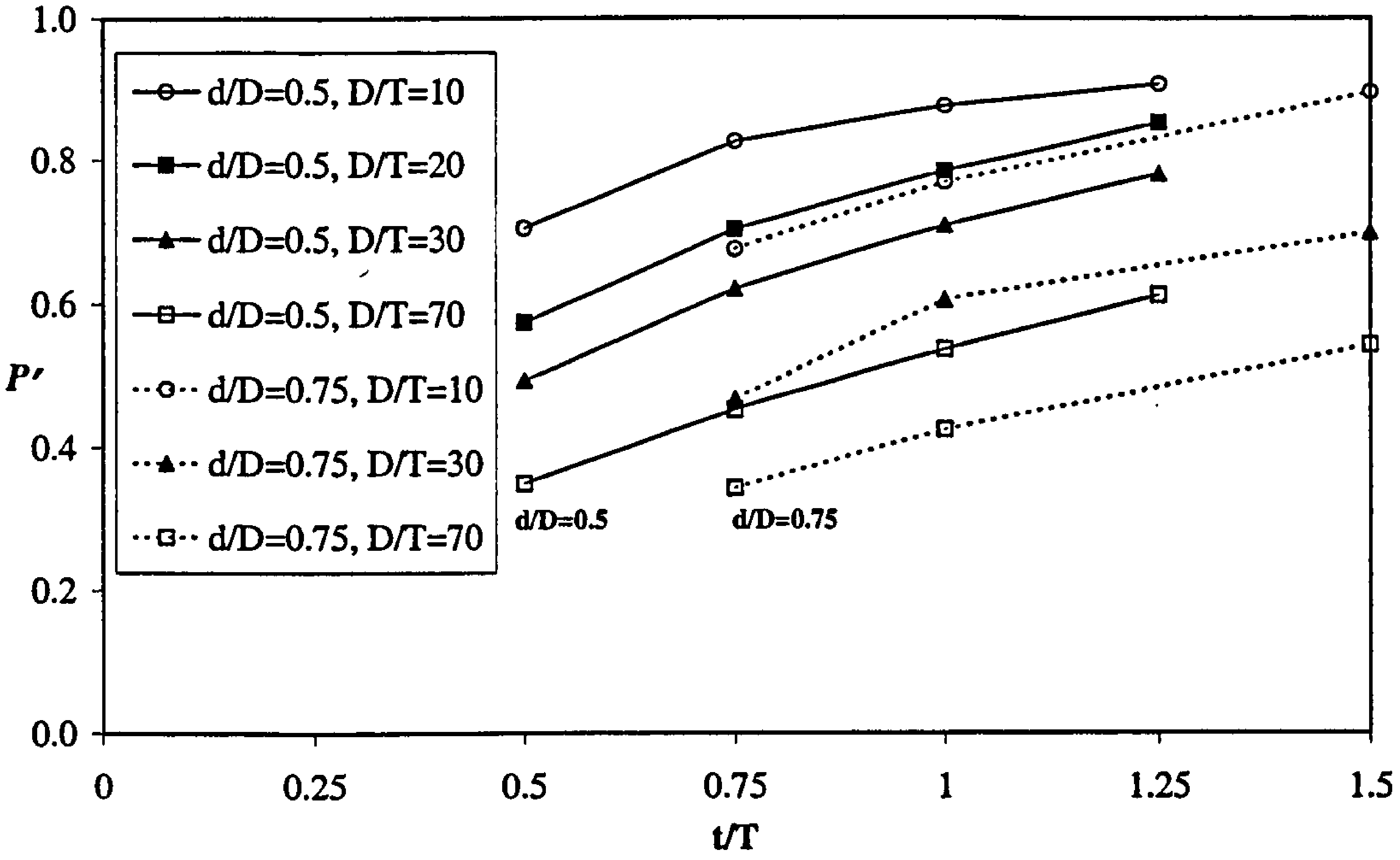

(a) Additional Cases

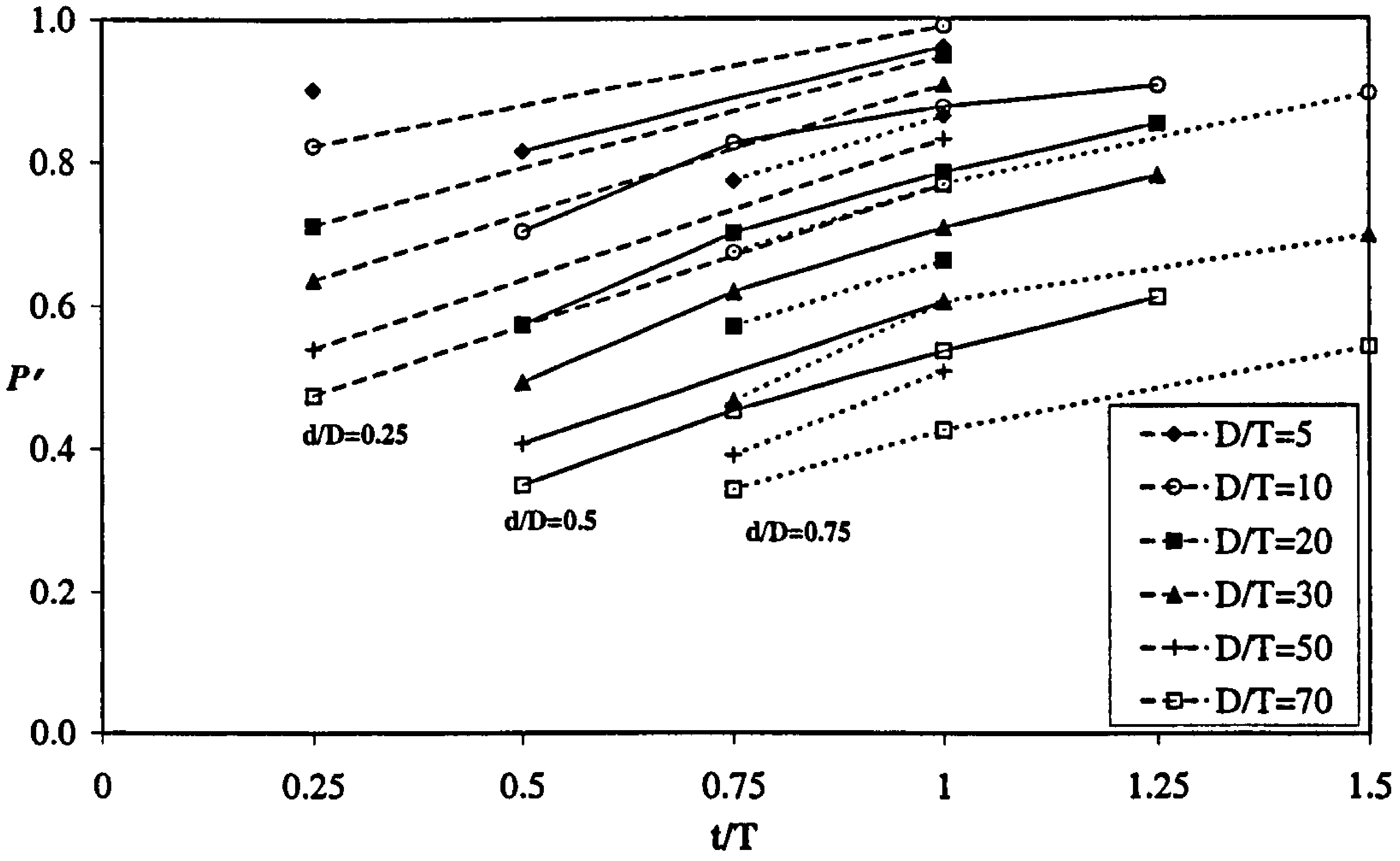

(b) All Cases

Figure 3.8: Normalised Limit Pressure Results versus t/T

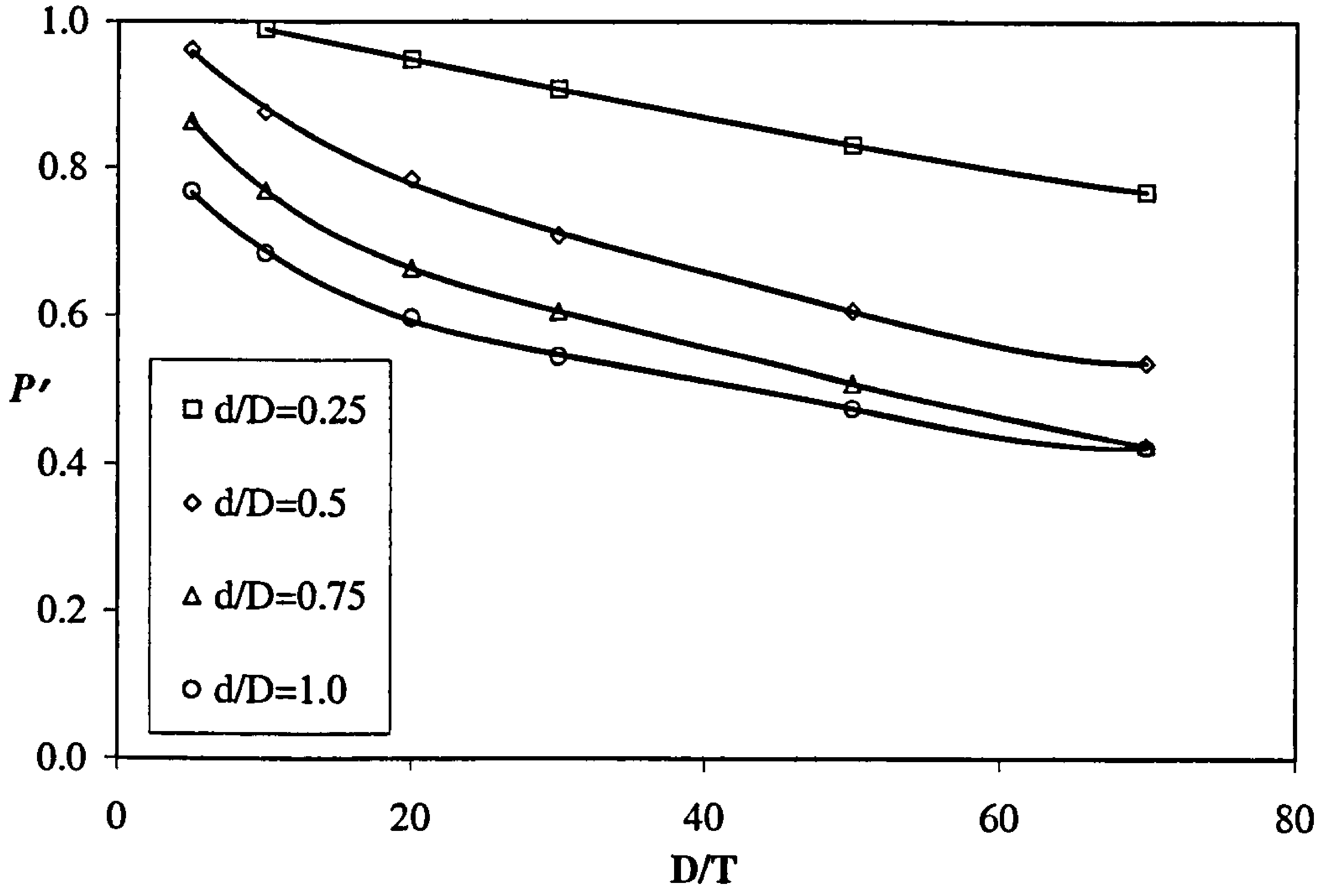

(a) t/T=1.0 Values

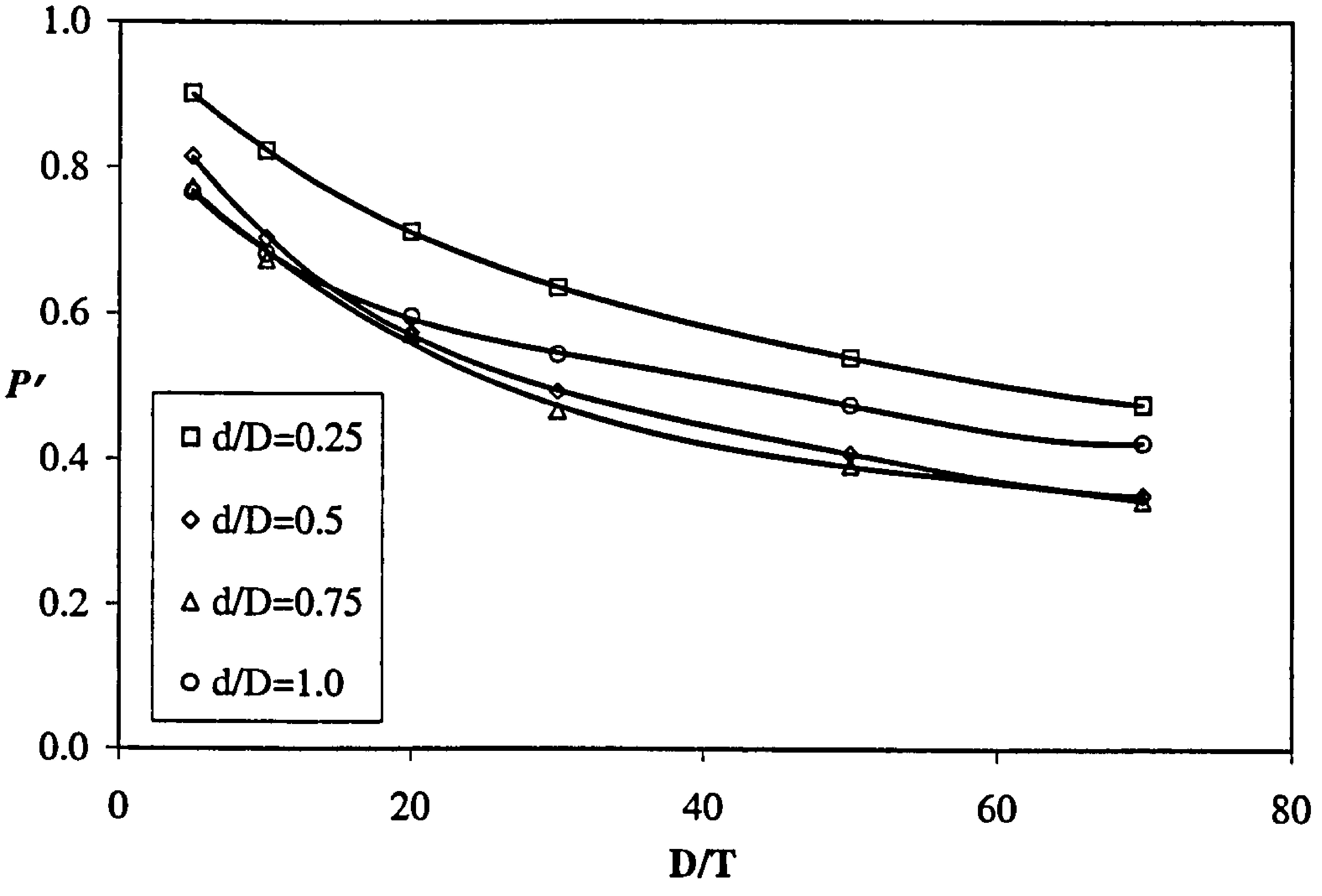

(b) t/T=d/D Values

Figure 3.9: Polynomial Curve Fitting to FE Results

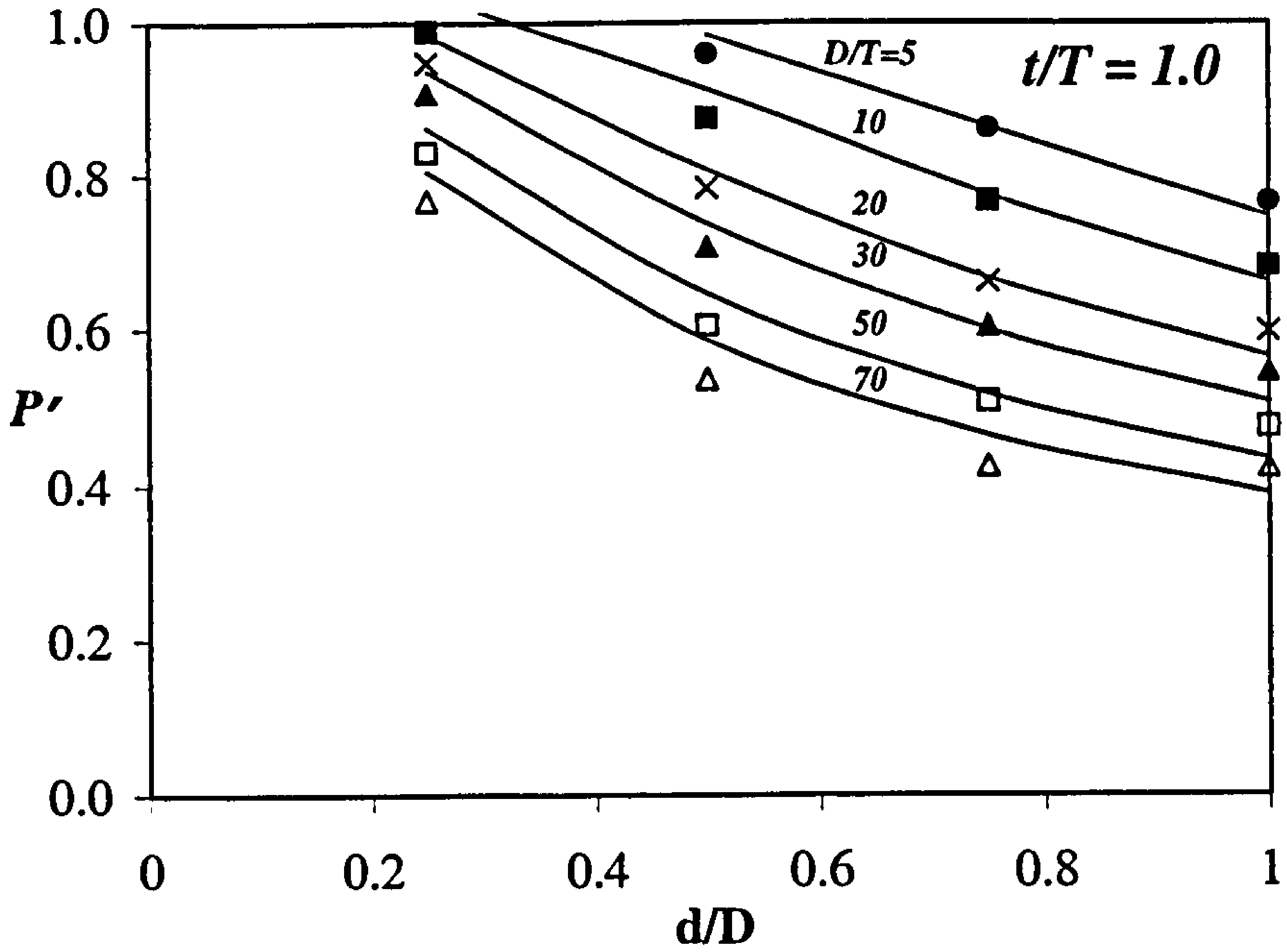

(a) t/T=1.0 Values

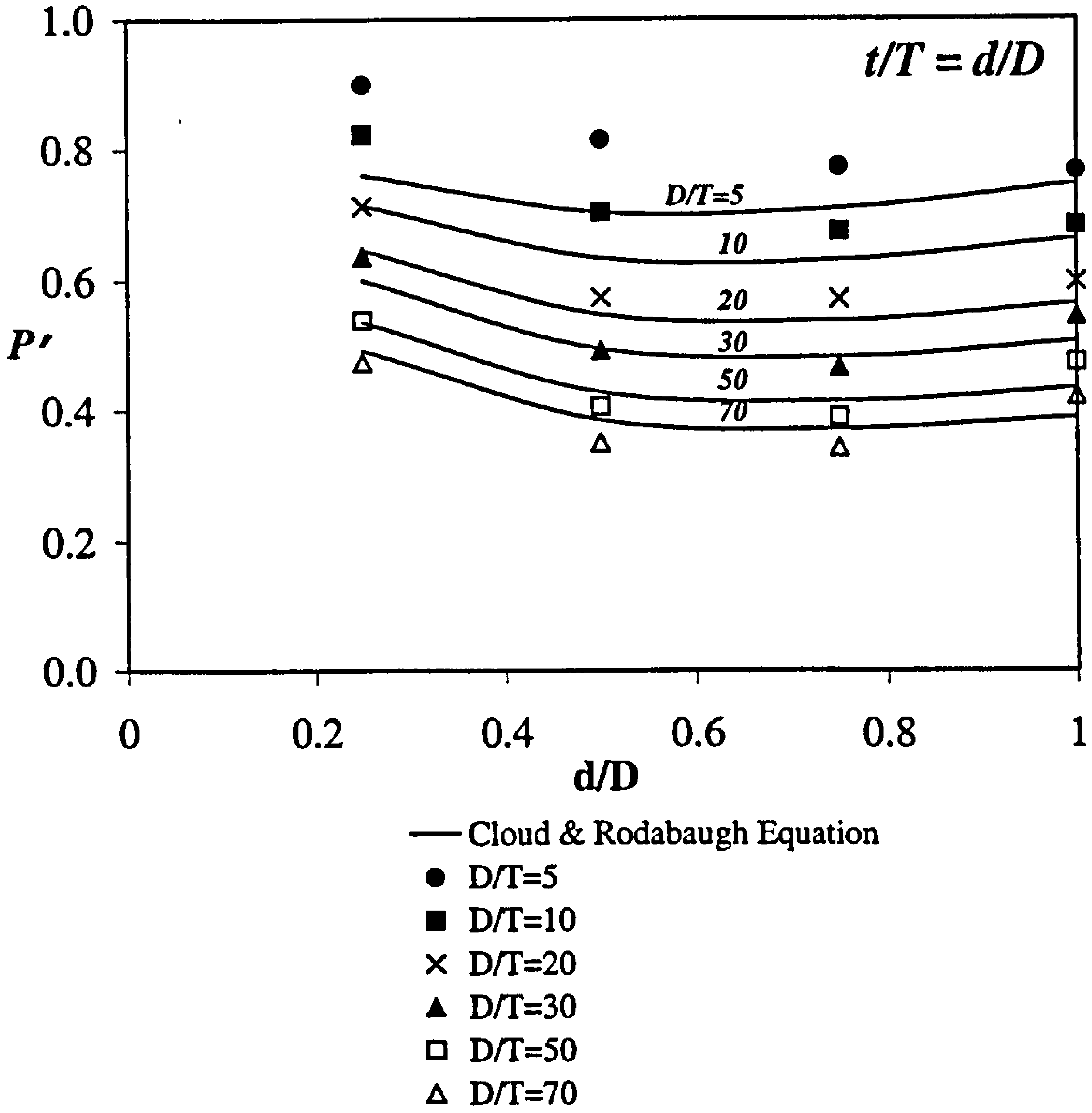

(b) t/T=d/D Values

Figure 3.10: Comparison of Cloud and Rodabaugh Equation with FE Results

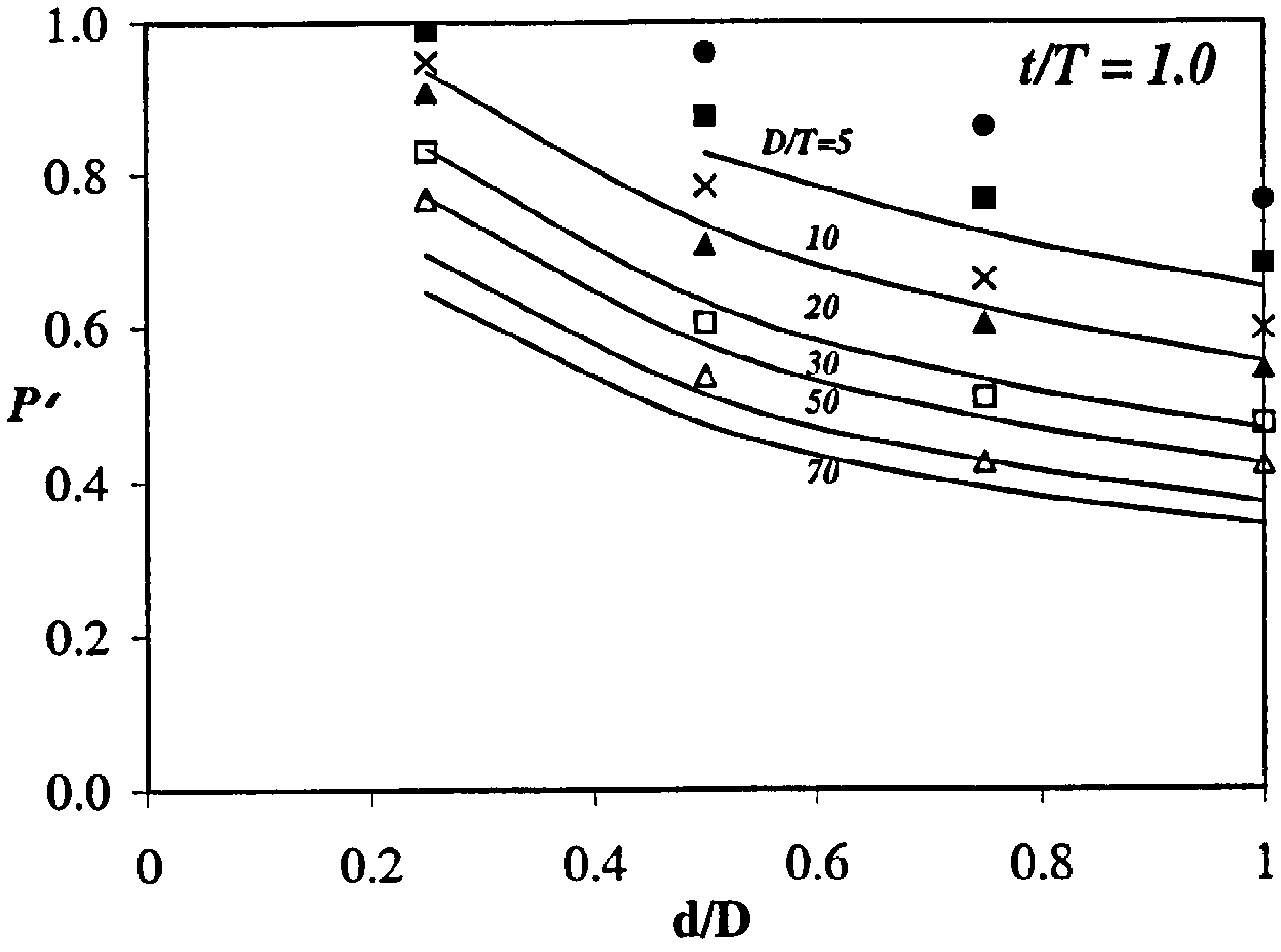

(a) t/T=1.0 Values

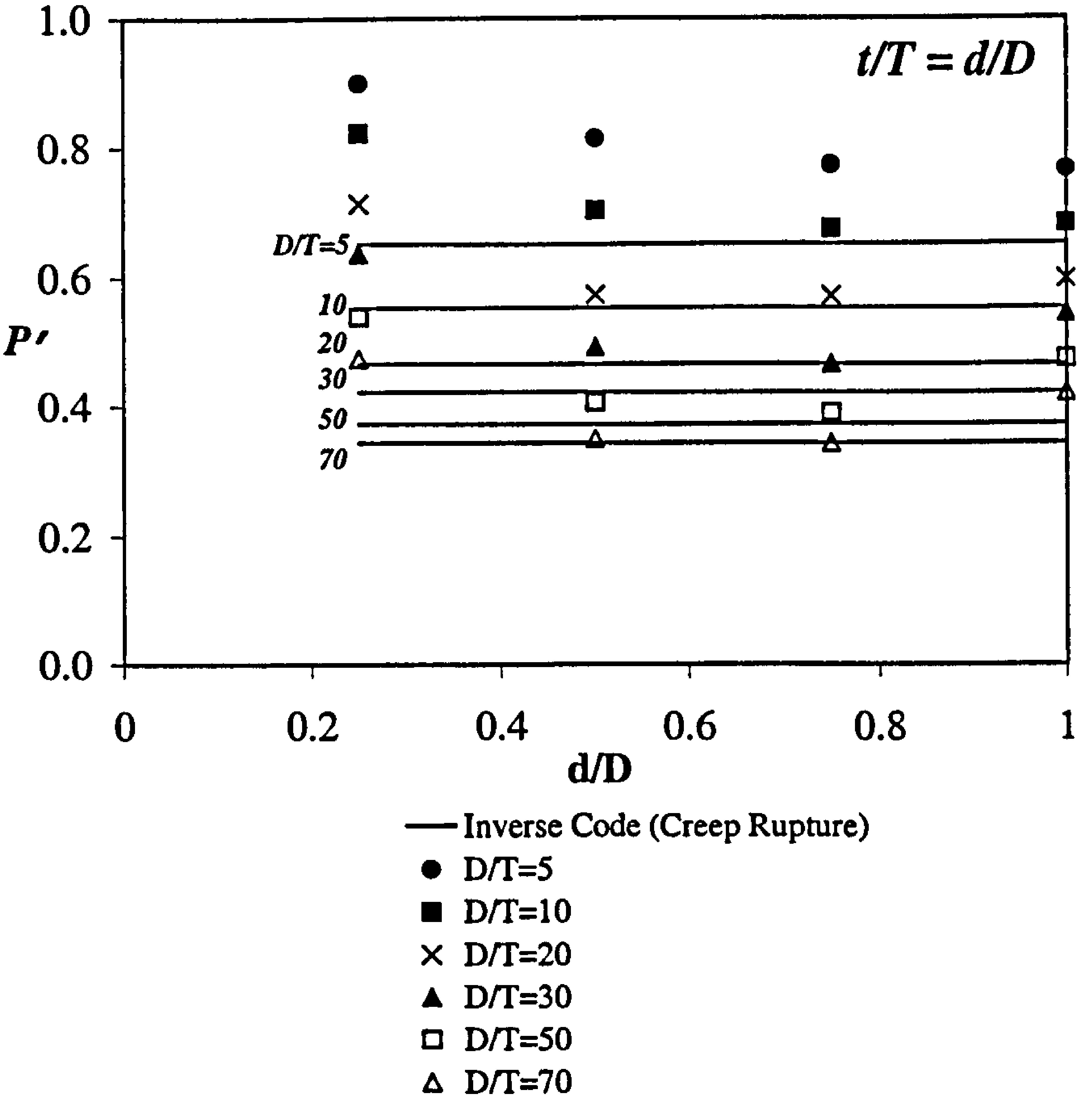

(b) t/T=d/D Values

Figure 3.11: Inverse Code Creep Rupture Pressure - Comparison with FE Results

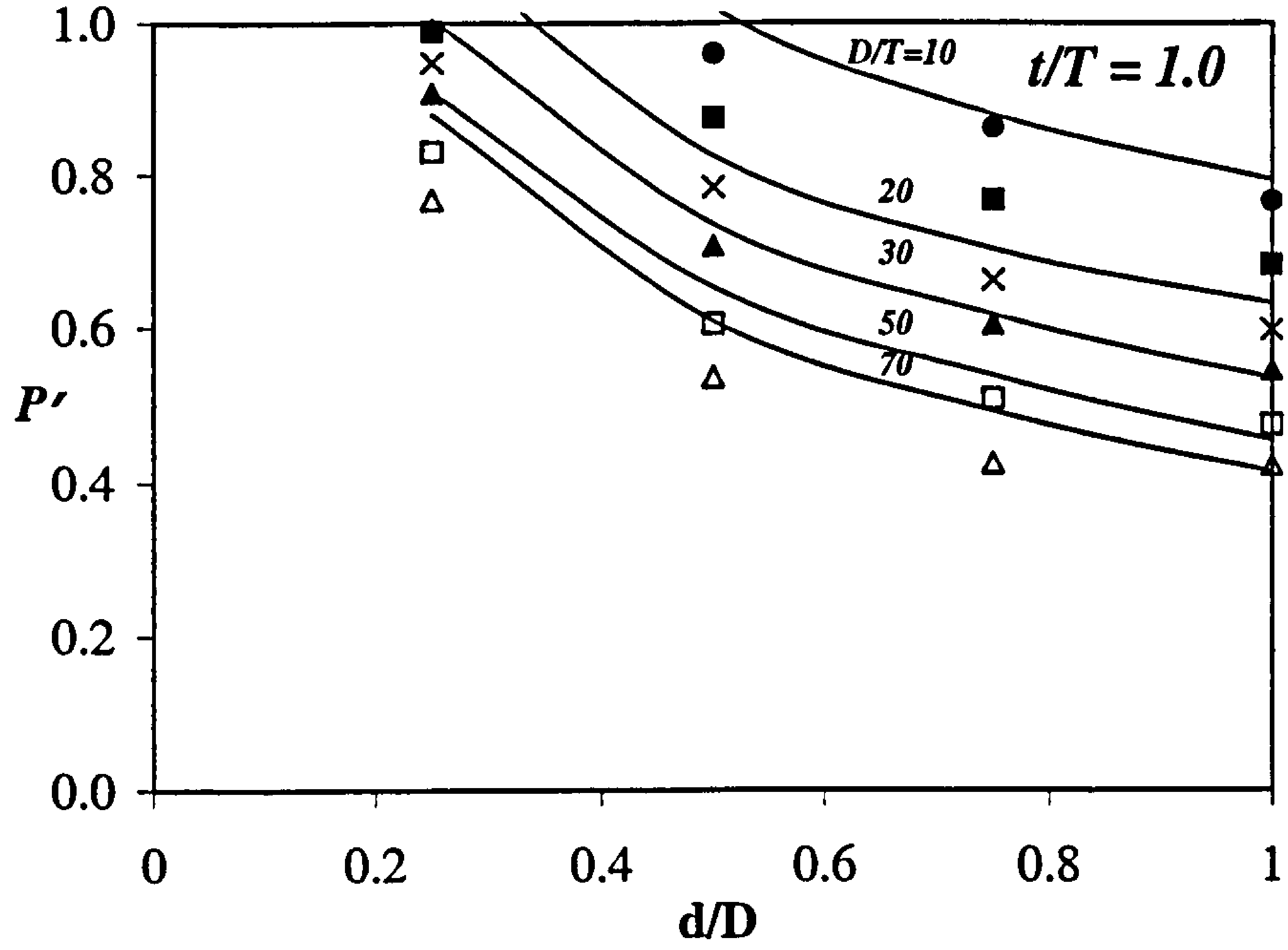

(a) t/T=1.0 Values

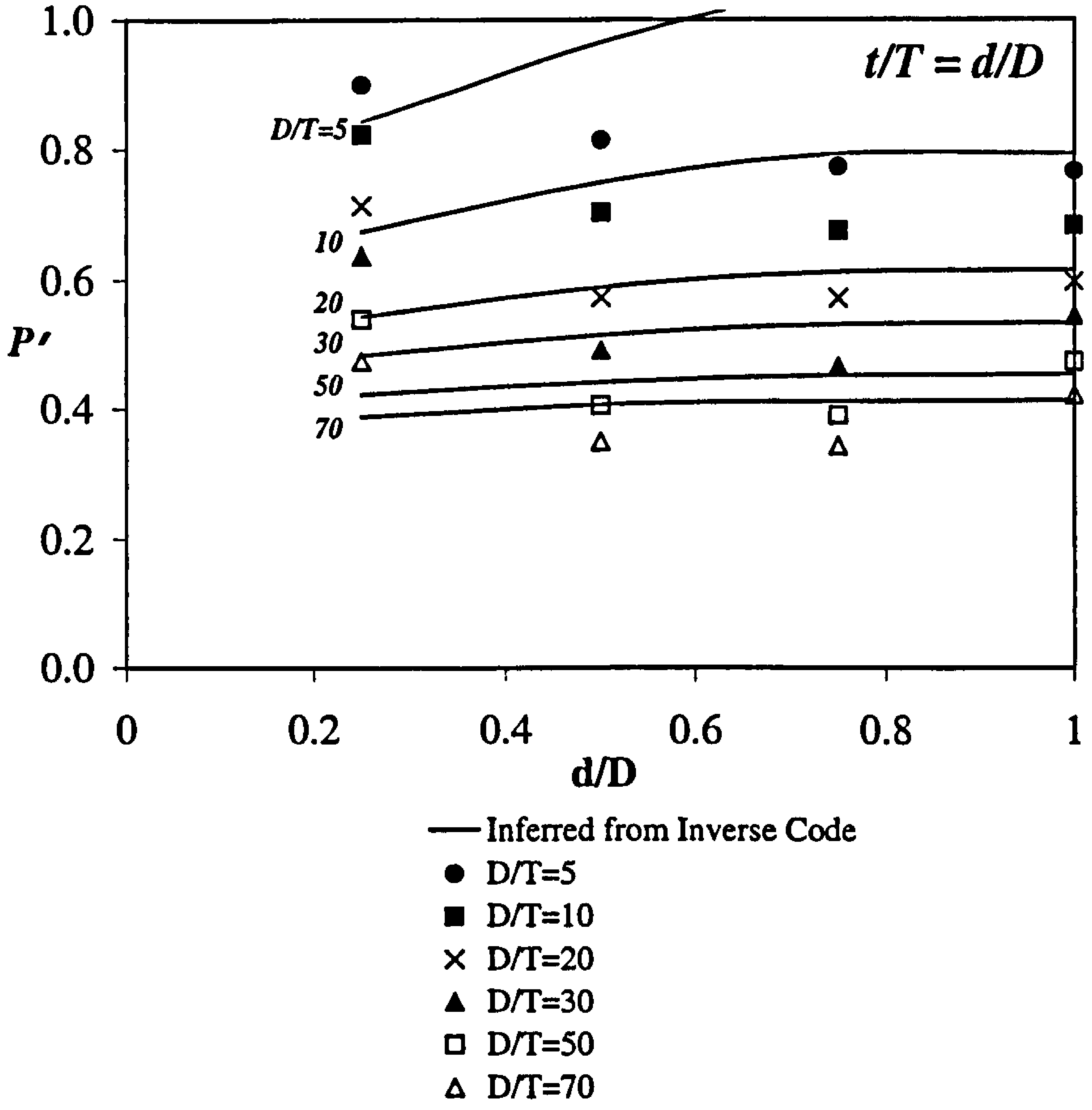

(b) t/T=d/D Values

Figure 3.12: Inferred Inverse Code Method - Comparison with FE Results

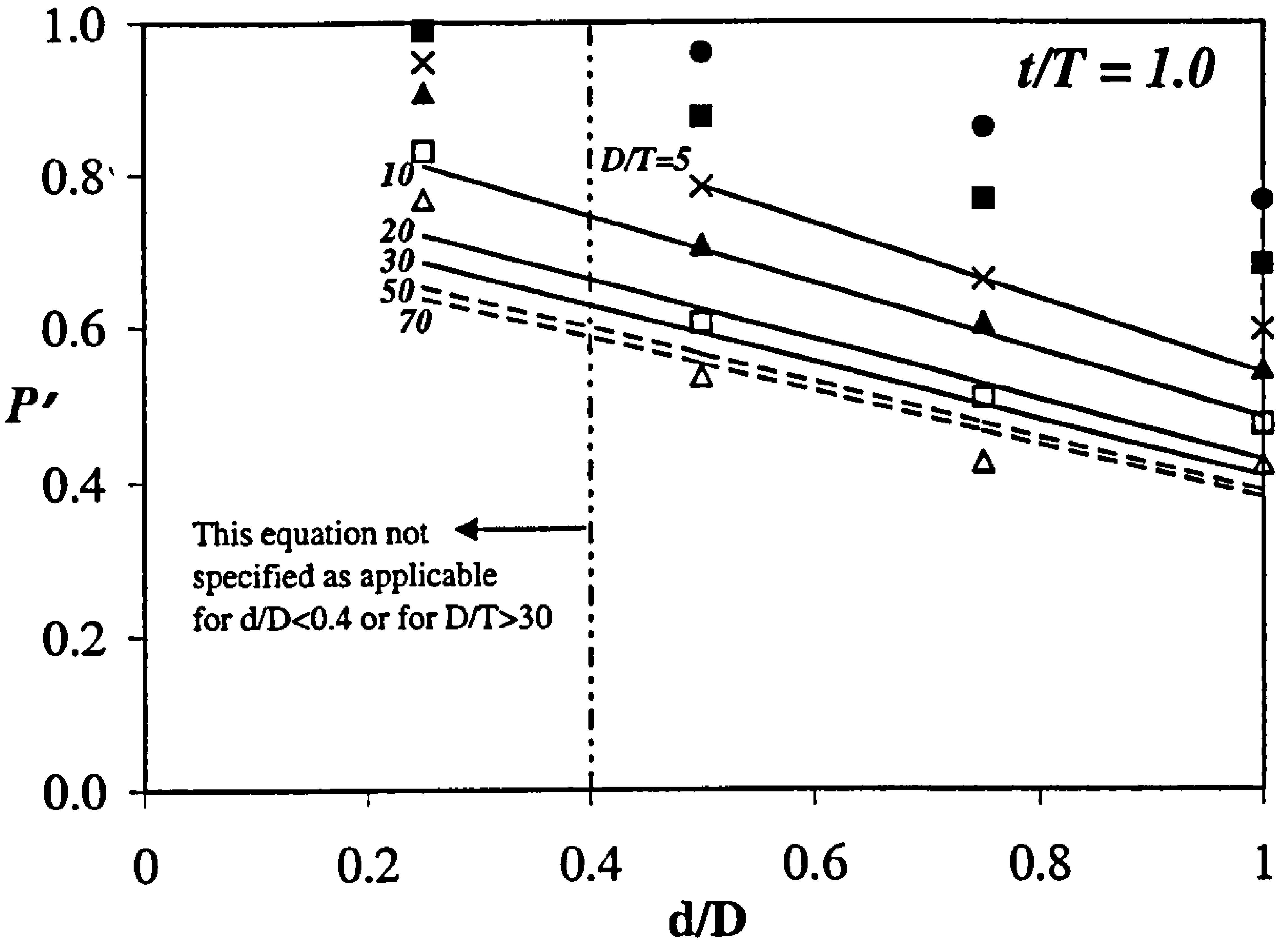

(a) t/T=1.0 Values

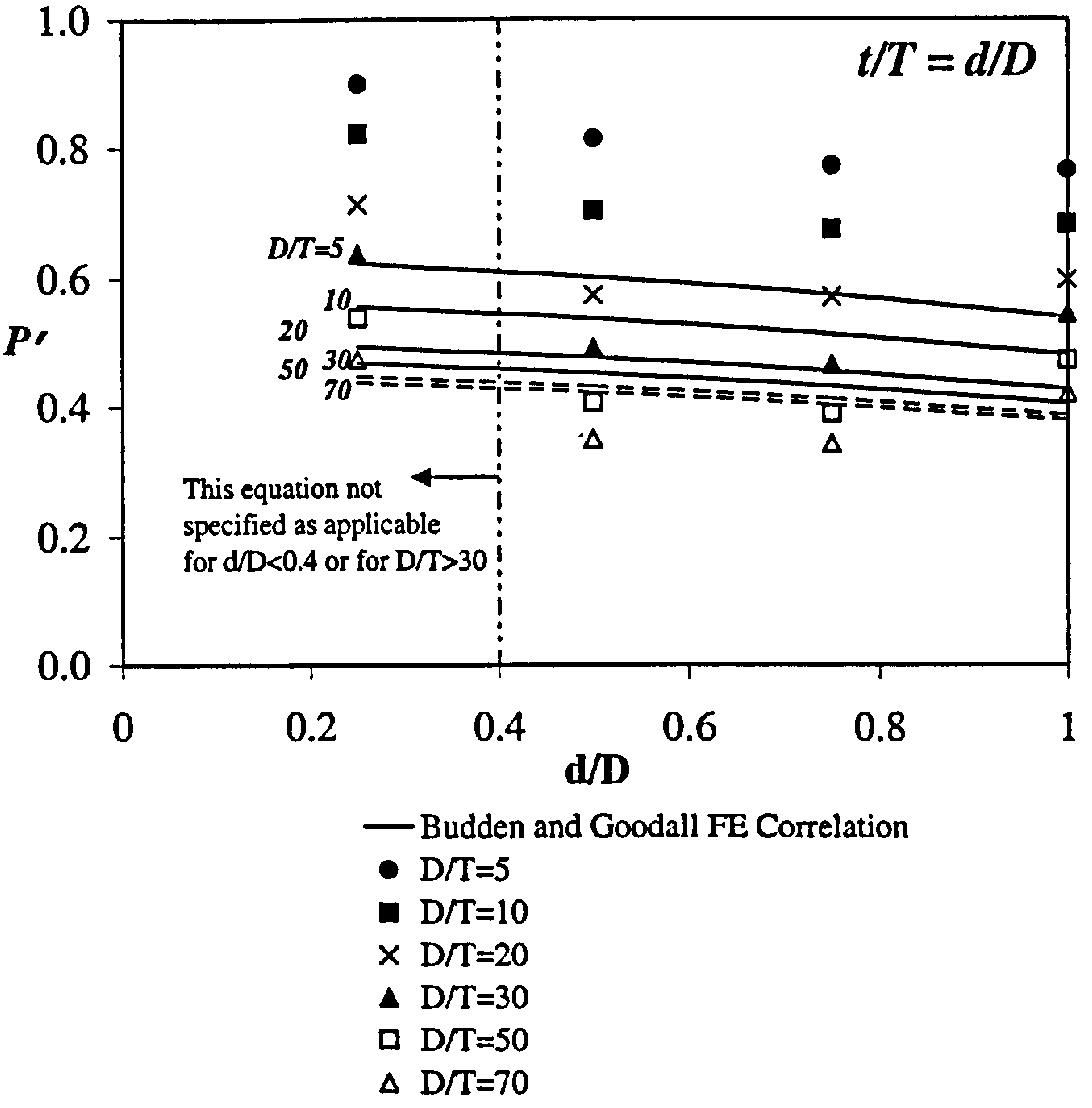

(b) t/T=d/D Values

Figure 3.13: Budden and Goodall FE Correlation - Comparison with FE Results

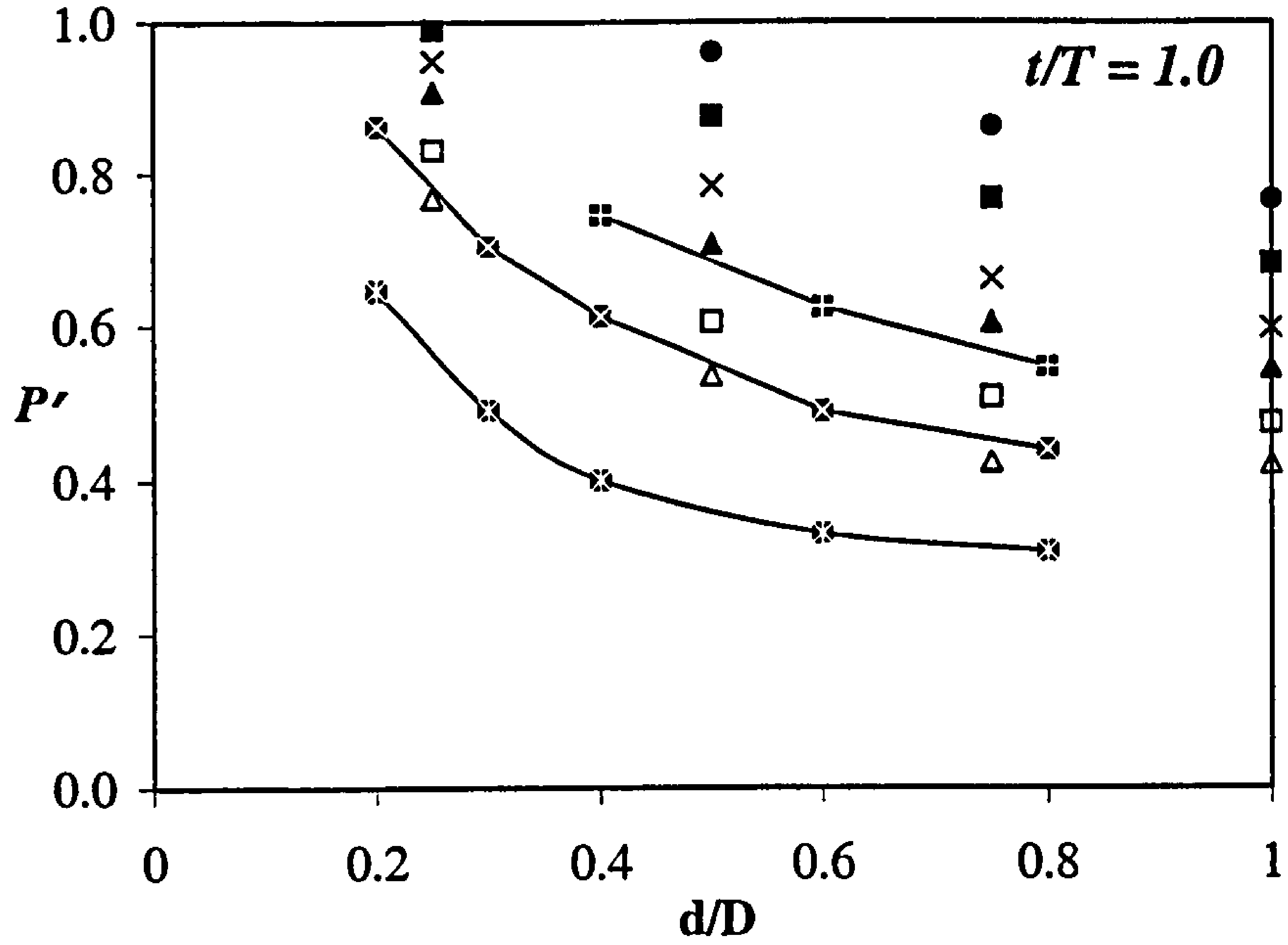

(a) t/T=1.0 Values

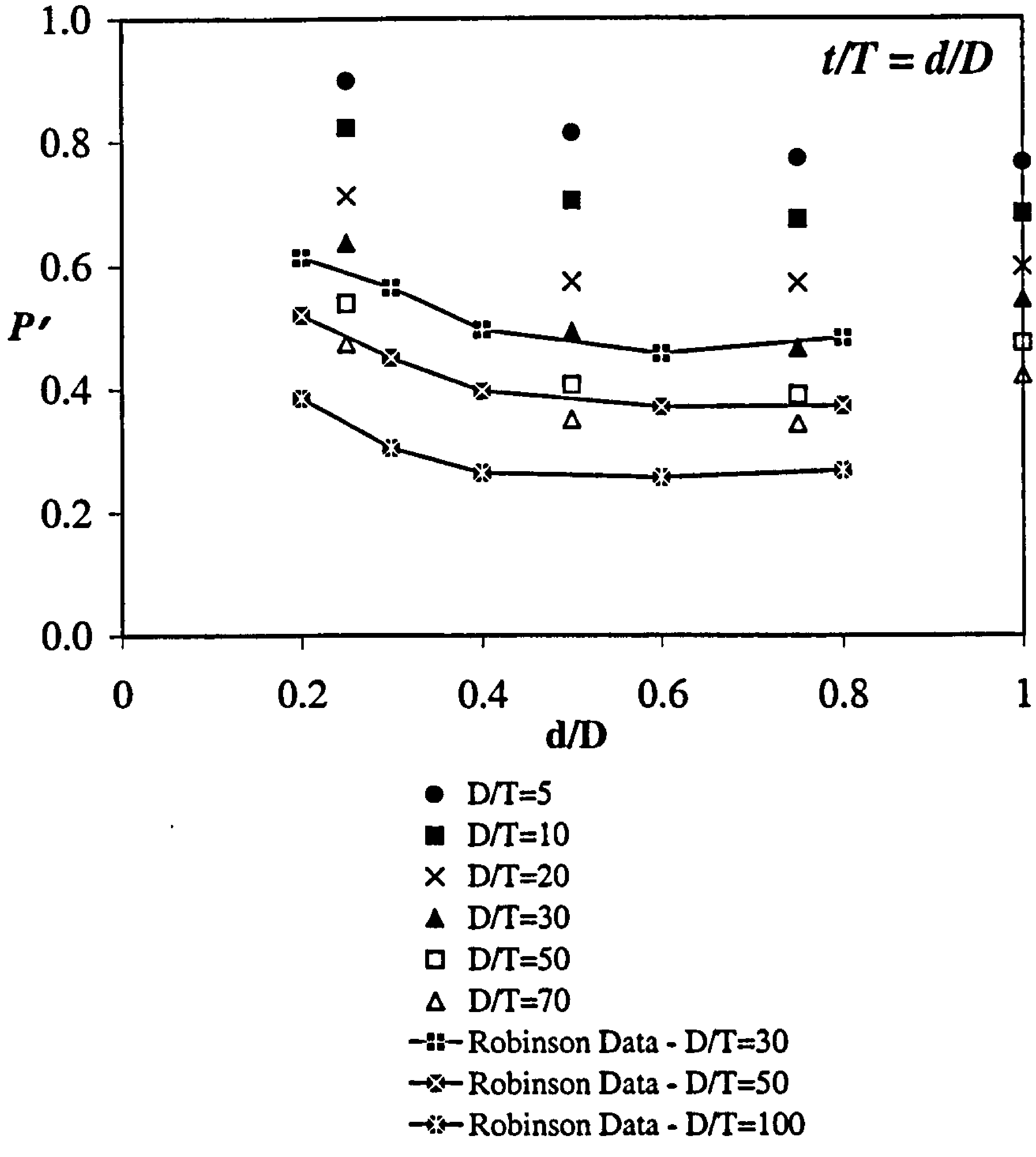

(b) t/T=d/D Values

Figure 3.14: Robinson Parametric Study Results - Comparison with FE Results

Chapter 4

Cracked Branch Junctions: Finite Element Parametric Study

4.1 Introduction

This Chapter presents a FE parametric study of limit loads for cracked piping branch junctions. The main loads considered are internal pressure, in-plane branch pipe bending and out-of-plane branch pipe bending. Results for single applications and combinations of these loads are presented for a range of junctions. The dimensional parameters studied were:

- d/D = 0.5, 0.75, 0.95
- D/T = 10, 20, 30
- t/T = 1.0
- Crack angle (length)
- a/t = 0.5, 0.75, 1.0

4.1.1 Crack Locations Studied

There are numerous possible crack locations for branch junctions, depending upon the loads applied, as explained in Chapter 1. However, it was not feasible for this study to cover in detail every combination described. Instead, the study gives a detailed assessment of the effects of cracks running around junction intersections, along the lower weld toe. This type of crack is common for out-of-plane branch pipe bending, pressure loading and in-plane branch pipe bending.

Out-of-plane Branch Pipe Bending

Out-of-plane branch bending was chosen as it is known to be the most severe of the six moment categories (see [8]). The peak elastic stress location for out-of-plane bending is at the lower weld toe on the flank of the junction, and so the cracks were centred about this location. A typical cracked junction (d/D=0.5) for out-of-plane bending is shown schematically in Figure 4.1(a), with the crack size defined by the angle 2α. The cracks were projected normally from the weld toe onto the inner surface of the run pipe, as shown in Figure 4.1(b).

Internal Pressure

Pressure loading produces peak elastic stresses at the crotch corner, but the flank of the junction is also typically a high stress location. This is known to be a location where pressure fatigue cracks occur [9], especially for larger branches (d/D $\geq$ 0.5). For this reason, the FE models used for out-of-plane bending were also subjected to pressure loading, both as a single load and in addition to the bending load (the loading techniques are described in Section 4.2.4).

In-plane Branch Pipe Bending

In-plane bending produces peak elastic stresses in the crotch, on the outside of the junction. The crack location was therefore chosen to run along the lower weld toe, centred about the crotch. The construction for these models was similar to the out-of-plane bending models, with the crack projected normally from the weld toe onto the inner surface of the run pipe. The crack location is shown schematically in Figure 4.2.

In-plane Run Pipe Bending

In addition to the above loads, exploratory work for cracked junctions subjected to in-plane run pipe bending is also presented. This work examined just one equal diameter (d/D=1) junction geometry, with D/T=10 and t/T=1, because an equal diameter junction would be considerably weaker than a junction with a smaller branch pipe. A common crack location for this loading case is known (from peak elastic stress locations described by Moffat [7] and from seismic work by Yahiaoui et al. [10]), and would be located on the branch pipe on the flank of the junction, with the crack orientated vertically, as shown in Figure 4.3. The effect of altering the length of such a crack was studied using two FE models with through-wall cracks, as shown in Figure 4.4, in addition to an uncracked FE model (the crack face nodes are highlighted in Figure 4.4). The cracked models included contact faces, deemed necessary to correctly model crack opening for this crack location. The 'l/D' ratio (where 'l' denotes the crack length) used for the FE models was either 0.34 or 0.82. It was the intention that further parameters would be altered for subsequent FE models. However, it soon became apparent that there was little reduction in limit load for the cracked models, even for a very long through-wall crack.

The results are shown in Figure 4.5(a) as normalised limit moments (M'), with M' defined as the limit moment divided by the plain pipe limit moment. The thick cylinder von Mises plain pipe equation was used:

$$M_{L(plain)} = \frac{\sigma_y}{6}\left[{D_o}^3 - {D_i}^3\right] \tag{4.1}$$

$$M' = \frac{M_L}{M_{L(plain)}} \tag{4.2}$$

The effect of the crack length on the limit load is shown in Figure 4.5(b), with M'/M'_U representing the normalised limit load (found by dividing each of the results by the uncracked limit load).

A through-wall crack with length almost equal to the pipe diameter only reduced the limit moment by 13%. The uncracked limit moment was equal to 90% of the plain pipe limit moment value. It was clear that there was little point in further study of the limit moment reduction for this type of crack and so the work subsequently concentrated on the crack types described for the other load cases.

4.1.2 Range of Junctions Studied

The study initially covered d/D=0.5 and d/D=0.95, for D/T=10, 20 and 30. All of the junctions had equal thickness in the branch and run pipes. Ideally, equal diameter junctions would have been modelled, but the nature of the out-of-plane bending cracks described above would result in sharp crack profiles at the flank of the junction, as shown in Figure 4.6. This could produce peak stress complications and would be an unrealistic crack profile. A slight reduction in the branch pipe was required in order to ensure a smooth crack profile. Hence, junctions with d/D=0.95 were modelled, providing data from which approximations could be made for equal diameter junctions.

For d/D=0.5 and d/D=0.95, each junction geometry had at least four FE models associated with it: one uncracked model and three cracked models. These cracked models were for through-wall cracks of varying crack angle (2α). In addition, selected part-penetrating cracks were also modelled to give an indication of the effect of the additional ligament strength, compared with a through-wall crack. For the through-wall cracks, the crack angle specified was an average of the angles on the inner and outer surfaces of the junction. The part-penetrating cracks were adapted from the relevant through-wall models and were assumed to have the same crack angle. This assumption was not strictly correct, as the average crack angle would alter if the crack depth was reduced, but the inner and outer crack angles were always close and hence the difference was insignificant.

After initial analysis of the results from the junctions with d/D=0.5 and d/D=0.95, it was decided to model an intermediate junction, with d/D=0.75 and D/T=20. Just two models were created for this junction: an uncracked model, and a model with a through-wall crack, the intention being to ensure that the relationships for d/D=0.5 and d/D=0.95 could be freely applied to intermediate cases.

The range of junctions studied, and the crack angles associated with them, are listed in Table 4.2. The part-penetrating cracks modelled were for the thickest junctions, with D/T=10. Just one part-penetrating crack length was modelled for d/D=0.5 and d/D=0.95, equivalent to the intermediate crack length for each of the respective through-wall models (Models T510-2 and T910-2). Two crack depths were analysed, a/t=0.5 and a/t=0.75. The construction of the FE models is described in the following Section.

4.2 Finite Element Modelling

4.2.1 General FE Mesh Generation

The FE analysis techniques were generally the same as those described for the uncracked parametric study in Chapter 3. The uncracked models of this study were created using the same geometry and meshing techniques (using ABAQUS [66] C3D20R 20-noded brick elements), with the weld geometry for d/D=0.5 and 0.75 defined using the data previously provided in Table 3.1. For the models with d/D=0.95, the weld dimensions are listed in Table 4.1. As before, all of the models were based on an internal run pipe diameter of 63.6mm and the length of the junction limbs, measured from the intersection of the run pipe and branch pipe centre lines, was equal to 200mm. The yield stress used was 308MN/m^2, Young's Modulus was 210GN/m^2 and Poisson's ratio was equal to 0.3.

As for the previous models, the number of elements through the thickness was reduced to one away from the intersection, and the mesh density around the run and branch pipes was also reduced as the distance from the intersection increased, in order to minimise the total number of elements in the model. The aspect ratio of the elements around the intersection was checked, using PATRAN, for each of the models created, a value of less than 5 being considered acceptable.

4.2.2 Cracked Models

The construction of the cracked models employed the same general modelling techniques as for the uncracked models. However, there were some different requirements to consider. In PATRAN [65], the mesh for a solid model is created around a template of solid objects. For an uncracked model the positioning of these 'solids' is not critical, providing the 'solid' can be meshed with the required element density. For cracked models it is preferable to position these 'solids' such that there is a boundary face of a solid in the plane of the required crack. The PATRAN solids for two typical branch junctions are shown in Figure 4.7. The solids at the junction intersection were created such that the solid faces between the lower weld toe and the inside of the run pipe were normal to the pipe surface. The crack profiles were defined using these faces.

The mesh was first defined on each edge and each individual solid was meshed. For an uncracked case, the nodes of the model would then be equivalenced: that is, nodes in adjacent solids occupying the same location at the solid boundaries would be transformed into a single node, thus joining adjacent solids together. To model the cracks, a technique, generally referred to as the 'node release method' was used. This method assumes that the cracks have zero width, with the nodes of two adjacent solid faces occupying the same location, without being connected. The cracks were created in PATRAN by equivalencing the entire mesh, except for the crack face location between two solids. The intended profiles for three through-wall cracks for out-of-plane bending (Models T520-1, T520-2 and T520-3), and the three through-wall cracks for in-plane bending (Models T520-6, T520-7 and T520-8) are marked in Figure 4.8, with the cracks running around the lower weld toe of the junction as described previously. The FE models for a selection of through-wall cracked models cracks are shown in Figures 4.9 and 4.10, for d/D=0.5 and d/D=0.95 respectively.

For part-penetrating cracks, the same principles were applied, but with the ligament of the crack included in the equivalencing selection. Part-penetrating crack profiles are displayed, in Figure 4.11. The mesh refinement and mesh density required for these cracked models is discussed in Section 4.2.5. After meshing of each model was complete, the crack profiles were verified in PATRAN using the free face display option, in conjunction with the clipping display tool. Examples of the FE models used for part-penetrating cracks are shown in Figure 4.12.

4.2.3 FE Analysis Techniques

The limit loads in this Chapter were obtained using the five-times elastic slope method, described in Chapter 3, Section 3.2.3. This criterion is an arbitrary one but has been used here to maintain consistency throughout this work and, in general, appeared to coincide with the plateau region of the limit load responses.

Gerdeen [3] recommended that, for limit load analysis, the selection of the deformation parameter should be such that 'the product of the load parameter and the deformation parameter should represent work'. This recommendation has been adhered to for moment loading, with moment-rotation curves used for evaluation of the limit moment (the rotation was recorded at the end of the branch pipe). For pressure loading the volumetric change should ideally be calculated. The difficulties associated with this have been described in Chapter 3, Section 3.2.3. For the additional uncracked (d/D=0.95) pressurised models in this section, the methods of evaluating the limit load values are the same as those in Section 3.2.3, with a combination of the two alternative parameters used. For the cracked models, two 'deformation' parameters were evaluated, using one of the d/D=0.5 models (model T510-2):

- the crotch corner hoop strain
- the rotation at the end of the branch pipe

The crotch corner hoop strain gave a limit pressure 2.6% higher than for the rotation parameter. Hence, the rotation of the branch pipe was used as a deformation parameter for the cracked pressure models.

4.2.4 Loading and Boundary Conditions

Out-of-plane Bending

For the out-of plane bending models, the bending was applied via rotation of a 'master' node, which was attached to the nodes at the end of the branch pipe (the master node was attached using the 'Beam' type of Multi-Point-Constraint in ABAQUS). For cracked cases, the bending was applied to the branch pipe so as to cause tension in the branch in the region of the crack; i.e. the crack would open under load. For moment acting in the opposite sense crack 'closure' (or compression) would occur, giving a higher limit load than for the crack opening case (contact faces would be required to correctly model the crack closure).

For branch out-of-plane bending, the cantilever model (i.e. with only one run pipe end clamped as recommended in [7] for defining moment loads) would require the full branch junction to be modelled, so that the moment could be reacted at just one end of the run pipe. However, a half-model (in the 1-2 plane as shown in Figure 4.1(a)) can be used if the applied moment is reacted out equally at the two ends of the run pipe by clamping each end of the run pipe: the two-run-ends-fixed (TREF) model.

To establish the typical difference between the limit moments for the cantilever model and the TREF models, a series of full FE models were created, for d/D=0.5 and d/D=0.95. Different sets of boundary conditions were applied for the two load cases:

- For the cantilever model, one end of the run pipe was fully clamped.
- For the TREF model the run pipe end was not fully clamped, but was allowed to move axially. This was done by constraining all of the nodes at the end of the run pipe in the 1 and 2 directions (as defined in Figure 4.1(a)) but not in the 3 direction.

The results of this boundary condition study are presented in Figure 4.13. The limit moments are presented as the normalised M' values, obtained using the plain pipe equation as described previously (equation (4.2)).

For d/D=0.5, the difference was found to be less than 0.3%. This is consistent with the work of Moffat et al. [72] which showed that, for branch moment loading, maximum elastic stress levels in branch junctions with $d/D \leq 0.5$ were not influenced significantly by the run pipe boundary conditions. However, for the d/D=0.95 case the limit moment was affected considerably by the run pipe boundary conditions. For the thickest case (D/T=10) the TREF limit moment was approximately 15% higher than that for the cantilever model. The results converged as D/T increased, and the results for D/T=30 were virtually identical.

As predicted [72], the cantilever model appears to be the most conservative estimate of limit moment, and hence the most desirable, but the inclusion of cracks leads to large numbers of elements (ranging from 4000 elements for a half-model of a through-wall crack in a d/D=0.5 junction, to around 10000 for a part-penetrating crack in a d/D=0.95 junction). To analyse a full model would require greatly increased analysis times compared with a half model. In addition, analysis of the cracked models using the cantilever model would cause asymmetrical loading about the centre of the crack profile. The crack profiles modelled were all symmetrical about the 1-2 plane of the junction (see Figure 4.1(a)), but for the cantilever model an asymmetrical crack profile would be expected at the flank of the junction in practice. This is because the clamped limb of the run pipe would experience greater loads than the free limb. The crack would thus tend to extend further into the clamped limb than the free limb. This effect implies that the cantilever model is unsuitable for such a crack on the flank. Symmetrical cracks would be more likely to occur for loading with the TREF boundary condition. Hence, all of the models were created as half models about the 1-2 plane (Figure 4.1(a)), with a symmetry boundary condition applied to the nodes on this plane of the model, and analysed using the TREF conditions described above.

Pressure Models and Combined Loading

Pressure was applied to the same cracked models described above for out-of-plane bending, both as an individual load and in combination with the bending.

For individual loading, pressure was applied to the inside faces of the junction, with an additional tensile stress applied to the end of the run and branch pipes to simulate closed end conditions. Pressure was not initially applied to the crack faces, as the original reason for using through-wall cracks was to provide conservative limit load estimates for cracks that had not yet propagated completely through the thickness. However, the additional weakening effect of pressure on the crack faces was investigated, for a selection of models, by applying a pressure load of half the internal pressure (0.5P) to both of the crack faces. This value of 0.5P was based on the assumption that the pressure varied linearly through the thickness, from P on the inner surface to zero on the outer surface. Hence, 0.5P was assumed to be the approximate mean crack face pressure. The effect of this pressure will be discussed in Section 4.3.2.

For the combined loading studies, the pressure was applied as described above, in addition to the application of out-of-plane bending described previously. There was no pressure loading applied to the crack faces. Proportional loading was used: a ratio of moment and pressure values was selected and the moment and pressure were then increased at the same rate, according to this ratio. Four different ratios were examined for each model (cracked and uncracked), giving a range of results from which interaction diagrams were constructed. As the loads were in a fixed ratio, it was only necessary to plot the limit load curve for one of the loads. The limit load for the other load was defined by the fixed ratio.

Alternative methods to proportional loading were also investigated for some of the models. Fixed pressure was applied initially, followed by increasing moment applied to the branch pipe. The reverse procedure, applying a fixed moment and increasing the pressure, was also tested. For both methods, the limit load results confirmed that there were no significant differences from those results obtained using the proportional loading method.

In-plane Bending Models

For in-plane bending the moment was applied using a master node at the end of the branch pipe, as described above for the out-of-plane bending models. The boundary conditions used were as for the cantilever model described previously. There were no complications in this case, as the crack was symmetrically loaded for the cantilever model. A half model was created about the 1-3 plane, with a symmetry condition applied to the nodes in this plane. One end of the run pipe was fully clamped, while the other was unconstrained. For the cracked models, there were two possible configurations, the first of which is shown in Figure 4.2, with the end of the cracked run pipe limb full clamped. Alternatively, the end of the run pipe on the uncracked limb could be clamped. The former case was expected to produce the lower limit loads, but both cases produce crack opening and have thus been investigated for a selection of models in order to quantify the effect of the run pipe boundary condition.

4.2.5 Mesh Convergence Study

A mesh convergence study was performed, using the branch junction geometry with d/D=0.5, D/T=10, for the uncracked model and two of the cracked models. Several mesh parameters were altered, with their influence on the out-of-plane limit moment and limit pressure recorded.

Uncracked Case

For the uncracked model the parameters varied were:

1. the number and size of elements approaching the intersection, in the run and branch pipes;
2. the number of elements around the circumference of the intersection;
3. the number of elements through the thickness at the intersection; and
4. the number of elements in the weld height.

It was found that these parameters made little difference to the resulting limit loads. The differences between the limit load of the coarsest mesh (one element through the thickness) and that of the finest mesh (five elements through the thickness), for moment and pressure loading, were only 1.3% and 0.6% respectively. Thereafter, the mesh parameters for the uncracked models were adjusted only to provide an aspect ratio for the elements of less than five, and to ensure that enough elements were used to define the geometric detail at the weld. For example, Model T510-U was derived from the quarter model used for the study described in Chapter 3. It had three elements through the thickness, six elements in the weld height and 24 elements around the circumference of the intersection (for a half-model).

Through-Wall Crack

Following the uncracked mesh convergence results, the effect of altering the element size at the crack tip upon the limit moment was examined for the intermediate size of through-wall crack. The parameters varied were:

1. the number of elements around the circumference of the intersection;
2. the size of the elements at the crack tip; and
3. the number of elements through the thickness at the intersection.

The coarsest mesh had three elements through the thickness and a uniform distribution of 24 elements around the circumference of the intersection (for a half model). This was then adjusted for subsequent models so that the element size was biased towards the crack tip: the size of the elements was reduced as the distance to the crack tip reduced. The finest mesh studied had five elements through the thickness and 32 elements around the circumference of the intersection. The coarsest mesh gave a limit moment just 2.5% higher than the finest mesh. Hence, the element size at the crack tip should be reduced if possible, but it is not critical to the limit moment value for through-wall cracks. All of the results subsequently presented are from cracked models with the elements biased towards the crack tip.

Part-Penetrating Crack

The most important issue to consider when modelling part-penetrating cracks, in addition to those considered for through-wall cracks, is to ensure adequate mesh refinement of the crack ligament. In a study by Yahiaoui et al. [17] for limit load work on cracked piping elbows, the number of elements through the crack ligament was found to produce considerable variation, particularly for long deep cracks.

The existing through-wall model mesh density was generally assumed to have sufficient mesh density to be suitable for a part-penetrating model, with the exception of the ligament. Examining junction T910-10 (d/D=0.95, D/T=10 and a/t=0.75), the number of elements through the ligament was varied from one to four, and the effect on the in-plane branch pipe bending moment studied. The % variation, calculated using the finest mesh result as the datum, is shown in Figure 4.14. It was found that the limit load for the coarsest mesh was only around 2% greater than the limit moment for the finest mesh analysed. Hence, the use of three elements through the ligament was found to be sufficient for a/t=0.75. The same models were used for a/t=0.5, with the crack depth reduced.

4.3 Results and Discussion

The results of the parametric study are presented and discussed in this Section. The study covers a range of junctions, both cracked and uncracked, all with t/T=1. The d/D ratio varied between 0.5 and 0.95, and the thickness ratio, D/T, varied between 10 and

30. The out-of-plane bending results presented are for the TREF boundary condition, previously discussed in Section 4.2.4. The single loading results are summarised in Table 4.3.

4.3.1 Uncracked Models - Moment Loading

It is important to understand the behaviour of the uncracked branch junctions before the cracked model results can be properly assessed. Uncracked pressure loading results have been discussed extensively in Chapter 3. However, moment loading behaviour has not yet been covered and so the uncracked moment results from this parametric study are examined in this Section.

The limit moment results were normalised using the plain pipe equation, as described previously for in-plane run pipe bending, but with the **branch pipe** dimensions:

$$M_{L(plain)} = \frac{\sigma_y}{6}\left[{d_o}^3 - {d_i}^3\right] \tag{4.3}$$

$$M' = \frac{M_L}{M_{L(plain)}} \tag{4.4}$$

The normalised moment results (M') for out-of-plane branch bending (OPB) and in-plane branch bending (IPB) are presented in Figure 4.15. Figure 4.15(a) shows the relationship between moment and D/T ratio. For d/D=0.5, the thickest junction moments (D/T=10) were clearly equal to the plain pipe value, reducing with increasing D/T (the value of M' reduced more for OPB than for IPB). For d/D=0.95, the limit moment was lower than the plain pipe value for all models. As D/T increased, the OPB and IPB limit moments reduced by similar amounts, and were also similar to the OPB results for d/D=0.5.

Figure 4.15(b) illustrates more clearly the effect of the d/D ratio on the limit moment. For IPB, M' always reduced with increasing d/D, with the lines showing the results for each thickness value having approximately the same slope. For OPB, M' reduced with increasing d/D for the thickest junctions. However, for the thinner junctions (D/T=20 and D/T=30) M' was greatest for d/D=0.95. The one d/D=0.75 result for OPB indicates that this increase in M' may only occur for d/D values approaching unity, but more models in the range 0.5≤d/D≤0.95 would be required to confirm this.

The loads applied to the run pipe are complex, due to the nature of the branch pipe loading. For the junctions with M' closest to unity, the run pipe is thick enough to withstand the loads applied to it by the branch moment and junction plastic deformation would mainly occur in the branch pipe, due to the limit moment of the branch pipe being reached. M' values of less than unity indicate that the run pipe would plastically deform in the region of the intersection, rather than the branch pipe. These different modes of deformation are illustrated for some sample cases for OPB and IPB, in Figures 4.16 and 4.17 respectively.

Hence, it can be stated that for junctions with D/T≤10 and d/D≤0.5, the limit moment can be obtained using the plain pipe limit moment for the branch pipe. The situation for D/T>10 or d/D>0.5 is more complex, and a larger range of FE models would be required to completely understand the limit moment trends.

The presented data is evaluated alongside existing solutions in Section 4.3.4.

4.3.2 Cracked Models - Single Loading

The limit moments are presented as M' values, with each limit moment result normalised to the relevant plain pipe limit moment to give M' (derived as before, using equations 4.3 and 4.4). The M' values were then plotted against the crack angle, 2α. The pressure results were normalised by dividing by the plain pipe limit pressure value for the run pipe, as described in Chapter 3:

$$P_{L(plain)} = \left(\frac{2}{\sqrt{3}}\right) \sigma_y \ \ln\left(\frac{R_o}{R_i}\right) \tag{4.5}$$

$$P' = \frac{P_L}{P_{L(plain)}} \tag{4.6}$$

The normalised limit pressures, P', were then plotted against the crack angle.

In addition, all of the normalised values were converted into the ratios M'/M'$_U$ or P'/P'$_U$, to show the reduction effect of the cracked models compared to the uncracked limit loads, M'$_U$ and P'$_U$. These values were plotted against crack angle to give an indication of the relationship between crack size and relative limit load reduction for each load case. The single loading limit load results are summarised in Table 4.3.

The limit load results were obtained from moment-rotation curves and pressure-rotation curves. Typical results for each of the three load cases are shown in Figure 4.18(a), (b) and (c) for OPB, pressure, and IPB respectively. The uncracked limit pressure curve is not shown in Figure 4.18(b) because this was plotted against diametric growth, although the limit pressure value is shown for comparison.

The single loading results are evaluated against existing methods in Section 4.3.5, resulting in recommendations for limit load assessment of cracked branch junctions.

Out-of-plane Bending and Pressure Models - a/t=1.0

The OPB and pressure limit load results are presented alongside each other, as the same FE models were used for both load cases.

The **through-wall** cracked results for **d/D=0.5** are presented in Figure 4.19. Figure 4.19(a) shows the normalised limit load results, illustrating the reduction in limit load with increasing D/T ratio and crack angle. Figure 4.19(b) illustrates the limit load reduction compared with the uncracked branch junction limit loads. It is interesting that the reduction in limit load with increasing crack size for each of these three thickness ratios was so similar, particularly in light of the the decreasing M' and P' values with increasing D/T (as shown in Figure 4.19(a)). The presence of a crack had a greater effect for OPB than for pressure loading. An approximate lower bound to each set of load results is given by the D/T=20 values for each case, as shown in Figure 4.19(b).

Figure 4.20 shows the **through-wall** cracked results for **d/D=0.95**. The normalised results for the thickest junction, shown in Figure 4.20(a), were lower than for d/D=0.5, but the results for D/T=20 and D/T=30 were similar. This shows that the trends for the uncracked junction, shown in Figure 4.15, continue to apply for junctions with cracks. For pressure loading, the normalised limit loads were lower than for d/D=0.5, as expected. Figure 4.20(b) shows that, as for d/D=0.5, the limit load reduction was almost independent of the junction thickness. Again, the OPB results were lower than the pressure results. A general approximation to a lower bound for both sets of data is again given by the D/T=20 values (with the exception of the D/T=10 model with the smallest crack, which was slightly below this line).

The typical spread of plasticity and deformed shape is shown for a selection of junctions in Figures 4.21 and 4.22, for OPB and pressure loading respectively. For the OPB cases shown, the displacements were unmagnified. For pressure loading 'dmag', the displacement magnification factor, is equal to 5. The load levels were all below the limit load value, with the ratio of the load to the limit load (M/M' or P/P') specified for each Figure. The variable plotted was the equivalent plastic strain (PEEQ in ABAQUS).

For the OPB models, there was little visible crack opening for the thick junction with the short crack, shown in Figure 4.21(a), but for the large crack in Figure 4.21(b) the crack opening was a combination of modes I and III. In both cases, the plasticity spread predominantly in the run pipe of the junctions. The flank area, 'below' the crack, and the area directly 'above' the crack did not experience much plasticity. This was because the presence of the crack largely removed the load bearing effect from this region, with the load distributed around the remaining circumference of the intersection.

The deformation for pressure loading is shown in Figures 4.22(a) and (b) for two of the intermediate crack angles. The crack opening for these models was predominantly Mode I, with some evidence of mode III opening. The plasticity spread into both the branch and run pipes for both junctions and, unlike OPB, there was considerable plasticity in the flank of the junction, although there was still no plasticity directly 'above' the crack. The presence of a crack for pressure loading results in high stress at the crotch corner (the peak location for uncracked junctions), in addition to the peak stress at the crack tip. This crotch corner stress resulted in a spread of plasticity quite separate to that from the crack tip (this is clearly visible in Figure 4.22(a)). This plasticity extended into both the branch and run pipes with increasing pressure. The flank area 'below' the crack location was still loaded for pressure, and hence there was some plasticity in this region. The area 'above' the crack was also loaded, but the d/t ratio for the branch pipe was lower than D/T (because t/T=1) and hence the branch pipe was less highly stressed.

For pressure loading, the crack faces were not pressurised as a rule, for the reasons described in Section 4.2.4. However, in order to quantify the expected weakening effect of pressure applied to crack faces, the d/D=0.95 cracked models (through-wall cases) were analysed with half of the internal pressure value applied to them. The resulting limit pressures are shown in Figure 4.23 as normalised limit pressures, P'. It is clear that pressurising the crack faces made little difference to the resulting limit pressure. The greatest reduction was for the thickest junctions (D/T=10) with large cracks, with the model with pressurised crack faces having a limit moment 8.8% lower than the standard case.

The limit load results for OPB and pressure loading cases, with through-wall cracks, are summarised in Figures 4.24(a) and 4.24(b) respectively, showing the lower bound approximations described above. The d/D=0.75 models, of which there was one uncracked and one through-wall cracked case, are also displayed. The results were remarkably similar for all d/D ratios analysed, even for large cracks of over one third of the intersection. Thus, the crack angle has been shown to be a useful means for comparing the relative effects of cracks on these limit loads.

In-plane Bending Models - a/t=1.0

The through-wall cracked results for d/D=0.5 are shown in Figure 4.25. The limit moment results are presented as for OPB, with the normalised M' results shown in Figure 4.25(a), and the results presented as M'/M'_U ratios in Figure 4.25(b). Considering Figure 4.25(a), there was a clear difference in behaviour between the D/T=10 results and the D/T=20 and D/T=30 results. For the smallest crack in the D/T=10 case, there was no reduction in limit moment compared with the uncracked case, while there was a clear reduction for greater D/T values. Obviously, small cracks have no effect on the limit moment for d/D=0.5 and D/T=10, and this principle can also be assumed for thicker junctions and junctions with smaller nozzles (i.e. with $D/T \leq 10$ and $d/D \leq 0.5$). Figure 4.25(b) clearly illustrates the increased strength of the D/T=10 models relative to the uncracked result, even for larger cracks. The thinner junctions gave similar reductions in the limit moment ratio for all of the crack angles analysed.

For d/D=0.95, the results are shown in Figure 4.26. Figure 4.26(a) shows that there was a reduction in limit load for all of the cracked cases. Figure 4.26(b) illustrates the relative reduction in limit moment for each model using two different sets of boundary conditions, as described previously in Section 4.2.4 (see Figure 4.2). As expected, the limit moment with the crack near the unconstrained end of the run pipe (b.c.2 in Figure 4.26(b)) gave less reduction in limit moment. Hence, the boundary condition with the crack near the fixed end of the run pipe (b.c.1 in Figure 4.26(b))was used as a conservative lower bound, with the thickest (D/T=10) cracked junctions actually giving the greatest reduction in limit load ratio with increasing crack angle: the opposite of the d/D=0.5 results.

The spread of plasticity for one of the junctions is shown in Figure 4.27. As for the OPB models, there was little plasticity in the cracked area. However, the plasticity had clearly spread around the junction intersection, with the junction just below the limit moment value.

Overall, the IPB results produced a similar response to the OPB and pressure results. An approximate lower bound to all of the results is provided by the d/D=0.5, D/T=20 (or D/T=30) results, shown in Figure 4.25(b).

Part-penetrating Cracks - a/t<1.0

A selection of models were analysed with **part-penetrating cracks**, as described in Section 4.1.2. The crack lengths used were equivalent to the corresponding intermediate crack angle for the relevant through-wall case. The limit load ratios, M'/M'_U and P'/P'_U have been plotted against a/t for the OPB, IPB, and pressure results, as shown in Figures 4.28(a) and 4.28(b), for d/D=0.5 and d/D=0.95 respectively. The through-wall and uncracked results were included. For d/D=0.5, the results for pressure were higher than for OPB, with the exception of the cracked a/t=0.75 case. For OPB and pressure loading for both d/D=0.5 and d/D=0.95, the ligament of the crack clearly strengthened the junction by approximately the same amount. However, for IPB the d/D=0.5 results (Figure 4.28(a)) showed that part-penetrating cracks of the length studied ($a/t \leq 0.75$) had no discernible reduction effect on the limit load. For d/D=0.95, this was not the case, although the IPB results did show the least reduction in strength of the three load cases. From the results, it was clear that cracks with $a/t \leq 0.5$ should have little effect on the limit load of the junction. The maximum reduction in limit load for a/t=0.5, compared with the uncracked result, was 11%.

The deformation and spread of plasticity is shown for each of the load cases in Figures 4.29, 4.30 and 4.31. The global deformation of the models tended to be less than for the through-wall cases, due to the constraining effect of the ligament (the displacement was magnified for all but one of the afore-mentioned figures). The spread of plasticity through the ligament is clear for each case, as is the crack opening.

4.3.3 Combined Loading Results

The combined loading results are presented using the non-dimensional parameters M'/M'_O and P'/P'_O, where, M'_O and P'_O represent the normalised single load case limit moment and pressure. The results are illustrated using a series of interaction diagrams. Figure 4.32 and Figure 4.33 show the combined loading results for d/D=0.5 and d/D=0.95, respectively. Each diagram shows the interaction behaviour for each of the through-wall cracked junctions for a specific junction geometry. The linear and circular interaction lines have been marked for comparison.

Considering the d/D=0.5 results, there was some overlapping of the interaction curves for the shortest crack and the uncracked case. This effect was observed for pressure dominated interaction results (i.e. with $P'/P'_O > 0.8$). The uncracked single loading results for pressure (P_O) were not directly compatible with the cracked P_O values, as a different displacement parameter was used for the uncracked single loading cases (described in Chapter 3). This resulted in the overlapping described, which was most pronounced for D/T=20 results in Figure 4.32. However, this was a minor effect and the overall message from the interaction diagrams was that the interaction tended towards circular interaction for uncracked junctions, and junctions with small cracks. For larger cracks, the behaviour tended towards linear interaction.

The d/D=0.95 results did not exhibit the overlapping of interaction curves that was found for d/D=0.5. The results were similar, with the uncracked junctions and junctions with small cracks tending towards circular interaction, and the interaction tending towards linear behaviour with increasing crack angle.

It is clear that the behaviour was similar for all junctions, with the uncracked results exhibiting essentially circular interaction, and the results for the longest cracks tending towards linear behaviour. The intermediate cracked models were distributed between the uncracked results and the longest crack results. The convexity theorem (see Chapter 1), stating that limit load combinations occurring within the linear interaction line are not possible, was confirmed by these results.

4.3.4 Comparison of Uncracked Moment Results with Existing Evaluation Methods

Similarly to the pressure results presented in Chapter 3, there are several existing methods for estimating the limit moments for uncracked branch junctions. These methods were described in Chapter 1, Section 1.4.3, and are examined here in order to compare them with the FE results presented for out-of-plane and in-plane bending.

Some of the methods presented were developed for tubular joints, as used in frameworks or offshore structures, rather than for branch junctions. In order to ensure that these methods were applicable, tubular joint models were developed for the uncracked junctions. This was done by adding an additional 'plug' of material to a selection of the existing FE models: in other words the run pipe no longer had an opening in its surface for the branch pipe connection. A typical tubular joint FE model (for d/D=0.95, D/T=10) is shown in Figure 4.34. The joints modelled were for d/D=0.5 and d/D=0.95, with D/T=10 and D/T=30 for each. These configurations were analysed under both OPB and IPB, and the difference between the limit moments obtained and the branch junction results was calculated. The % variation from the branch junction limit moment for each case is shown in Figure 4.35. Clearly, the additional material in the tubular joints had little effect for d/D=0.5. However, for d/D=0.95 there were considerable strengthening effects, with the the limit moment for OPB being up to 6% higher than the branch junction value, and the limit moment for IPB increasing by as much as 37%, for the D/T=30 model. Clearly, any assessment for tubular joints using the present branch junction data should be treated with caution for junctions other than those with $d/D \leq 0.5$.

Plain Pipe Solution [20]

As mentioned previously, Miller [20] has suggested that, for a well designed model with suitable reinforcement, the limit load for a plain cylinder can be used to approximate the limit load of the branch junction. The junctions presented in this study did not include reinforcement regions, and so this principle was not expected to apply. The results have been presented normalised to the plain pipe values, as shown in Figure 4.15. It is clear that the plain pipe gives a reasonable approximation for thick junctions with small nozzles, but is not appropriate for thinner junctions. The results show a reduction from the plain pipe value of over 50% for junctions with D/T=30. The plain pipe limit moment value is recommended for branch junctions with d/D≤0.5 and D/T≤10. For thinner junctions, and junctions with larger d/D values, alternative methods of assessment are required.

Rodabaugh Recommendation [27]

As mentioned in Chapter 1, Rodabaugh [27] discussed limit moment solutions for uncracked branch junctions and concluded that the following equation for the branch out-of-plane moment gives the best agreement with test data on tubular joints (note that limit load data is not strictly derived directly from experimental data). The equation was only specified to be applicable for 35<D/T<98 and 0.19<d/D<0.9, but has been applied here to the entire range of junction geometry presented for the FE results. Rodabaugh stated that out-of-plane bending should be used as a lower bound to all limit moment results, as this was the most severe of the moment loads. The equation was as follows:

$$M^* = M_L/M_{LP} = [1.4 + 9.8\,(d/D)]\,/\,[(D/T)\,(d/D)\,(t/T)]\,; \leq 1.0 \tag{4.7}$$

where M_{LP} was the simple shell plain pipe result. In order to compare the FE results with this equation, the values obtained from equation (4.7) were divided by the corresponding values from equation (4.3), giving:

$$M' = \frac{M^* d^2 t \sigma_y}{\frac{\sigma_y}{6}\left[{d_o}^3 - {d_i}^3\right]} \tag{4.8}$$

A comparison of this equation with the FE results for d/D=0.5 and d/D=0.95 is shown in Figure 4.36. The agreement with the OPB FE data was good, with the exception of the FE model with d/D=0.95 and D/T=10. Considering the comparison for D/T≥20, the equation gave a lower bound to the FE results for IPB and OPB, with the exception of the junction with d/D=0.5 and D/T=20, which had a slightly lower limit moment. Hence, this equation is recommended for assessment of junctions with D/T≥20, although IPB limit moments for junctions with d/D=0.5 would be significantly under-estimated.

SINTAP Compendium [22]

The SINTAP compendium [22] includes a limit moment formula for in-plane and out-of-plane branch bending of a **tubular T-joint**, as described in Chapter 1, Section 1.4.3. The formula originated from design guidance for offshore installations [44] and is not stated to be a lower bound limit load solution. The solutions were calculated using the formula:

$$M_L = Q_u Q_f \sigma_y T^2 d_o \tag{4.9}$$

where,

Q_f = a factor to allow for the presence of axial and moment loads in the run pipe ($Q_f = 1.0$ for single branch moment loading)

Q_u = a strength factor which varies with the joint and load type

For in-plane bending: $Q_u = 5\beta\gamma^{0.5}$

For out-of-plane bending: $Q_u = (1.6 + 7\beta)\, Q_\beta$

$\beta = d_o/D_o$

$\gamma = D_o/2T$

Q_β = a geometric modifier defined as:

$Q_\beta = 1.0$ for $\beta \leq 0.6$ $\qquad Q_\beta = \frac{0.3}{\beta(1-0.833\beta)}$ for $\beta > 0.6$

The results are presented in Figure 4.37, alongside the FE results. The equation was clearly non-conservative for all cases, except for d/D=0.5 OPB loading, and is not recommended as an evaluation method for branch junctions.

API Offshore Recommended Practice RP2A [45]

The API publication [45] covering working stresses for offshore platforms includes formulae for the calculation of allowable loads for tubular joints under axial loads and branch in-plane and out-of-plane moments. The allowable moments (M_a) obtained using these formulae have been included here for comparison with the limit moment data for the corresponding branch junction. The equation used was:

$$M_a = Q_u Q_f \frac{\sigma_y T^2}{1.7}\, 0.8\, d_o \tag{4.10}$$

where the definitions are the same as for [22] with the exception of Q_u:

For in-plane bending: $Q_u = (3.4 + 19\beta)$

For out-of-plane bending: $Q_u = (3.4 + 7\beta)\, Q_\beta$

The equation did give a lower bound to the FE results (assuming that M'≤1.0) but was generally over-conservative. However, this method did give a good estimate of the limit moments for the d/D=0.95, D/T=10 case, but is otherwise not recommended.

CIDECT Design Guide [46]

The CIDECT design guide [46] is aimed at the design of tubular joint structures and includes formulae for the design strength of such joints under branch in-plane and out-of-plane bending. The equations for IPB and OPB design moments (M^*) were:

$$M^*_{IPB} = 4.85\sigma_y T^2 \gamma^{0.5} \beta d_o \tag{4.11}$$

$$M^*_{OPB} = \sigma_y T^2 \frac{2.7}{1 - 0.81\beta} d_o \tag{4.12}$$

where, β and γ are defined as above for [22].

These formulae are compared with the FE limit moment results for the corresponding branch junctions, as shown in Figure 4.39. The results were very similar to the results using equation 4.9 above, with the equations only giving conservative estimates for the d/D=0.5 junctions under OPB. Hence, this technique is not recommended.

Assessment Recommendations for Uncracked Moment Loading

The plain pipe solution should be used to obtain the limit moment for branch junctions with d/D≤0.5 and D/T≤10. For junctions with d/D=0.95 and D/T=10, the API method gives a good approximation, but is otherwise over-conservative. The Rodabaugh equation gives a lower bound to all moment data, with the exception of d/D=0.95, D/T=10.

Using the limited range of FE data presented, a curve fitting exercise has been performed (using the 'trendline' facility in Microsoft Excel, as in Chapter 3) to enable limit moment estimation within the range of parameters studied. A lower bound equation was produced for the diameter ratios d/D=0.5 and d/D=0.95, using the OPB results. For d/D=0.5:

$$M' = 0.0014\frac{D}{T}^2 + 0.0854\frac{D}{T} + 1.712 \qquad (4.13)$$

Similarly, for d/D=0.95:

$$M' = 0.0006\frac{D}{T}^2 + 0.0448\frac{D}{T} + 1.2222 \qquad (4.14)$$

The curves representing the above equations are shown in Figure 4.40, and give estimates of M' for junctions with t/T=1.0 and thickness ratios in the range: 10 ≤ D/T ≤ 30. Further equations could be produced if more accurate prediction of the IPB limit moment is required.

4.3.5 Comparison of Cracked Results with Existing Methods

In this section, the accuracy and conservatism of simplified limit load estimation methods are examined for cracked branch junctions under pressure and branch moments. This has been done by comparing each of the methods with the FE limit load results presented in Section 4.3.2.

Evaluation methods aimed specifically at cracked branch junctions or tubular joints are sparse. Only one such method is presented, for moment loading. In addition, it has been suggested [35] that the limit load (F_L) for a cracked branch junction can be obtained from that for the uncracked junction (F_{LU}) by using a scale factor based on the ratio of the cracked to uncracked limit load for an equivalent plain pipe:

$$\frac{F_L\,(Cracked\ Branch\ Junction)}{F_L\,(Uncracked\ Branch\ Junction)} = \frac{F_L\,(Cracked\ Plain\ Pipe)}{F_L\,(Uncracked\ Plain\ Pipe)} = \frac{F_L}{F_{LU}} \tag{4.15}$$

This approach has been examined by comparing various plain pipe limit load assessment methods.

Limit Moment - Cracked Tubular Joint Solution

As mentioned in Chapter 1, a tubular joint estimation equation could be used to estimate the limit moment for cracked branch junctions. The equation, originating from [58], is applicable for branch pipe moments (as stated in [57]), and is based upon the crack area as a fraction of the total weld area. The equation results in an area reduction factor, F_{AR}, which indicates the reduction in strength compared with the uncracked case. F_{AR} is equivalent to M', and is defined as:

$$F_{AR} = \left(1 - \frac{Crack\ Area}{Weld\ Length \times T}\right)\left(\frac{1}{Q_\beta}\right)^{m_q} \tag{4.16}$$

Q_β has been defined previously for the uncracked tubular joint solutions (equation (4.9)). The value of m_q (either 1 or 0) depends on the approach used to estimate the uncracked strength. The uncracked strength is not evaluated here, as the solution is compared directly with normalised FE results. Although the use of m_q=1 would give the most conservative results, this value was designed for use with the API solution (described previously in equation (4.10)) and appeared to be purely a method of aligning the API uncracked values with HSE [44] values. Hence, m_q=0 has been used here, removing the influence of d/D from equation (4.16).

The F_{AR} results are shown in Figure 4.41, alongside the FE branch junction results for a/t=1.0. The F_{AR} relationship gives reasonable approximations for small through-wall cracks, but became considerably non-conservative for OPB as the crack size increased.

Overall, this method gives a reasonable guide to the reduction in limit moment for branch junctions. As might be expected, the prediction is generally non-conservative, as the method was designed for use with tubular joints.

Limit Moment - Cracked Plain Pipe Solution

As discussed above, the ratio of the limit load for a cracked plain pipe to the equivalent uncracked plain pipe is sometimes used to obtain the limit load for a branch junction (see equation (4.15)). This assumes the ability to determine the limit load for the uncracked branch junction.

For moment loading of the branch pipe, the method employed is based on the branch pipe dimensions, using the solution for a plain pipe with a circumferential crack. The solution used was taken from the R-code defect assessment software compendium [73]. For external, part-penetrating, semi-elliptic cracks:

$$M_L = \frac{4\sigma_y}{3}\left[(r_o - a)^3 - r_i^3 + \left(r_o^3 - (r_o - a)^3\right)\left(\cos\frac{\alpha}{2} - \frac{1}{2}\sin\alpha\right)\right] \tag{4.17}$$

For fully penetrating cracks (i.e. a=t) equation 4.17 reduces to:

$$M_L = \frac{4\sigma_y}{3}\left[\left(r_o^3 - r_i^3\right)\left(\cos\frac{\alpha}{2} - \frac{1}{2}\sin\alpha\right)\right] \tag{4.18}$$

As the crack depth, a, and angle, α, tend to zero, these solutions give the thick pipe uncracked solution described previously (equation (4.3)).

The above solutions were divided by the plain pipe value from equation (4.3) to give M'/M'_U, which was then compared directly with the cracked FE results. Considering the through-wall crack comparison, shown in Figure 4.42(a), the theoretical plain pipe solution (equation (4.18)) clearly gives a lower bound to the results, without being over-conservative. Similarly, the part-penetrating comparison in Figure 4.42(b) shows that the theoretical solution (equation (4.17)) gives a lower bound for part-penetrating cracks. These equations are thus recommended for the scaling of the limit moment for a cracked piping branch junction, using the uncracked limit moment value.

Limit Pressure - Cracked Plain Pipe Solution

For pressure loading, the geometry of a piping branch junction with a flank crack is sometimes approximated to that of a plain pipe, of the run pipe dimensions, with an equivalent axial crack. There are a number of analytical limit pressure solutions available for pipes with axial cracks. Here, the global solution from the R-Code compendium

[73] has been examined. For part-penetrating semi-elliptic cracks:

$$P_L = \sigma_y \left[\frac{a}{(R_o - a)\,N} + \ln \left[\frac{R_o - a}{R_i} \right] \right] \tag{4.19}$$

where,

$$N = \left[1 + \frac{1.61L^2}{4\,(R_o - a)\,a} \right]^{\frac{1}{2}} \tag{4.20}$$

As the crack depth, a, and crack length, L, tend to zero, this solution gives the thick pipe solution defined by equation (4.5). When the crack depth, a, is set equal to the pipe thickness, the solution reduces to the R-code [73] solution for a fully penetrating crack in a cylinder:

$$P_L = \sigma_y \left[\frac{T}{R_i N} \right] \tag{4.21}$$

with N defined in equation (4.20).

The plain limit pressures were normalised by dividing them by the uncracked value from equation (4.5). This resulted in the ratio P'/P'_U, which was compared directly with the FE results. The crack length assumed for the FE models was taken by measuring the axial distance (in the run pipe direction) between the crack tips.

Figure 4.43 shows the comparison between the FE results and the normalised limit pressure from equation (4.21), for fully penetrating (a/t=1.0) cracks. The plain pipe theoretical values always gave a lower bound, but were too over-conservative to be of practical use. The part-penetrating solutions were not compared, due to the poor agreement found for a/t=1.0.

It has been shown, using Figures 4.19(b) and 4.20(b), that the OPB load case gives the greatest reduction in limit load of the three load cases considered, compared with uncracked limit load values, for through-wall cracks of similar size. In addition, examining the results for part-penetrating cracks, shown in Figure 4.28, the pressure results were never more than 6% lower than the OPB results. Hence, the recommended approach for assessing branch junctions under pressure is to use the plain pipe reduction factor for moment loading, described above for OPB and IPB. This reduction factor, when used with uncracked limit pressure for branch junctions, would give an accurate lower bound solution for through-wall cracks, and an indication of the effect of the additional ligament strength for part-penetrating cracks.

Summary of Cracked Junction Assessment Recommendations

The use of the equation for the limit moment of a cracked plain pipe with a circumferential crack (equation (4.17)) is recommended, as a scaling factor for the uncracked branch junction limit load (see equation (4.15)). This relationship has been found to give conservative limit load estimates for cracked junctions under in-plane and out-of-plane branch pipe bending, and also for pressure loading. The relationship has been shown to be applicable for junctions in the range: $0.5 \leq d/D \leq 0.95$ and $10 \leq D/T \leq 30$. Considering the lack of variation in the relationship between limit load and crack angle, regardless of the values of d/D and D/T, it is thought likely that the relationship would apply to junctions outside the range studied. The use of this approach assumes the correct assessment of the limit load for the corresponding uncracked branch junction.

4.4 Concluding Remarks

This parametric study of limit loads for cracked piping branch junctions has presented a series of results for out-of-plane branch pipe bending, in-plane branch pipe bending and pressure loading. These results were compared with existing assessment methods, and recommendations have been made for future assessment. In addition, uncracked limit moment results were evaluated for OPB and IPB, and limited evaluation of cracked junctions under in-plane run pipe bending were also presented.

The overall conclusions are provided, for each Chapter, in Chapter 7. This will summarise the assessment recommendations for cracked and uncracked branch junctions. The following experimental work will reinforce the validity of the techniques used for this limit load study through a series of tests on cracked and uncracked branch junctions, comparing the results with the appropriate FE results.

Table 4.1: Weld Dimensions for d/D=0.95

d/D	D/T	w_{hc} [mm]	w_{bc} [mm]	w_{bf} [mm]
0.95				
	10	8.426	5.189	0.500
	20	3.992	2.459	0.237
	30	2.610	1.607	0.155

Table 4.2: Branch Junction Model Parameters

	Out-of-plane Branch Bending and Pressure			**In-plane Branch Bending**		
	Model Ref.	2α [deg.]	a/t	Model Ref.	2α [deg.]	a/t
d/D=0.5	T510-U	0	0	T510-U	0	0
D/T=10	T510-1	52.01	1	T510-6	40.72	1
	T510-2	98.87	1	T510-7	81.88	1
	T510-3	140.27	1	T510-8	128.38	1
	T510-4	98.87	0.5	T510-9	81.88	0.5
	T510-5	98.87	0.75	T510-10	81.88	0.75
d/D=0.5	T520-U	0	0	T520-U	0	0
D/T=20	T520-1	49.00	1	T520-6	42.42	1
	T520-2	95.08	1	T520-7	84.93	1
	T520-3	137.59	1	T520-8	130.65	1
d/D=0.5	T530-U	0	0	T530-U	0	0
D/T=30	T530-1	48.08	1	T530-6	42.76	1
	T530-2	93.92	1	T530-7	86.06	1
	T530-3	136.9	1	T530-8	131.54	1
d/D=0.75	T720-U	0	0	T720-U	0	0
D/T=20	T720-2	85.71	1	T720-7	94.29	1
d/D=0.95	T910-U	0	0	T910-U	0	0
D/T=10	T910-1	51.63	1	T910-6	52.47	1
	T910-2	95.79	1	T910-7	84.21	1
	T910-3	136.78	1	T910-8	128.37	1
	T910-4	95.79	0.5	T910-9	84.21	0.5
	T910-5	95.79	0.75	T910-10	84.21	0.75
d/D=0.95	T920-U	0	0	T920-U	0	0
D/T=20	T920-1	48.41	1	T920-6	45.91	1
	T920-2	91.52	1	T920-7	88.48	1
	T920-3	134.09	1	T920-8	131.59	1
d/D=0.95	T930-U	0	0	T930-U	0	0
D/T=30	T930-1	47.60	1	T930-6	46.51	1
	T930-2	90.40	1	T930-7	89.6	1
	T930-3	133.49	1	T930-8	132.4	1

Table 4.3: Normalised Limit Load Results

	Out-of-plane Branch Bending and Pressure					**In-plane Branch Bending**		
	Model Ref.	M'	M'/M'_U	P'	P'/P'_U	Model Ref.	M'	M'/M'_U
d/D=0.5 D/T=10	T510-U	1.000	1.000	0.876	1.000	T510-U	1.000	1.000
	T510-1	0.847	0.847	0.770	0.879	T510-6	1.000	1.000
	T510-2	0.614	0.614	0.605	0.691	T510-7	0.899	0.899
	T510-3	0.422	0.422	0.432	0.494	T510-8	0.659	0.659
	T510-4	0.888	0.888	0.788	0.900	T510-9	1.000	1.000
	T510-5	0.786	0.786	0.657	0.750	T510-10	0.998	0.998
d/D=0.5 D/T=20	T520-U	0.571	1.000	0.784	1.000	T520-U	0.798	1.000
	T520-1	0.485	0.849	0.683	0.871	T520-6	0.708	0.887
	T520-2	0.360	0.630	0.533	0.679	T520-7	0.559	0.700
	T520-3	0.240	0.420	0.367	0.468	T520-8	0.395	0.494
d/D=0.5 D/T=30	T530-U	0.426	1.000	0.708	1.000	T530-U	0.614	1.000
	T530-1	0.365	0.857	0.644	0.910	T530-6	0.551	0.896
	T530-2	0.272	0.637	0.517	0.731	T530-7	0.428	0.697
	T530-3	0.181	0.425	0.352	0.498	T530-8	0.296	0.482
d/D=0.75 D/T=20	T720-U	0.532	1.000	0.663	1.000	T720-U	0.720	1.000
	T720-2	0.319	0.599	0.448	0.675	T720-7	0.532	0.738
d/D=0.95 D/T=10	T910-U	0.838	1.000	0.691	1.000	T910-U	0.828	1.000
	T910-1	0.690	0.823	0.592	0.856	T910-6	0.741	0.895
	T910-2	0.487	0.581	0.477	0.690	T910-7	0.600	0.725
	T910-3	0.305	0.363	0.358	0.518	T910-8	0.460	0.555
	T910-4	0.762	0.910	0.614	0.888	T910-9	0.768	0.928
	T910-5	0.660	0.788	0.568	0.822	T910-10	0.704	0.850
d/D=0.95 D/T=20	T920-U	0.581	1.000	0.595	1.000	T920-U	0.599	1.000
	T920-1	0.475	0.817	0.506	0.850	T920-6	0.553	0.922
	T920-2	0.338	0.581	0.402	0.676	T920-7	0.460	0.767
	T920-3	0.215	0.370	0.252	0.424	T920-8	0.364	0.607
d/D=0.95 D/T=30	T930-U	0.452	1.000	0.535	1.000	T930-U	0.482	1.000
	T930-1	0.371	0.820	0.447	0.836	T930-6	0.447	0.929
	T930-2	0.271	0.598	0.356	0.666	T930-7	0.374	0.777
	T930-3	0.176	0.390	0.230	0.430	T930-8	0.299	0.658

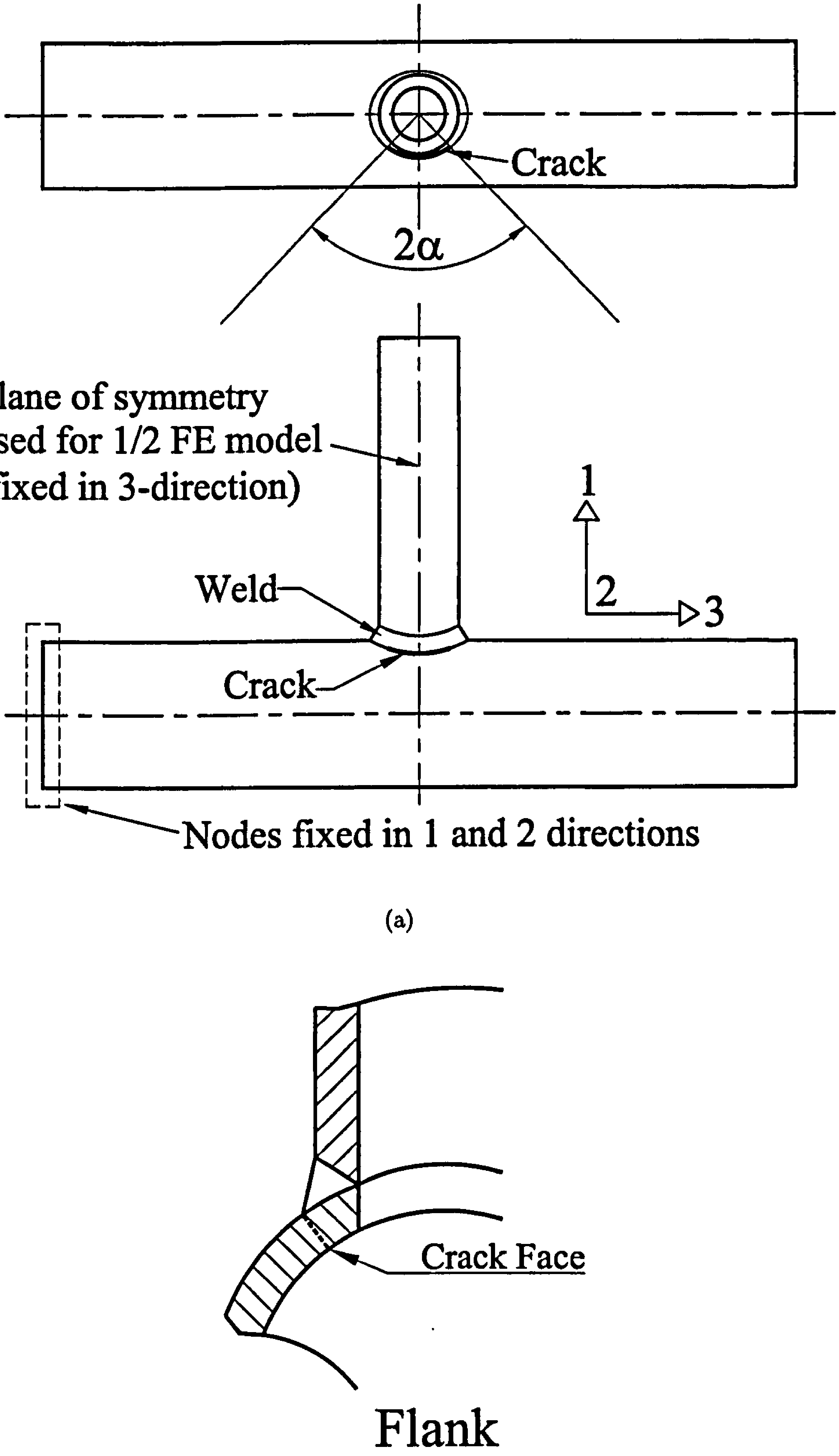

(a)

(b)

Figure 4.1: Configuration for Out-of-plane Branch Pipe Bending

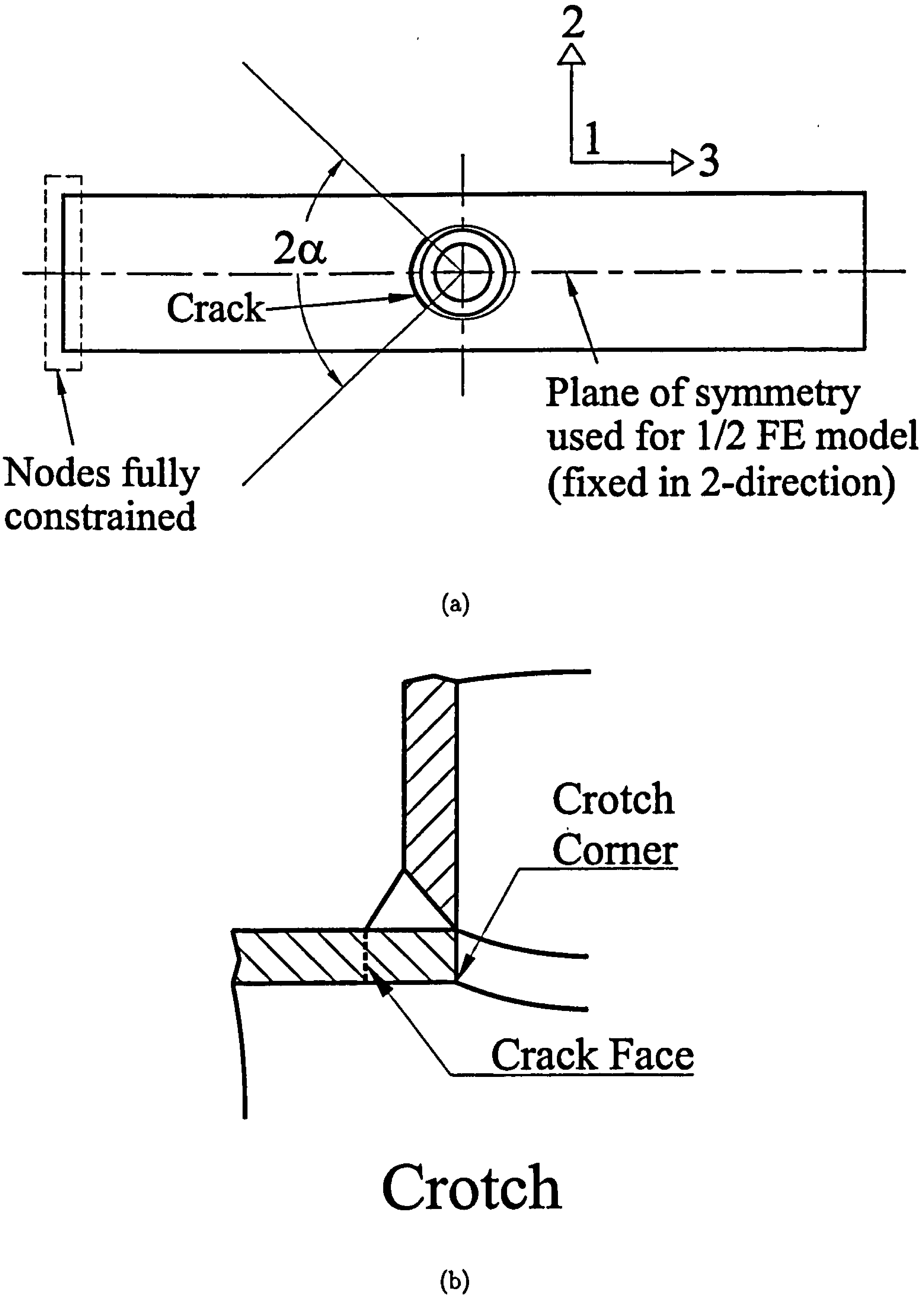

Figure 4.2: Configuration for In-plane Branch Pipe Bending

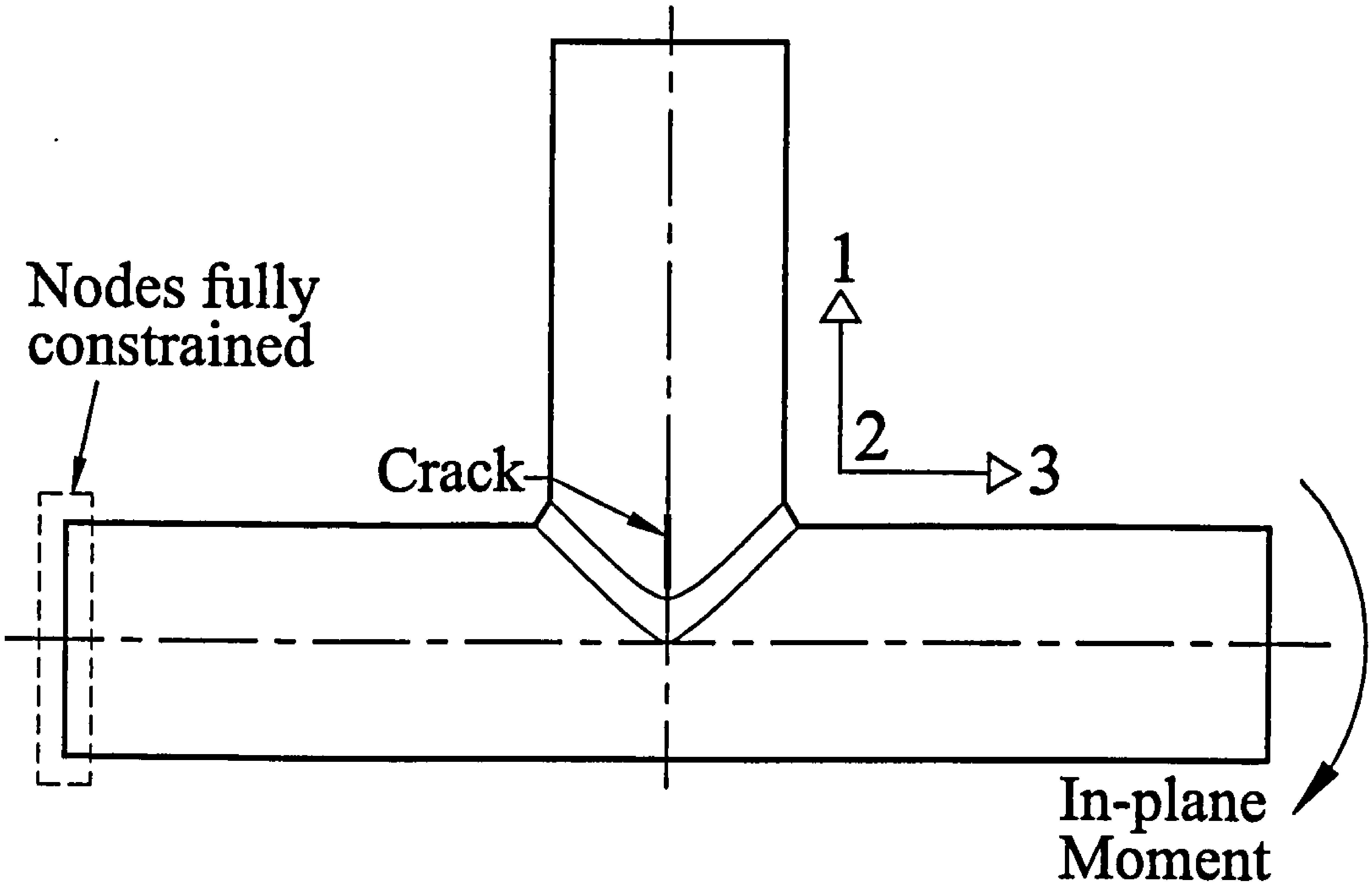

Figure 4.3: Configuration for In-plane Run Pipe Bending

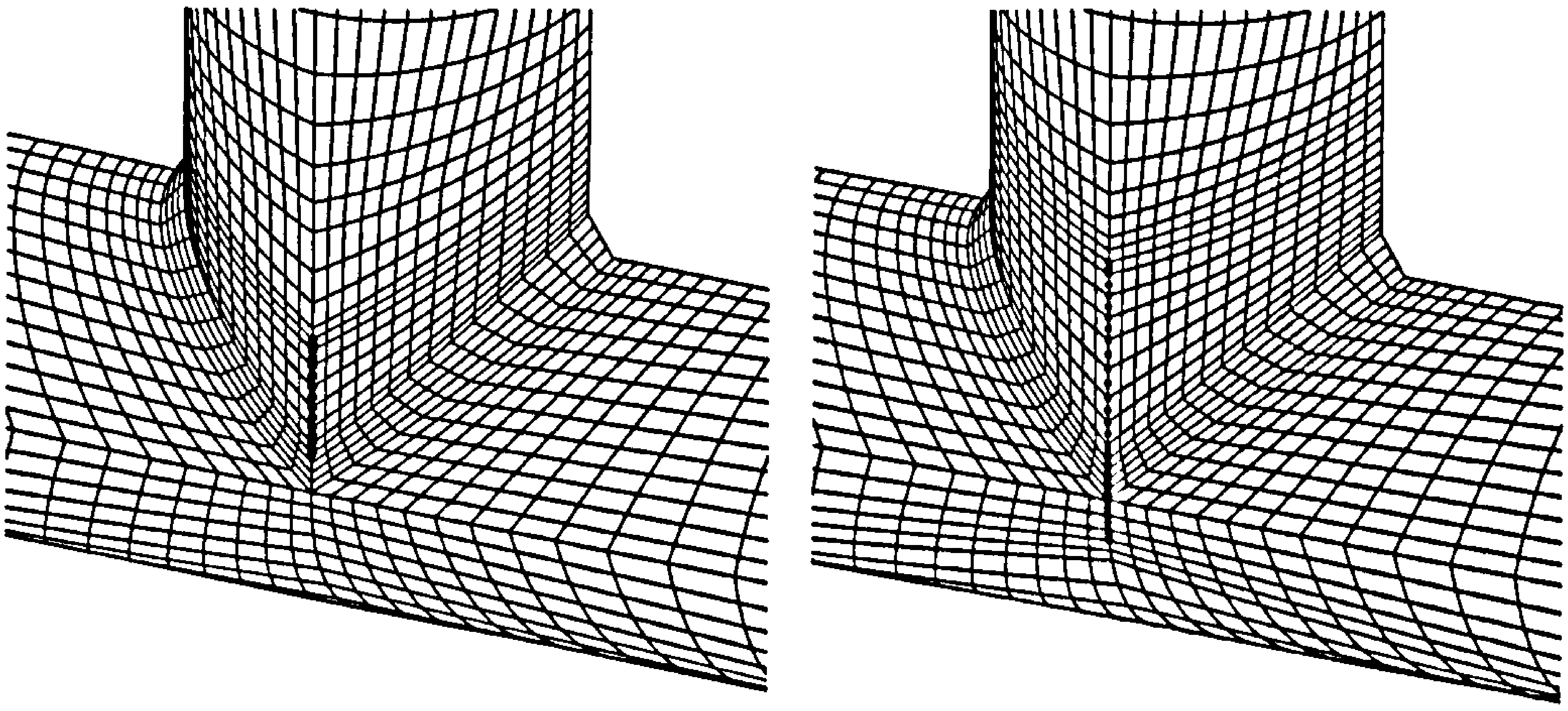
(a) l/D=0.34

(b) l/D=0.82

Figure 4.4: Cracked FE Models for In-plane Run Pipe Bending

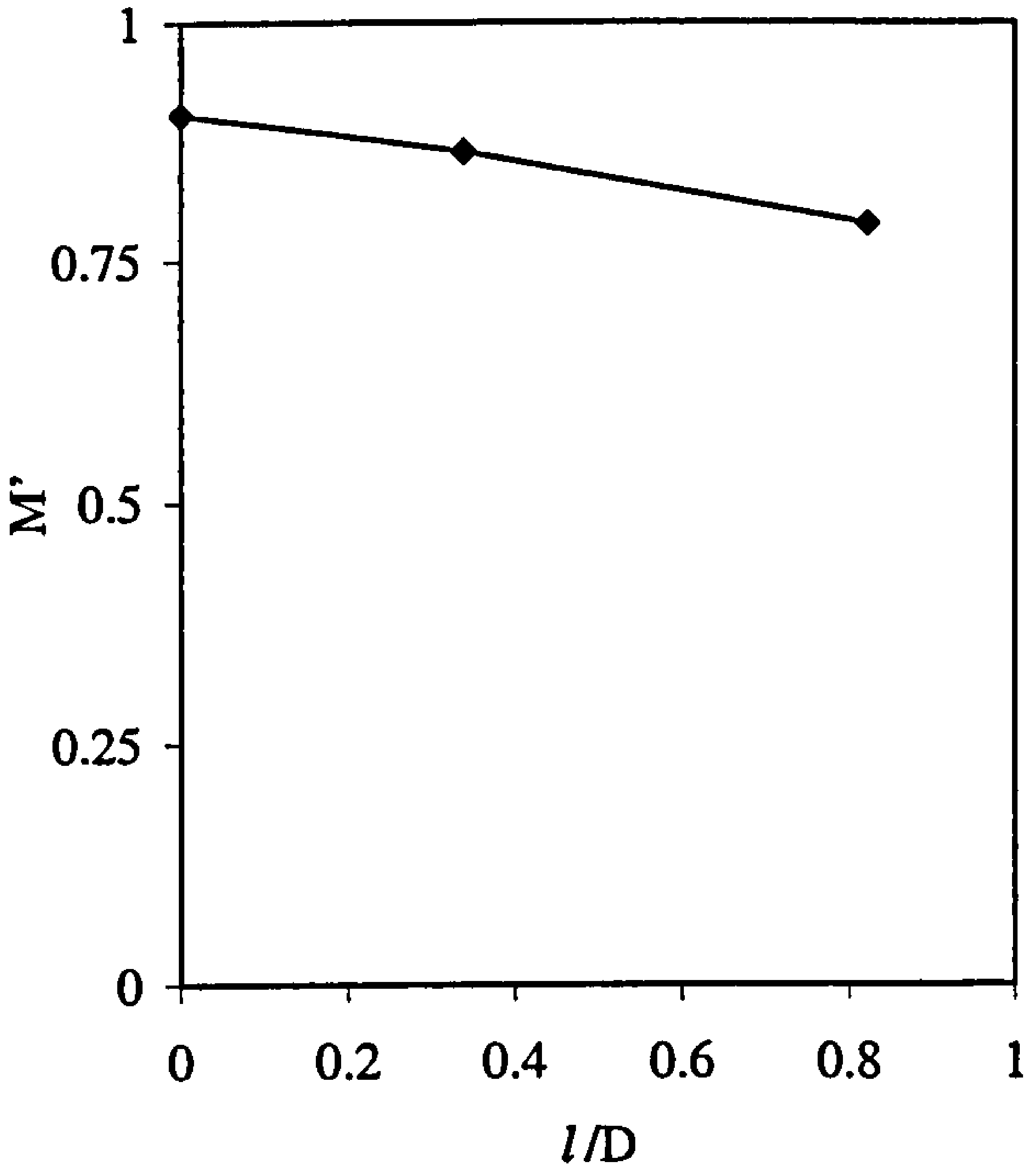

(a) Normalised to Plain Pipe Moment

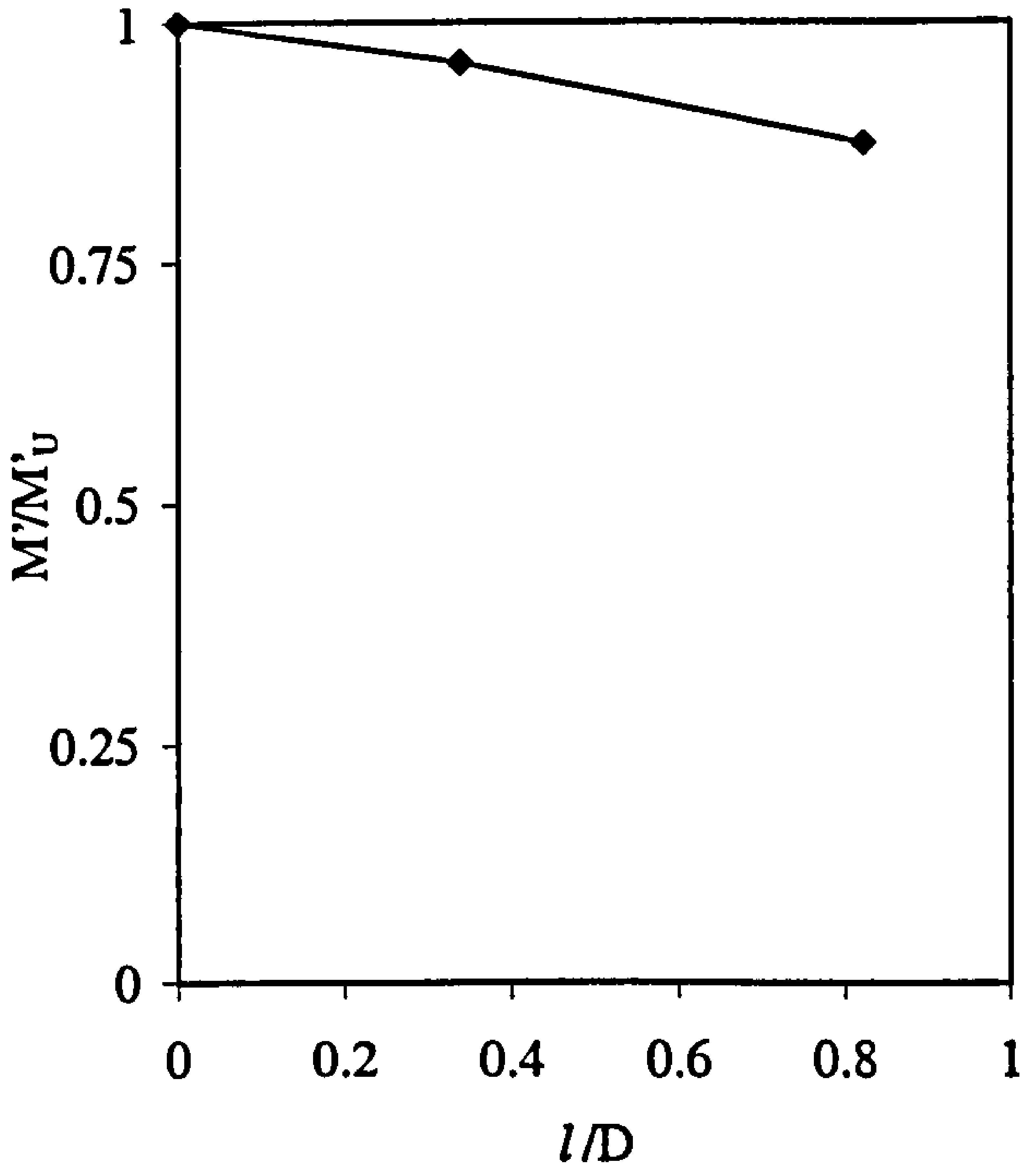

(b) Normalised to Uncracked Moment

Figure 4.5: Limit Moment Results for In-plane Run Pipe Bending

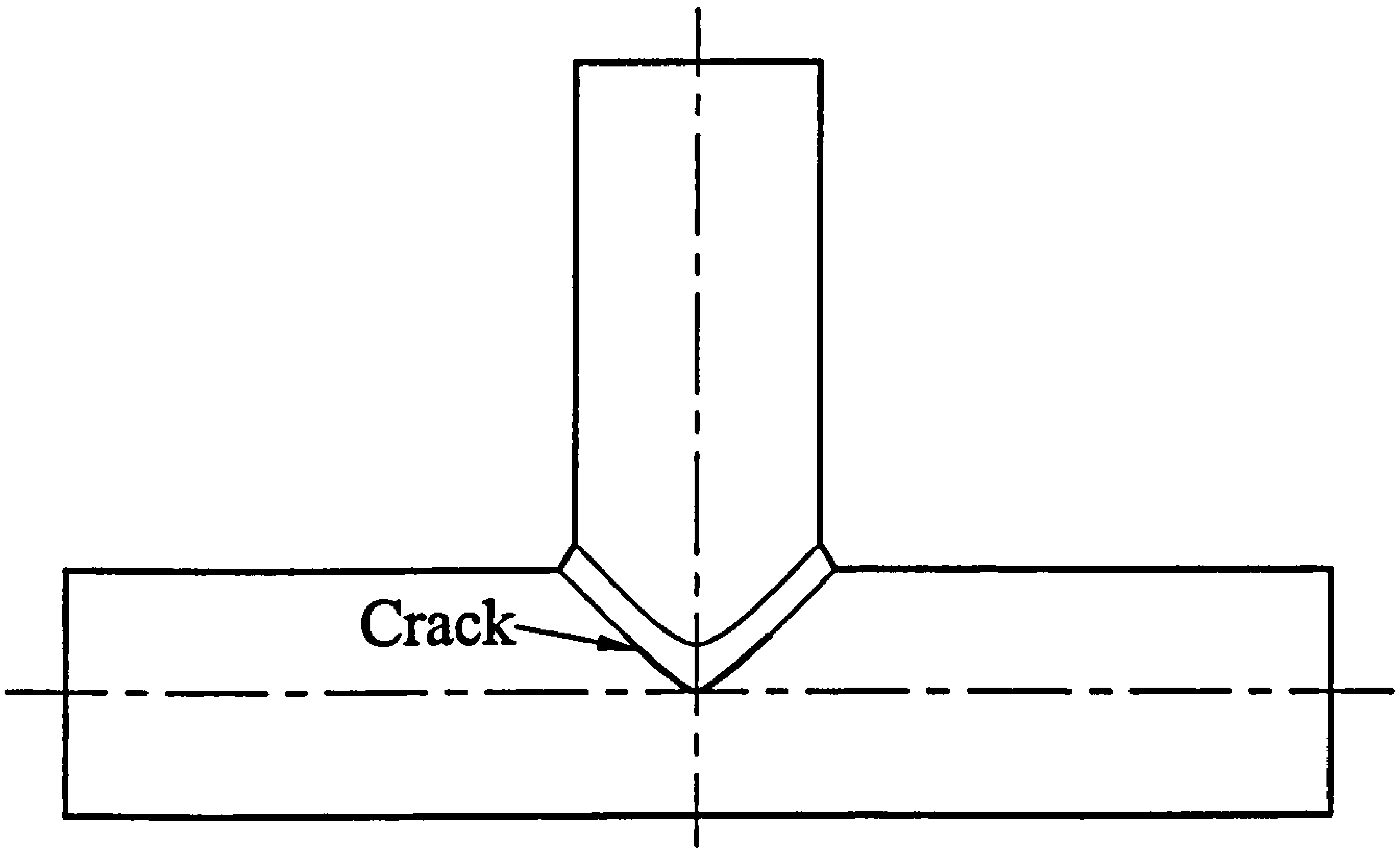

Figure 4.6: Crack Location for Out-of-plane Branch Bending - d/D=1.0

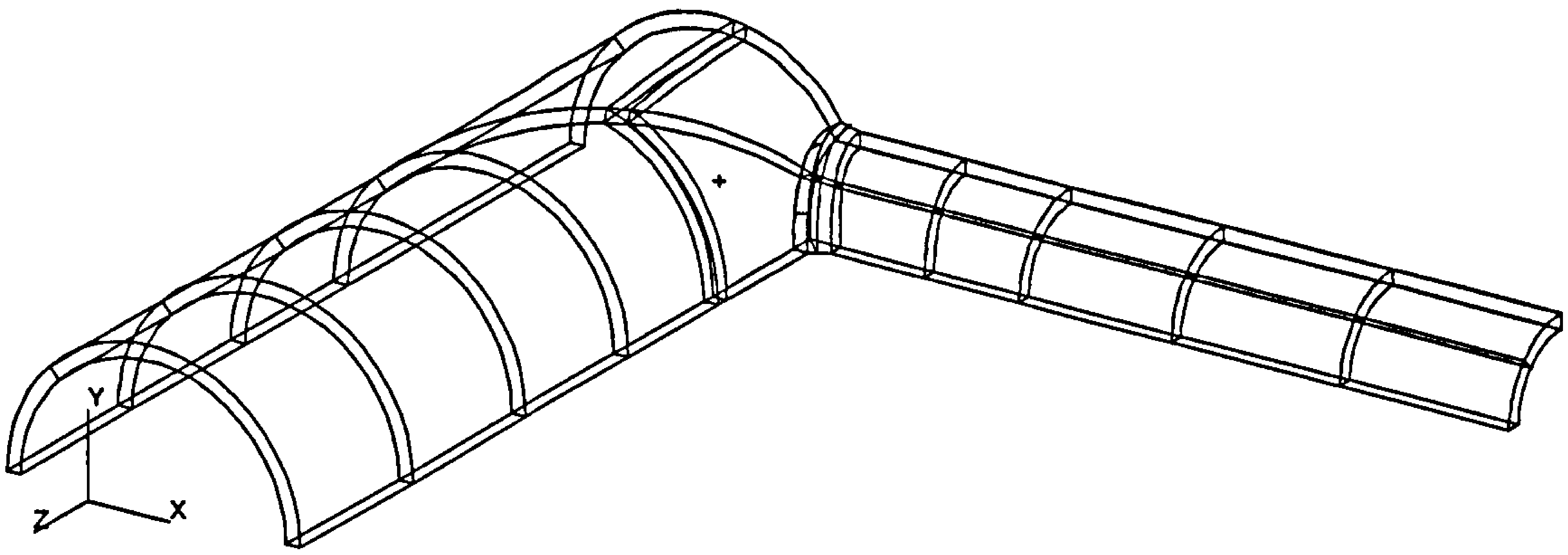

(a) d/D=0.5, D/T=20

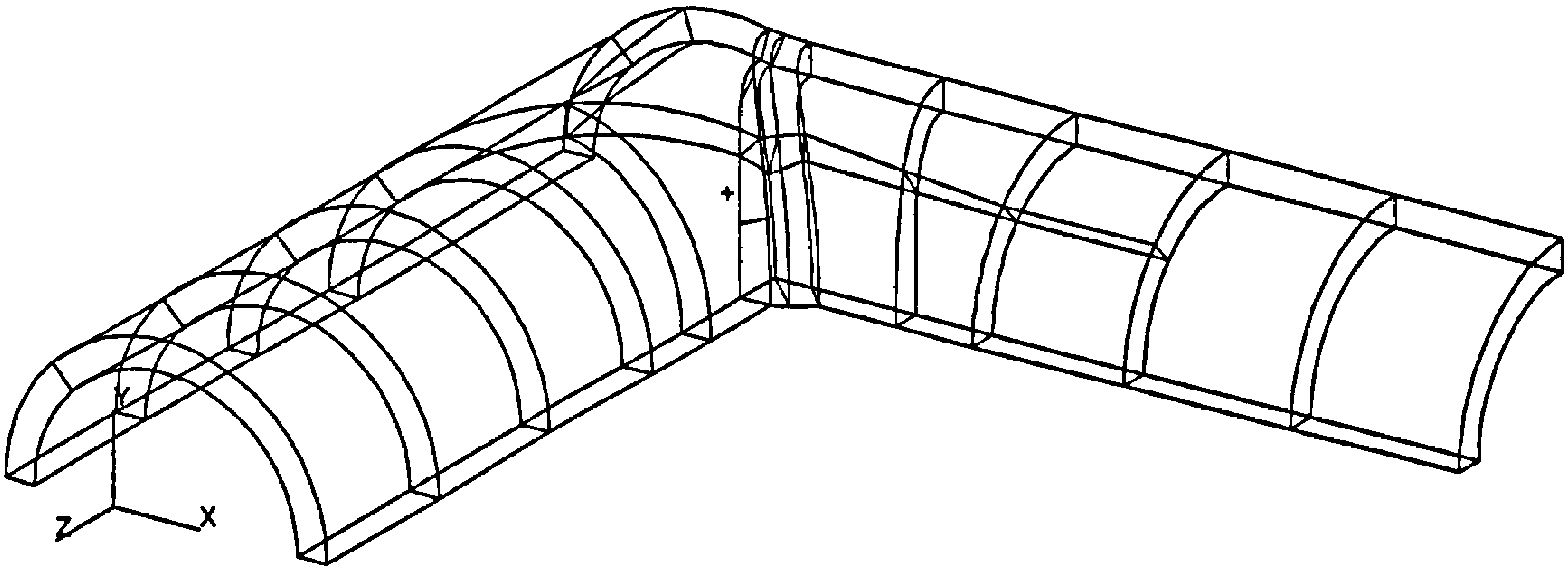

(b) d/D=0.95, D/T=10

Figure 4.7: Typical Solid Geometry for FE Models: generated using PATRAN

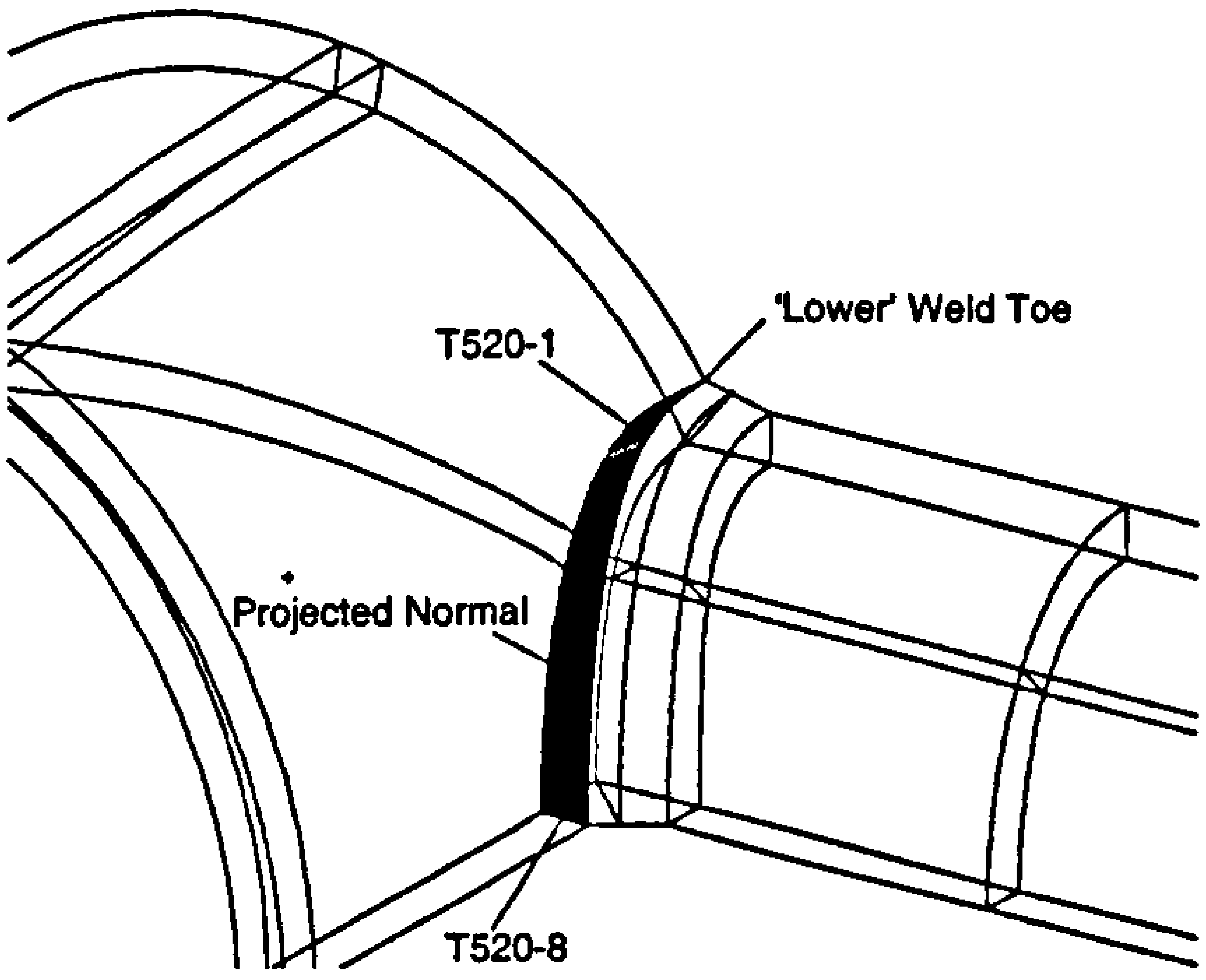

(a) Geometry for Models T520-1 and T520-8

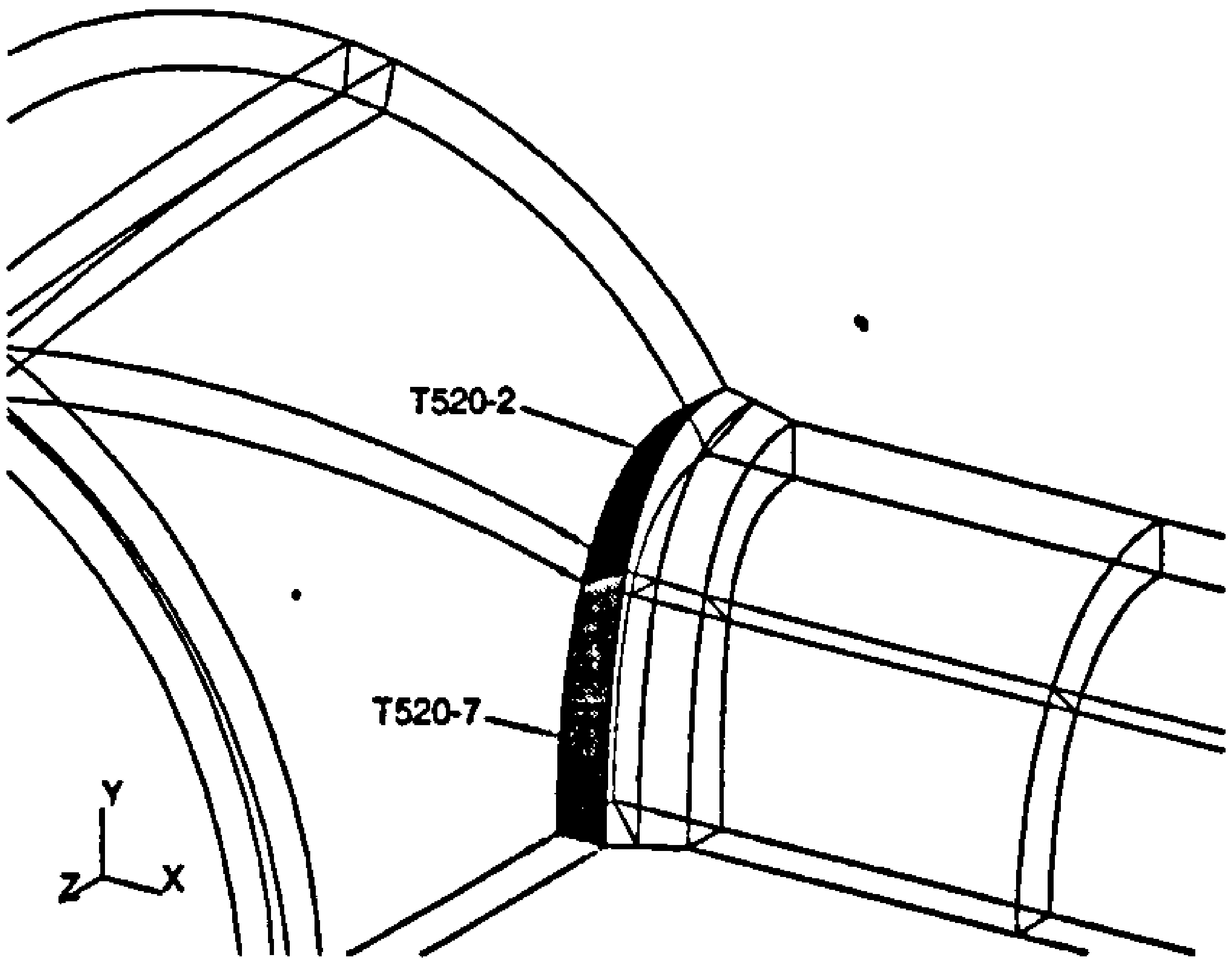

(b) Geometry for Models T520-2 and T520-7

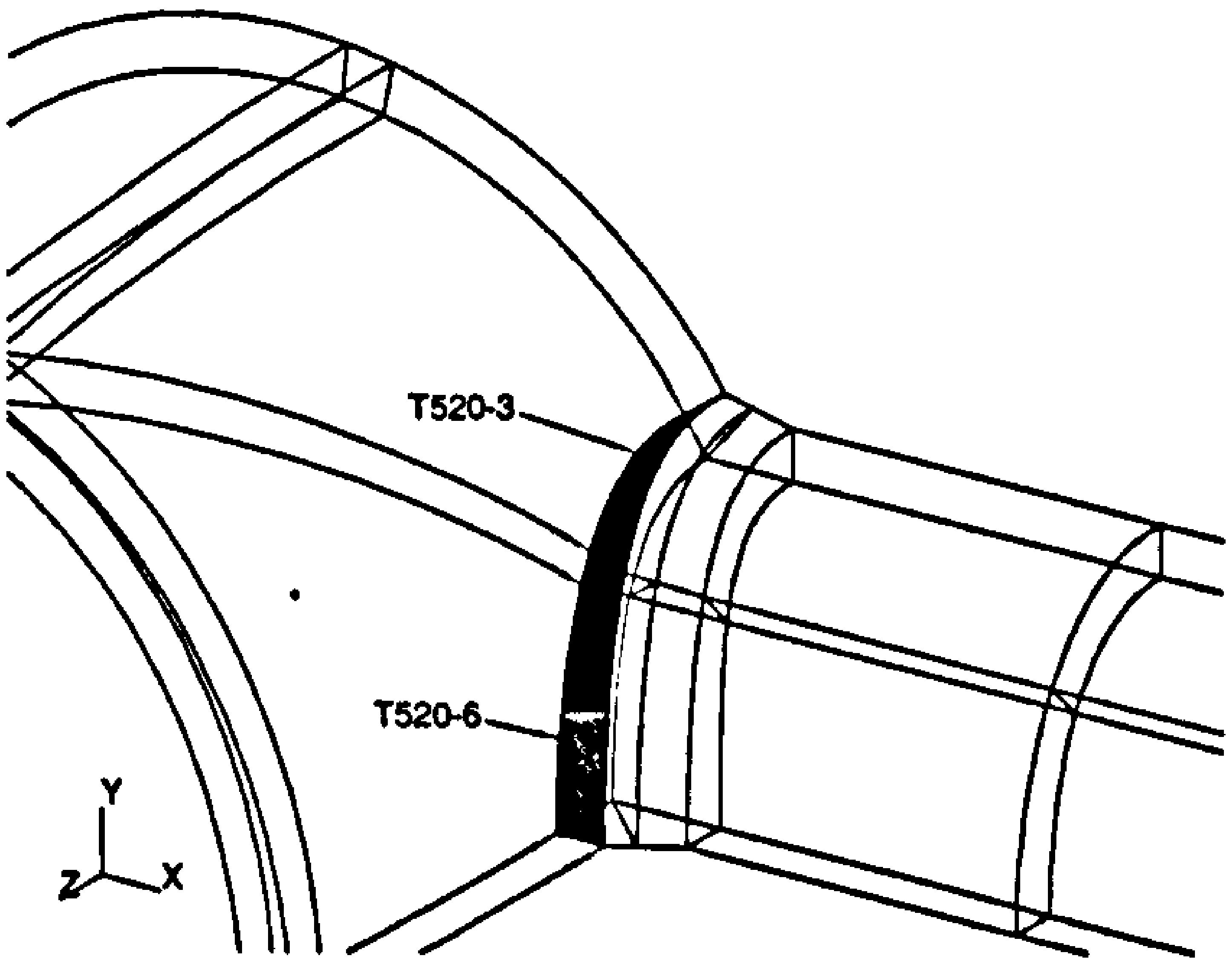

(c) Geometry for Models T520-3 and T520-6

Figure 4.8: Typical Crack Profiles for Through-wall Cracked Models

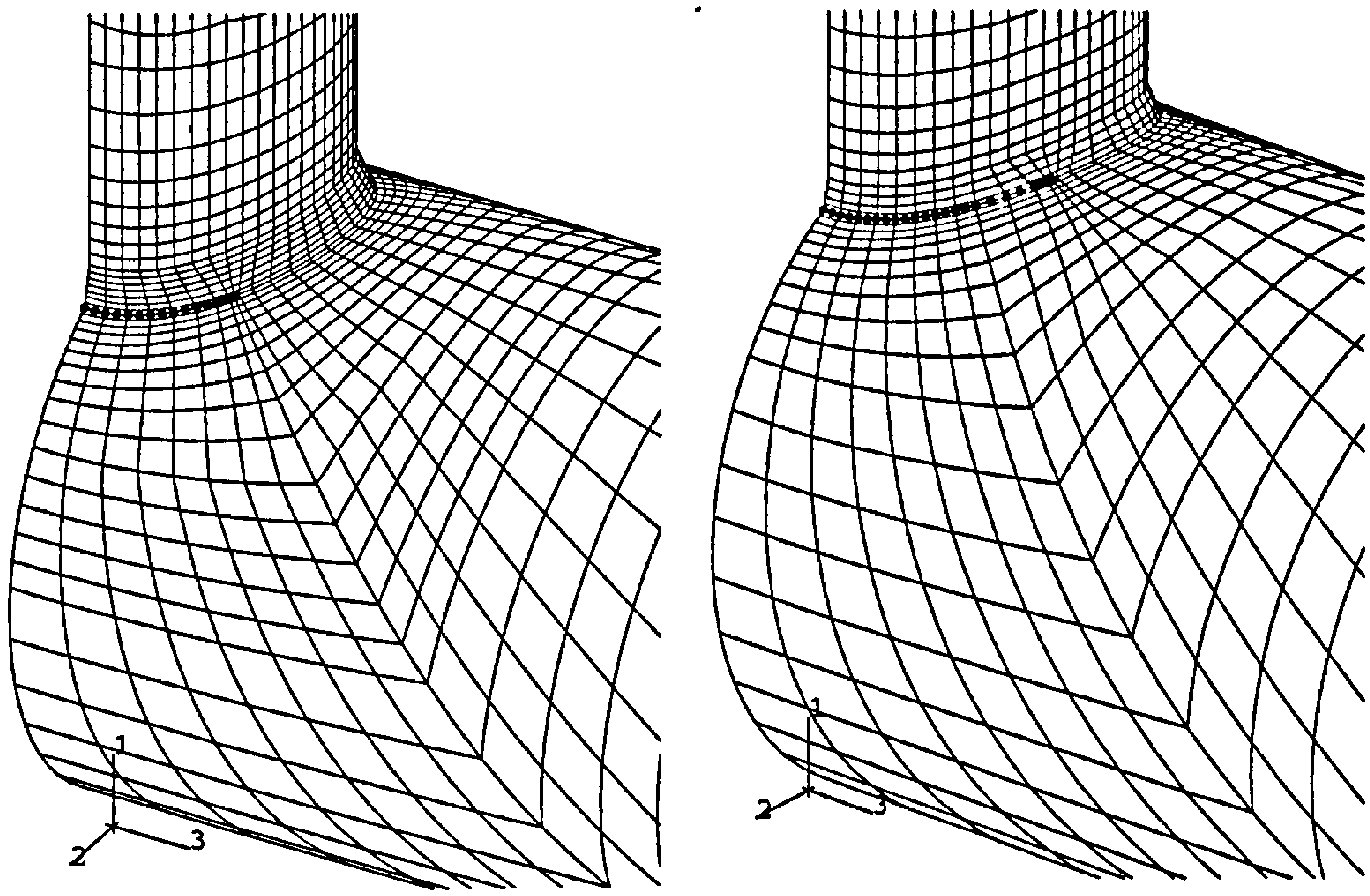

(a) Model T520-2 (b) Model T530-3

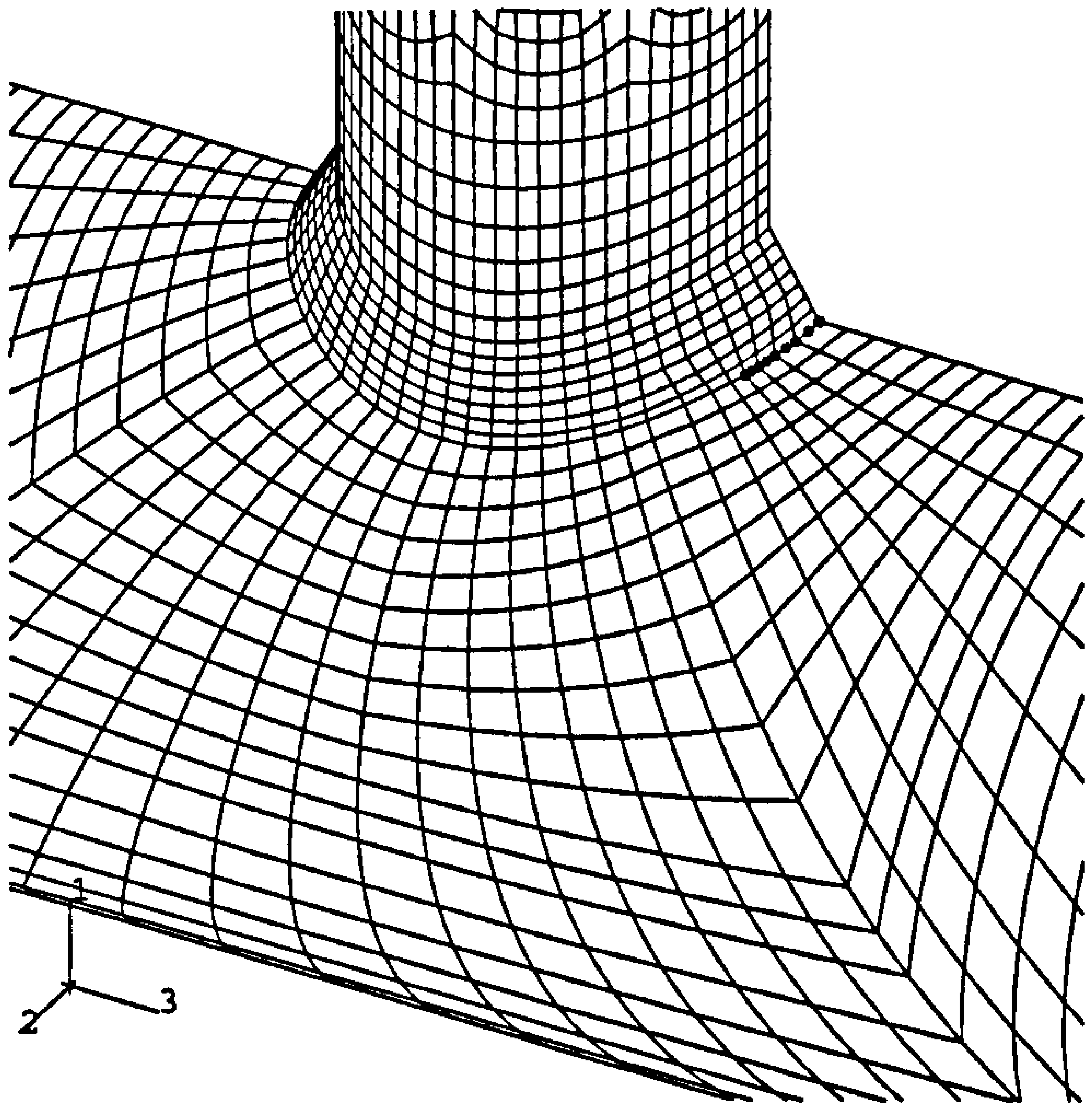

(c) Model T510-6

Figure 4.9: Typical FE Models used for d/D=0.5 Cracked Junctions (a/t=1.0)

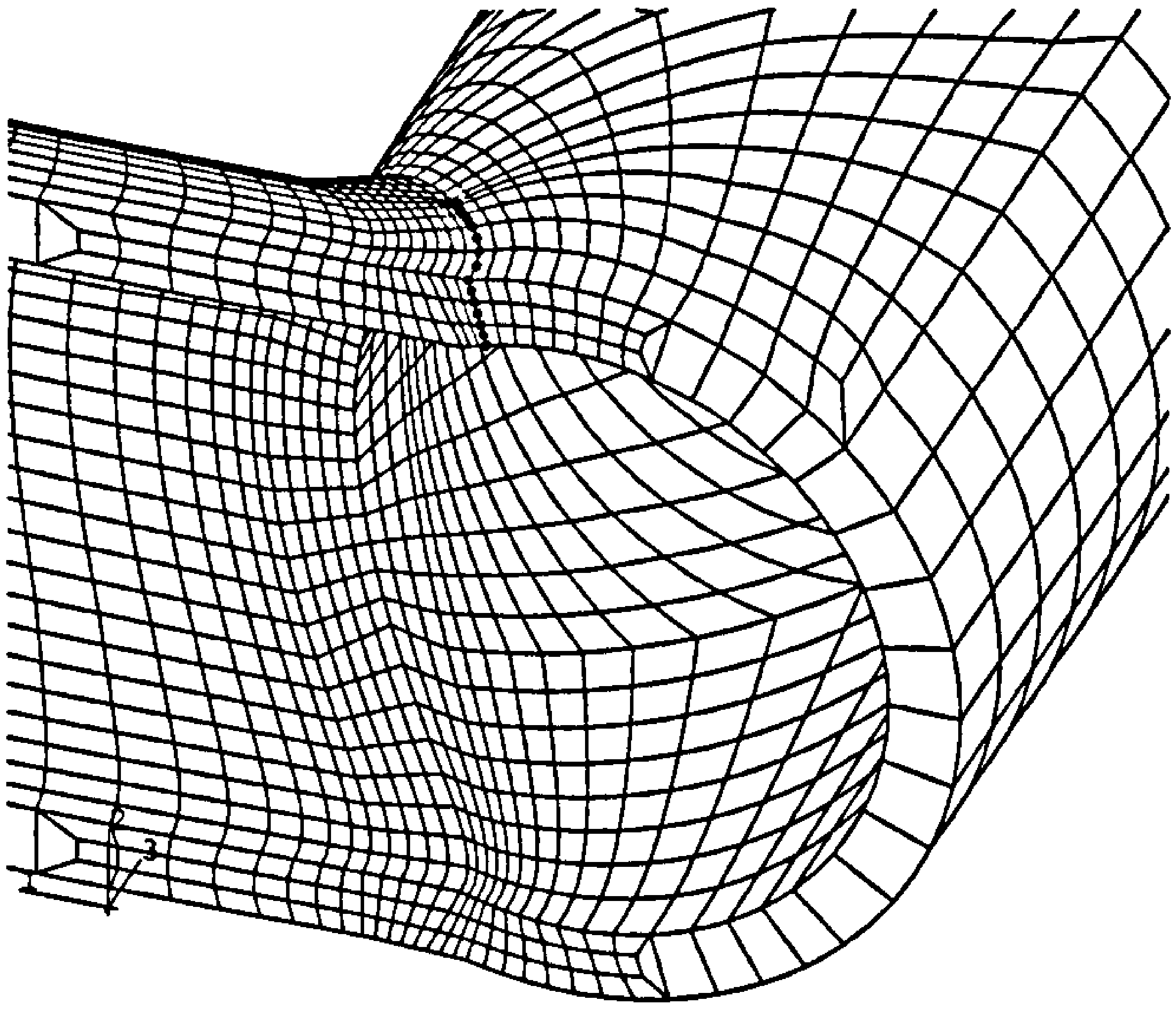

(a) Model T910-1

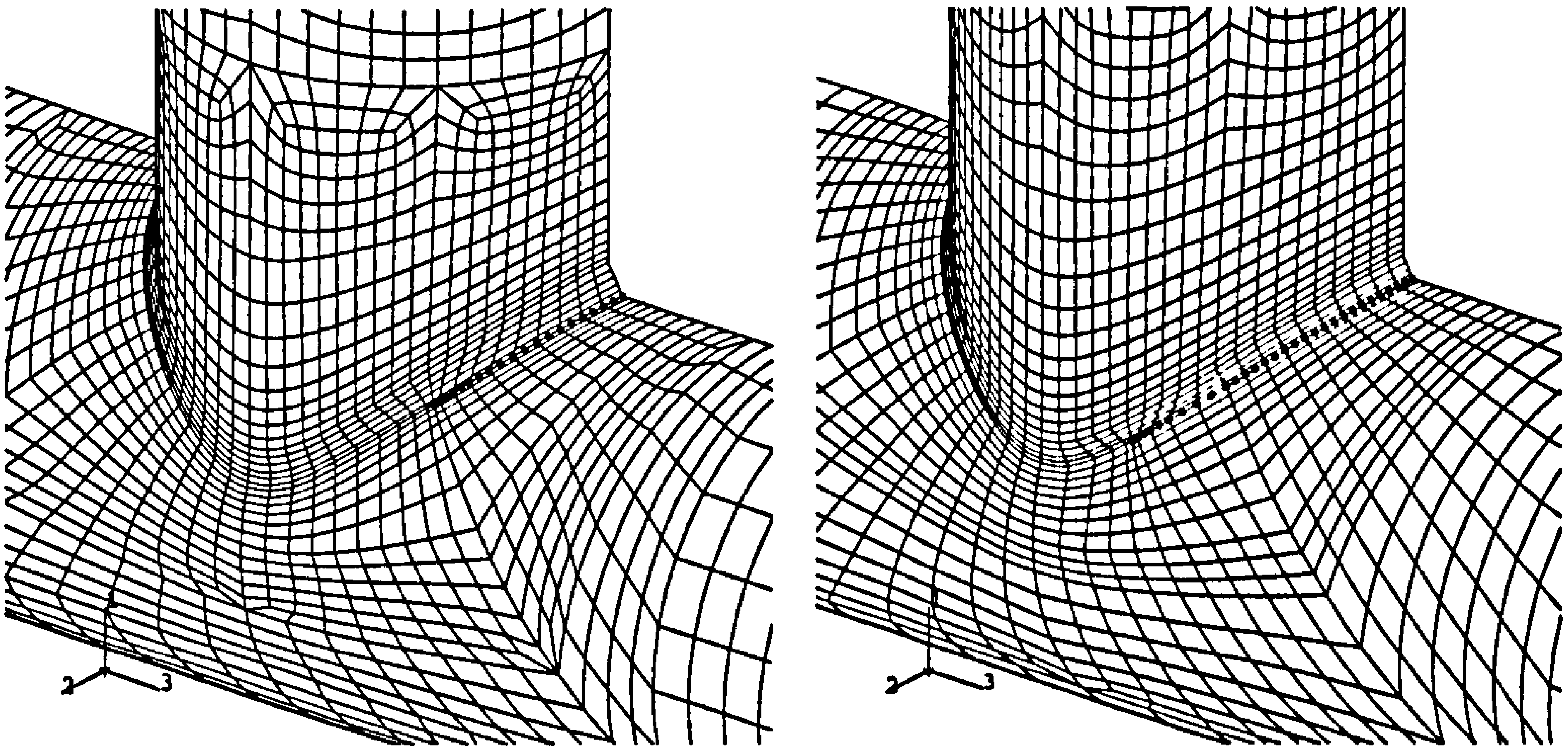

(b) Model T920-7

(c) Model T910-8

Figure 4.10: Typical FE Models used for d/D=0.95 Cracked Junctions (a/t=1.0)

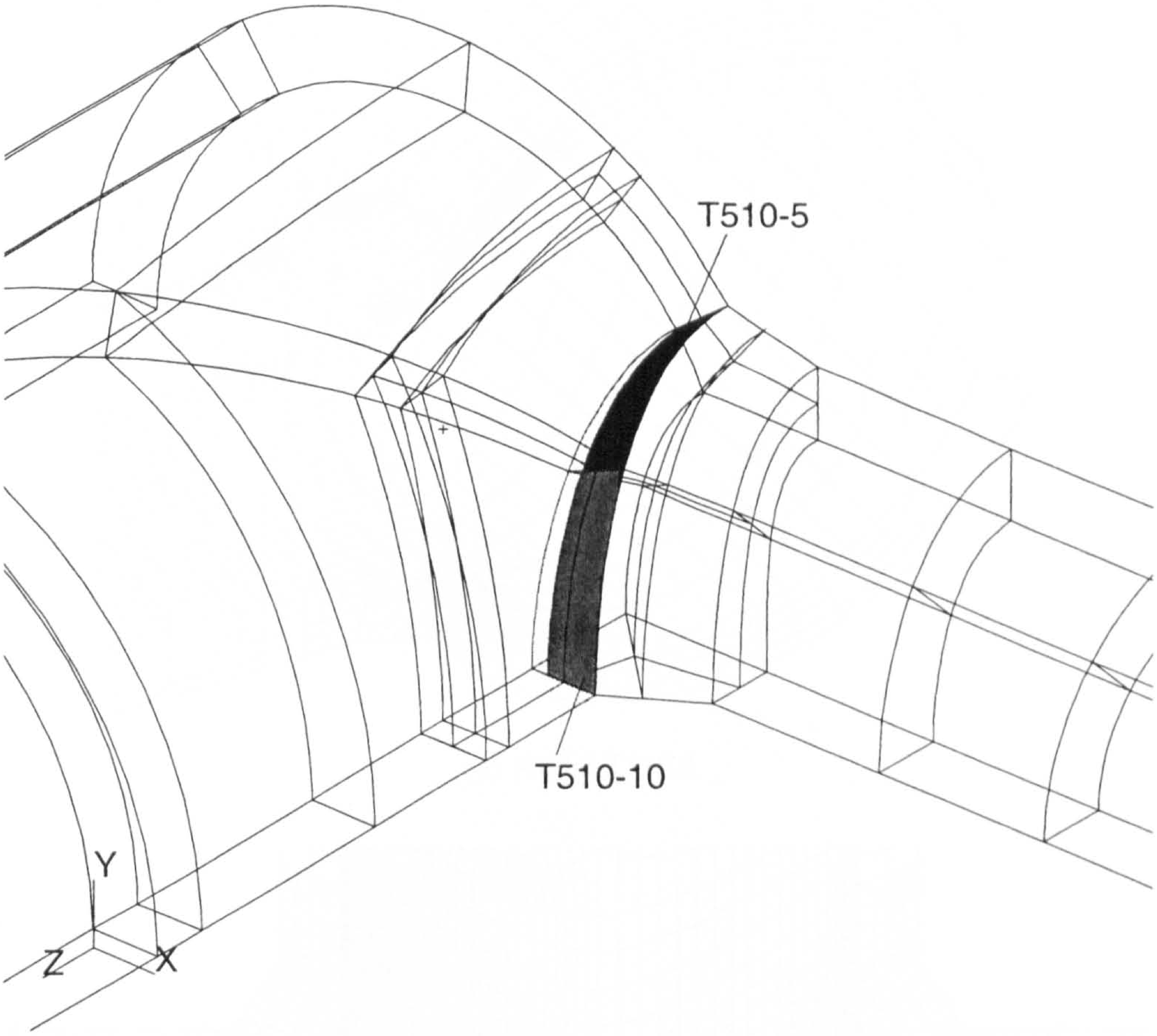

(a)

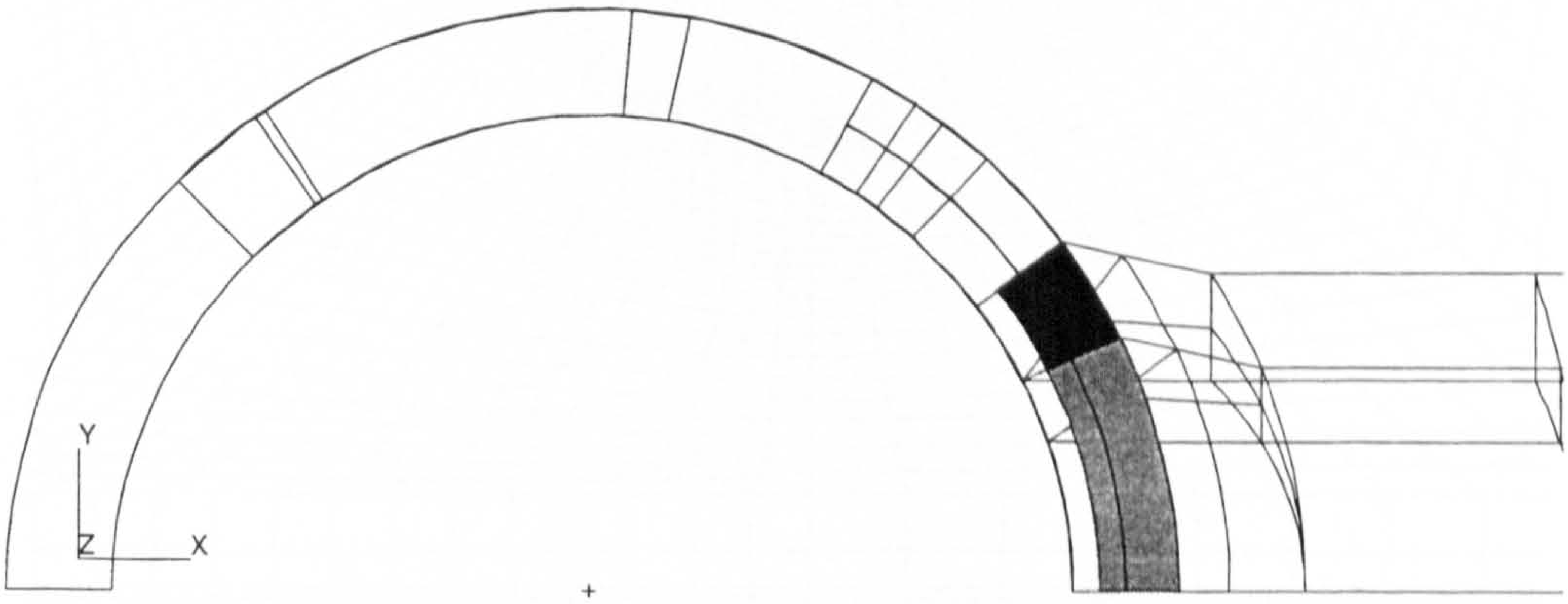

(b)

Figure 4.11: Typical Profiles for Part-Penetrating Cracks: Models T510-5 and T510-10

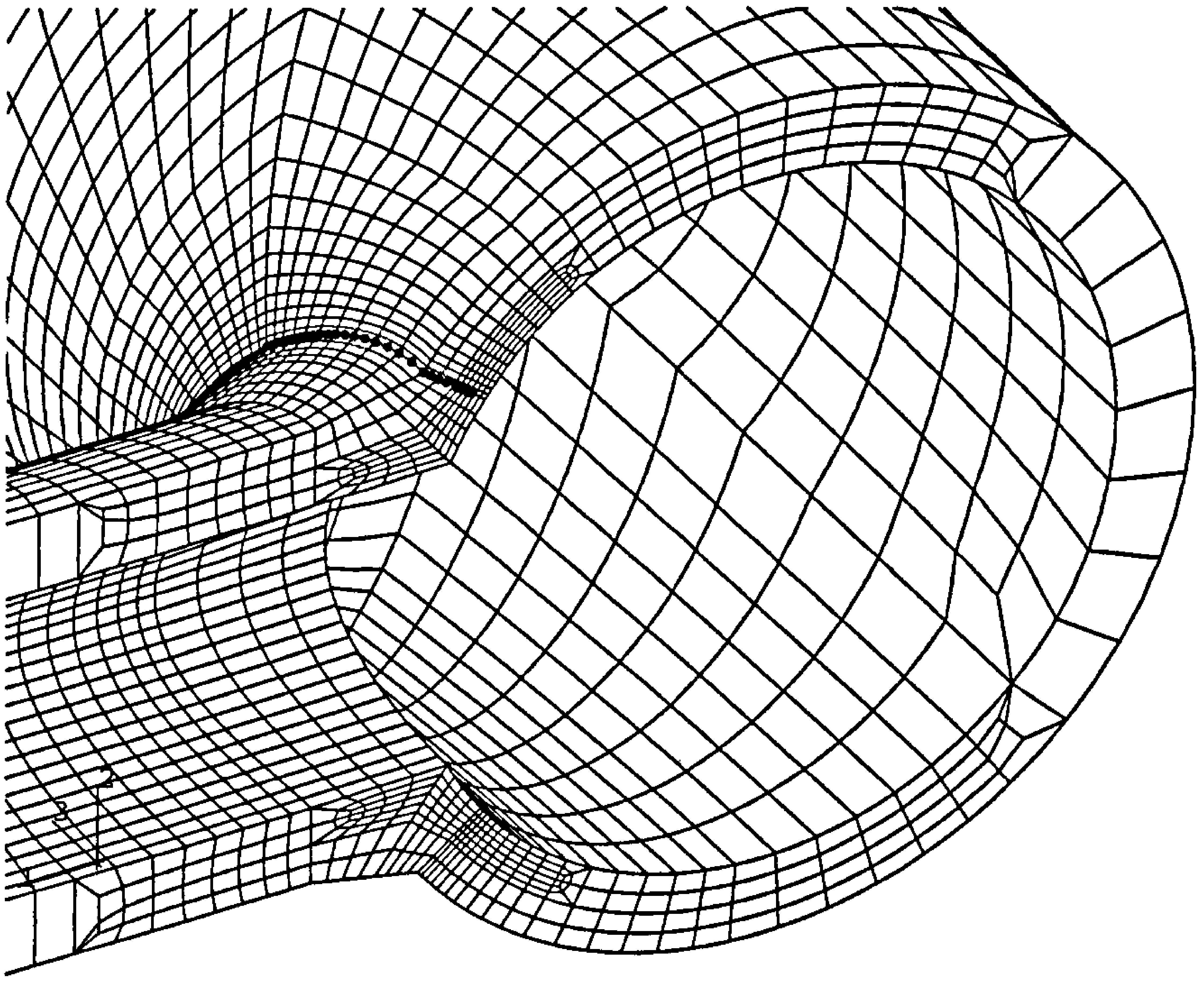

(a) Model T510-5

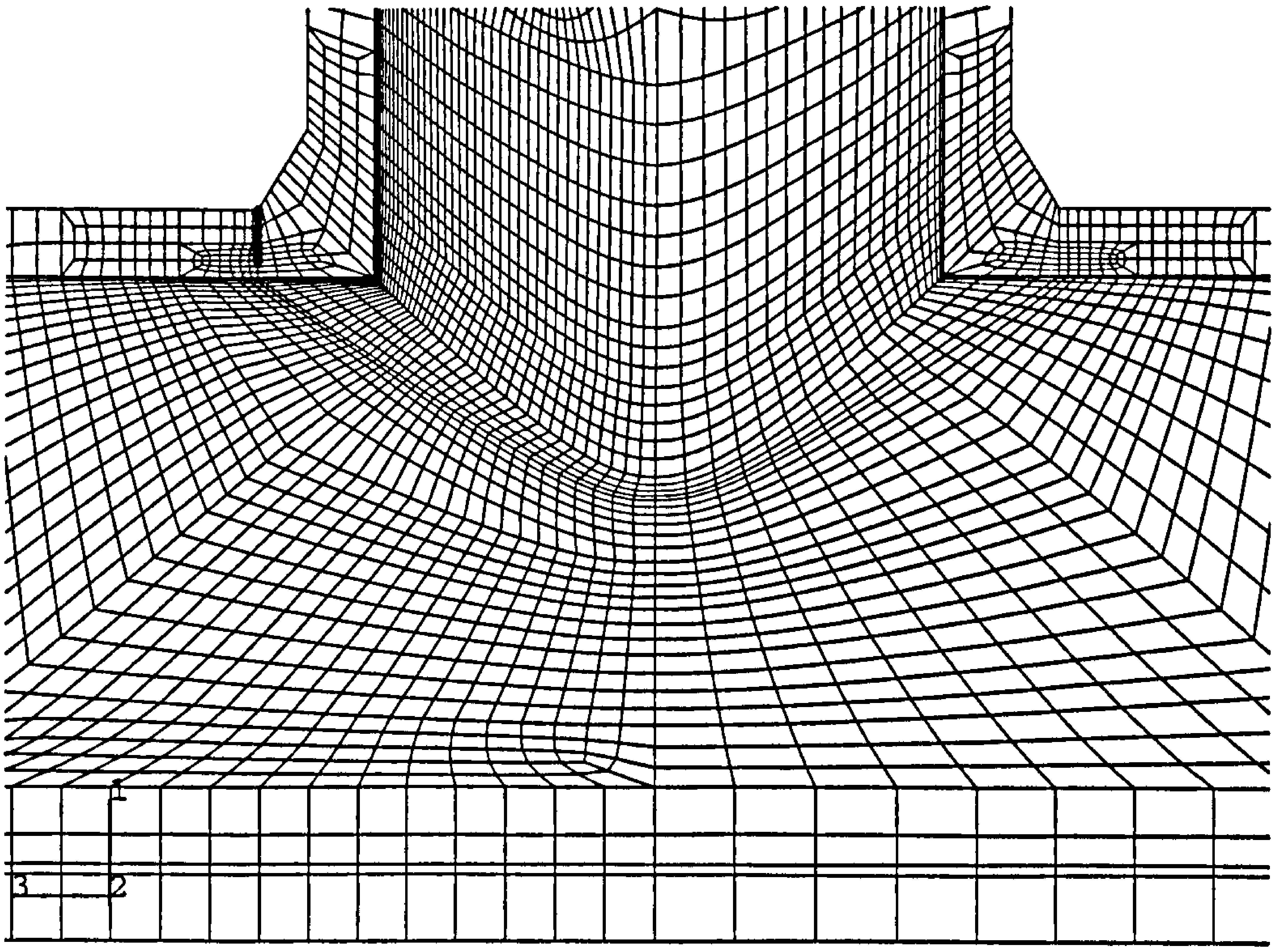

(b) Model T910-10

Figure 4.12: Typical FE Models used for Part-Penetrating Cracks

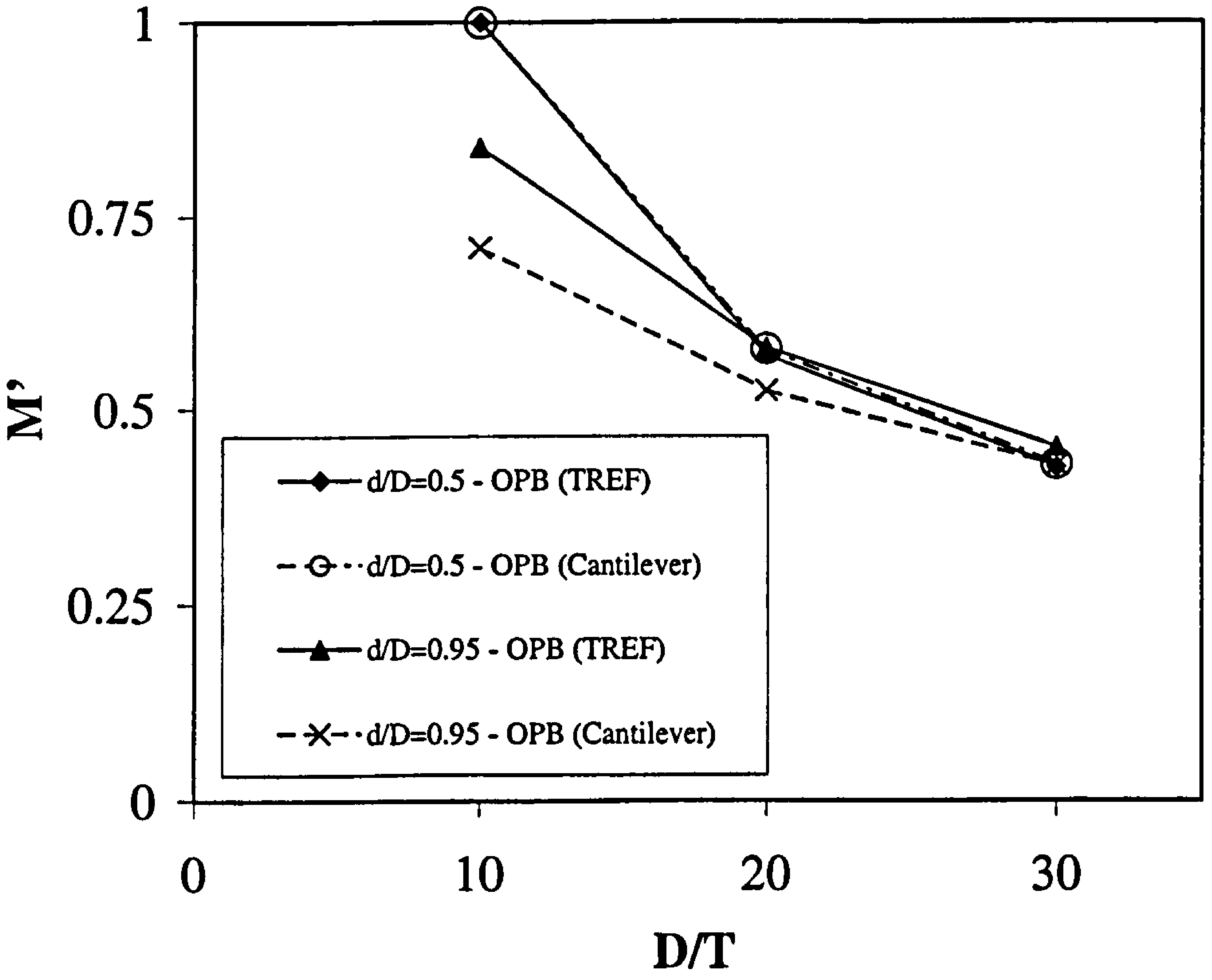

Figure 4.13: Effect of Run Pipe Boundary Conditions for Out-of-plane Branch Bending

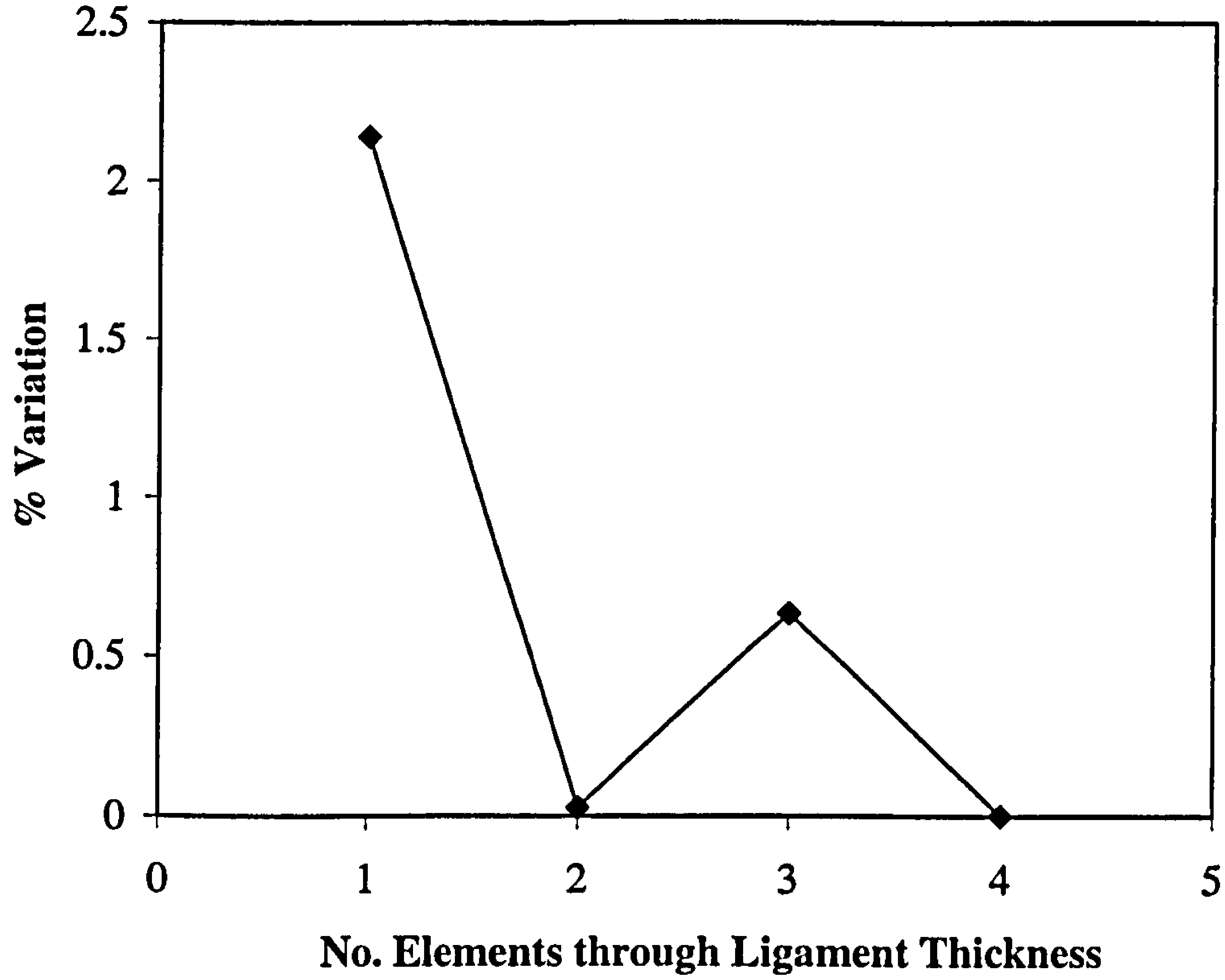

Figure 4.14: Mesh Convergence Study: Variation of Limit Moment for IPB (a/t=0.75)

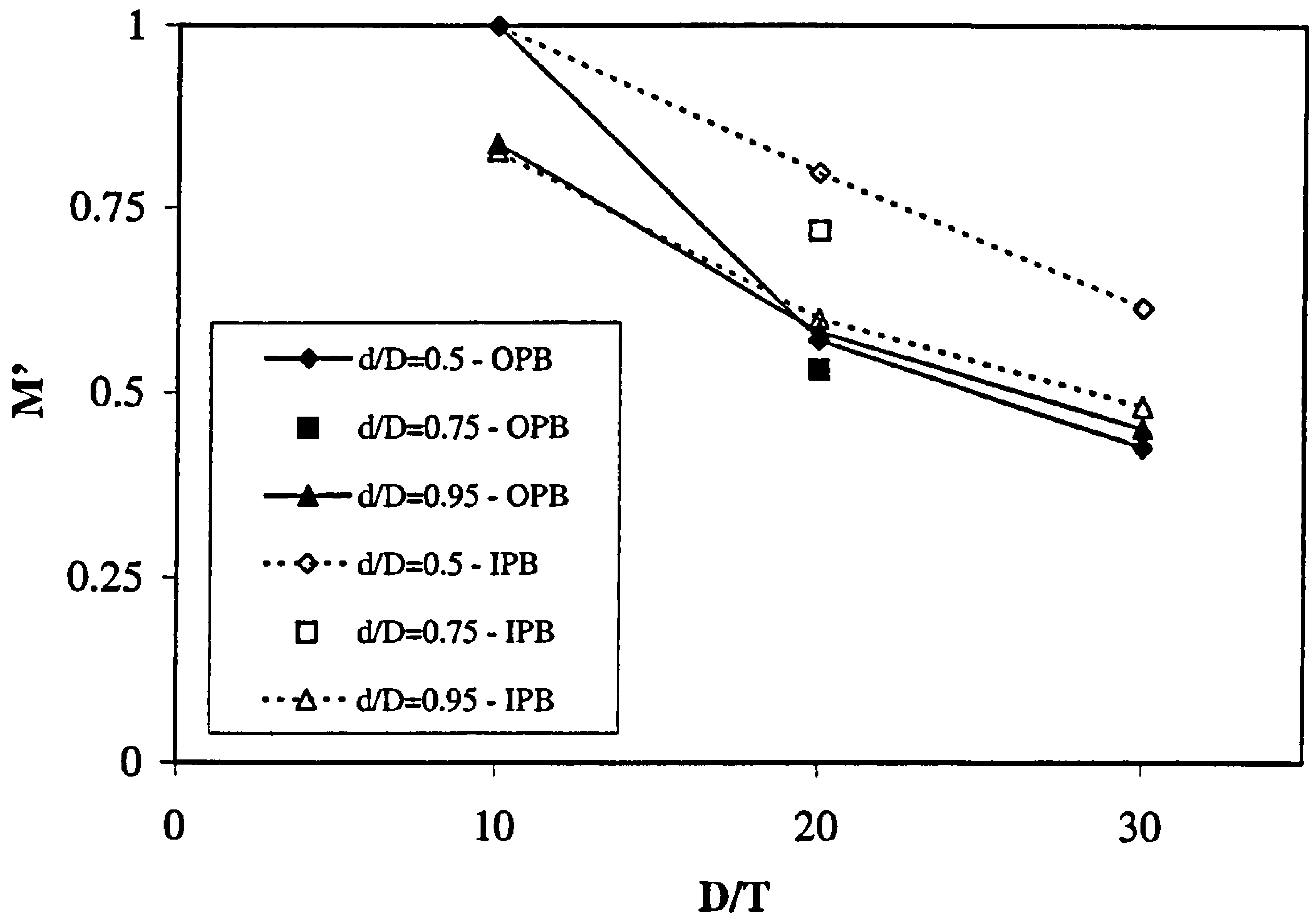

(a) Results plotted versus D/T

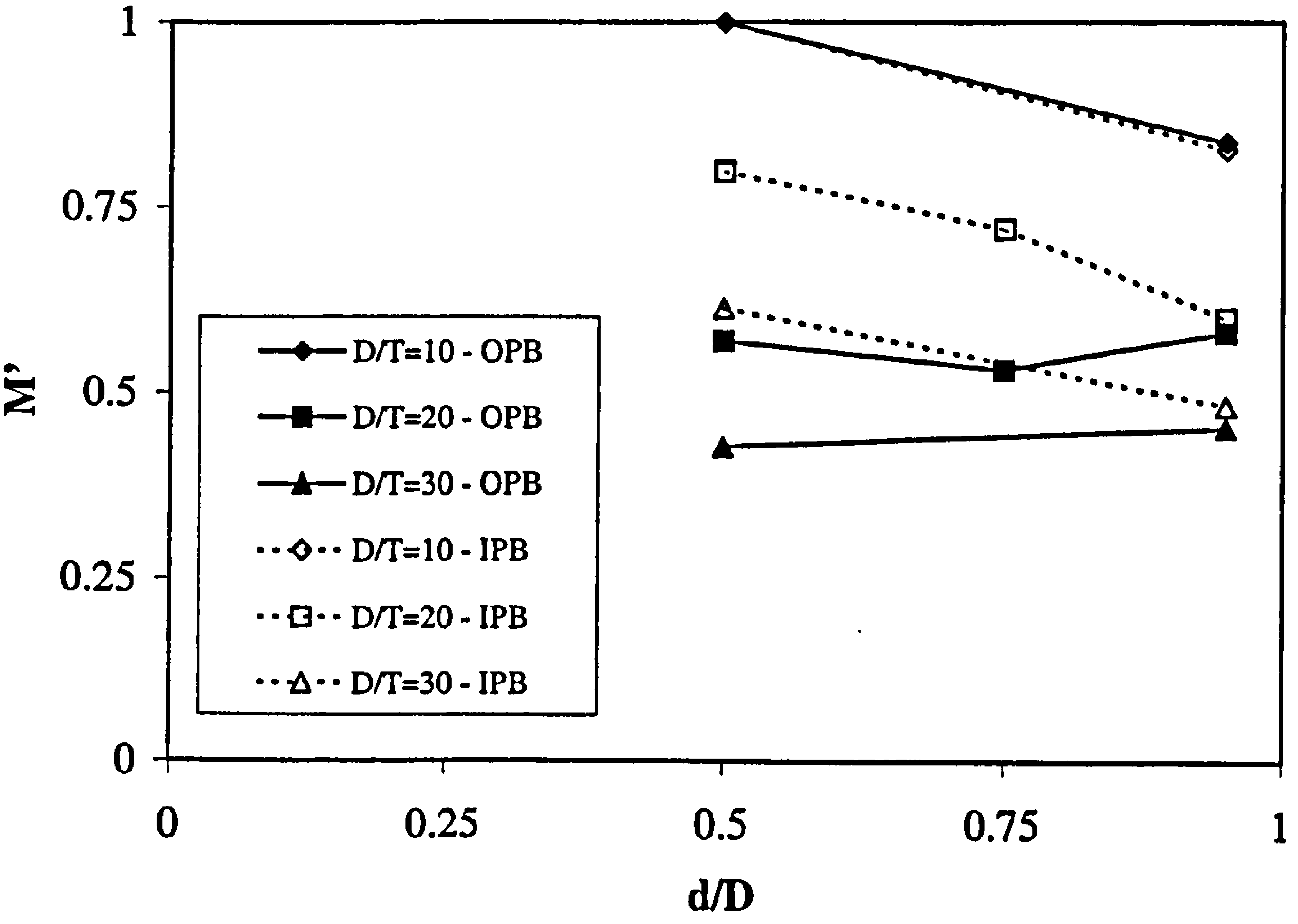

(b) Results plotted versus d/D

Figure 4.15: Uncracked Moment Results - Normalised using Plain Pipe Limit Moment

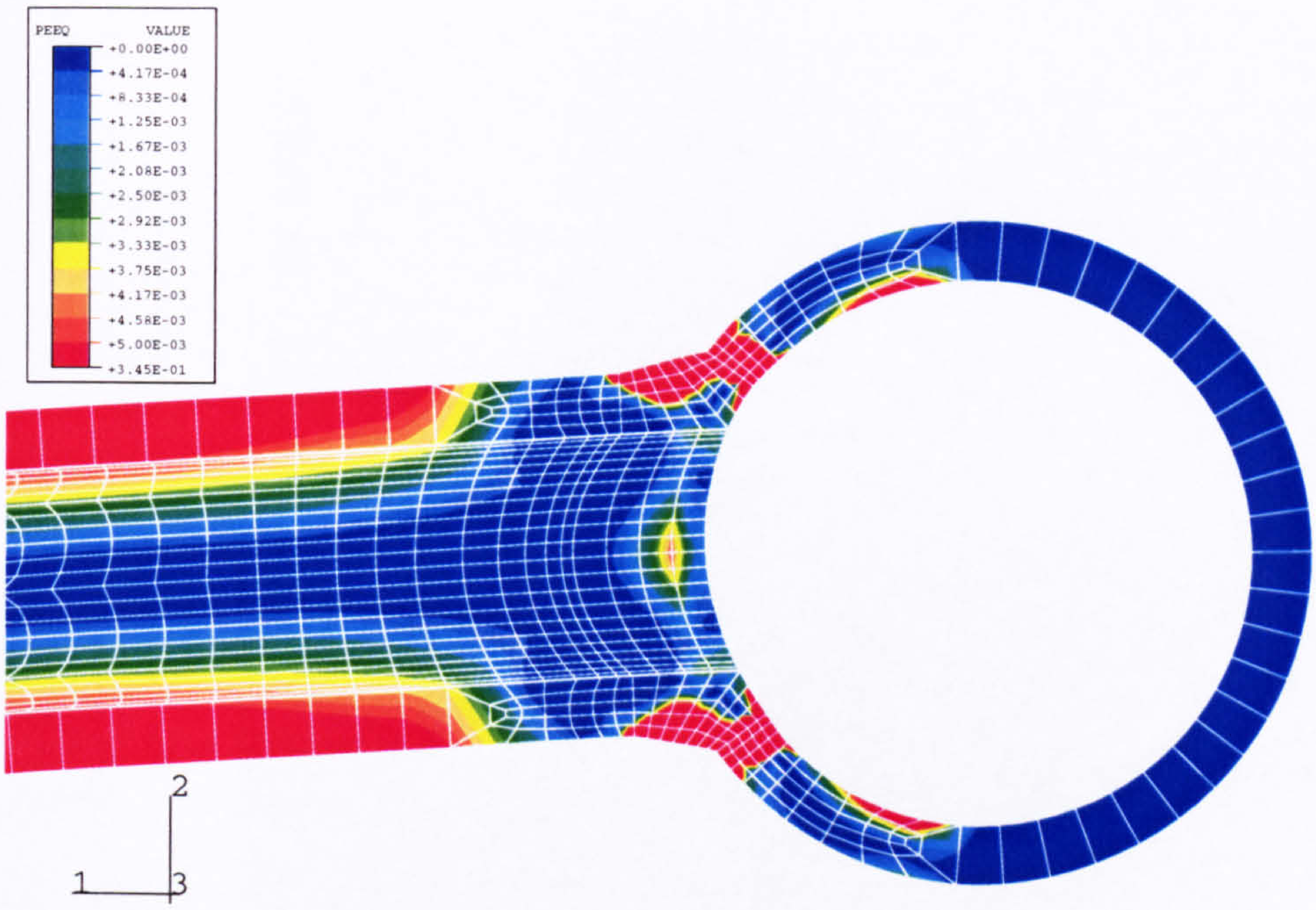

(a) d/D=0.5, D/T=10

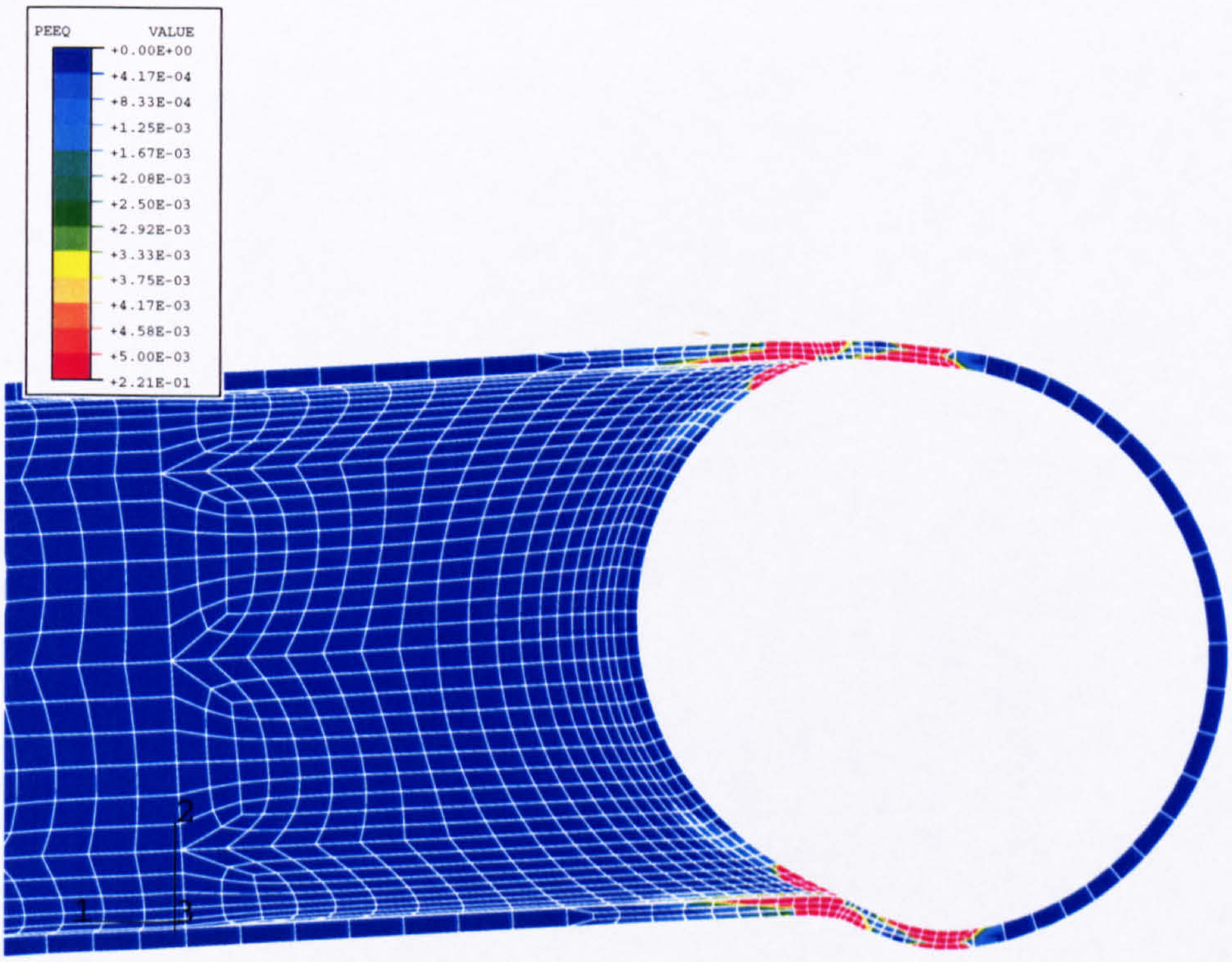

(b) d/D=0.95, D/T=30

Figure 4.16: Spread of Plasticity for Uncracked Out-of-plane Branch Pipe Bending

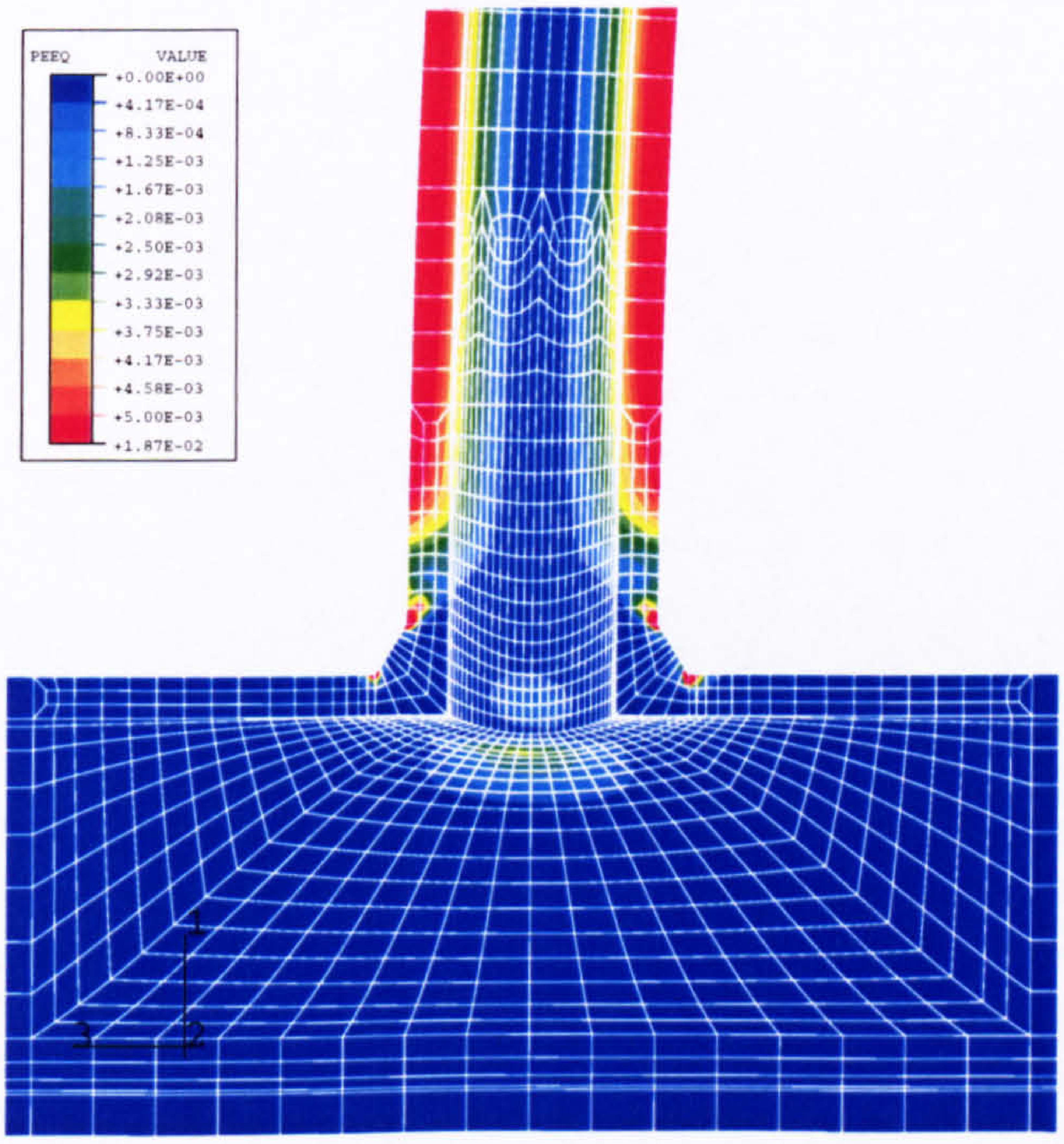

(a) d/D=0.5, D/T=10

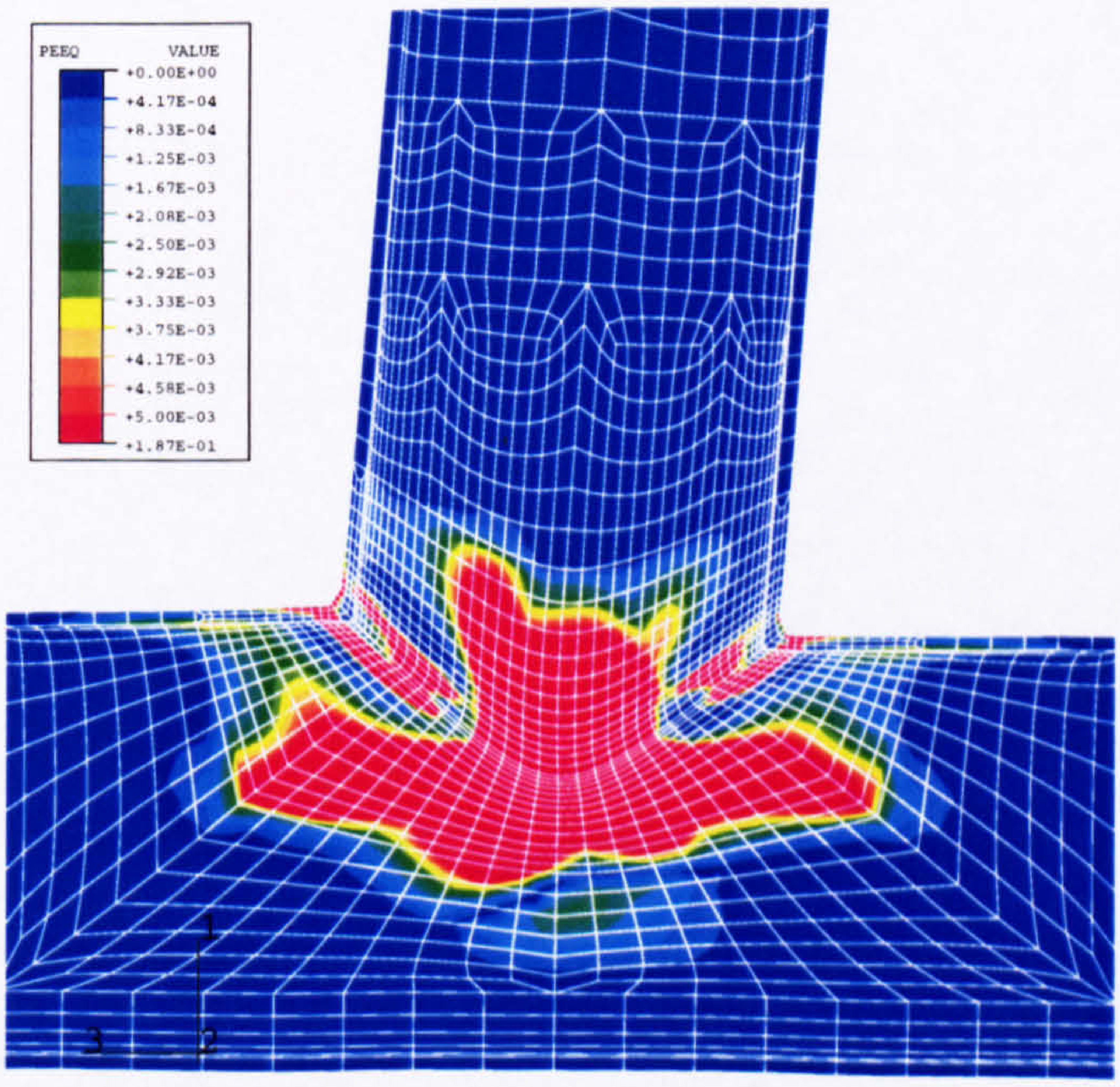

(b) d/D=0.95, D/T=30

Figure 4.17: Spread of Plasticity for Uncracked In-plane Branch Pipe Bending

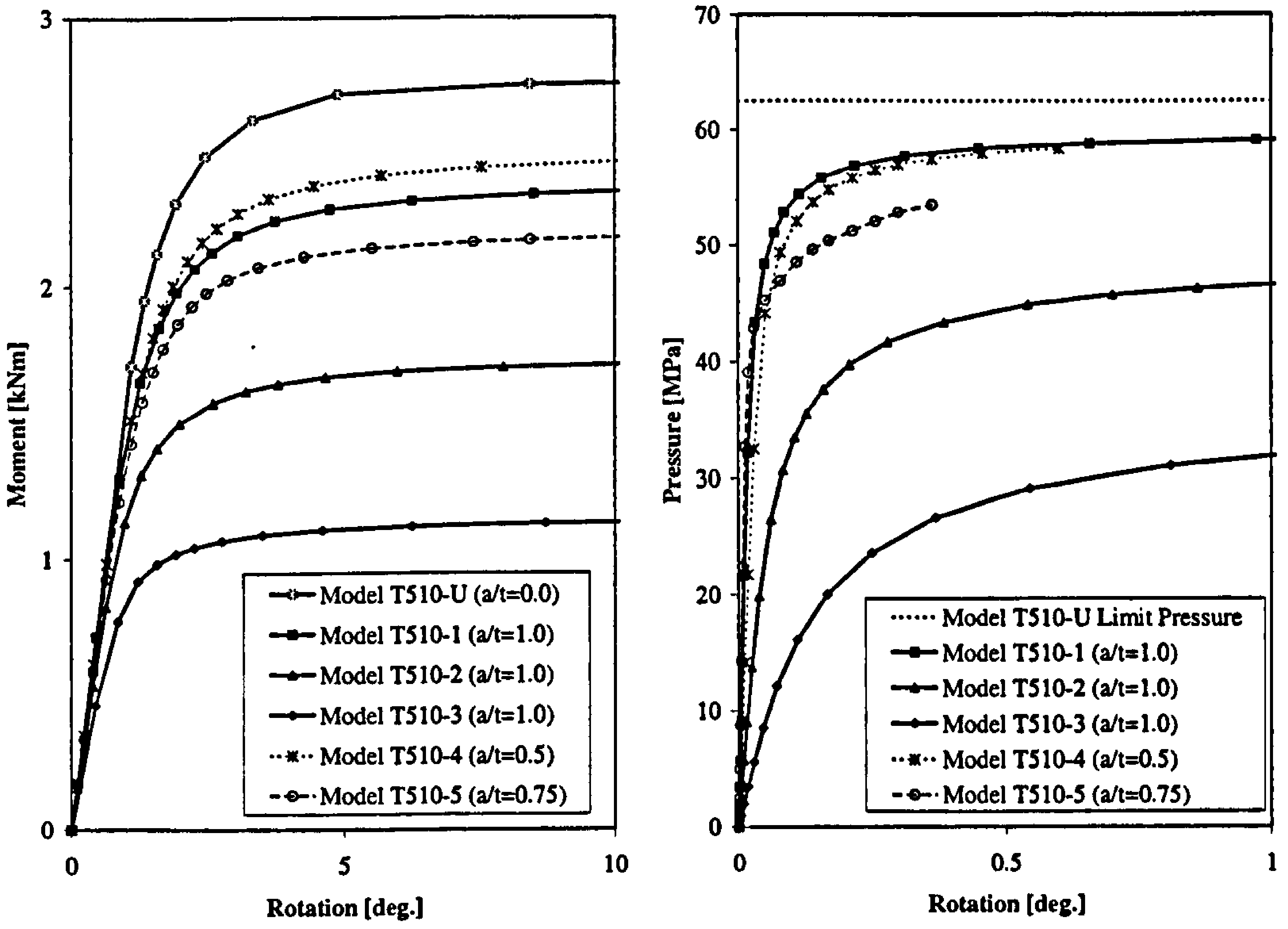

(a) OPB - d/D=0.5, D/T=10 (b) Pressure - d/D=0.5, D/T=10

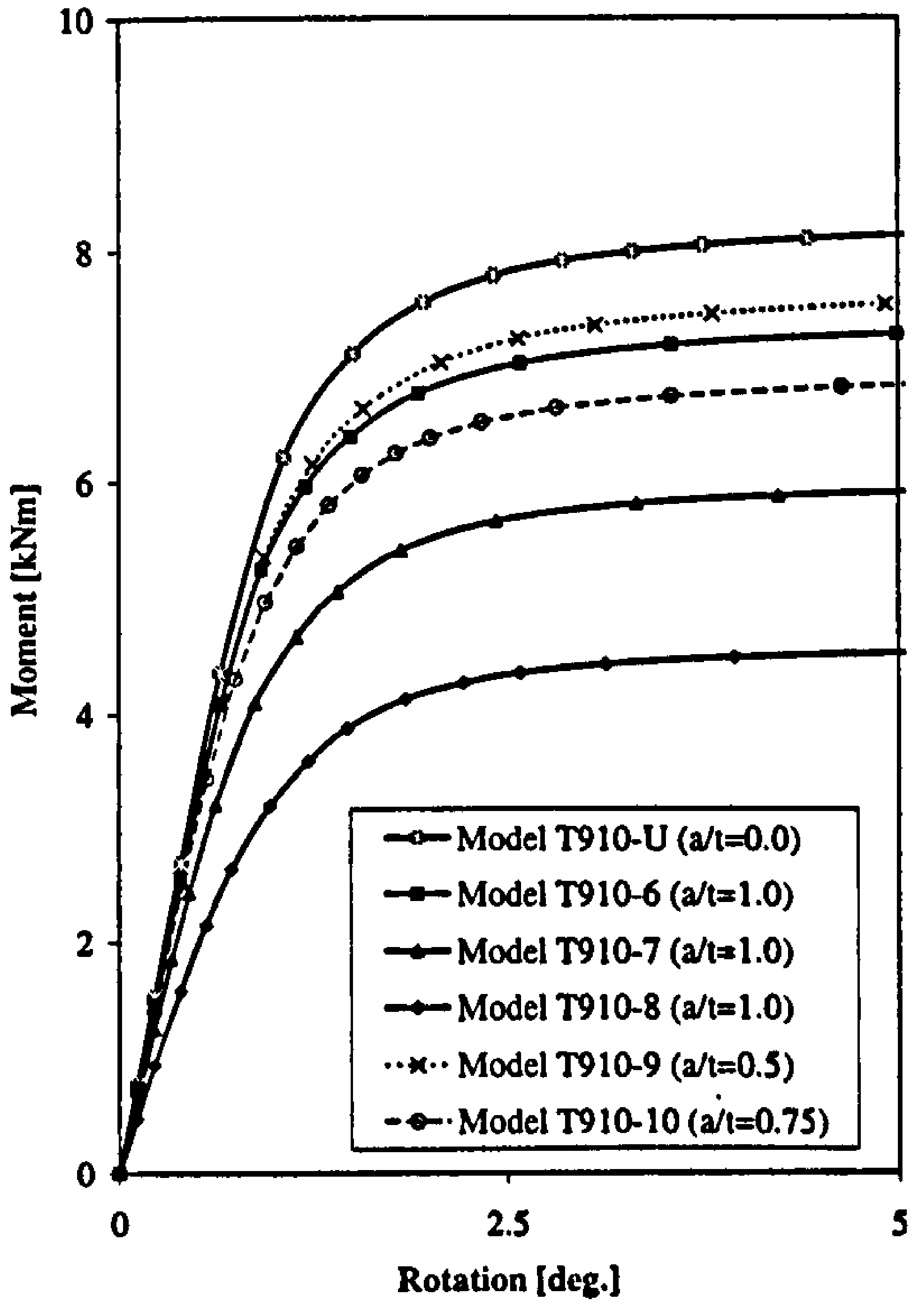

(c) IPB - d/D=0.95, D/T=10

Figure 4.18: Typical Load versus Rotation Curves

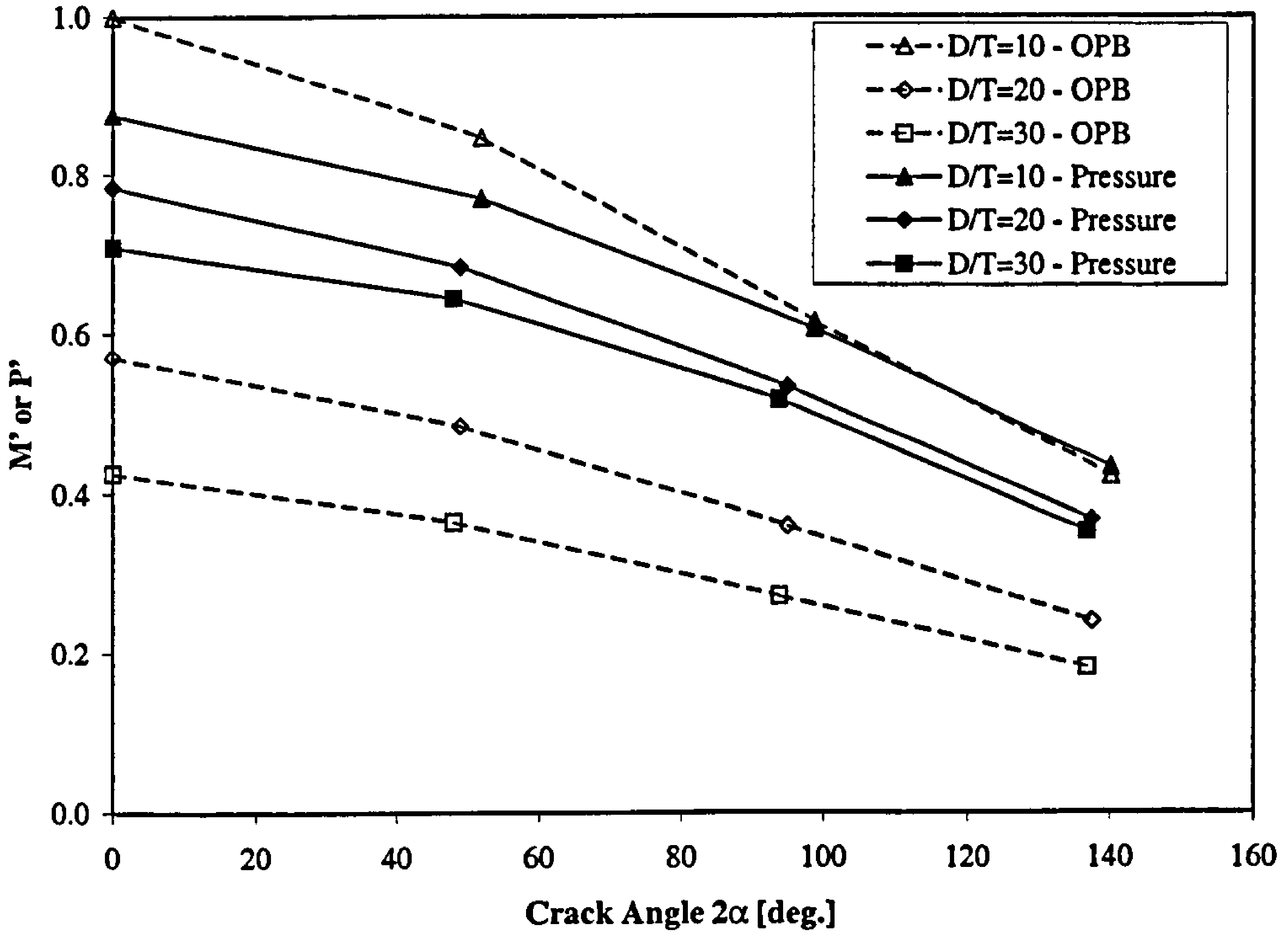

(a) Results Normalised using Plain Pipe Values

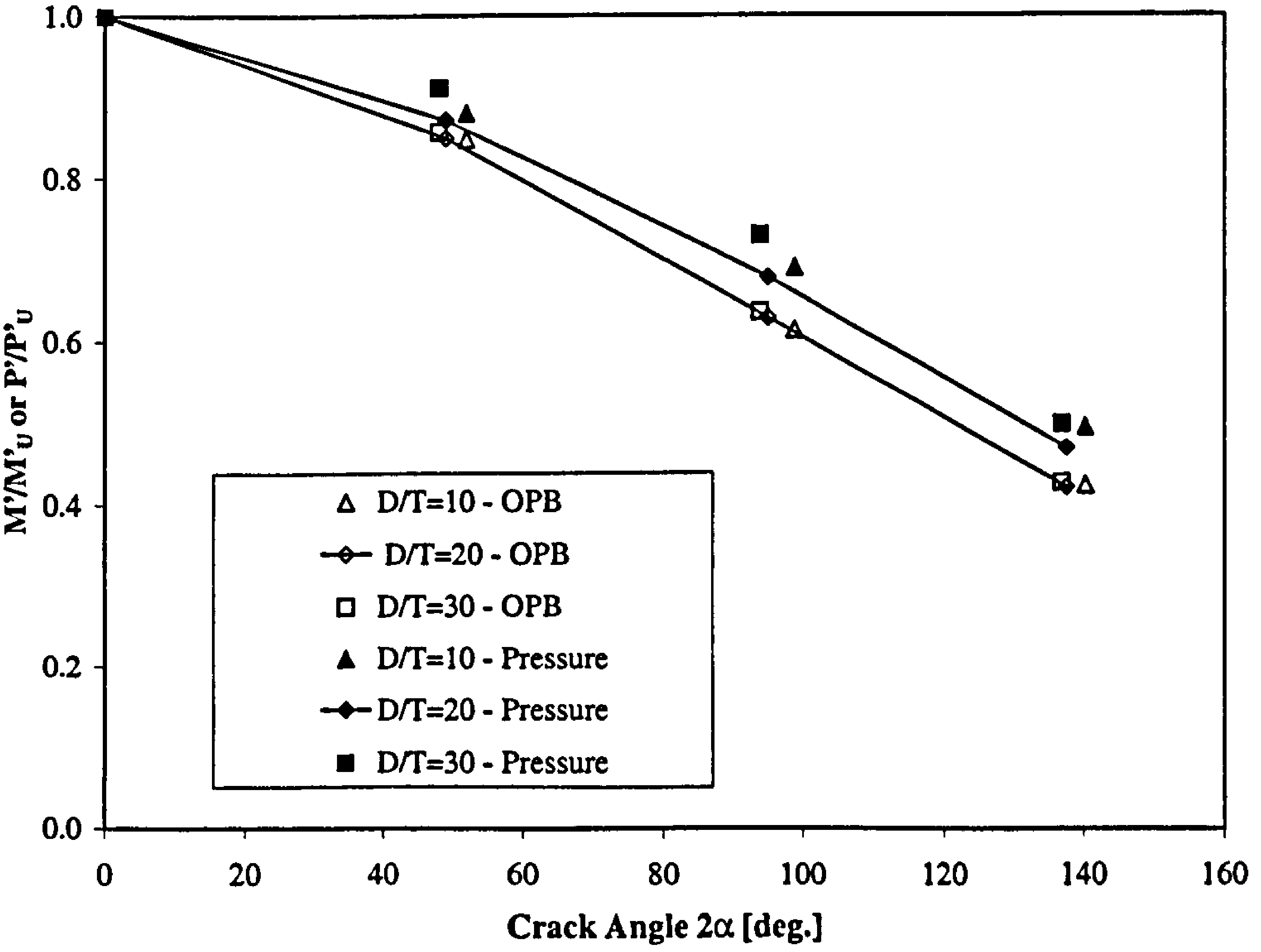

(b) Results Normalised using Uncracked Limit Load

Figure 4.19: Variation of OPB and Pressure Results with Crack Angle: d/D=0.5, a/t=1.0

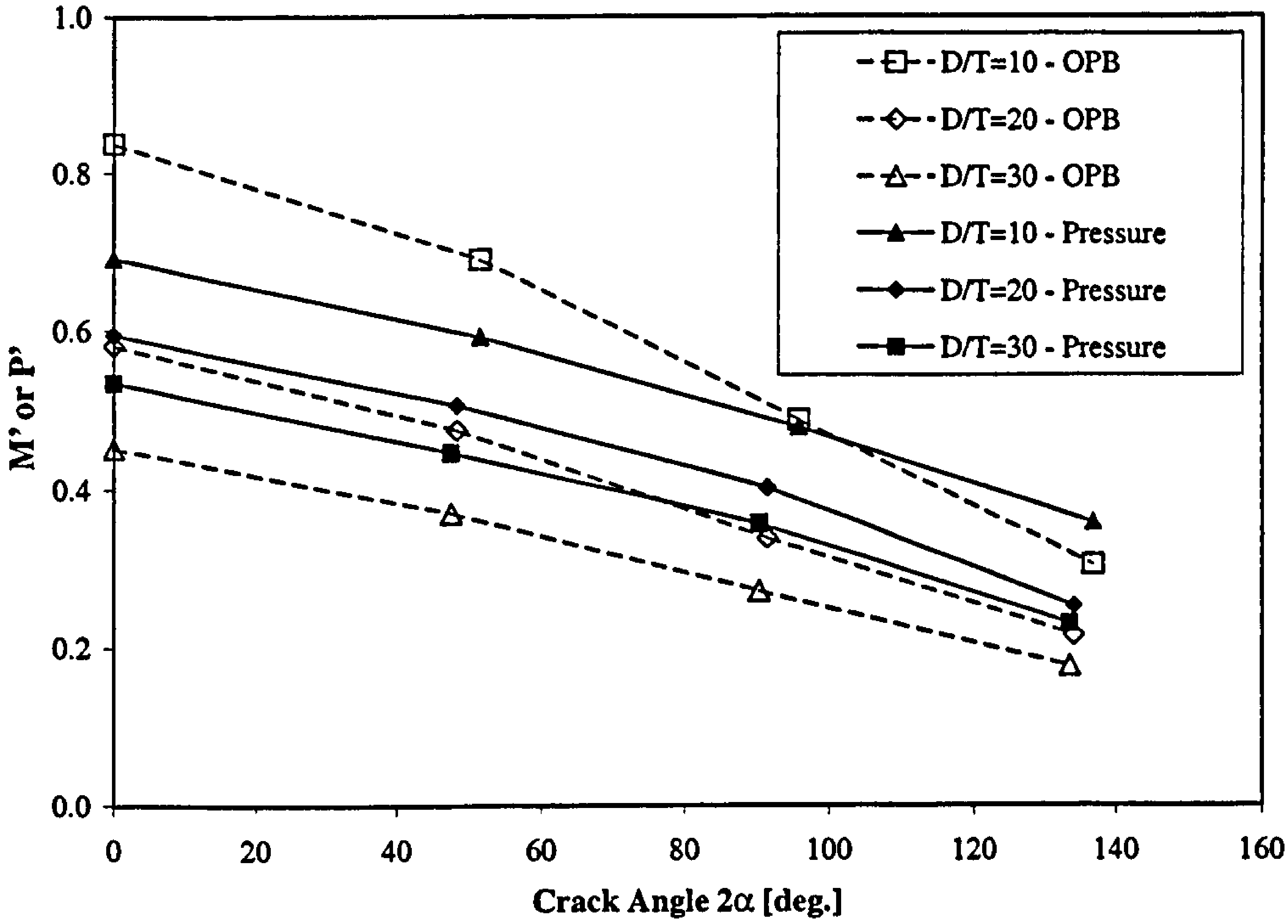

(a) Results Normalised using Plain Pipe Values

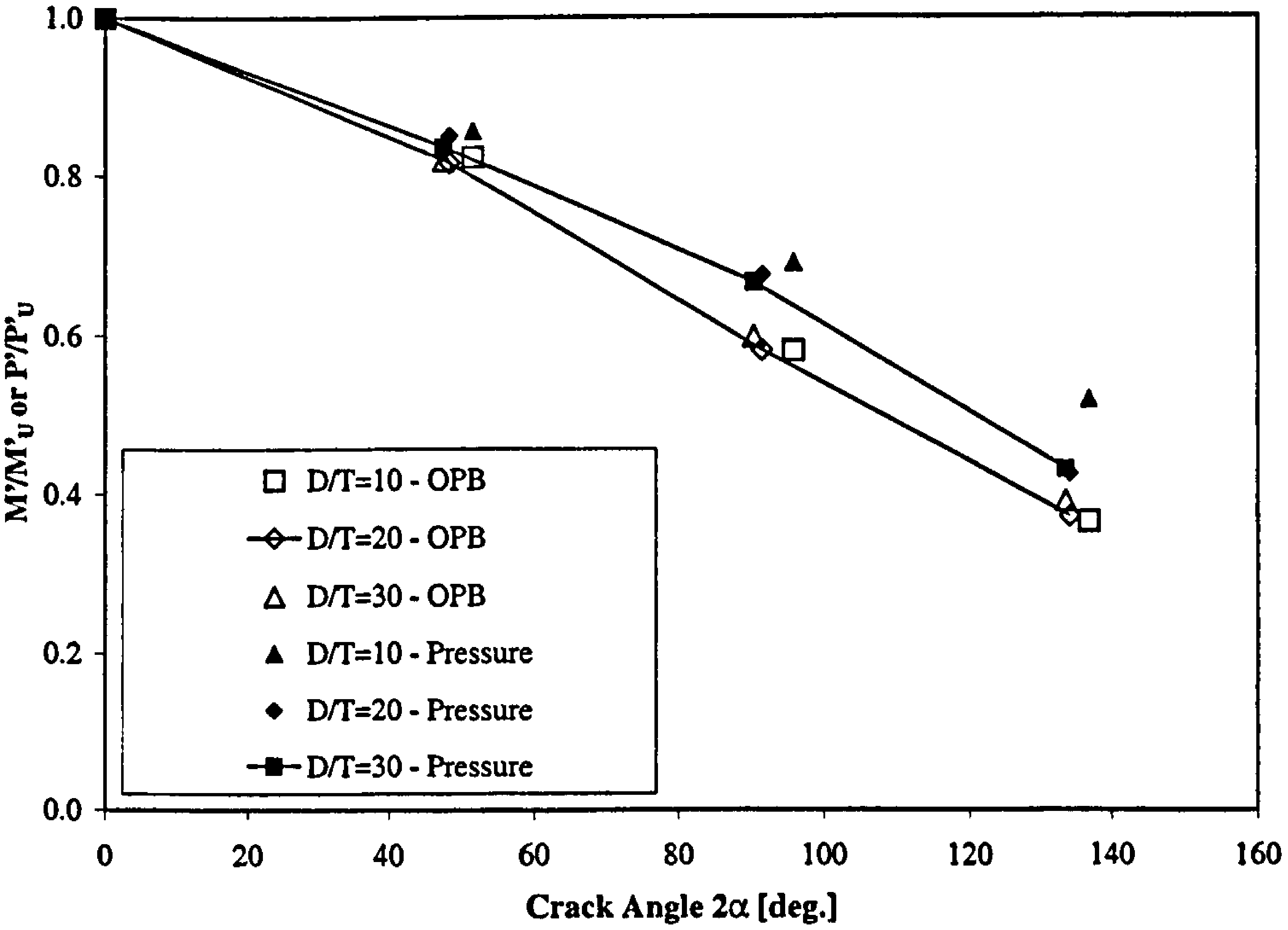

(b) Results Normalised using Uncracked Limit Load

Figure 4.20: Variation of OPB and Pressure Results with Crack Angle: d/D=0.95, a/t=1.0

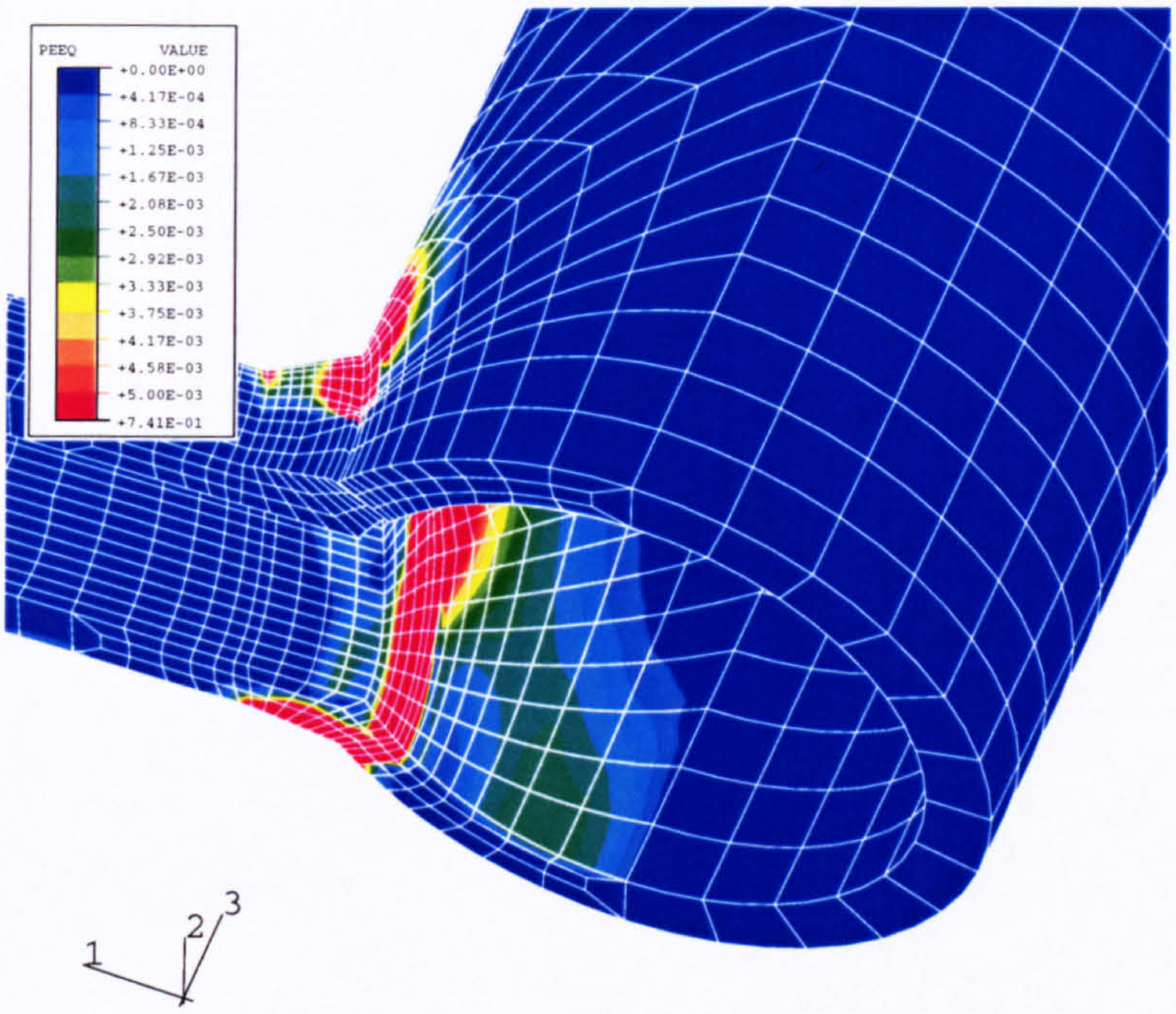

(a) Model T510-1 - d/D=0.5, D/T=10 (M/M'=0.94)

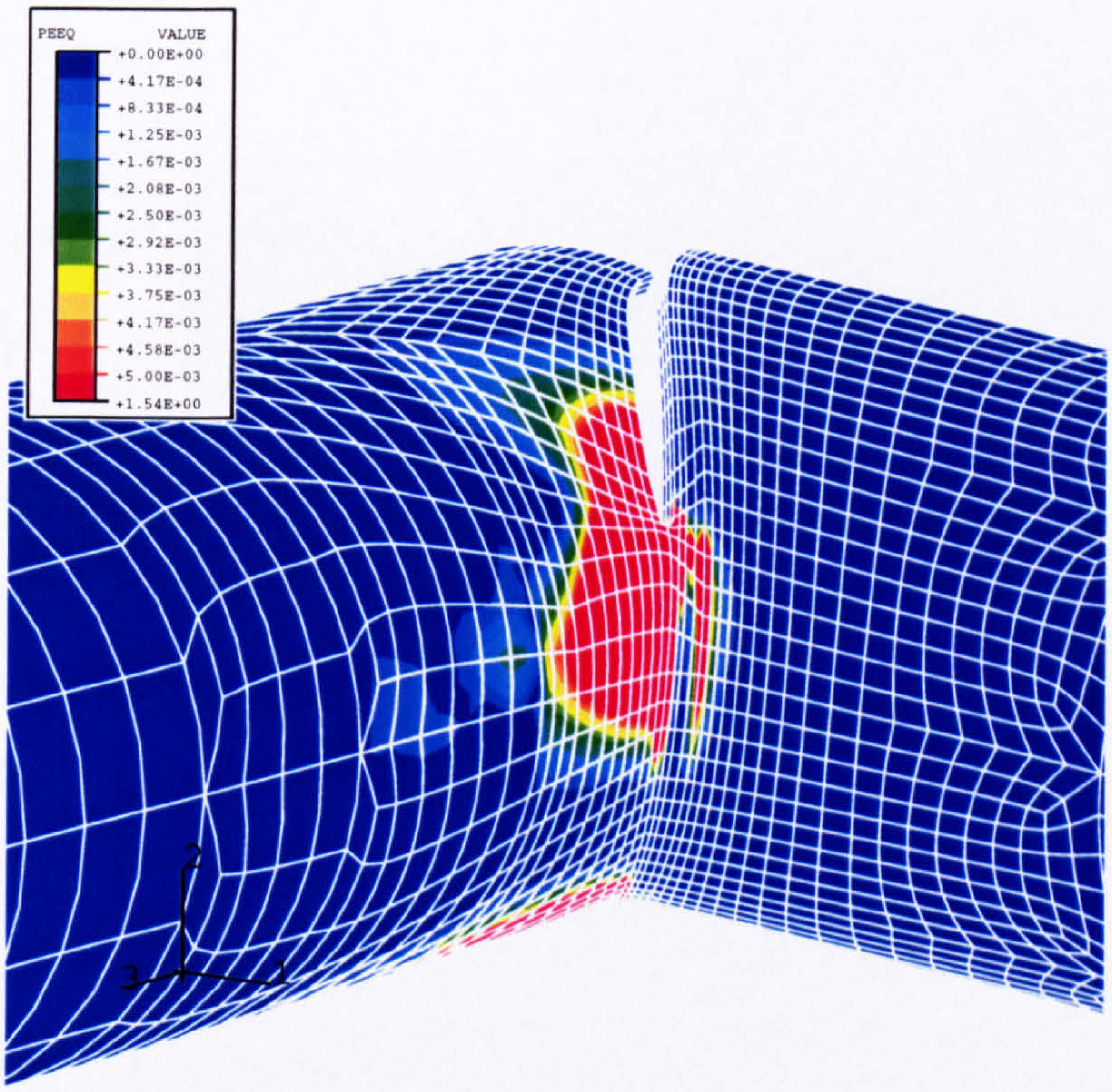

(b) Model T530-3 - d/D=0.95, D/T=30 (M/M'=0.95)

Figure 4.21: Spread of Plasticity for Cracked Junctions under Out-of-plane Bending

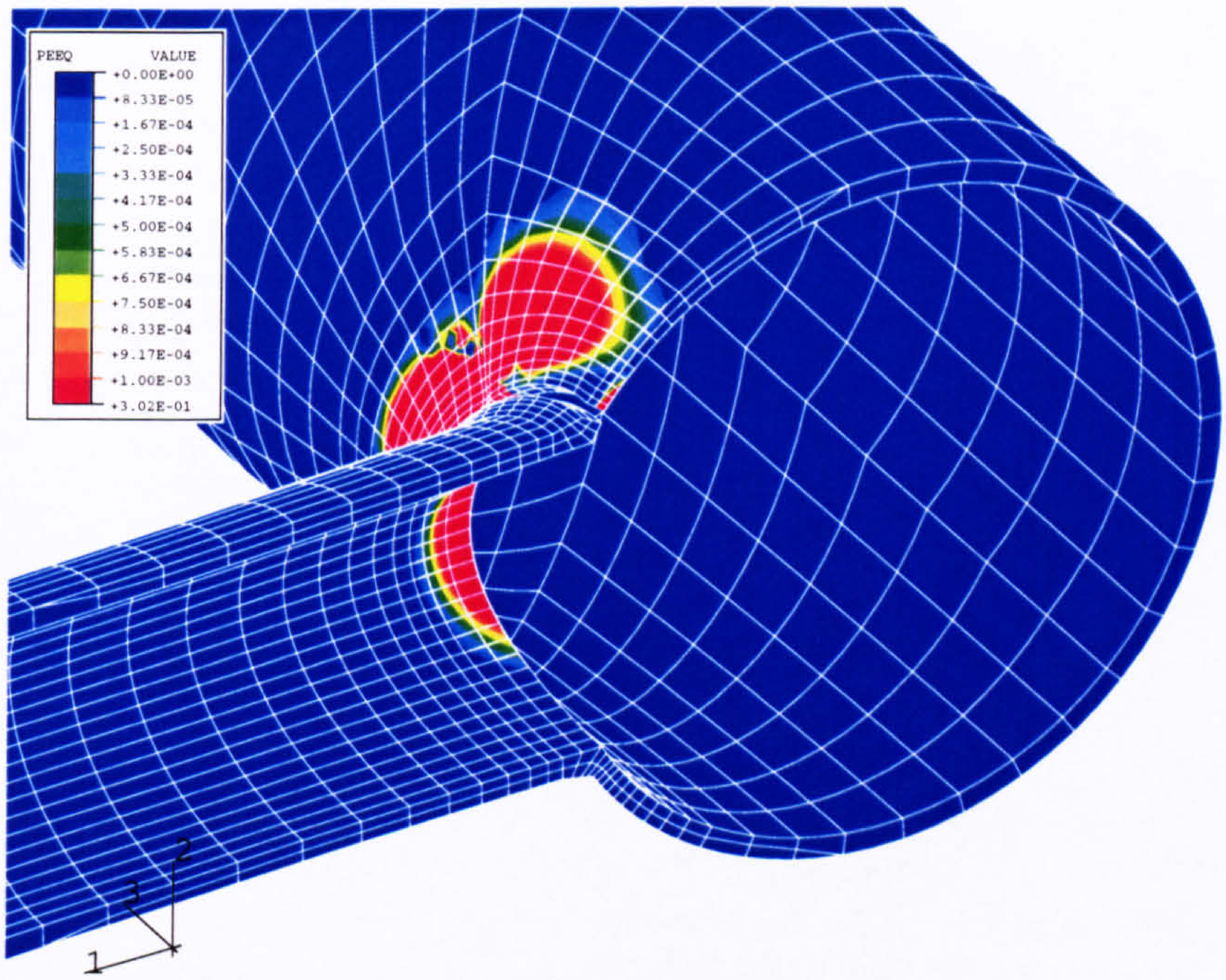

(a) Model T530-2 - d/D=0.5, D/T=30 (P/P'=0.93; dmag=5)

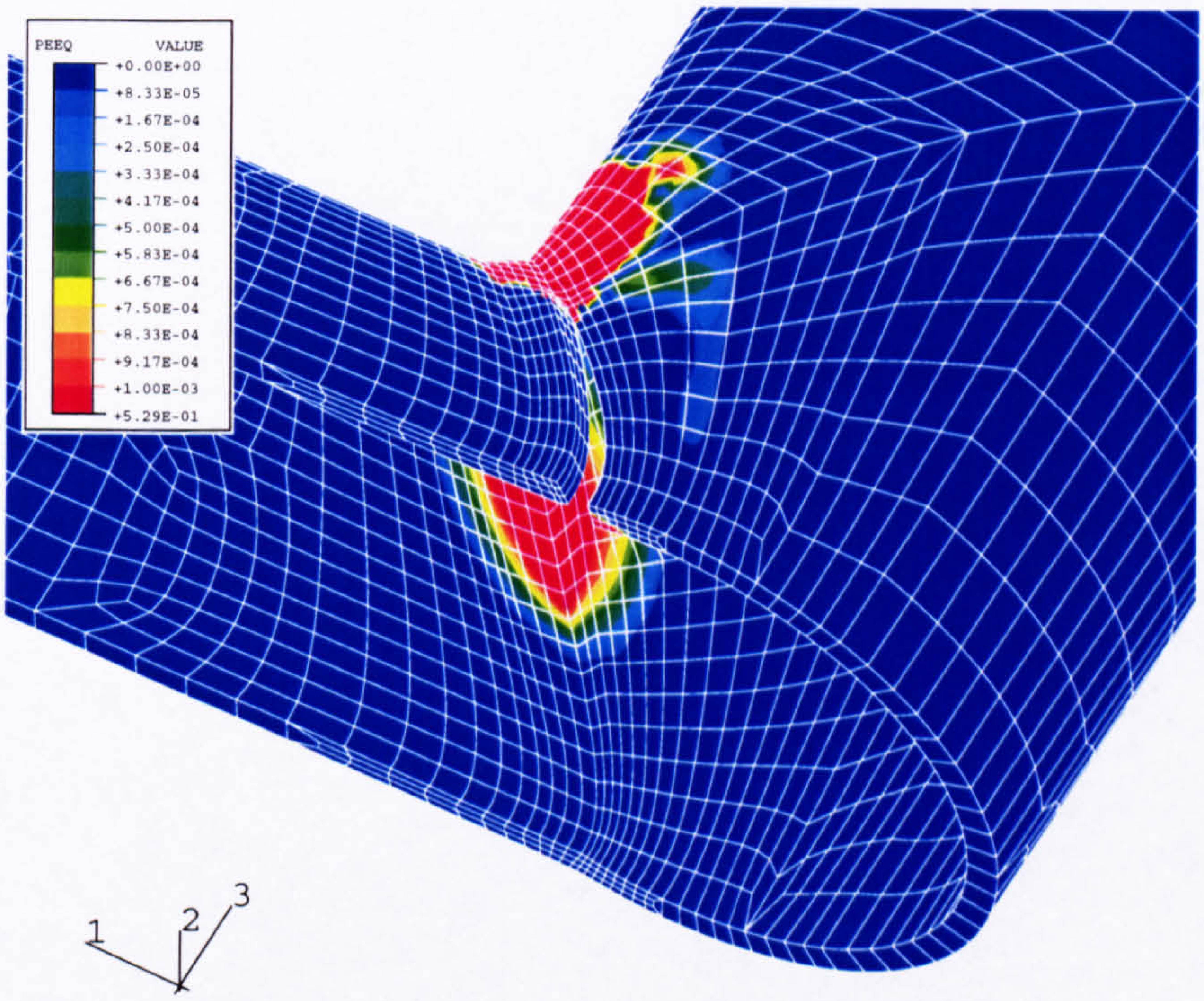

(b) Model T920-2 - d/D=0.95, D/T=20 (P/P'=0.93; dmag=5)

Figure 4.22: Spread of Plasticity for Cracked Junctions under Pressure

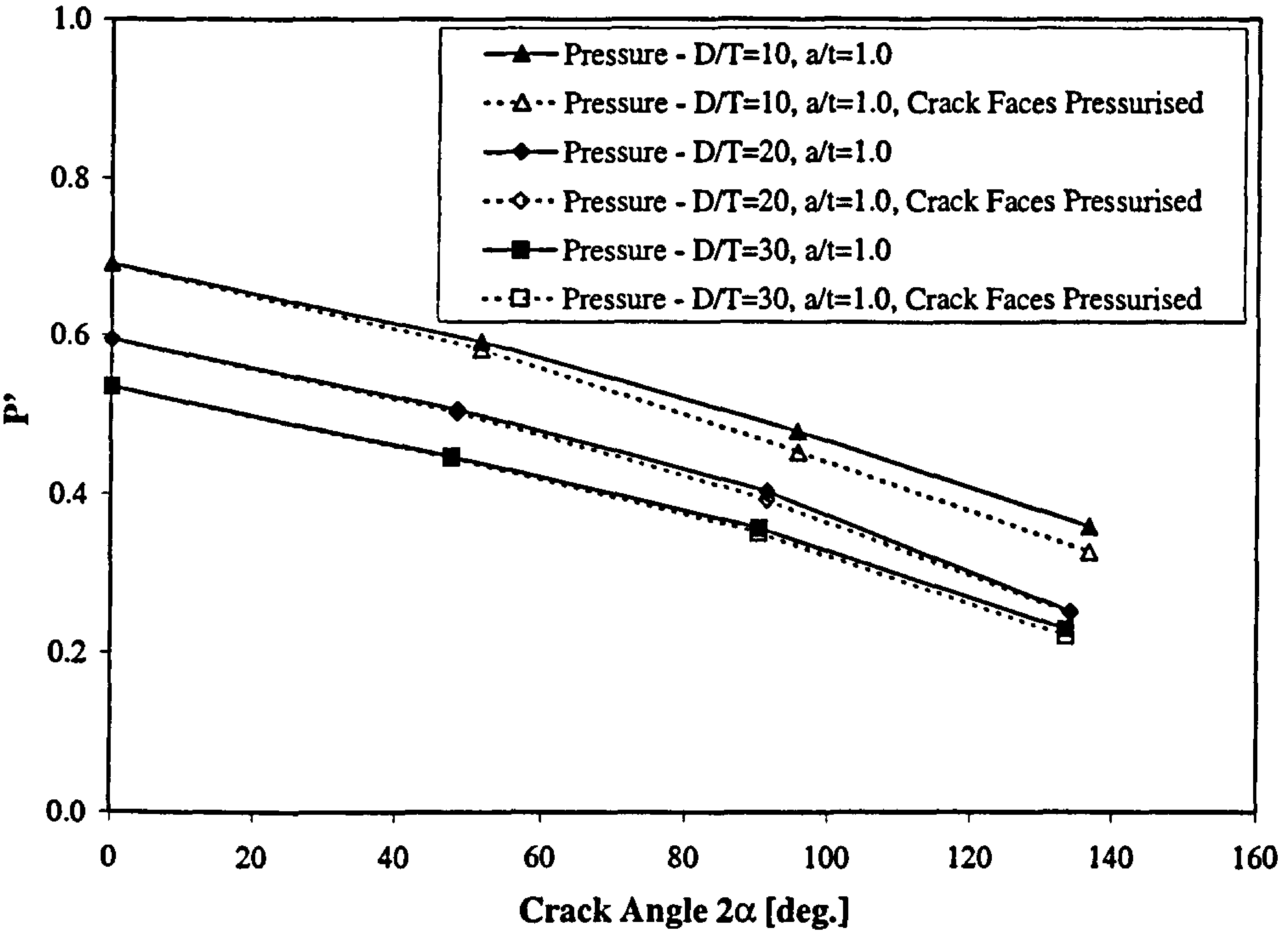

Figure 4.23: Effect of Pressurising Crack Faces - d/D=0.95, a/t=1.0

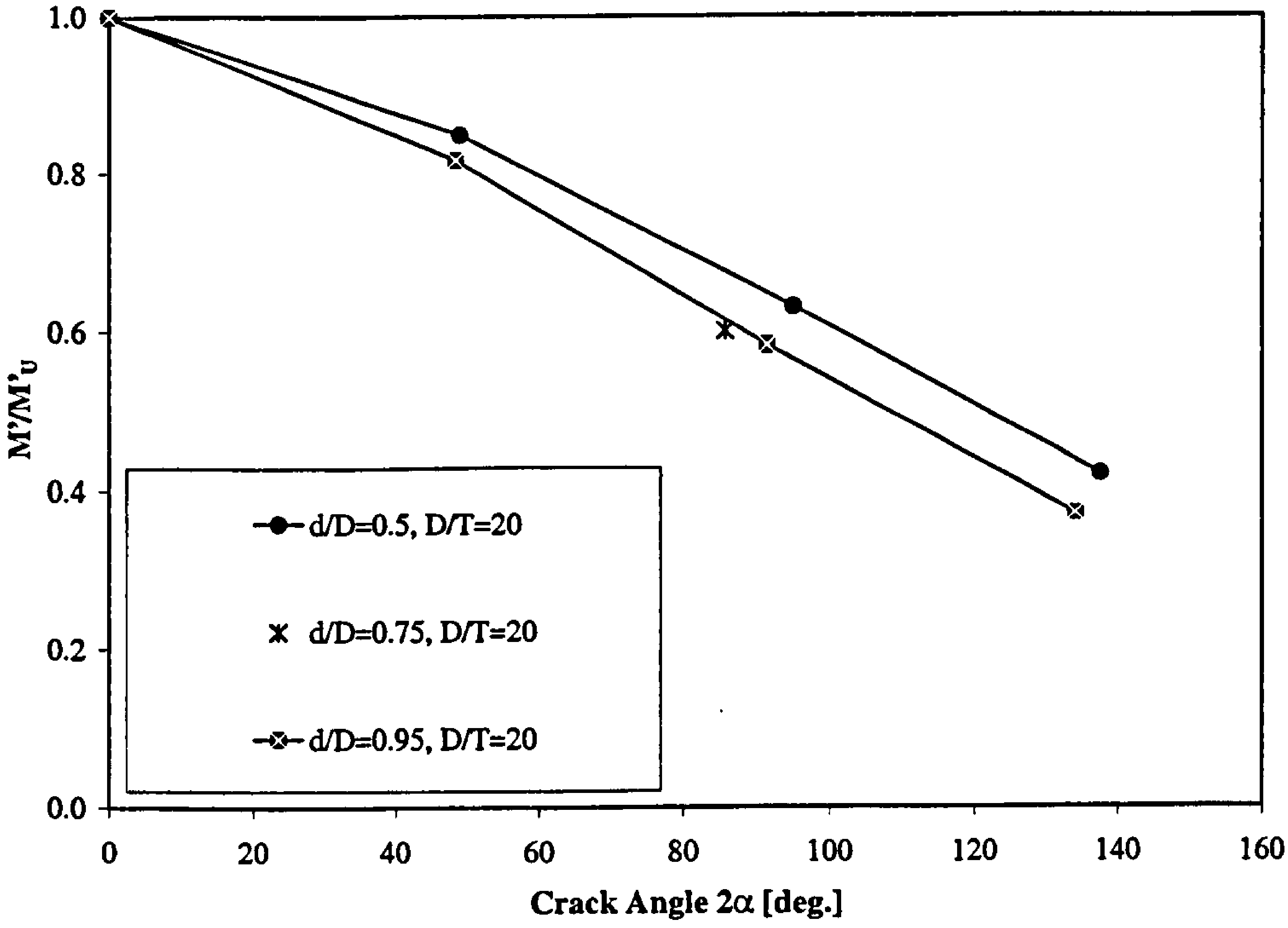

(a) OPB Summary

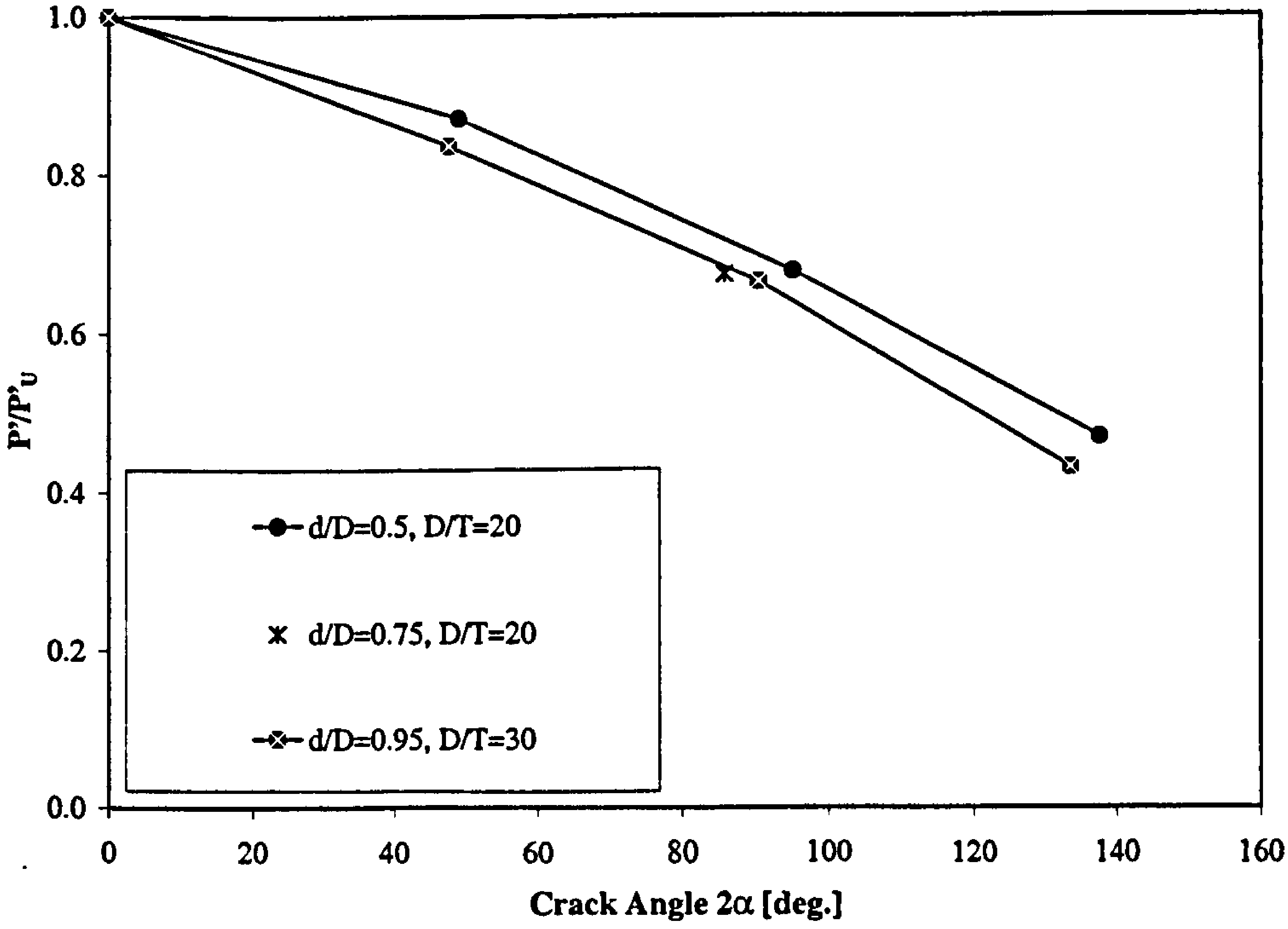

(b) Pressure Summary

Figure 4.24: Summary of Limit Load Results for Cracked OPB and Pressure (a/t=1.0)

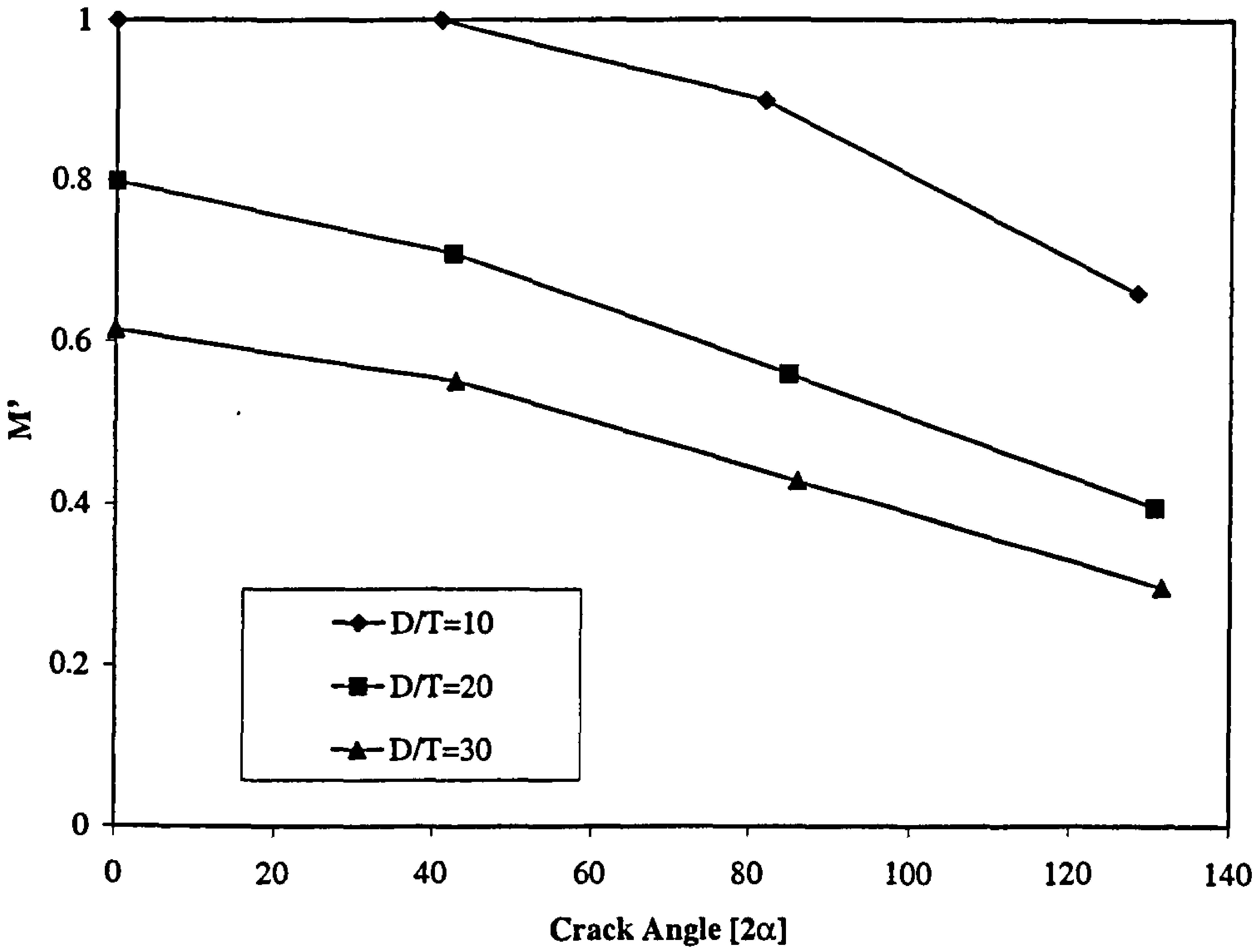

(a) Results Normalised using Plain Pipe Values

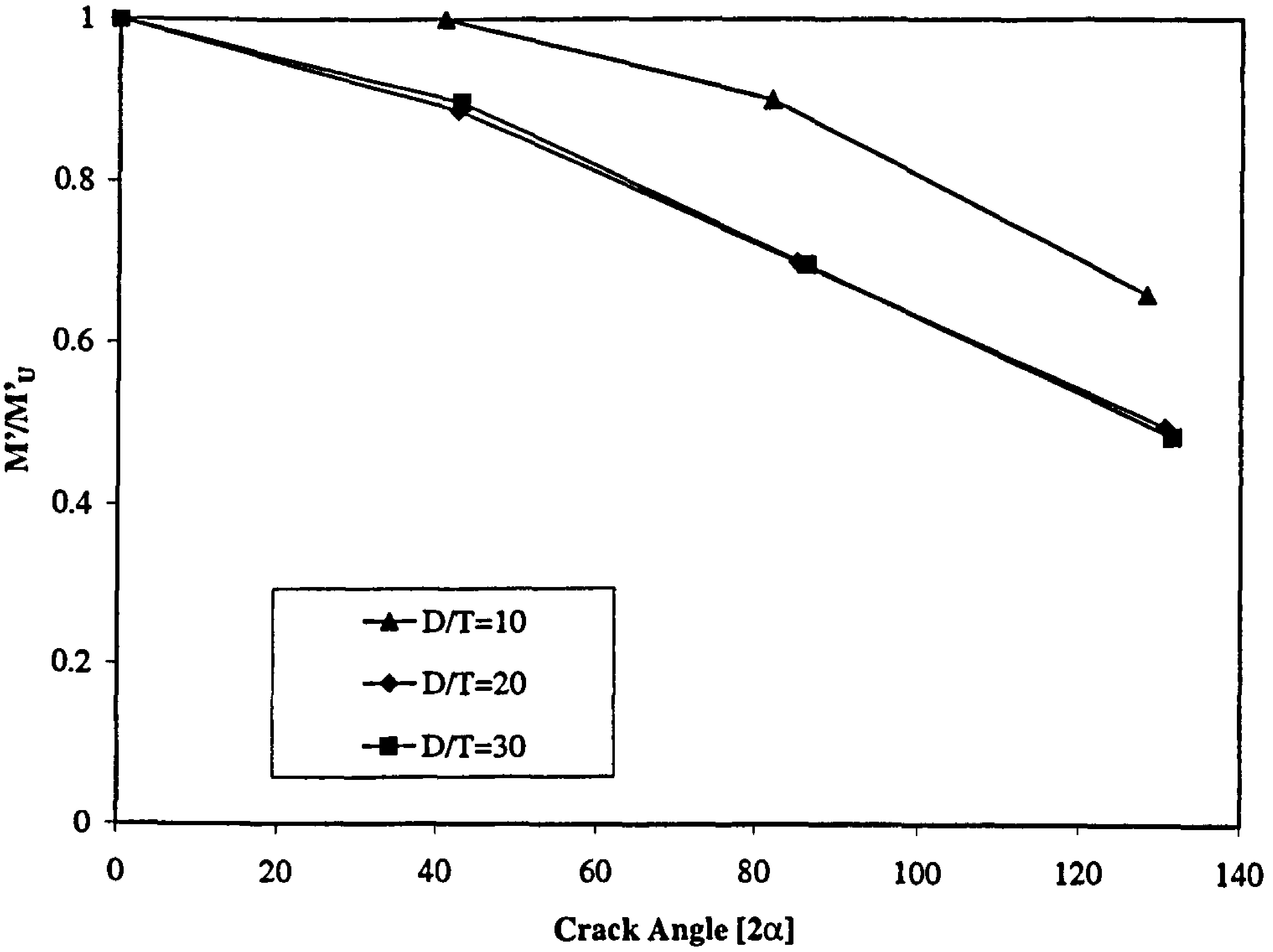

(b) Results Normalised using Uncracked Limit Load

Figure 4.25: Variation of IPB Results with Crack Angle: d/D=0.5, a/t=1.0

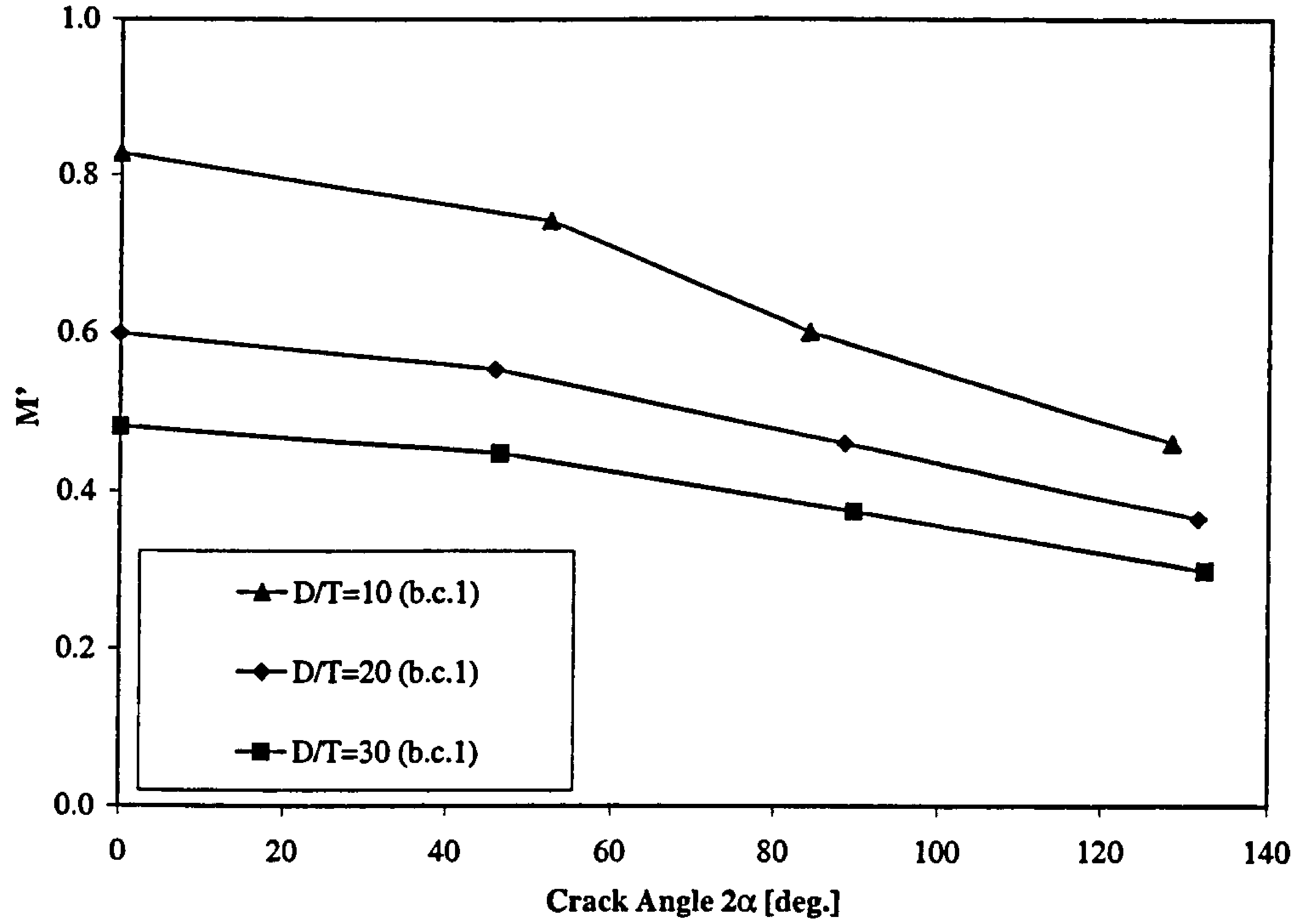

(a) Results Normalised using Plain Pipe Values

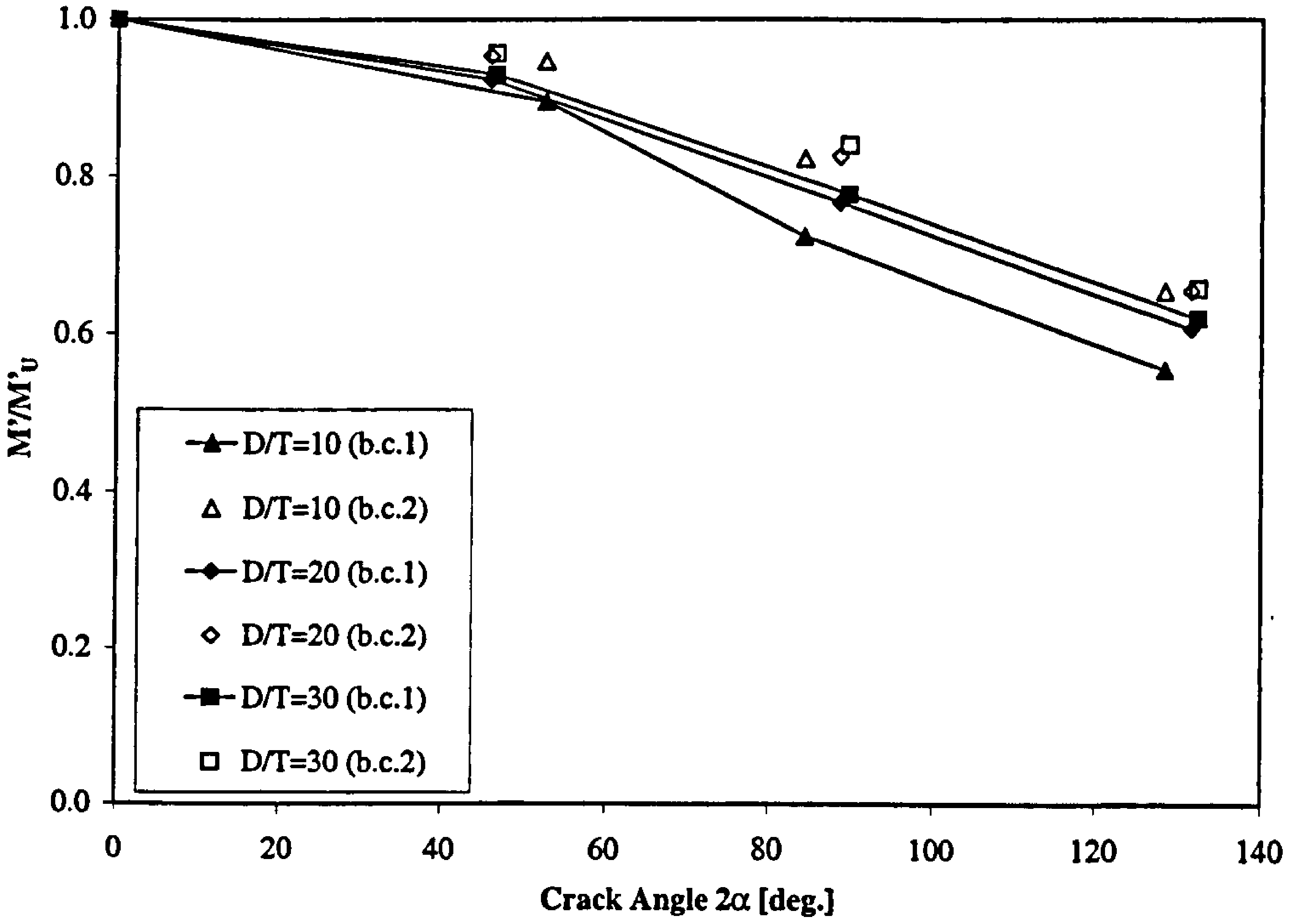

(b) Results Normalised using Uncracked Limit Load

Figure 4.26: Variation of IPB Results with Crack Angle: d/D=0.95, a/t=1.0

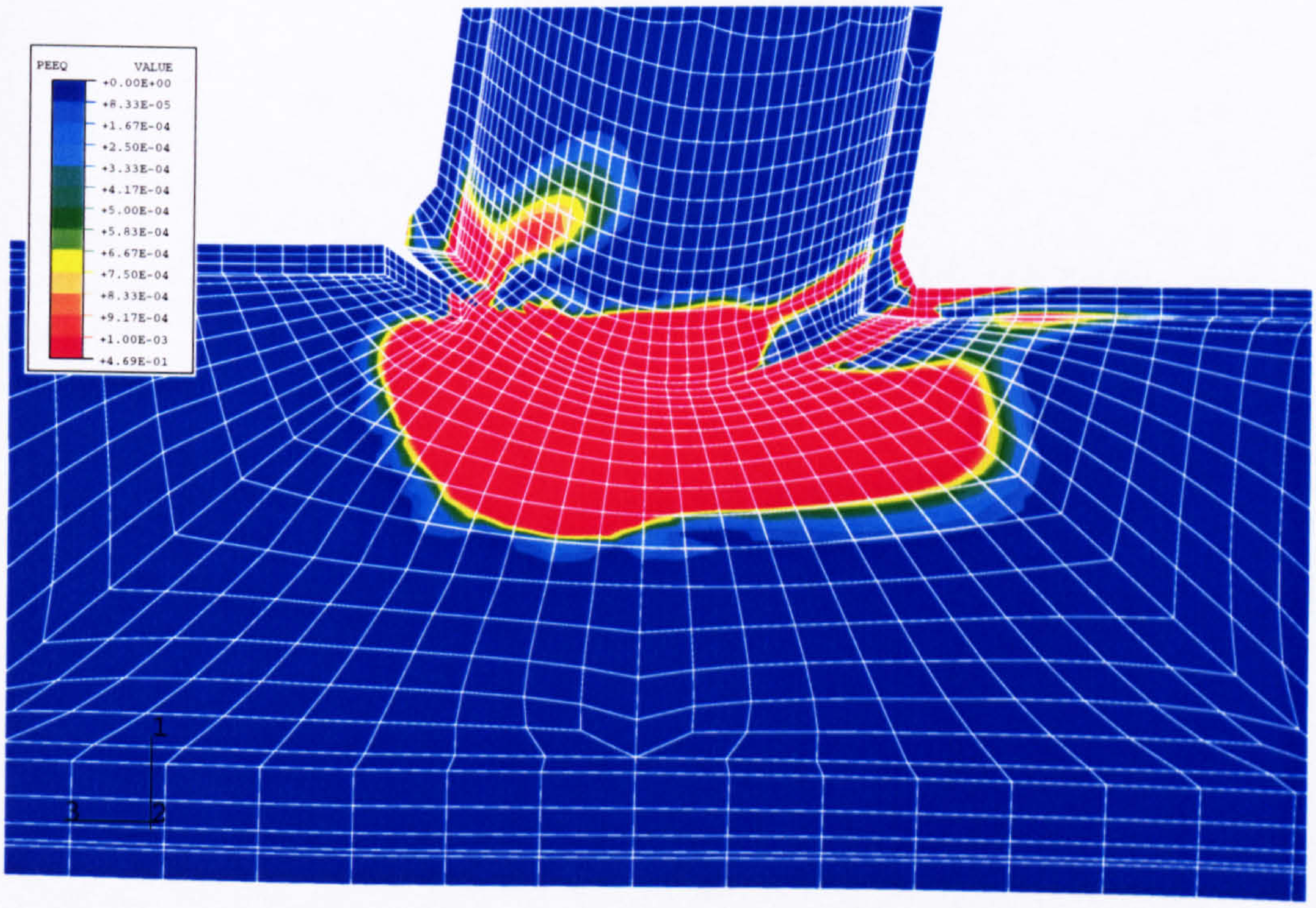

Figure 4.27: Spread of Plasticity for In-plane Bending:
Model T720-7 (M/M'=0.89, dmag=5)

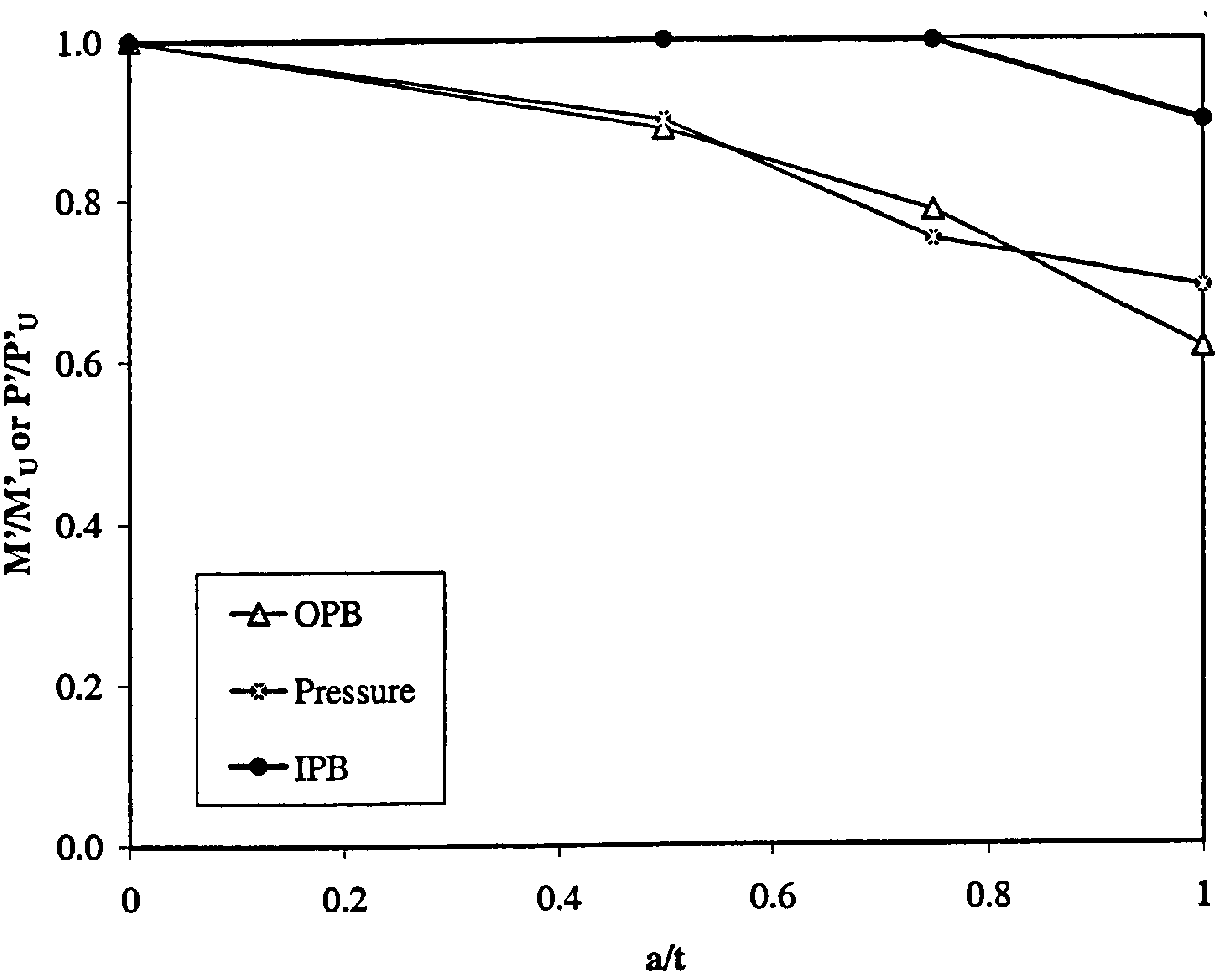

(a) d/D=0.5, D/T=10 - Normalised using Uncracked Limit Load

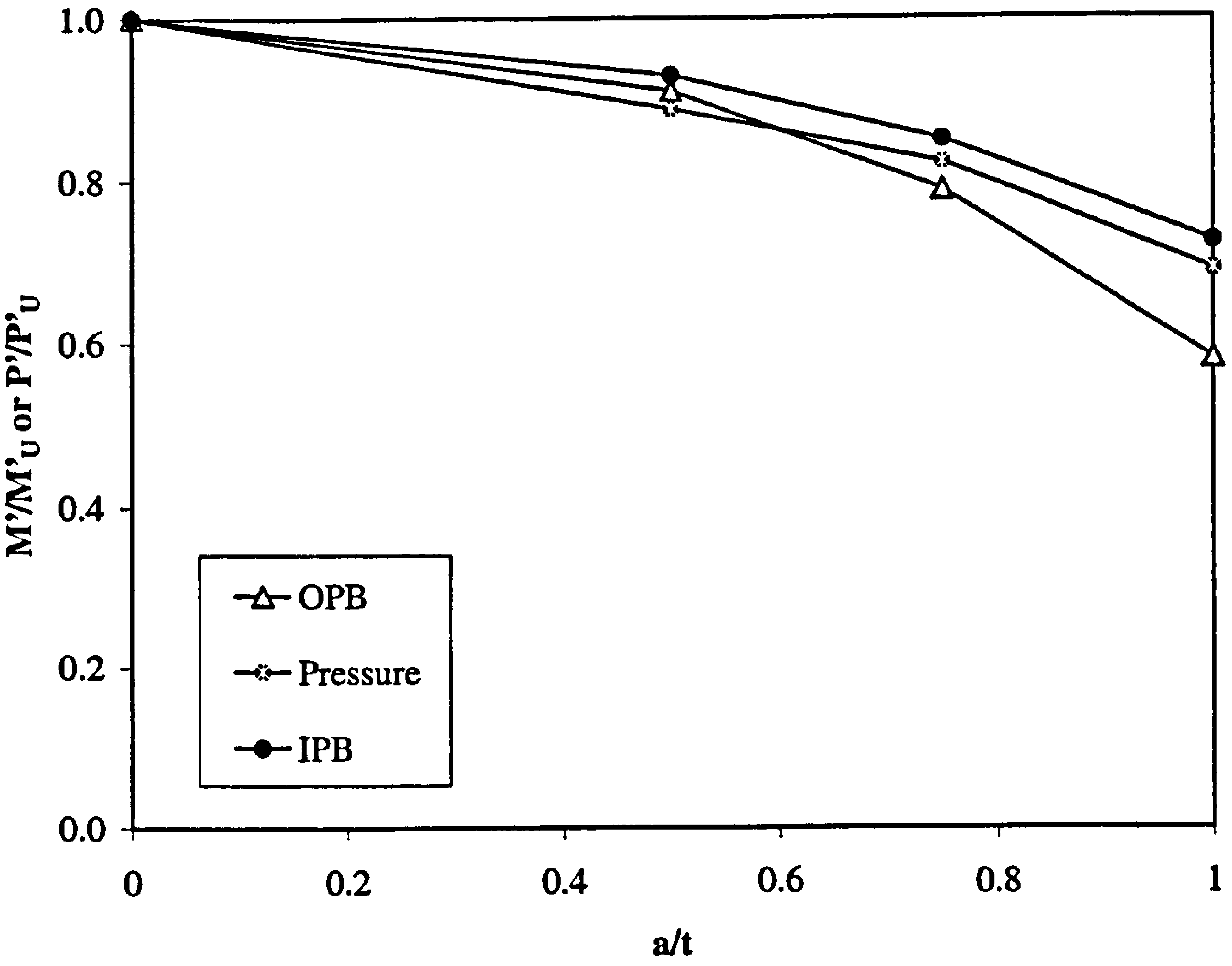

(b) d/D=0.95, D/T=10 - Normalised using Uncracked Limit Load

Figure 4.28: Variation of Limit Load Results with Crack Depth

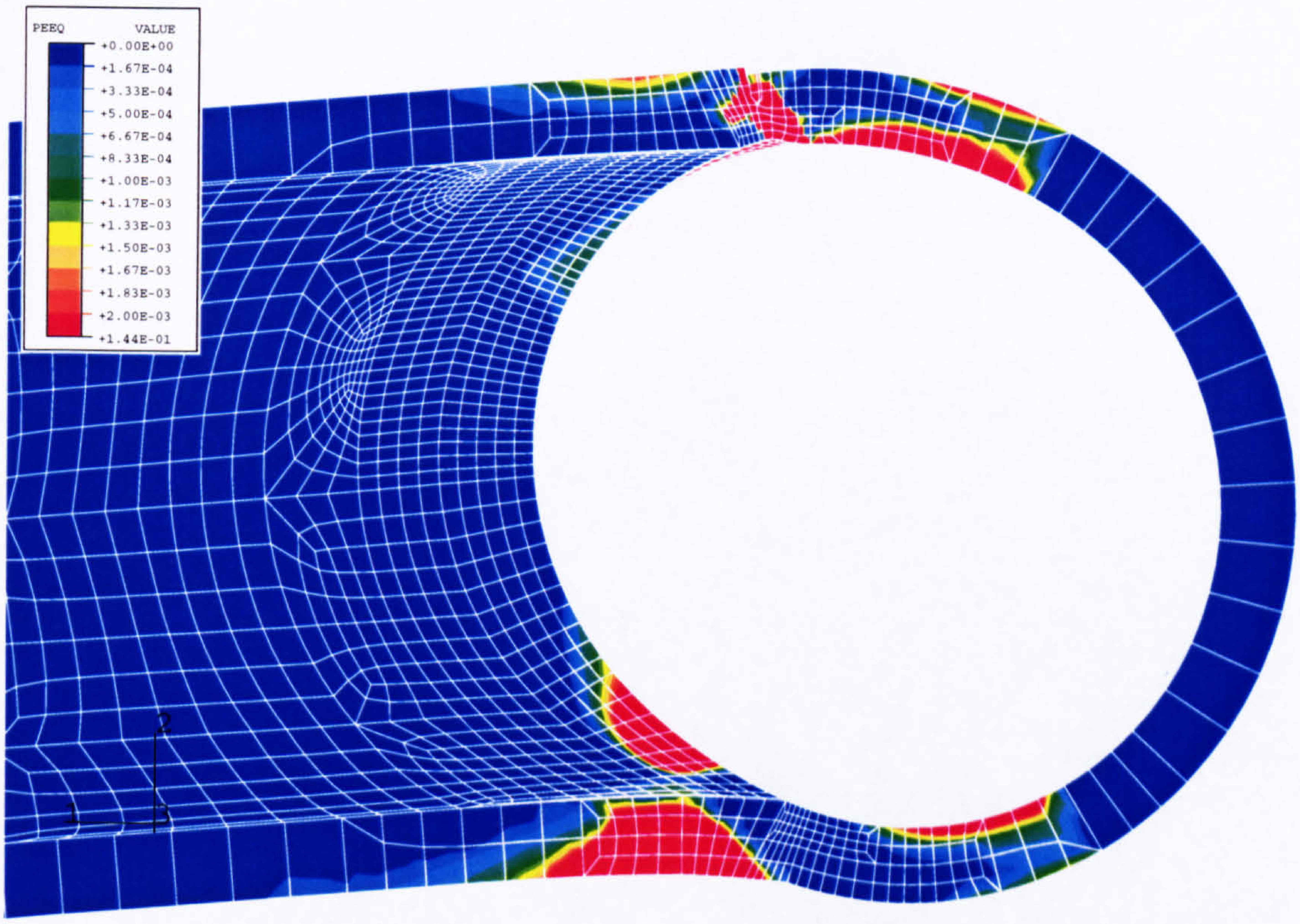

Figure 4.29: Part-penetrating Cracks - Spread of Plasticity for Out-of-plane Bending: Model T910-4 - d/D=0.95, D/T=10, a/t=0.5 (M/M'=0.83, dmag=5)

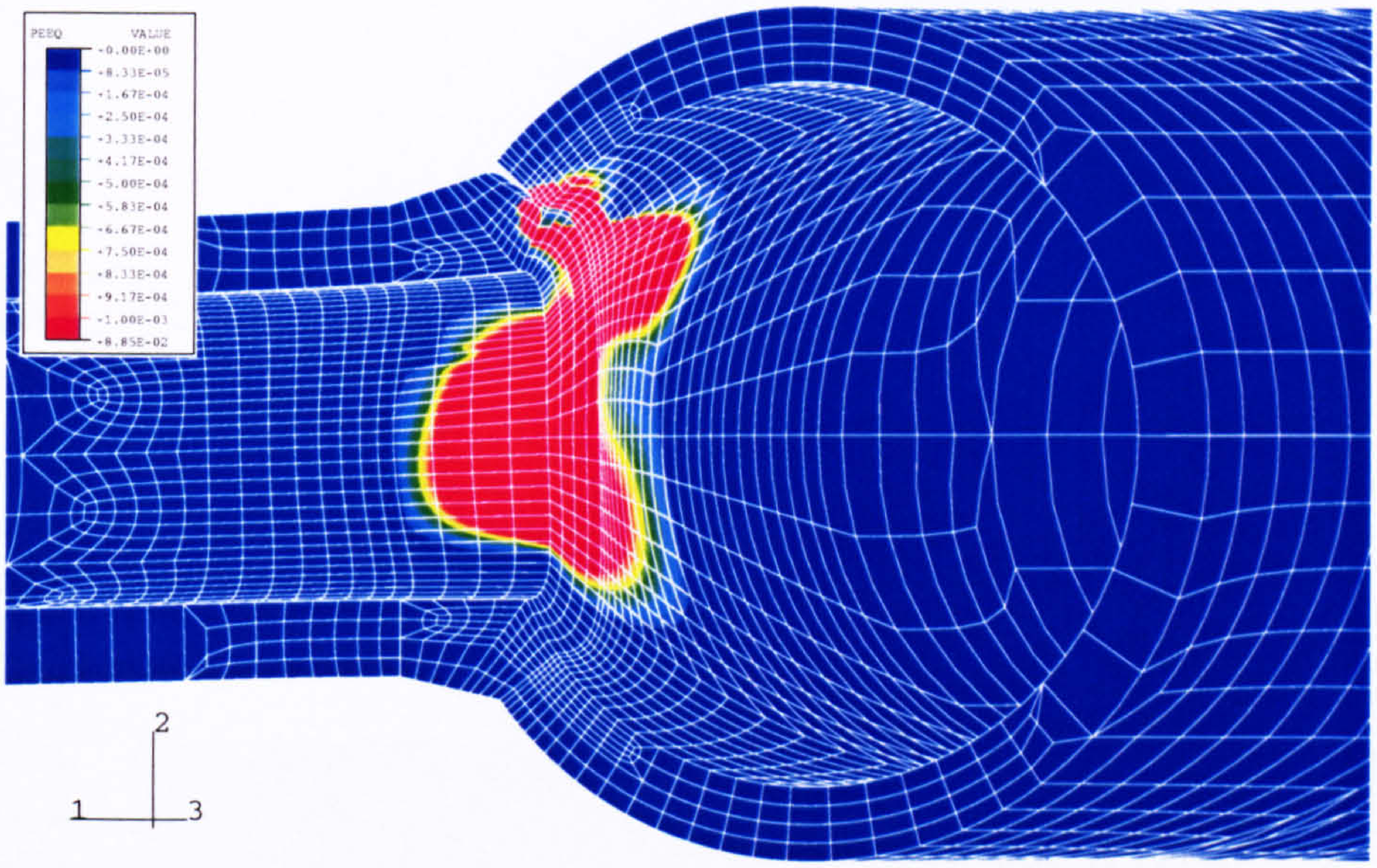

(a) Model T510-5 - d/D=0.5, D/T=10, a/t=0.75 (P/P'=1.0, dmag=1.0)

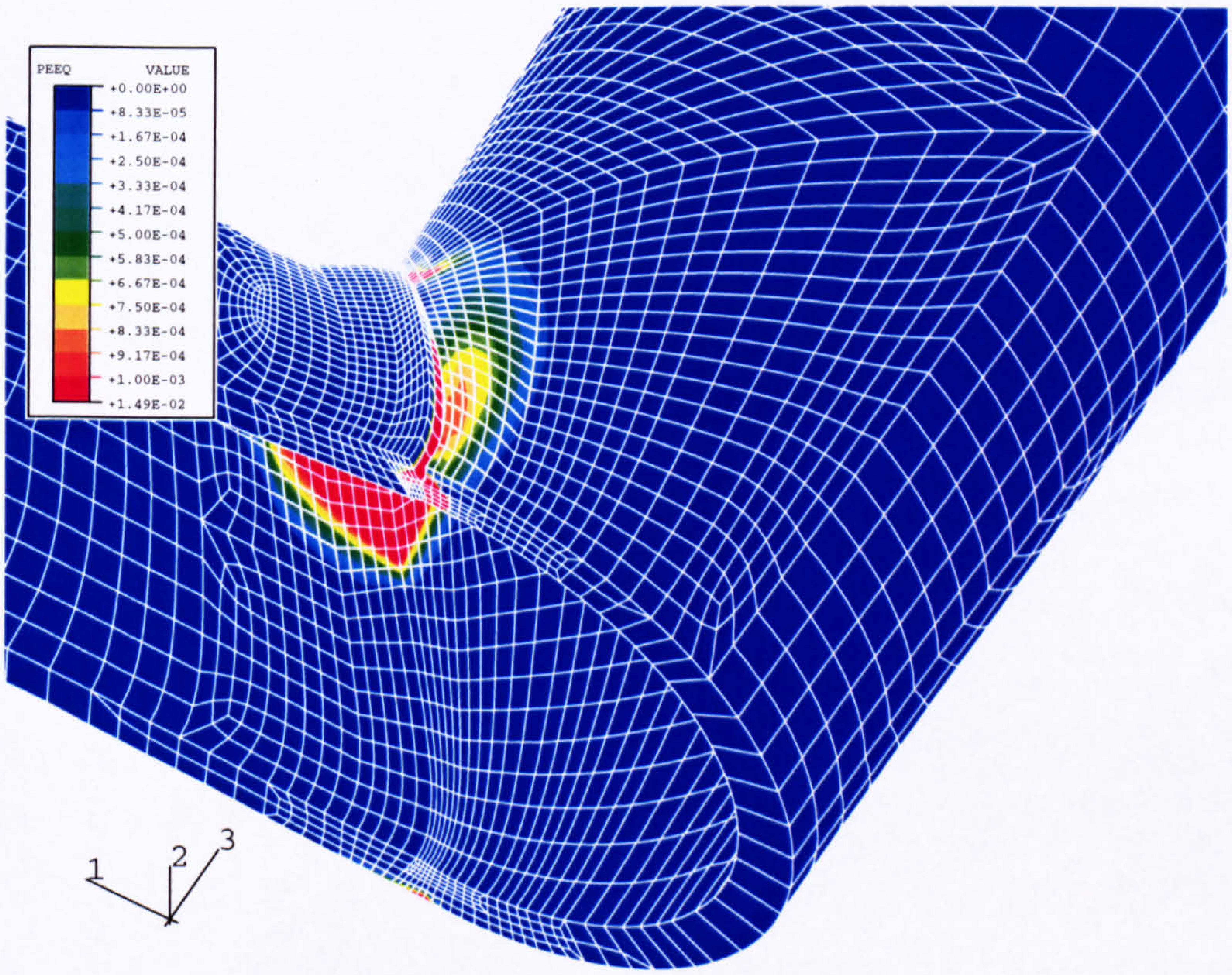

(b) Model T910-4 - d/D=0.95, D/T=10, a/t=0.5 (P/P'=0.78, dmag=30)

Figure 4.30: Part-penetrating Cracks - Spread of Plasticity for Pressure Loading

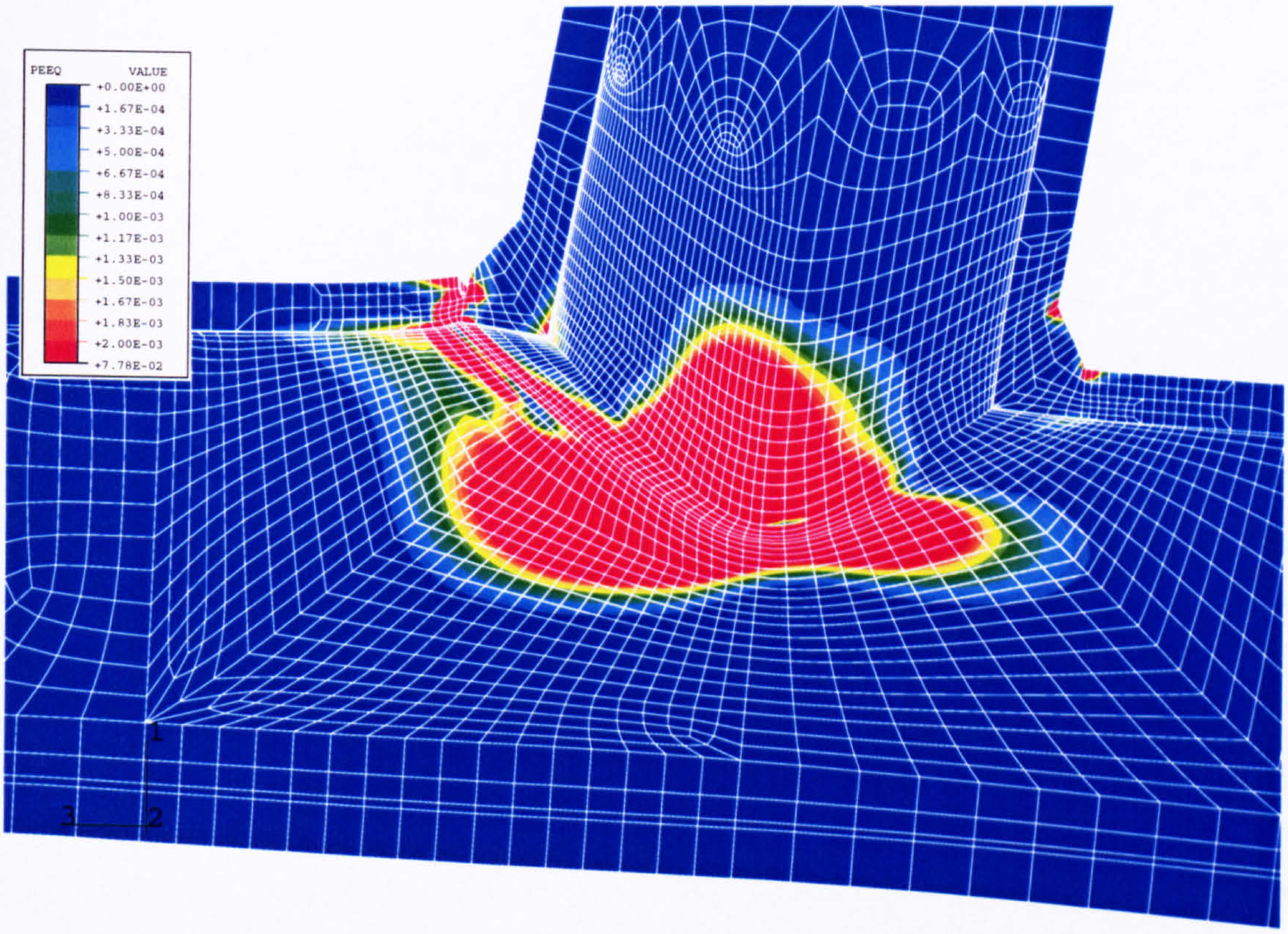

Figure 4.31: Part-penetrating Cracks - Spread of Plasticity for In-plane Bending: Model T910-10 - d/D=0.95, D/T=10, a/t=0.5 (M/M'=0.81, dmag=10)

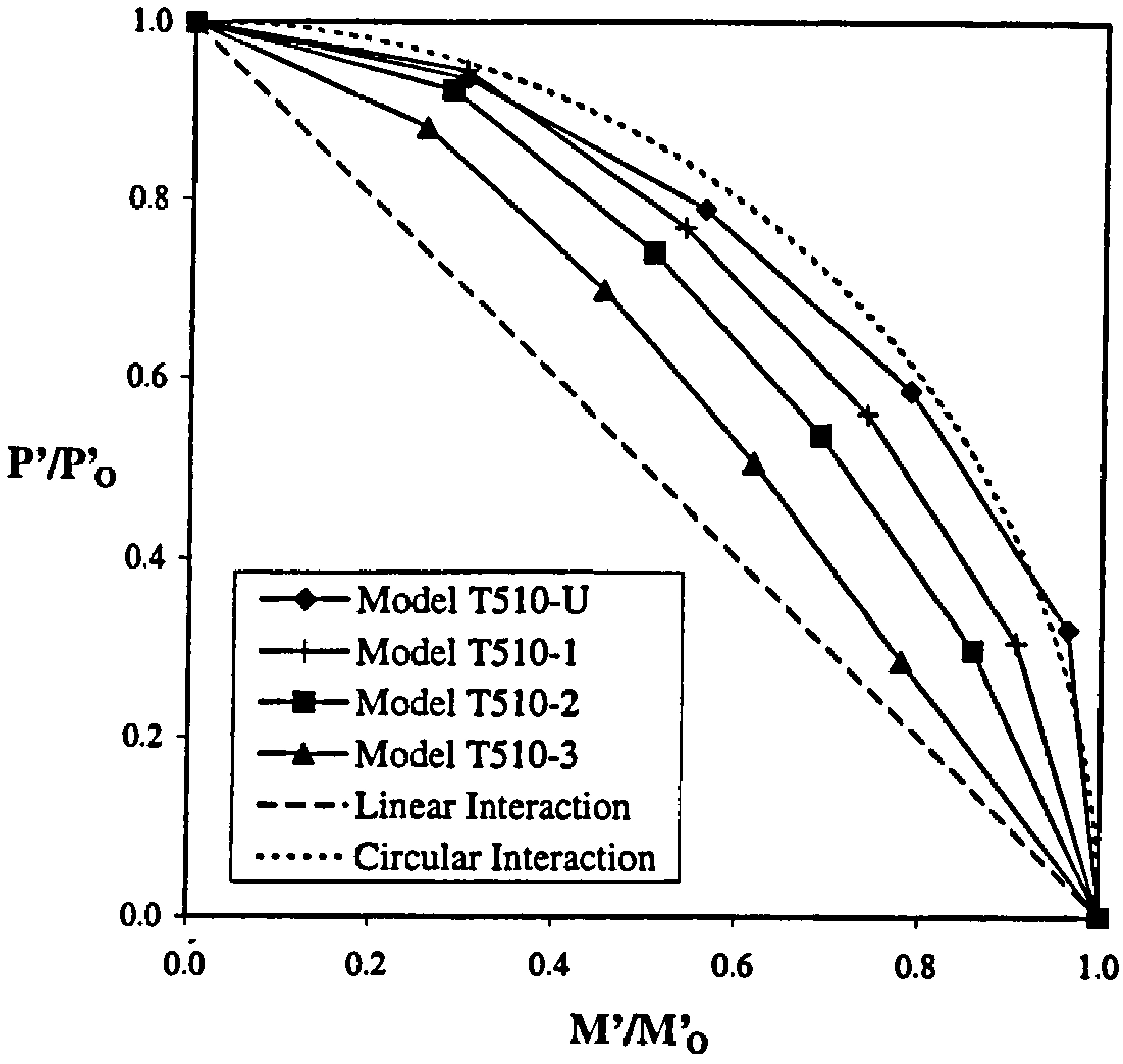

Figure 4.32: (a) Interaction Diagram: d/D=0.5, D/T=10, a/t=1.0

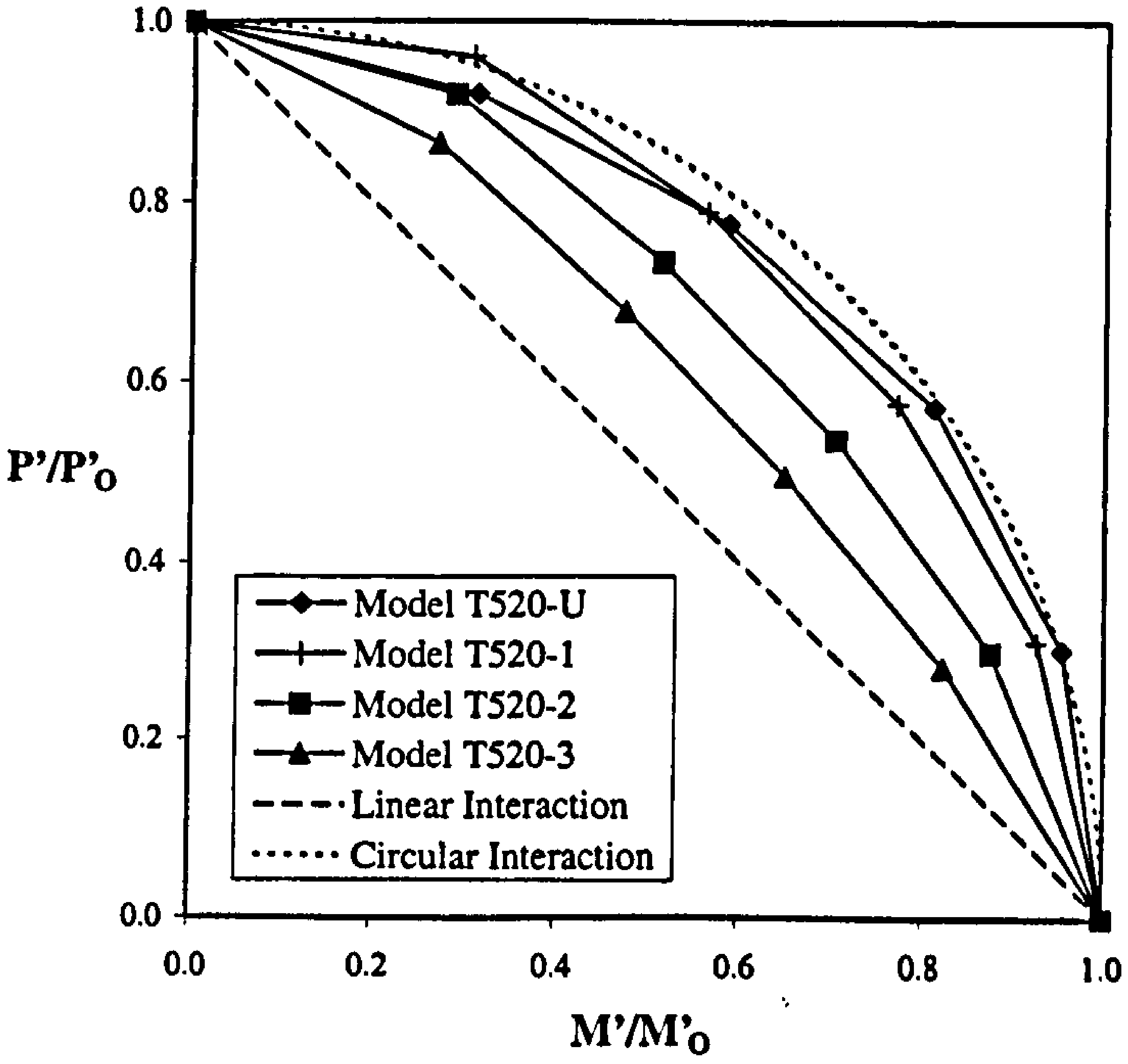

Figure 4.32: (b) Interaction Diagram: d/D=0.5, D/T=20, a/t=1.0

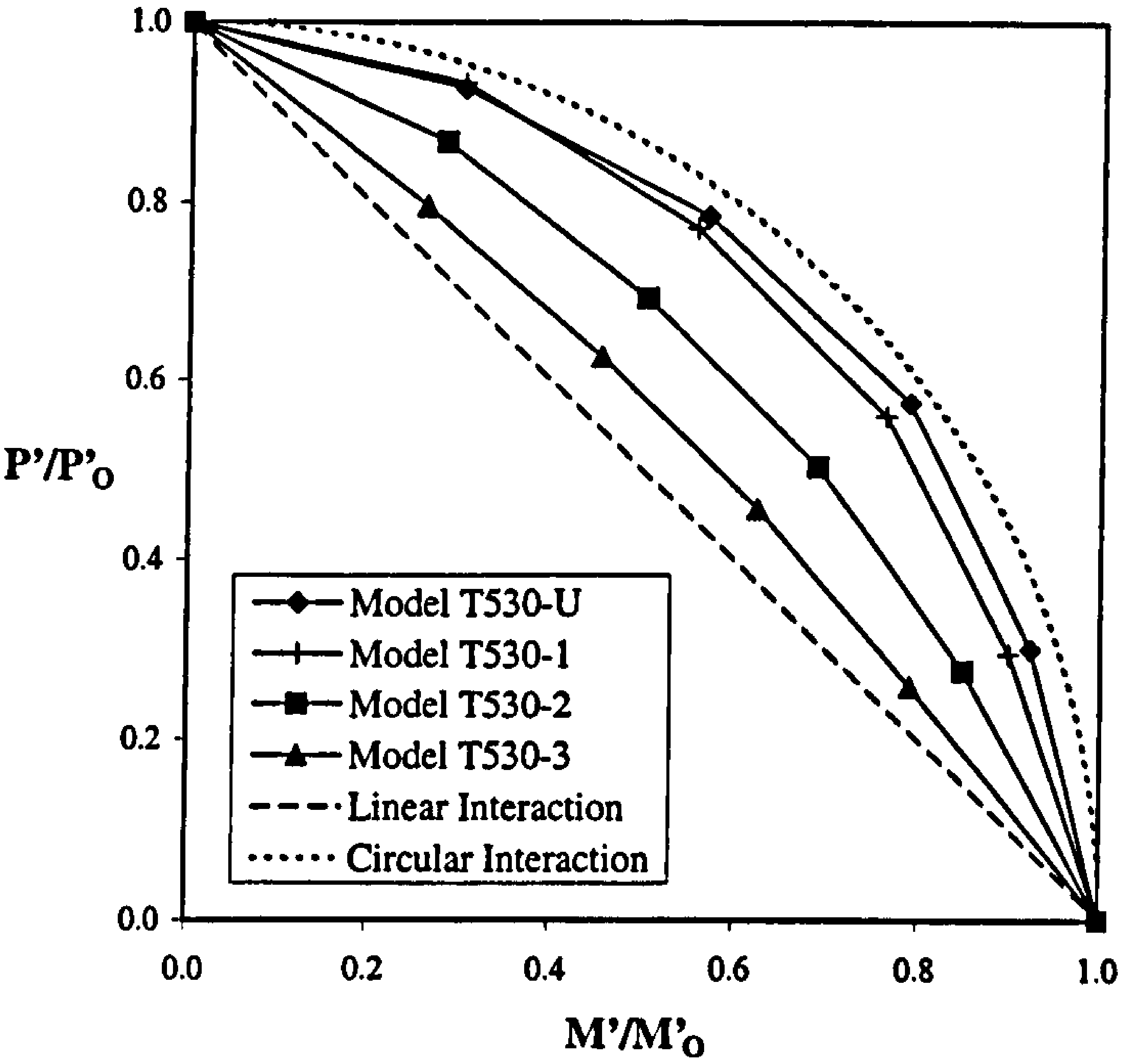

Figure 4.32: (c) Interaction Diagram: d/D=0.5, D/T=30, a/t=1.0

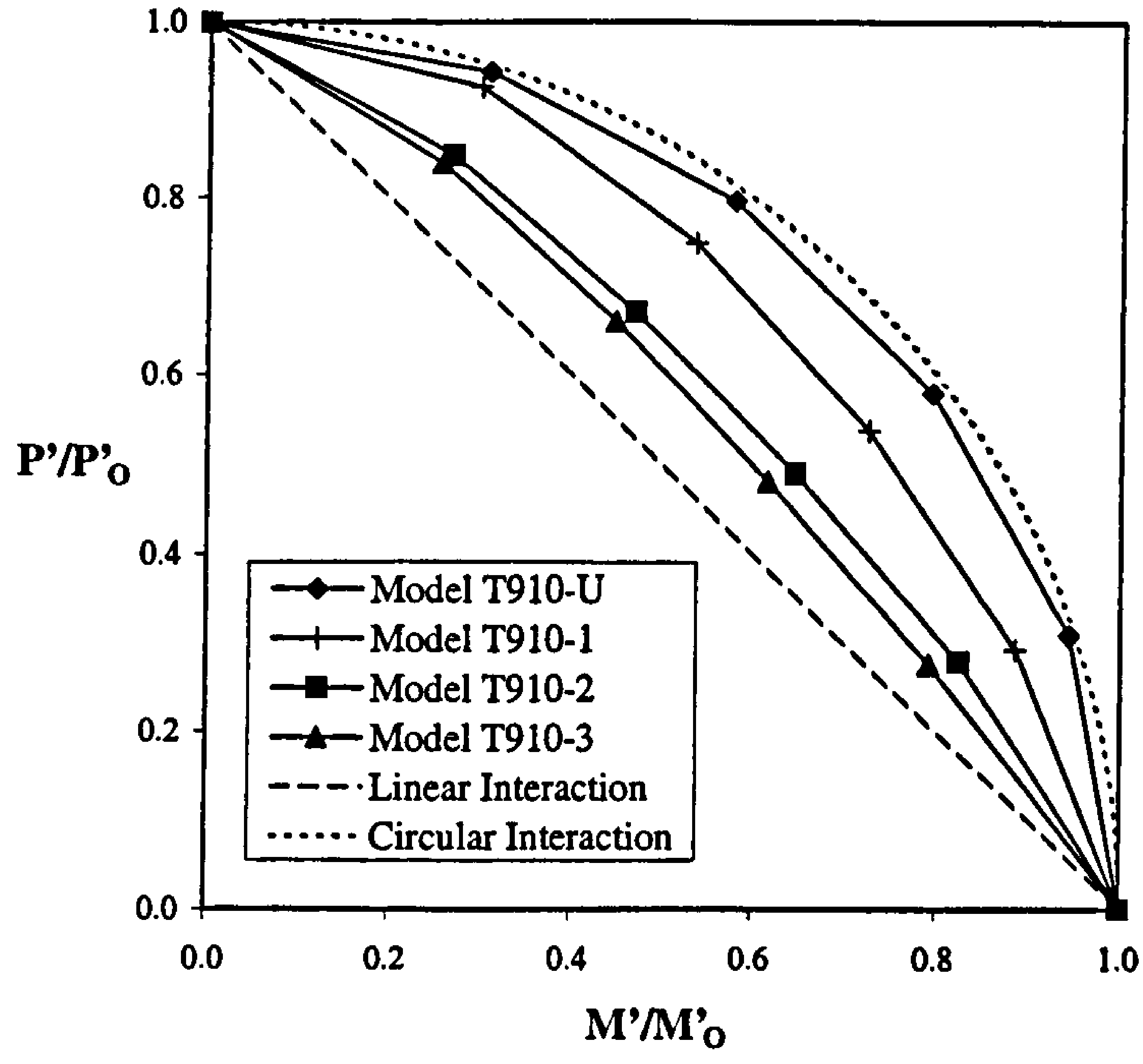

Figure 4.33: (a) Interaction Diagram: d/D=0.95, D/T=10, a/t=1.0

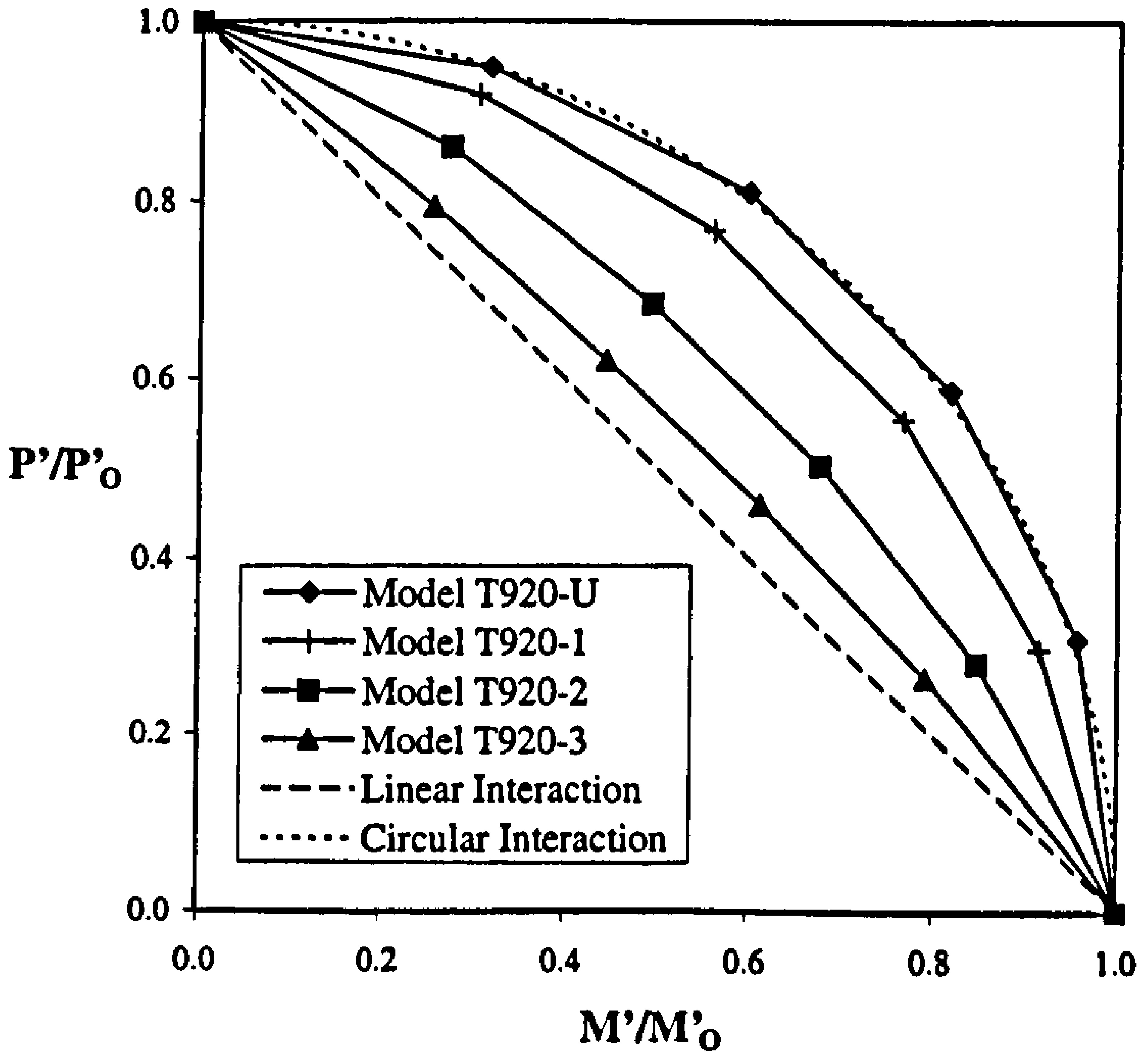

Figure 4.33: (b) Interaction Diagram: d/D=0.95, D/T=20, a/t=1.0

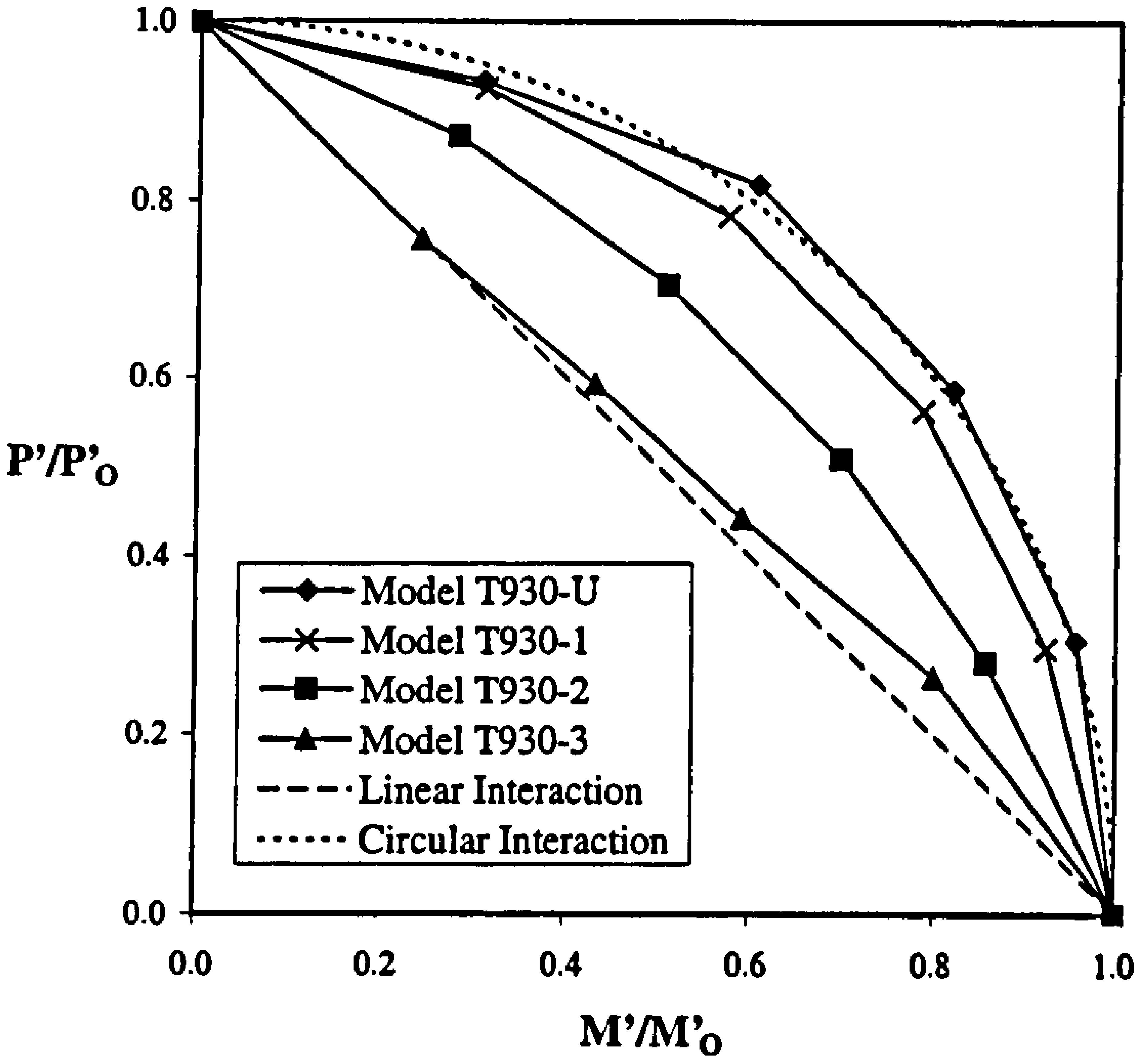

Figure 4.33: (c) Interaction Diagram: d/D=0.95, D/T=30, a/t=1.0

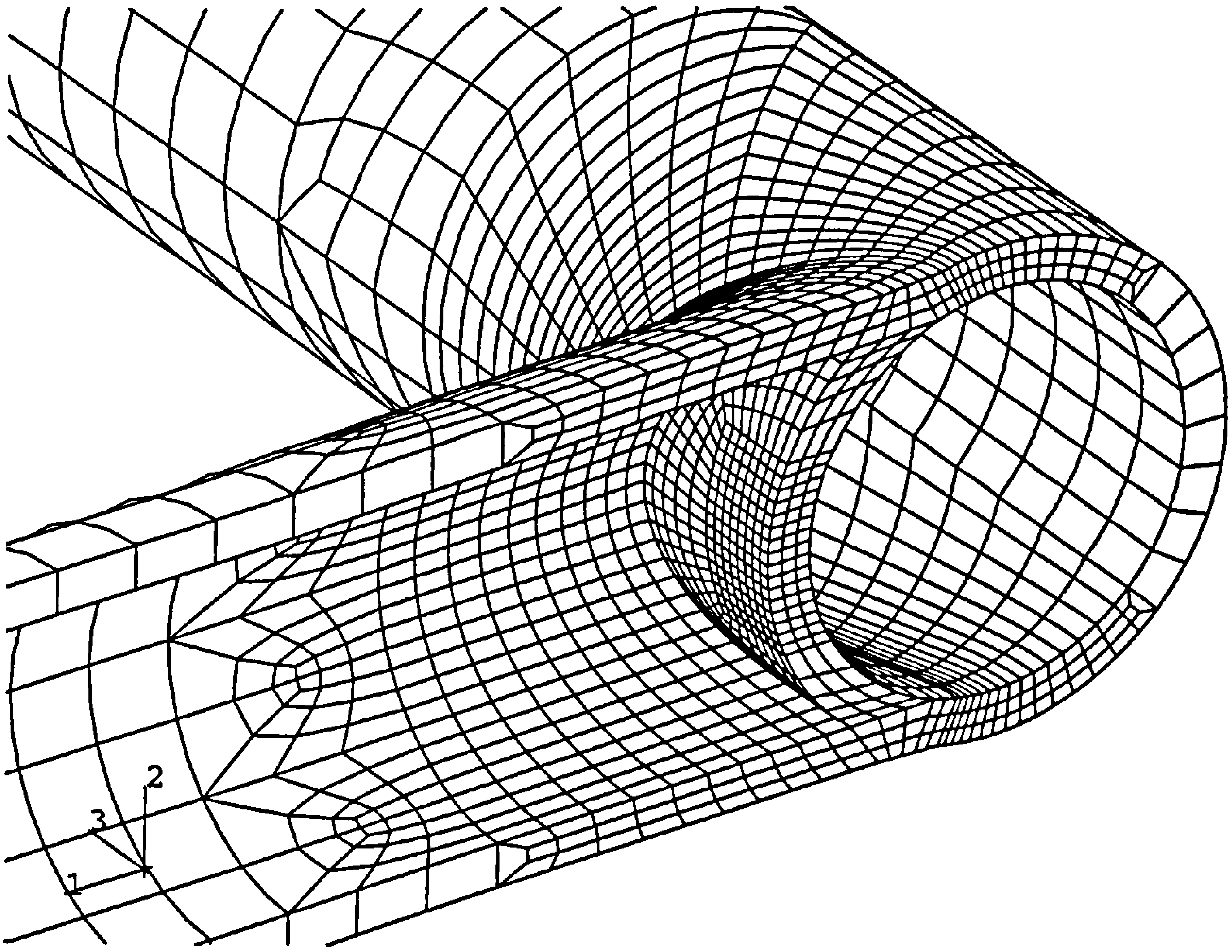

Figure 4.34: FE Model for Tubular Joint - d/D=0.95, D/T=10

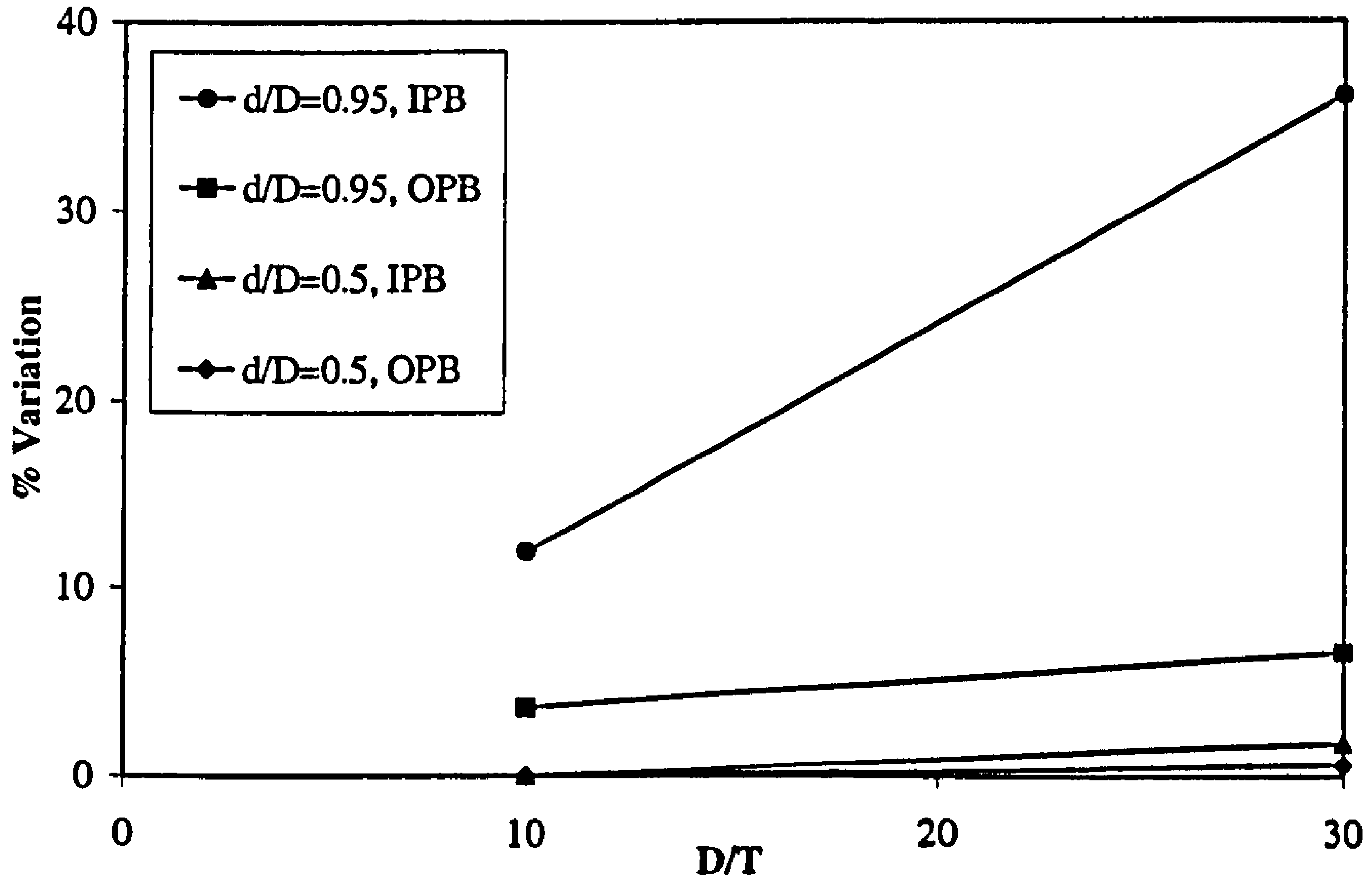

Figure 4.35: Variation of Tubular Joint Limit Moments from Branch Junction Results

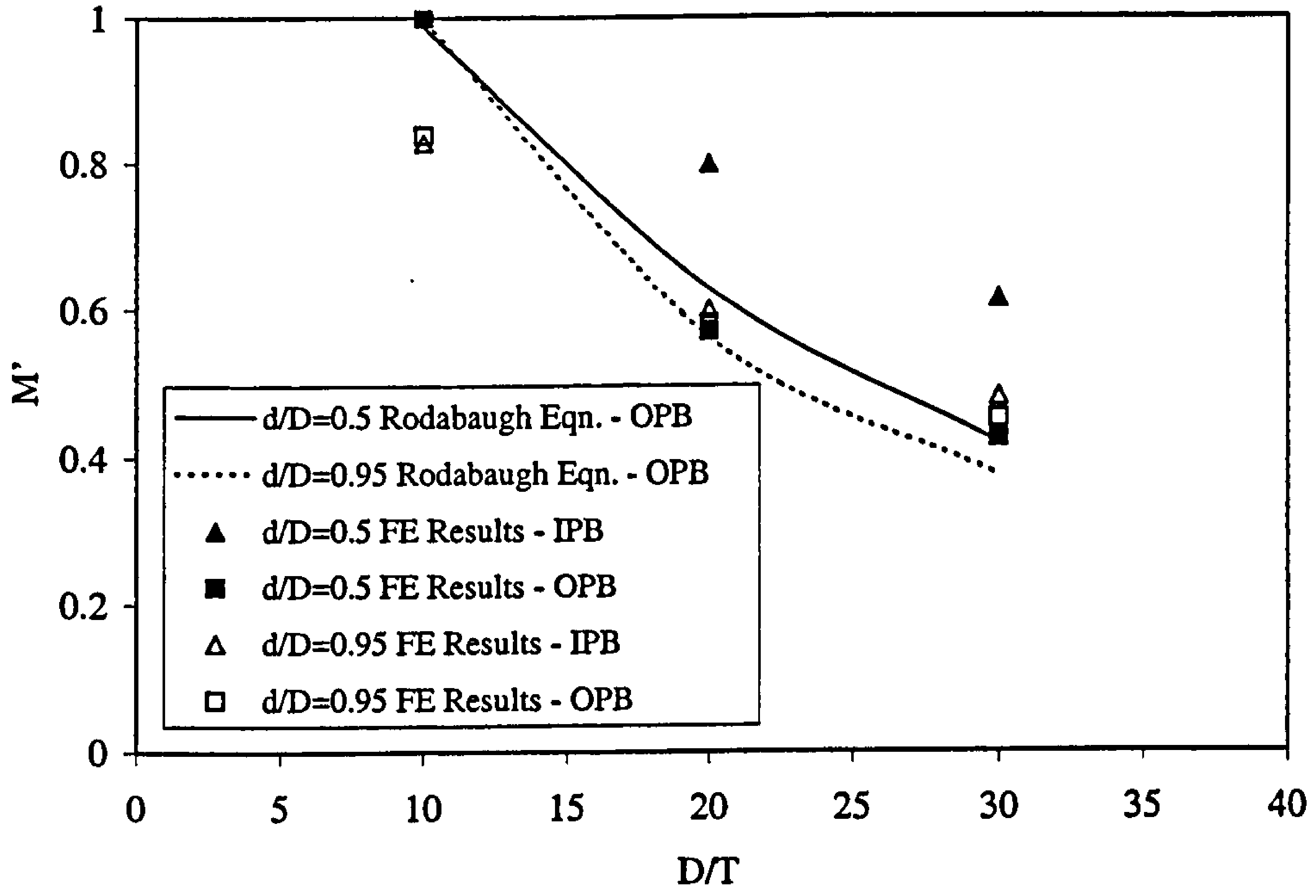

Figure 4.36: Rodabaugh Equation - Comparison with FE Results

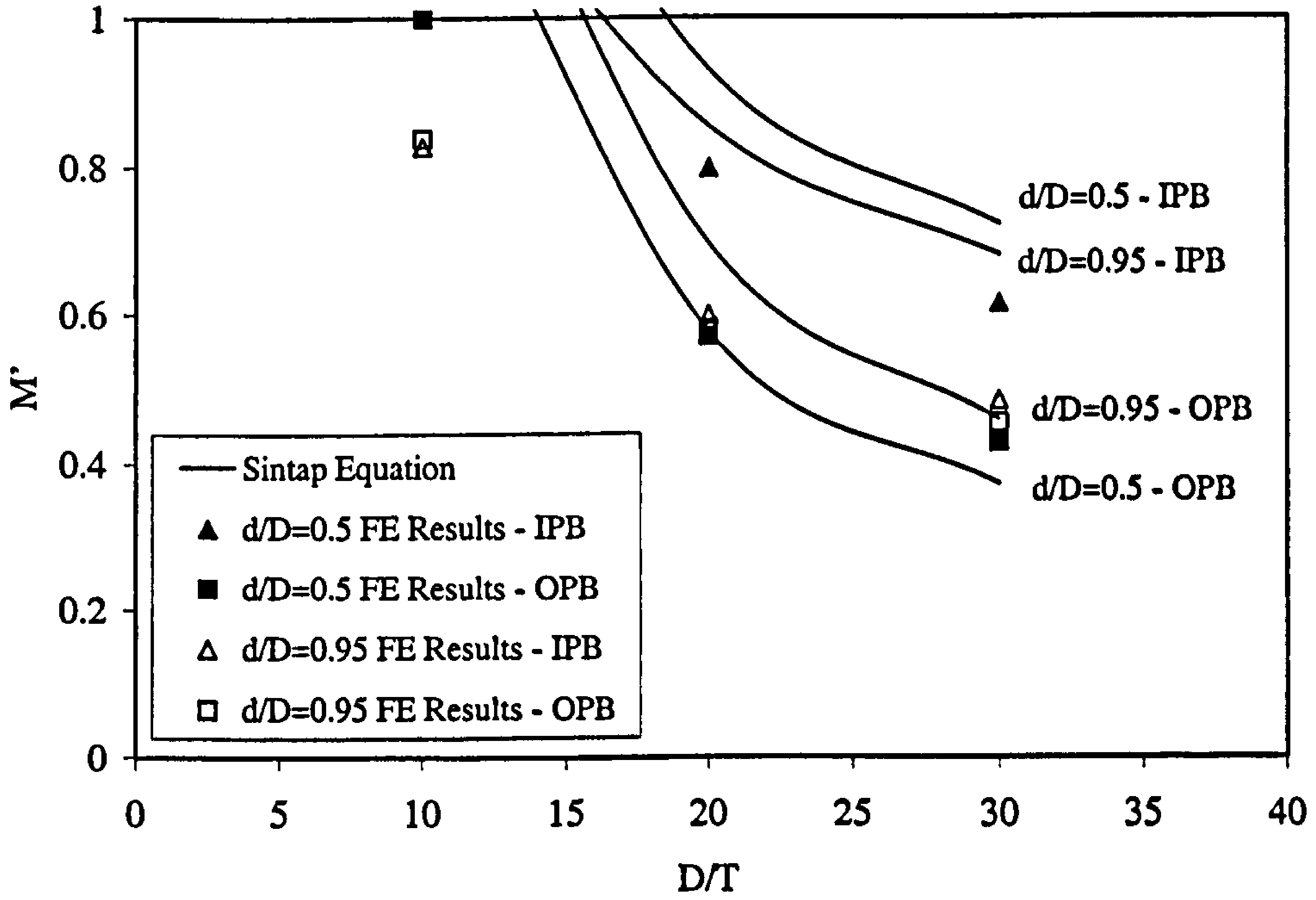

Figure 4.37: Sintap Compendium Equation - Comparison with FE Results

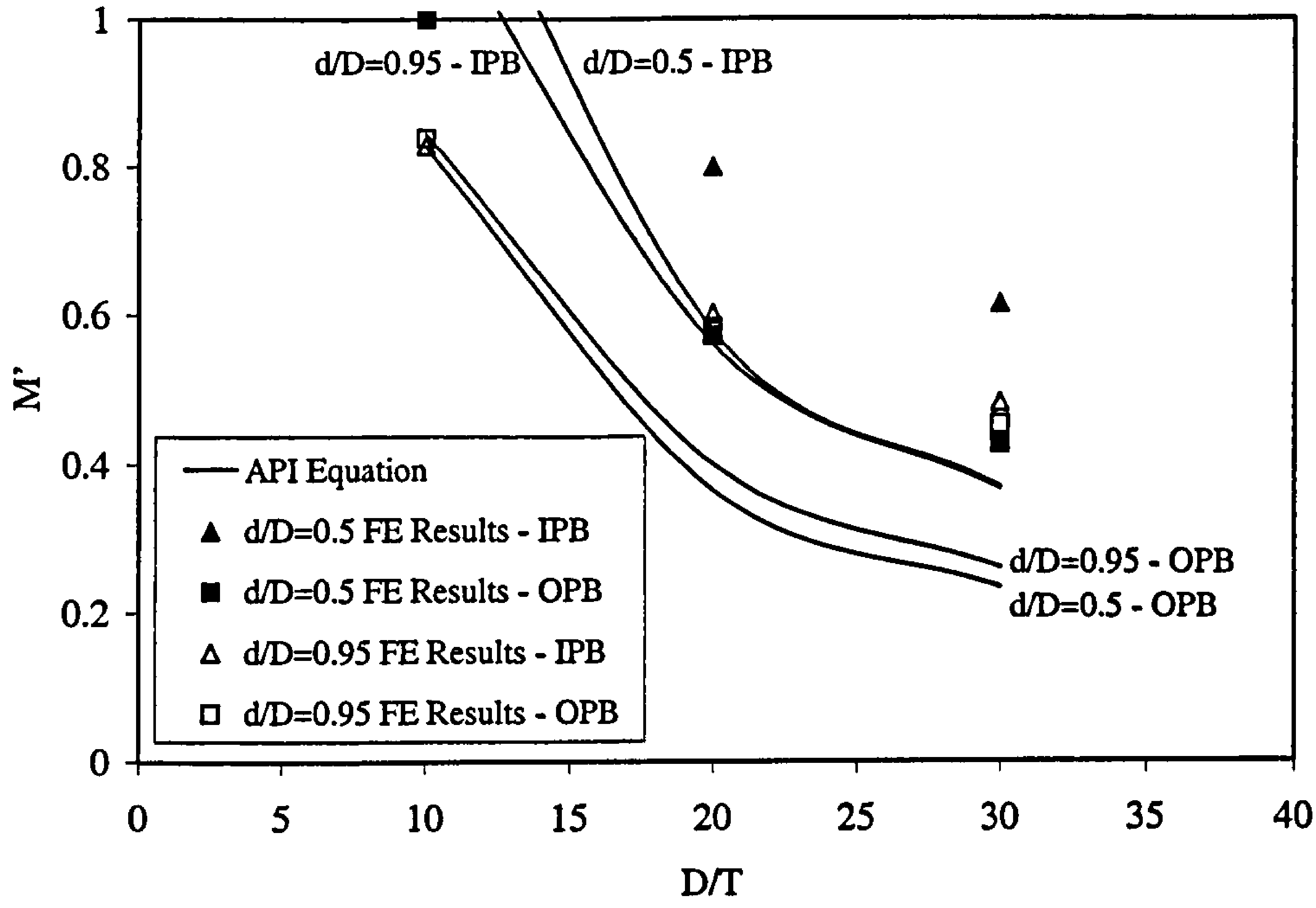

Figure 4.38: API equation - Comparison with FE Results

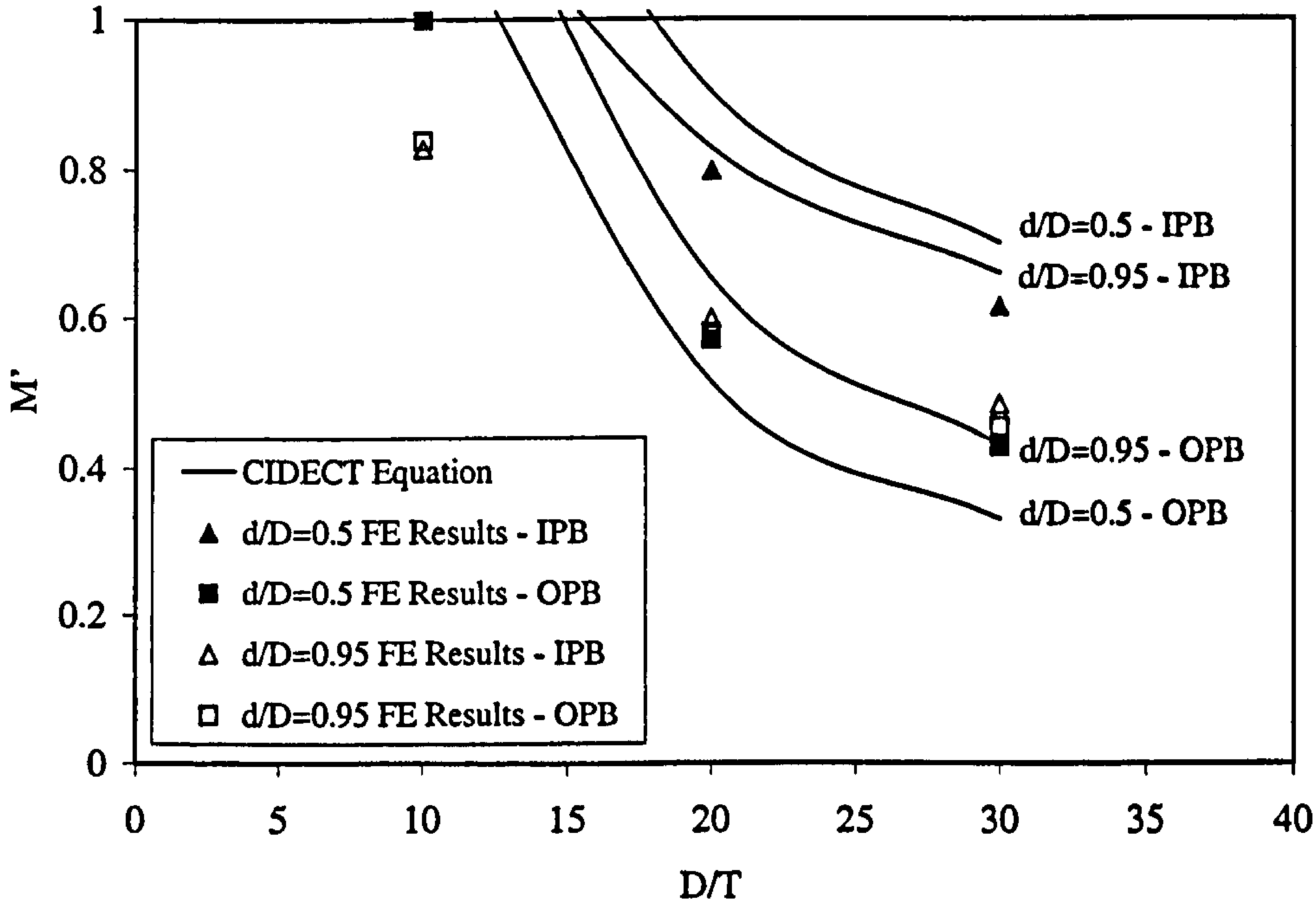

Figure 4.39: CIDECT equation - Comparison with FE Results

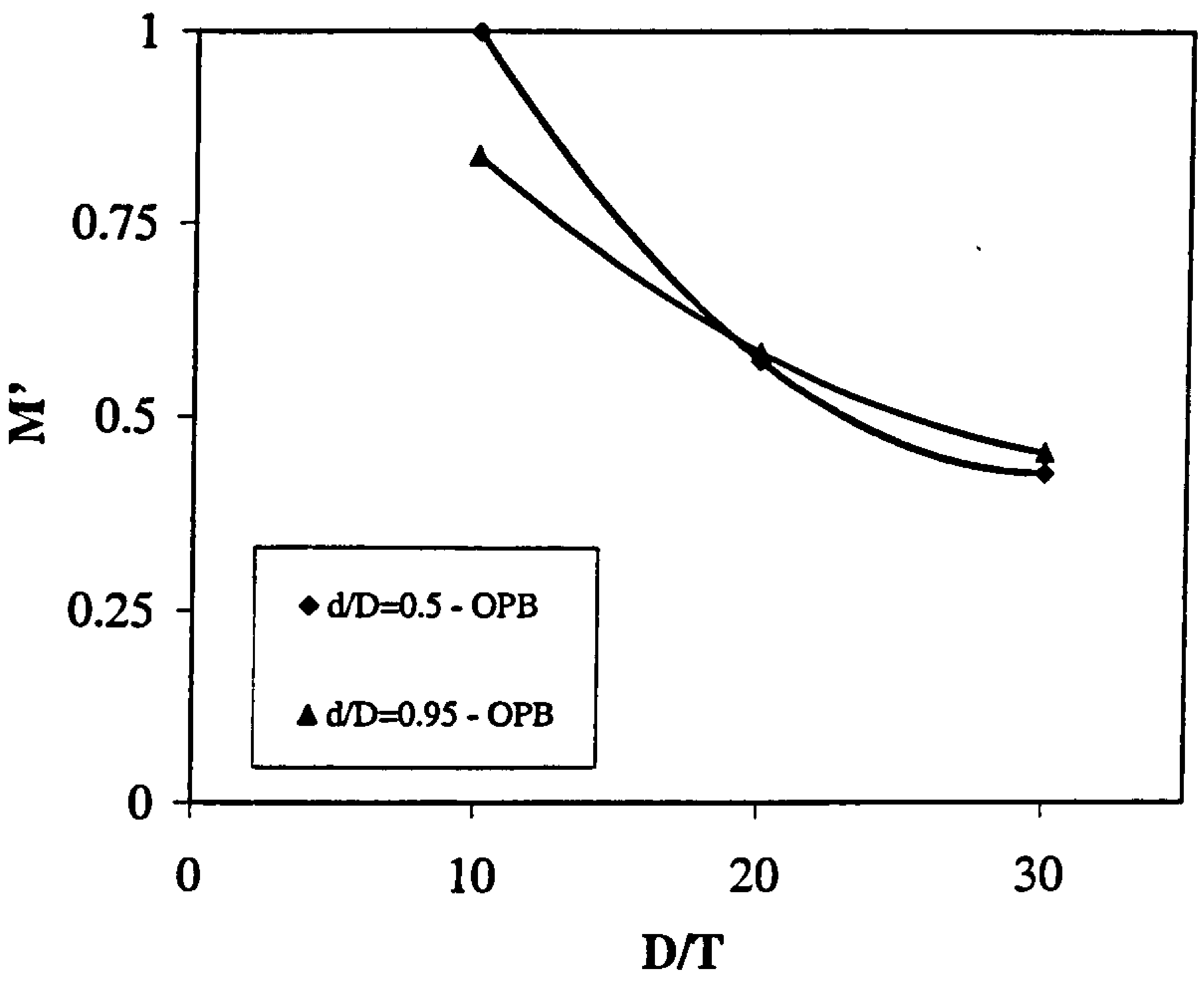

Figure 4.40: Polynomial Curve Fitting to FE Results for OPB

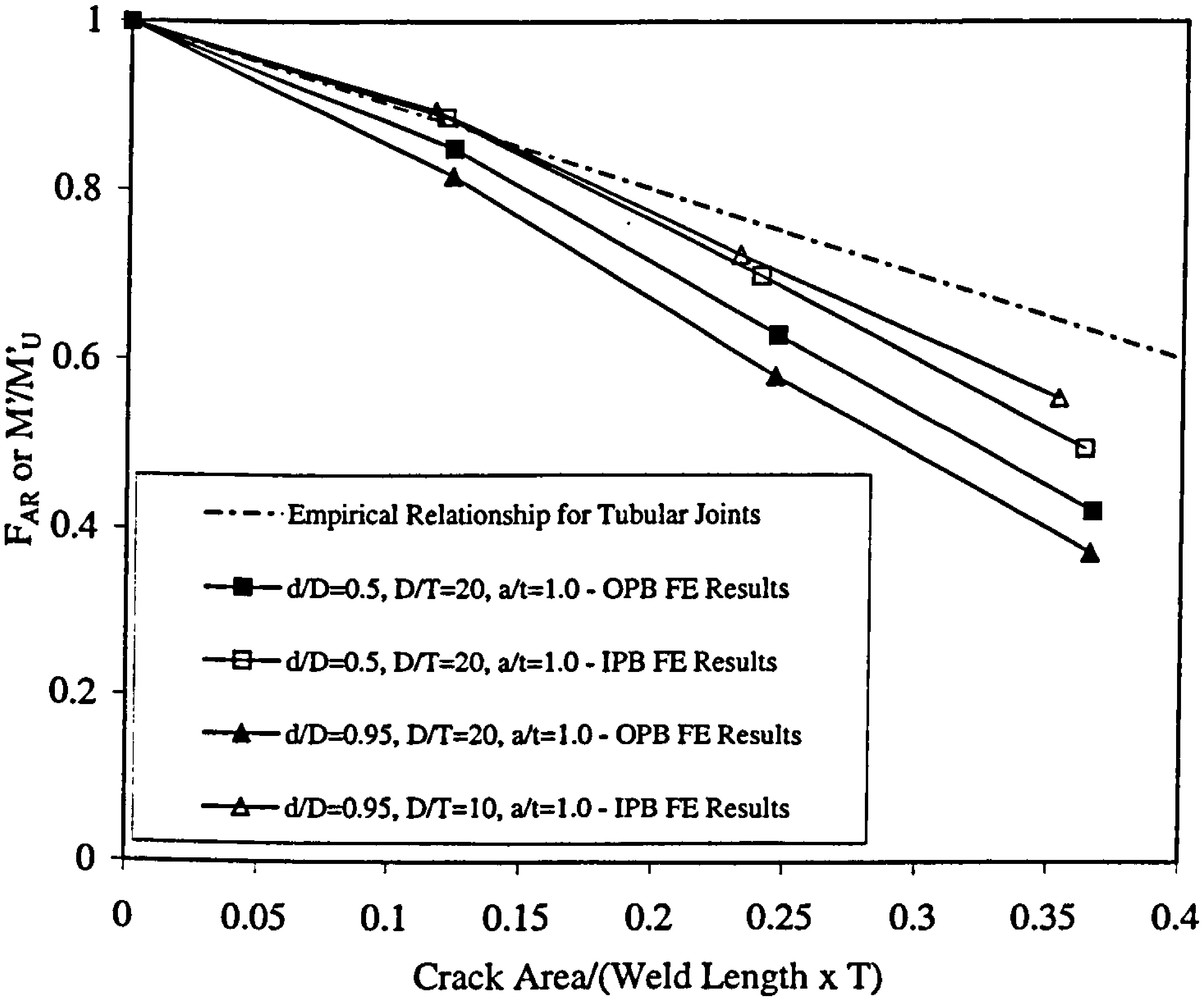

Figure 4.41: Area Reduction factor - Comparison with FE Results

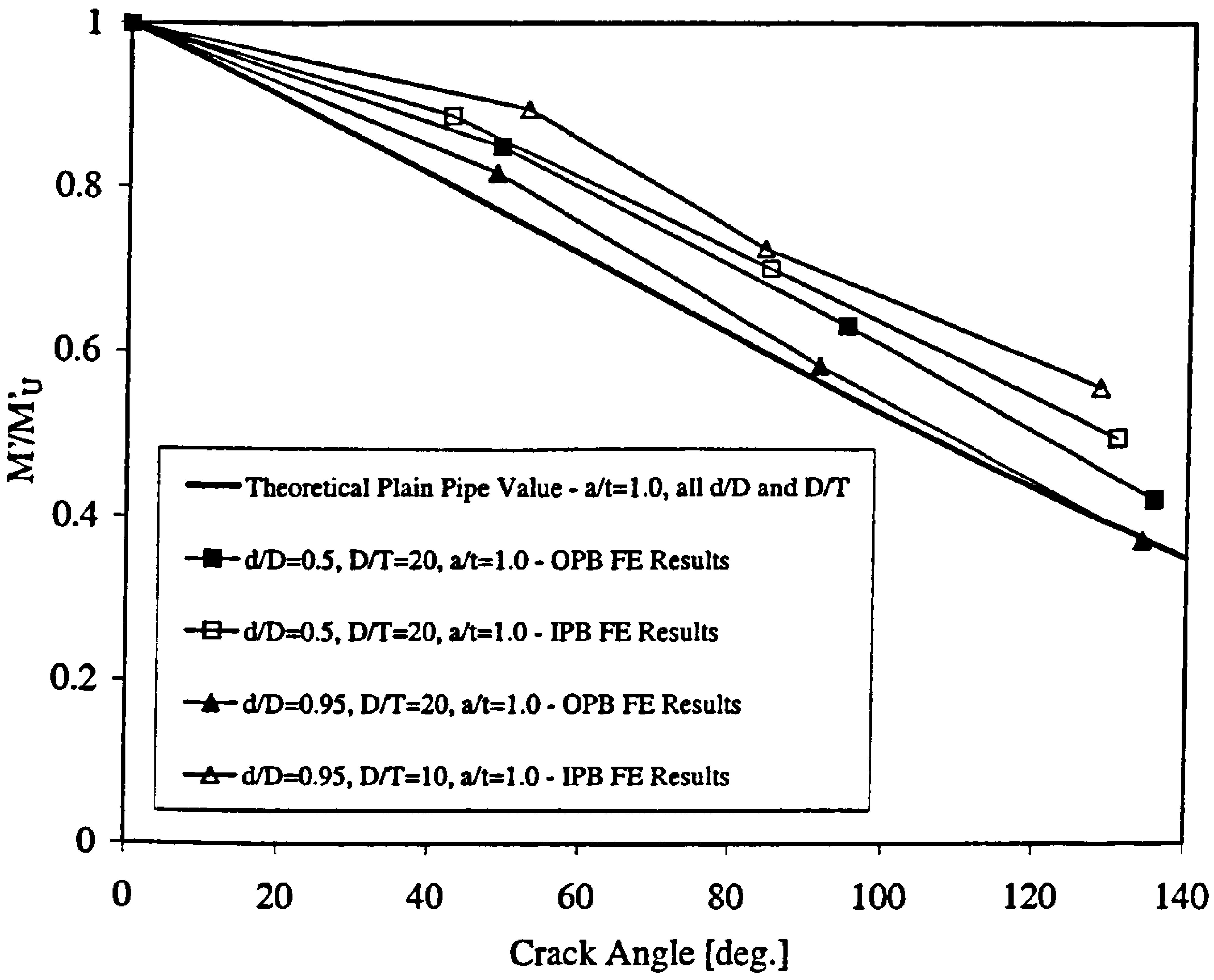

(a) Through-wall Cracks

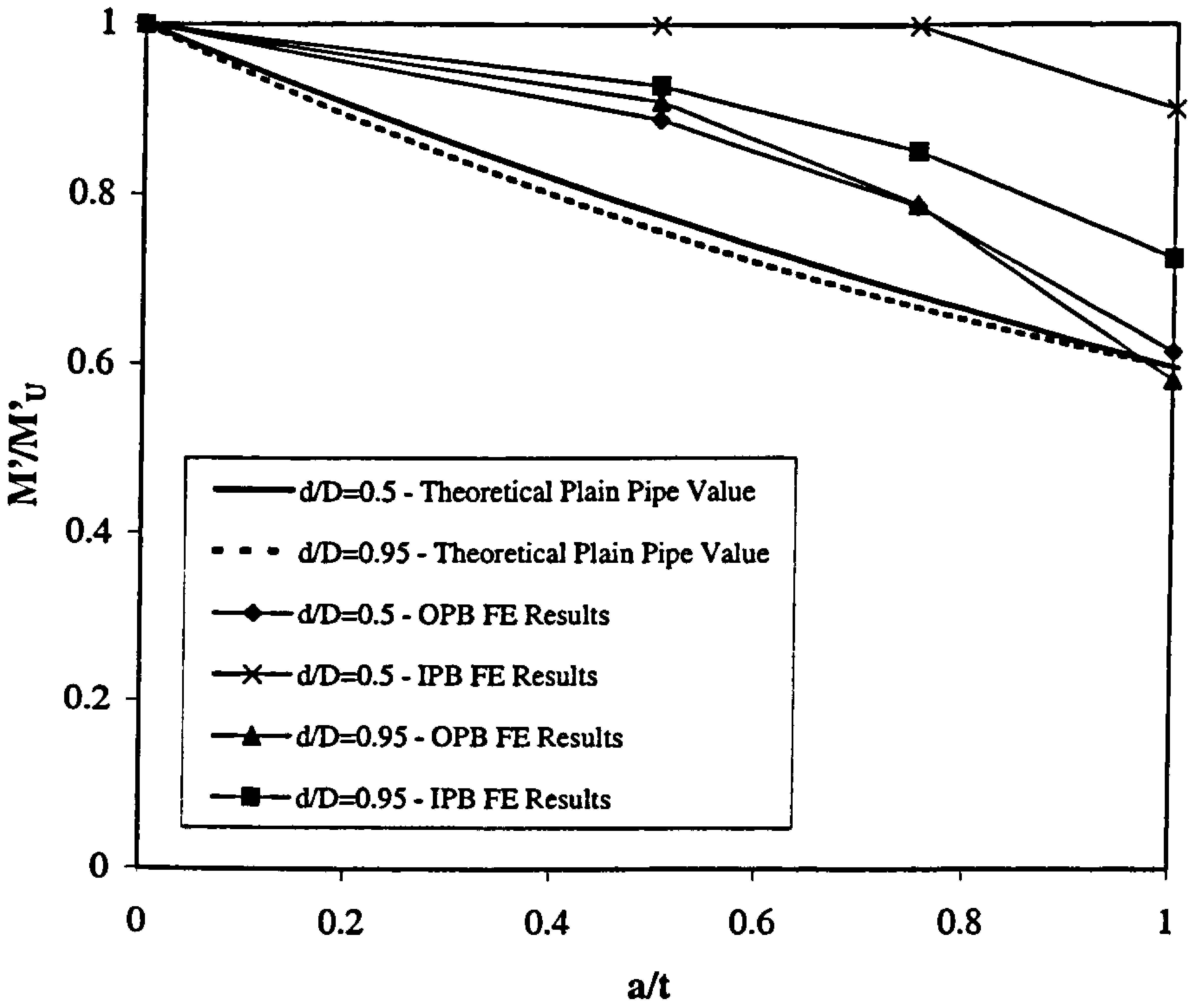

(b) Part-penetrating Cracks

Figure 4.42: Cracked Plain Pipe Limit Moment - Comparison with FE Results

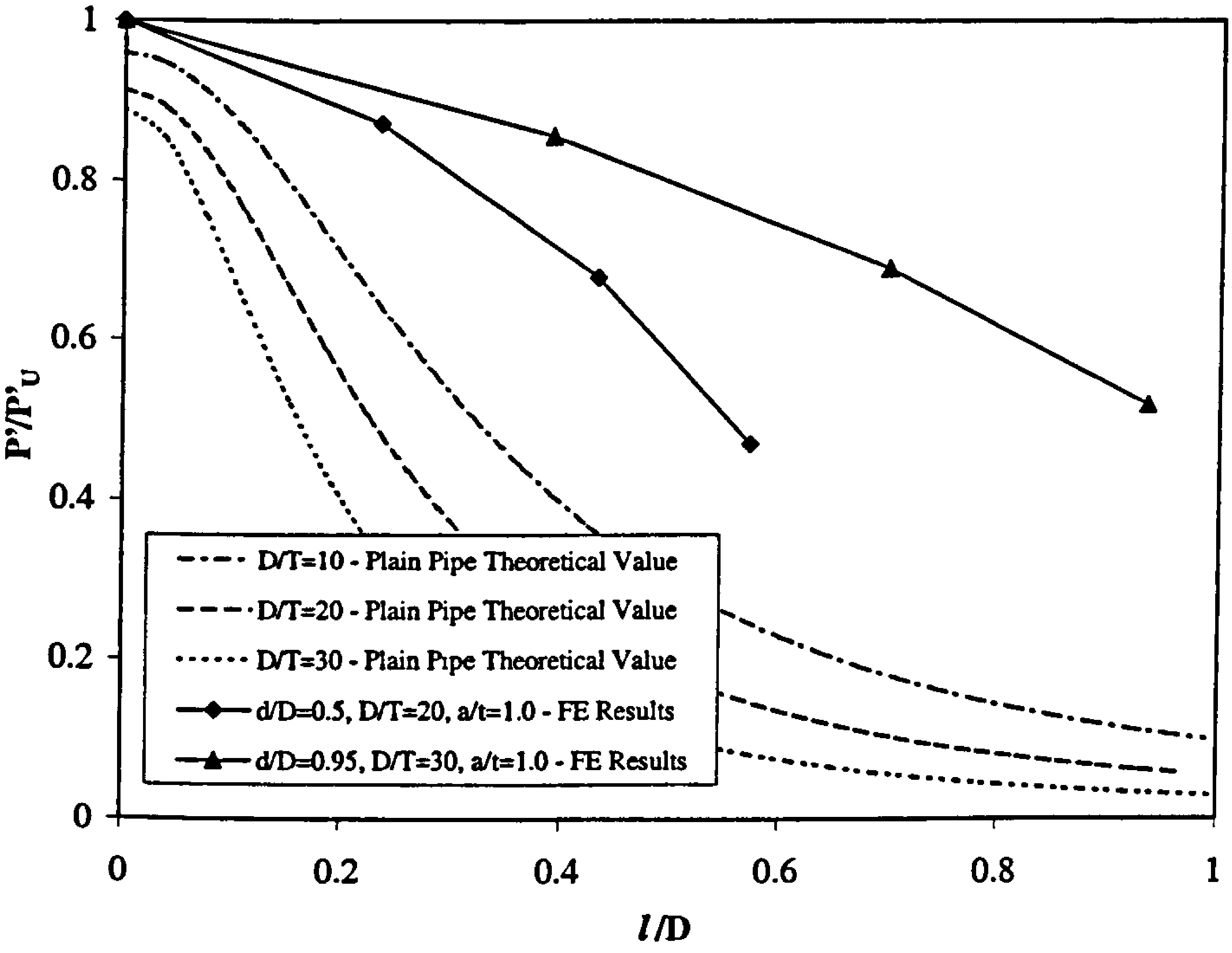

Figure 4.43: Cracked Plain Pipe Limit Pressure Comparison with FE Results (a/t=1.0)

Chapter 5

Experimental Methods

The objective of the experimental work was to confirm that the parametric study FE results produced, for both uncracked and cracked junctions, were valid. It was not deemed necessary to produce a wide range of different branch junctions to do this, but rather a few cases for one specific geometry were selected for testing. The experimental results could not be compared directly with the limit load FE results, further FE analyses being required to include the material and geometric non-linearities. However, if the experimental and FE non-linear results compared well, then this would provide the necessary validation for the less complex limit load studies.

The load cases tested were limited to internal pressure and in-plane bending. There were only a limited number of test specimens available and so out-of plane bending was not considered. Out-of-plane bending is difficult to perform experimentally on branch junctions, and the methods required may produce complex loading rather than pure out-of-plane bending (as described by Yahiaoui et al. [19]). For this reason in-plane bending was chosen, as the test arrangement used to simulate this loading case is comparatively straightforward.

5.1 Model Specification

The branch junctions in question are the same type as those studied in Chapters 3 and 4. The weld geometry was present, but material property variations in the weld material were not accounted for, these being assumed identical to those of the branch junction. Experimentally, the only way to remove the influence of the weld material for the cylinder-cylinder type of branch junction is to machine the entire junction from solid material. This method is more expensive than fabricating junctions with welds, but it was important to remove one of the variables from the experimental study. In addition to the removal of the weld material variations, there was more control over the dimensions and tolerances involved than for fabricated junctions.

The junctions studied had the parameters: d/D=0.95, D/T=10, and t/T=1.0. These parameters were also used in the cracked model FE parametric study (described in Chapter 4). Ideally, a d/D value of 1.0 would have been preferred, as this junction is one of the most commonly used types and has the lowest limit pressure for the equal thickness case (t/T=1.0 - see Chapter 3). However, for cracked junctions with the crack positioned on the flank (along the lower weld toe) the use of d/D=1.0 presented some problems, as explained in Chapter 4. Hence, d/D=0.95 was the largest value considered for cracked models. The thickness value, D/T=10, was the thickest assessed in the cracked parametric study and all of the cracked models had t/T=1.0.

The loads applied to the test specimens were restricted to two distinct types of loading. For each type, an uncracked model was tested in addition to any cracked models. A total of five junctions were tested:

- In-plane bending of branch pipe - uncracked
- In-plane bending of branch pipe - part-penetrating (PP) crack
- In-plane bending of branch pipe - through-wall (TW) crack
- Internal pressure loading - uncracked
- Internal pressure loading - part-penetrating crack

The loading of these models will be described in detail in 5.4

5.1.1 Geometry of Junctions

General Dimensions

The junction geometry was based on the parameters specified above and is shown in Figure 5.1. The sizes were all based upon the bore diameter (63.6mm) of a previously manufactured junction (used in [10]) for which the machining mandrel was still available. This mandrel was designed for an equal diameter junction, so the branch section was re-machined for d/D=0.95. The manufacturing processes are described in Section 5.2.

There were differences between the limit load FE model (see Chapter 4) and the experimental model. These were caused by the radius of the machine tool used at the junction intersection. It was decided that no attempt would be made to machine the weld profile (of the FE model) but to use the curvature provided by the machine tool to represent the weld. The geometric differences between the FE model and the machined model are shown in Figure 5.2 for the crotch and flank locations. It is clear that there is a small amount of additional reinforcement material with the FE model, particularly at the crotch.

Crack Locations and Dimensions

Experimentally, the cracks were machined using Electric Discharge Machining (EDM). This procedure requires an electrode with the dimensions of the required defect or crack. For the FE limit load models assessed in Chapter 4 the crack profile was projected normally from the lower weld toe on the outside of the junction onto the inside surface of the junction, forming the plane of the crack. However, this produces complicated crack profiles with double curvature, due to the changing angle of the normal direction along the crack length. Cracks with double-curvature cannot be produced using standard EDM techniques, as the electrode can only be used to machine in one direction. Hence, an approximation to these crack profiles was required, so that an electrode could be manufactured with a single curvature specification. In other words, the crack profile on the outer diameter was projected in one direction, as explained below. The manufacture of the cracks is described in Section 5.2.2.

The crack profile dimensions were all determined from the FE model geometry. This was done so that the experimental models would be comparable with the FE models, despite there being no clear weld toe experimentally. The cracks were therefore located where the weld toe would be for the FE model. PATRAN [65] was used to determine the crack geometry from the original FE model. For part-penetrating cracks the value of a/t was defined as the ratio of the crack depth to the thickness in the plane of the crack. The length of the plane of the crack through the junction was greater then the nominal junction thickness 't', as the crack was not projected normally.

The crack locations for each of the three cracked junctions were based upon the peak stress locations for the relevant loading condition. Crack locations for each loading case are discussed in detail for the limit load study in Chapter 4.

For the in-plane bending models, both of the cracks were located at the crotch of the junction, running along the lower weld toe. One of the cracks was a through-wall crack (a/t=1.0) and the other was an external, part-penetrating crack (a/t=0.75). The cracks were of equal length and were equivalent to the 'middle' crack length of the three crack lengths assessed in the limit load study. The model geometry and crack profile are shown in Figure 5.3(a), for a quarter-model in PATRAN. The through-wall crack is an extension of the part-penetrating case. The projected normal line used for the crack profile of the limit load study is also shown for comparison (the limit load crack was projected from the weld toe, normal to the surface). The electrode position has also been marked and will be discussed in the following Section. A section through the run pipe is shown to illustrate the crack profile more clearly (Figure 5.3(b)). The cracks were created by projecting the weld toe in the global vector direction: (-1.0, 0.0, -0.4), equivalent to an angle of 21.80° from the branch pipe, as shown in Figure 5.3(c).

The crack in the pressure model was located on the flank of the junction, again at the lower weld toe, as shown in Figure 5.4(a) for a quarter-model. The crack length was again chosen to be equivalent to the 'middle' crack length of the limit load study. The normal line for the limit load case is labelled. The crack was part-penetrating, with a/t=0.75 (obviously, through-wall cracks could not be tested experimentally under pressure loading). The crack can be seen more clearly by taking a section view along the inside of the run pipe, as in Figure 5.4(b). The crack for the experimental case was projected in the global vector direction [-0.5, -1.0, 0.0], equivalent to an angle of 26.57°, as illustrated in Figure 5.4(b). The electrode position has again been marked and will be discussed in the following Section.

The profile and manufacture of the cracks is discussed in more detail in Section 5.2.2.

5.2 Manufacturing of Experimental Models

5.2.1 Production of Branch Junctions

The branch junctions were machined from mild steel plate. The machining methods used had been previously established, as described in [10]. The plate was flame-cut into a series of oversize 'T' sections. Initial rough machining was then performed on the specimens: the limbs were turned and the branch and run pipes were bored to be oversize. The specimens were then subjected to stress relief by heating in a furnace at 650°C for one hour, followed by natural cooling. The bores of the specimen were then finally machined, so that the specimen could be located on the location mandrel. This mandrel enabled the intersecting area of the junction to be machined. The machining was performed using a 'Marwin' four axis milling machine, equipped with a CNC control system. The tool-path was generated using an existing program [10].

The specimen was machined in two runs, one run for each side of the junction. The mandrel allowed the specimen to be rotated so that the opposing half could be machined using the same datum position. The mandrel arrangement is shown in Figure 5.5. The cutter path is shown in Figure 5.6 (the tool had a radius of 8mm). The final junction specification is shown in Figure 5.1. A total of six junctions were manufactured, only five being intended for testing with the extra junction saved in case of any problems. Additionally, one of the original 'T' sections was left unmachined, but was subjected to the same heat treatment as the junctions. This 'T' section was then used for the tensile test specimens (discussed in Section 5.3).

Dimensional Survey

An extensive dimensional survey was performed on each of the junctions, to evaluate any dimensional variations. The external diameter and thickness were measured at a series of locations, shown in Figure 5.7. The maximum, minimum and average values are summarised in Table 5.1, and the % difference values from the specified dimensions (Figure 5.1) are also shown (the upper and lower % difference values indicate the range of the readings taken).

The greatest % variation from the specified dimensions was 2.4% for the branch pipe thickness of the junction with the through-wall crack. Generally, the % variation was much lower than this and was deemed acceptable.

5.2.2 Production of Cracks

The insertion of crack-like defects (also referred to as cracks herein) into three of the junctions was a complicated procedure, due to the curved geometry and the positioning of the defects. The first, and most time-consuming, step was to devise a method for machining the electrodes. The copper plate used for the electrodes was 1mm thick. The subsequent machining of the defects was fairly routine.

Machining of Electrodes

1. The **in-plane bending electrodes** were considered first. The general geometry and location of the electrodes required for the two cracks is shown in Figure 5.3. A local coordinate system was set up for the electrode in PATRAN (coordinate system '2' in Figure 5.3(a)). This enabled the required geometry to be assessed, by taking the coordinates of a series of points along the crack profile, for both a/t values. It was apparent from the plot in the local x-y plane that the curvature could be assumed to be constant, with a radius of 49.38mm. Hence, the dimensions in PATRAN were altered to generate the correct machining coordinates for the electrode. The overall dimensions for the required electrodes are shown for the local coordinate system '2' in Figure 5.8, with the coordinates generated from PATRAN applied to the inner surface of the electrode, rather than adjusting

them to the thickness of the electrode material (the PATRAN coordinates were used in this way for all of the electrodes manufactured). The copper electrode material was mounted on a cylinder with radius of 49.38mm. The copper was rolled onto this cylinder and fixed in place. The electrode profile could then be machined into the end of this copper section.

The machining of the electrode profile was performed on a three axis milling machine and required compensation for the tool radius. This was done using a CNC G-code (G129) developed by Moreton et al [74]. G129 is a modification of the G29 tool compensation code. This code enabled the profile to be machined into the copper on the end of the mounting cylinder for each of the two electrodes.

2. The **electrode for the pressure model** was then considered. The geometry of this electrode is shown in Figure 5.4(a). The coordinates of the required geometry were assessed in the same way as for the in-plane bending electrodes, described above. The general geometry of the electrode required is shown for the local coordinate system in Figure 5.8. It was clear that the profile for this electrode could not be approximated to a cylinder. Hence, the electrode profile was extrapolated to a flat plane and the resulting profile was machined into a flat section of copper, using standard tool compensation techniques. It was necessary to produce a mandrel to match the required dimensions of the electrode. The copper section was then mounted on the mandrel, applying a curvature to match the mandrel profile, and secured in place using a series of screws.

Machining of Cracks and Dimensional Survey

The cracks were inserted into the junctions using EDM techniques (performed by a subcontractor). The angle specification and points of first contact were specified, to enable the junctions to be positioned correctly for the machining. The required displacement of the electrodes, measured from the point of first contact, was also specified.

For in-plane bending, the setup specification for the two cracked junctions is shown in Figure 5.9. A collar was used (Figure 5.10) to position each electrode correctly. This was placed over the branch pipe until the edge was resting against the crack midpoint (equivalent to Contact Point (TW) in Figure 5.9). The electrode was positioned along the guide edge and adjusted until contact with the run pipe surface was made (the contact points were different for the two cases, as shown in Figure 5.9). This ensured that the crack would be in the correct position. The collar was then removed prior to machining.

For the cracked pressure case, the positioning and contact point specification is shown in Figure 5.11. The angle of the junction was altered so that the required electrode movement was in the vertical direction. The setup for machining is shown in Figure 5.12. The crack location was obtained from a vertical edge against the run pipe.

The finished cracks are shown in Figures 5.13 and 5.14 for in-plane bending and pressure respectively. The in-plane bending model shown is the part penetrating model, but the profile was the same for the through-wall model. The cracked pressure model is shown after completion of the test, and has the COD transducer in place (described in Section 5.4.1).

After machining, a dimensional survey was performed on the cracks. To ensure that the cracks were located correctly, and were symmetrical, the crack tip and the mid-crack locations on the junctions were measured using a vernier height gauge, with the specimen placed on a flat measuring table. As would be expected, considering the careful setup of the electrodes, the crack locations were very close to those desired.

In order to check that the crack profiles were correct, impressions were taken by pouring a quick-setting, cold-curing acrylic resin into each of the cracks (this was not done for the through-wall crack). When this resin had cured, it was removed and the casting dimensions were checked: the depth and thickness of the casting were measured at several points.

For the in-plane bending model (with $a/t=0.75$), the crack thickness was equal to 1.20mm ±.02. The depth measurements varied between +1.12% and -3.40% of the depth at the equivalent location in the PATRAN model.

For the pressure model, the thickness was constant and equal to 1.17mm. The maximum depth variation measured was between 1.5% and 5.7% greater than the depth from the PATRAN model.

These measured values were considered acceptable for each of the models.

5.2.3 Overall Fabrication of the Models

The model limbs were extended in length by welding an additional piping section to each of the limbs. The extension pipe dimensions are shown in Figure 5.15, for the branch and run pipe dimensions. They were machined down from thick mild steel pipe.

The end connections required for the branch junctions were different for pressure and in-plane bending. Existing components were modified to match the junction dimensions. For in-plane bending, only two limbs required end connections, so that the junctions could be attached to the Dartec loading faces, by means of pinned connections. For pressure loading, an end connection was obviously required for each limb. Each of these had a small bleed screw (not shown) to assist in the removal of any trapped air, while only one required a connection for attachment to the pressure pump. The geometry of the end connections for in-plane bending and pressure is shown in Figure 5.15.

The components for each test specimen were butt-welded together, using V-blocks to align the various components. The in-plane bending specimen with the part-penetrating crack had an internal strain gauge (described in Section 5.4.1), which had to be attached prior to welding because access would be restricted with the extension limbs in place. For this specimen, it was important to minimise the temperature at the strain gauge, otherwise the installation would be damaged. This was done using numerous wet cloths, applied to the junction immediately following each weld run. When the junction had cooled the next weld run was applied. Heat resistant cable was used for the gauge wiring, which was additionally protected from any weld 'splatter' using thin copper inserts at the pipe connections. For the remainder of the junctions all of the strain gauges were applied after welding.

5.3 Material Properties

In order to check the general material properties of the original steel plate, four tensile test specimens were machined from the previously mentioned additional 'T' section. This section had been subjected to the same heat treatment as the sections used for the branch junctions, but no further machining had taken place. Two specimens were taken from the branch pipe direction, and two from the run pipe direction, in order to check for any material property differences. (The specimens were basically of the same design as those used for the cylinder tests in Chapter 2 - Figure 2.11). Three of the specimens were routinely tested in a uniaxial tensile testing machine, using extensometer readings to calculate the strain values. A displacement rate of 1mm/min was used. There were no significant differences between the results for these three tests, as shown for Tests 1-3 in Figure 5.16.

The fourth specimen had two strain gauges attached to it, in the axial direction. One gauge was placed on each side, so that any bending could be taken into account. This specimen was tested at a displacement rate of 0.2mm/min (equivalent to a strain rate of 6.4 micro-strain/s, after removing test machine stiffness), compared with 1mm/min (equivalent to 300 micro-strain/s) for the first three tests (the rate was increased to 2mm/min in the plastic region for all four tests). The results for this test (Test 4 in Figure 5.16) showed a significant reduction (approximately 10%) in the lower yield stress. A reduction in yield stress would be expected for mild steel with a reduced strain rate, as explained in [75].

It was decided that tests should be performed on specimens taken from the untested spare branch junction, in order to have material properties for the closest available material to that tested. These tensile tests were actually performed after the branch junction tests were completed, so it was known that the spare junction was not required. Two test specimens were machined from the junction, one from each flank. In order to decide upon the test rates used, the test data from the uncracked junction tests was examined (the uncracked tests were used to avoid the complications of the crack-tip strains). The rate of increase of strain from the gauges at the peak strain locations was used as a guide. For the pressure case, there was no gauge at the peak location (the crotch corner) and so the FE strain values were used to calculate the strain, relative to strain gauge results for other locations, at this point. The rates were only examined at the start of the test, prior to yield. For the in-plane bending case, the strain rate was approximately 1.8 micro-strain/s. For the pressure case the rate was approximately 4.1 micro-strain/s.

The tensile test specimens both had strain gauges attached, as for Test 4. The required machine displacement rate was found by loading one of the specimens in the elastic region at a variety of different rates (the displacement of the machine included the machine deflection and so could not be used to calculate the strain rate directly). It was decided that a rate of 0.03 mm/min should be used. This was expected to give a value of below 2 micro-strain/s. Both specimens were tested at this displacement rate. The true stress-strain results are shown in Figure 5.17 (Tests 5 & 6). The two tests showed no significant differences. despite the lower strain rate, the yield plateau value was actually between that of tests 1-3 and test 4, although the difference in material history of the specimens for tests 5 and 6 was thought to be the reason for this.

For the purposes of the FE modelling (described in Chapter 6) a single true stress-strain curve was produced from the average of curves for tests 5 & 6, as shown in Figure 5.17. The method for converting engineering stress-strain curves to true stress-strain curves is explained in [68]. Due to the nature of the stress-strain curves, first yield was lower than the yield 'plateau', at 230.5MN/m^2. The yield 'plateau' was between 237.7MN/m^2 and 239.2MN/m^2. This is shown in the magnified region in Figure 5.17.

5.4 Experimental Arrangements

The experimental arrangements for each test are described in this section. As with the cylinder work described in Chapter 2, the primary objective of the experiments was to obtain some form of load-displacement plot for each case. For each model a different set of displacement values was recorded, as described below.

In addition, the spread of plasticity around the junction, particularly from a crack tip, was of interest. This kind of data is used to confirm FE strain values from full non-linear analysis (i.e. with true stress-strain curve and non-linear geometry considered). If these FE models were then analysed under limit load conditions, the strains could be used to assess local limit loads, as opposed to the global limit loads obtained from load-displacement plots. Hence, a series of strain gauges were applied to each specimen, as described below. The locations of the gauges were based upon the spread of plasticity from preliminary FE analyses.

Where 'pairs' of gauges are referred to, there were two independent gauges arranged at right angles on a rosette. The gauge pairs all had a gauge length of 1.57mm. Where 'rosettes' are referred to, there were three independent gauges present on a rosette, at 0°, 45° and 90°, as shown in Figure 5.18. These rosettes enabled the principal strain direction to be derived at a particular location, and had a gauge length of 1.5mm.

It should be noted that the gauges were not positioned directly onto the intersection transition surface (the area between the branch and the run pipes), unless required because of the crack location, as this area had double curvature. Any gauge in this area would probably detach at lower strain levels than for a gauge on a surface with single curvature.

5.4.1 In-Plane-Bending

The experimental arrangement and loading procedure was nominally identical for each of the in-plane bending branch junctions. For the cracked models, the crack opening displacement (COD) was recorded, as described below. The general arrangement of the junctions in the Dartec testing machine is shown in Figure 5.19, for one of the cracked junctions. The test arrangement did not give a constant bending response throughout the intersection, as the moment would alter with the distance from the loading axis. However, the correct moment at the intersection could be calculated if the moment offset length was known. The horizontal offset of the junction was measured throughout each test, so that the correct moment could be calculated from the crosshead load value. The moment was given by the equation:

$$\text{Moment} = \text{Load} \times (\text{Original Length - Offset}) \tag{5.1}$$

For all of the bending tests, a diametral displacement transducer was positioned at the flank of the junction, as marked in Figure 5.19. From the FE data, the diametral value was expected to decrease overall, so the transducer range was adjusted accordingly.

The lengths of the extension limbs for each test setup varied slightly. The values of l_x, l_r, l_b and the original moment offset, l_{off}, are given in Figure 5.19.

The specific test arrangements and strain gauge details are described below. The strain gauge positions stated are the actual measured positions rather than the original specified positions.

Uncracked Model

There were five strain gauge pairs attached to this junction, as shown in Figure 5.20. In addition, there was a single gauge placed axially on the loaded run pipe extension limb, to compare with FE nominal strain (this gauge was in line with gauge pairs 1 and 2, at a distance of 176mm from the branch pipe).

Cracked Models

For the cracked models, a COD transducer was positioned across the crack opening, as shown in Figure 5.21. The mounts for this transducer were machined to match the curvature of relevant mounting area and then soldered in place. The minimum distance that the COD transducer could measure between the two mounts ('c' in Figure 5.21) was 7mm. The distance 'c' was measured for each of the cracked cases: for the part-penetrating crack c=8mm, for the through-wall crack c=9mm.

The strain gauge positions were nominally the same for the part-penetrating and through wall cracked cases. The locations for each case are shown in Figure 5.22. An additional single gauge was placed on the inside surface of the part-penetrating model (prior to welding of the extension limbs) in order to monitor the spread of plasticity in the crack ligament. The location of this gauge is shown in Figure 5.23.

5.4.2 Internal Pressure

The procedure for pressure loading of the uncracked and cracked junctions was similar, but very different measurements were taken for each case. Ideally, the product of the parameters used in load-deformation plots should be equal to work (as defined by Gerdeen [3] and discussed in Chapter 1). Therefore, for pressure loading the displacement parameter should be the change in volume of the pressurised fluid. However, with the apparatus available this was difficult to measure. This parameter was also found to be difficult to evaluate from the FE models. Hence alternative (more practical) deformation parameters were used for these tests - these are described below.

Both junctions were tested inside a testing chamber, in order to contain any spillages. Oil was used as the pressurised medium, with the pressure monitored by means of a pressure transducer (with a strain gauge arrangement). The pressure was applied using a manually operated pump, with a maximum rating of 10000psi (69MPa). All of the parameters were recorded using a data logger.

Uncracked Model

The measured displacement parameter was the diametral growth of the run pipe at the flank location. As this was the only displacement parameter measured, two diametral growth transducers were used, in case of any problems with recording data during the test. The positions of the transducers are shown in Figure 5.24.

The positions of the strain gauges around the intersection are shown in Figure 5.24. Just four pairs of gauges were attached for this case. Their positions were based upon the peak strain areas (i.e. the crotch and the flank). A pair was placed on each flank of the run pipe, in line with the intersection centreline, as this area was of particular interest with regard to the crack location for the cracked junction. One pair of gauges was located on the outer run pipe opposite the crotch corner. (The crotch corner is the peak strain location for uncracked pressure loading, but it is difficult to apply and monitor strains inside a pressurised junction and was deemed unnecessary for the uncracked case). The final pair of gauges was placed on one of the extension limbs, to ensure the nominal strains were correct (and hence provide confidence that the rest of the strains had been recorded correctly).

Cracked Model

For this model there were two measured displacement parameters:

- The Crack Opening Displacement was measured using a standard strain gauge transducer, as for the in-plane bending tests. The COD transducer required two fixing blades, one on each side of the crack. Each blade was machined to match the curvature of the relevant mounting area and then soldered in place. The transducer arrangement is shown in Figure 5.25. For this case, c=7.2mm.
- The rotation of the branch pipe, relative to the run pipe of the junction was also measured. From FE limit load studies, it was found that the diametral growth of

the junction (as used for the uncracked junction) was not useful for the cracked junction, as the value would increase to a certain limit and then decrease as the plasticity spread around the intersection. This was further complicated by the non-symmetrical nature of the cracked junctions. Hence, the rotation of the branch junction was used as a displacement parameter, as this was the parameter used when assessing the limit pressures for the cracked FE study.

The arrangement for recording this rotation is shown in Figure 5.26 and is shown schematically in Figure 5.27(a). A bar was attached (welded) to each end of the run pipe, from which another bar (Reference bar 1 in Figure 5.27(a)) was suspended above the branch pipe. A second reference bar (Reference bar 2) was extended from the end of the branch pipe. Two displacement transducers were attached between these two reference bars and the rotation of the end of the branch pipe could be calculated from the displacements of these two transducers. A schematic representation of the arrangement under loading is shown in Figure 5.27(b). Assuming that the rotation of the branch direction was small enough that the transducers could be assumed to always be horizontal, the rotation was calculated using the equation:

$$\text{Angle of Rotation} = tan^{-1}\left(\frac{displacement\ a - displacement\ b}{250}\right) \qquad (5.2)$$

The pressure could then be plotted against this rotation value to evaluate the response of the junction.

The strain gauge arrangement for these cracked models is shown for the intersection area in Figure 5.28 (all of the gauges shown are single gauges). There were single gauges placed at each end of the crack, one parallel and the other perpendicular to the crack face. Other single gauges were positioned around the crack based upon strain readings from the FE model and to examine the spread of plasticity around the crack. A gauge pair was placed on the flank, on the opposite side of the junction to the crack (in a similar position to Gauge pair 1P in Figure 5.24). Finally, a single gauge was placed on one of the extension limbs to monitor the nominal hoop strain.

5.5 Concluding Remarks

The manufacture and experimental arrangements have been described in detail for the branch junction tests. The test results and comparisons with FE results are discussed in Chapter 6.

Table 5.1: Results of Branch Junction Dimensional Survey

Uncracked In-Plane Bending

	D	T	T'	d	t	t'
Max. [mm]	78.060	7.165	7.150	74.440	7.105	7.095
Min. [mm]	77.900	7.090	7.000	74.260	6.940	6.915
Mean [mm]	77.981	7.117	7.064	74.344	7.028	7.007
Upper % Diff.	0.412	1.344	1.132	0.310	0.495	0.354
Lower % Diff.	0.206	0.283	-0.990	0.067	-1.839	-2.192
Mean % Diff.	0.310	0.664	-0.085	0.181	-0.596	-0.889

Part-Penetrating Cracked In-Plane Bending

	D	T	T'	d	t	t'
Max. [mm]	77.910	7.070	7.055	74.380	7.030	7.055
Min. [mm]	77.680	6.930	6.970	74.130	6.935	6.980
Mean [mm]	77.803	6.985	7.001	74.260	6.991	7.015
Upper % Diff.	0.219	0.000	-0.212	0.229	-0.566	-0.212
Lower % Diff.	-0.077	-1.980	-1.414	-0.108	-1.909	-1.273
Mean % Diff.	0.081	-1.202	-0.981	0.067	-1.111	-0.778

Through-Wall Cracked In-Plane Bending

	D	T	T'	d	t	t'
Max. [mm]	77.900	7.125	7.070	74.370	7.115	7.105
Min. [mm]	77.660	6.910	6.915	74.180	6.970	6.900
Mean [mm]	77.779	7.004	6.989	74.259	7.046	7.011
Upper % Diff.	0.206	0.778	0.000	0.216	0.636	0.495
Lower % Diff.	-0.103	-2.263	-2.192	-0.040	-1.414	-2.405
Mean % Diff.	0.051	-0.939	-1.146	0.065	-0.344	-0.828

Uncracked Pressure

	D	T	T'	d	t	t'
Max. [mm]	77.960	7.130	7.140	74.410	7.075	7.060
Min. [mm]	77.860	7.010	7.010	74.330	7.020	7.025
Mean [mm]	77.923	7.060	7.058	74.381	7.044	7.038
Upper % Diff.	0.283	0.849	0.990	0.270	0.071	-0.141
Lower % Diff.	0.154	-0.849	-0.849	0.162	-0.707	-0.636
Mean % Diff.	0.235	-0.141	-0.174	0.231	-0.364	-0.455

Part-Penetrating Pressure

	D	T	T'	d	t	t'
Max. [mm]	77.98	7.105	7.180	74.570	7.095	7.215
Min. [mm]	77.76	6.975	6.970	74.280	6.965	7.090
Mean [mm]	77.862	7.051	7.046	74.407	7.031	7.156
Upper % Diff.	0.309	0.495	1.556	0.485	0.354	2.051
Lower % Diff.	0.026	-1.344	-1.414	0.094	-1.485	0.283
Mean % Diff.	0.157	-0.263	-0.335	0.266	-0.556	1.222

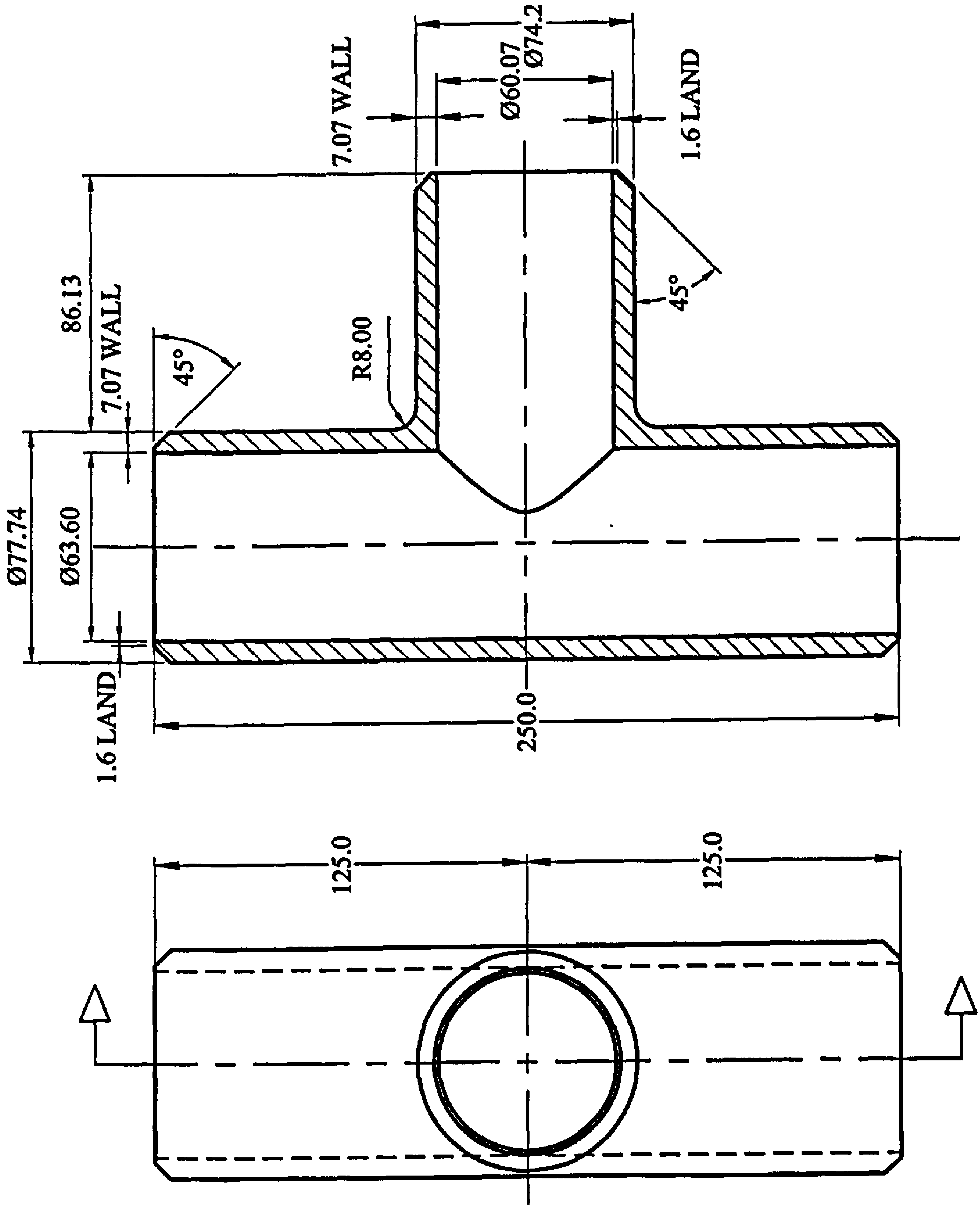

Figure 5.1: Specified Model Dimensions

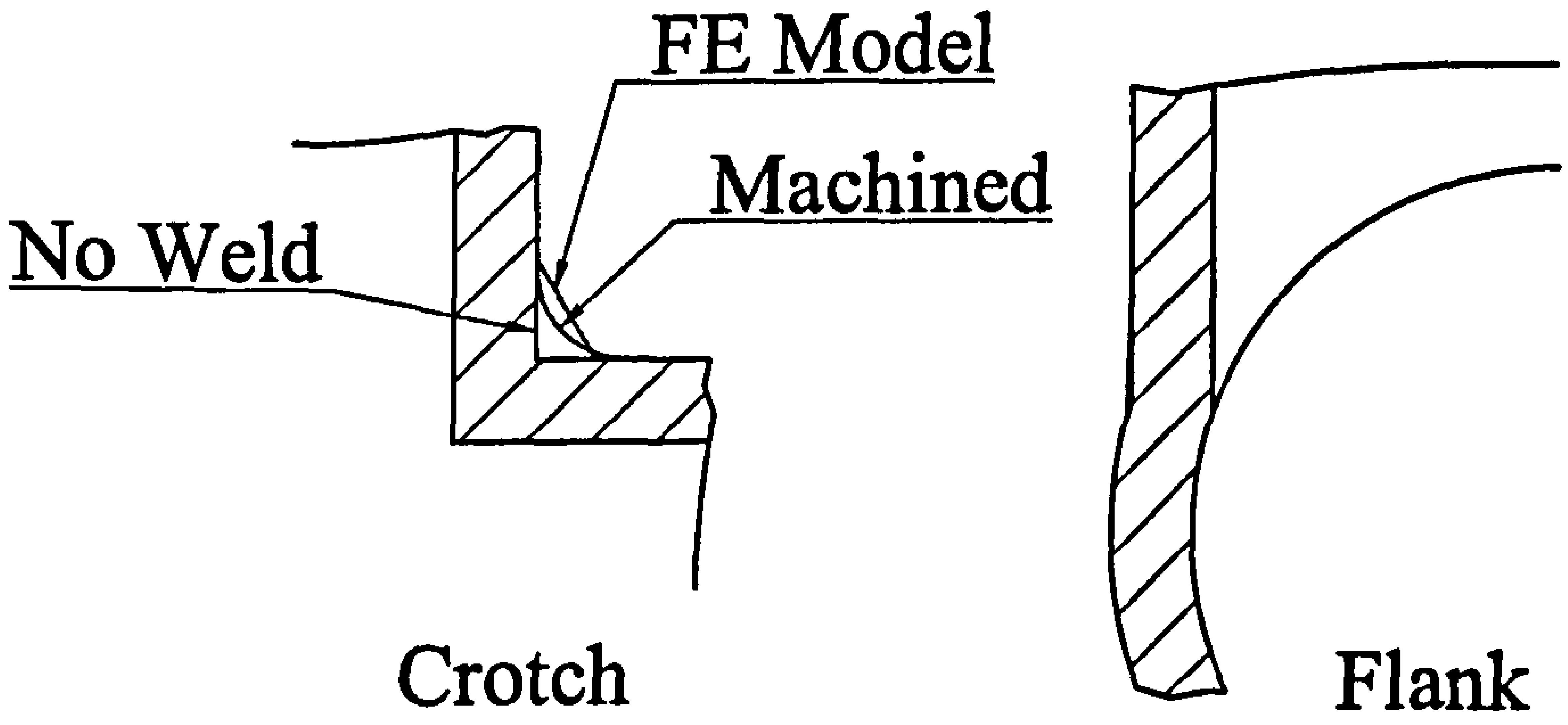

Figure 5.2: Comparison of Intersections of FE and Experimental Models

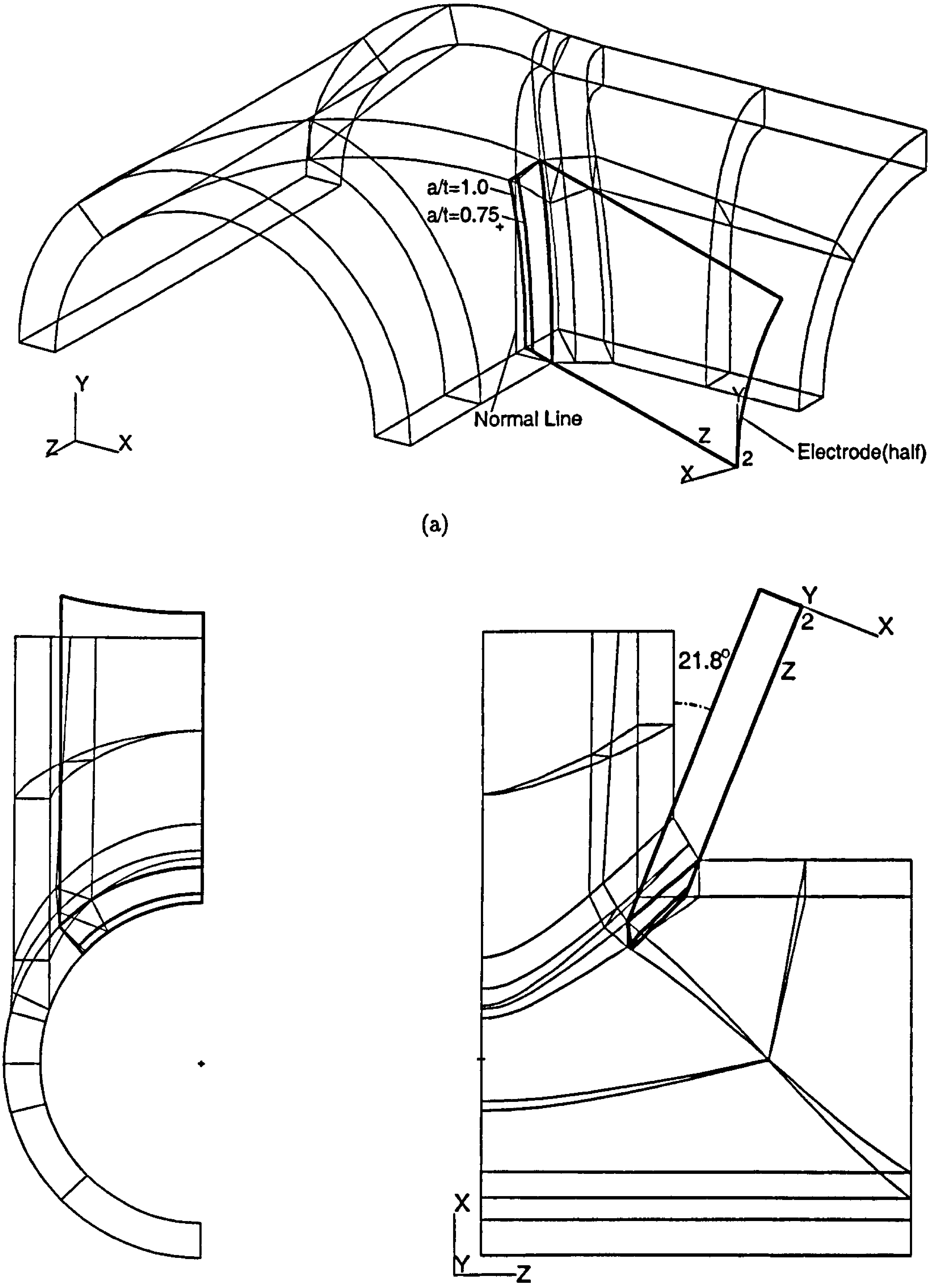

(a)

(b)

(c)

Figure 5.3: In-Plane Bending Models - Crack and Electrode Positions

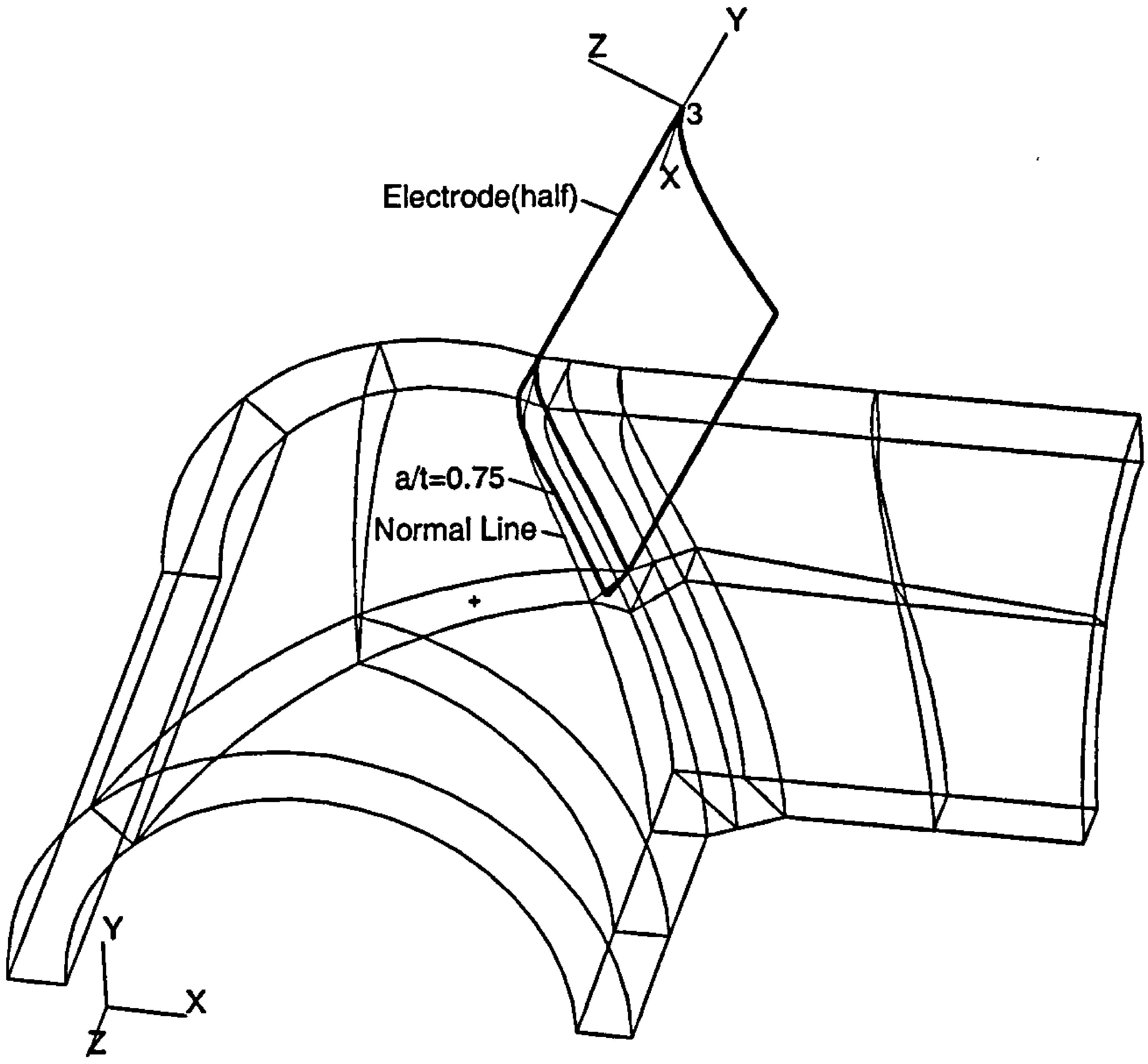

(a)

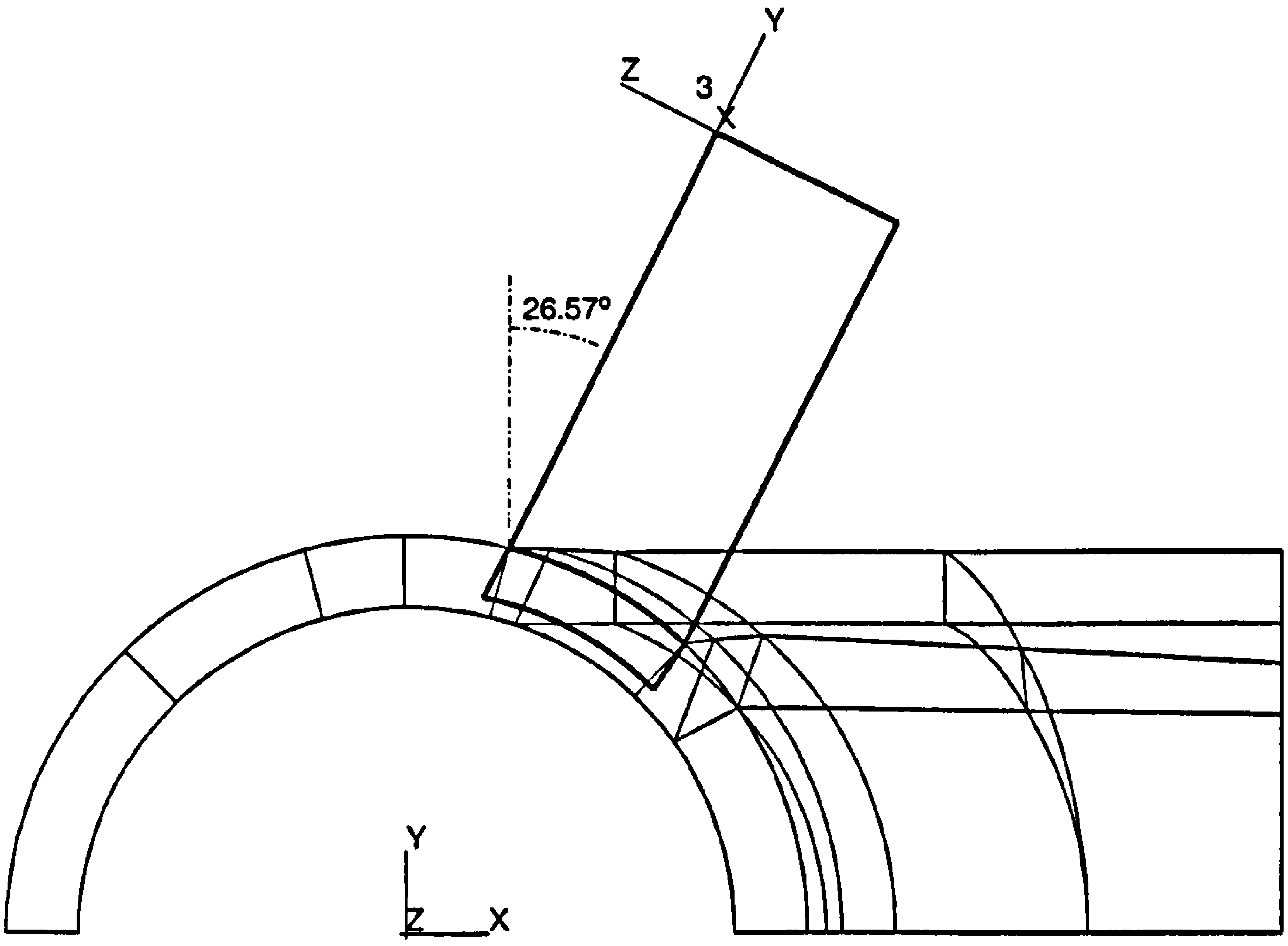

(b)

Figure 5.4: Cracked Pressure Model - Crack and Electrode Positions

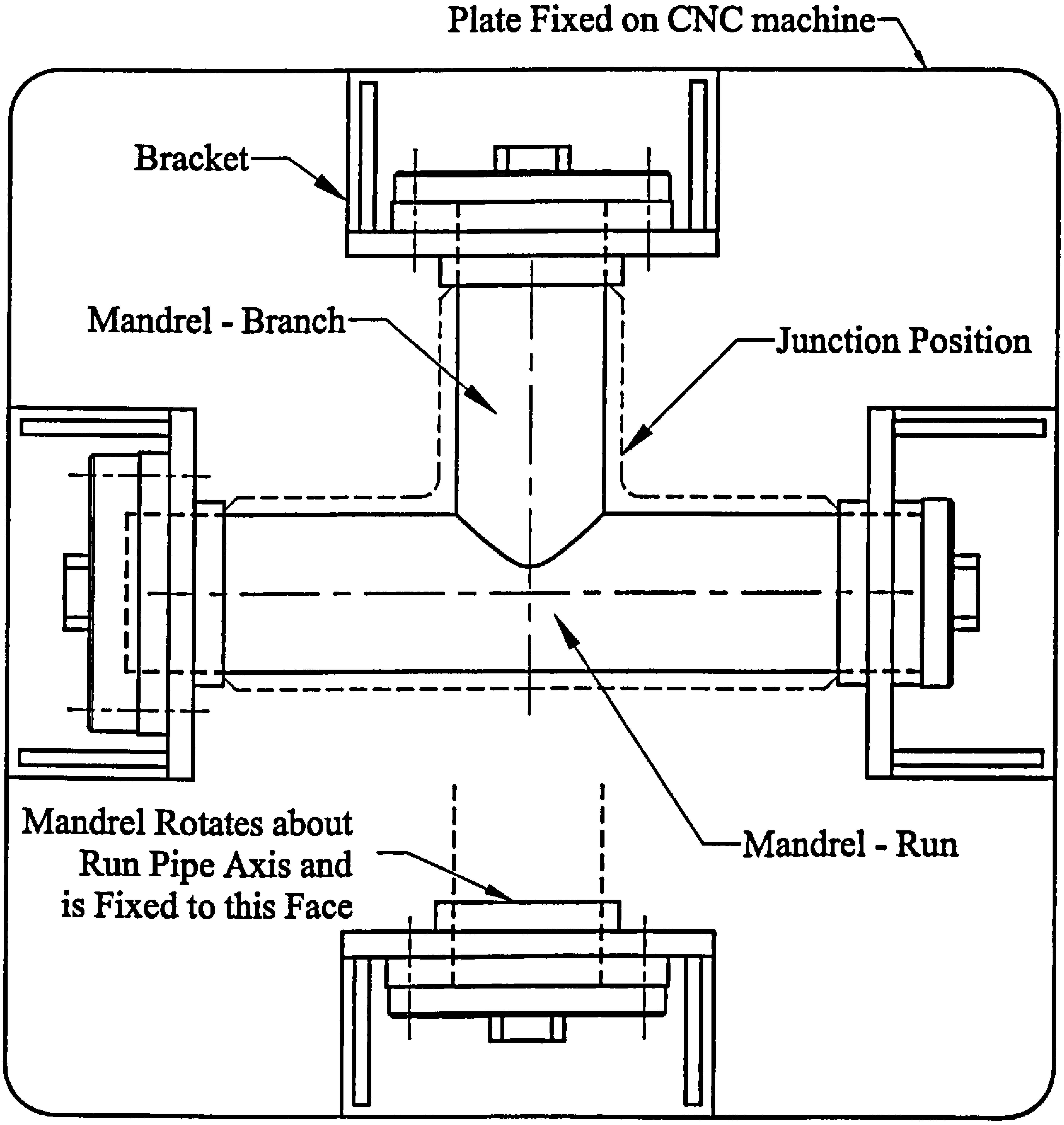

Figure 5.5: Mandrel Setup for Machining of Junctions

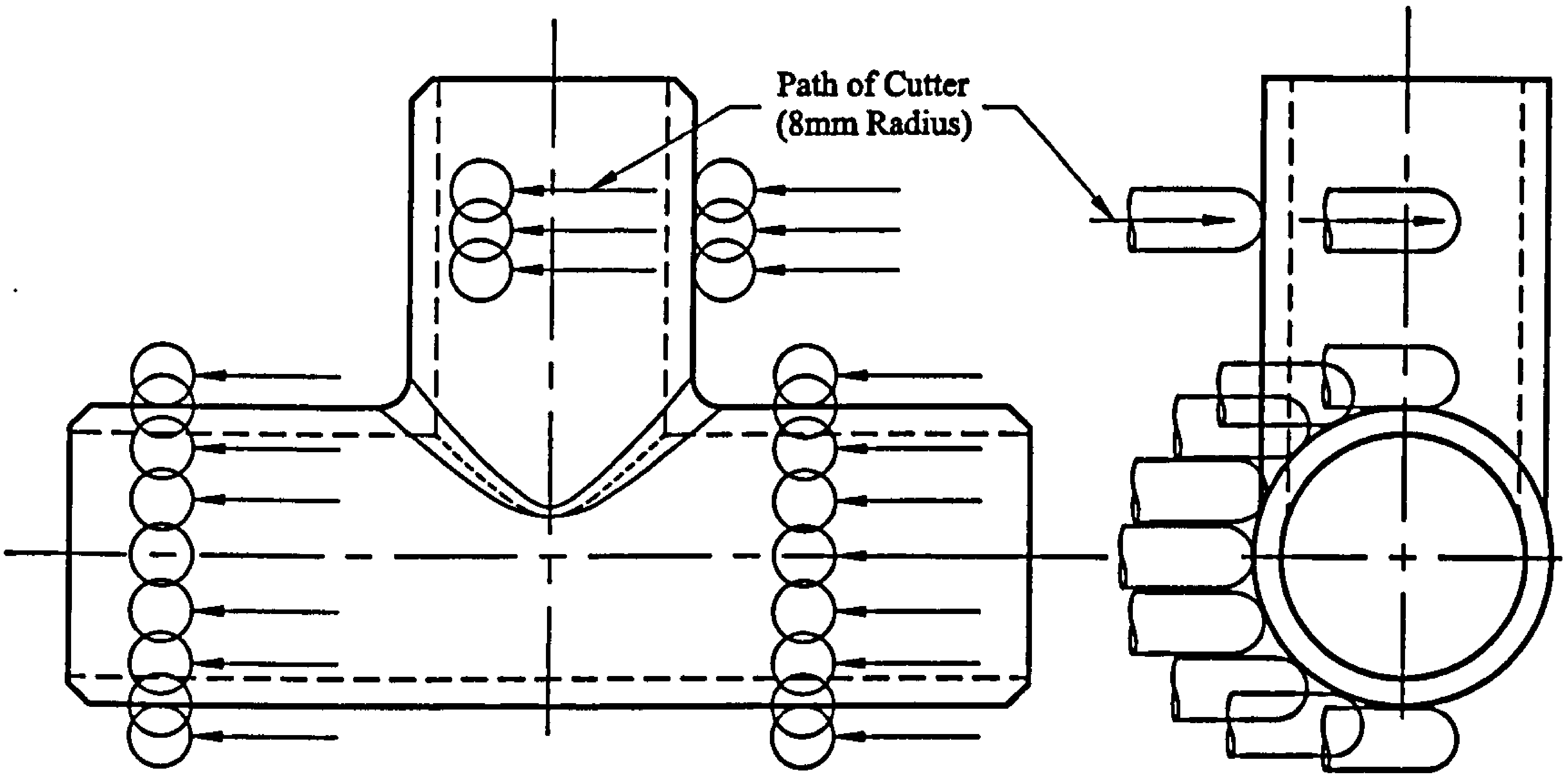

Figure 5.6: Cutter Path for Machining of Junction

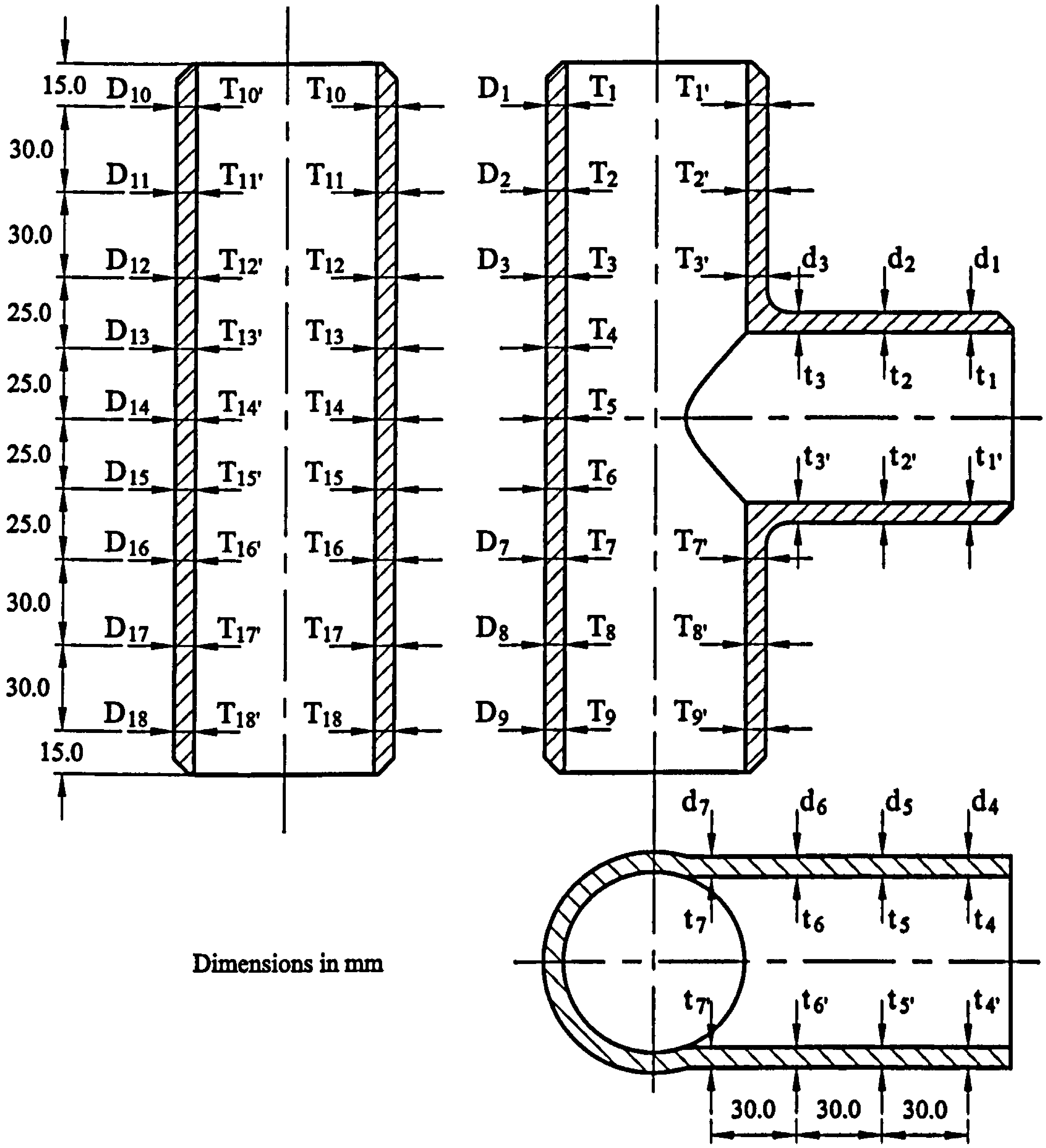

Figure 5.7: Dimensional Survey Measurement Locations

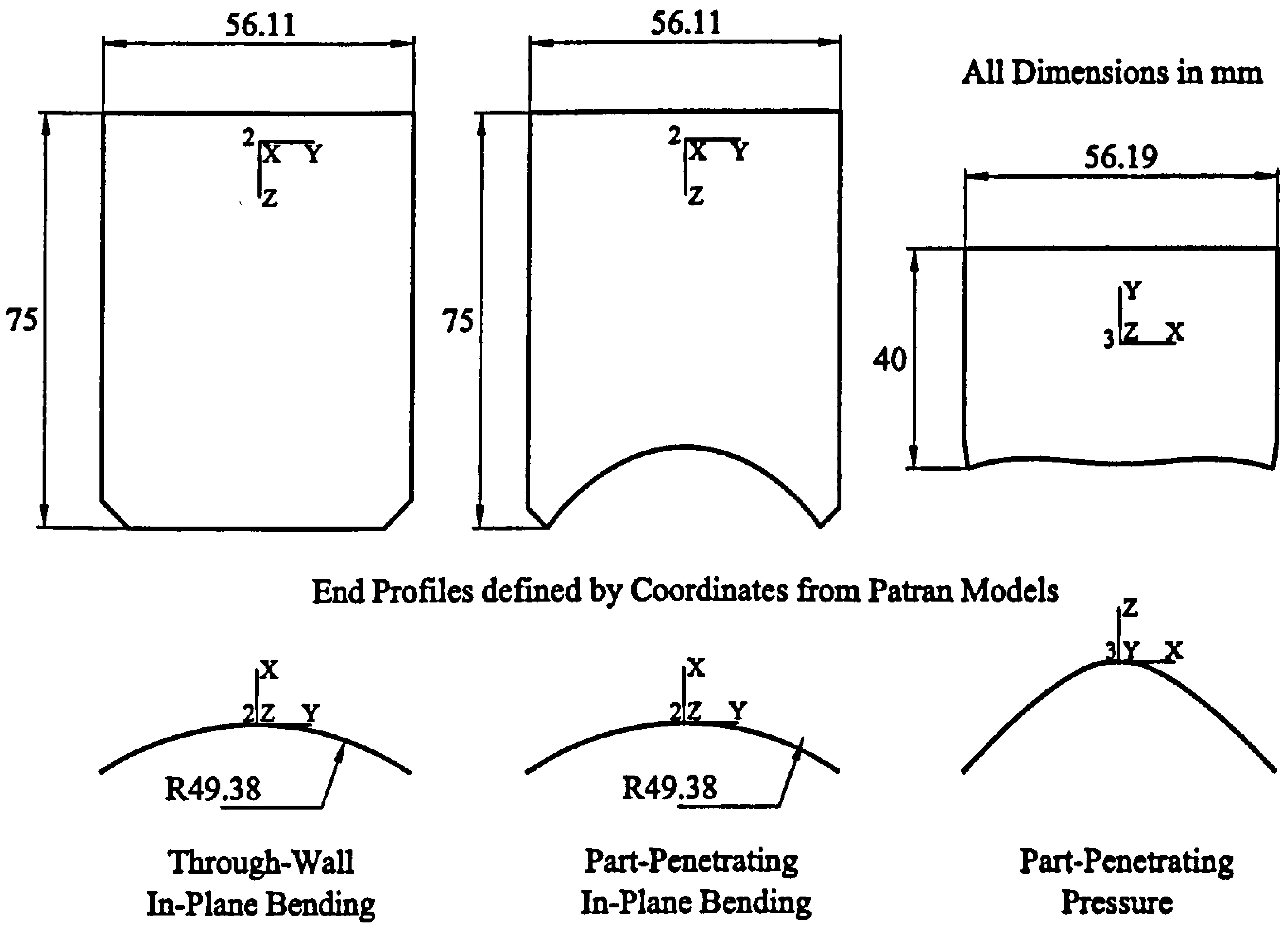

Figure 5.8: Electrode Dimensions

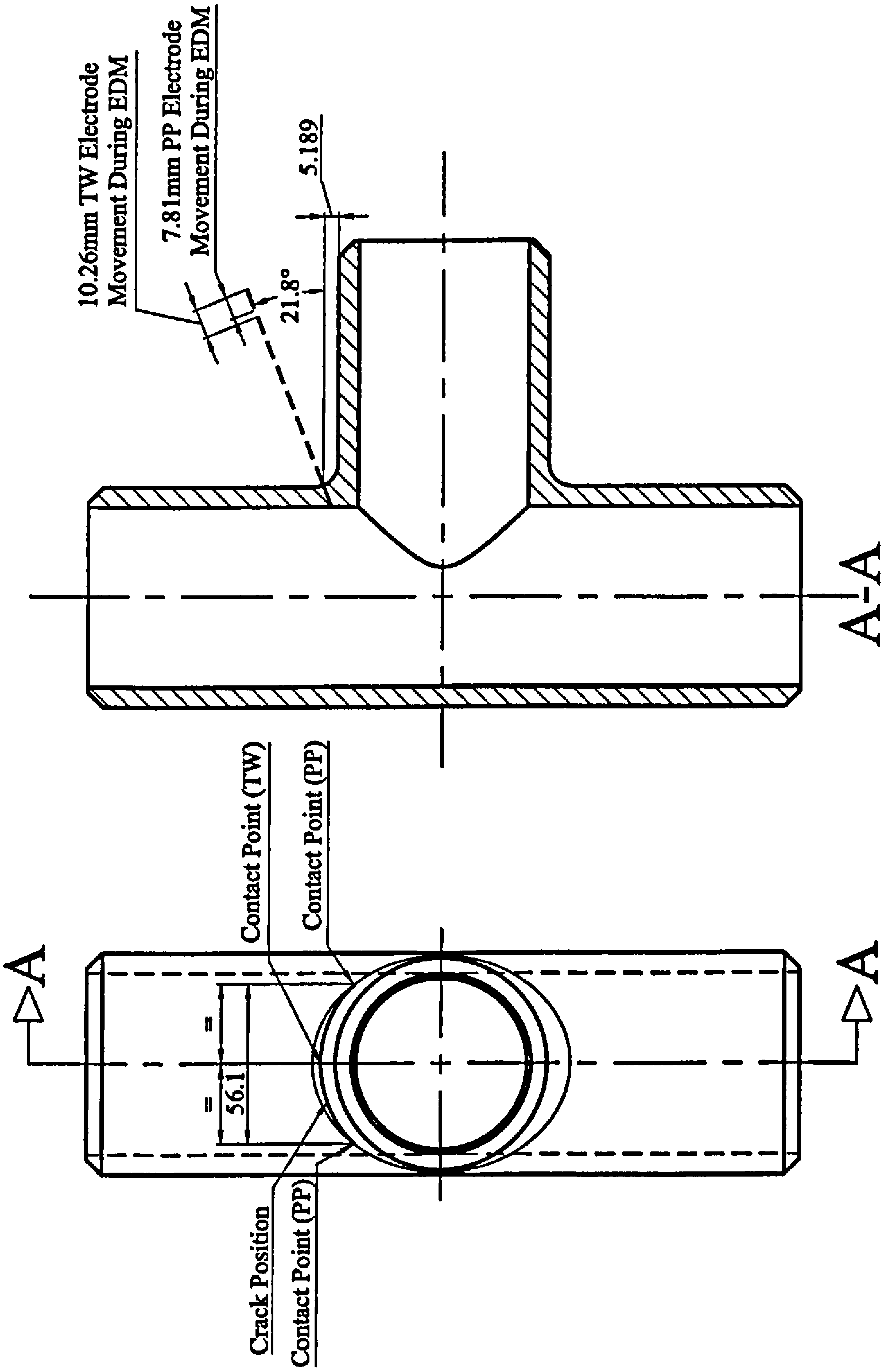

Figure 5.9: Specification for EDM of In-Plane Bending Models

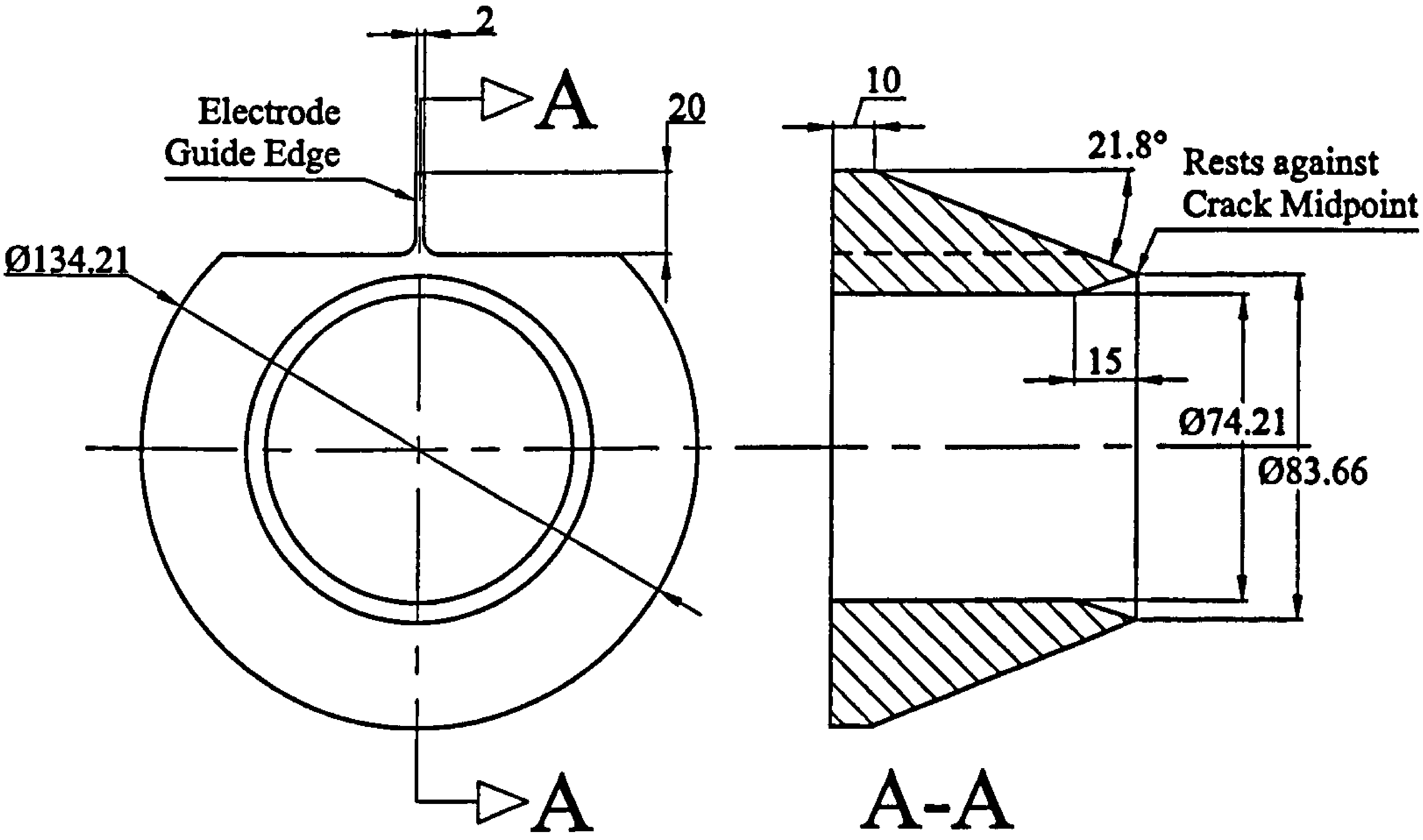

Figure 5.10: Setup Collar for EDM of In-Plane Bending Models

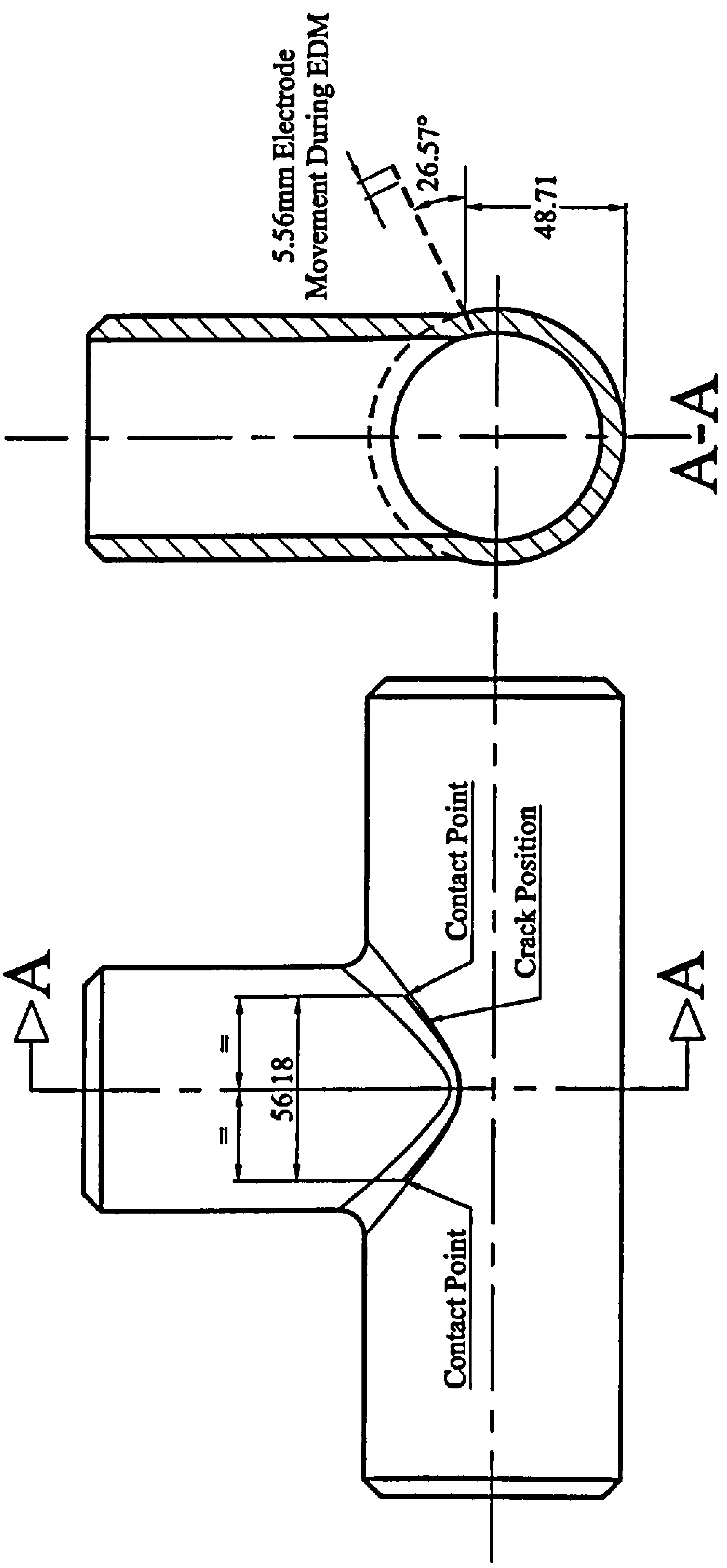

Figure 5.11: Specification for EDM of Pressure Model

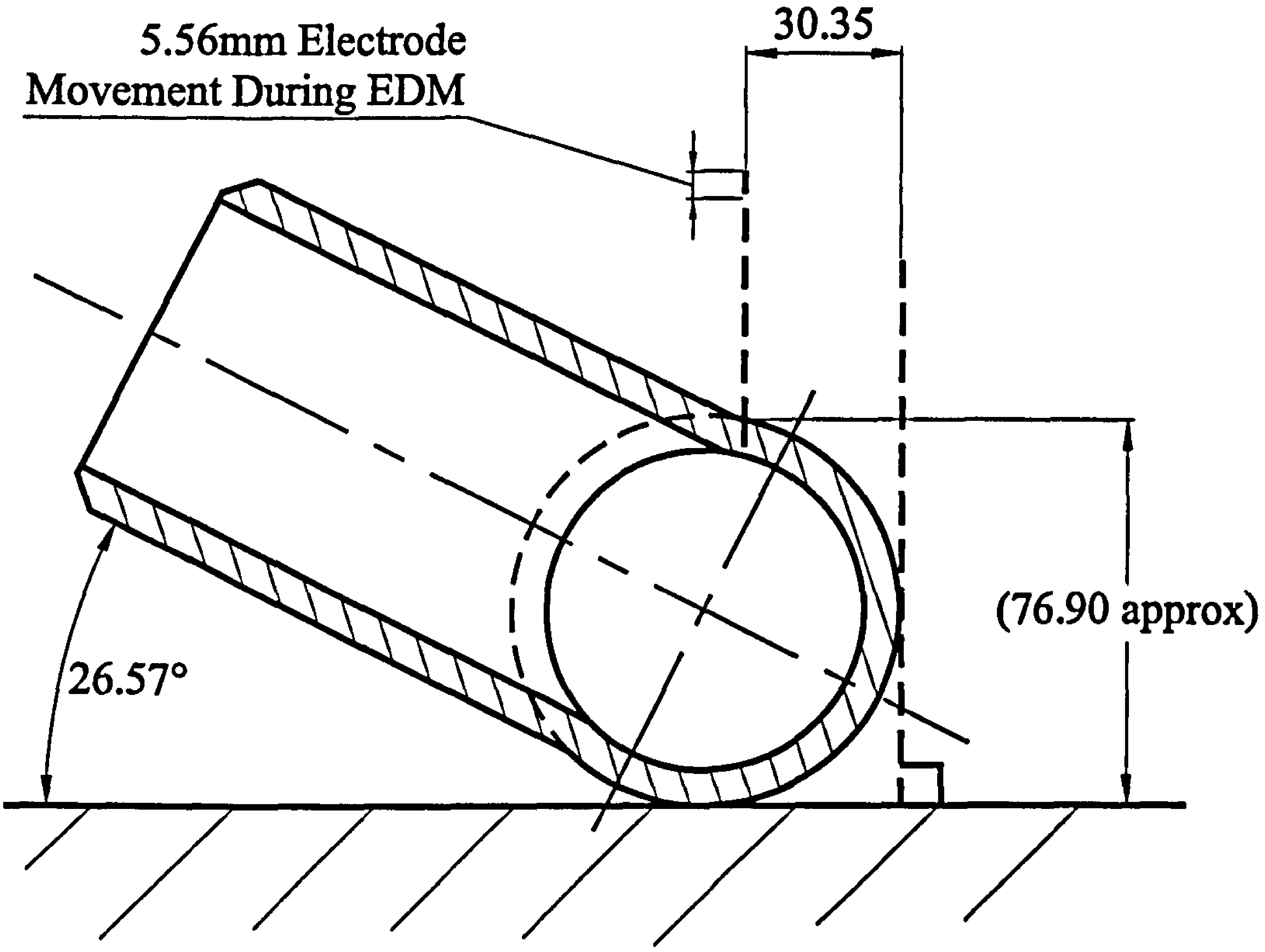

Figure 5.12: Setup for EDM of Pressure Model

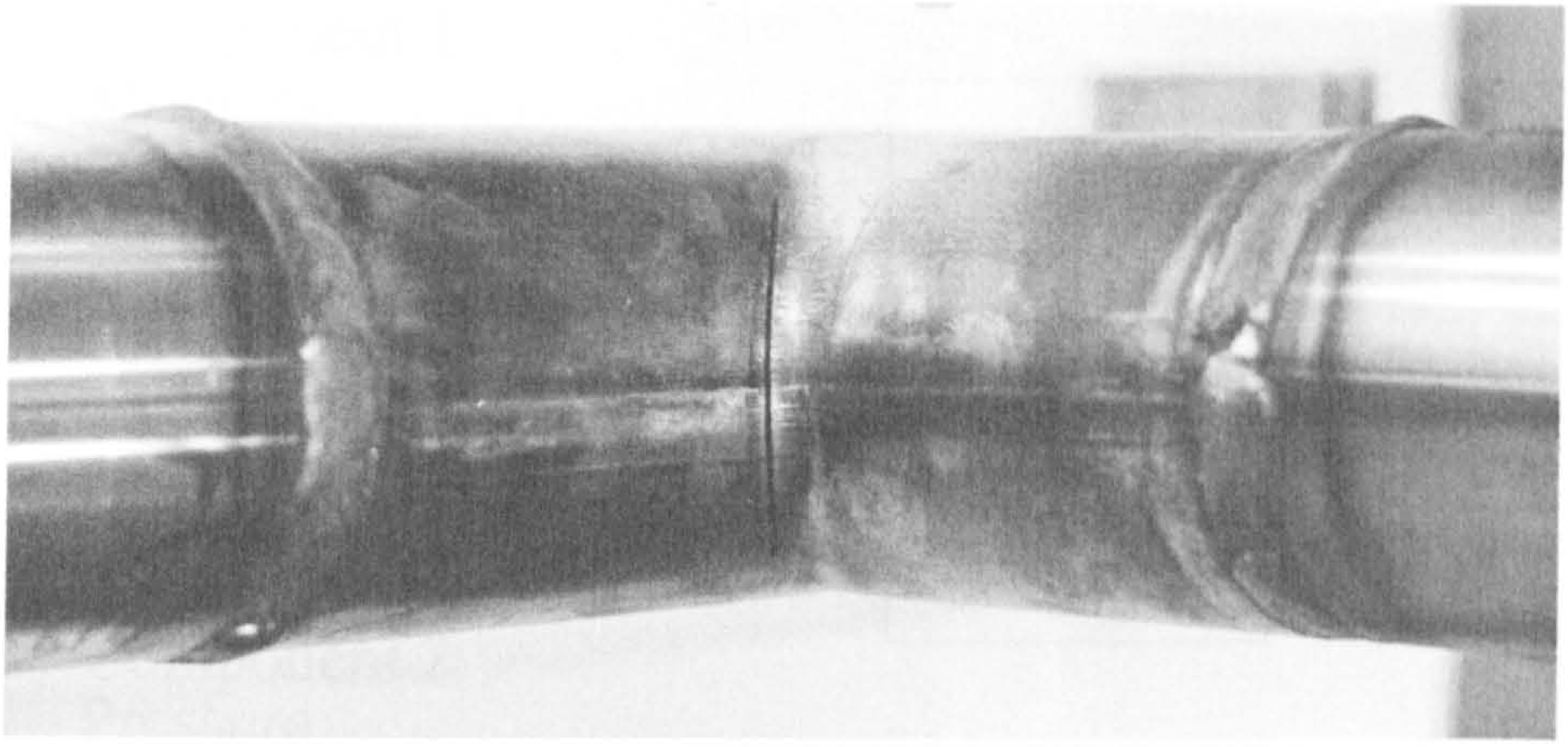

Figure 5.13: Part-Penetrating In-Plane Bending Crack

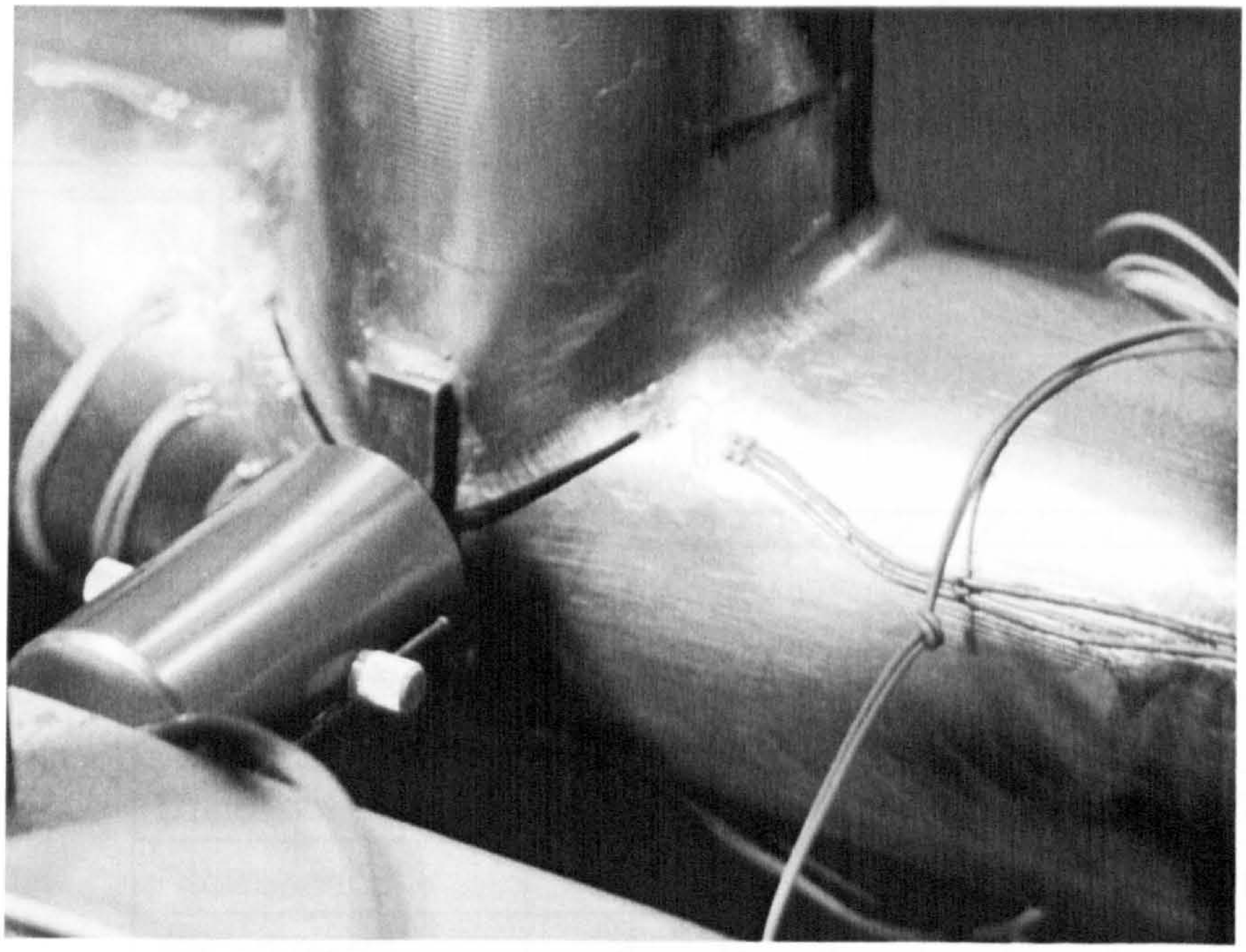

Figure 5.14: Part-Penetrating Pressure Crack

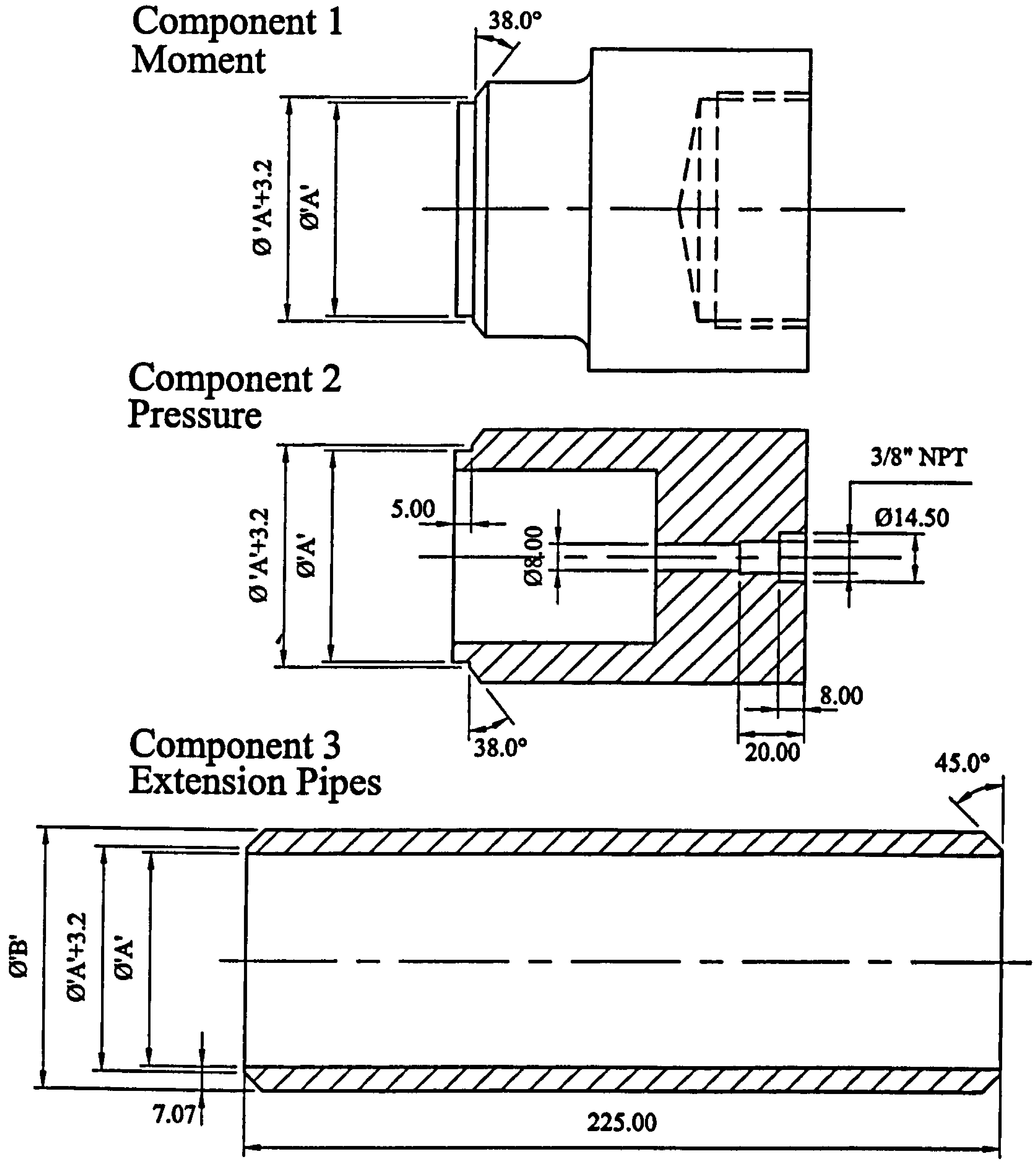

Component No.	1 and 2		3	
Dimension 'A'	63.60	60.07	63.60	60.07
Dimension 'B'	--	--	77.74	74.21
No. off (each)	4	2	12	6

Figure 5.15: End-Component and Extension-Limb Dimensions

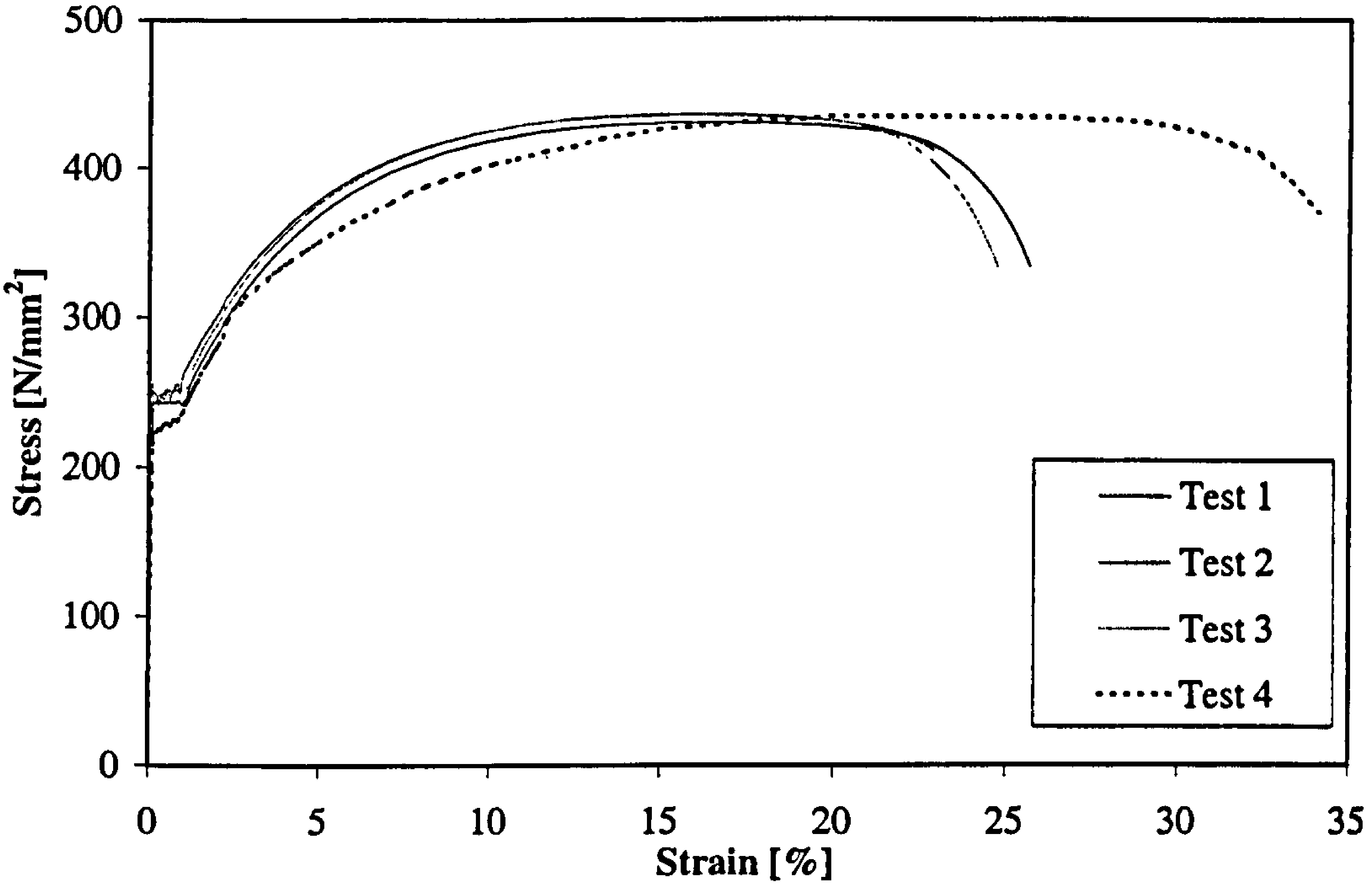

Figure 5.16: Tensile Test Results - Engineering Stress/Strain

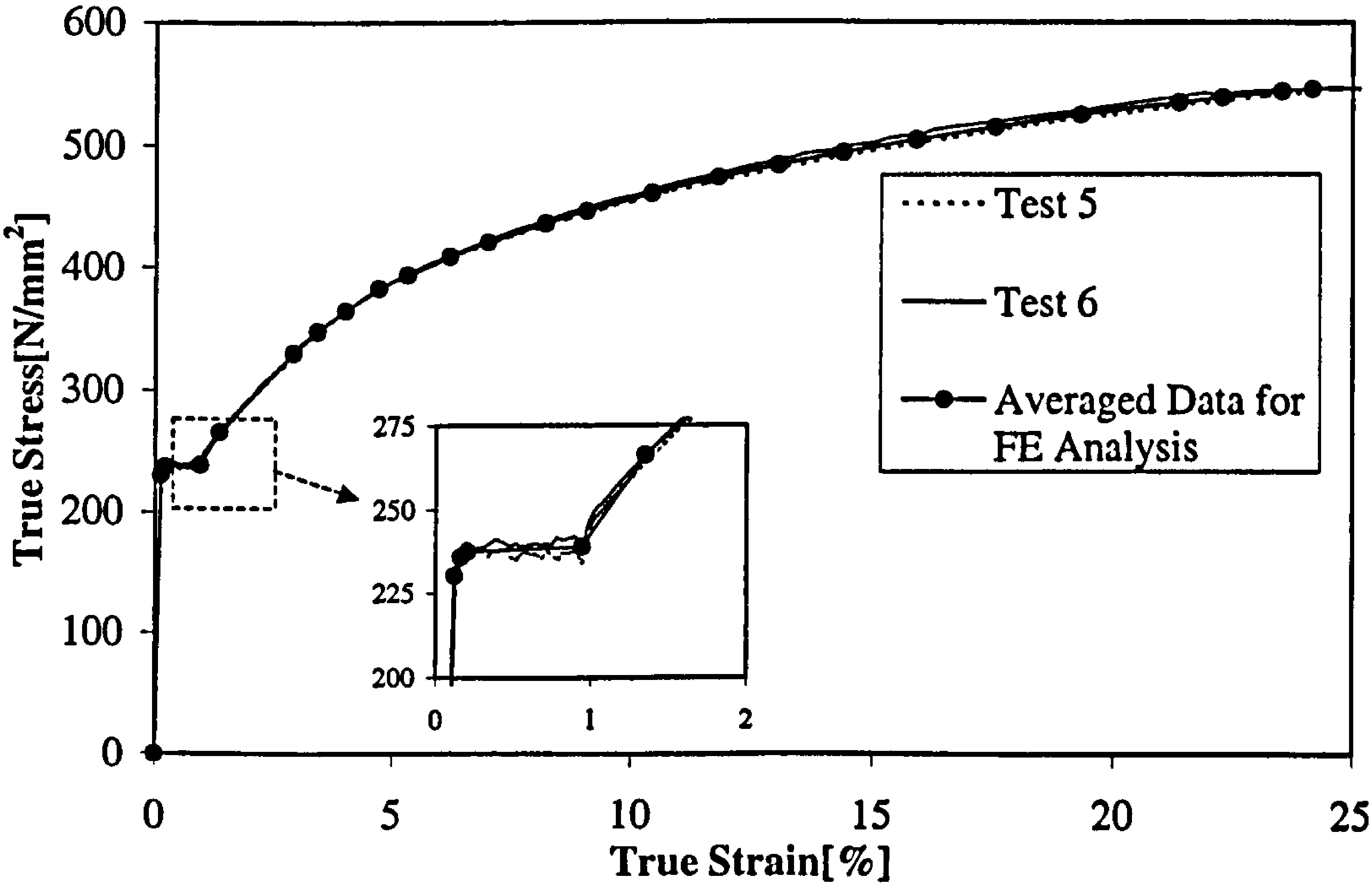

Figure 5.17: True Stress/Strain Results for Specimens 5 and 6

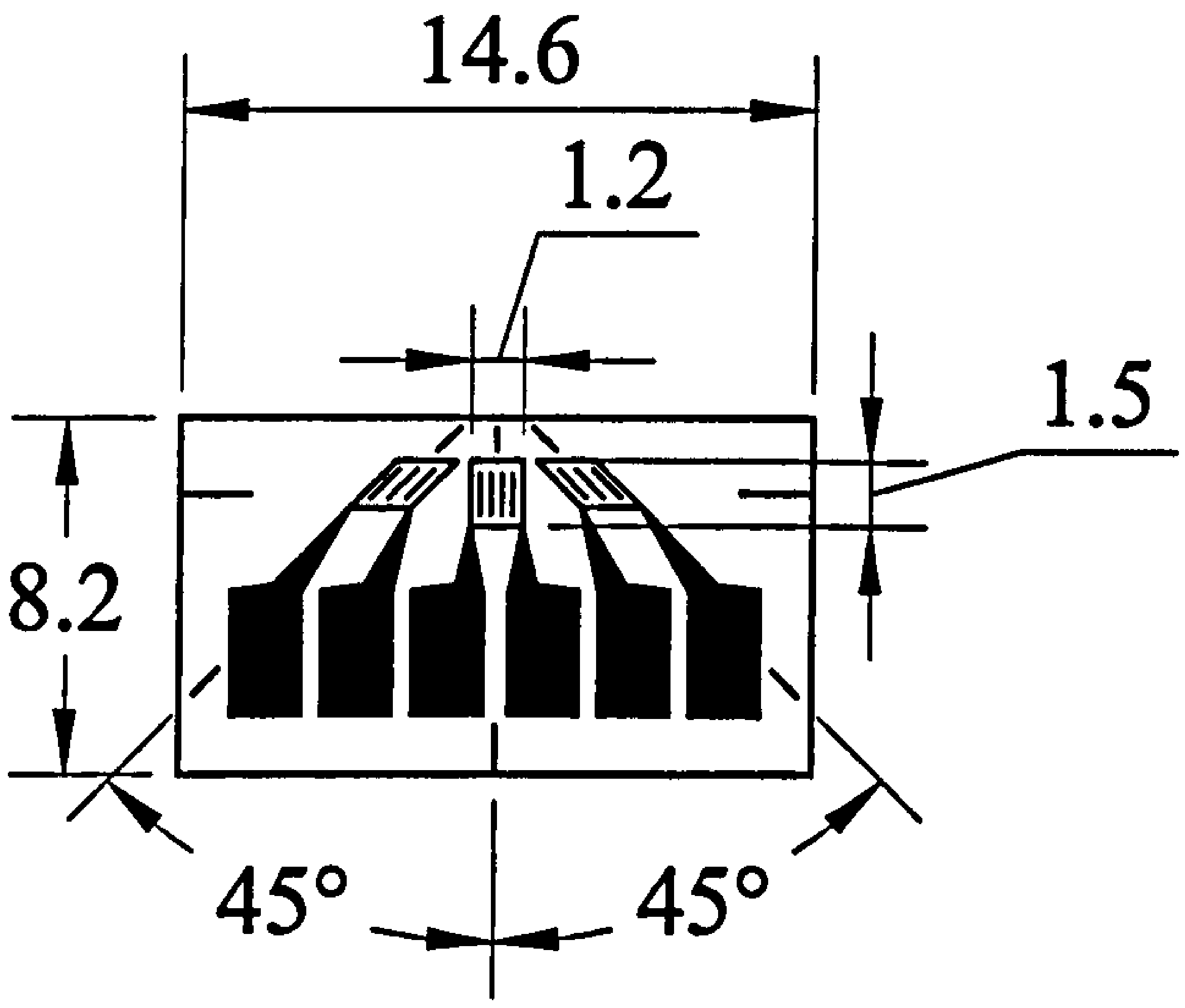

Figure 5.18: Strain Gauge Rosette

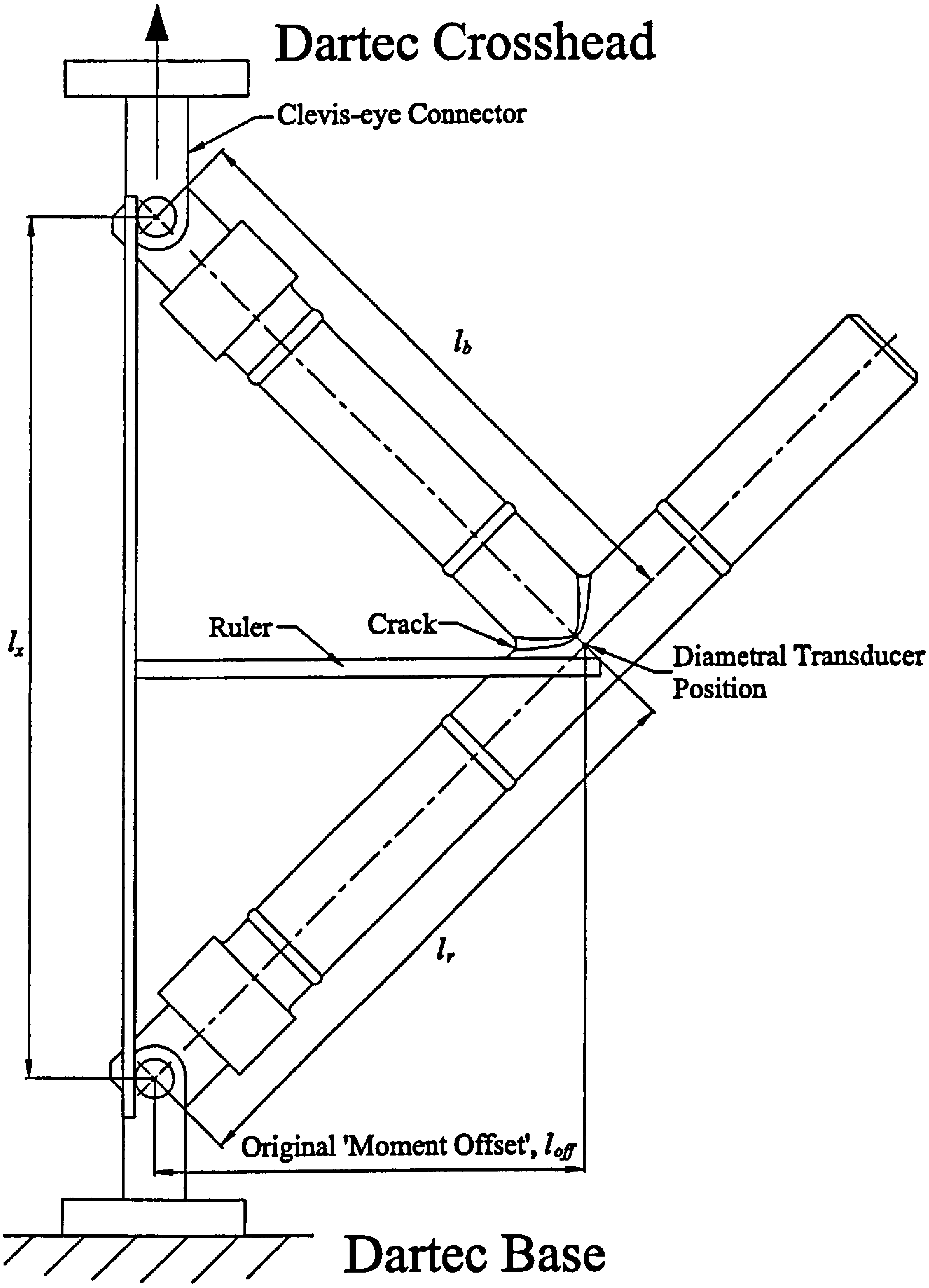

Junction	l_x [mm]	l_r [mm]	l_b [mm]	l_{off} [mm]
Uncracked	728	514	514.5	361
Part-Penetrating Crack	719	509	509	359
Through-Wall Crack	730	515.5	516	361

Figure 5.19: Experimental Arrangement for In-Plane Bending

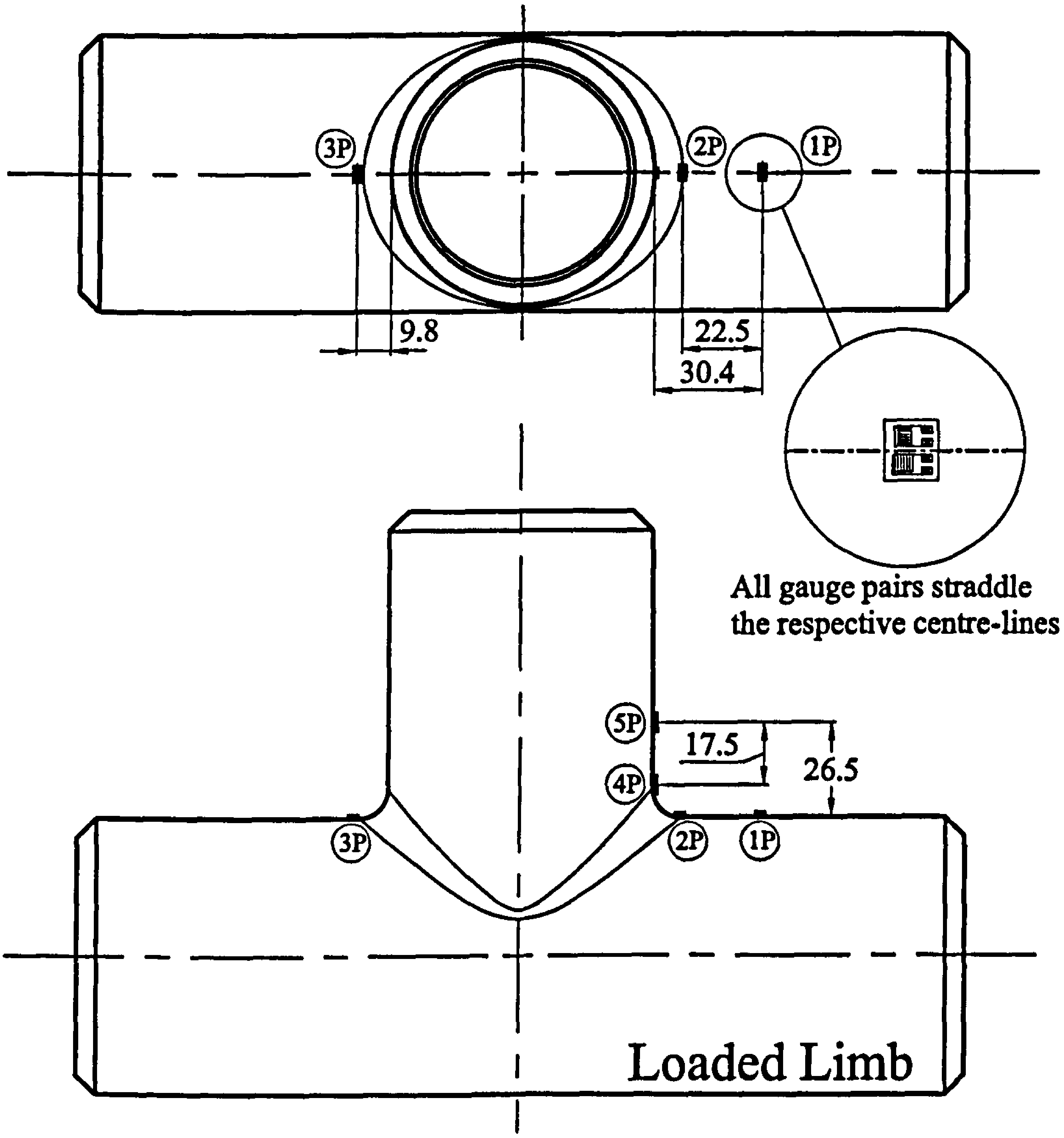

Figure 5.20: Strain Gauge Arrangement for Uncracked In-Plane Bending

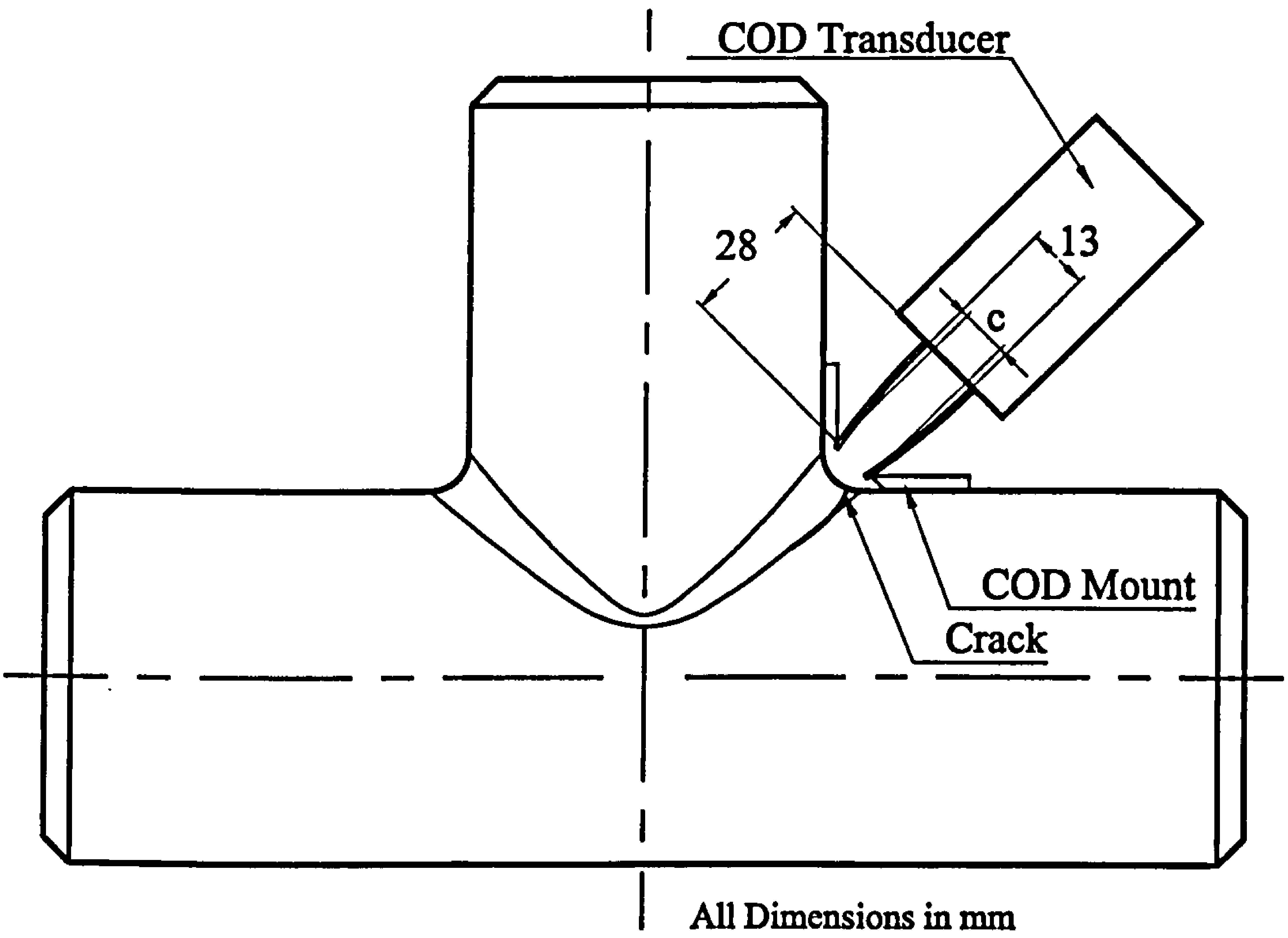

Figure 5.21: COD Transducer for In-Plane Bending

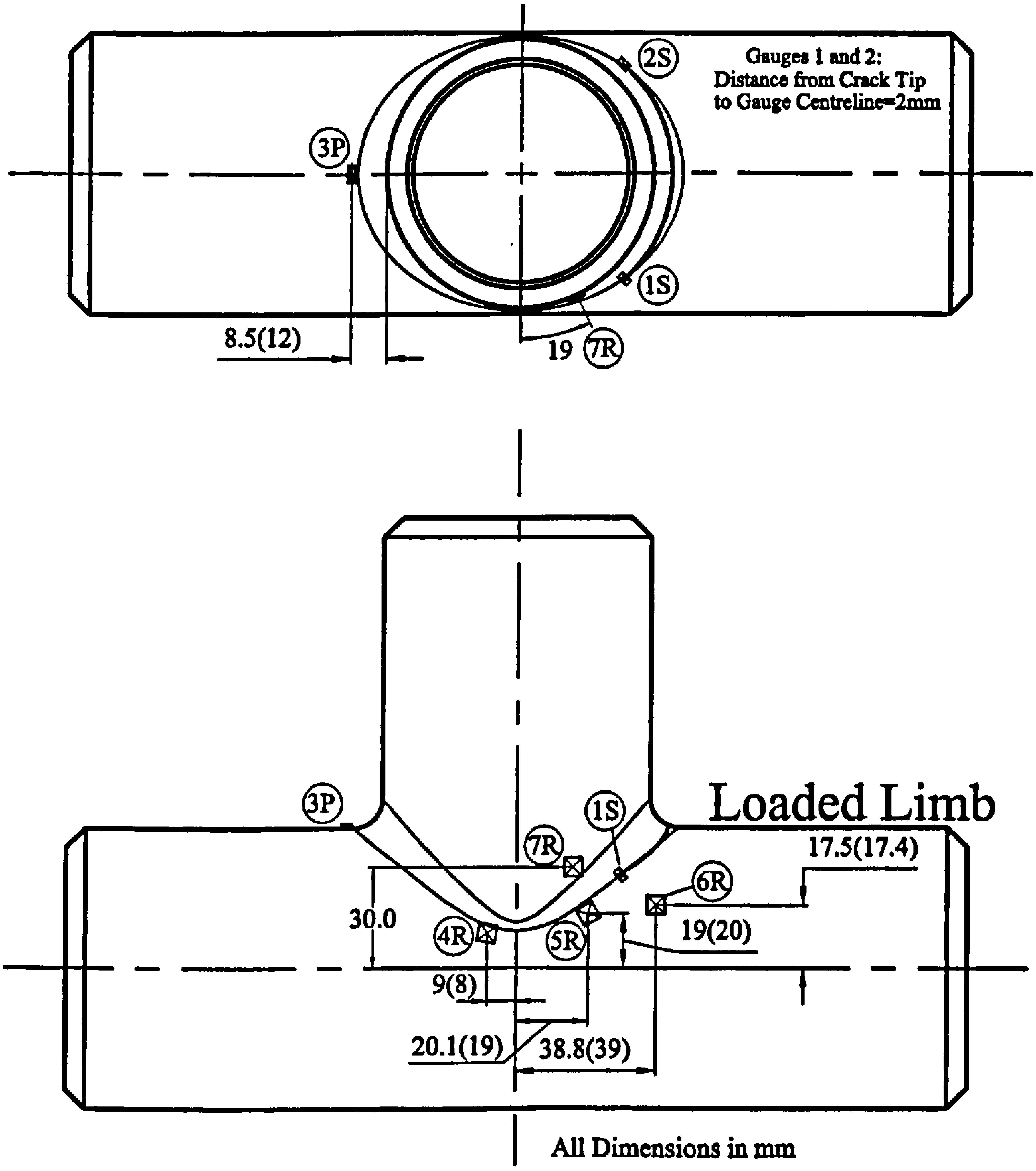

Figure 5.22: Strain Gauge Arrangement for Cracked In-Plane Bending (Part-Penetrating Model Dimensions in Parentheses; S = single gauge, P = gauge pair, R = gauge rosette)

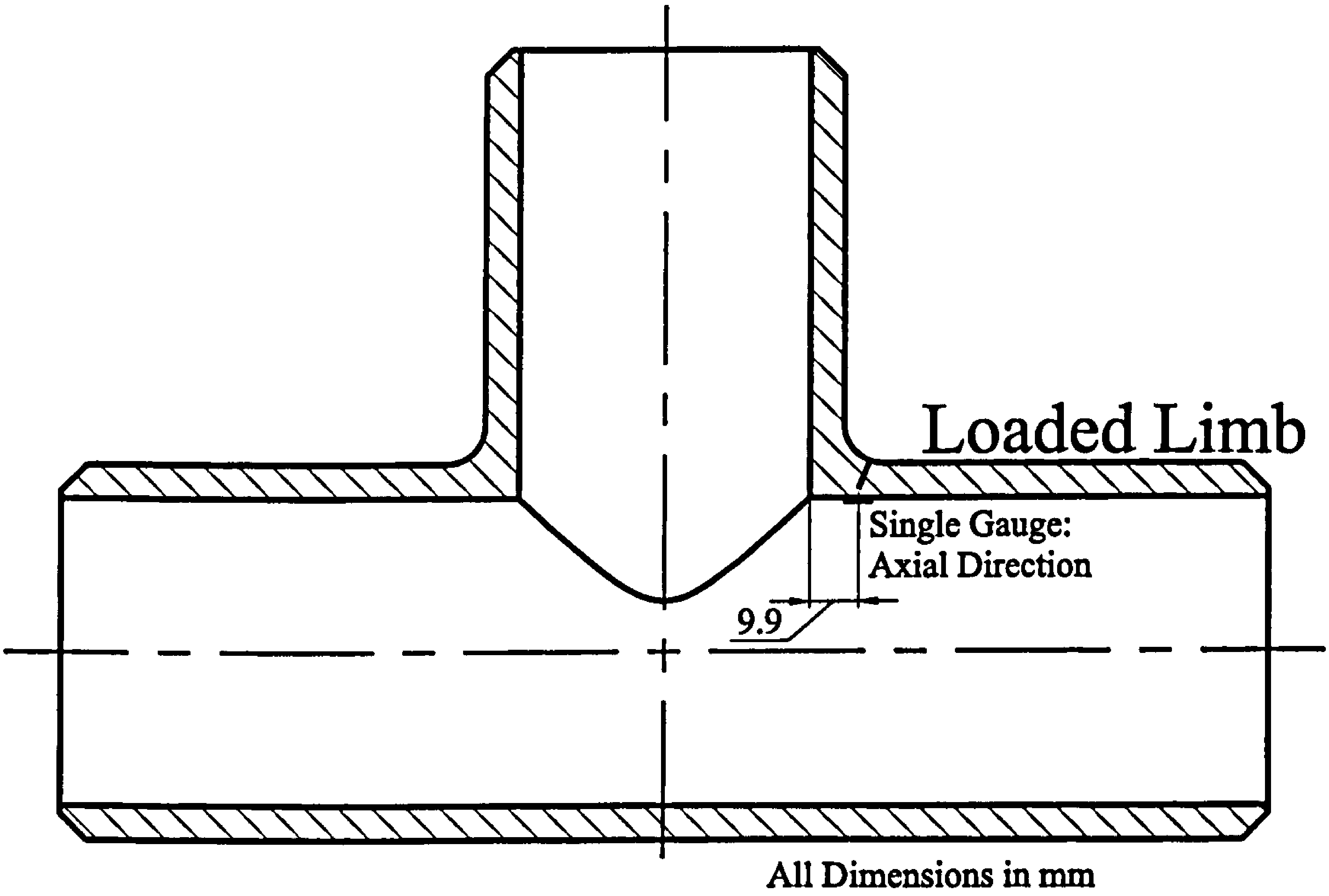

Figure 5.23: Additional Internal Gauge for Part-Penetrating In-Plane Bending

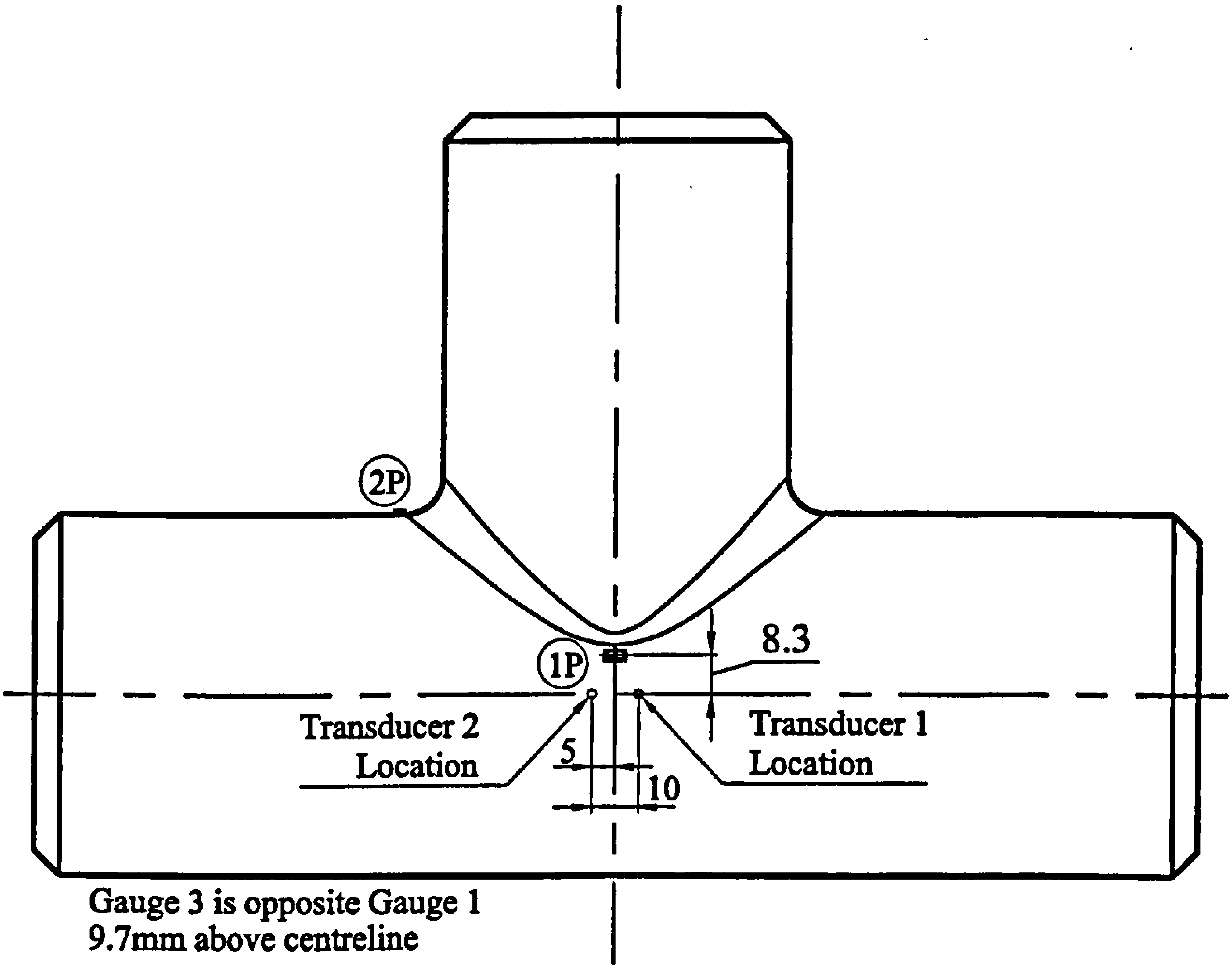

Figure 5.24: Strain Gauge Arrangement for Uncracked Pressure

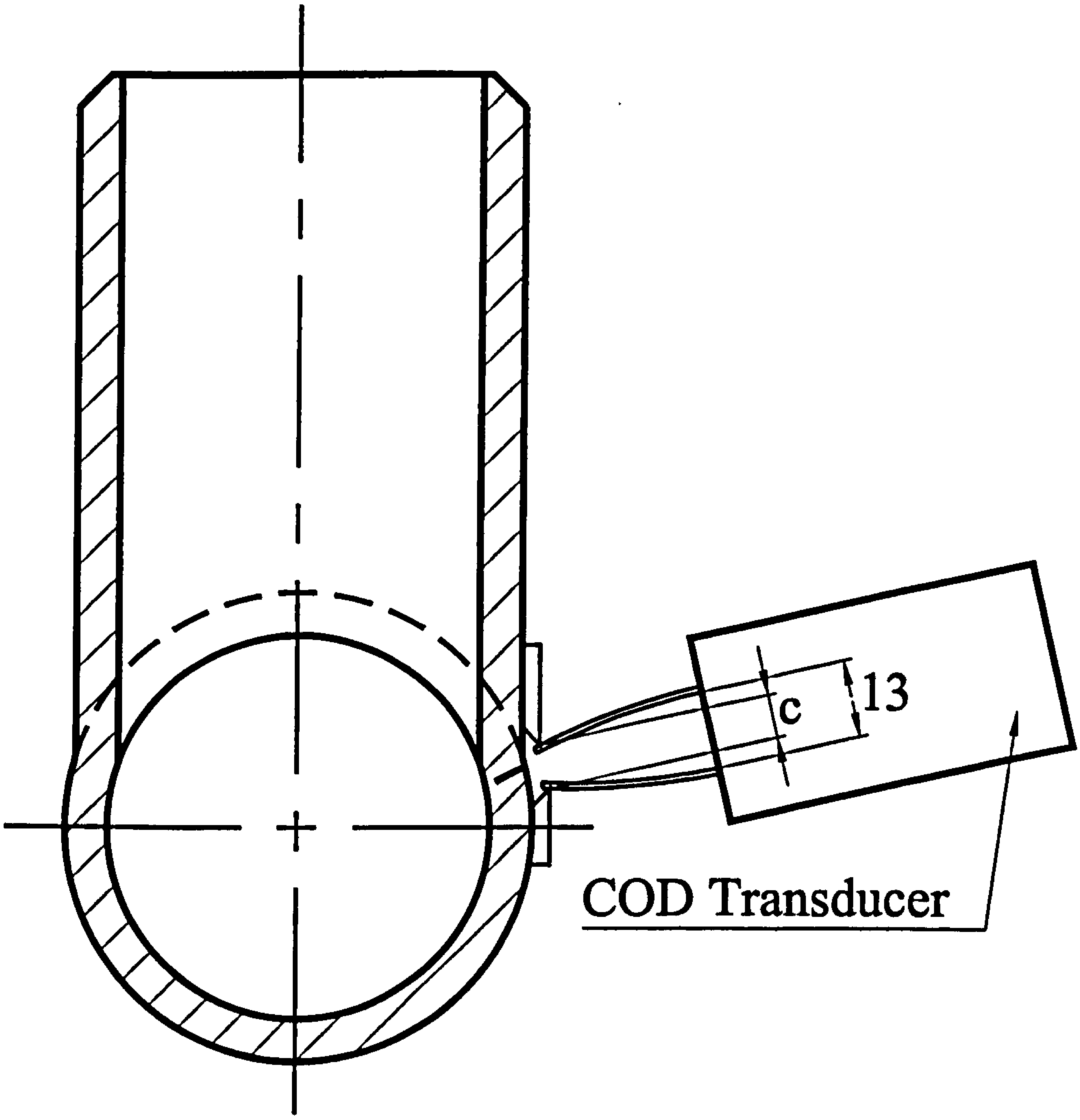

Figure 5.25: COD Transducer for Cracked Pressure Component

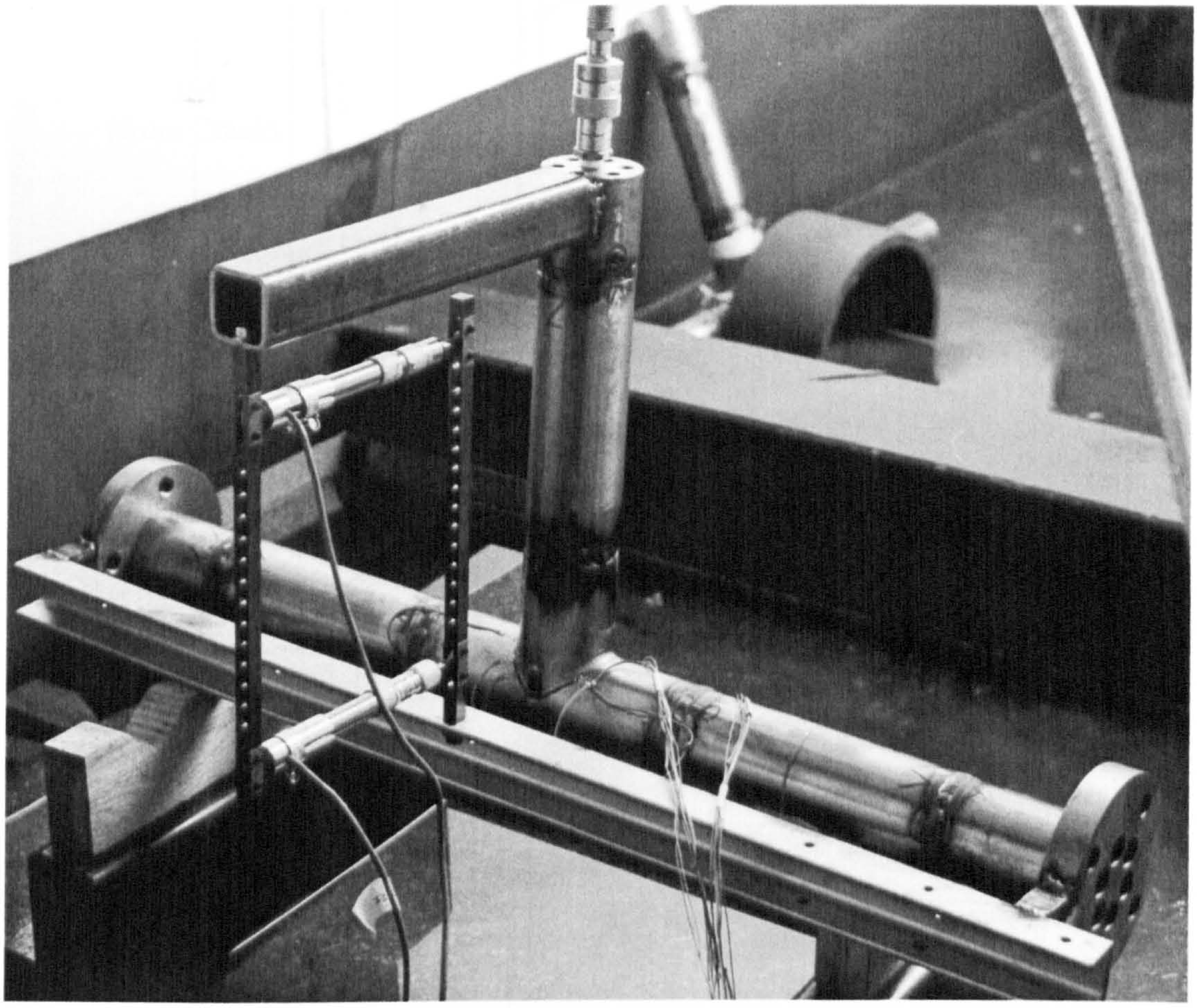

Figure 5.26: Experimental Arrangement for Cracked Pressure Component

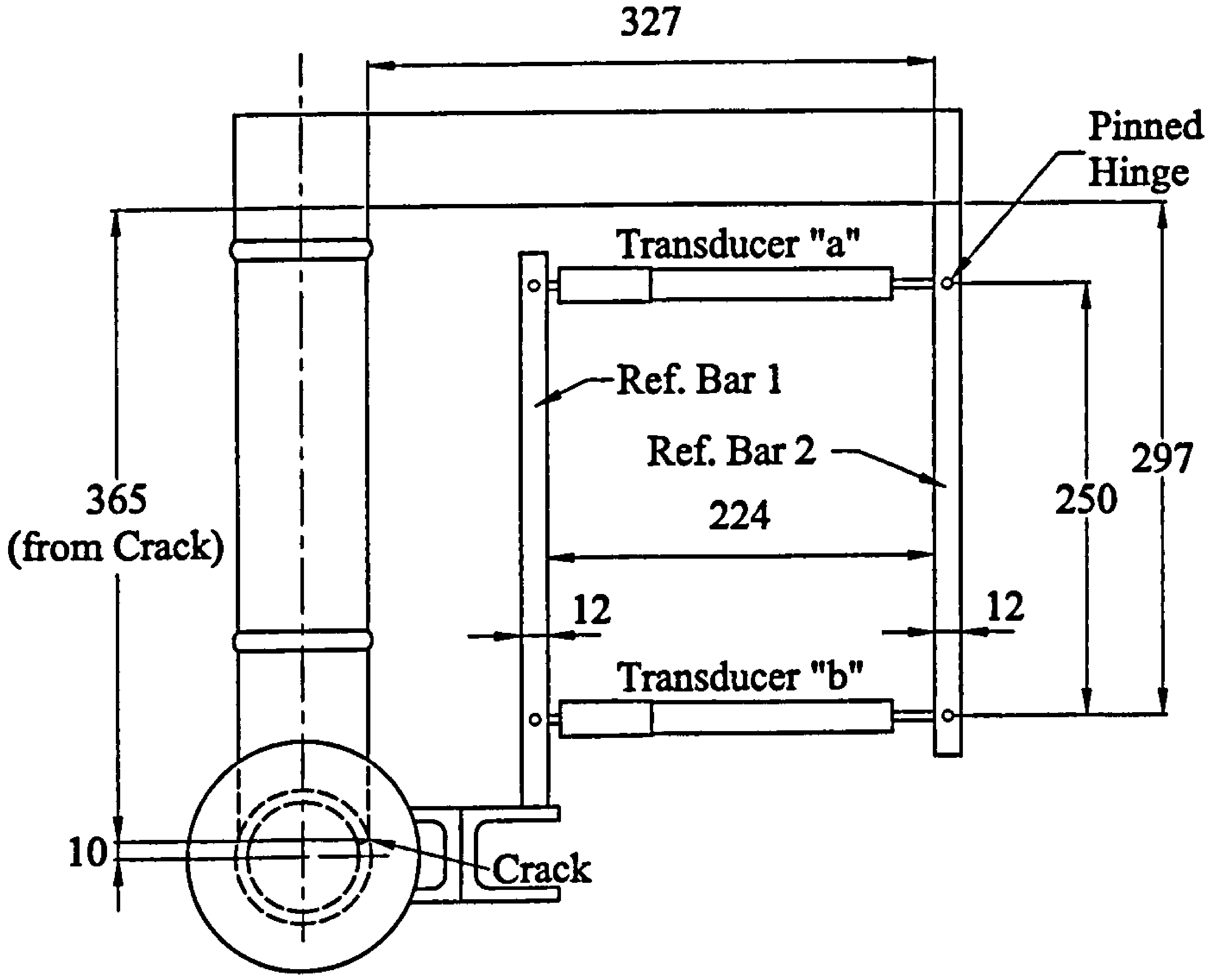

(a) Original Position

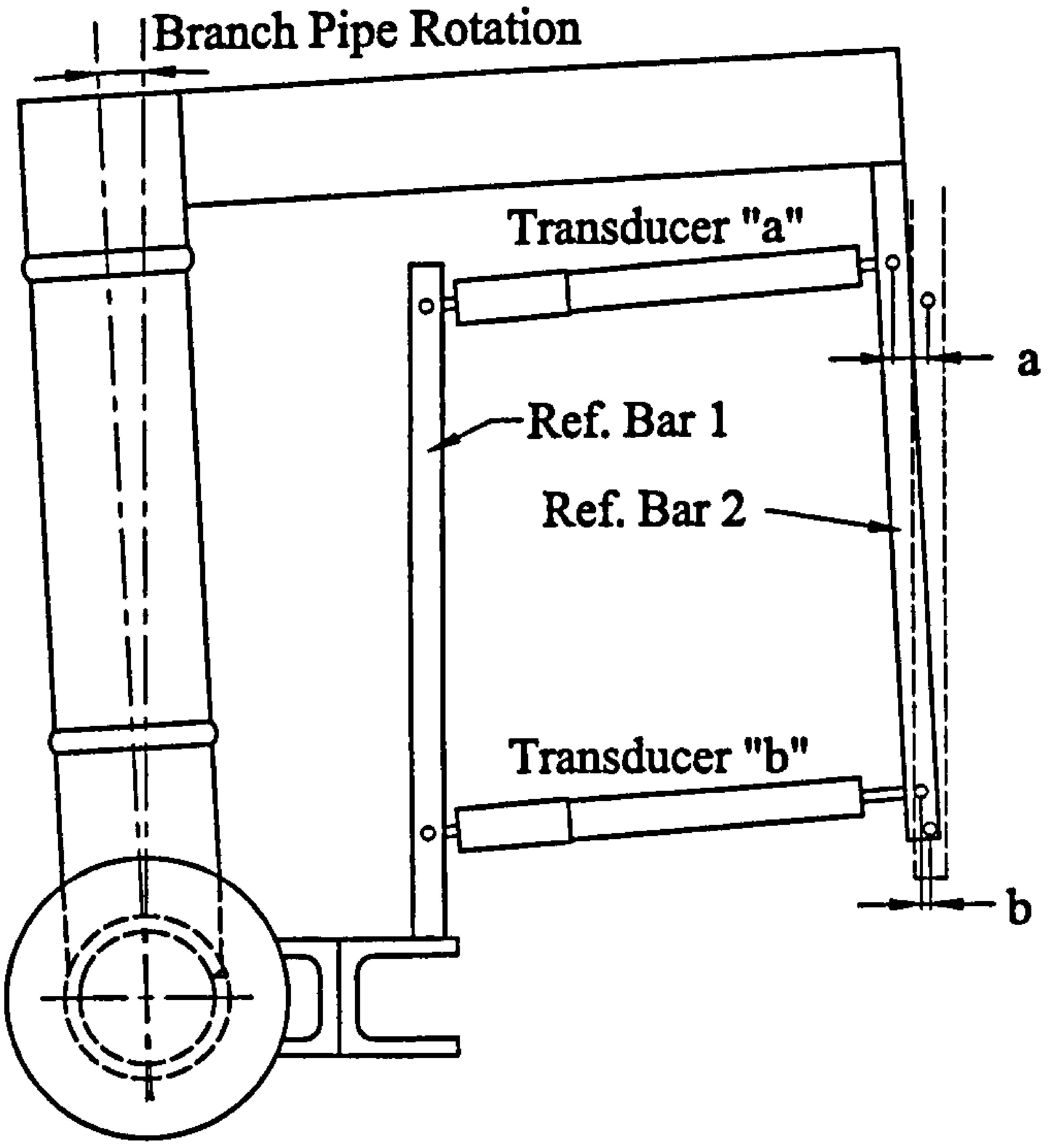

(b) Displaced Position

Figure 5.27: Transducer Arrangement for Cracked Pressure Component

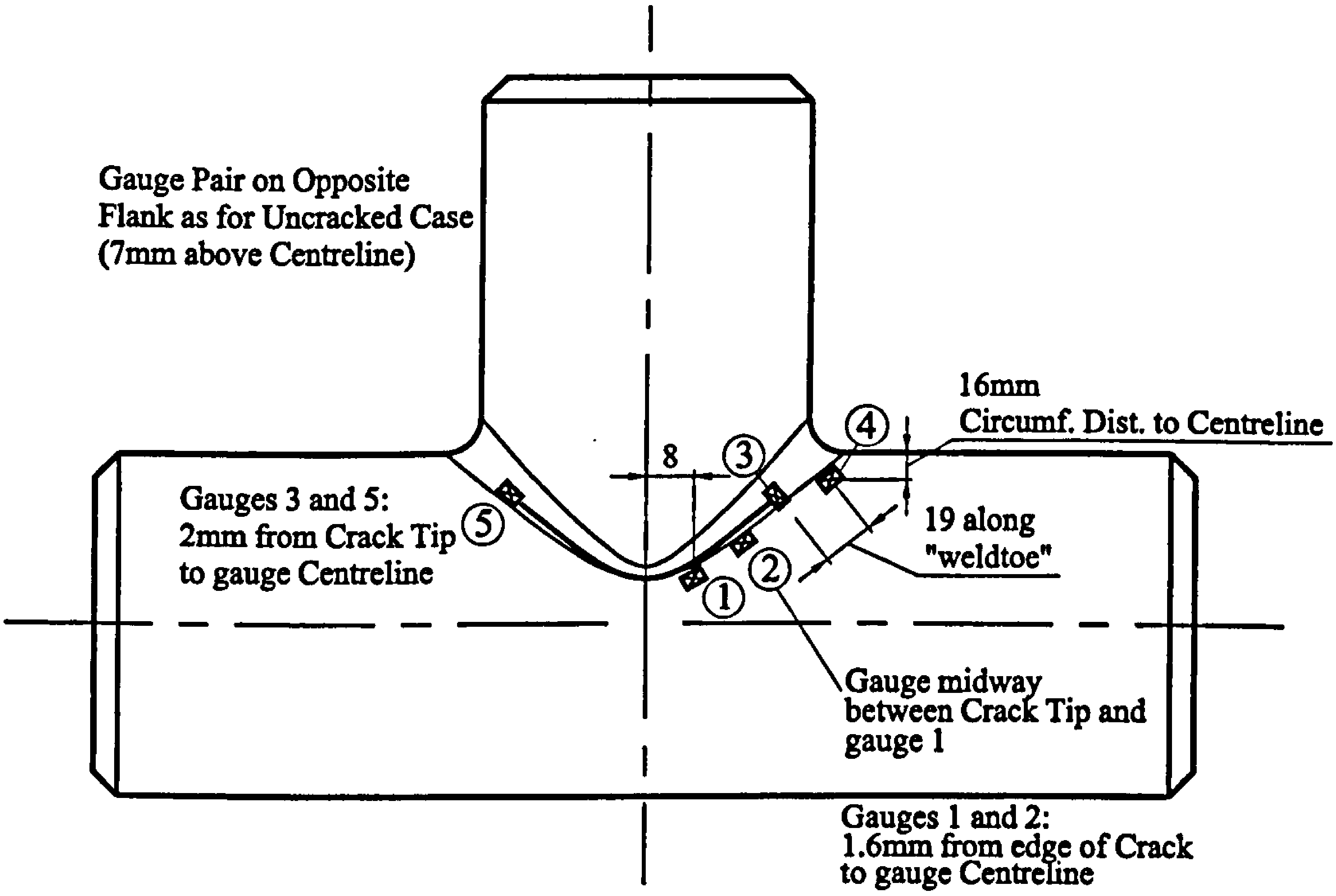

Figure 5.28: Strain Gauge Arrangement for Part-Penetrating Pressure Model

Chapter 6

Experimental Results and Comparison with FE Results

This chapter presents the results from the experimental work described in Chapter 5 and compares them with the corresponding FE results. The FE modelling techniques used for these experimental cases are also described.

6.1 FE Modelling Techniques

The general construction of the FE models was similar to that used for the cracked models described in Chapter 4. However, the geometry of the cracks for these experimental cases was different to the limit load cases, as described previously in Chapter 5. The crack profile was projected in one direction from the outer weld toe, rather than normally to the surface. The material properties have been described in Section 5.3. The true stress-strain curve that was used is shown in Figure 5.17. For all of the experimental models, non-linear geometric changes were also accounted for (i.e. the NLGEOM option was used in ABAQUS [66]). For the in-plane bending case, there were significant differences in the methods of loading, compared with the previous limit load cases.

6.1.1 Loading and Boundary Conditions

In-Plane Bending Models

The experimental setup has been described previously and is shown in Figure 5.19. For the FE limit load cases in Chapter 4, the in-plane bending was applied by means of a pure moment at a master node at the end of the branch pipe. The run pipe was fully clamped at one end, with the other end free, giving the cantilever model (as described by Moffat [7]). However, this pure moment arrangement is difficult to reproduce experimentally and so it was decided that the moment should be applied by the method shown in Figure 5.19. This setup was reproduced for the FE model. The nodes at the end of each of the two loaded limbs were attached to a master node at the centre of the pipe diameter, using rigid beam constraints (this technique was described for the limit load cases in Chapter 4). The appropriate pinned boundary conditions were employed at each of the master nodes, as shown for the deformed model in Figure 6.1. The master node at the end of the run pipe was clamped in the three translational degrees of freedom (DOFs), but the rotational degrees of freedom were unconstrained, so that rotation about the pin axis was possible. The master node at the end of the branch pipe was only clamped in the lateral direction. A displacement was applied in the appropriate direction to the master node at the end of the branch pipe.

A half-model was required for each of the three cases, as all of the models were symmetrical about the '1-3' plane (see Figure 6.1) - a plane of symmetry was specified in the FE model to account for this. The length of each of the limbs, measured from the intersection of the run pipe and branch pipe centre lines, was equal to 500mm. The methodology for calculating the moment at the centre of the junction was the same as for the corresponding experimental case, described previously in Section 5.4.1.

One difference between the experimental and FE arrangements was the absence of the end connections from the FE models. The FE models simply assumed a straight pipe of the same length as these connections. Theoretically, this could effect the deformation response of the junction. To ensure that this was not the case, the uncracked model was altered to include the stiffness of the end connector. The results for the two cases were found to be identical, as shown in Figure 6.2, and hence the inclusion of the end connection stiffness was not required.

Pressurised Models

The setup for the uncracked pressure model was very similar to that of the FE limit load cases in Chapter 3. A quarter model was used for the uncracked case, with symmetry boundary conditions applied to the two planes of symmetry. The branch pipe was fully clamped, with an axial force applied to the end of the run pipe to simulate the closed end condition.

For the cracked case, the boundary conditions were slightly different to the limit load models described in Chapter 4. The branch pipe was fully clamped (as for the uncracked pressure model described above) with an end pressure applied to the end of the run pipe to simulate closed end conditions. The out-of-plane branch pipe rotation was actually measured from the rotation of the end of the run pipe (nominally the same value). A half model was used, with a symmetry face about the centre of the crack length.

6.1.2 FE Model Geometry

Uncracked Models: Effect of Intersection Geometry

Initially, the welded geometry was used for each of the FE models (this was also used in Chapter 5 to derive the electrode profiles). The mesh density used was similar to those used for the limit load cases in Chapter 4. The uncracked models had five elements through the thickness near the intersection of the branch and run pipes. 40 elements were used around the intersection (for a half model). The uncracked, welded FE model is shown in Figure 6.3, and was analysed for both in-plane bending and pressure loading.

After initial comparisons were made between the uncracked FE and experimental results, it was decided that the influence of the extra reinforcement present in the welded FE model (described in Section 5.1.1) should be examined, because the FE results were higher than expected. Firstly, an uncracked model was created from two plain pipes, without any weld reinforcement or smoothing of the intersection between the pipes. This model produced a lower moment and pressure response than the original welded model, especially for in-plane bending, implying that the intersection profile was an important feature.

It was deemed necessary to model the machined junction (as specified in Figure 5.1), with the radius of the machine tool as a basis for the intersection profile. This machined junction geometry was produced and an uncracked model was created, as shown in Figure 6.4. The mesh density was similar to that of the welded junction described previously, but with 48 elements around the (half model) circumference at the intersection. The FE results for the three uncracked cases are shown in Figures 6.5(a) and (b), for in-plane bending and pressure respectively. For both in-plane bending and pressure, the machined model loads were lower than for the original welded model. For in-plane bending, the 'no-weld' model gave significantly lower moments than the machined model, but for pressure the 'no-weld' model was very close to the machined model.

The machined model was subsequently used for all cases, in order to remove one of the potential sources of variation between the FE analysis and the experiments.

Cracked Models

FE models for the three cracked cases were derived from the machined geometry. The crack locations were modelled in the identical locations as for the welded model, as this was the geometry used to position the cracks in Chapter 5. This requirement created difficulties with the construction of the models, particularly for the in-plane bending models, as the crack no longer ran along the weld toe but actually overlapped onto the curvature created by the tool radius between the run and branch pipes. This is shown in Figure 6.6 at the crotch of the junction for the in-plane bending, part-penetrating crack. The ligament thickness, alteration of which could significantly affect the load capacity of the junction, was kept constant and the crack depth was extended to account for the change in geometry. This change in depth reduced away from the crotch of the junction. For the cracked pressure case the crack profile only overlapped slightly onto the curved intersection and was therefore assumed to lie on the run pipe with the curvature adjusted slightly to accommodate this.

Significant modifications were required in PATRAN to model the cracks for the machined geometry. The cracked models all had a much finer mesh around the intersection than the uncracked model. The FE models with part-penetrating cracks are shown in Figure 6.7 and Figure 6.8 for in-plane bending and pressure loading respectively. (For in-plane bending, the through wall crack model used the same mesh as the part-penetrating case, but with additional nodes released). The technique for mesh construction for the cracks in these models was identical to that described previously in Chapter 4.

The cracked models had a total of eight elements through the thickness at the intersection. These were not distributed evenly: there were 6 elements through the lower half of the junction thickness and two through the upper half. This was done to ensure that the mesh through the crack ligament was adequate (this was shown to be important for cracked cylinders in tension in Chapter 2) and this mesh arrangement gave three elements through the ligament for a/t=0.75. The mesh density for these models was higher than for the original welded models as the intersection region between the branch and run pipes was smaller. In order to achieve a reasonable element aspect ratio more elements were required around the intersection: for the cracked in-plane bending models, 64 elements were used (for a half model) and for the cracked pressure model 56 elements were used.

These machined models were the basis for the all of the subsequent FE results, and were used for the comparisons with the experimental results (Section 6.2).

6.1.3 Techniques for comparing FE Results

Displacement Results

The techniques for comparing the FE results with the experimental data were straightforward. The FE models were loaded in the same way, with the same boundary conditions. Hence, the same measurements were taken as for the experiments. The displacements of the relevant nodes were used to obtain the displacement parameters.

The only exception to the above was for the comparison with the Crack Opening Displacement (COD) Transducer (described in Chapter 5). The COD transducer was located on two mounts (for example, see Figure 5.21) and had a minimum opening of approximately 7mm. This setup meant that the displacement at the crack opening was not the parameter recorded, rather the distance between two mounts near to the crack. For the FE models, the opening of the centre of the crack at the surface was initially examined. Although this gave reasonable results it was decided to postulate the positions of the mount tips, and hence calculate the distance between them, in order to give a more correct comparison with the experimental data.

The method for assessing the positions of the mount tips involved the identification of two nodes at the mount locations in each FE model. The technique is shown schematically in Figure 6.9 for in-plane bending. During the analysis, the position of each pair of nodes, and the gradients between them, were used to calculate the new position of the mounts' tips. The 'position nodes' were used to calculate the global position of each mount. The 'guide nodes' were used to calculate the slope of the mount and thus, the angular position of each mount tip. A simple calculation of the distance increase between these two mount tip positions resulted in the COD parameter. In Figure 6.9 the initial distance between the two mount tips is marked 'c', with the additional COD parameter defined for the displaced case. The previously calculated opening at the centre of the crack is marked CFOD (crack face opening displacement). This technique was used for each of the cracked cases. The COD and CFOD results will be presented in Section 6.2.

Strain Results

The strain results (calculated at the integration points of elements) were extrapolated and averaged at the nodes on the surface (an output option in ABAQUS), enabling direct comparison with the strain gauge data. For each of the gauge positions, the FE values of strain were taken from the node nearest to the actual gauge location.

For the single-element gauges and the gauge pairs, the strain results were compared with the strain in the appropriate direction in the FE model.

The strains from the three-element gauge rosettes were converted into principal strains. This experimental maximum principal strain was then compared with the maximum principal strain from the FE model, at each rosette location.

Twice Elastic Slope Method

The merits and inadequacies of the twice-elastic-slope method for evaluating plastic loads were discussed in Chapter 1. The major drawback was the difference that the elastic portion of a component could make to the resulting plastic load. However, it is legitimate to use the method for comparison here, as the limb length for each model was nominally identical and the primary function of the experiments was to ensure the modelling techniques for the FE limit load models were adequate.

Hence, the twice-elastic-slope has been used to compare the plastic loads for a variety of the parameters in Section 6.2. This enables evaluation of the deformation parameters for each model, and also allows the effect of the cracks on the strength of the components to be assessed.

6.2 Results and Discussion

The primary results of interest for each case were the global moment-deformation or pressure-deformation response for the various deformation parameters measured. These are presented for each test, alongside the corresponding FE results. The plastic load was determined, for suitable parameters, using the twice-elastic-slope method (M_{TES} or P_{TES}, for moment and pressure respectively). In addition, a limit load analysis has been performed for each model, so that comparisons between limit load and plastic loads can be made. A yield stress of 238N/mm^2 was used for the elastic/perfectly-plastic material.

The strain results were of secondary interest. The main purpose of the strain gauge data was to gain a better understanding of the behaviour of each structure and also to verify that the FE models were suitable. For some of the strain gauges, there is a case for using the data to derive a 'local' plastic load.

The resulting plastic and limit loads are summarised in Table 6.1 and Table 6.2, for in-plane bending and pressure loading respectively.

6.2.1 In-Plane Bending: Uncracked

Displacement Results

The moment versus crosshead displacement results are shown in Figure 6.10(a). It is clear that the comparison between the FE and experimental results was fairly good, with the FE giving slightly higher moment values. Experimentally, M_{TES} was equal to 6.42kNm, with the FE M_{TES} value just 5.1% higher (6.75kNm). The experimental plastic moment was 5.6% lower than the limit moment of 6.78kNm.

The diametral growth comparison is shown in Figure 6.10(b). The comparison was again good, the only significant difference being the positive displacement at low moment levels for the experimental case. This effect was also observed for the cracked cases (see Sections 6.2.2 and 6.2.3). The general sensitivity of the transducer to small displacements was good, as shown by the smooth response in Figure 6.10(b).

Strain Results

For this test, the hoop and axial strain distributions were plotted around the crotch region of the intersection (between the loaded limbs) using the FE strain data, for four different moment levels. The experimental strain gauge data from gauge numbers 1-4 (see Figure 5.20) was then plotted against this data. The distributions are shown in Figures 6.10(c) and 6.10(d), for axial and hoop strain respectively. The maximum moment level of 5.13 kNm was chosen with reference to Figure 6.10(a), so that the difference between the FE and experimental global response was not too great.

The FE data compared exceptionally well with the strain gauge results, for both hoop and axial strains, confirming the peak strain locations. This area of the junction was clearly dominated by axial strain, as expected.

6.2.2 In-Plane Bending: Part-Penetrating Crack (a/t=0.75)

Displacement Results

The moment-displacement curves are shown in Figure 6.11(a). The FE data compared well with the experimental results. Experimentally, M_{TES} was 5.68kNm, just 1.4% lower than the FE value of 5.76kNm, and 0.4% lower than the limit moment of 5.66kNm. The curves diverged only slightly with increasing crosshead displacement, until crack propagation started. Crack propagation was first observed at approximately 32mm displacement (marked in Figure 6.11(a)) and the moment level began to drop immediately after this as the crack increased in size. Propagation began at the bottom of the crack, at the midpoint of its length. The crack proceeded to grow through the ligament, breaking completely through the thickness after 41mm displacement. The crack simultaneously extended along the length of the ligament, basically becoming a through-wall crack, and then continued to extend in length around the intersection area. The final condition of the junction, after 84mm crosshead displacement, is shown in Figure 6.11(b).

The FE model did not include any consideration for crack propagation, and hence the FE data was not useful after 32mm displacement. However, this was well beyond the plastic moment level, which was the main parameter of interest.

The moment-diametral displacement results are shown in Figure 6.11(c). As for the uncracked test, there was initially some positive displacement experimentally, followed by a return to the expected negative displacement i.e. reduction in diameter. The FE displacement values were always negative, and agreed fairly well with the experimental results at higher displacements.

The COD results are compared in Figure 6.11(d). The CFOD response is shown to illustrate the difference between the techniques described in Section 6.1.3, and is clearly higher than the COD response. The TES values were taken for COD and experimental values only. The FE and experimental values of M_{TES} were close, at 4.81kNm and 4.72 kNm respectively: a difference of just 1.9%.

Strain Results

The COD results should be considered alongside the ligament strain results, shown in Figure 6.11(e), as both of these measurements refer to the behaviour of the crack ligament. Experimentally the ligament strain appeared to relax at around 1.7kNm. There was no obvious reason for this and it can only be assumed that it was a genuine measurement. This relaxation caused the M_{TES} value obtained to be greater than expected (5.36kNm), as the elastic slope was taken prior to this relaxation. For the FE analysis, no corresponding relaxation was found, so the M_{TES} value was 6.9% lower than the experimental value, at 4.99kNm. Considering the ligament strain response alongside the overall moment-displacement response (Figure 6.11(a)), the ligament strain response reversed in direction near the moment level at which crack propagation was first observed. Gauge failure occurred soon after, at a relatively low strain of around -5000 microstrain. It is uncertain if this reversal in strain direction was simply the gauge de-bonding from the surface of the component, or if it was a real effect, although the latter seems quite feasible.

The crack tip strains, shown in Figure 6.11(f) were also considered a possible source for a local plastic load value. As expected, the strains were greatest perpendicular to the crack faces, while the strains parallel to the crack faces were negligible in comparison. Assessing M_{TES} for the perpendicular strains, the FE value of 3.35kNm was 14.7% higher than the experimental value of 2.92kNm. Considering the high strain gradients around a crack tip, and that the gauge measured strain along the gauge length and not at a single point as was assumed, the comparison is good.

The remaining strain results are shown in Figures 6.11(g)-(j). The comparison between the FE and experimental results was good, in general, for these gauges.

6.2.3 In-Plane Bending: Through-Wall Crack (a/t=1.0)

Displacement Results

The moment-displacement curves for this case are shown in Figure 6.12(a). The comparison between the FE and experimental data was good, with the experimental value of M_{TES} equal to 4.42kNm, just 3.8% lower than the FE value of 4.59kNm. The experimental M_{TES} value was 6.1% lower than the limit load of 4.69kNm.

Crack propagation was initially observed at a crosshead displacement of 35mm, from just one end of the crack. Unlike the part-penetrating case, this initial propagation did not have a great effect on the moment-displacement response until the crack had extended by around 4mm, at a crosshead displacement of 50mm. At this point, propagation was also observed at the opposite end of the crack, measuring 1mm in length. The moment level began to fall after this, with both ends of the crack quickly extending in length around the intersection. The final condition of the junction, after 95mm crosshead displacement, is shown in Figure 6.12(b).

The moment-diametral displacement results are shown in Figure 6.12(c). The behaviour of this junction was very similar to that of the other bending tests described. Experimentally, there was some initial diametral growth, followed by the diametral reduction predicted by the FE analysis. Neglecting this initial discrepancy, the comparison between the FE and experimental results was again good.

The COD results are presented in Figure 6.12(d). The results are very similar in behaviour to the part-penetrating results. However, the difference between the FE and experimental M_{TES} values was greater for this case. Experimentally, M_{TES} was 3.61kNm and the FE value was 3.98kNm: a difference of 10.2%.

As the crosshead displacement increased for this model, there was some overlapping of the crack faces (a combination of 'Mode 1' and 'Mode 3' crack opening), as shown in Figure 6.12(e) for the FE model. This was not as significant for the other cracked cases because the ligament tended to constrain the crack to 'Mode 1' type opening.

Strain Results

The crack tip strains are presented in Figure 6.12(f). Generally the comparison between FE and experimental results was good, with the FE correctly predicting the trends of the experimental strains. However, the M_{TES} values for the strains perpendicular to the crack faces did not compare well. The FE value of 1.88kNm was nearly double the experimental result of 0.95kNm. One difficulty involved with evaluating M_{TES} using strains in a peak location, such as a crack tip, is the initial determination of the elastic slope. Figure 6.12(f) illustrates this point, with no apparent linear region for the experimental strain. In fact, the FE elastic slope was used, which may have led to the large difference in M_{TES} values.

The remaining strain results are shown in Figure 6.12(g)-(k). In general the comparison of the FE data with the strain gauge results was good.

6.2.4 Summary of Bending Cases

The moment-displacement responses for all three bending cases are shown in Figures 6.13(a) and 6.13(b), for experimental and FE results respectively. Experimentally, it was clear that the part-penetrating case approached the through-wall cracked case as crack propagation progressed through the ligament.

Evaluation of the effect of a crack on a junction's plastic load was carried out by comparing the various M_{TES} values. All of the M_{TES} values have been normalised to the respective experimental or FE uncracked junction value (obtained using the moment-displacement response) and plotted against a/t. The results are shown in Figure 6.14. M_{TES} values obtained using crosshead displacement and COD exhibited good comparisons between the experimental and FE results, and would be suitable measures for global and local plastic loads respectively. In addition, the reduction for the limit load results was very similar to that of the plastic load results.

The ligament strain comparison was not as good, for the reasons discussed in Section 6.2.2. However, this parameter is worth considering for plastic load analysis, as it gives a reliable indication of ligament collapse. A maximum allowable strain level could be set for the ligament, above which the structure could be said to have reached the local plastic load.

The M_{TES} values from the crack tip strains gave very large reductions in plastic load for the through-wall crack, particularly for the experimental results. The comparison between the experimental and FE values was reasonable, considering the high strain gradients around the crack tips. The crack tip strain is not thought to be a meaningful parameter to use for local plastic load evaluation.

6.2.5 Pressure: Uncracked

Displacement Results

The pressure was plotted against the diametral displacement (from one of the two transducers used: the results from the transducers were virtually identical and so only one set has been presented) as shown in Figure 6.15(a). The comparison between the experimental and FE results was fair, with the experimental P_{TES} value of 32.8MPa 9.1% lower than the value predicted by FE analysis of 35.8MPa. Both the FE and experimental P_{TES} values were lower than the limit pressure of 37.5MPa. The junction did not reach its ultimate collapse load as the pump used had insufficient capacity available.

Strain Results

The strain values for this test compared reasonably well. The strain response for gauge-pair 2, located at the outer crotch, is shown in Figure 6.15(b). At pressure greater than 25MPa comparison of the magnitudes of the strain was disappointing. However, the trends of the strains were correctly identified, with the reversal of the strain in the axial direction apparent. The strain at this location was hoop dominated as expected.

The flank strain values are shown in Figures 6.15(c) and 6.15(d), for gauge-pairs 1 and 3 respectively. Again, the comparisons were not remarkable but the trends exhibited by the strain gauge data were as predicted.

6.2.6 Pressure: Part-Penetrating Crack (a/t=0.75)

Displacement Results

The response of the cracked pressurised junction is shown in Figure 6.16(a). The junction failed when leakage occurred through the crack ligament at a pressure of 38.7MPa. The P_{TES} values are illustrated in Figure 6.16(b). The general comparison of the experimental and FE data appeared disappointing, although the difference between the experimental P_{TES} value of 24.0MPa and the FE value of 26.2MPa was 9.2%: only slightly greater than for the uncracked junction. The experimental rotation did not register any reading until 8MPa, indicating a lack of sensitivity of the measuring setup to very small rotations. The elastic slope for the experimental case was therefore extrapolated from the initial positive rotation data (i.e. above 8MPa), as marked in Figure 6.16(b). The final deformation of the junction is shown in Figure 6.16(c), illustrating the crack opening.

The pressure-COD response is shown in Figure 6.16(d). As for the in-plane bending results, the COD method (described in Section 6.1.3) provided an improved comparison with the experimental results. The comparison between the experimental and FE (using COD) P_{TES} values was excellent, with the FE result of 27.3MPa just 2.2% higher than the experimental value of 26.7MPa.

Strain Results

The crack tip strain response is illustrated in Figure 6.16(e). As for the in-plane bending junctions, the strain perpendicular to the crack faces was the higher of the two directions measured (although the strains parallel to the crack faces were also high for this case) and was assessed for P_{TES}. Experimentally, P_{TES} was 20.4MPa, just 0.5% lower than the FE value of 20.5MPa. The typical plastic strain around the crack is displayed in Figure 6.16(f), for equivalent plastic strain (PEEQ variable in ABAQUS). The main plasticity spread around the run pipe side of the crack rather than the branch pipe side.

The remaining strain values are shown in Figures 6.16(g) and (h), and show the predicted FE strains to be reasonably accurate.

6.2.7 Summary of Pressure Cases

The various P_{TES} values were normalised with respect to the respective FE or experimental uncracked result. These normalised values have been plotted against a/t, as shown in Figure 6.17. The reduction in plastic load for the cracked model was almost identical for the FE and experimental global results (i.e. using diametral growth and branch pipe rotation). Examining the P_{TES} results for the COD value, the experimental value was actually higher than the global response, while the FE value was equal to it, implying that COD cannot be used as a local plastic load indicator for this case. The P_{TES} values from the crack tip strains were both lower than the global plastic load and could be used to provide a local plastic load.

6.3 Concluding Remarks

The comparison between the FE and experimental results was good, in general. The global plastic loads obtained from the experimental results were always within 9.2% of the FE predicted plastic loads. The agreement was particularly good for the bending cases which were all within 5.1%.

For local plastic loads, the COD gave useful results for the bending tests, but not for the pressurised crack test. The ligament strain is also shown to be a useful guide to ligament collapse for part-penetrating cracks. The crack tip strain results for in-plane bending did not appear suitable, but gave good agreement for the pressure case.

The primary objective of the experimental work was to instill confidence in the existing limit load results of Chapter 4 by studying experimental cases and using the same FE modelling techniques to simulate them. This objective has been fulfilled.

Table 6.1: Plastic Moment and Limit Moment Results

a/t	0			0.75			1.0		
M_{TES} Parameter	Exp. [kNm]	FE [kNm]	%	Exp. [kNm]	FE [kNm]	%	Exp. [kNm]	FE [kNm]	%
Displacement	6.42	6.75	5.1	5.68	5.76	1.4	4.42	4.59	3.8
COD				4.72	4.81	1.9	3.61	3.98	10.2
Crack Tip Strain				2.92	3.35	14.7	0.95	1.88	97.9
Ligament Strain				5.36	4.99	-6.9			
Limit Moment [kNm]	6.78			5.66			4.69		

Table 6.2: Plastic Pressure and Limit Pressure Results

a/t	0			0.75		
P_{TES} Parameter	Exp. [MPa]	FE [MPa]	%	Exp. [MPa]	FE [MPa]	%
Displacement/Rotation	32.8	35.8	9.1	24.0	26.2	9.2
COD				26.7	27.4	2.2
Crack Tip Strain				20.4	20.5	0.5
Limit Pressure [MPa]	37.5			30.5		

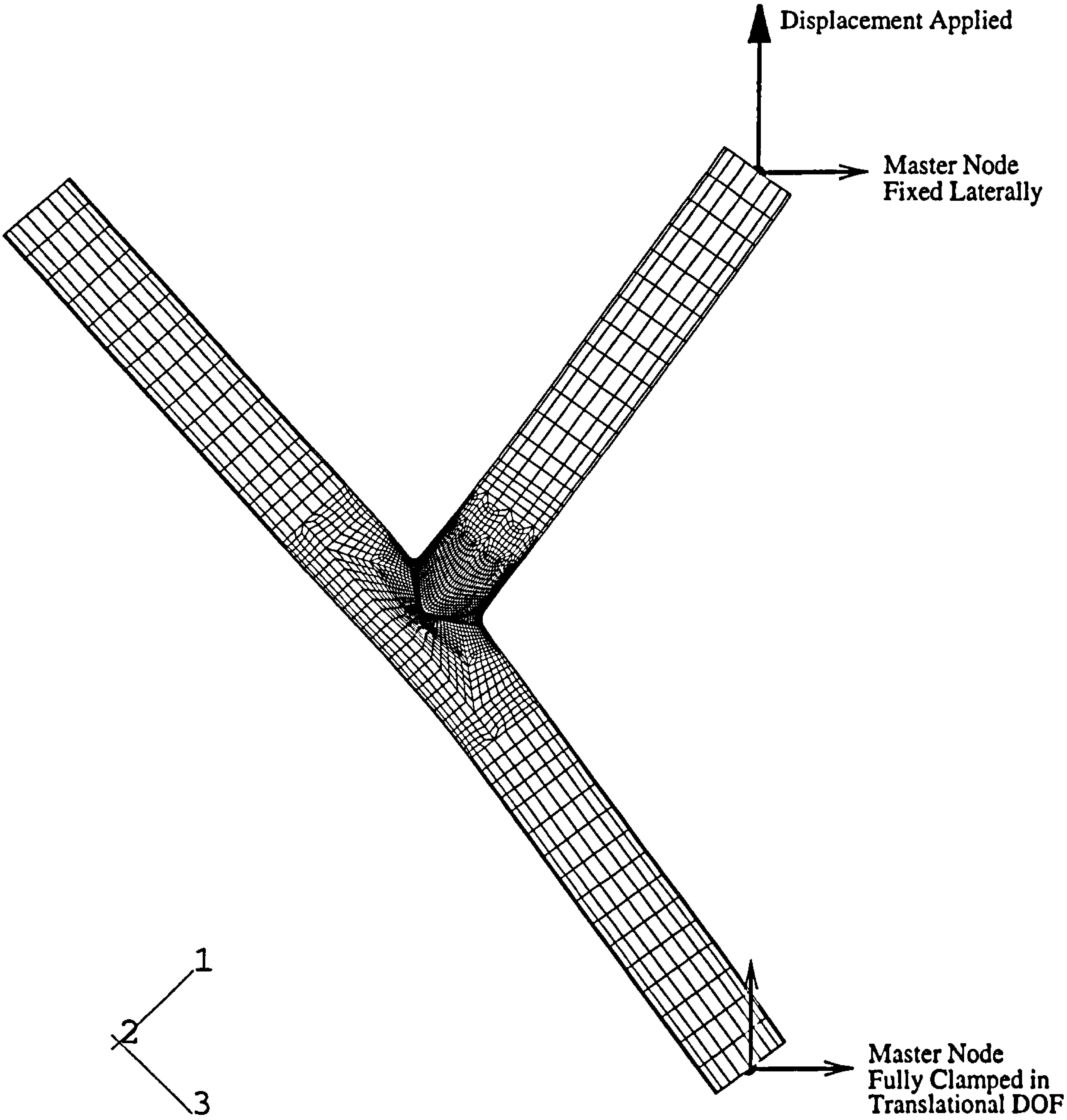

Figure 6.1: Deformed FE Model for Uncracked In-Plane Bending

(Crosshead Displacement = 65.5mm)

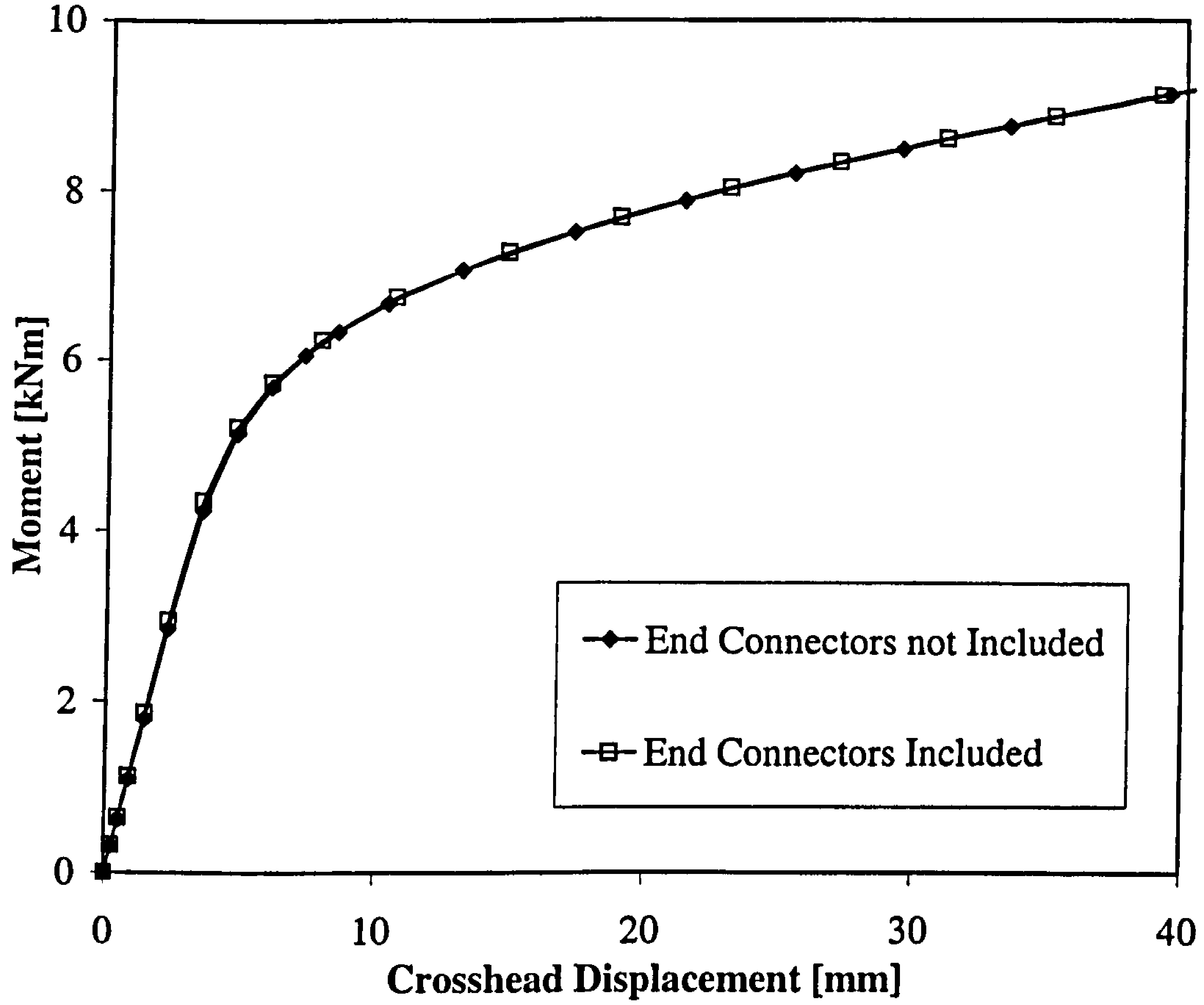

Figure 6.2: Effect of Including Rigid End Connectors for Uncracked In-Plane Bending

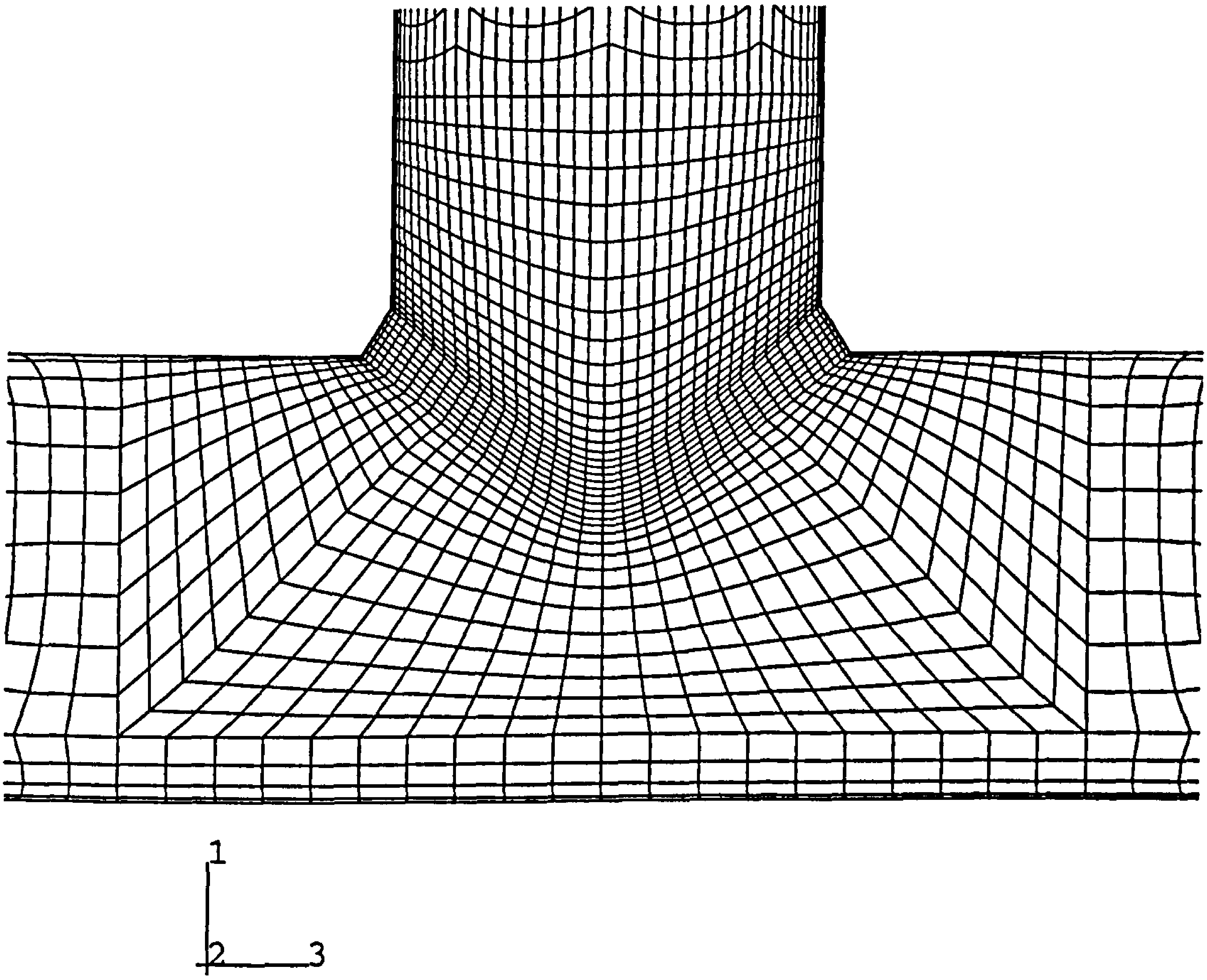

Figure 6.3: Uncracked FE Mesh for Welded Geometry

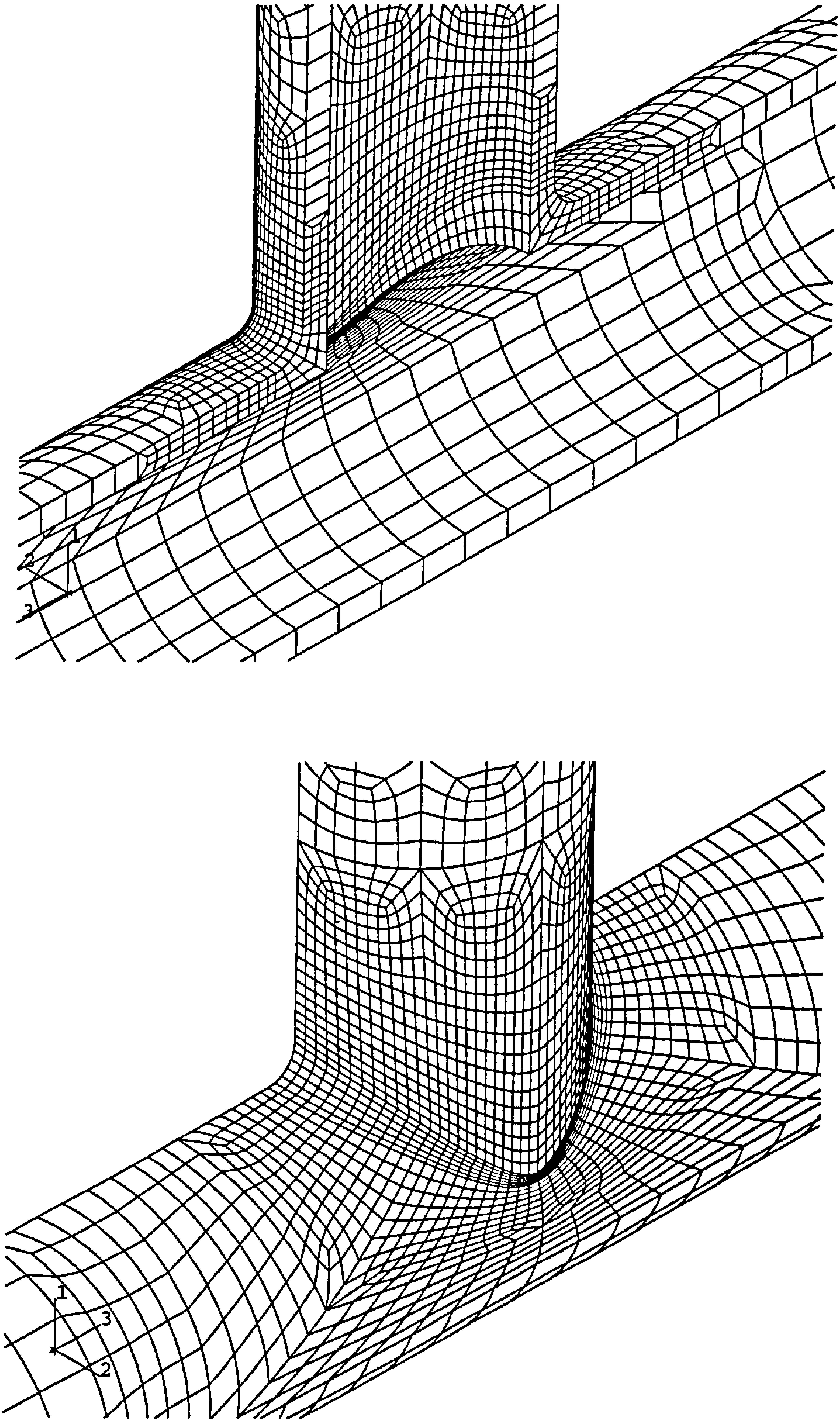

Figure 6.4: Uncracked FE Model for Machined Geometry

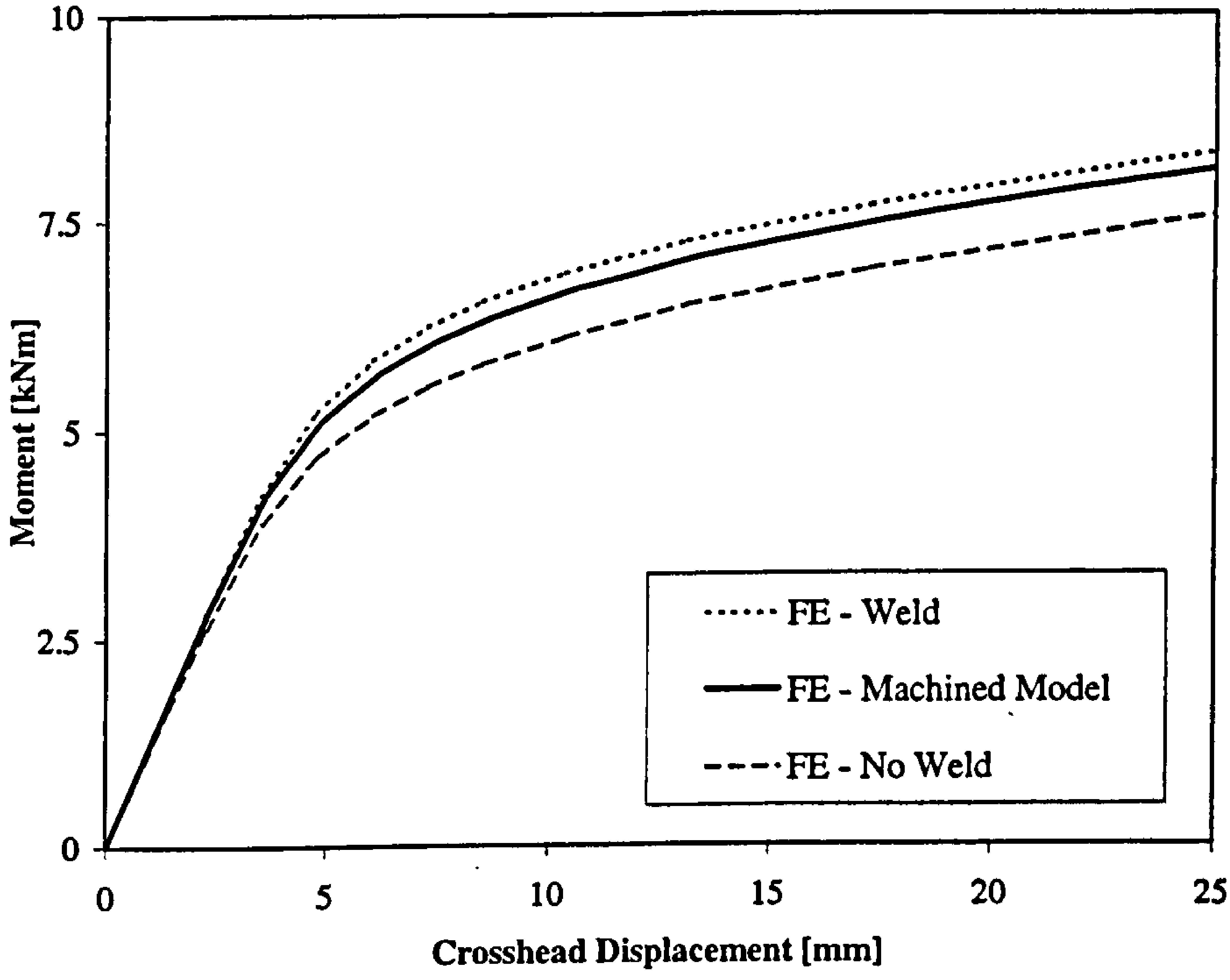

(a)

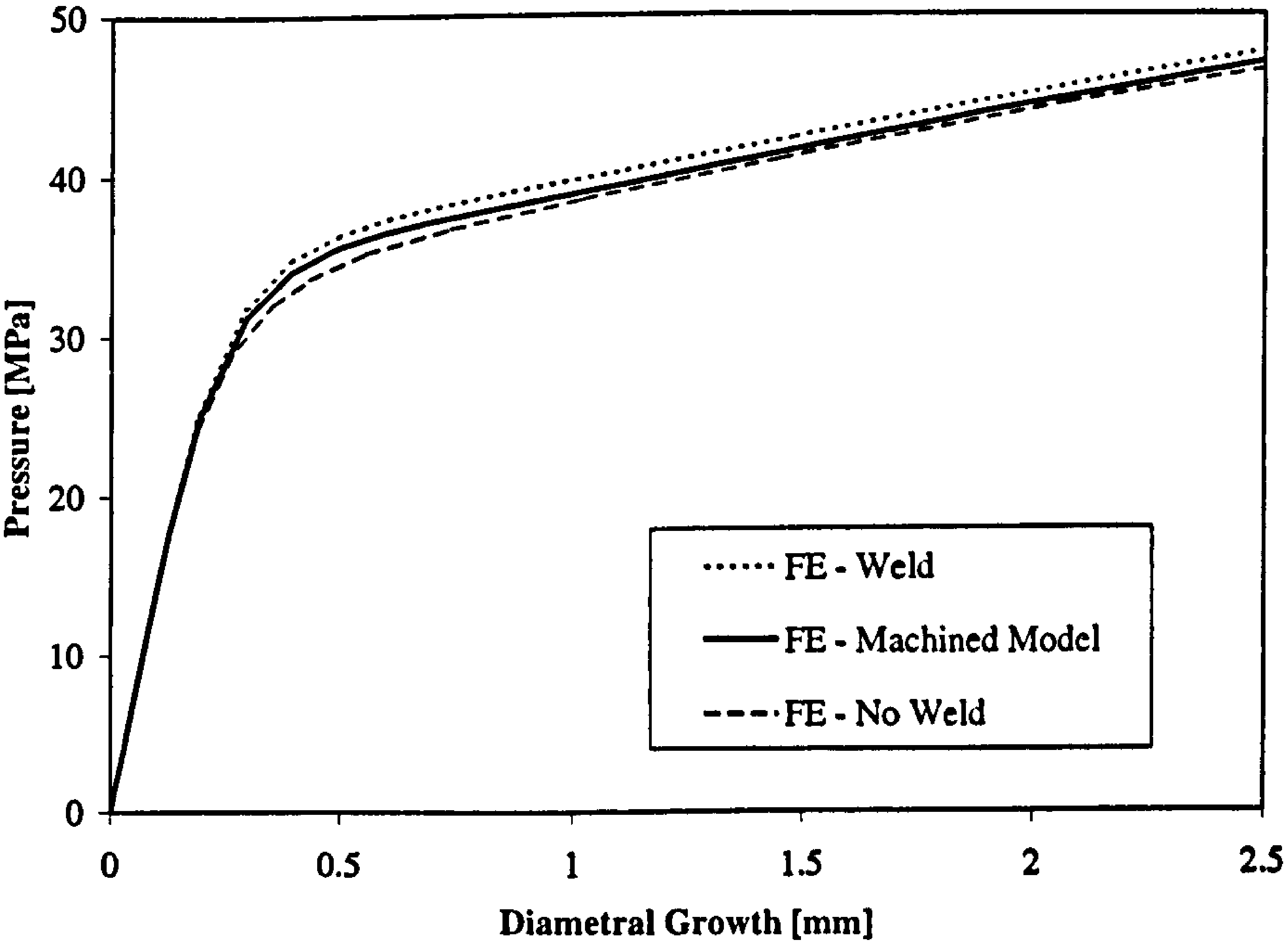

(b)

Figure 6.5: Comparison of Load-Displacement Curves for Different Uncracked FE Models: (a) In-Plane Bending (b) Pressure

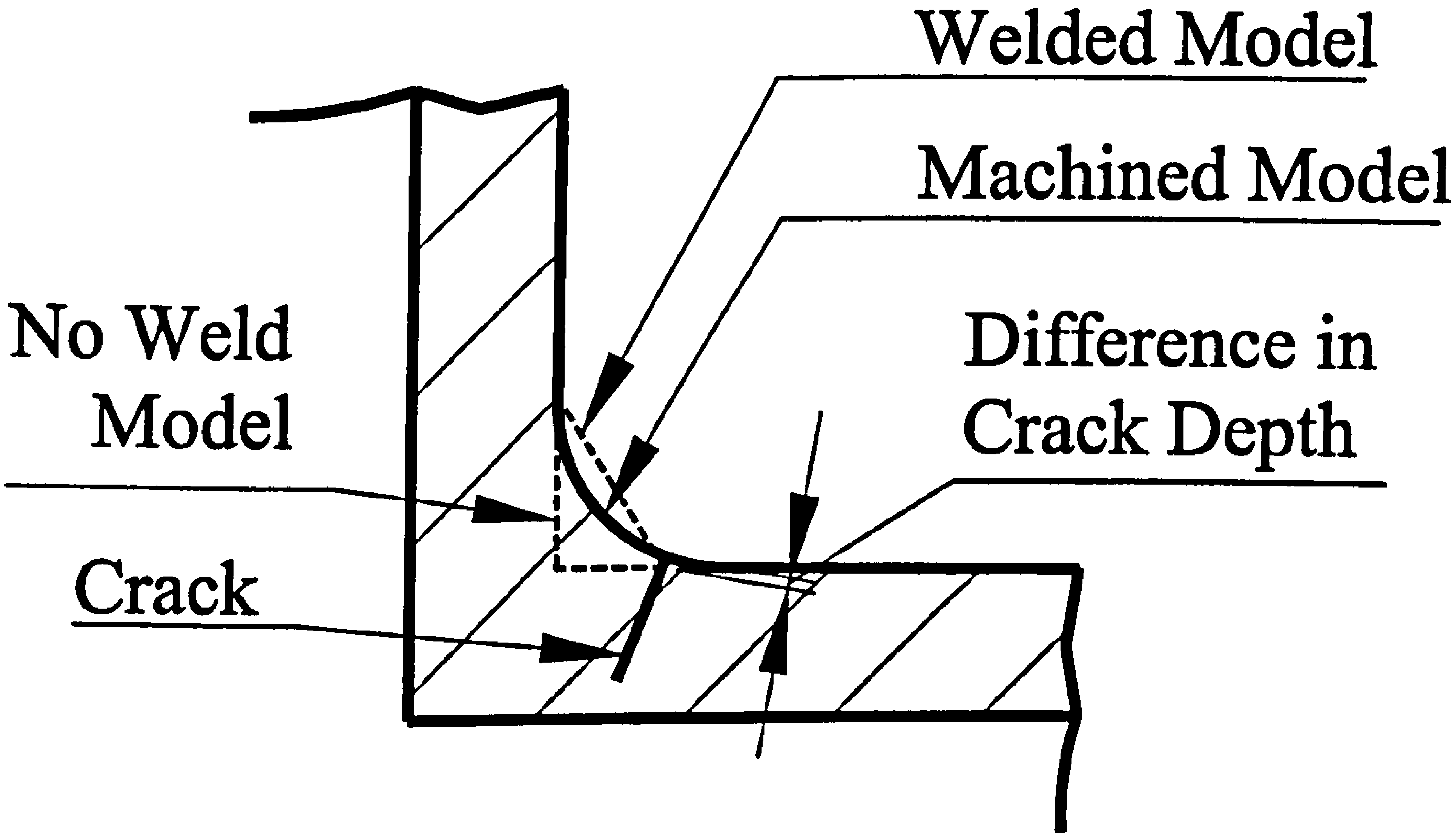

Figure 6.6: Position of Crack for Machined FE Model

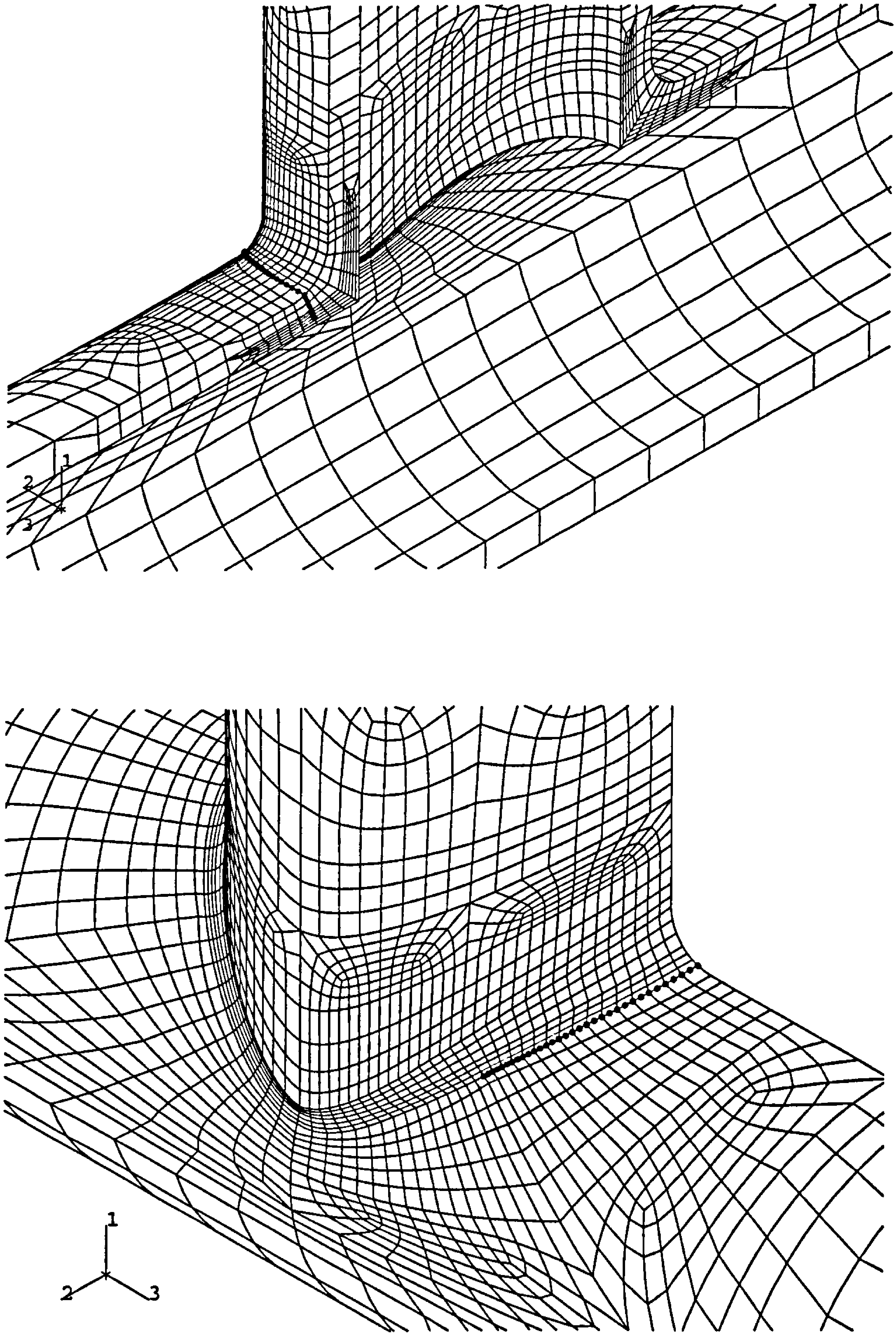

Figure 6.7: Cracked In-Plane Bending FE Model for Machined Geometry (a/t=0.75; Crack Face Nodes Marked)

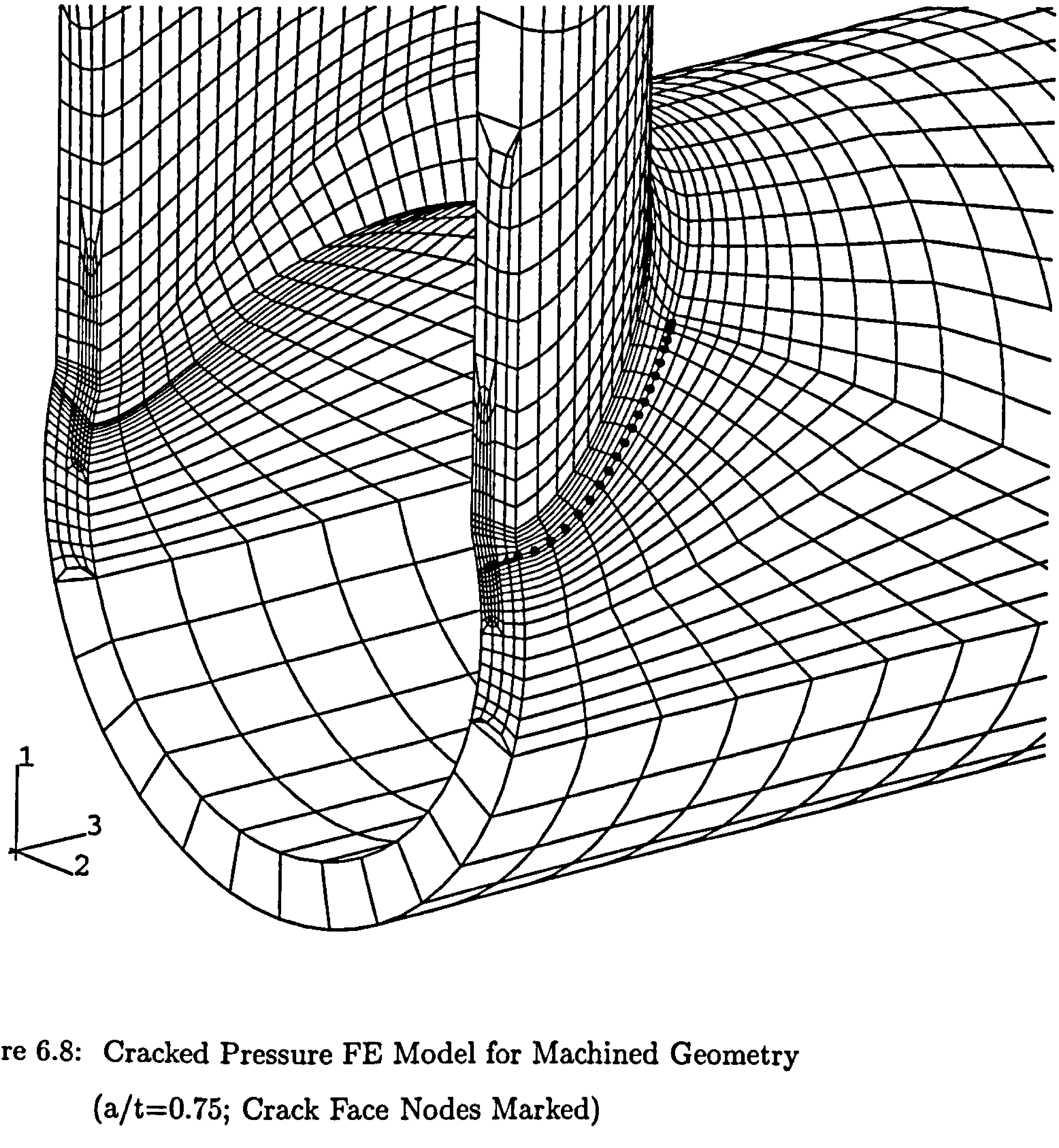

Figure 6.8: Cracked Pressure FE Model for Machined Geometry (a/t=0.75; Crack Face Nodes Marked)

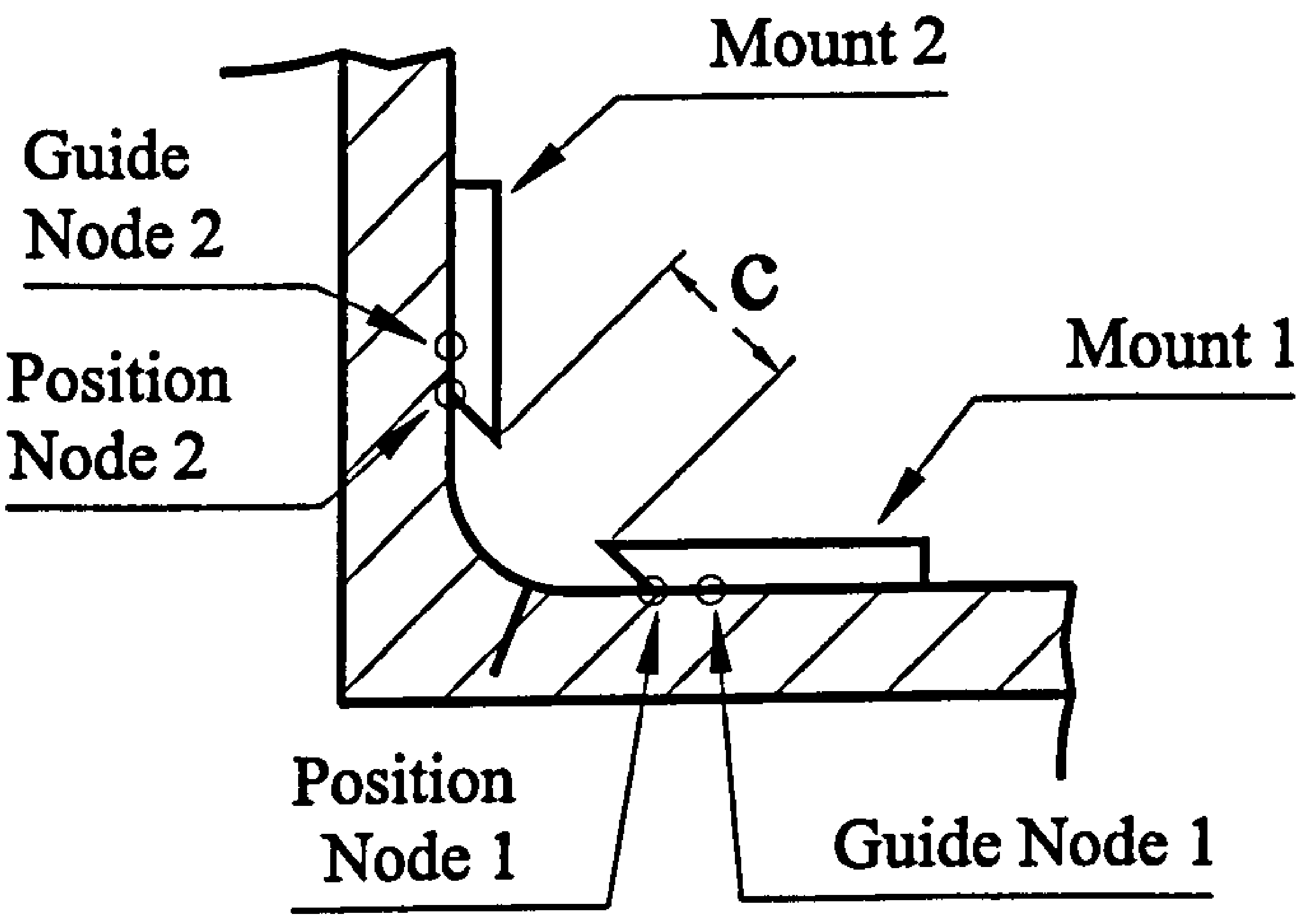

ORIGINAL

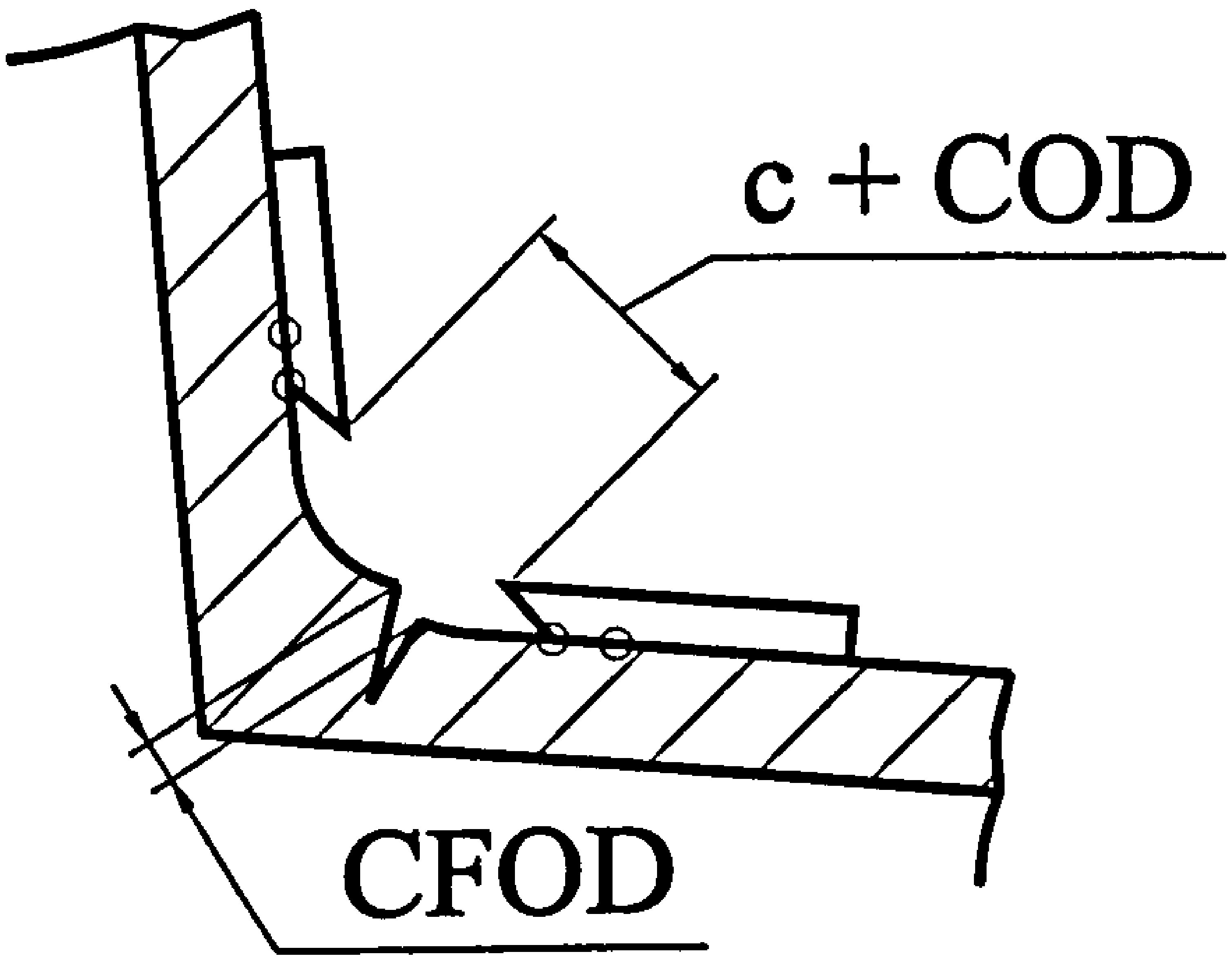

DISPLACED

Figure 6.9: Calculation of COD from Nodal Displacements

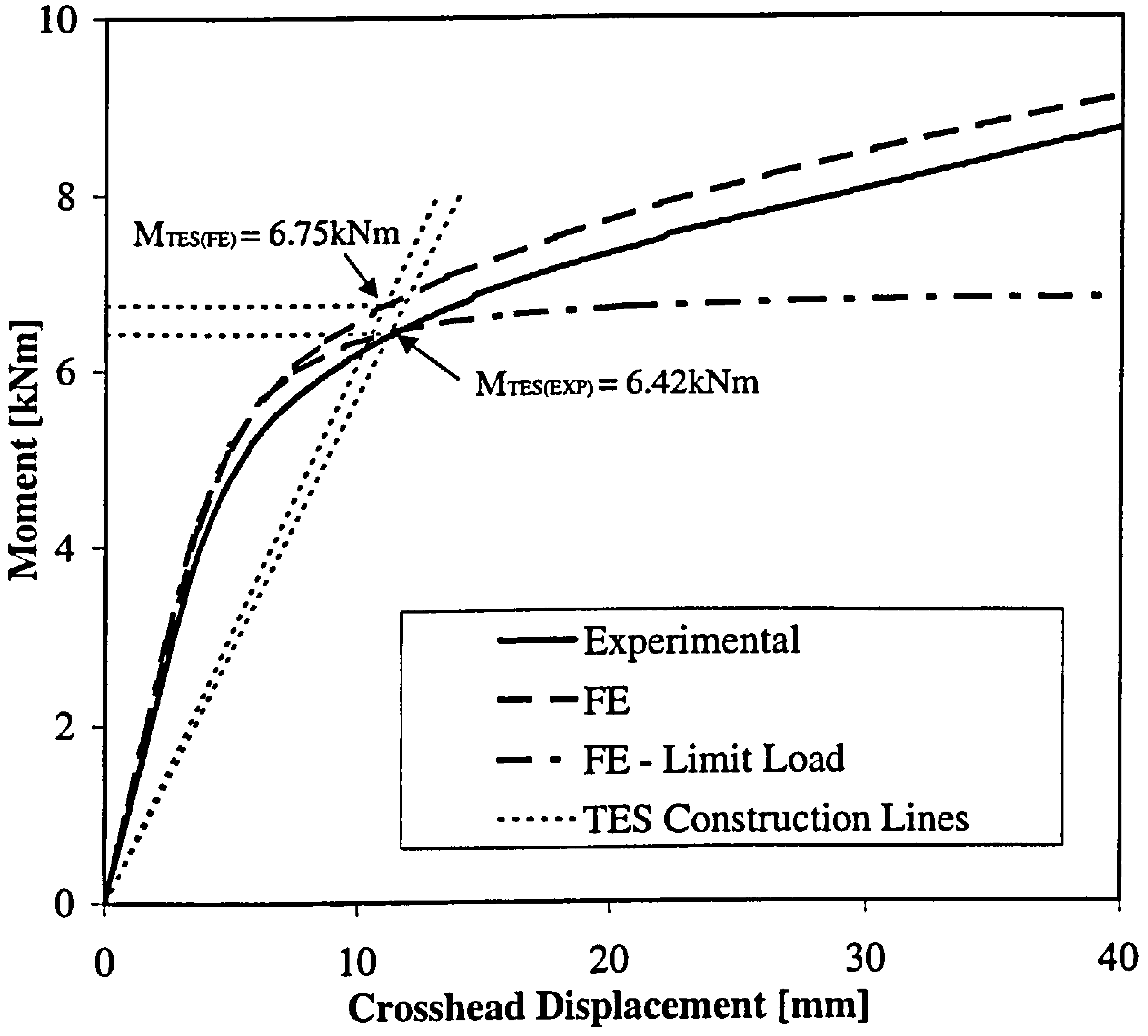

Figure 6.10: (a)Uncracked In-Plane Bending: Moment v Crosshead Displacement

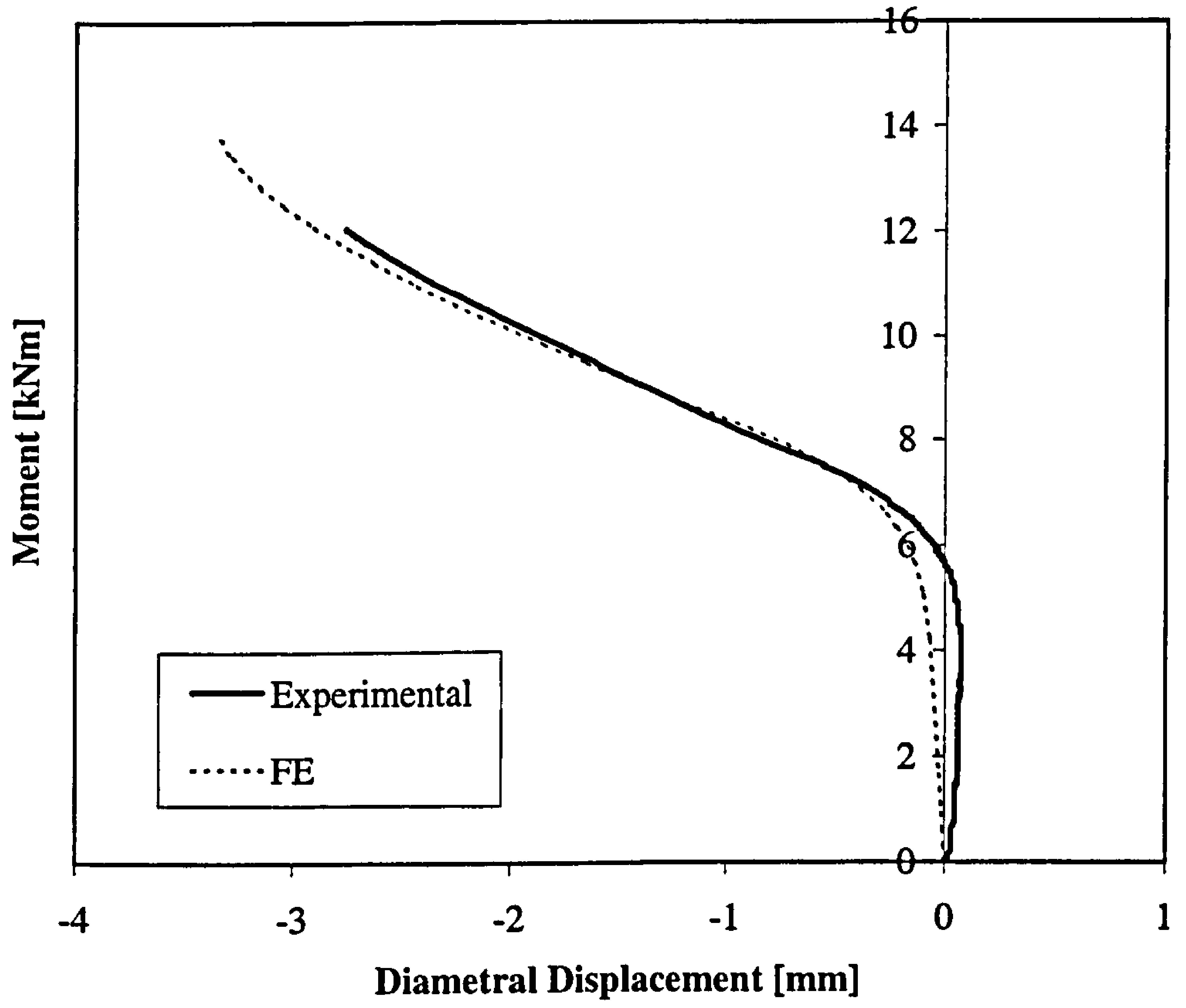

Figure 6.10: (b)Uncracked In-Plane Bending: Moment v Diametral Displacement

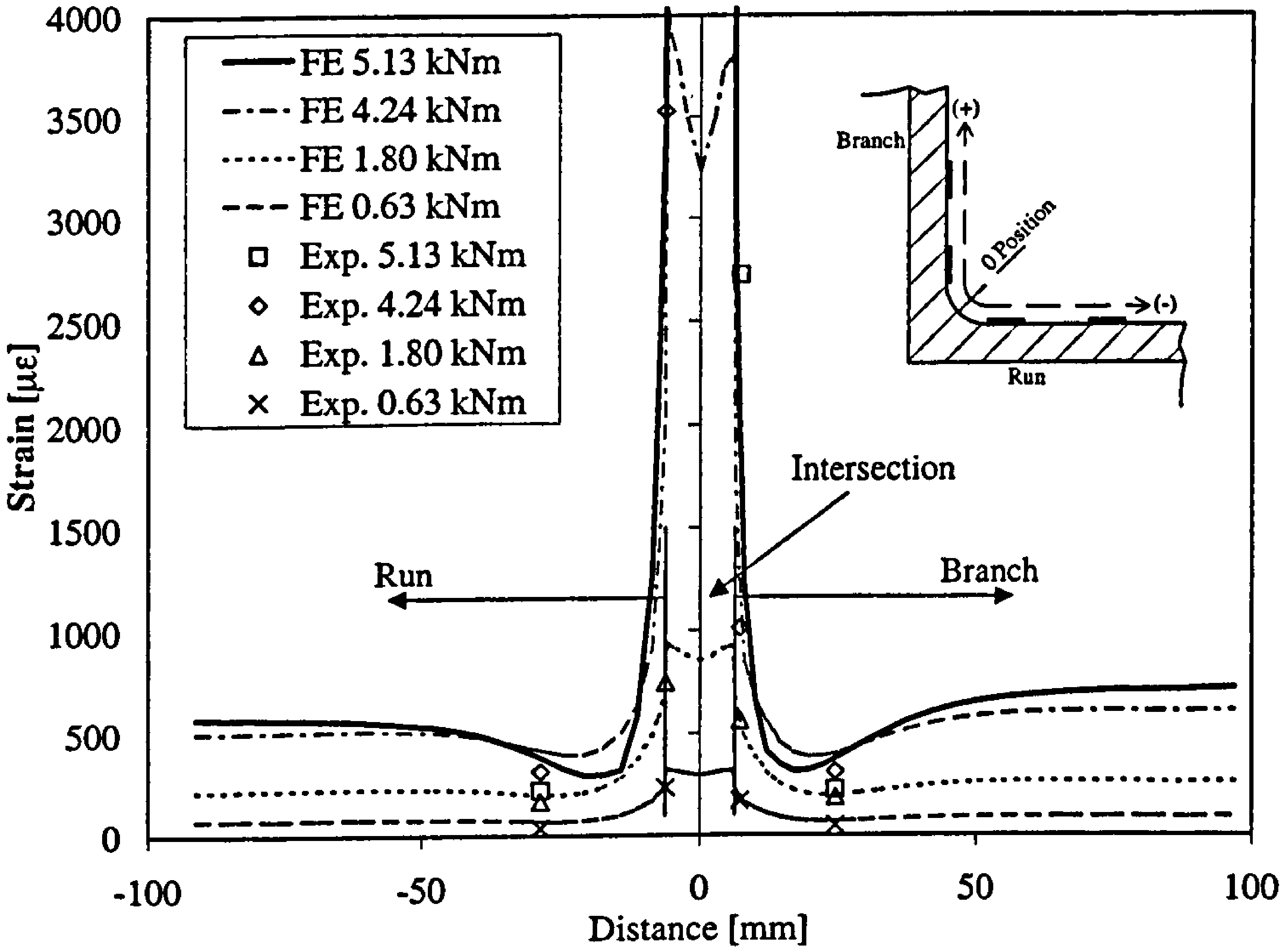

Figure 6.10: (c)Uncracked In-Plane Bending: Axial Strain Distribution

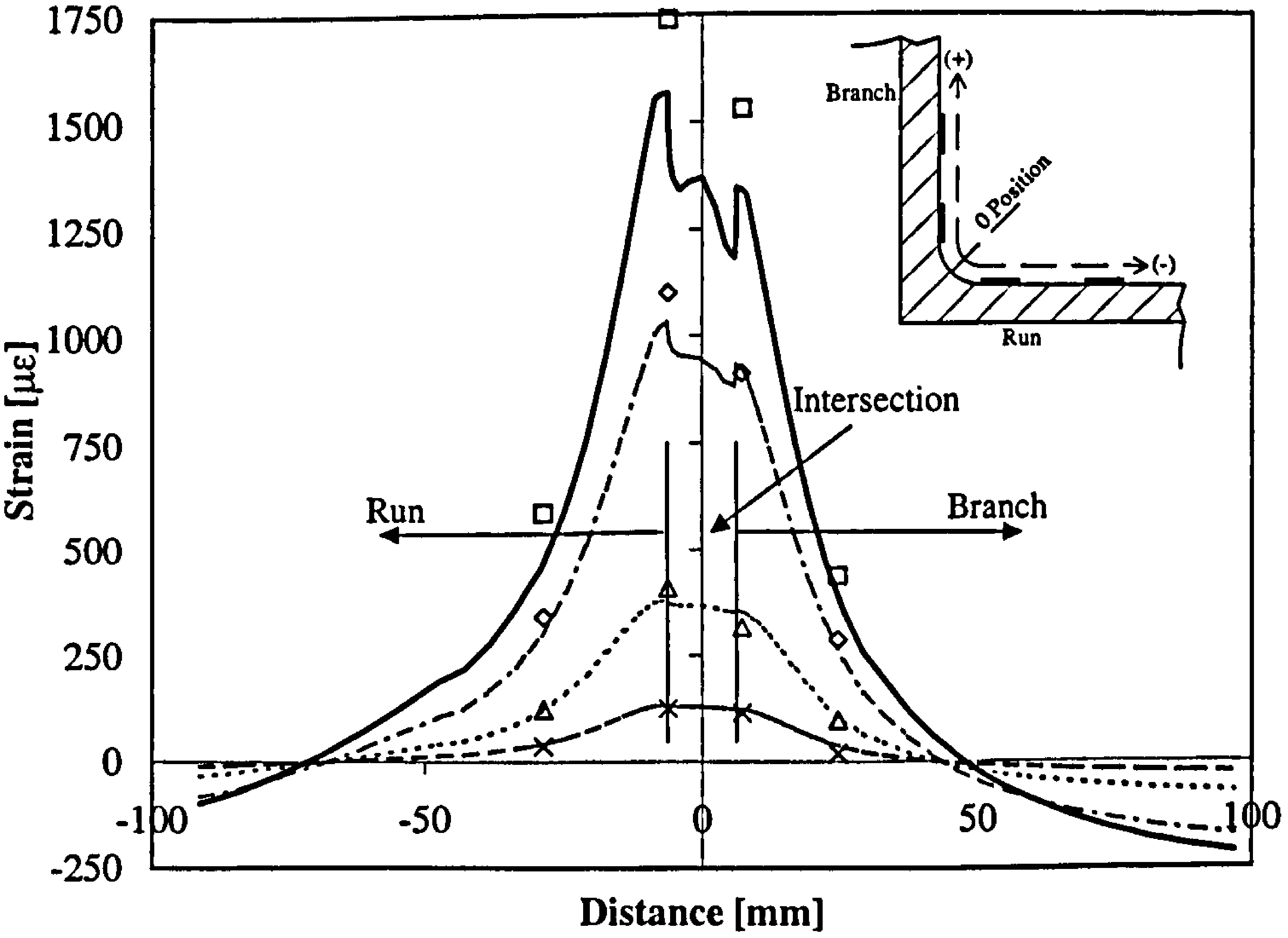

Figure 6.10: (d)Uncracked In-Plane Bending: Hoop Strain Distribution

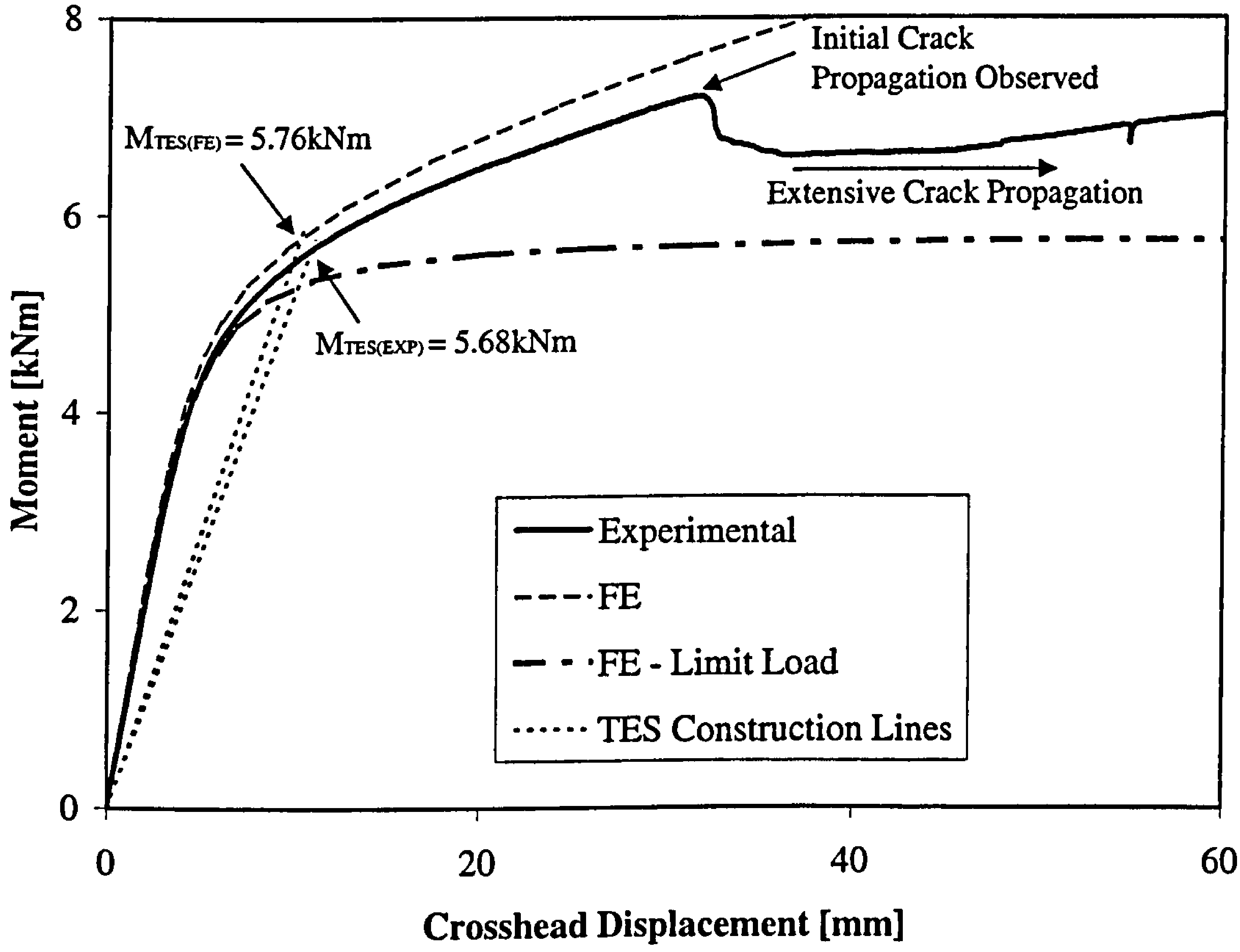

Figure 6.11: (a)PP Crack, In-Plane Bending:Moment v Crosshead Displacement

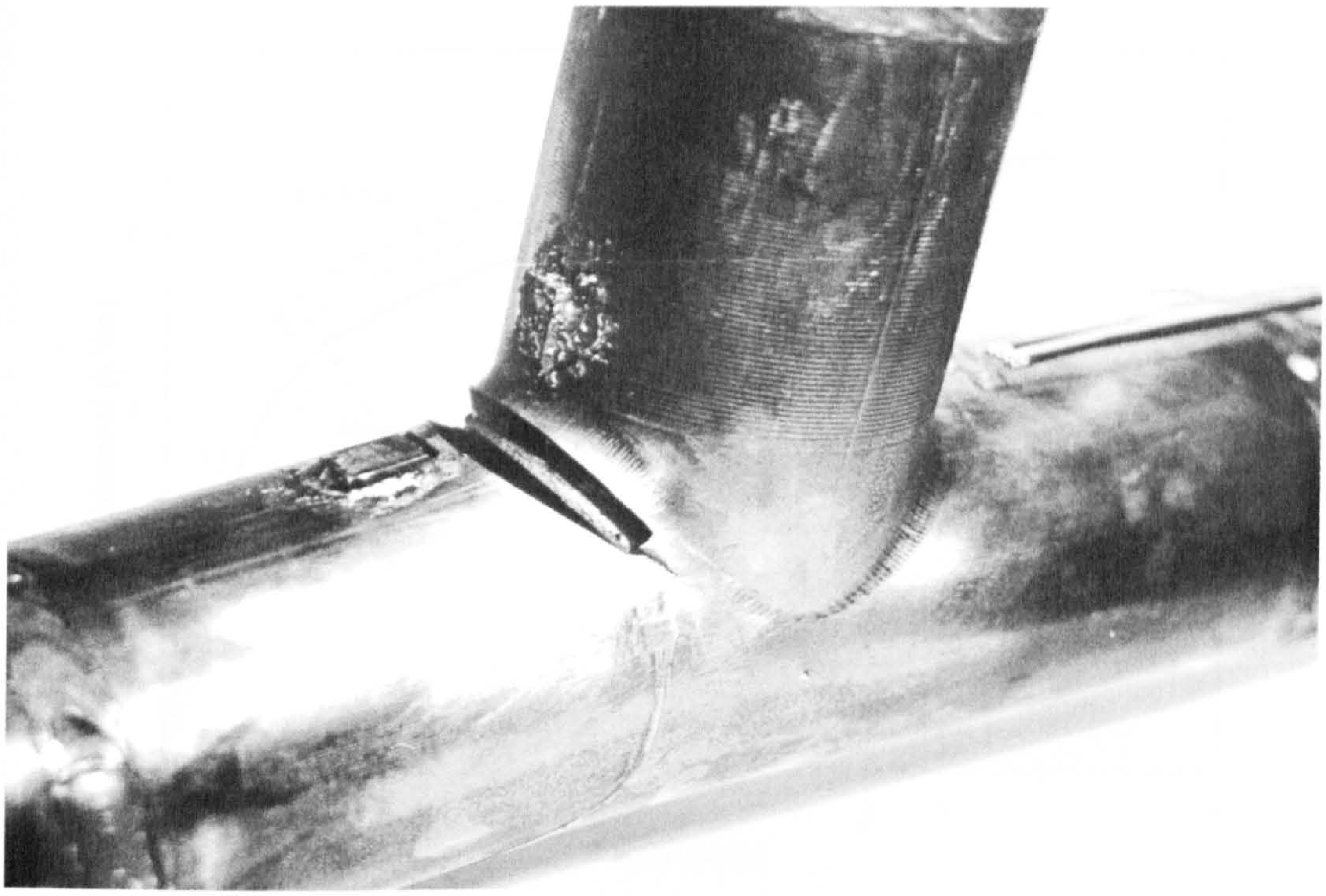

Figure 6.11: (b)PP Crack, In-Plane Bending: Final Condition of Junction

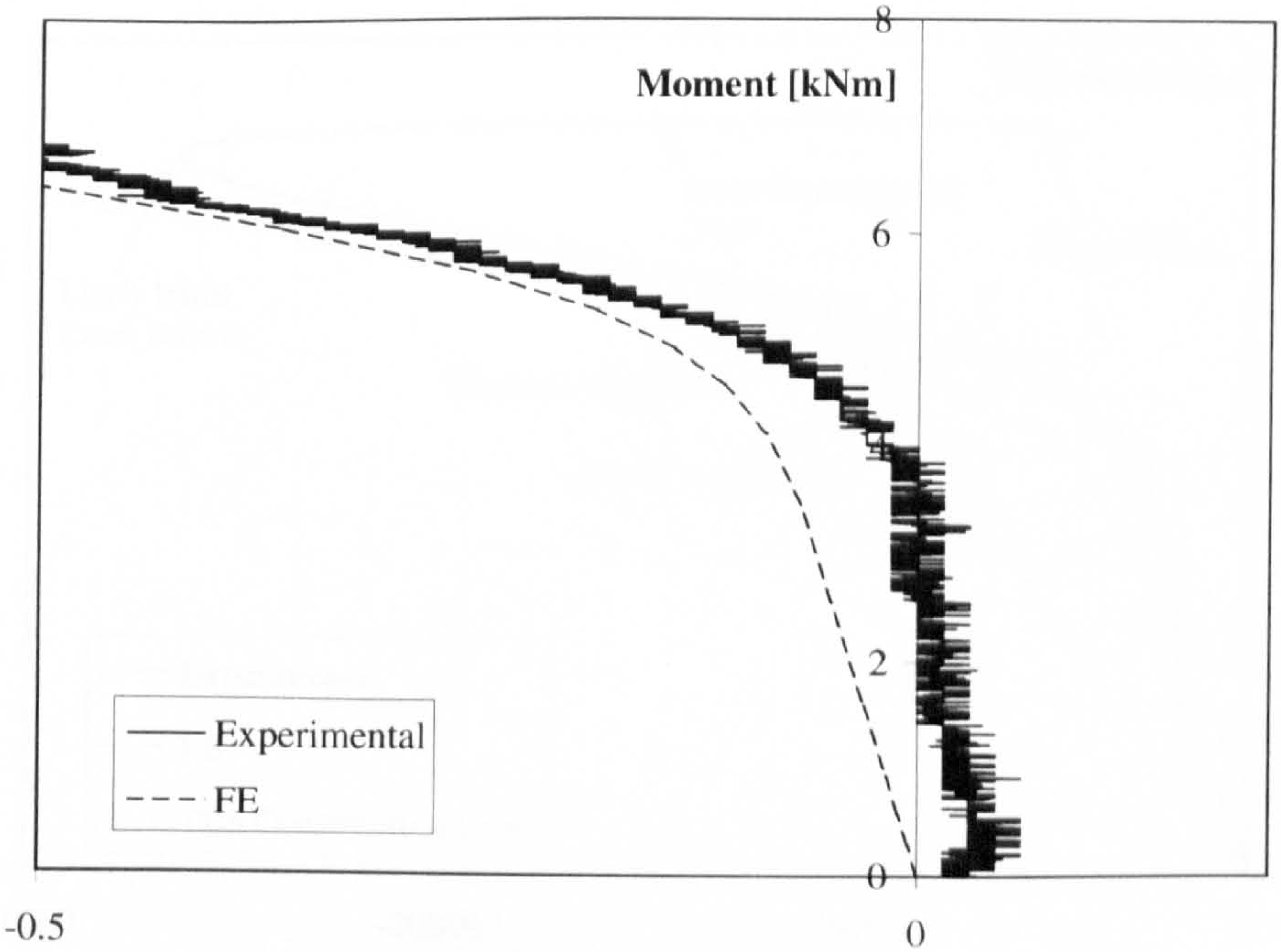

Figure 6.11: (c)PP Crack, In-Plane Bending:Moment v Diametral Displacement

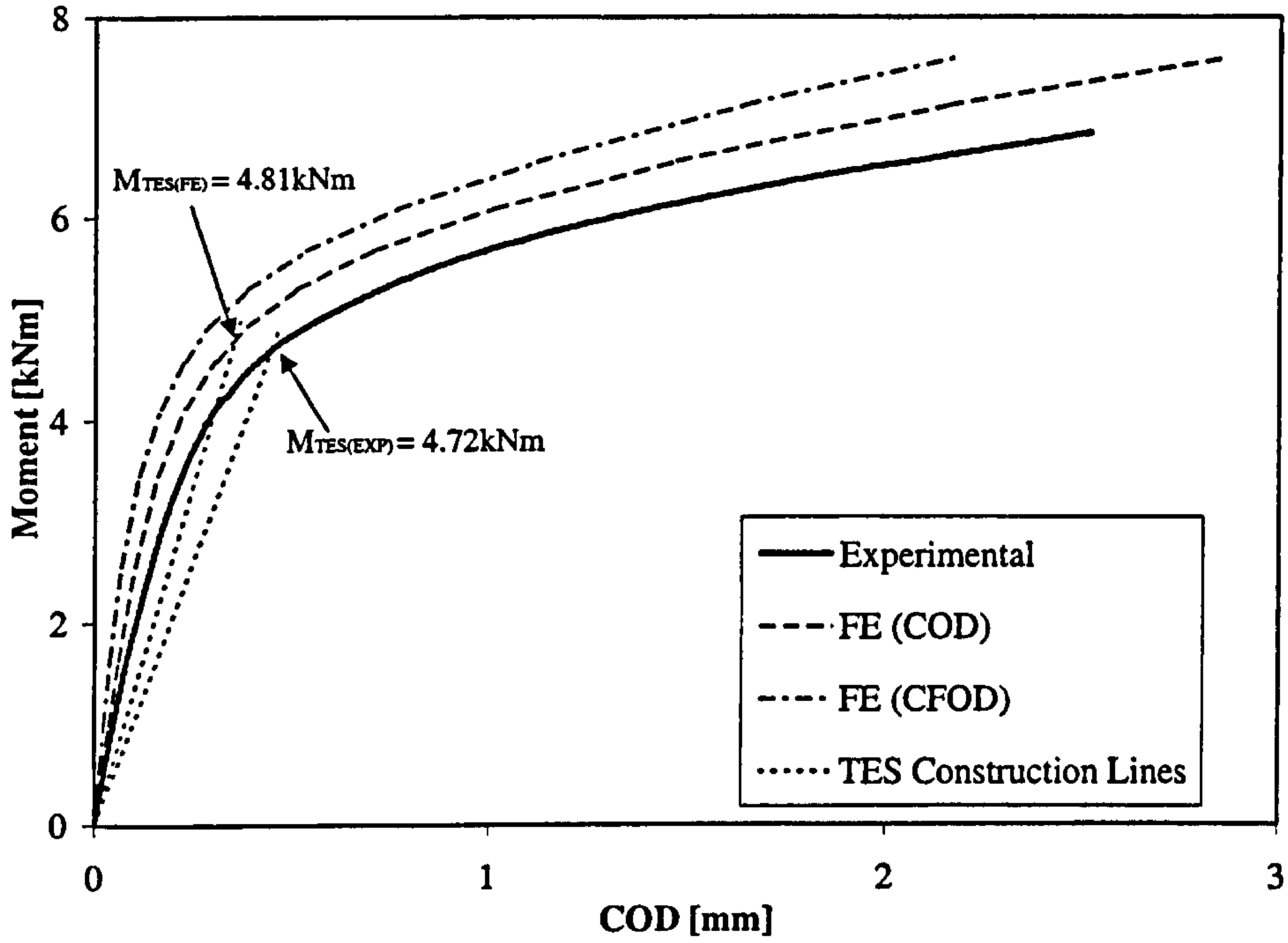

Figure 6.11: (d)PP Crack, In-Plane Bending:Moment v COD

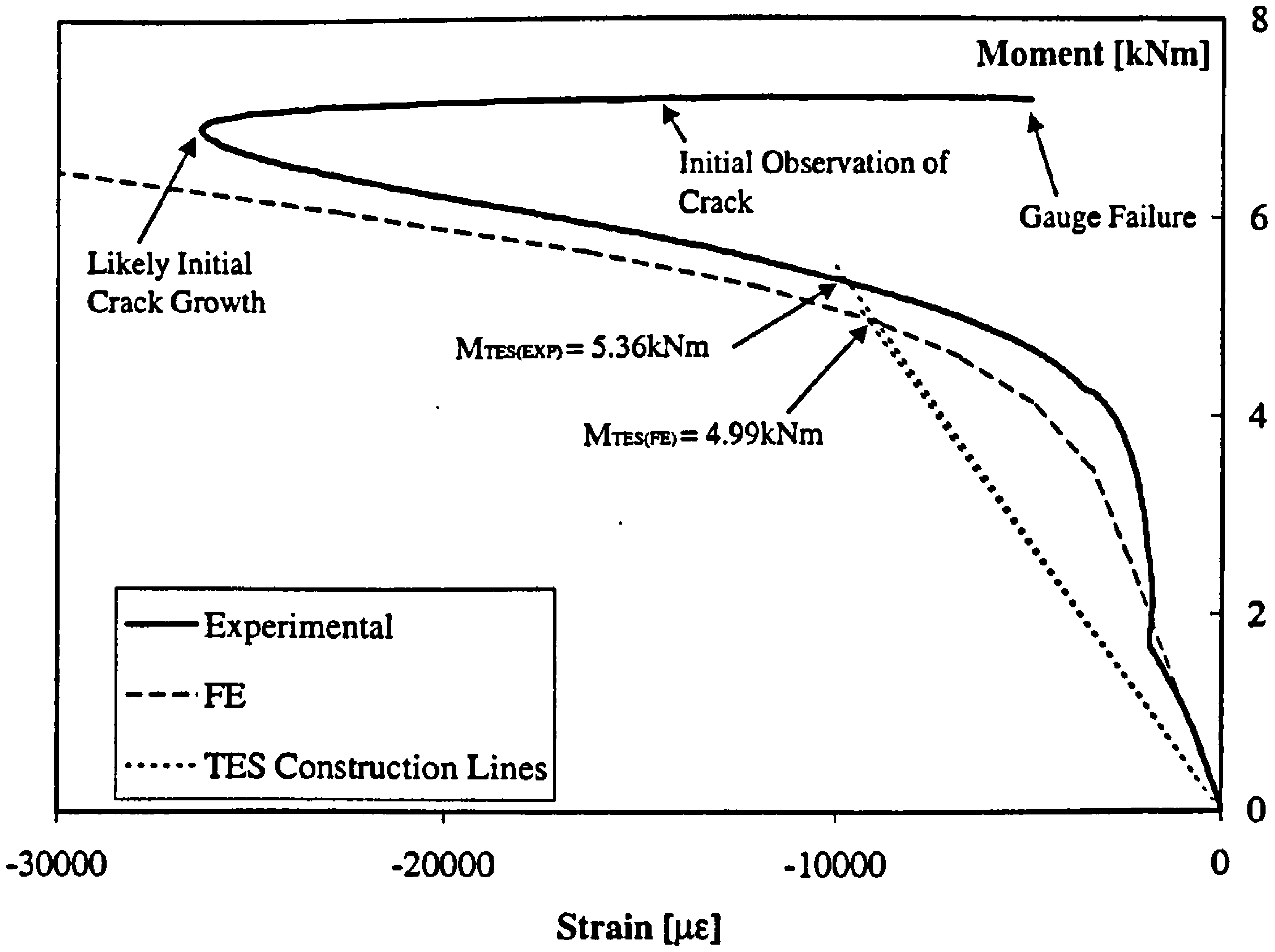

Figure 6.11: (e)PP Crack, In-Plane Bending:Moment v Ligament Strain

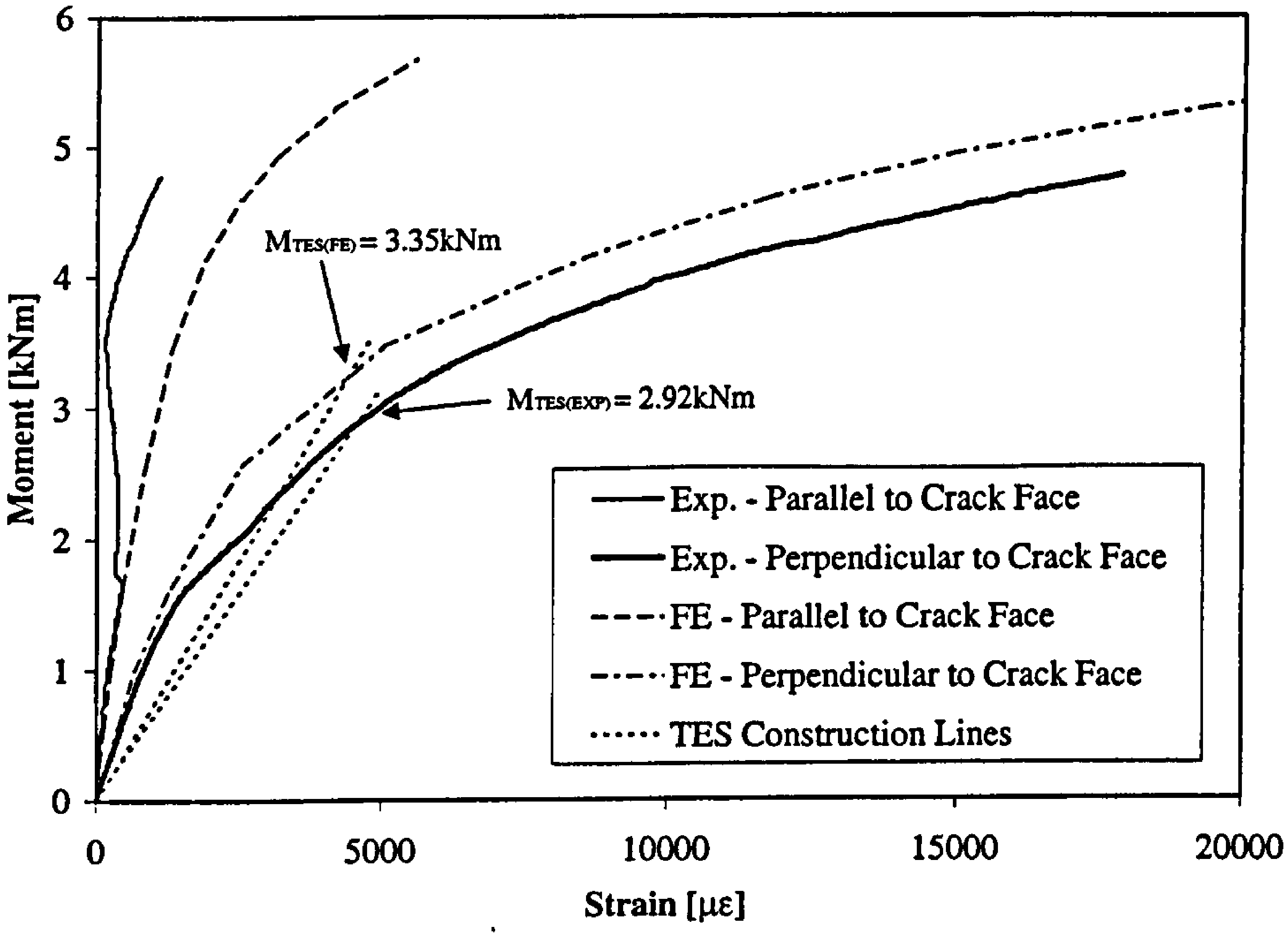

Figure 6.11: (f)PP Crack, In-Plane Bending: Moment v Crack Tip Strains

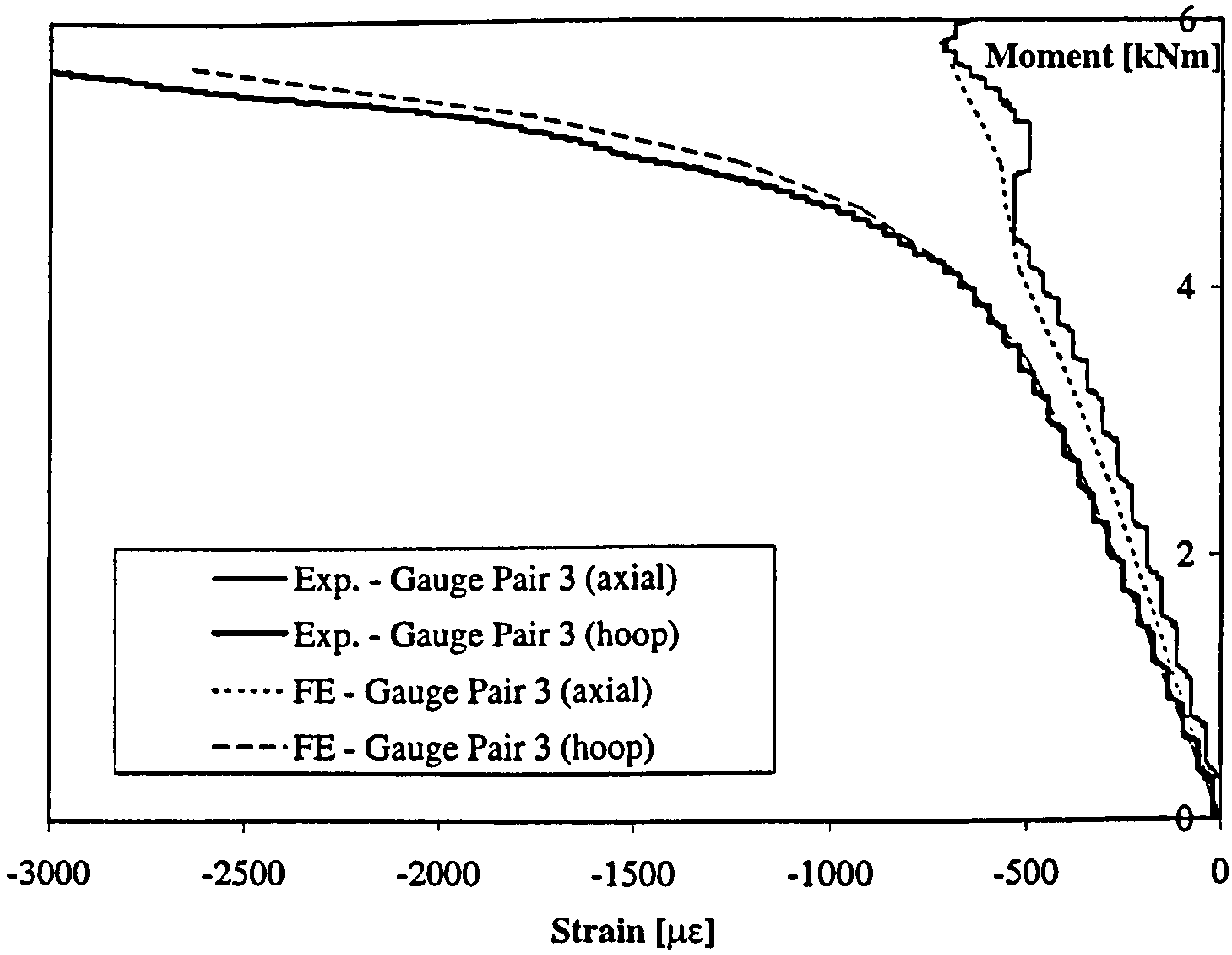

Figure 6.11: (g)PP Crack, In-Plane Bending: Moment v Gauge Pair 3 Strains

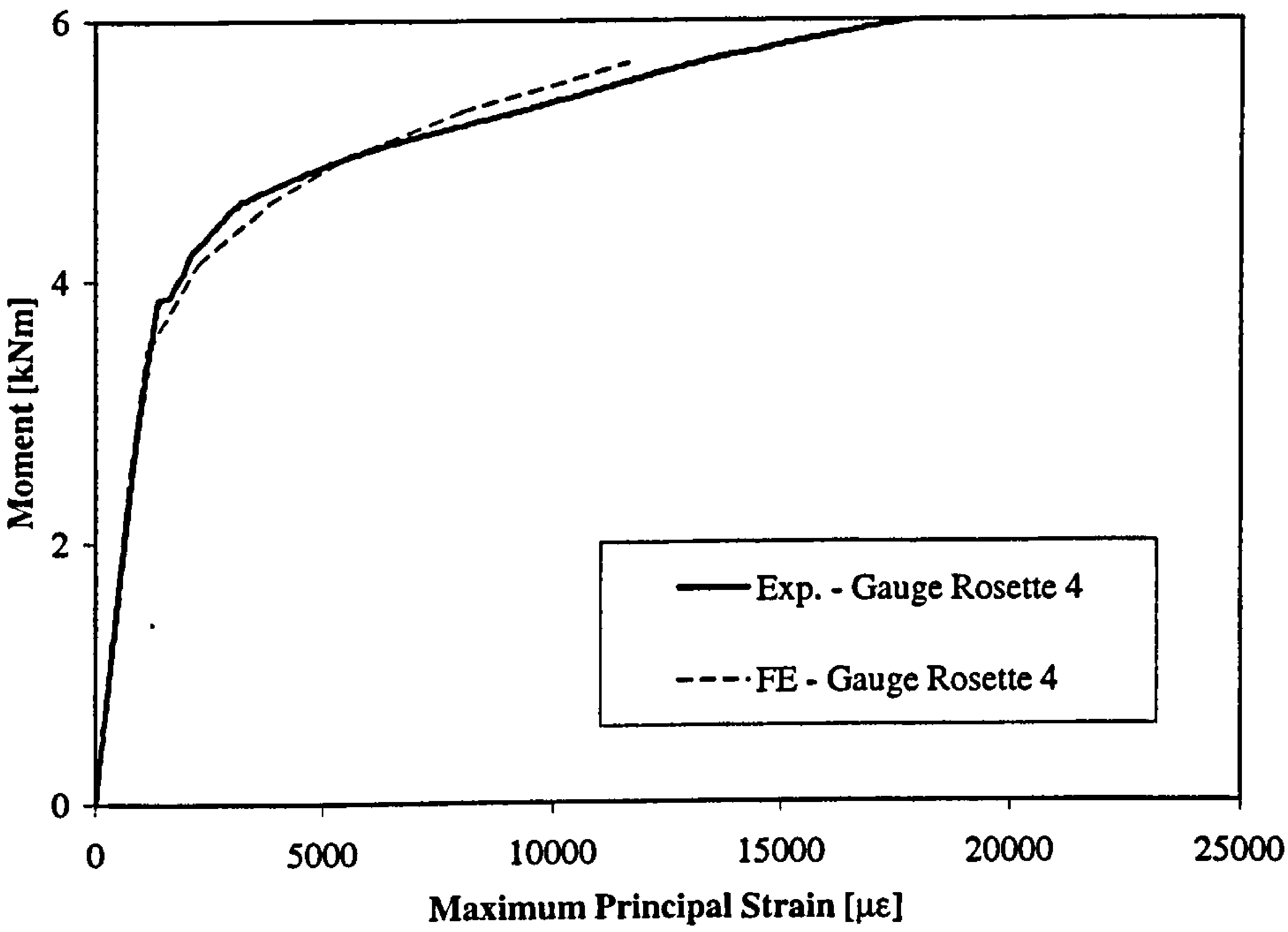

Figure 6.11: (h)PP Crack, In-Plane Bending: Moment v Gauge 4 Strain

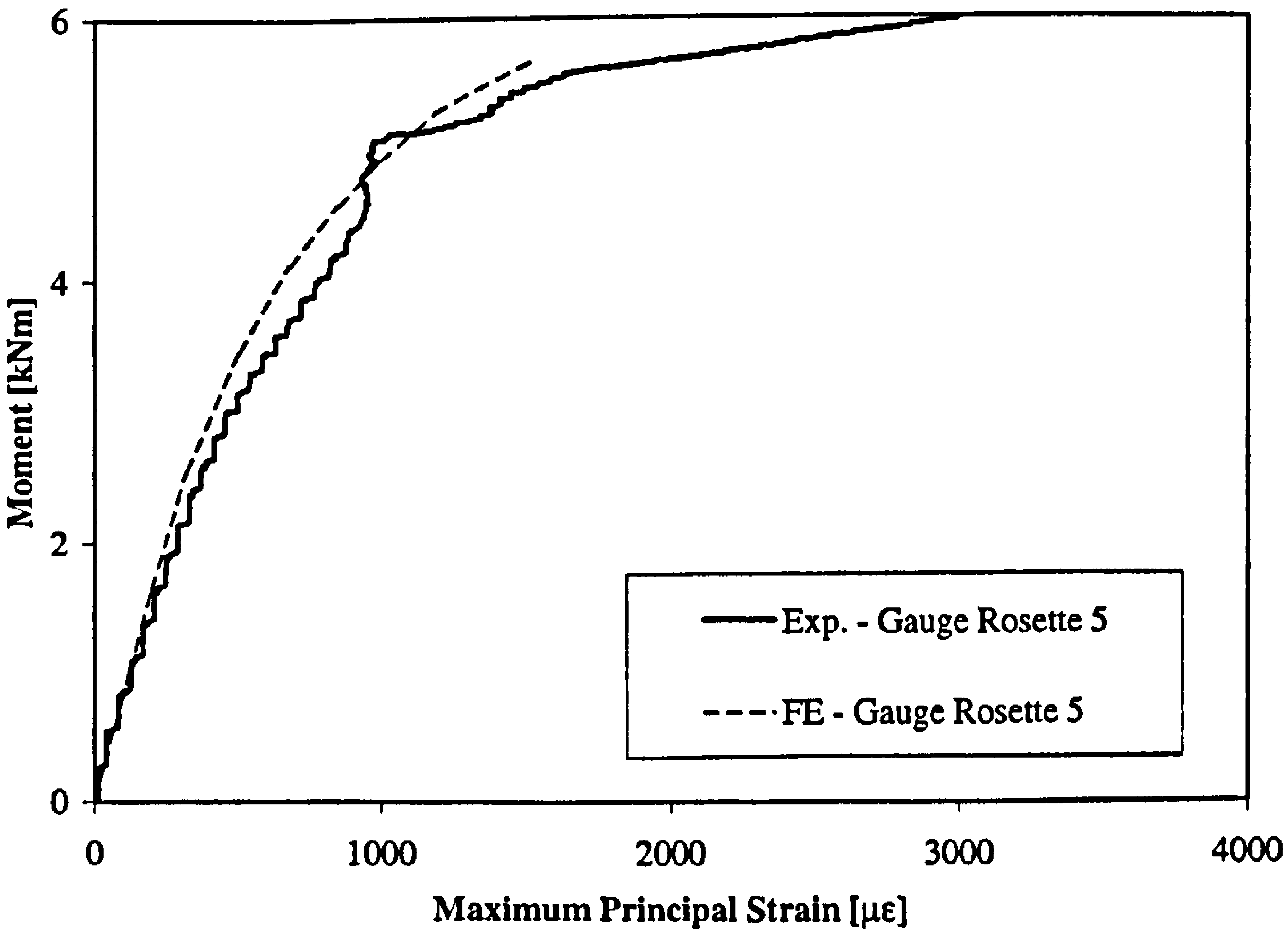

Figure 6.11: (i)PP Crack, In-Plane Bending: Moment v Gauge 5 Strain

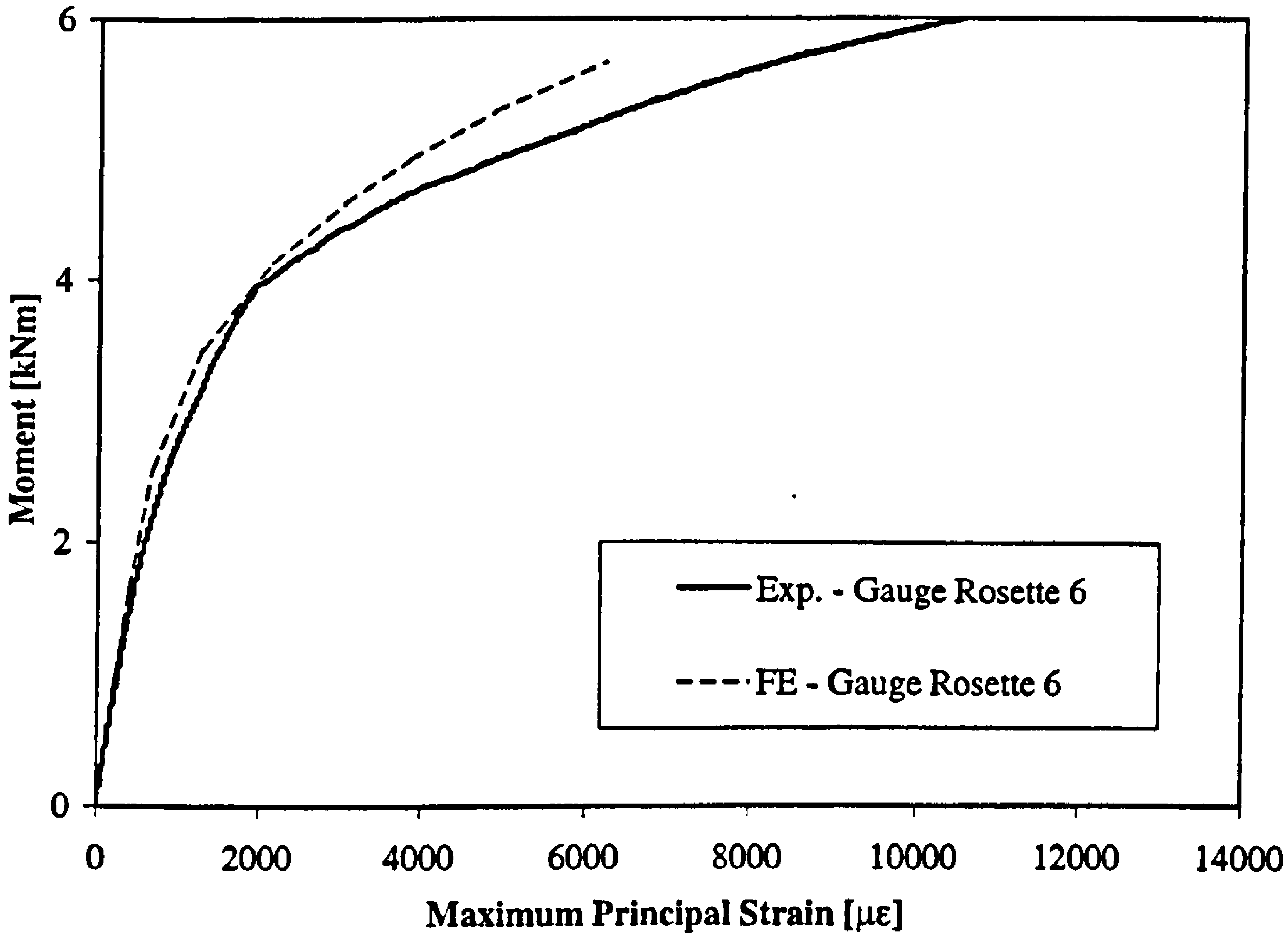

Figure 6.11: (j)PP Crack, In-Plane Bending: Moment v Gauge 6 Strain

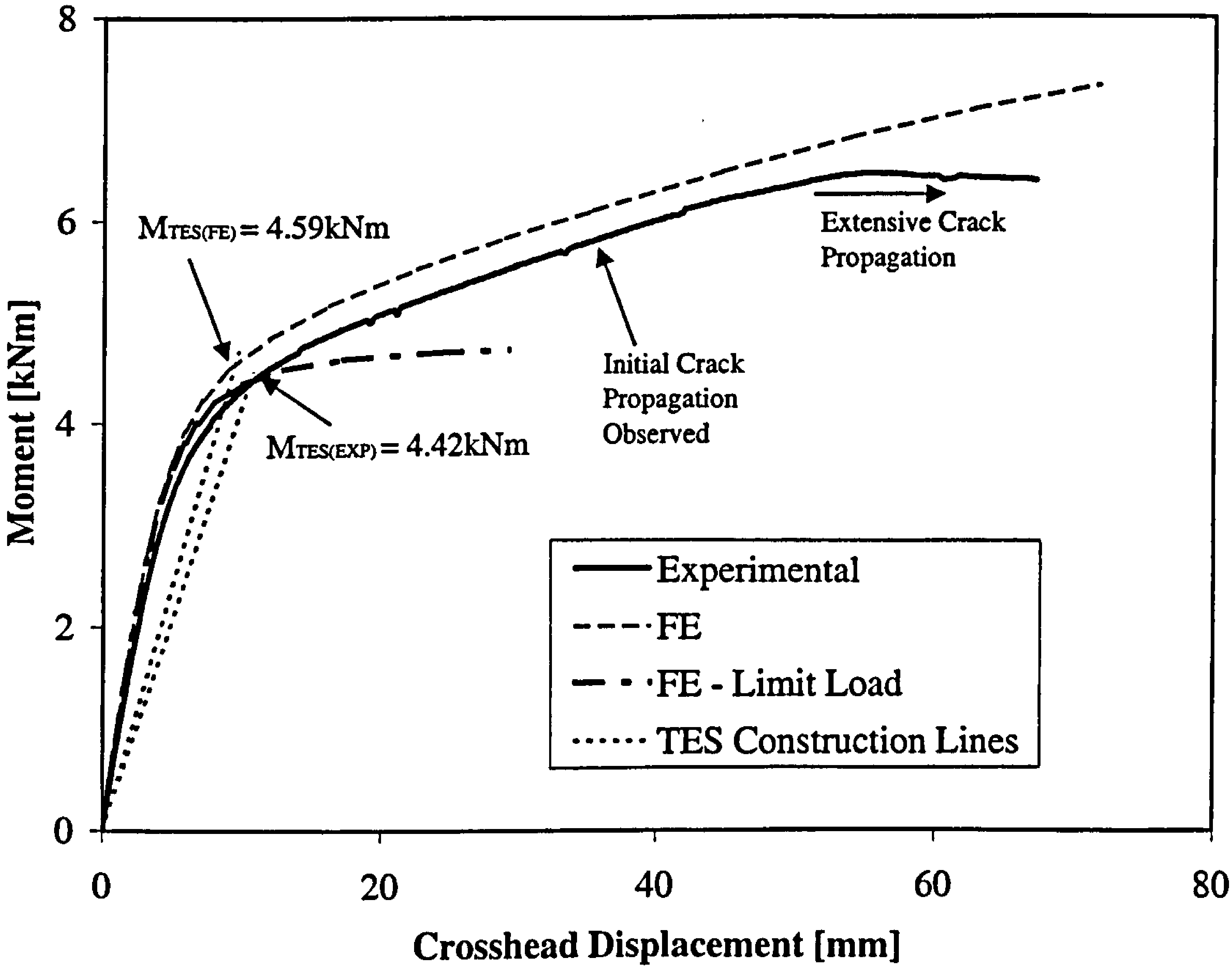

Figure 6.12: (a)TW Crack, In-Plane Bending: Moment v Crosshead Displacement

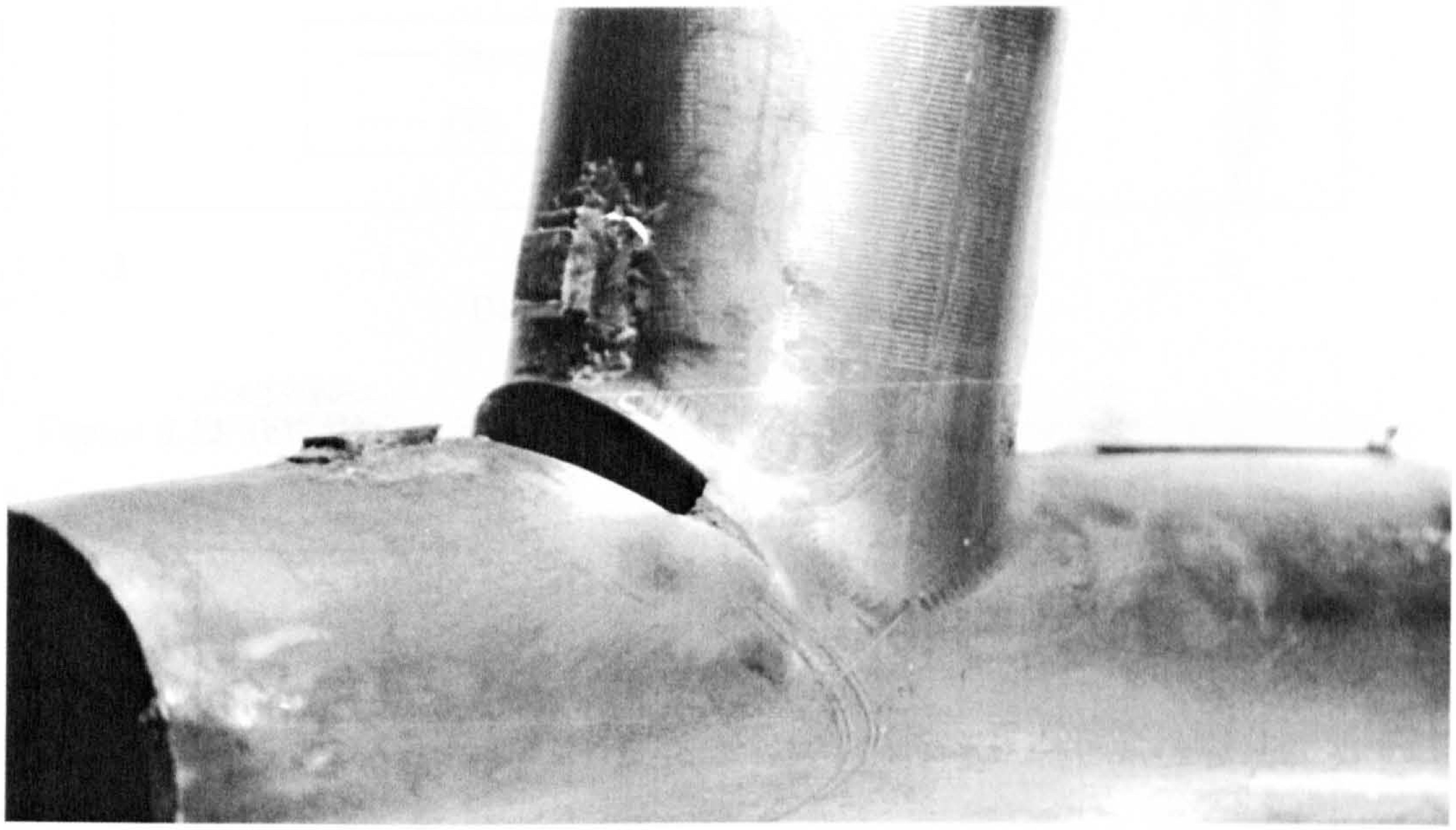

Figure 6.12: (b)TW Crack, In-Plane Bending: Final Condition of Junction

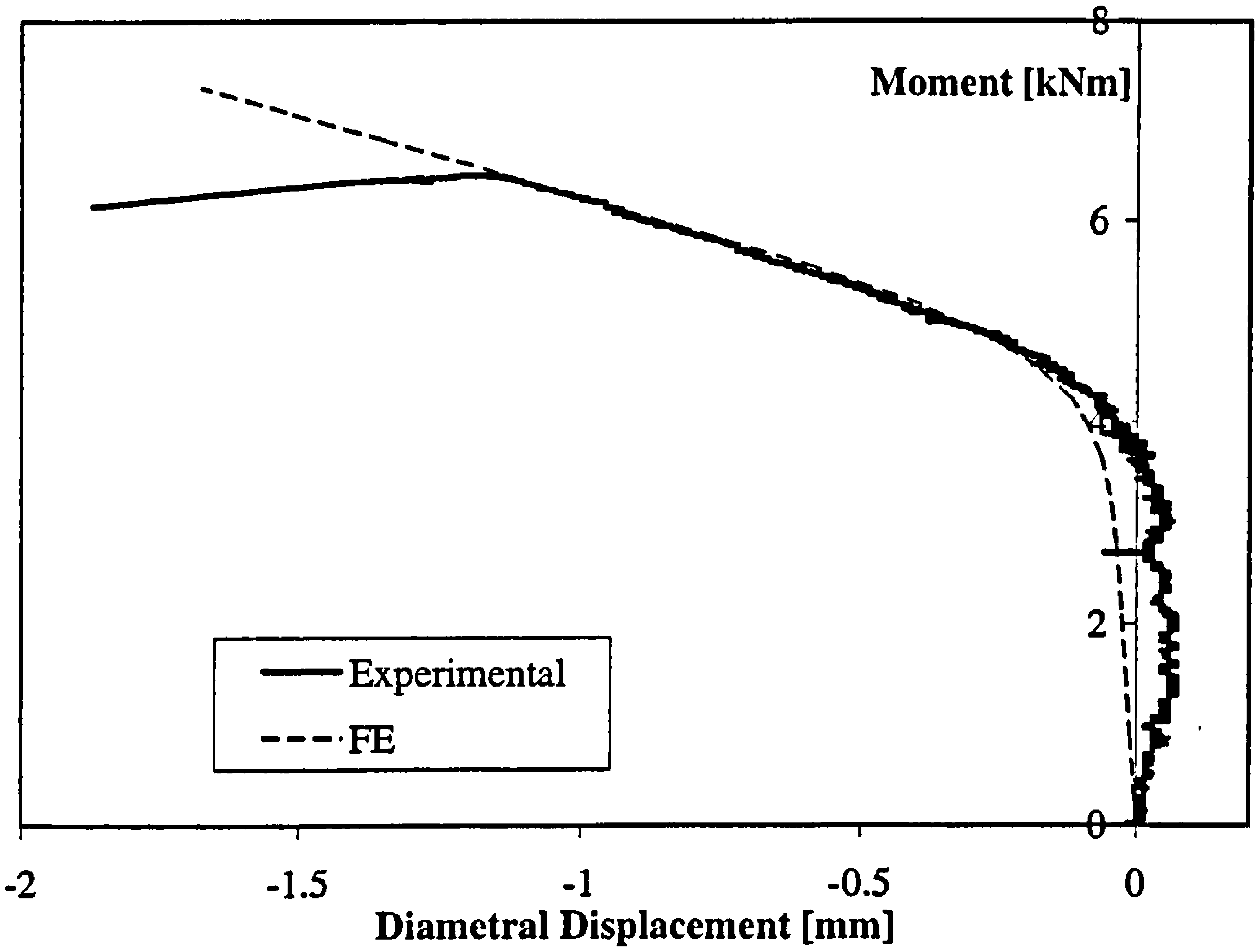

Figure 6.12: (c)TW Crack, In-Plane Bending: Moment v Diametral Displacement

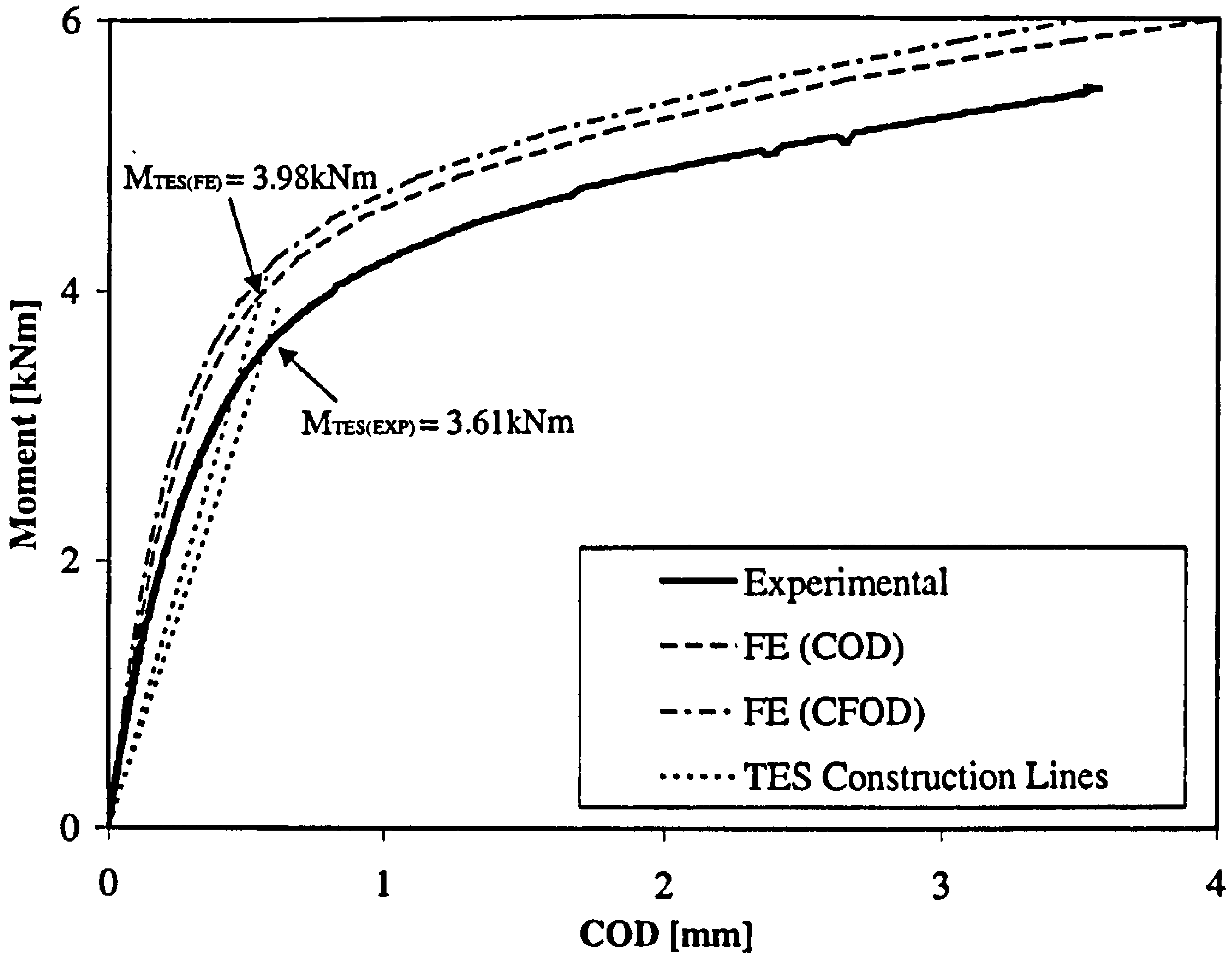

Figure 6.12: (d)TW Crack, In-Plane Bending: Moment v COD

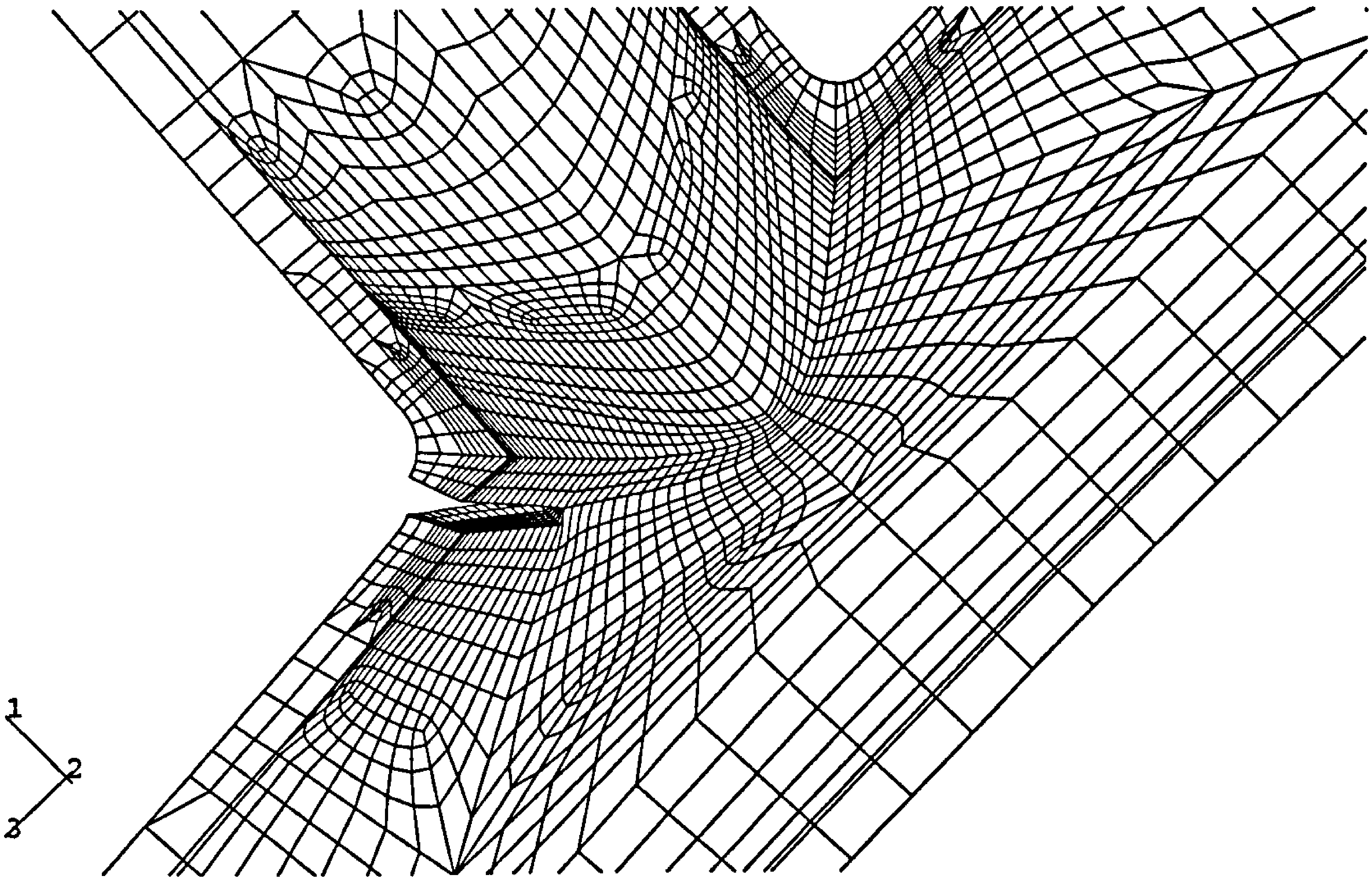

Figure 6.12: (e)TW Crack, In-Plane Bending: Typical Crack Opening Mode

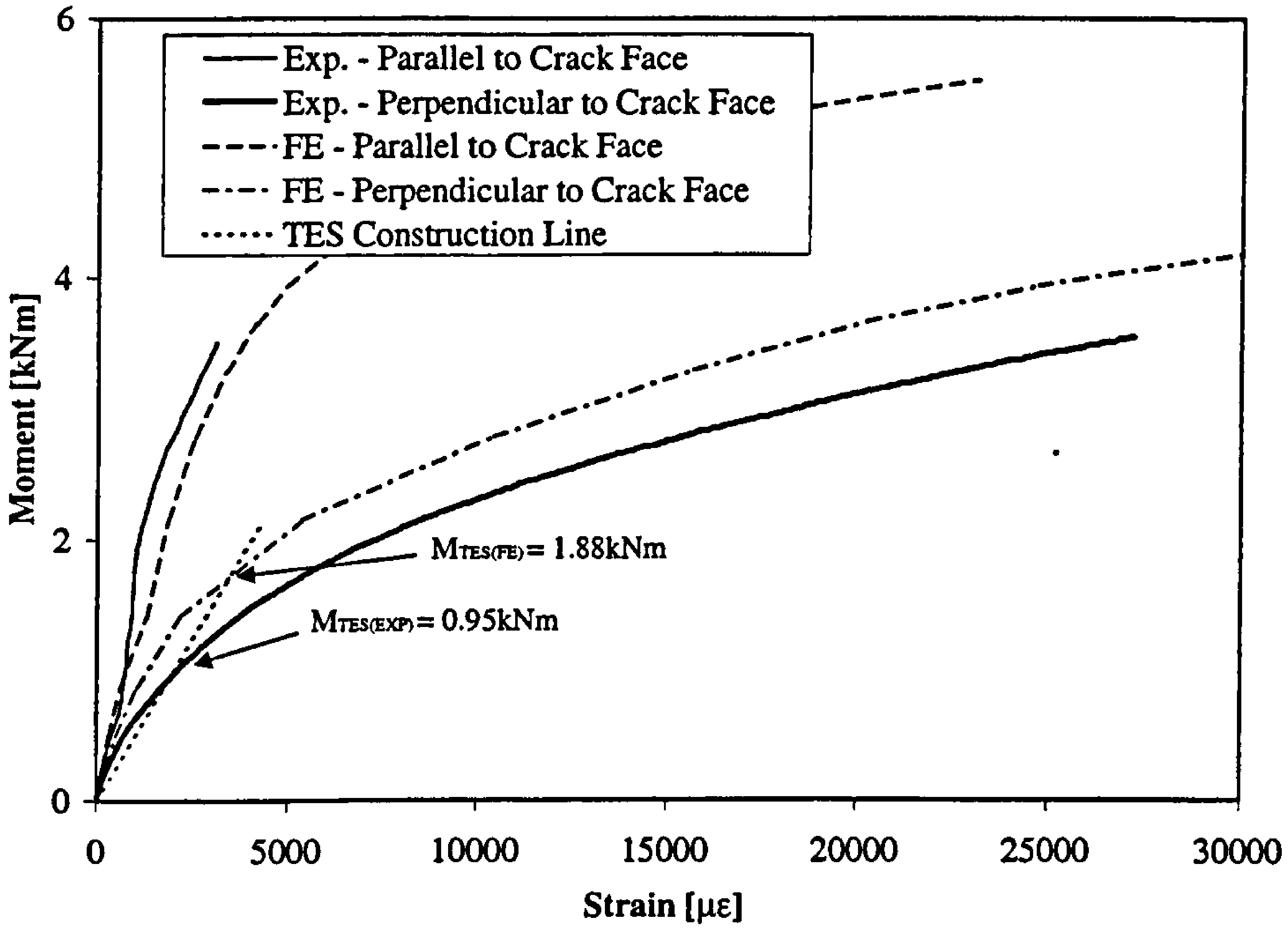

Figure 6.12: (f)TW Crack, In-Plane Bending: Moment v Crack Tip Strains

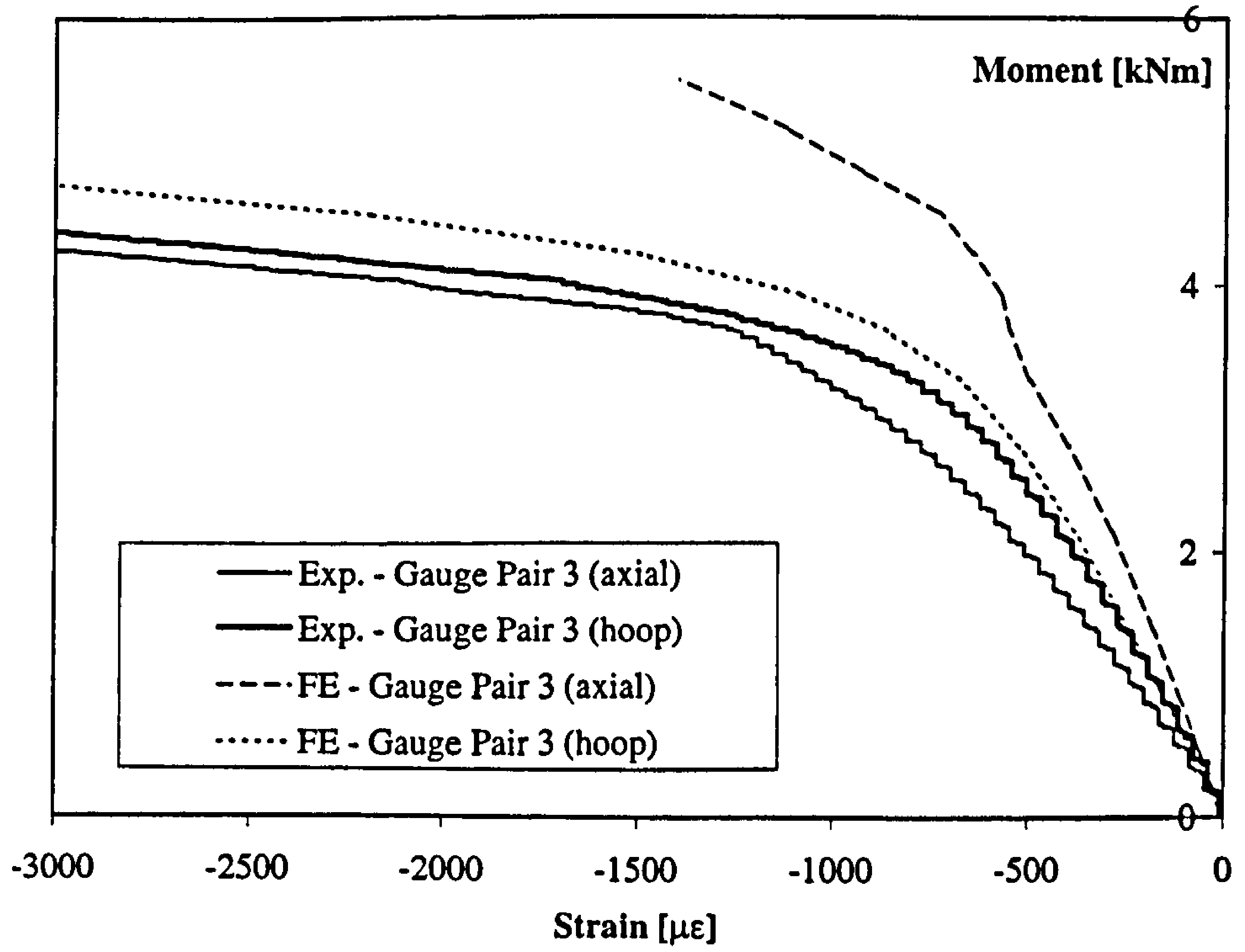

Figure 6.12: (g)TW Crack, In-Plane Bending: Moment v Gauge Pair 3 Strains

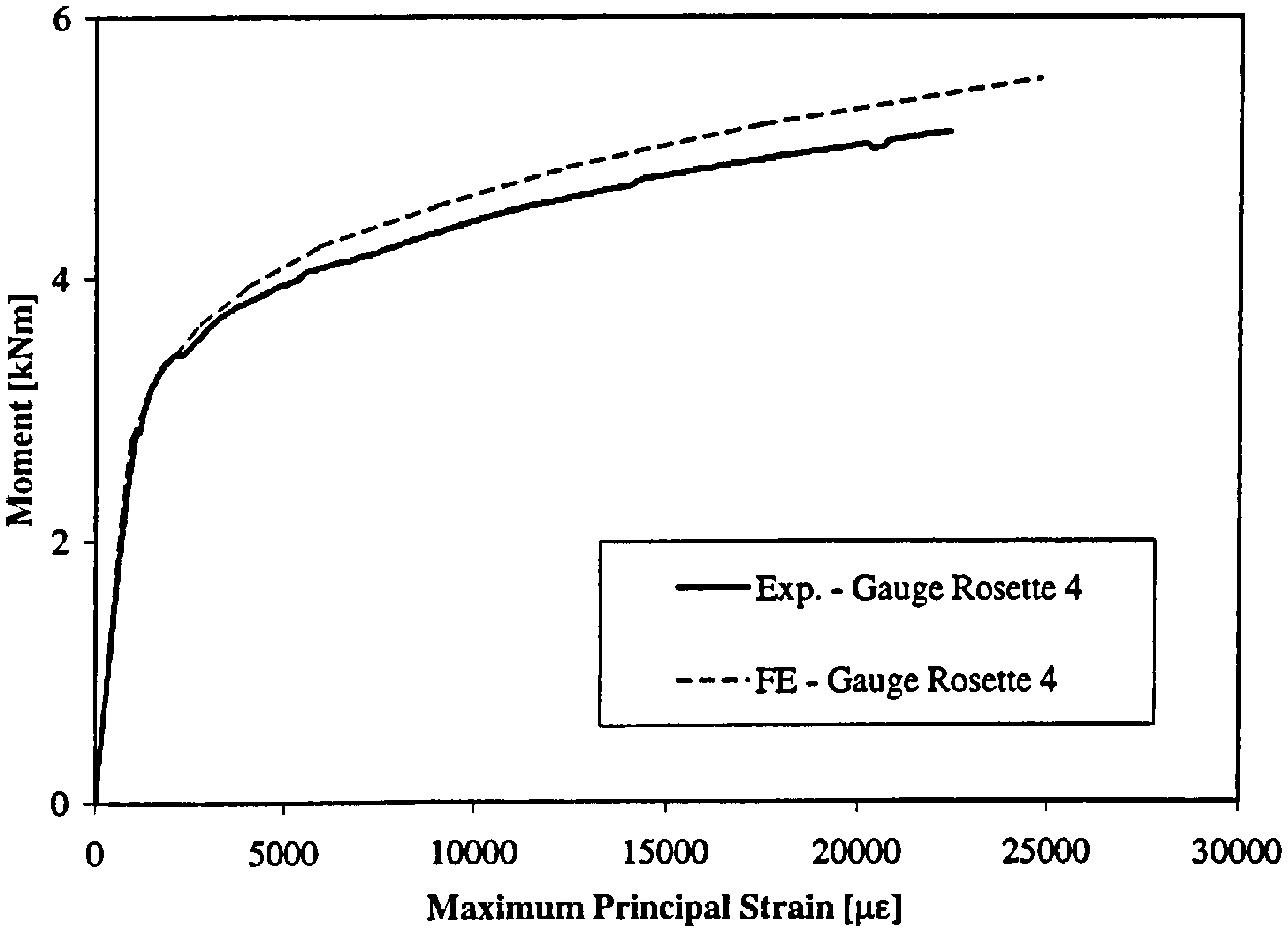

Figure 6.12: (h)TW Crack, In-Plane Bending: Moment v Gauge 4 Strain

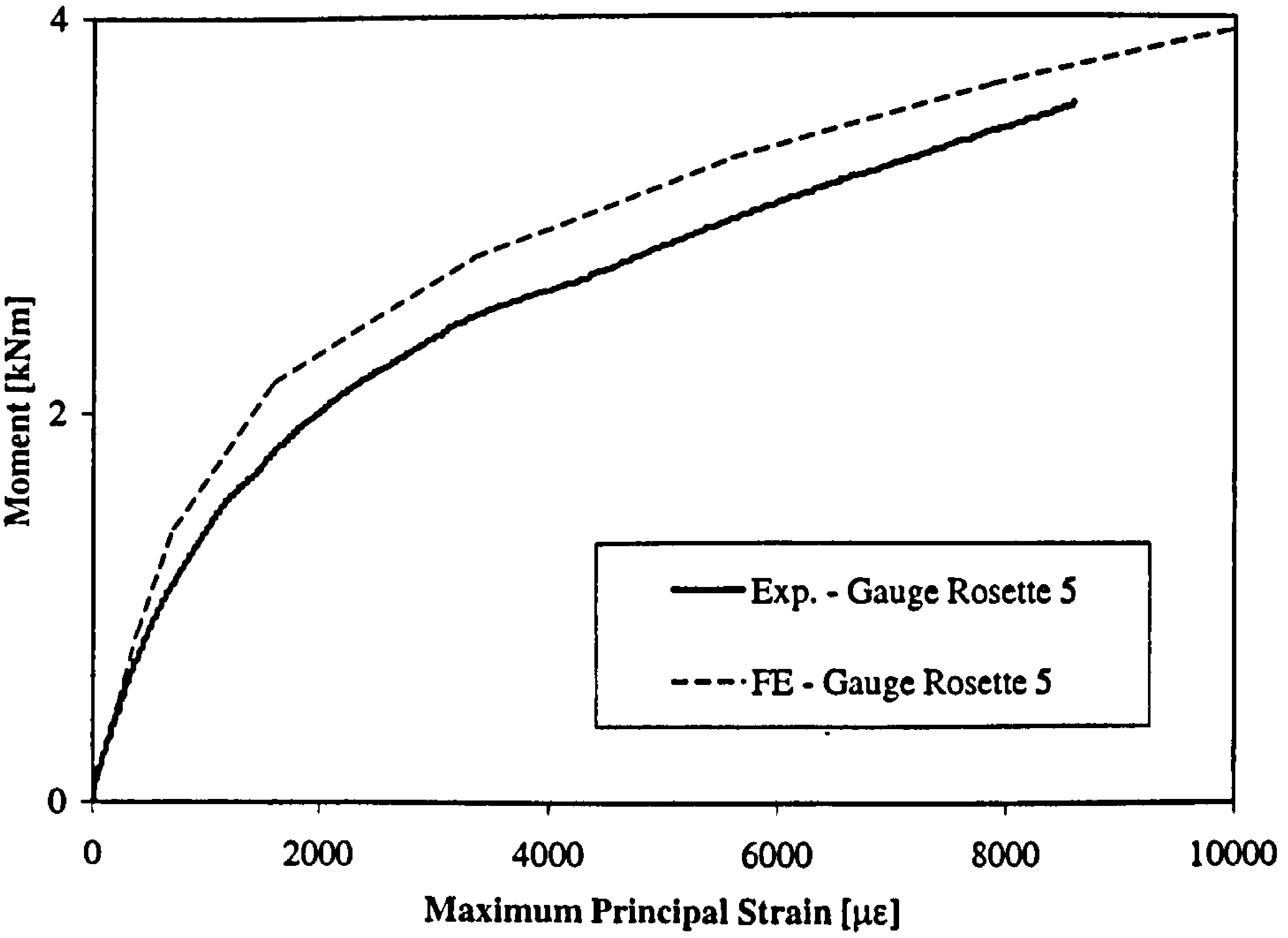

Figure 6.12: (i)TW Crack, In-Plane Bending: Moment v Gauge 5 Strain

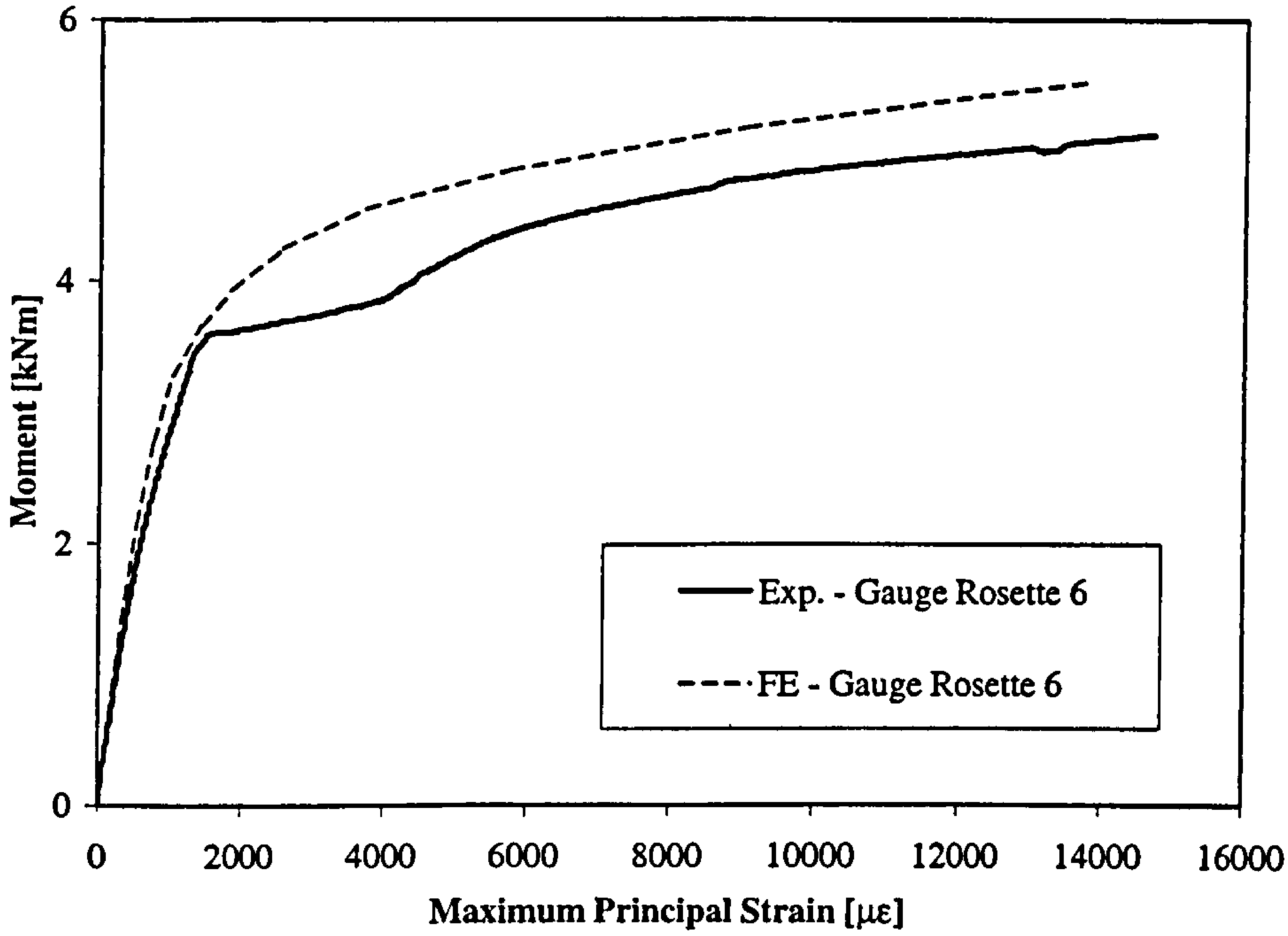

Figure 6.12: (j)TW Crack, In-Plane Bending: Moment v Gauge 6 Strain

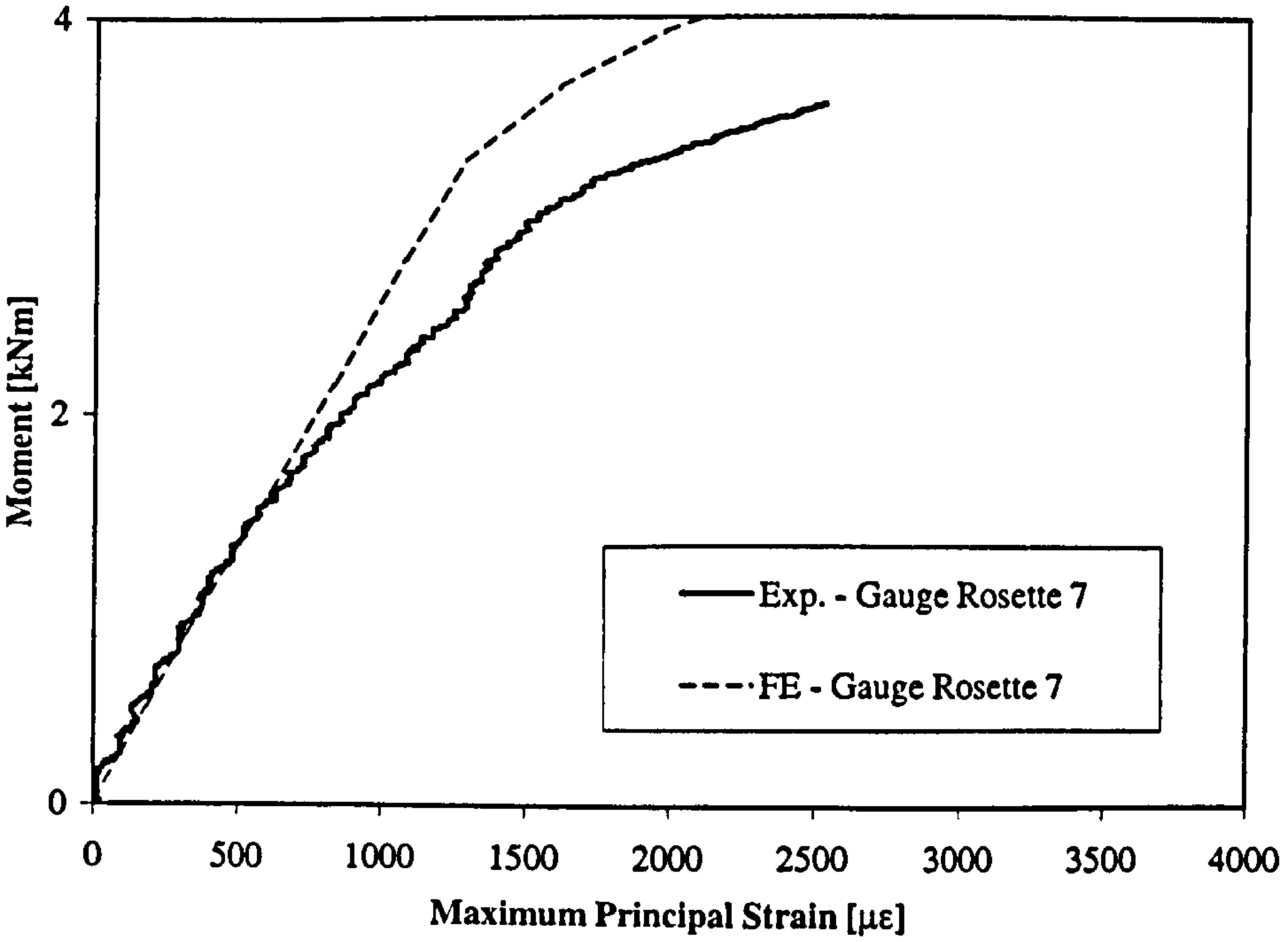

Figure 6.12: (k)TW Crack, In-Plane Bending: Moment v Gauge 7 Strain

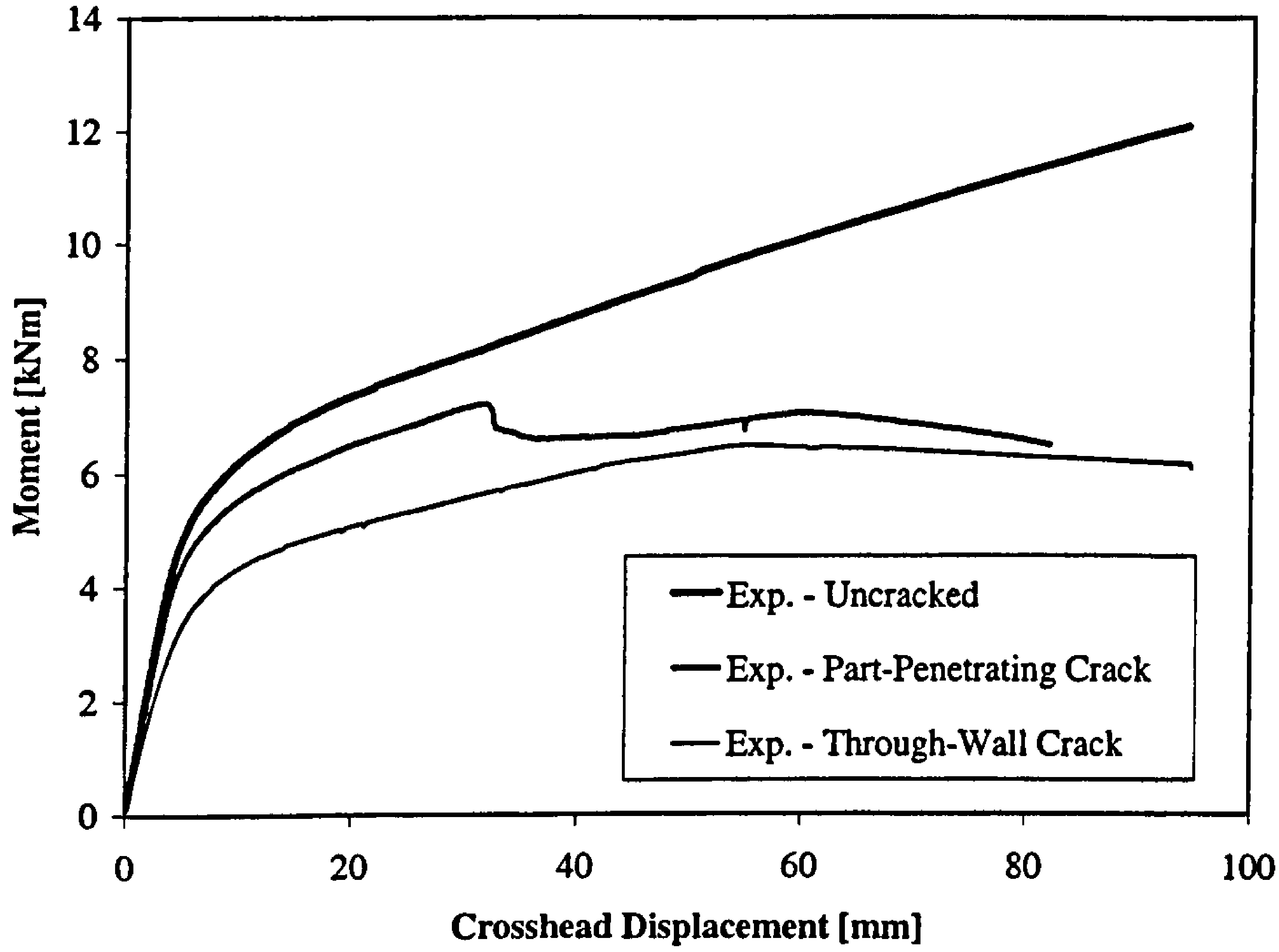

Figure 6.13: (a)Load v Crosshead Displacement: Experimental Results

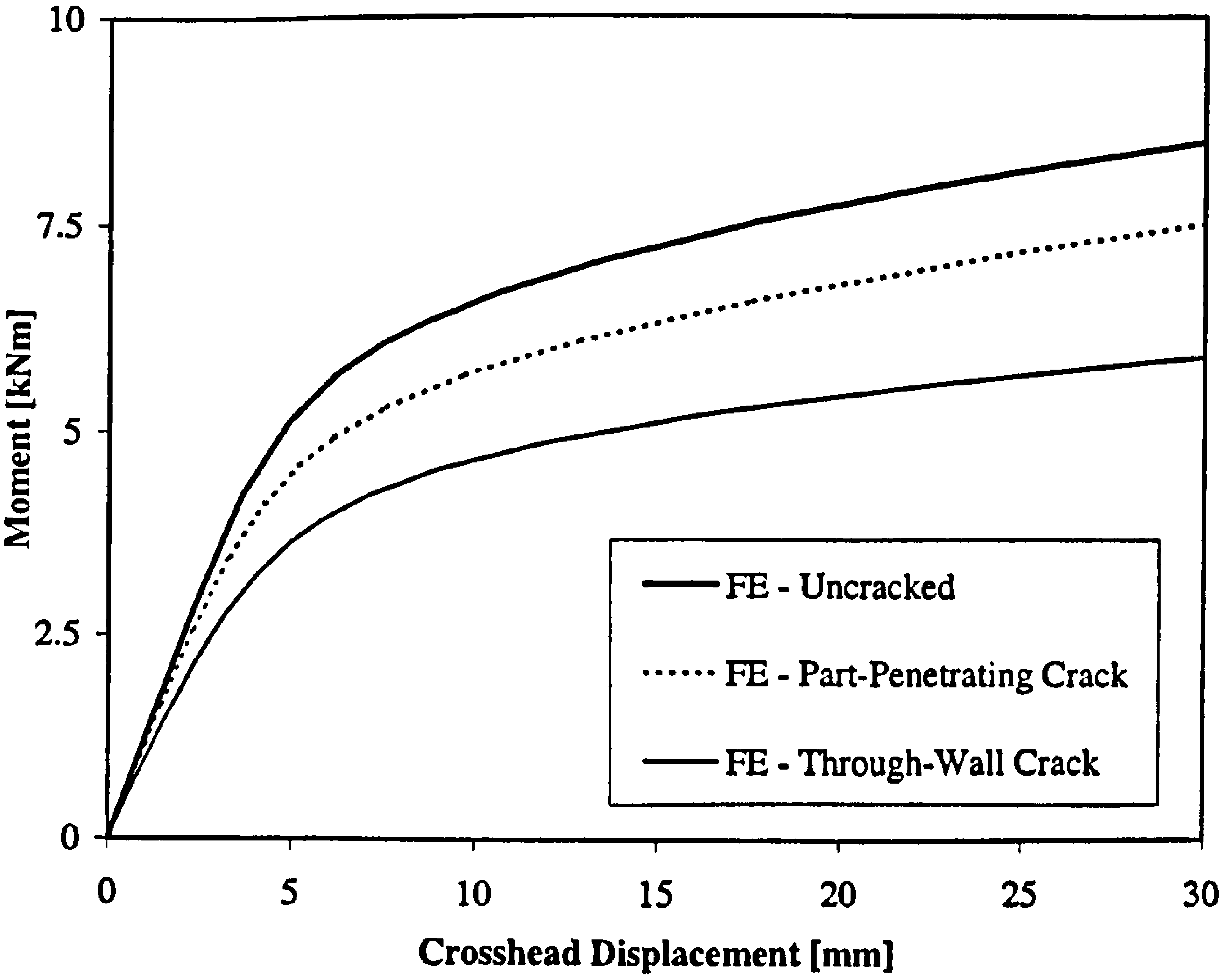

Figure 6.13: (b)Load v Crosshead Displacement: FE Results

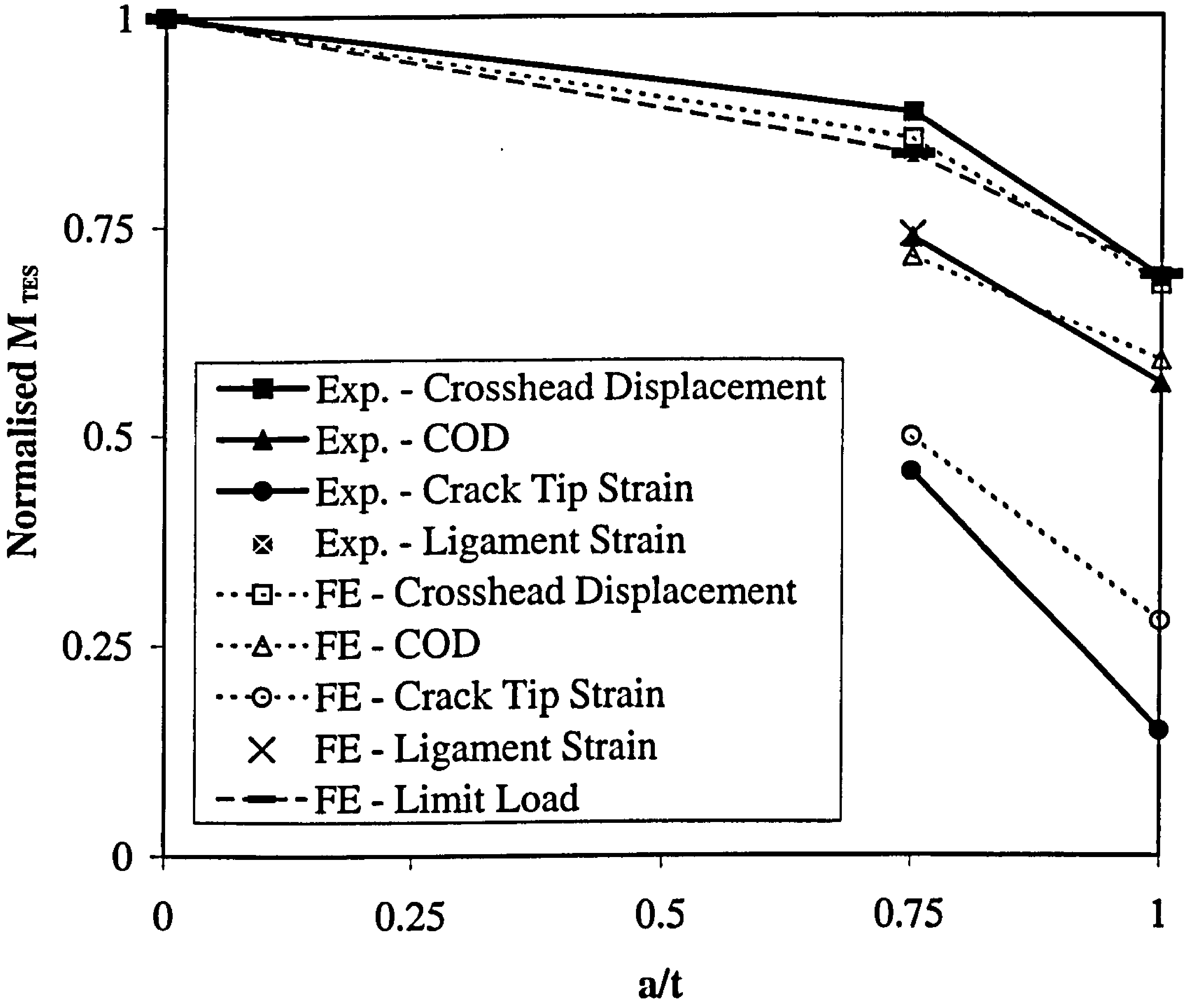

Figure 6.14: M_{TES} Results, Normalised to Respective Uncracked Values

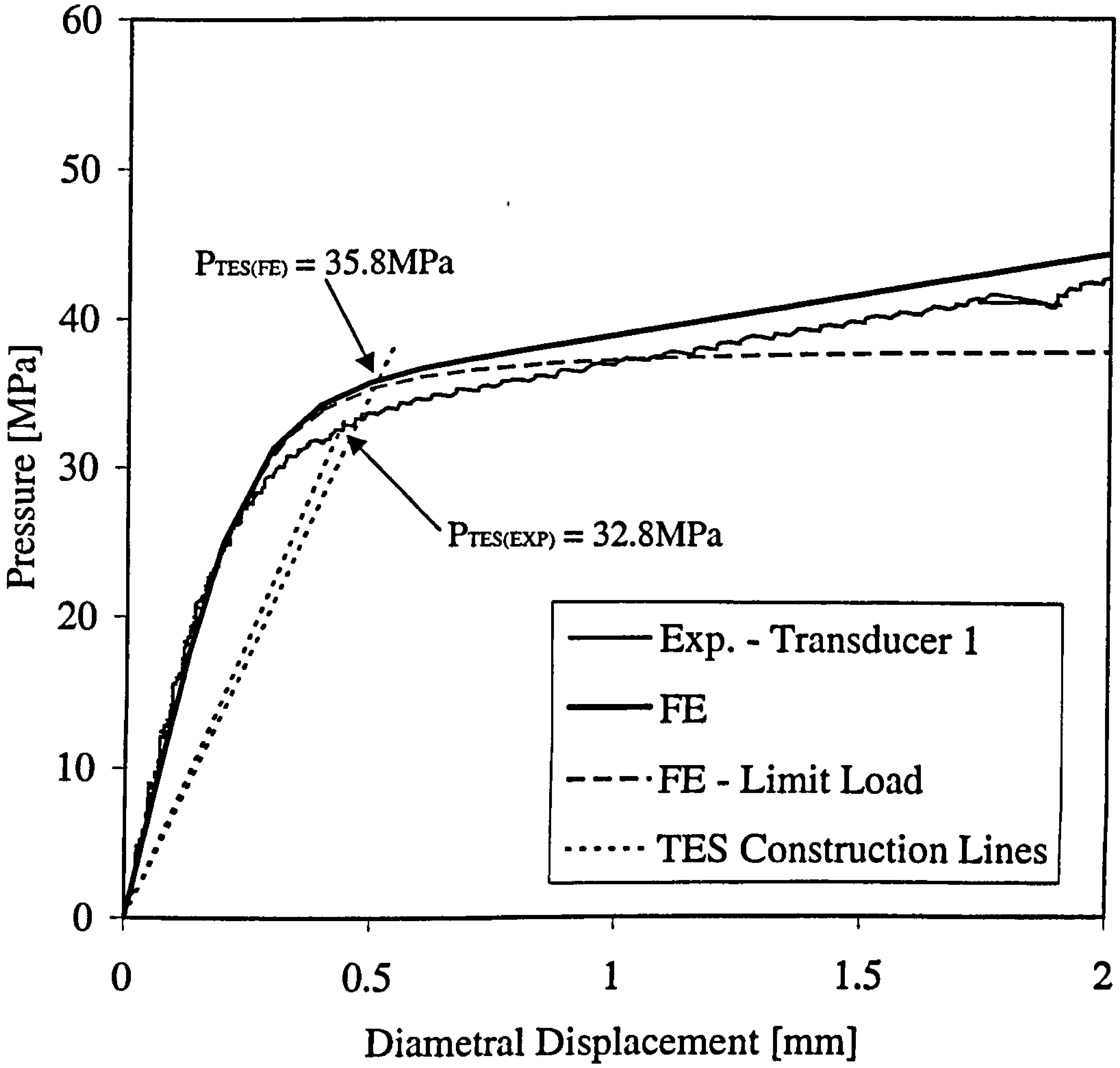

Figure 6.15: (a)Uncracked Pressure: Pressure v Diametral Displacement

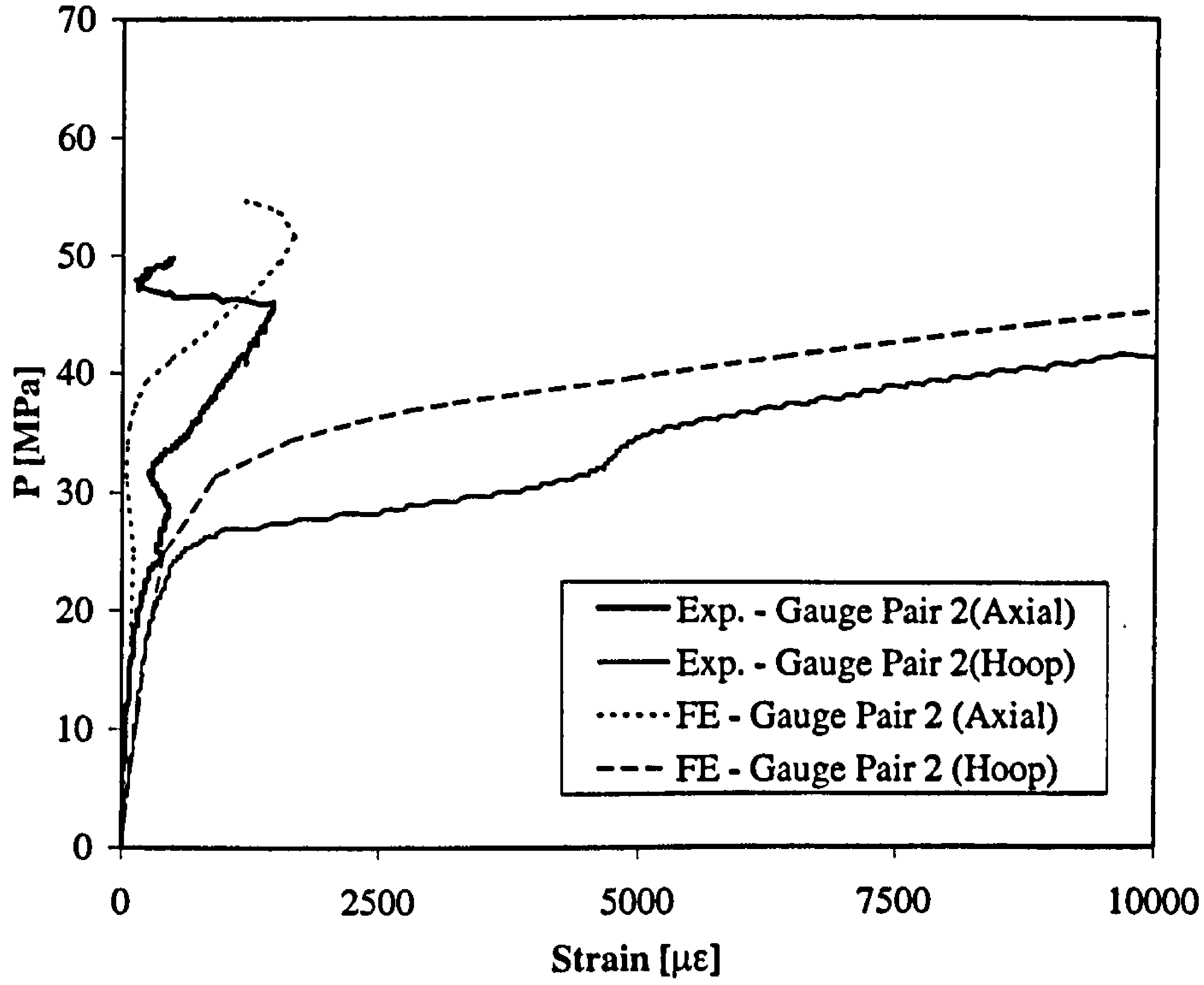

Figure 6.15: (b)Uncracked Pressure: Pressure v Crotch Strains (Gauge Pair 2)

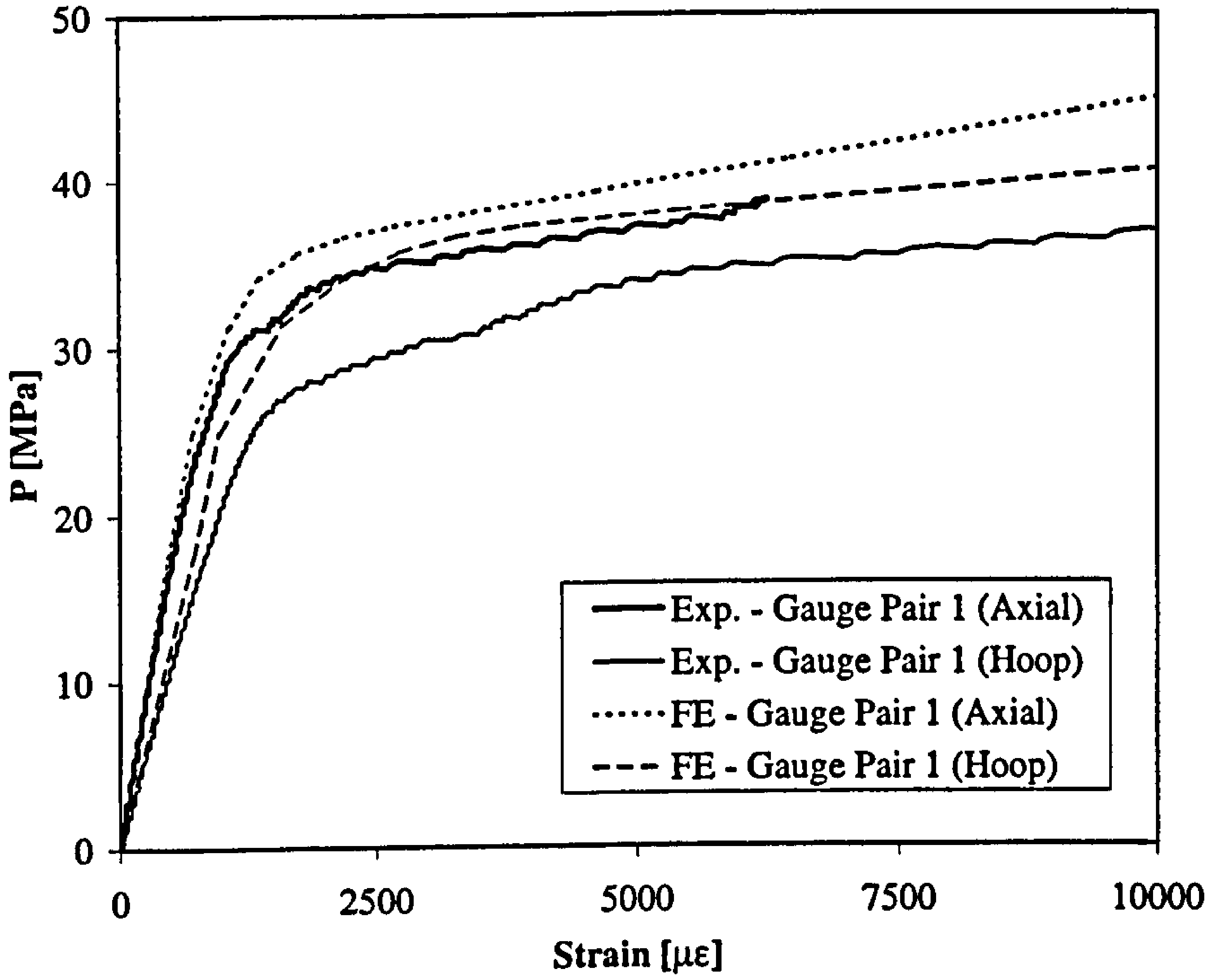

Figure 6.15: (c)Uncracked Pressure: Pressure v Flank Strains (Gauge Pair 1)

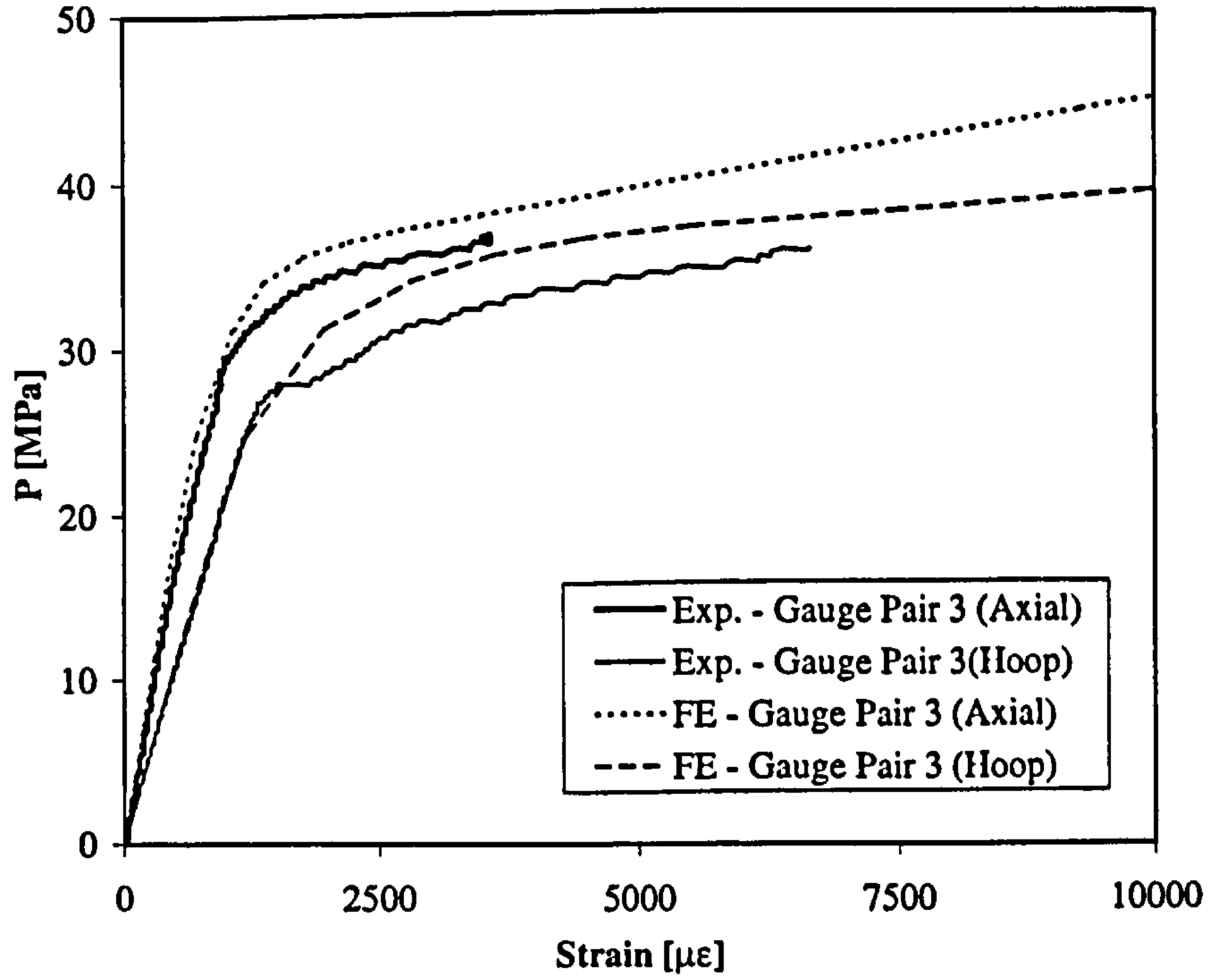

Figure 6.15: (d)Uncracked Pressure: Pressure v Flank Strains (Gauge Pair 3)

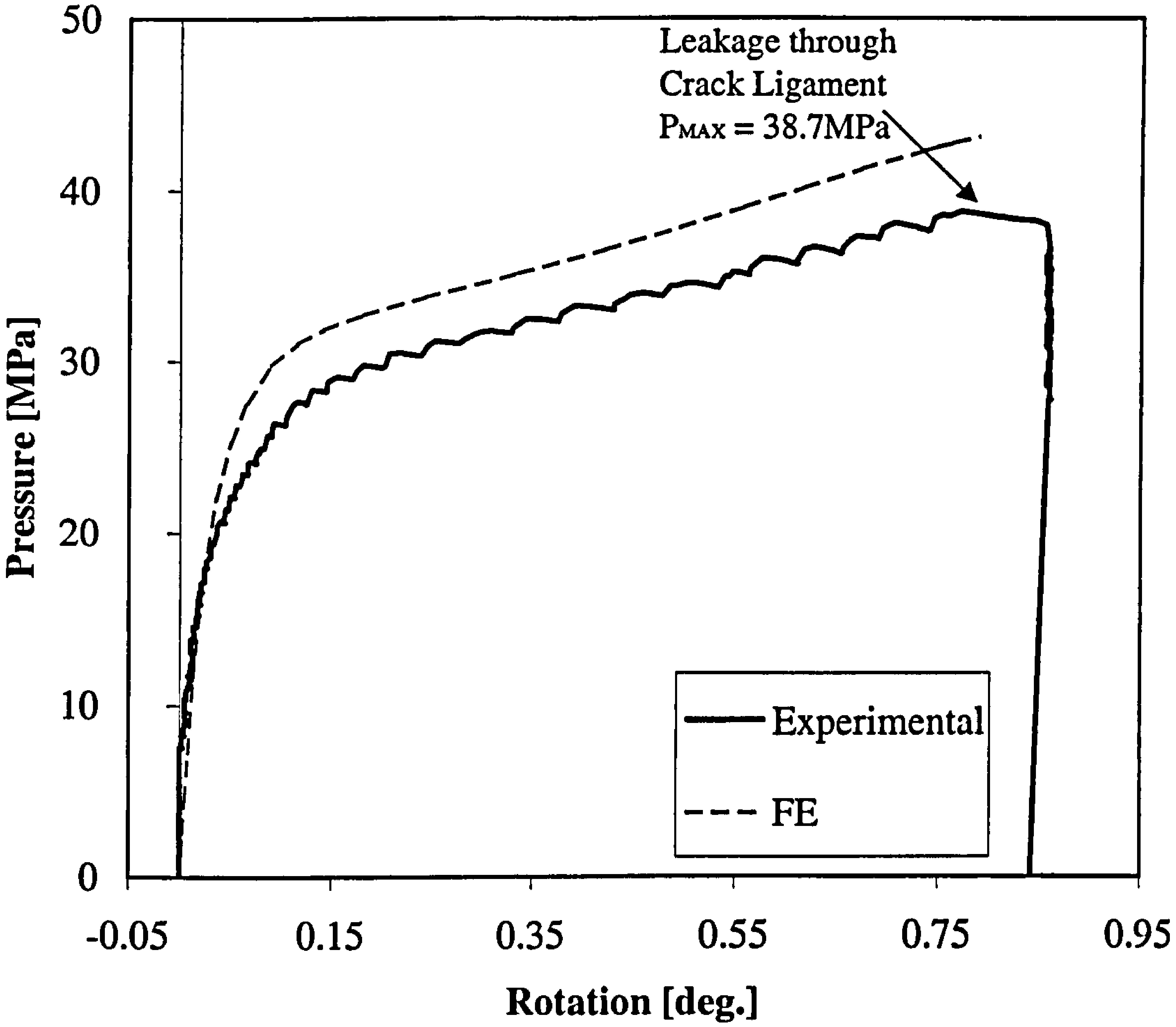

Figure 6.16: (a)PP Cracked Pressure: Pressure v Branch Pipe Rotation

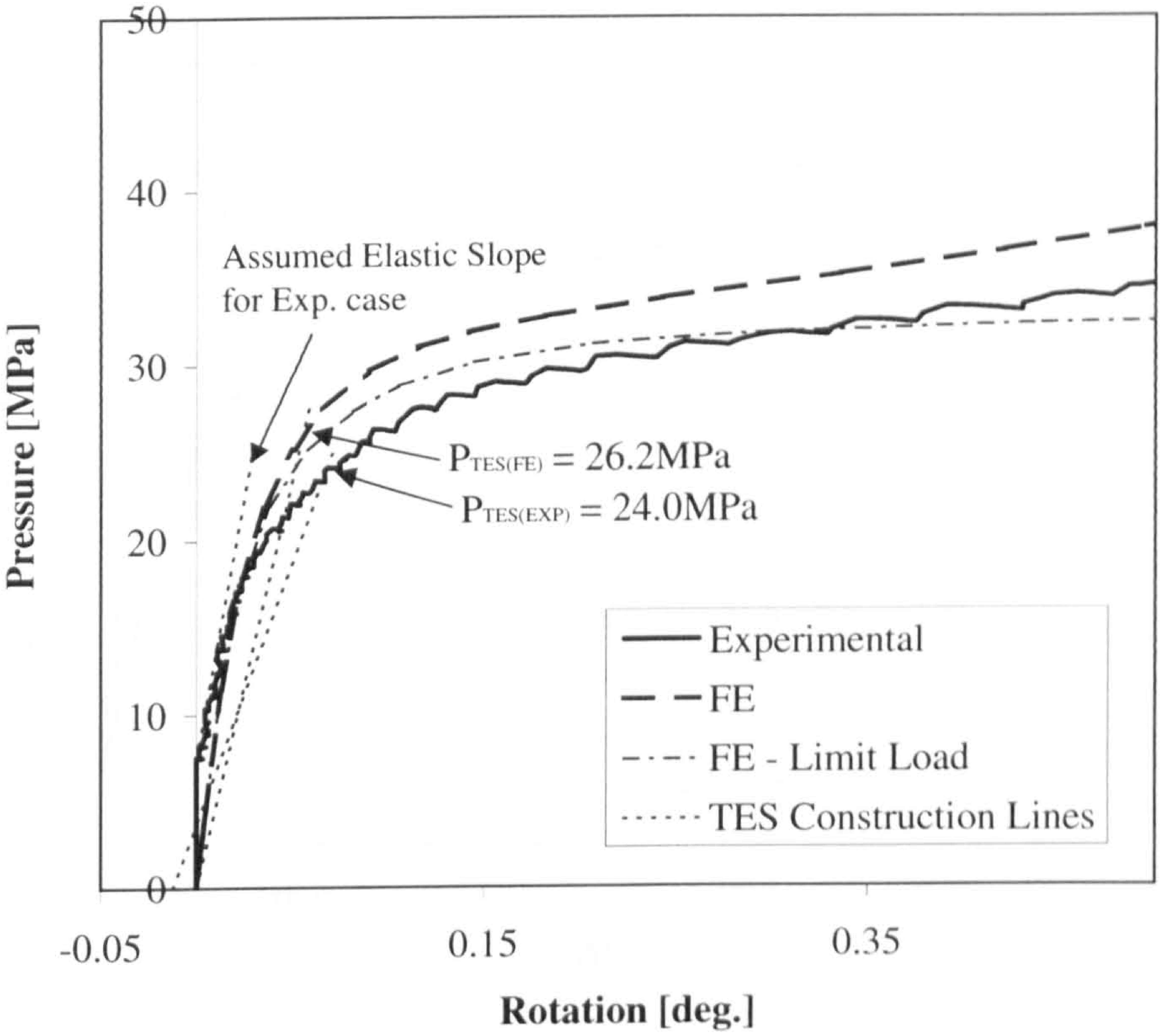

Figure 6.16: (b)PP Cracked Pressure: Pressure v Branch Pipe Rotation (P_{TES} Calculation)

Figure 6.16: (c)PP Cracked Pressure: Cross-Section of Deformed Junction

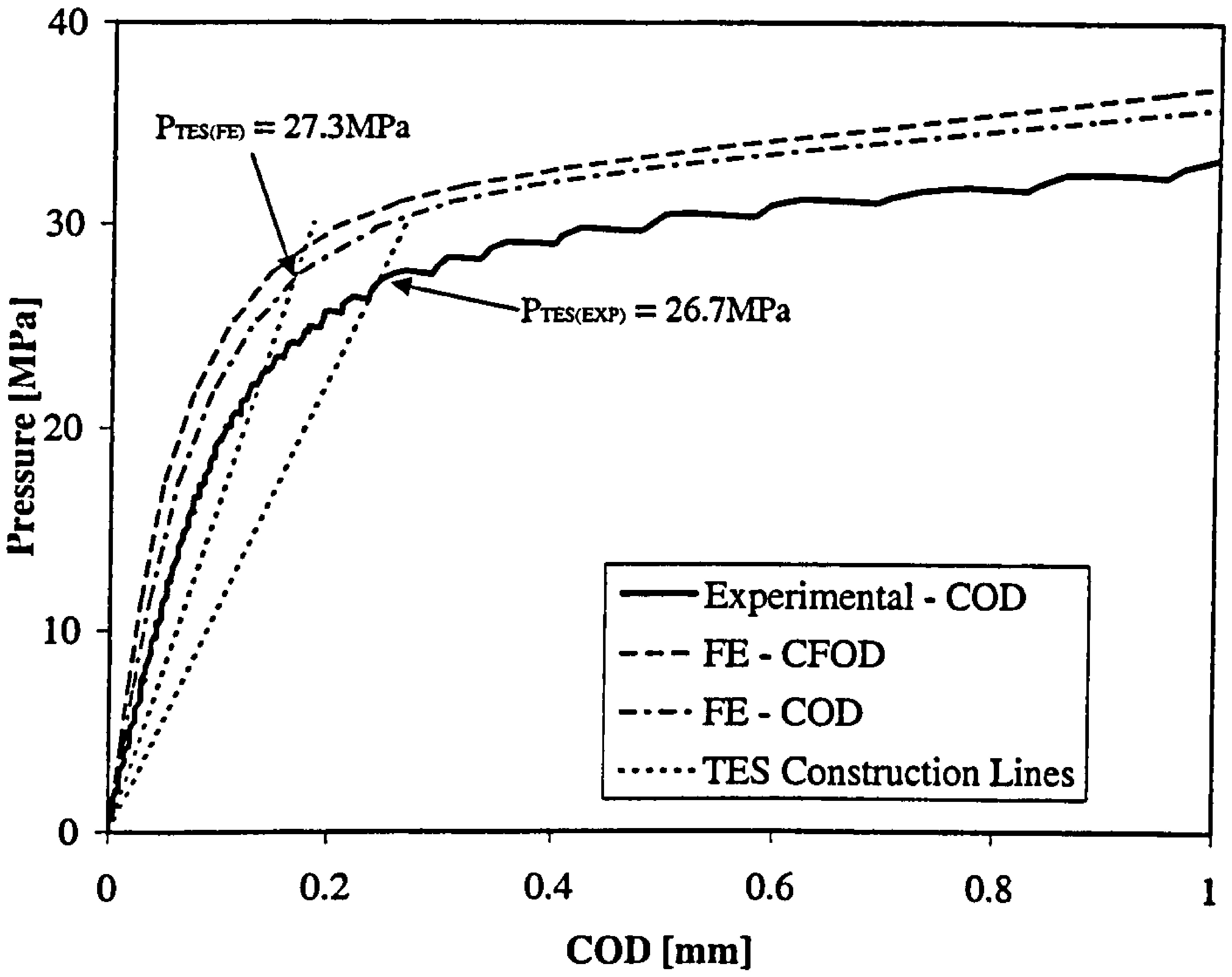

Figure 6.16: (d)PP Cracked Pressure: Pressure v COD

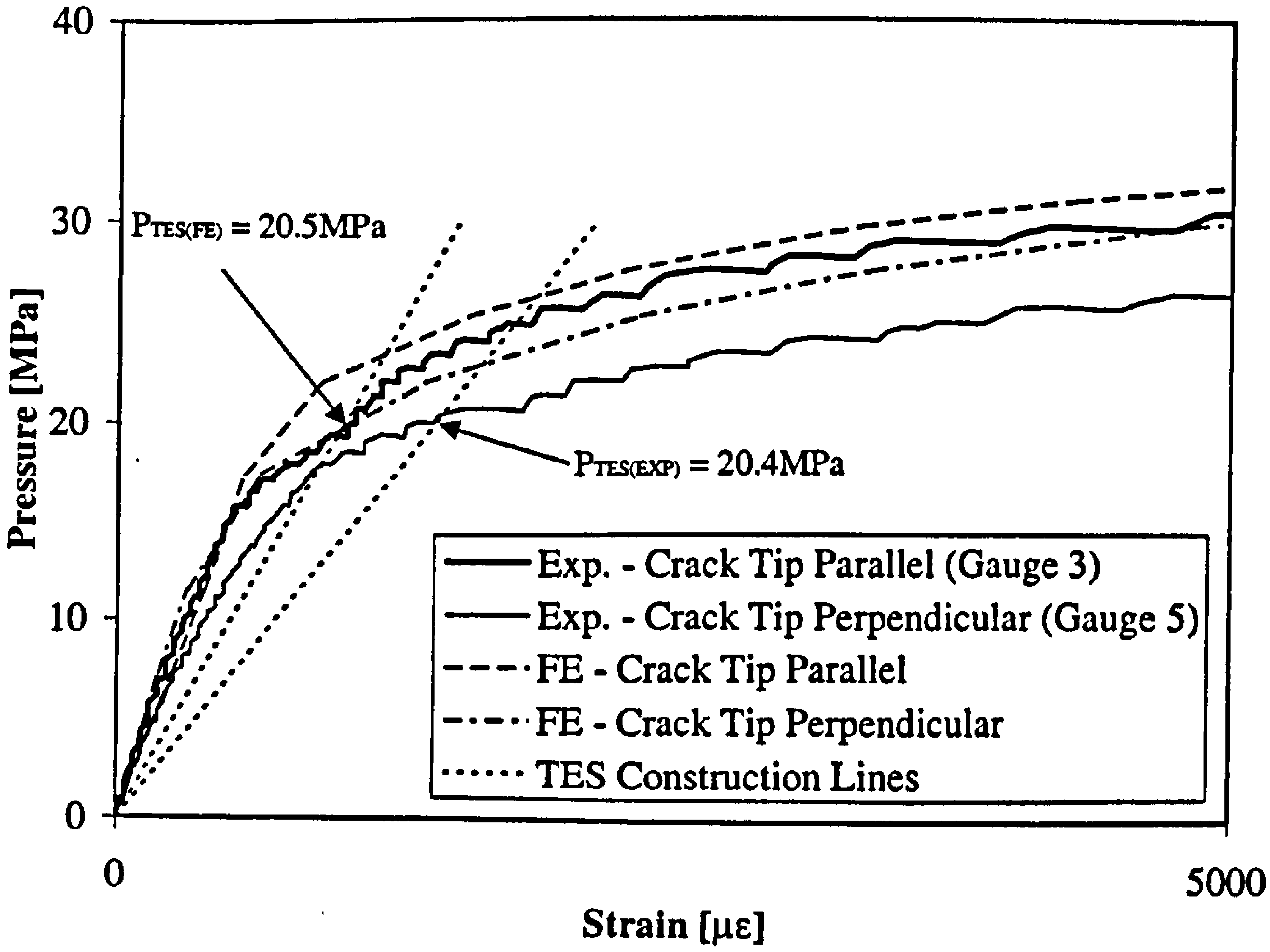

Figure 6.16: (e)PP Cracked Pressure: Pressure v Crack Tip Strains

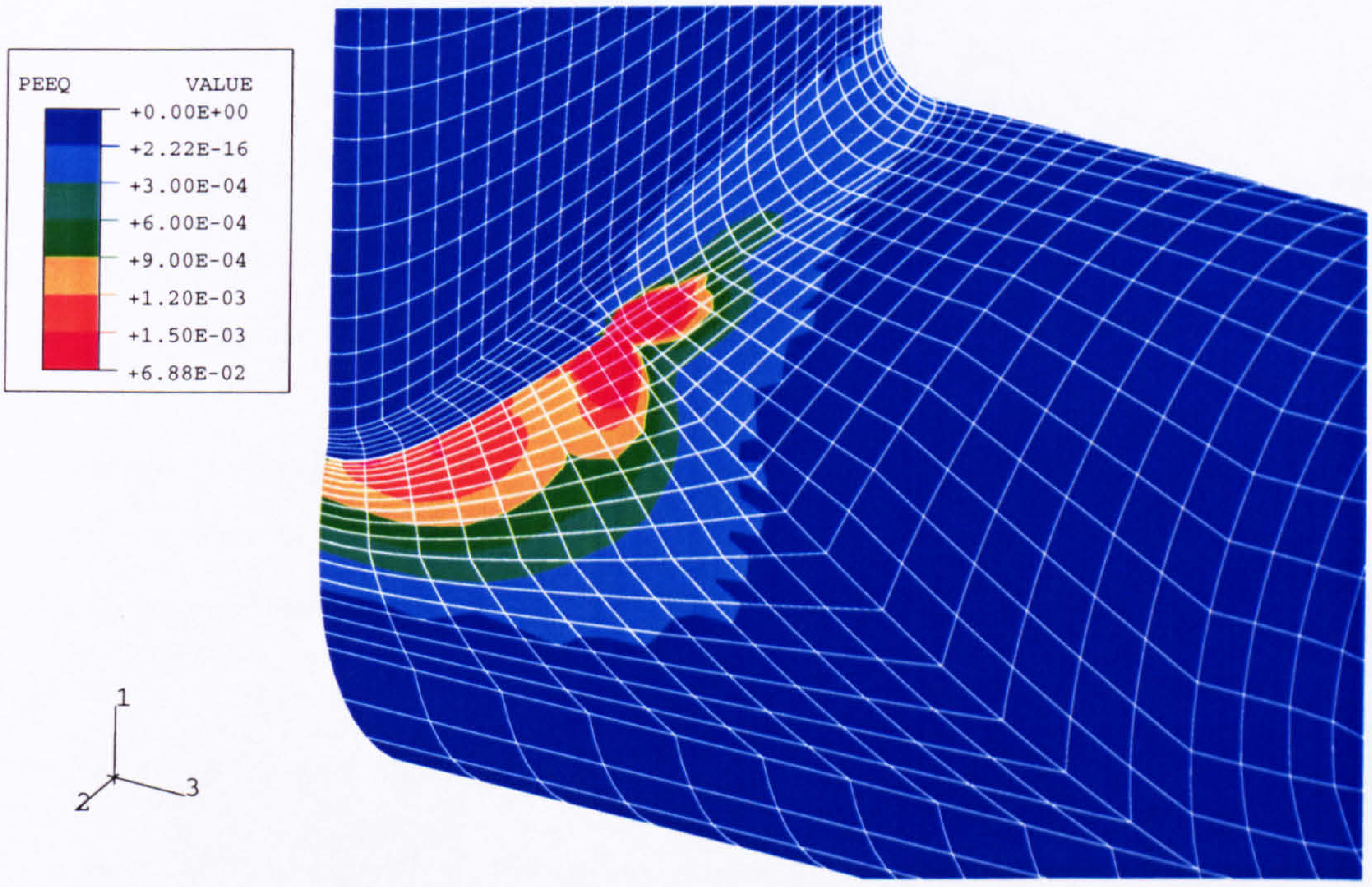

Figure 6.16: (f)PP Cracked Pressure: Equivalent Plastic Strain Distribution (P=27.6MPa)

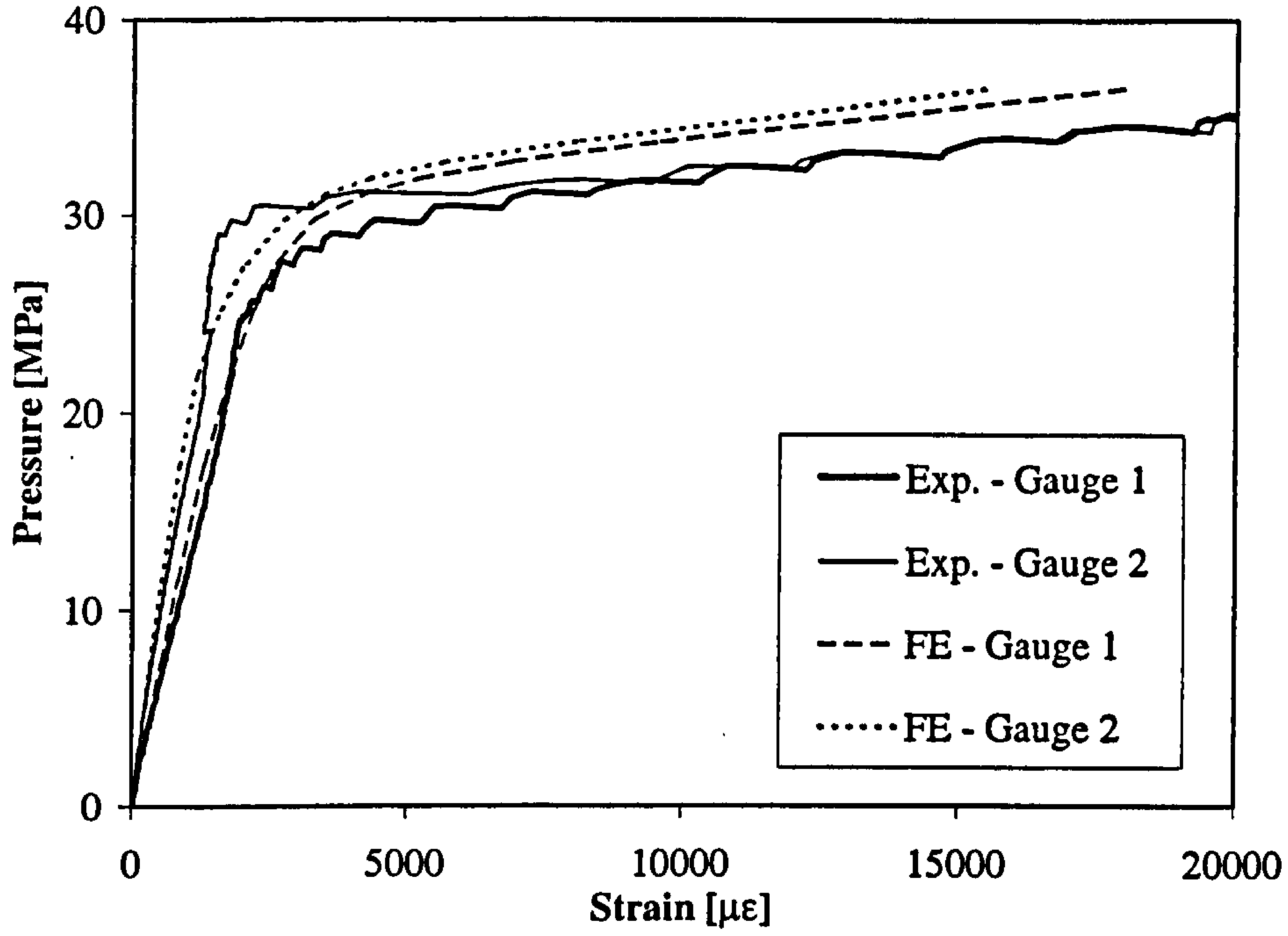

Figure 6.16: (g)PP Cracked Pressure: Pressure v Strain (Gauges 1 and 2)

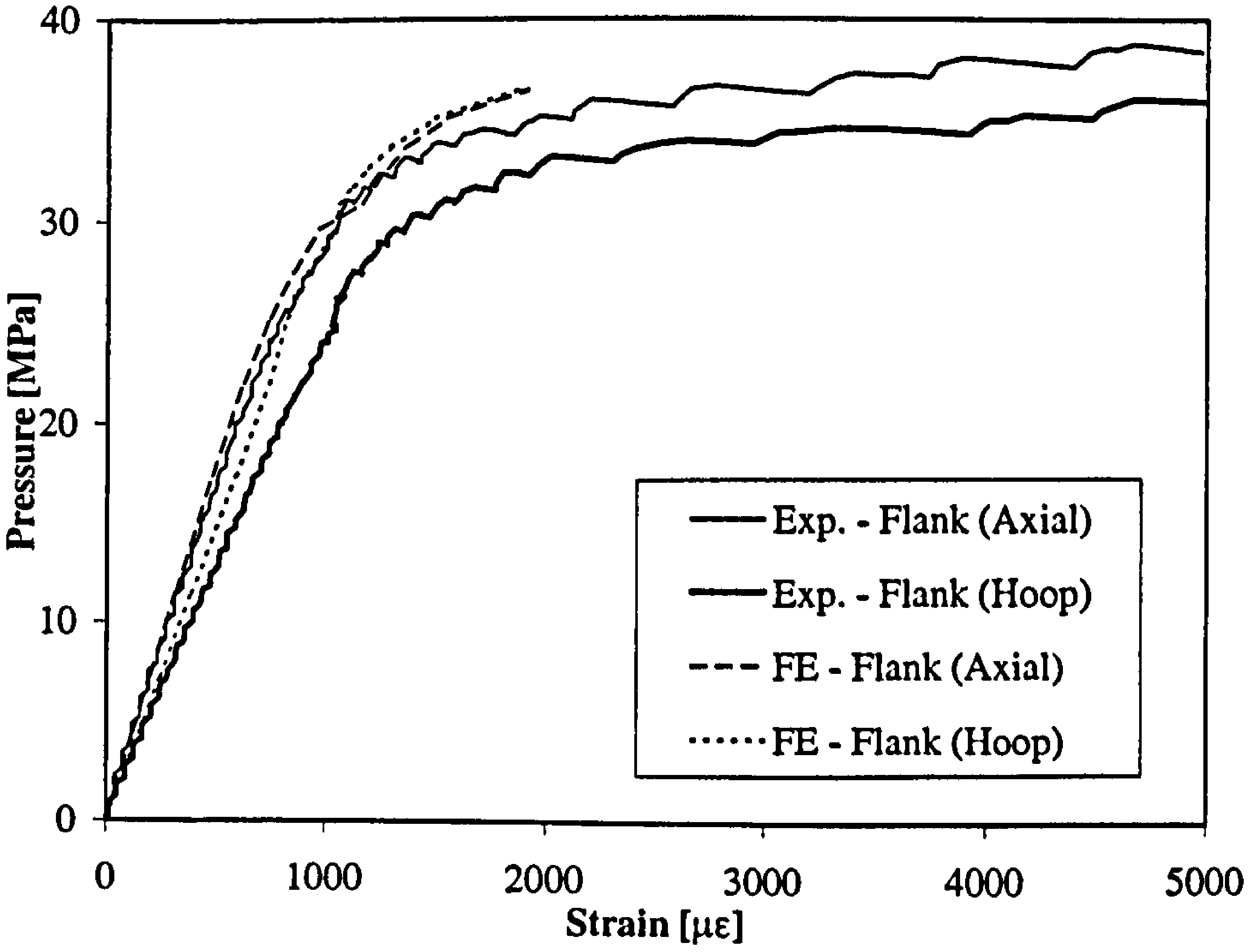

Figure 6.16: (h)PP Cracked Pressure: Pressure v Strain (Flank Gauge Pair)

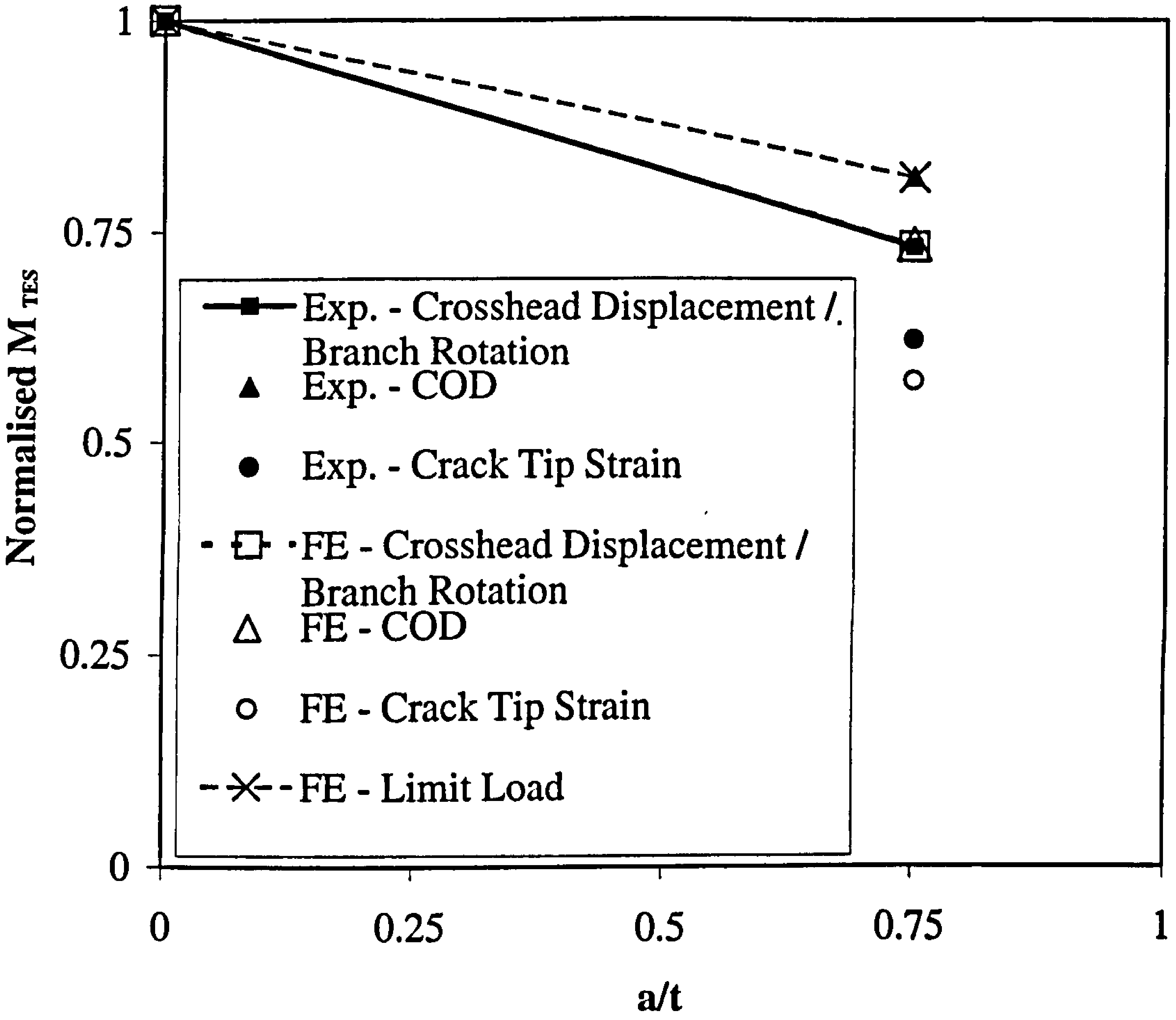

Figure 6.17: P_{TES} Results, Normalised to Respective Uncracked Values

Chapter 7

Conclusions and Future Work

This Chapter summarises the most significant observations and conclusions from the previous Chapters. Suggestions for possible future work are also provided in Section 7.5. It should be noted that the conclusions presented are based solely upon the geometric range examined for each component.

7.1 Cracked Cylinders in Tension

1. The theoretical limit load described in Section 2.2 has been verified using the results of a FE mesh convergence study. The usual net section theoretical solution was found to underestimate the limit load - there was a difference of 15.5% for cracks with $a/t \geq 0.366$.
2. The focused mesh was found to be the most economical method of evaluating the limit load accurately, in terms of number of elements used. However, a standard mesh with the elements biased towards the crack tip also gave results that were close to the theoretical limit load.
3. The overall agreement between the experimental and non-linear FE results was good, both in terms of the load-displacement response and the strain levels. The predicted FE peak strain locations agreed well with the experimental strain peaks.
4. There was a factor of approximately 1.6 between the theoretical limit load and the ultimate load for each test specimen.

7.2 Limit Loads for Uncracked Branch Junctions

Conclusions are presented below from uncracked parametric studies of branch junctions subjected to pressure and branch pipe moment loadings. Combined loading was also assessed, for pressure and out-of-plane branch bending, as part of the cracked parametric study. The conclusions for combined loading are presented alongside the cracked junction results in Section 7.3.2.

7.2.1 Pressure Loading

1. An extensive parametric study has been successfully completed, for junctions within the geometric range: $0.25 \leq d/D \leq 1.0$, $5 \leq D/T \leq 70$ and $0.25 \leq t/T \leq 1.5$.
2. Using the equations presented in Section 3.3.1 (equations (3.3) and (3.4), it is possible to estimate the limit pressure for any branch junction within the range studied.
3. Several existing methods for evaluating the limit pressure have also been compared with parametric study results. The most useful comparison methods were deemed to be the Cloud and Rodabaugh equation (equation (3.9))and the Inverse Code method (equation (3.13)) for creep rupture pressure.

7.2.2 Moment Loading

1. A limit moment study for uncracked branch junctions was carried out alongside the subsequent cracked junction study. The range of geometric parameters was more limited than that described above for pressure loading: $0.5 \leq d/D \leq 0.95$, $10 \leq D/T \leq 30$ and $t/T=1.0$. The moment loads studied were out-of-plane branch pipe bending (OPB) and in-plane branch pipe bending (IPB).
2. The limit moment solution (OPB and IPB), for junctions with $d/D \leq 0.5$ and $D/T \leq 10$, reduced to the theoretical plain pipe limit moment solution for the branch pipe.
3. For $D/T \geq 20$, the Rodabaugh solution (equation (4.7)) generally gave conservative values compared with the FE results.

4. The OPB results gave an approximate lower bound to the limit moments.

5. Curve fitting was performed using the OPB FE results, for d/D=0.5 and d/D=0.95. Two equations have been presented (equations (4.13) and (4.14)), from which a limit moment estimate can be calculated for junctions within the range $10 \leq D/T \leq 30$. Limit moments for junctions with intermediate d/D values could be estimated by linear interpolation.

6. A comparison of branch junction and tubular joint FE models showed that the additional material of the tubular joint had little effect on the limit moments for d/D=0.5. However, for components with d/D=0.95 there were considerable strengthening effects, with the limit moment for IPB being up to 37% higher than the branch junction value. The increase in limit moment was a maximum of 6% for OPB.

7.3 Limit Loads for Cracked Branch Junctions

An extensive limit load study for piping branch junctions with cracks has been presented. The geometric parameters studied were:

- d/D = 0.5, 0.75, 0.95
- D/T = 10, 20, 30
- t/T = 1.0
- Crack angle (length)
- a/t = 0.5, 0.75, 1.0

The main load cases studied were internal pressure, in-plane branch pipe bending and out-of-plane branch pipe bending. For these cases, the cracks studied were located running around junction intersections, along the lower weld toe. A small selection of junctions, with through-wall cracks, subjected to in-plane run pipe bending were also evaluated. However, these junctions exhibited little reduction in limit moment, even for large cracks.

7.3.1 Single Loading

1. The reduction in limit load for through-wall cracks was generally similar, with respect to crack angle, for in-plane branch pipe bending, out-of-plane branch pipe bending, and pressure loading.

2. For part-penetrating cracks, there was a clear reduction from the uncracked limit load for all junctions studied, with the exception of the junctions with d/D=0.5 and D/T=10 subjected to in-plane branch pipe bending. These junctions showed no reduction in limit load for part-penetrating cracks.

3. For branch pipe moment loadings, the ratio of the theoretical limit moment solution, for a plain pipe with a circumferential crack (see equations (4.17) and (4.18)), to the corresponding uncracked plain pipe solution (equation (4.3)) has been shown to be similar to the cracked to uncracked limit load ratio for branch junctions. The limit load relationship was relationship used was:

   $$\frac{F_L\,(Cracked\ Branch\ Junction)}{F_L\,(Uncracked\ Branch\ Junction)} = \frac{M_L\,(Cracked\ Plain\ Pipe)}{M_L\,(Uncracked\ Plain\ Pipe)} \qquad (7.1)$$

   This resulted in limit moment estimates for branch junctions with cracks around the branch pipe intersection. The use of this relationship relies on accurate estimation of the limit load for the relevant uncracked branch junction. Good agreement was found for FE results from through-wall and part-penetrating cracks.

4. The cracked plain pipe limit pressure solution, assuming an axial crack in the run pipe, did not give good agreement with the FE results. However, because the limit load reduction for pressure was similar to that for moment loads with similar cracks, the use of the scaling factor from the plain pipe limit moment equations, as described in equation (7.1), could also be used to provide a lower bound limit pressure estimate.

7.3.2 Combined Loading

1. Limit load interaction diagrams have been presented for pressure versus out-of-plane branch pipe bending. The cracked junctions analysed were all through-wall

cracked junctions, with the geometric parameters: d/D=0.5 or 0.95 and D/T=10, 20 or 30. The corresponding uncracked junctions were also analysed.

2. The uncracked limit load results exhibited essentially circular interaction.
3. For the cracked junctions, there was a distinct trend towards linear interaction as the crack angle extended.

7.4 Experimental Study for Branch Junctions

The experimental study was intended to provide confidence in the aforementioned limit load FE results, by validating the FE techniques used with experimental data. A series of five components were tested, for pressure loading and in-plane branch pipe bending. The nominal dimensions specified were the same for all components, with d/D=0.95, D/T=10 and t/T=1.0. An uncracked component was tested for each load case, followed by three cracked components with a/t=1.0 or a/t=0.75. The conclusions from this study are presented below.

1. Branch junctions were successfully machined from solid billets of material, using CNC machining. Electrodes were machined for the insertion of cracks into three of the junctions. This was performed using EDM techniques, resulting in cracks with negligible variation from the nominal dimensions.
2. The FE models for the machined junctions required the inclusion of the curved intersection to achieve good agreement with the experimental results.
3. Tensile tests should be performed at a similar strain rate to that used for testing the branch junctions.
4. The comparison between the FE and experimental results was generally good. The global plastic loads obtained from the experimental results were always within 9.2% of the FE predicted plastic loads. The agreement was particularly good for the bending cases, which were all within 5.1%.
5. For local plastic loads, the crack opening displacement (COD) gave useful results for the bending tests, but not for the pressurised crack test. The ligament strain

value was also shown to give a good indication of ligament collapse for part-penetrating cracks. The crack tip strain results gave good agreement for the pressure case.

6. The primary objective of the experimental work was to instill confidence in the limit load results presented previously. This objective has been fulfilled.

7.5 Recommendations for Future Work

- The scope of the uncracked branch junction limit load studies should be expanded to incorporate the remaining branch junction moment loads, and to extend the existing uncracked moment load data. The existing FE models of the pressure study in Chapter 3 provide a basis from which half and full FE models could be created, as required.

- The recommendations for the assessment of cracked branch junctions, summarised above, may be applicable for limit loads of junctions outside the parametric range analysed. The parametric limits of applicability should be checked by creating and analysing a selection of junctions outside this range.

- Other common crack locations should be assessed using similar techniques. For example, there is sparse data for limit pressures for junctions with crotch corner cracks.

- Crack opening areas could be calculated from the existing FE models, in order to contribute to the 'leak-before-break analysis' requirements of the R6 procedure [1].

- The existing cracked junction models should be re-analysed to derive 'J-integral' values, thus addressing the fracture mechanics aspect of the R6 procedure [1]. Sub-modelling techniques could be used to refine the FE mesh at the crack location, if necessary.

References

[1] I. Milne, R.A. Ainsworth, A.R. Dowling, and A.T. Stewart. Assessment of the Integrity of Structures Containing Defects. *British Energy Generation Ltd, Document Ref. R/H/R6, Revision 3*, 2000.

[2] A.R. Dowling and S.H.A. Townley. The Effect of Defects on Structural Failure: A Two-Criteria Approach. *Int. J. Pressure Vessels and Piping*, 3:77–107, 1975.

[3] J.C. Gerdeen. *A Critical Evaluation of Plastic Behaviour data and a United Definition of Plastic Loads for Pressure Components.* PVRC Welding Research Council bulletin 254, 1979.

[4] C.R. Calladine. *Plasticity for Engineers.* Ellis Horwood Ltd., Chichester, UK, 1985.

[5] K. Yahiaoui, D.G. Moffat, and D.N. Moreton. The Collapse Behaviour of a Forged Piping Branch Junction under Internal Pressure. *9th Int. Conf. Pressure Vessel Technology, Sydney*, 2000.

[6] SST Systems Inc. *CAEPIPE, Version 5.02H, San Jose, California, USA.*

[7] D.G. Moffat. Experimental Stress Analysis of Four Fabricated Equal Diameter Branch Pipe Intersections Subjected to Moment Loadings and the Implications on Branch Junction Design. *Proc. Instn. Mech. Engrs A*, 199(4):261–284, 1985.

[8] D.G. Moffat, J.A.M. Mwenifumbo, S.H. Xu, and J. Mistry. Effective Stress Factors Due to Internal Pressure and External Moment Loads. *Journal of Strain Analysis*, 26(2):85–101, 1989.

[9] J. Decock. Determination of Stress Concentration Factors and Fatigue Assessment of Flush and Extruded Nozzles in Welded Pressure Vessels. *Proc. Second Int. Conf. Pressure Vessel Technology, Part II, ASME*, pages 821–835, 1973.

[10] K. Yahiaoui, D.G. Moffat, and D.N. Moreton. Single Frequency Seismic Loading Tests on Pressurised Branch Pipe Intersections Machined from Solid. *Journal of Strain Analysis*, 28(3):197–207, 1993.

[11] M.G. Kirkwood. *Plastic Loads for Branch Pipe Junctions Subjected to Combined Internal Pressure and In-Plane Moments.* PhD Thesis, University of Liverpool, 1989.

[12] *CEN Draft European Standard, prEN 13445-3, Unfired Pressure Vessels-Part 3: Design.* Draft European Standard, 1999.

[13] D.G. Moffat, M.F. Hsieh, and M.A. Lynch. An Assessment of ASME III and CEN TC54 Methods of Determining Plastic and Limit Loads for Pressure System Components. *Journal of Strain Analysis*, 36(3):301–313, 2001.

[14] *ASME Boiler and Pressure Code, Section III, Division 1, Subsection NB.* New York, 1998.

[15] M.F. Hsieh, D.G. Moffat, and J. Mistry. Nozzles in the Knuckle Region of a Torispherical Head: Limit Load Interaction under Combined Pressure and Piping Loads. *9th Int. Conf. Pressure Vessel Technology, Sydney*, 2000.

[16] K. Yahiaoui, D.G. Moffat, and D.N. Moreton. Experimental Plastic Loads of Cracked Plain Pipes Subjected to Internal Pressure and Bending. *Proc. 8th Int. Conf. Pressure Vessels and Piping, ASME*, 404:55–69, 2000.

[17] K. Yahiaoui, D.G. Moffat, and D.N. Moreton. Piping Elbows with Cracks. Part 1: A Parametric Study of the Influence of Crack Size on Limit Loads due to Pressure and Opening Bending. *Journal of Strain Analysis*, 35(1):35–46, 2000.

[18] K. Yahiaoui, D.G. Moffat, and D.N. Moreton. Piping Elbows with Cracks. Part2: Global Finite Element and Experimental Plastic Loads under Opening Bending. *Journal of Strain Analysis*, 35(1):47–57, 2000.

[19] K. Yahiaoui, D.G. Moffat, and D.N. Moreton. Plastic Loads of Cracked Forged Piping Branch Junctions: Experimental Results and Comparison with Numerical Data. *Int. Journal of Pressure Vessels and Piping*, 77:249–260, 2000.

[20] A.G. Miller. Review of Limit Loads of Structures Containing Defects. *Int. Journal Pressure Vessels and Piping*, 32:191–327, 1988.

[21] M.R. Jones and J.M. Eshelby. Limit Solutions for Circumferentially Cracked Cylinders under Internal Pressure and Combined Tension and Bending. *Nuclear Electric Technology Division Report, TD/SID/REP/0032, Barnwood, Gloucester, UK*, 1990.

[22] S. Al Laham. Stress Intensity Factor and Limit Load Handbook (SINTAP Compendium). *Nuclear Electric Report EPD/GEN/REP/0316/98, Issue 2.*

[23] D.G. Moffat, J. Mistry, and S.E. Moore. Effective Stress Factor Correlation Equations for Piping Branch Junctions under Internal Pressure Loading. *ASME J. of Pressure Vessel Technology*, 121:121–126, 1999.

[24] J.S. Blair. Reinforcement on Branch Pieces. *Engineering, London*, 1947.

[25] R.L. Cloud and E.C. Rodabaugh. Approximate Analysis of the Plastic Limit Pressure of Nozzles in Cylindrical Shells. *Trans. ASME, J. Eng. Power*, 90:171–176, 1968.

[26] E.C. Rodabaugh and R.L. Cloud. Assessment of the Plastic Strength of Pressure Vessel Nozzles. *Trans. ASME, J. Eng. for Industry.*

[27] E.C. Rodabaugh. A Review of Area Replacement Rules for Pipe Connections in Pressure Vessels and Piping. *WRC Bulletin 335*, 1998.

[28] J. Schroeder and P. Rangarajan. Upper Bounds to Limit Pressures of Branch Pipe Lateral Connections. Part I: Bounds for Branch/Pipe Diameter Ratios Smaller than 0.7. *ASME Paper No. 71-PVP-44, Pressure Vessel and Piping Conf., San Francisco, California*, 1971.

[29] F. Ellyin and N. Turkkan. Lower Bound to Limit Pressure of Nozzle-to-cylindrical Shell Attachment. *ASME Paper No. 71-PVP-38, Pressure Vessel and Piping Conf., San Francisco, California*, 1971.

[30] M. Robinson. Lower-Bound Limit Pressures for the Cylinder-Cylinder Intersection: A Parametric Survey. *Trans. ASME J. Press. Vess. Technology*, 100:65–73, 1978.

[31] C.J. Tabone and H.R. Mallet. Pressure-plus-moment Limit Load Analysis for a Cylindrical Shell Nozzle. *Proc. Pressure Vessels and Piping, San Diego, California, ASME*, 120:131-136, 1987.

[32] M.G. Kirkwood and D.G. Moffat. Plastic Loads for Piping Branch Junctions subjected to Combined Pressure and In-plane Moment Loads. *I.Mech.E. Procs. E., J. Mechanical Process Engineering*, 208:31–43, 1994.

[33] Z.F. Sang, L.P. Xue, Y.J. Lin, and G.E.O. Widera. Limit and Burst Pressures of Cylindrical Shell Intersections with a Large Diameter Ratio. *9th Int. Conf. on Pressure Vessel Technology, Sydney*, 2000.

[34] A. Zahoor. Ductile Fracture Handbook. *Electric Power Institute, Palo Alto, CA - Report EPRI NP-6301-D/N14*, 1-3, 1991.

[35] Calculation of Reference Stresses and Stress Intensity Factors. *Assessment Procedure R5, Volume 7 Issue 2, Appendix A3 (draft)*, 2000.

[36] P.J. Budden and I.W. Goodall. Creep Life of Pressure Vessel Branch Connections: The Reference Stress Approach. *Nuclear Electric Report TD/SID/REP/0123*, 1990.

[37] S.J. Booth. The Calculation of Operating Stresses at Branches and End Caps for Use in GOM101 Creep Life Assessments. *CEGB Report SWR/SSD/0447/N/84*, 1984.

[38] D. Galt. Parametric Study of Limit Pressures for Cylinder-Cylinder Intersection. *Babcock Energy Ltd. Report, SES/44/BNL/78221/D001*, 1992.

[39] J. Schroeder and P. Rangarajan. Part I - Upper Bounds to In-plane and Out-of-plane Limit Couples Applied to the Branch for Branch/Pipe Diameter Ratios Smaller than 0.8. *Proc. Second ASME Int. Conf. Pressure vessel Technology, Part 1, Design and Analysis, San Antonio, Texas*, pages 291-303, 1973.

[40] F. Ellyin and N. Turkkan. Out-of-plane Limit Couples of Nozzles in Cylindrical Vessels or Branch Pipes in Tee Connections. *Proc. Second ASME Int. Conf. Pressure vessel Technology, Part 1, Design and Analysis, San Antonio, Texas*, pages 361–373, 1973.

[41] F. Ellyin and N. Turkkan. Limit In-plane Couples of Nozzles in Cylindrical Vessels and Branch Connections in Piping Systems. *Proc. of the Second Int. SMIRT Conf., Brussels, Belgium*, 3, 1973.

[42] ASME Boiler and Pressure Code. *Section III, Division I, Subsection NB-3600, New York*, 1998.

[43] C.J. Billington, M. Lahani, and E. Tebbett. Background to New Formulae for the Ultimate Limit State of Tubular Joints. *Proc. Offshore Technology Conf., Houston, Texas*, 1982.

[44] Offshore Installations: Guidance on Design, Construction and Certification. *UK Health and Safety Executive, London, Fourth Edition*, 1990.

[45] Recommended Practice for Planning, designing and Constructing Fixed Offshore Platforms. *API RP2A 20th Edition, American Petroleum Institute, Washington*, 1993.

[46] J. Wardenier, Y. Kurobane, J.A. Packer, D. Dutta, and N. Yeomans. Design Guide for Circular Hollow Section (CHS) Joints under Predominantly Static Loading. *CIDECT Publication*, 1991.

[47] D.G. Moffat and J. Mistry. Interaction of External Moment Loads and Internal Pressure on a Variety of Branch Pipe Intersections. *Proc. 6th Int. Conf. Pressure Vessel Technology, Beijing*, 1988.

[48] C. Nadarajah, D. Mackenzie, and J.T. Boyle. Limit and Shakedown Analysis of Nozzle/Cylinder Intersections under Internal Pressure and In-plane Moment Loading. *Int. Journal Pressure Vessels and Piping*, 68:261–272, 1996.

[49] H.D. Schulze, U. Brenner, and H. Fuhlrott. Application of Fracture Mechanics for Safety Assessments of Cracked Pipes. *ASME, Circumferential Cracks in Pressure Vessels and Piping*, 1:129–140, 1984.

[50] Th. Schwarz, K.H.Herter, P. Julisch, and W. Stoppler. Experimental Investigations on the Strength and Fracture Behaviour of Degraded Piping Components. *Proc. of the 12th Int. SMIRT Conf.*, pages 87–92, 1993.

[51] X. Schuler, D. Blind, U. Eisele, K.H. Herter, and W. Stoppler. Fracture Mechanics Evaluation of Cracked Components with Consideration of Multiaxiality of Stress State. *Nuclear Eng. and Design*, 151:291–305, 1994.

[52] D. Plancq and M.N. Berton. Limit Analysis based on Elastic Compensation Method of Branch Pipe Tee Connection under Internal Pressure and Out-of-Plane Moment Loading. *Int. Journal Pressure Vessels and Piping*, 75:819–825, 1998.

[53] S. Chapuliot, D. Moulin, G. Goudet, and J. Bourg. Behavior of Cracked Branch Pipes Subject to Out-of Plane Bending. *9th ICF, Sydney*, 1997.

[54] S. Chapuliot and D. Moulin. Experimental and Numerical Study on the Behavior of Cracked Branch Pipes. *ASME PVP ??*, 365:115–120, 1998.

[55] S. Chapuliot and D. Moulin. Effect of Internal Pressure on the Tearing of a Surface Crack in a Branch Pipe Submitted to Out-of-plane Bending. *Proc. of the 14th Int. SMIRT Conf., Lyon*, 1997.

[56] A. Stacey, J.V. Sharp, and N.W. Nichols. The Influence of Cracks on the Static Strength of Tubular Joints. *15th Int. Conf. on Offshore Mechanics and Arctic Eng., Florence*, 1996.

[57] A. Stacey, J.V. Sharp, and N.W. Nichols. Static Strength Assessment of Cracked Tubular Joints. *15th Int. Conf. on Offshore Mechanics and Arctic Eng., Florence*, 1996.

[58] M.J. Cheaitani and F.M. Burdekin. Ultimate Strength of Cracked Tubular Joints. *Tubular Structures VI, Proc. 6th Int. Symp. Tubular Structures, Melbourne*, pages 607–616, 1994.

[59] *BS7910: Guide on Methods for Assessing the Acceptability of Flaws in Metallic Structures.* British Standards Institution, 1999.

[60] J.J. Cao, G.J. Yang, J.A. Packer, and F.M. Burdekin. Crack Modelling in FE Analysis of Circular Tubular Joints. *Engineering Fracture Mechanics*, 61:537–553, 1998.

[61] A.J. Carter. A Library of Limit Loads for FRACTURE.TWO. *Nuclear Electric Report, Issue 2*, 1999.

[62] M.A. Lynch, D.G. Moffat, D.N. Moreton, and R.A. Ainsworth. Limit Loads for Cylinders with Fully Circumferential Internal Cracks in Tension: Comparison of Analytical and Finite Element Data. *9th Int. Conf. Pressure Vessel Technology, Sydney*, 2000.

[63] R.A. Ainsworth. Internal Technical Note. *British Energy Internal Document*, 1999.

[64] A. Mendelson. *Plasticity: Theory and Application.* Collier-MacMillan Ltd., 1968.

[65] PDA Engineering. *PATRAN, Version 8.5, Santa Ana, California, USA.*

[66] Karlsson Hibbitt and Inc. Sorenson. *ABAQUS/Standard Users Manual, Version 5.8.*

[67] T.L. Anderson. *Fracture Mechanics: Fundamentals and Applications.* CRC Press Inc., USA, 1991.

[68] G.E. Dieter. Mechanical Behaviour of Materials under Tension. *Metals Handbook, 9th edition*, 8. Mechanical Testing.

[69] M.J. Fagan. *Finite Element Analysis: Theory and Practice.* Addison Wesley Longman Ltd., England, 1992.

[70] Y. Wang and A. Kuo. Development of Guidelines for FEA Modelling of Cylinder-to-Cylinder Intersections (Draft Report). *Optimal Corporation (for PVRC)*, 1999.

[71] BS806. *Design and Construction of Ferrous Piping Installations for and in Connection with Land Boilers, Appendix H.* British Standards Institution, 1992.

[72] D.G. Moffat, J. Mistry, and J.A.M. Mwenifumbo. Moment Loads on Branch-pipe Junctions: The Effect of Run-pipe Fixing on Elastic Stress Levels and its Implications on Plastic Limit Loads. *Int. Journal Pressure Vessels and Piping*, 38(4):249–259, 1989.

[73] R-Codes User Guide, Software for Assessing the Integrity of Structures Containing Defects. *British Energy Generation Ltd*, 1999.

[74] D.N. Moreton and R. Durnford. Three-Dimensional Tool Compensation for a Three-Axis Turning Centre. *Int. J. Advanced Manufacturing Technology*, 15:649–654, 1999.

[75] N. Jones and T. Wierzbicki. *Structural Crashworthiness.* Butterworth and Co., 1983.